

Oceanologia

Official Journal of the Polish Academy of Sciences: Institute of Oceanology and Committee on Maritime Research



EDITOR-IN-CHIEF

Janusz Pempkowiak
Institute of Oceanology Polish Academy of Sciences, Sopot, Poland

MANAGING EDITOR

Agata Bielecka - abielecka@iopan.pl

Editorial Office Address

Institute of Oceanology Polish Academy of Sciences (IO PAN)
Powstańców Warszawy 55
81-712 Sopot, Poland
Mail: editor@iopan.pl

ADVISORY BOARD

Prof. Xosé Antón Álvarez Salgado

Marine Research Institute, Spanish Research Council (CSIC), Vigo, Spain

Dr Boris Chubarenko

P.P. Shirshov Institute of Oceanology, Russian Academy of Sciences, Kaliningrad, Russia

Prof. Mirosław Darecki

Institute of Oceanology, Polish Academy of Sciences, Sopot, Poland

Prof. Jerzy Dera

Institute of Oceanology, Polish Academy of Sciences, Sopot, Poland

Prof. Agnieszka Herman

Institute of Oceanography, University of Gdańsk, Gdynia, Poland

Prof. Genrik Sergey Karabashev

P.P. Shirshov Institute of Oceanology, Russian Academy of Sciences, Moscow, Russia

Prof. Alicja Kosakowska

Institute of Oceanology, Polish Academy of Sciences, Sopot, Poland

Prof. Zygmunt Kowalik

Institute of Marine Science, University of Alaska Fairbanks (UAF), USA

Prof. Matti Leppäranta

Institute of Atmospheric and Earth Sciences, University of Helsinki, Finland

Prof. Ewa Łupikasza

Faculty of Earth Sciences, University of Silesia, Sosnowiec, Poland

THEMATIC EDITORS

Prof. Stanisław Massel – Institute of Oceanology, Polish Academy of Sciences, Sopot, Poland

Prof. Tymon Zieliński – Institute of Oceanology, Polish Academy of Sciences, Sopot, Poland

Prof. Hanna Mazur-Marzec

Institute of Oceanography, University of Gdańsk, Gdynia, Poland

Prof. Dag Myrhaug

Norwegian University of Science and Technology (NTNU), Trondheim, Norway

Prof. Sergej Olenin

Coastal Research and Planning Institute, Klaipeda University CORPI, Klaipeda, Lithuania

Prof. Tarmo Soomere

Tallinn University of Technology, Estonia

Prof. Hans von Storch

Institute of Coastal Research, Helmholtz Center Geesthacht, Germany

Prof. Dariusz Stramski

Scripps Institution of Oceanography, University of California, San Diego, USA

Prof. Piotr Szefer

Department of Food Sciences, Medical University of Gdańsk, Poland

Prof. Antoni Śliwiński

Institute of Experimental Physics, University of Gdańsk, Poland

Prof. Muhammet Türkoğlu

Çanakkale Onsekiz Mart University, Turkey

Prof. Jan Marcin Węśławski

Institute of Oceanology, Polish Academy of Sciences, Sopot, Poland

This journal is supported by the Ministry of Science and Higher Education, Warsaw, Poland

Indexed in: ISI Journal Master List, Science Citation Index Expanded, Scopus, Current Contents, Zoological Record, Thomson Scientific SSCI, Aquatic Sciences and Fisheries Abstracts, DOAJ

IMPACT FACTOR ANNOUNCED FOR 2016 IN THE 'JOURNAL CITATION REPORTS' IS 1.500; 5-year IF is 1.341

Publisher

Elsevier Sp. z o.o.
22, Jana Pawła II Avenue
00-133 Warsaw, Poland

Associate Publisher

Justyna Kasprzycka
j.kasprzycka@elsevier.com
+31 20 485 3846

ISSN 0078-3234



Available online at www.sciencedirect.com

ScienceDirect

journal homepage: www.journals.elsevier.com/oceanologia/



ORIGINAL RESEARCH ARTICLE

Bioactive metabolites produced by *Spirulina subsalsa* from the Baltic Sea

Karolina Szubert^a, Magda Wiglusz^a, Hanna Mazur-Marzec^{a,b,*}

^a Institute of Oceanography, University of Gdańsk, Gdynia, Poland

^b Institute of Oceanology, Polish Academy of Sciences, Sopot, Poland

Received 2 September 2017; accepted 17 November 2017

Available online 6 December 2017

KEYWORDS

Spirulina subsalsa;
Cyanometabolites;
Cytotoxicity;
Proteases inhibitors;
Mass spectrometry

Summary Cyanobacteria are known producers of compounds with possible medical applications. So far, the biotechnological potential of *Spirulina subsalsa* has been explored in few studies. They were mainly focused on the use of this cyanobacterium as a bioremediation agent. In our study, seven fractions from Baltic-derived *S. subsalsa* CCNP1310 were obtained and their cytotoxic effect on the T47D breast cancer cell line as well as inhibitory effects against elastase, trypsin, thrombin, chymotrypsin, and carboxypeptidase A were examined. Four fractions revealed a significant decrease in relative viability of cancer cells. Two inhibited the activity of chymotrypsin and one carboxypeptidase A, but at a moderate level. No effect was observed against other tested proteases. Active fractions were screened with liquid chromatography tandem mass spectrometry (LC–MS/MS) optimized for the detection of peptides, for preliminary characterization of bioactive compounds. We identified three groups of compounds which share the same fragment ions and are possibly linked with effects observed in conducted tests. Our research indicates for the first time that compounds produced by Baltic strain of *S. subsalsa* not only have high activity against T47D cancer cells but also seem to work selectively as they do not have strong inhibitory effect against the tested enzymes. That indicates the existing potential of the cyanobacterium to be used as a source of important cytotoxic agents.

© 2017 Institute of Oceanology of the Polish Academy of Sciences. Production and hosting by Elsevier Sp. z o.o. This is an open access article under the CC BY-NC-ND license (<http://creativecommons.org/licenses/by-nc-nd/4.0/>).

* Corresponding author at: Institute of Oceanology, Polish Academy of Sciences, Powstańców Warszawy 55, 81-712 Sopot, Poland.

E-mail addresses: karolina.szubert@phdstud.ug.edu.pl (K. Szubert), magda.wiglusz@phdstud.ug.edu.pl (M. Wiglusz), biohm@iopan.gda.pl (H. Mazur-Marzec).

Peer review under the responsibility of Institute of Oceanology of the Polish Academy of Sciences.



Production and hosting by Elsevier

<https://doi.org/10.1016/j.oceano.2017.11.003>

0078-3234/© 2017 Institute of Oceanology of the Polish Academy of Sciences. Production and hosting by Elsevier Sp. z o.o. This is an open access article under the CC BY-NC-ND license (<http://creativecommons.org/licenses/by-nc-nd/4.0/>).

1. Introduction

Cyanobacteria, as primary producers, are important components of the phytoplankton community. In eutrophic ecosystems, and under favorable conditions, they can develop into blooms. The ecosystem consequences of the blooms are complex and still not fully recognized (Havens, 2008; Peng et al., 2017; Šulčius et al., 2017). At least part of the effects of cyanobacteria on co-occurring organisms can be attributed to the activity of secondary metabolites produced and released to the environment (Karjalainen et al., 2007). Recently, these metabolites have attracted a lot of scientific attention, as beside environmental significance they can find application in different branches of our life, including agriculture and food industry. Cyanobacterial products are also seriously considered as potential drugs and cosmetics (Rastogi and Sinha, 2009; Singh et al., 2011). For this reason, the species from *Arthrospira* genus, mainly *Arthrospira platensis*, have been widely explored (Ciferri and Tiboni, 1985; Gademann, 2011; Hosseini et al., 2013). Unfortunately, in the majority of the reports, the cyanobacterium was wrongly classified as belonging to *Spirulina* genus. The situation is further complicated by the fact that products from *Arthrospira* are sold on the market under the name of *Spirulina*. To solve the problem, Tomaselli et al. (1996) suggested that in scientific published materials only the proper generic name of the cyanobacterium could be used. In all other cases, such as commercial products, the common name “*Spirulina*” could be accepted, if the correct scientific denomination of the organism is provided.

Spirulina genus was primarily described by Turpin (1827) as *Spirulina oscillarioides*. The author observed filamentous structures, usually in clusters or in fine mats which were macroscopically visible. The tightly and regularly screw-like coiled filaments were composed of cylindrical cells and intensely motile (rotating) trichomes. Later, Stizenberger (1852) introduced morphologically similar genus named *Arthrospira*. In subsequent years, the classification of these two genera remained a matter of dispute. Main morphological criteria dividing these two organisms are: trichome diameter, type of helicity, visibility of cross walls, cell wall pore pattern, mode of trichome fragmentation and presence of cylindrical bodies (Vonshak and Tomaselli, 2000). In recent years, the taxonomic classification of cyanobacteria has undergone extensive revision with the advent of phylogenetic analyses based on molecular sequence data. These analyses confirmed and justified the separation of these two genera. Currently, *Spirulina* is classified to Spirulinales order, while *Arthrospira* belongs to Oscillatoriales order (Komarek et al., 2014).

Spirulina subsalsa Oersted ex Gomont, used in our work, was first described by Gomont in 1892. The cyanobacterium occurs in salt and fresh waters all over the world (*S. subsalsa* Oersted ex Gomont.: Algaebase). In the Baltic Sea, it was reported for the first time by Witkowski in 1993. The trichomes of Baltic-derived *S. subsalsa* are 3.0–5.0 μm wide and form tightly coiled spirals. They glide with typical oscillatory, screw-like movements over the substrate. The cyanobacterium forms mat structures, usually of blue-green color but in the Baltic pinkish-red filaments were also observed (Włodarska-Kowalczyk et al., 2014). *S. subsalsa*

was found to be one of the components of cyanobacterial blooms that have harmful effects on lesser flamingos in lake Bogoria, Kenya (Ballot et al., 2004; Krienitz et al., 2003) and on blue shrimps, after they were stocked into pre-cleaned algal raceways (Lightner, 1978). However, there is no evidence that it produces any of the known cyanotoxins. Krienitz et al. (2003) and Ballot et al. (2004) found that *S. subsalsa* is one of the most abundant components of cyanobacterial communities in Kenyan lakes yet neither produces microcystins nor anatoxin-a, which were identified in flamingo stomach contents and their fecal pellets. Lightner (1978) did not identify the agent responsible for blue shrimps hemorrhagic enteritis, however, results of his work suggested that under certain conditions *S. subsalsa* produces a weak toxin that is mildly toxic to shrimps, but only when relatively large quantity of fresh cyanobacterial biomass was consumed.

So far, the potential biotechnological application of *S. subsalsa* has been explored in few studies. They were mainly focused on the use of this cyanobacterium as bioremediation agent for the accumulation of pollutants and industrial leftovers (Chakraborty et al., 2011; Huang and Zhihui, 2002; Jiang et al., 2015; Zhang et al., 2014; Zhihui and Guolan, 2000). *S. subsalsa* was also used as a biosensor for toxicity assessment of estuarine waters (Campanella et al., 2001). This species is also a source of polyhydroxyalkanoates (PHA), the environmentally friendly biopolymers which can find application among others in the production of implants and artificial tissues (Shrivastav et al., 2010).

In previous screening studies, *S. subsalsa* CCNP1310 was found to produce biologically active metabolites such as commercially important enzymes and unknown enzyme inhibitors, as well as agents promoting the growth of several bacterial strains (Mazur-Marzec et al., 2015). The results of the tests indicated that this organism is a promising candidate for further studies into the potential application of its metabolites. However, in the tests, crude extracts, containing a complex mixture of metabolites were used. The rich matrix of the samples could have attenuating or enhancing effects on the results of the performed assays. Therefore, the aim of our current work was to extend the existing knowledge of the activity of metabolites produced by the Baltic cyanobacterium *S. subsalsa* CCNP1310 by fractionation of crude extract (1) and application of series of biochemical assays (2). Attempts to characterize the active agent(s) were also made.

2. Material and methods

The list of reagents used in the study for extraction, separation and biochemical tests is presented in supplementary materials.

2.1. Culture, extraction, and fractionation of *S. subsalsa*

S. subsalsa, from Culture Collection of Northern Poland, strain CCNP1310 (accession number in GenBank KJ161437) was isolated from Puck Bay in 2009. Monospecies culture of the cyanobacterium was grown for biomass in Z8 medium (Kotai, 1972; Mazur-Marzec et al., 2015) supplemented with NaCl and MgSO₄ to obtain salinity at 7 [PSU], at room tem-

perature ($25 \pm 1^\circ\text{C}$) and continuous light of $10 [\mu\text{M photons m}^{-2} \text{s}^{-1}]$ provided by standard cool white fluorescent lamps (36 [W]). Biomass was harvested between 3 and 4 weeks of the culture, in the mid exponential growth phase. Freeze-dried cyanobacterial biomass (2 g) was extracted with 75% methanol (20 ml) by vortexing for 10 min, followed by 10 min bath sonication. Then, the extract was centrifuge ($10,000 \times g$) for 10 min. The obtained supernatant was dissolved in water so that the methanol content did not exceed 15%. The sample was loaded onto the 10-[g] SPE cartridge (Sep-Pak; C18 cartridge, Waters, Milford, USA). The cartridge was first washed with MiliQ water and then the sorbed substances were eluted with aqueous solutions of methanol, gradually increasing the strength of the eluent from 40% to 100%, at 10% step. The collected fractions were evaporated to dry residue.

2.2. Screening for enzyme inhibitors

The enzyme inhibition assays were performed according to protocols described by [Pluotno and Carmeli \(2005\)](#), [Ocampo Bennet \(2007\)](#), and [Kwan et al. \(2009\)](#). The detailed conditions of the five enzymatic assays are presented in [Table 1](#). Serial dilutions (from 10 times to 100,000 times) of the solid-phase extraction (SPE) fractions were prepared in MiliQ water. Standard inhibitors were dissolved either in water or in 1% DMSO (as indicated by the producer); the enzyme and the substrate were dissolved in a buffer solution or in water ([Table 1](#)). The mixtures containing the sample or standard inhibitor (positive control), enzyme and buffer were preincubated in microplates for 5–20 min. Then, the substrate solution was added and the mixture was incubated for the next 10–20 min, depending on the enzyme ([Table 1](#)). The absorbance was measured with a microplate reader (Versa Max Tunable Microplate Reader, Sunnyvale, USA). Data were obtained from three independent experiments; in each test, the samples were assayed in triplicate.

2.3. Cytotoxic activity

Human breast adenocarcinoma cell line was obtained from CLS Cell Lines Service GmbH (Eppelheim, Germany). Monolayer cultures of T47D cells were maintained in RPMI 1640 medium supplemented with 10% (v/v) fetal bovine serum and 1% antibiotics mixture (penicillin and streptomycin). Cells were incubated at 37°C in CO_2 (5%) incubator (New Brunswick Galaxy 170s, Eppendorf, Germany). Cell viability was determined by MTT method as described by [Felczykowska et al. \(2015\)](#). For this purpose, T47D cells were seeded at a density of 4×10^3 (for 24 h of incubation) and 2×10^3 (for 48 h of incubation) per well of 96-well plate and allowed to attach overnight. Next, the medium was replaced with a fresh portion of medium containing *S. subsalsa* SPE fractions at concentrations 25, 50, 100 and $200 \mu\text{g ml}^{-1}$. Then, $100 \mu\text{l}$ of MTT solution (4 mg ml^{-1}) was added to each well. After 2 h of incubation, the medium was removed and formazan was dissolved in $100 \mu\text{l}$ of added DMSO. The absorbance of the reaction mixtures was measured at 570 nm (with reference wavelength 660 nm) with a microplate reader. Data from three independent experiments were collected. In MTT

assay, cell viability drop below 50% was considered as significant.

2.4. Mass spectrometry analysis

The SPE fractions were transferred to chromatographic vials and analyzed by liquid chromatography tandem mass spectrometry (LC–MS/MS) as described in [Mazur-Marzec et al. \(2015\)](#). The instrument was equipped with Agilent 1200 (Agilent Technologies, Waldboronn, Germany) coupled online to a hybrid triple quadrupole/linear ion trap mass spectrometer (QTRAP5500, Applied Biosystems, Sciex, Concord, ON, Canada). A turbo ion source (550°C , 5.5 kV) operating in positive mode was used. To determine the content of the SPE fractions, the information-dependent acquisition method (IDA) was used. Enhanced product ion spectra (EPI) were acquired at the interval 50–1000 Da with 50 V collision energy and 20 V collision energy spread. Data were gathered and processed with Analyst QS (Version 1.5.1, Applied Biosystems/MDS Analytical Technologies, Concord, ON, Canada, 2008).

3. Results

As a result of solid phase extraction, eight fractions from *S. subsalsa* extract were collected. In the text, they were denoted by numbers corresponding to the methanol concentration [%] in the eluent.

3.1. Inhibition of enzyme activity

Inhibitory activity of SPE fractions against proteases was assessed using elastase, trypsin, thrombin chymotrypsin and carboxypeptidase A. Results of the assays are shown in [Table 2](#). No inhibitory effect was observed for elastase, trypsin or thrombin. Fractions 70 and 80 revealed moderate effect for chymotrypsin. Fraction 90 inhibited carboxypeptidase A, but only at the highest concentration.

3.2. Cytotoxicity against human breast cancer cells

The activity of eight SPE fractions from *S. subsalsa* extract toward T47D human breast cancer cell line was evaluated using MTT viability test. As shown in [Fig. 1](#), fractions 40, 60, 80 and 90, revealed the highest potency in decreasing T47D cancer cell viability. The strongest effect was observed for fraction 40 and 60 with IC_{50} values $25 \mu\text{g ml}^{-1}$, yet concentration-dependency in case of those fractions were low. Cytotoxic and concentration-dependent effects were observed for fractions 80 and 90 with IC_{50} values $100 \mu\text{g ml}^{-1}$. Of all tested samples, the highest decrease in T47D cancer cell viability was recorded for fraction 90 applied at concentration $200 \mu\text{g ml}^{-1}$ (mean relative viability 17.5%).

3.3. LC–MS/MS analysis

The content of the active fractions was analyzed with LC–MS/MS system optimized for the detection of peptides. Using IDA mode, the m/z values, retention time and a peak area of the detected ions were determined ([Table 3](#)). For the most intensive peaks, which could be responsible for the observed

Table 1 Enzyme inhibition assay.

	Chymotrypsin	Trypsin	Elastase	Thrombin	Carboxypeptidase-A
Enzyme	Chymotripsin 0.1 mg ml ⁻¹ Solvent: buffer solution Volume: 10 µl	Trypsin 1 mg ml ⁻¹ Solvent: buffer solution Volume: 10 µl	Elastase 75 µg ml ⁻¹ Solvent: buffer solution Volume: 10 µl	Thrombin 0.5 mg ml ⁻¹ Solvent: water Volume: 10 µl	Carboxypeptidase-A 1.6 µM Solvent: buffer solution Volume: 10 µl
Inhibitor (or sample)	Aprotinine 50–500 µg ml ⁻¹ Solvent: water Volume: 10 µl	Aprotinine 10–60 µg ml ⁻¹ Solvent: water Volume: 10 µl	Elastatinal 5–125 µg ml ⁻¹ Solvent: 1% DMSO Volume: 10 µl	4-(2-Aminoethyl) benzenesulfonyl fluoride hydrochloride (AEBSF) 60–2400 µg ml ⁻¹ Solvent: water Volume: 10 µl	CPI 5–100 µg ml ⁻¹ Solvent: water Volume: 10 µl
Buffer	50 mM Tris–HCl 100 mM NaCl 1 mM CaCl ₂ , pH 7.5 Volume: 100 µl	50 mM Tris–HCl, 100 mM NaCl, 1 mM CaCl ₂ , pH 7.5 Volume: 100 µl	0.2 M Tris–HCl, pH 8.0 Volume: 150 µl	0.2 M Tris–HCl, pH 8.0 Volume: 170 µl	50 [mM] Tris–HCl, pH 7.5 Volume: 160 µl
Preincubation	5 min at 25°C	5 min at 25°C	20 min at 30°C	10 min at 25°C	10 min at 25°C
Substrate	Suc-Gly-Gly-pnitroanilide 2 mM Solvent: buffer solution Volume: 100 µl	Nα-benzoyl-L-arginine-4- nitroanilide hydrochloride BAPNA; 2 mM Solvent: buffer solution Volume: 100 µl	N-succinyl-Ala-Ala-Ala-p- nitroanilide 2 mM Solvent: buffer solution Volume: 30 µl	N-p-tosyl-Gly-Pro-Lys-p- nitroanilide acetate salt 0.5 mg ml ⁻¹ Solvent: buffer solution Volume: 20 µl	N-4-Metoxypheylazofornyl- Phe-OH potassium salt; 0.2 mM Solvent: 1% DMSO Volume: 20 µl
Incubation	20 min at 25°C	20 min at 25°C	10 min at 30°C	10 min at 25°C	10 min at 25°C
Wavelength	405 nm	405 nm	405 nm	405 nm	350 nm
Reference	(Ocampo Bennet, 2007)	(Pluotno and Carmeli, 2005)	(Kwan et al., 2009)	(Ocampo Bennet, 2007)	(Ocampo Bennet, 2007)

Table 2 Inhibition of serine proteases by SPE fractions from *Spirulina subsalsa* CCNP1310; Inhibitory effects against the enzymes were studied by microplate test method as described in Section 2. Results are mean of tests done in triplicate; “+” inhibition observed up to 100 x dilution; “–” no effect observed.

Fraction	0	40	50	60	70	80	90	100
Elastase	–	–	–	–	–	–	–	–
Trypsin	–	–	–	–	–	–	–	–
Thrombin	–	–	–	–	–	–	–	–
Chymotrypsin	–	–	–	–	+	+	–	–
Carboxypeptidase A	–	–	–	–	–	–	+	–

activity, the product ion spectra were collected (Supplementary materials Fig. 15). We identified three groups of ion peaks which share the same fragment ions and are possibly linked with effects observed in conducted tests. Presence of ions characterized by m/z at 677 (in fractions 40 and 50) and 832, (in fraction, 90) (1) and doubly charged ions with m/z 602 (fractions 60 and 70) and 594 (fraction 60) (2), corresponds to cytotoxicity revealed in MTT test. Ion peak at $m/z = 649$ was detected in fractions 70 and 80 which showed inhibitory activity against chymotrypsin (3).

4. Discussion

In the search for agents effective in the treatment of incurable or/and persistent diseases, the marine environment with its unexplored biodiversity appears to be of high importance. Seas and oceans are inhabited by 92.3 million species and marine organisms make up 95% of the biomass on Earth. However, only 10% of publications on biodiversity refers to marine organisms and only slightly over 0.1% of published genomes describe marine species (Titilade and Olalekan,

2015). Also, the knowledge about secondary metabolites produced by marine organisms is limited. Among marine microorganisms, cyanobacteria are one of the most effective producers of compounds which show strong and diverse biological activity. It was estimated that approximately 24% of marine natural products commercially available for biomedical research are of cyanobacterial origin (Gerwick and Moore, 2012). Due to diverse mechanisms of action and potent activity, the compounds are highly attractive as potential drug candidates (Felczykowska et al., 2015; Gerwick and Moore, 2012; Herfindal et al., 2005; Humisto et al., 2016; Mazur-Marzec et al., 2015; Oftedal et al., 2010). Bioactive cyanobacterial products were mainly identified in organisms from tropical waters. However, recent studies revealed that also cyanobacteria from temperate regions, such as the Baltic Sea, can be explored as sources of metabolites with the potential biotechnological application.

In order to select natural products with desired activity, screening studies with application of different bioassays are conducted. In the tests, the effect of metabolites on the specific proteolytic activity of the enzyme can be studied. Proteases are fundamental for the functioning of live structures and occur in all organisms (Patel, 2017). Compounds, which deregulate activity of such proteases as chymotrypsin, trypsin, elastase, and thrombin, can find application in the treatment of several metabolic disorders, such as urticaria, contact dermatitis, asthma, inflammatory bowel disease, blood clogging, neurological disorders or cancer (Patel, 2017; Sapio and Fricker, 2014).

Several strains of Baltic cyanobacteria were proven to produce metabolites with inhibitory effect against serine proteases (Table 4). Neither of the previously tested crude extracts from 27 Baltic cyanobacteria (Mazur-Marzec et al., 2015), nor SPE fractions from *S. subsalsa* CCNP1310 examined in this study, were active against elastase. That can indicate the rare occurrence of elastase inhibitors among metabolites produced by these microorganisms. Separated fractions from

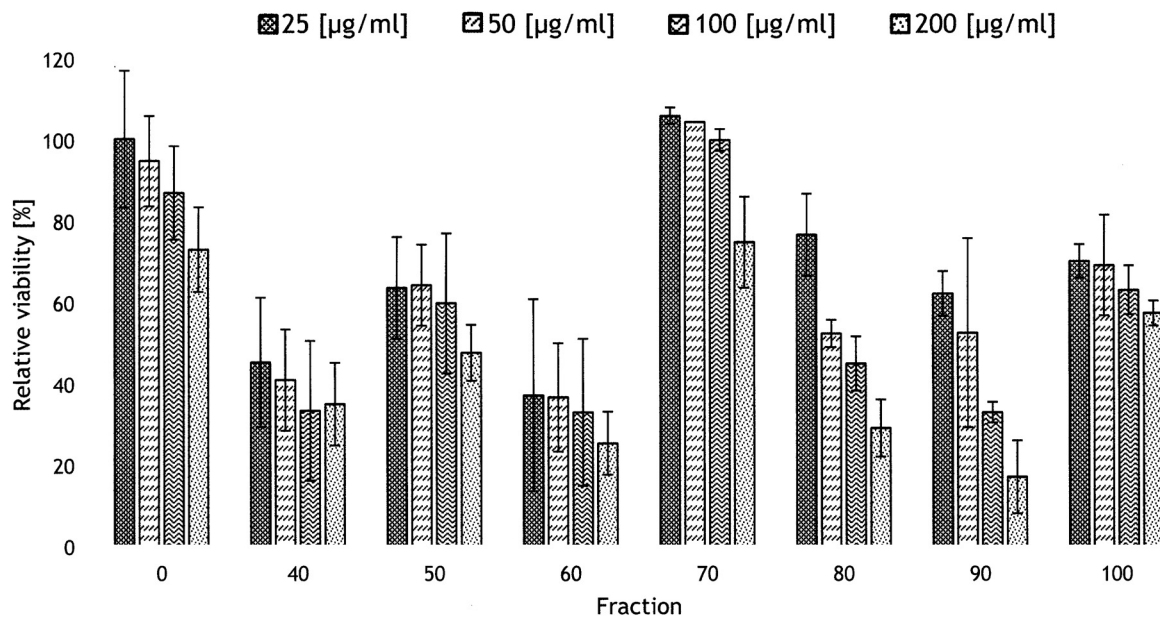


Figure 1 The effects of SPE fractions from *Spirulina subsalsa* CCNP1310 extract on the viability of T47D human breast cancer cells assayed by MTT method as described in Section 2. Each bar represents a mean (\pm SD) of three experiments performed in triplicate.

Table 3 Characteristics of ions detected by LC–MS/MS in *Spirulina* CCNP1310 fractions.

Fraction	Retention time [min]	Peak area of extracted ion	<i>m/z</i>	Fragment ions
40	9.23	2.81×10^{10}	677	70, 86, 103, 120
	10.45	1.11×10^{10}	633	271, 289, 299, 317
	10.50	2.29×10^9	573	
	10.93	3.18×10^9	557	195, 213, 281, 299, 367, 385, 453, 471
50	4.63	2.89×10^9	621	70, 170, 243, 534, 541, 626, 643
	5.59	1.47×10^9	518	127, 151, 210, 271, 415, 474
	9.24	1.19×10^{10}	677	70, 86, 103, 120
	9.47	5.28×10^9	500	127, 145, 379, 397, 456
	11.68	6.92×10^9	659	120, 379, 395, 511, 572, 599
60	9.68	2.59×10^{10}	1203/602 ^a	70, 112, 138, 180, 209, 350, 378
	10.35	3.75×10^9	1187/594 ^a	70, 138, 180, 209, 350, 595, 633, 762, 886
70	9.68	6.41×10^9	1203/602 ^a	70, 112, 138, 180, 209, 350, 378
	9.79	6.51×10^9	1050/524 ^a	86, 136, 183, 262, 308, 326, 432, 478, 562, 747, 860, 975
	10.45	2.31×10^9	547	105, 173, 323, 349, 385, 529
	11.10	4.25×10^9	647	159, 323, 385, 347, 485
	11.78	1.01×10^{10}	649	109, 171, 259, 421, 487
80	1.96	1.15×10^9	641	109, 139, 183, 297, 413, 527, 605
	11.09	3.78×10^9	647	86, 104, 125, 166, 184, 502
	11.55	5.79×10^9	649	109, 171, 259, 421, 487
	11.79	1.71×10^{10}	650	347, 487
90	9.71	1.25×10^{10}	832	70, 86, 103, 120
100	11.59	1.34×10^9	883	347, 405, 467, 482, 500, 629, 657, 721
	11.65	3.28×10^9	500	144, 236, 438, 482, 500

^a Doubly charged ions.

CCNP1310 had also no effect against trypsin and thrombin, although such activity was previously revealed in the crude extract from this cyanobacterium. The possible explanations for this discrepancy are that during SPE procedure some compounds were lost and/or some were separated into several different fractions. As a consequence, their concentration in the tested samples could have been too low to exert any effect on the enzyme. We revealed the moderate activity of fractions 70 and 80 from *S. subsalsa* CCNP1310 against chymotrypsin for the first time. As in both fractions, ion peak at *m/z* = 649 was detected, the link between its presence and the inhibitory activity against chymotrypsin can be assumed. Carboxypeptidase A was found to be inhibited by components of fraction 90 and this result confirms previous effects observed in tests performed on a crude extract from the cyanobacterium (Mazur-Marzec et al., 2015).

To discover anticancer natural products, cell based methods are the most common. The T47D cell line applied in our tests derives from a 54-year-old woman and is one of the most widely used cell line in breast cancer studies. It was shown to be an ideal experimental model to elucidate the progesterone-specific effects of a luminal A subtype of breast cancer (Yu et al., 2017). Cytotoxic activity against cancer cells have been revealed in many strains of cyanobacteria, but only in several cases, the active agents were identified (Rastogi and Sinha, 2009; Singh et al., 2011). The range of cellular targets of cytotoxic cyanobacterial metabolites is wide and include cytoskeletal structures, as well as enzymes (Table 5).

In addition, there are numerous natural anticancer agents whose mechanism of action has not been elucidated yet, e.g.: dragonamides, minutissamides, and almiramides (Humisto et al., 2016).

As for Baltic cyanobacteria, Herfindal et al. (2005) and Oftedal et al. (2010) found that extracts from benthic strains of *Anabaena* sp. induced apoptosis of acute myeloid leukemia cells. Further research of Humisto et al. (2016) confirmed that Baltic-derived *Anabaena* strains produce the most promising leukemia drug candidate. In studies carried out by Felczykowska et al. (2015), ethanol extracts from Baltic strains of *Pseudanabaena* sp., *Microcystis aeruginosa*, and *Pseudanabaena cf. galeata* had cytotoxic activity toward breast cancer cells and uterine cervix origin, but not against normal dermal fibroblasts. Although in several studies a potential of Baltic cyanobacteria to synthesized novel bioactive compounds was demonstrated, the metabolites responsible for cytotoxic effects were not identified. In our work, we proved that some SPE fractions from of *S. subsalsa* CCNP1310 cells contain metabolites cytotoxic against human breast cancer cells, line T47D. As active fractions were separated by non-active one, we presume that *S. subsalsa* CCNP1310 produces more than one cytotoxic agent.

Mass spectrometry analysis conducted in our study revealed that in the TIC of fraction 90, only one major ion peak was present, which strongly links it with the observed cytotoxic activity against the T47D cells. The ion detected in IDA mode is characterized by *m/z* 832, and fragment ions at *m/z* 70, 86,

Table 4 Marine cyanobacterial metabolites of known inhibitory properties against selected proteases.

Compound	Species	Class of compound	Place of isolation	Target (protease)	Reference
Bouillomides A–B	<i>Lyngbya bouillonii</i>	Depsideptides	Guam	Elastase, chymotrypsin	Rubio et al. (2010)
Kempopeptin A	<i>Lyngbya</i> sp.	Cyclic depsipeptide	Grassy Kay	α -Chymotrypsin, elastase	Taori et al. (2008)
Kempopeptin B	<i>Lyngbya</i> sp.	Cyclic depsipeptide	Grassy Kay	Trypsin	Taori et al. (2008)
Largamides A–C	<i>Lyngbya confervoides</i>	Cyclic depsipeptides	No data	Elastase	Plaza and Bewley (2006)
Largamides D–G	<i>Oscillatoria</i> sp.	Cyclic depsipeptides	No data	α -Chymotrypsin	Plaza and Bewley (2006)
Lyngbyastatin 4	<i>Lyngbya confervoides</i>	Cyclic depsipeptide	Florida	α -Chymotrypsin, elastase	Matthew et al. (2007)
Lyngbyastatin 5–7	<i>Lyngbya</i> spp.	Cyclic depsipeptides	South Florida	Elastase	Taori et al. (2007)
Lyngbyastatin 8–10	<i>Lyngbya semiplena</i>	Cyclic depsipeptides	Guam	Elastase	Kwan et al. (2009)
Molassamide	<i>Dichothrix utahensis</i>	Depsideptide	Molasses	α -Chymotrypsin, elastase	Gunasekera et al. (2008)
Pompanopeptin A	<i>Lyngbya confervoides</i>	Cyclic peptide	Florida	Trypsin	Matthew et al. (2008)
Symplocamide	<i>Symploca</i> sp.	Cyclic peptide	Papua New Guinea	Chymotrypsin, trypsin	Linnington et al. (2008)
Tiglicamides A–C	<i>Lyngbya confervoides</i>	Cyclic depsipeptides	Florida	Elastase	Matthew et al. (2009)
Somamide B	<i>Lyngbya majuscula</i>	Cyclic depsipeptide	South Florida	Elastase, chymotrypsin	Taori et al. (2007)
Aeruginosins	<i>Schizothrix assemblage</i> <i>Microcystis viridis</i> , <i>Oscillatoria agardhii</i> , <i>Microcystis aeruginosa</i>	Lipopeptide	No data	Trypsin, thrombine	Ersmark et al. (2008)
Pitipeptolides A- B	<i>Lyngbya majuscula</i>	Cyclic depsipeptides	No data	Elastase	Costa et al. (2012)
Anabenopectin	<i>Oscillatoria agardhii</i>	Cyclic peptides	No data	Trypsin	Burja et al. (2001)
Aeruginosins	<i>Nodularia spumigena</i>	Linear peptides	Baltic Sea	Trypsin, thrombine	Fewer et al. (2013)
Spumigins	<i>Nodularia spumigena</i>	Linear peptides	Baltic Sea	Trypsin	Fewer et al. (2009)
Anabenopectines	<i>Nodularia spumigena</i>	Cyclic peptides	Baltic Sea	Trypsin, carboxypeptidase A, elastase	Spoof et al. (2015)
Pseudoaeruginosins	<i>Nodularia spumigena</i>	Peptide	Baltic sea	Trypsin	Fewer et al. (2013)

Table 5 Marine cyanobacterial metabolites of known structure and anticancer properties.

Compound	Species	Place of isolation	Molecular targets	Cancer cell line	Reference
Apratoxin A	<i>Lyngbya majuscula</i>	Finger's Reef, Apra Harbor, Guam	JAK/STAT pathway; inhibits Hsp90 function	KB, LoVo	Luesch et al. (2001b)
Aurilide	<i>L. majuscula</i>	Papua New Guinea	Prohibitin 1	NCI-H460, Neuro-2a	Han et al. (2006)
Bisebromoamide	<i>Lyngbya</i> sp.	Okinawa Prefecture	Actin filaments	HeLa	Teruya et al. (2009)
Carmaphycins A and B	<i>Symploca</i> sp.	Curaçao	Proteasome	H-460, HTC-116	Pereira et al. (2012)
Curacin A	<i>L. majuscula</i>	Curaçao	Microtubules	MCF-7, MDA-MB231, PC-3, OV-2008	Wipf et al. (2004)
Dolastatins 10 and 15	<i>Symploca</i> sp.	Ulong Channel, Palau	Microtubules	KB, LoVo	Luesch et al. (2001a)
Hoiamide D	<i>L. majuscula</i> and <i>Phormidium gracile</i>	Papua New Guinea	Inhibits MDM2/p53 interaction	NCI-H460, Neuro-2a	Pereira et al. (2009)
Isomalylngamides A and A1	<i>L. majuscula</i>	Taiwan	Inactivation of cellular kinases	MCF-7, MDA-MB-231	Chang et al. (2011)
Lagunamide A	<i>L. majuscula</i>	Pulau Hantu, Singapore	Prohibitin 1	P388, A549, PC3, HCT8, SK-OV3, HCT8, MCF7	Tripathi et al. (2012)
Largazole	<i>Symploca</i> sp.	Key Largo, Florida	Class 1 histone deacetylase	MDA-MB-231, U2OS, HT29, IMR-32	Taori et al. (2007)
Somocystinamide A	<i>L. majuscula</i>	Somo Somo, Fiji	Caspase-8-dependent cell death pathway	Neuro-2a	Nogle and Gerwick (2002)
Symplocamide A	<i>Symploca</i> sp.	Sunday Island, Papua New Guinea	Chymotrypsin	H-460, Neuro-2a	Linnington et al. (2008)
Tubercidin	<i>Plectonema radiosum</i>	Fiji	Microtubules	KB, HL-60	Stewart et al. (1988)

120. These low mass ions are probably immonium ions of Pro (or Arg), Leu/Ile and Phe, respectively, and indicate the peptidic structure of the compound. Trace amounts of the ion in fraction 80 was detected in enhanced ion product mode. As ion at m/z 677, present in cytotoxic fractions 40 and 50, also gave these product ions, it can be concluded that it represents structural analogue of the same class of peptide as a compound in fraction 90. The TIC of fraction 60, which was also active in MTT assay against the breast cancer cells, was characterized by the presence of major ion peak at m/z 602 and less intense ion peak at m/z 594. Both ions have several fragment ions in common, therefore they can also be classified to the same group of compounds. Ion peak at m/z 602 can be observed also in TIC of fraction 70. This fraction, however, was not active in MTT assay, which can be explained by the four-times lower content of the compound.

In our study, the activity of *S. subsalsa* metabolites against T47D cells was revealed. Although an extract from a small amount (2 g) of lyophilized material was used, significant effects were observed even at $25 \mu\text{g ml}^{-1}$ concentration of the tested material. In similar studies conducted on crude extracts from 1 g of Baltic-derived cyanobacteria, activity against cancer cells was also observed, but never at concentrations lower than $50 \mu\text{g ml}^{-1}$ (Felczykowska et al., 2015). This could indicate that *S. subsalsa* metabolites are highly active and exert an effect on T47D cells even at small amounts. Low amounts of bioactive compounds produced by organisms might make the process of their identification difficult. In such cases, the mass cultivation of cyanobacteria is indispensable to isolate sufficient quantities of the active molecule and to proceed to further steps of drug discovery process.

Cytotoxic activity of metabolites of *S. subsalsa* has never been reported. Our research indicates that compounds produced by this cyanobacterium not only have strong activity against T47D cancer cells but also seem to work selectively, as they do not have strong inhibitory effect against the tested enzymes, especially in the case of fractions 40 and 60. Although in conducted research, the compounds responsible for the observed activity were not unequivocally identified, some characteristic features of their structure were described. This improves the quality of the work, compared to studies where only activity of crude cyanobacterial extract was documented. The tests showed for the first time the existing potential of the Baltic *S. subsalsa* to be used as a source of important cytotoxic agents. In view of these promising results, further studies are worth to be continued.

Acknowledgments

This study was financially supported by the National Science Centre in Poland (project number NCN 2016/21/B/NZ9/02304; The grant holder Hanna Mazur-Marzec HMM). We thank Justyna Kobos and Anna Krakowiak (Institute of Oceanography, University of Gdańsk, Gdynia, Poland) for all the support during cultivation process.

Appendix A. Supplementary data

Supplementary material related to this article can be found, in the online version, at [doi:10.1016/j.oceano.2017.11.003](https://doi.org/10.1016/j.oceano.2017.11.003).

References

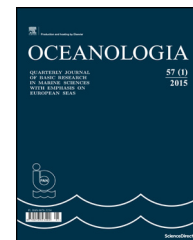
- Ballot, A., Krienitz, L., Kotut, K., Wiegand, C., Metcalf, J.S., Codd, G.A., Pflugmacher, S., 2004. Cyanobacteria and cyanobacterial toxins in three alkaline Rift Valley lakes of Kenya—Lakes Bogoria, Nakuru and Elmenteita. *J. Plankton. Res.* 26 (8), 925–935, <http://dx.doi.org/10.1093/plankt/fbh084>.
- Burja, A., Banaigs, B., Abou-Mansour, E., Burgess, G.J., Wright, P.C., 2001. Marine cyanobacteria – a prolific source of natural products. *Tetrahedron* 57, 9347–9377, [http://dx.doi.org/10.1016/S0040-4020\(01\)00931-0](http://dx.doi.org/10.1016/S0040-4020(01)00931-0).
- Campanella, L., Cubadda, F., Sammartino, M.P., Saoncella, A., 2001. An algal biosensor for the monitoring of water toxicity in estuarine environments. *Water Res.* 35 (1), 69–76, [http://dx.doi.org/10.1016/S0043-1354\(00\)00223-2](http://dx.doi.org/10.1016/S0043-1354(00)00223-2).
- Chakraborty, N., Banerjee, A., Pal, R., 2011. Accumulation of lead by free and immobilized cyanobacteria with special reference to accumulation factor and recovery. *Bioresource Technol.* 102 (5), 4191–4195, <http://dx.doi.org/10.1016/j.biortech.2010.12.028>.
- Chang, T.T., More, S.V., Lu, I.-H., Hsu, J.-C., Chen, T.-J., Jen, Y.C., Lu, C.-K., Li, W.-S., 2011. Isomalyngamide A, A-1 and their analogs suppress cancer cell migration in vitro. *Eur. J. Med. Chem.* 46 (9), 3810–3819, <http://dx.doi.org/10.1016/j.ejmech.2011.05.049>.
- Ciferri, O., Tiboni, O., 1985. The biochemistry and industrial potential of *Spirulina*. *Annu. Rev. Microbiol.* 39, 503–526, <http://dx.doi.org/10.1146/annurev.mi.39.100185.002443>.
- Costa, M., Costa-Rodriguez, J., Fernandes, M.H., Barros, P., Vasconcelos, V., Martins, R., 2012. Marine cyanobacteria compounds with anticancer properties: a review on the implication of apoptosis. *Mar. Drugs* 10, 2181–2207, <http://dx.doi.org/10.3390/md10102181>.
- Ersmark, K., Del Valle, J.R., Hanessian, S., 2008. Chemistry and biology of the aeruginosin family of serine protease inhibitors. *Angew. Chem. Int. Ed.* 47, 1202–1223, <http://dx.doi.org/10.1002/anie.200605219>.
- Felczykowska, A., Pawlik, A., Mazur-Marzec, H., Toruńska-Sitarz, A., Narajczyk, M., Richert, M., Węgrzyn, G., Herman-Antosiewicz, A., 2015. Selective inhibition of cancer cells' proliferation by compounds included in extracts from Baltic Sea cyanobacteria. *Toxicol.* 108, 1–10, <http://dx.doi.org/10.1016/j.toxicol.2015.09.030>.
- Fewer, D.P., Jokela, L., Rouhiainen, J., Wahlsten, M., Koskenniemi, K., Stal, L.J., Sivonen, K., 2009. The non-ribosomal assembly and frequent occurrence of the protease inhibitors spumigins in the bloom-forming cyanobacterium *Nodularia spumigena*. *Mol. Microbiol.* 73 (5), 924–937, <http://dx.doi.org/10.1111/j.1365-2958.2009.06816.x>.
- Fewer, D.P., Jouni, J., Paukku, E., Osterholm, J., Wahlsten, M., Permi, P., Aitio, O., Rouhiainen, L., Gomez-Saez, G.V., Sivonen, K., 2013. New structural variants of aeruginosin produced by the toxic bloom forming cyanobacterium *Nodularia spumigena*. *PLOS ONE* 8 (9), 1–10, <http://dx.doi.org/10.1371/journal.pone.0073618>.
- Gademann, K., 2011. Out in the green: biologically active metabolites produced by cyanobacteria. *Chimia* 65 (6), 416–419, <http://dx.doi.org/10.2533/chimia.2011.416>.
- Gerwick, W.H., Moore, B.S., 2012. Lessons from the past and charting the future of marine natural products drug discovery and chemical biology. *Chem. Biol.* 19 (1), 85–98, <http://dx.doi.org/10.1016/j.chembiol.2011.12.014>.
- Gomont, M., 1892. *Monographie des Oscillariées (Nostocacées Homocystées)*. Deuxième partie. – Lyngbyées. *Annales Des Sciences Naturelles, Botanique* 7 (16), 91–264.
- Gunasekera, S.P., Ross, C., Paul, V.J., Matthew, S., Luesch, H., 2008. Dragonamides C and D, linear lipopeptides from the marine cyanobacterium brown *Lyngbya polychroa*. *J. Nat. Prod.* 71, 887–890, <http://dx.doi.org/10.1021/np0706769>.

- Han, B., Gross, H., Goeger, D.E., Mooberry, S.L., Gerwick, W.H., 2006. Aurilides B and C, cancer cell toxins from a Papua New Guinea collection of the marine cyanobacterium *Lyngbya majuscula*. J. Nat. Prod. 69 (4), 572–575, <http://dx.doi.org/10.1021/np0503911>.
- Havens, K.E., 2008. Cyanobacteria blooms: effects on aquatic ecosystems. Adv. Exp. Med. Biol. 619, 733–747, http://dx.doi.org/10.1007/978-0-387-75865-7_33.
- Herfindal, L., Oftedal, L., Selheim, F., Wahlsten, M., Sivonen, K., Døskeland, S.O., 2005. A high proportion of Baltic Sea benthic cyanobacterial isolates contain apoptogens able to induce rapid death of isolated rat hepatocytes. Toxicol. 46 (3), 252–260, <http://dx.doi.org/10.1016/j.toxicol.2005.04.005>.
- Hosseini, S.M., Khosravi-Darani, K., Mozafari, M.R., 2013. Nutritional and medical applications of *Spirulina* microalgae. Mini-Rev. Med. Chem. 13 (8), 1231–1237, <http://dx.doi.org/10.2174/1389557511313080009>.
- Huang, G.-L., Zhihui, S., 2002. Immobilization of *Spirulina subsalsa* for removal of triphenyltin from water. Artif. Cell. Blood Sub. 30 (4), 293–305, <http://dx.doi.org/10.1081/BIO-120006120>.
- Humisto, A., Herfindal, L., Jokela, J., Karkman, A., Bjørnstad, R., Choudhury, R.R., Sivonen, K., 2016. Cyanobacteria as a source for novel anti-leukemic compounds. Curr. Pharm. Biotechnol. 17 (1), 78–91, <http://dx.doi.org/10.2174/1389201016666150826121124>.
- Jiang, L., Pei, H., Hu, W., Ji, Y., Han, L., Ma, G., 2015. The feasibility of using complex wastewater from a monosodium glutamate factory to cultivate *Spirulina subsalsa* and accumulate biochemical composition. Bioresource Technol. 180, 304–310, <http://dx.doi.org/10.1016/j.biortech.2015.01.019>.
- Karjalainen, M., Engström-Ost, J., Korpinen, S., Peltonen, H., Pääkkönen, J.-P., Rönkkönen, S., Suikkanen, S., Viitasalo, M., 2007. Ecosystem consequences of cyanobacteria in the northern Baltic Sea. Ambio 36 (2–3), 195–202, [http://dx.doi.org/10.1579/0044-7447\(2007\)36\[195:ECOCIT\]2.0.CO;2](http://dx.doi.org/10.1579/0044-7447(2007)36[195:ECOCIT]2.0.CO;2).
- Komarek, J., Kastovsky, J., Mares, J., Johansen, J.R., 2014. Taxonomic classification of cyanoprokaryotes (cyanobacterial genera) 2014, using a polyphasic approach. Preslia 86, 295–335.
- Kotai, J., 1972. Introduction for Preparation of Modified Nutrient Solution Z8 for Algae. Norwegian Insti. Water Res. Publ. B-11/69, Oslo, 5 pp.
- Krienitz, L., Ballot, A., Kotut, K., Wiegand, C., Pütz, S., Metcalf, J. S., Codd, G.A., Pflugmacher, S., 2003. Contribution of hot spring cyanobacteria to the mysterious deaths of lesser Flamingos at Lake Bogoria, Kenya. FEMS Microbiol. Ecol. 43 (2), 141–148, <http://dx.doi.org/10.1111/j.1574-6941.2003.tb01053.x>.
- Kwan, C.J., Taori, K., Paul, J.V., Luesch, H., 2009. Lyngbyastatins 8–10, elastase inhibitors with cyclic depsipeptide scaffolds isolated from the marine cyanobacterium *Lyngbya semiplena*. Mar. Drugs 7, 528–538, <http://dx.doi.org/10.3390/md7040528>.
- Lightner, D.V., 1978. Possible toxic effects of the marine blue-green alga, *Spirulina subsalsa*, on the blue shrimp, *Penaeus stylirostris*. J. Invertebr. Pathol. 32 (2), 139–150, [http://dx.doi.org/10.1016/0022-2011\(78\)90023-X](http://dx.doi.org/10.1016/0022-2011(78)90023-X).
- Linnington, R.G., Edwards, D.J., Shuman, C.F., McPhail, K.L., Matainaho, T., Gerwick, W.H., 2008. Symplocamide A, a potent cytotoxin and chymotrypsin inhibitor from the marine Cyanobacterium *Symploca* sp. J. Nat. Prod. 71 (1), 22–27, <http://dx.doi.org/10.1021/np070280x>.
- Luesch, H., Moore, R.E., Paul, V.J., Mooberry, S.L., Corbett, T.H., 2001a. Isolation of dolastatin 10 from the marine cyanobacterium *Symploca* species VP642 and total stereochemistry and biological evaluation of its analogue symplostatin 1. J. Nat. Prod. 64 (7), 907–910, <http://dx.doi.org/10.1021/np010049y>.
- Luesch, H., Yoshida, W.Y., Moore, R.E., Paul, V.J., Corbett, T.H., 2001b. Total structure determination of apratoxin A, a potent novel cytotoxin from the marine cyanobacterium *Lyngbya majuscula*. J. Am. Chem. Soc. 123 (23), 5418–5423, <http://dx.doi.org/10.1021/ja010453j>.
- Matthew, S., Ross, C., Rocca, J.R., Paul, V.J., Luesch, H., 2007. Lyngbyastatin 4, a dolastatin 13 analogue with elastase and chymotrypsin inhibitory activity from the marine cyanobacterium *Lyngbya confervoides*. J. Nat. Prod. 70, 124–127, <http://dx.doi.org/10.1021/np060471k>.
- Matthew, S., Ross, C., Paul, V.J., Luesch, H., 2008. Pompanopeptins A and B, new cyclic peptides from the marine cyanobacterium *Lyngbya confervoides*. Tetrahedron Lett. (64), 4081–4089, <http://dx.doi.org/10.1016/j.tet.2008.02.035>.
- Matthew, S., Paul, V.J., Luesch, H., 2009. Tiglicamides A–C, cyclopeptideptides from the marine cyanobacterium *Lyngbya confervoides*. Phytochemistry (70), 2058–2063, <http://dx.doi.org/10.1016/j.phytochem.2009.09.010>.
- Mazur-Marzec, H., Błaszczak, A., Felczykowska, A., Hohlfeld, N., Kobos, J., Toruńska-Sitarz, A., Devi, P., Montalvão, S., D'souza, L., Tammela, P., Mikosik, A., Bloch, S., Nejman-Faleńczyk, B., Węgrzyn, G., 2015. Baltic cyanobacteria – a source of biologically active compounds. Eur. J. Phycol. 50 (3), 343–360, <http://dx.doi.org/10.1080/09670262.2015.1062563>.
- Nogle, L.M., Gerwick, W.H., 2002. Somocystinamide A, a novel cytotoxic disulfide dimer from a Fijian marine cyanobacterial mixed assemblage. Org. Lett. 4 (7), 1095–1098, <http://dx.doi.org/10.1021/ol017275j>.
- Ocampo Bennet, X., 2007. Peptide au seiner Cyanobakterien Wasserblüte (1998) aus dem Wannensee/Berli: Strukturen and biologische Wirksamkeit. Univ. Freiburg, Freiburg, 28 pp.
- Oftedal, L., Selheim, F., Wahlsten, M., Sivonen, K., Døskeland, S.O., Herfindal, L., 2010. Marine benthic cyanobacteria contain apoptosis-inducing activity synergizing with daunorubicin to kill leukemia cells, but not cardiomyocytes. Mar. Drugs 8 (10), 2659–2672, <http://dx.doi.org/10.3390/md8102659>.
- Patel, S., 2017. A critical review on serine protease: key immune manipulator and pathology mediator. Allergol. Immunopathol. 45 (1), 1–13, <http://dx.doi.org/10.1016/j.aller.2016.10.011>.
- Peng, Y., Liu, L., Jiang, L., Xiao, L., 2017. The roles of cyanobacterial bloom in nitrogen removal. Sci. Total Environ. 609, 297–303, <http://dx.doi.org/10.1016/j.scitotenv.2017.03.149>.
- Pereira, A., Cao, Z., Murray, T.F., Gerwick, W.H., 2009. Hoiamide a, a sodium channel activator of unusual architecture from a consortium of two Papua new Guinea cyanobacteria. Chem. Biol. 16 (8), 893–906, <http://dx.doi.org/10.1016/j.chembiol.2009.06.012>.
- Pereira, A.R., Kale, A.J., Fenley, A.T., Byrum, T., Debonis, H.M., Gilson, M.K., Valeriote, F.A., Moore, B.S., Gerwick, W.H., 2012. The Carmaphycins: new proteasome inhibitors exhibiting an α,β -epoxyketone warhead from a marine cyanobacterium. Chembiochem 13 (6), 810–817, <http://dx.doi.org/10.1002/cbic.201200007>.
- Plaza, A., Bewley, C.A., 2006. Largamides A–H, unusual cyclic peptides from the marine cyanobacterium *Oscillatoria* sp. J. Org. Chem. 71, 6898–6907, <http://dx.doi.org/10.1021/jo061044e>.
- Pluotno, A., Carmeli, S., 2005. Banyasin A and banyasides A and B, three novel modified peptides from a water bloom of the cyanobacterium *Nostoc* sp. Tetrahedron 61, 575–583, <http://dx.doi.org/10.1002/chin.200517196>.
- Rastogi, R.P., Sinha, R.P., 2009. Biotechnological and industrial significance of cyanobacterial secondary metabolites. Biotechnol. Adv. 27 (4), 521–539, <http://dx.doi.org/10.1016/j.biotechadv.2009.04.009>.
- Rubio, B.K., Parish, S.M., Yoshida, W., Schupp, P.J., Schils, T., Williams, P.G., 2010. Depsipeptides from a Guamanian marine cyanobacterium, *Lyngbya bouillonii*, with selective inhibition of serine proteases. Tetrahedron Lett. 51 (51), 6718–6721, <http://dx.doi.org/10.1016/j.tetlet.2010.10.062>.
- Sapio, M.R., Fricker, L.D., 2014. Carboxypeptidases in disease: insights from peptidomic studies. Proteom. Clin. Appl. 8 (5–6), 327–337, <http://dx.doi.org/10.1002/prca.201300090>.
- Shrivastav, A., Mishra, S.K., Mishra, S., 2010. Polyhydroxyalkanoate (PHA) synthesis by *Spirulina subsalsa* from Gujarat coast of India. Int. J. Biol. Macromol. 46 (2), 255–260, <http://dx.doi.org/10.1016/j.ijbiomac.2010.01.001>.

- Singh, R.K., Tiwari, S.P., Rai, A.K., Mohapatra, T.M., 2011. Cyanobacteria: an emerging source for drug discovery. *J. Antibiot.* 64 (6), 401–412, <http://dx.doi.org/10.1038/ja.2011.21>.
- Spirulina subsalsa* Oersted ex Gomont: Algaebase. http://www.algaebase.org/search/species/detail/?species_id=23781 (retrieved 13.04.17).
- Spoof, L., Błaszczuk, A., Meriluoto, J., Cegłowska, M., Mazur-Marzec, H., 2015. Structures and activity of new anabaenopeptins produced by Baltic Sea cyanobacteria. *Mar. Drugs* 14 (1), 8 pp., <http://dx.doi.org/10.3390/md14010008>.
- Stewart, J.B., Bornemann, V., Chen, J.L., Moore, R.E., Caplan, F.R., Karuso, H., Larsen, L.K., Patterson, G.M., 1988. Cytotoxic, fungicidal nucleosides from blue green algae belonging to the Scytonemataceae. *J. Antibiot.* 41 (8), 1048–1056, <http://dx.doi.org/10.7164/antibiotics.41.1048>.
- Stizenberger, E., 1852. *Spirulina* und *Arthrospira* (nov. gen.). *Hedwigia* 1, 32–34.
- Šulčius, S., Montvydienė, D., Mazur-Marzec, H., Kasperovičienė, J., Rulevičius, R., Cibulskaitė, Ž., 2017. The profound effect of harmful cyanobacterial blooms: from food-web and management perspectives. *Sci. Total Environ.* 609, 1443–1450, <http://dx.doi.org/10.1016/j.scitotenv.2017.07.253>.
- Taori, K., Matthew, S., Rocca, J.R., Paul, V.J., Luesch, H., 2007. Lyngbyastatins 5-7, potent elastase inhibitors from Floridian marine cyanobacteria, *Lyngbya* spp. *J. Nat. Prod.* 70 (10), 1593–1600, <http://dx.doi.org/10.1021/np0702436>.
- Taori, K., Paul, V.J., Luesch, H., 2008. Kempopeptins A and B, serine protease inhibitors with different selectivity profiles from a marine cyanobacterium *Lyngbya* sp. *J. Nat. Prod.* 71, 1625–1629, <http://dx.doi.org/10.1021/np8002172>.
- Teruya, T., Sasaki, H., Fukazawa, H., Suenaga, K., 2009. Bisebromamide, a potent cytotoxic peptide from the marine cyanobacterium *Lyngbya* sp.: isolation, stereostructure, and biological activity. *Org. Lett.* 11 (21), 5062–5065, <http://dx.doi.org/10.1021/ol9020546>.
- Titilade, P.R., Olalekan, E.I., 2015. The importance of marine genomics to life. *J. Ocean Res.* 3 (1), 1–13, <http://dx.doi.org/10.12691/jor-3-1-1>.
- Tomaselli, L., Palandri, M.R., Tredici, M.R., 1996. On the correct use of the *Spirulina* designation. *Algological Studies/Archiv Für Hydrobiologie, Supplement Volumes* 539–548.
- Tripathi, A., Fang, W., Leong, D.T., Tan, L.T., 2012. Biochemical studies of the lagunamides, potent cytotoxic cyclic depsipeptides from the marine cyanobacterium *Lyngbya majuscula*. *Mar. Drugs* 10 (5), 1126–1137, <http://dx.doi.org/10.3390/md10051126>.
- Turpin, P.J.F., 1827. *Spirulina oscillarioide*. *Dictionnaire Des Sciences Naturelles* 50, 309–310.
- Vonshak, A., Tomaselli, L., 2000. Arthrospira (Spirulina): systematics and ecophysiology. In: Whitton, B.A., Potts, M. (Eds.), *The Ecology of Cyanobacteria*. Springer, Netherlands, 505–522, http://dx.doi.org/10.1007/0-306-46855-7_18.
- Wipf, P., Reeves, J.T., Day, B.W., 2004. Chemistry and biology of curacin A. *Curr. Pharm. Des.* 10 (12), 1417–1437, <http://dx.doi.org/10.2174/1381612043384853>.
- Witkowski, A., 1993. *Microphytobenthos*. In: Korzeniowski, K. (Ed.), *Puck Bay. Inst. Oceanogr. Univ. Gdańsk.*, Gdańsk, 395–415.
- Włodarska-Kowalczyk, M., Balazy, P., Kobos, J., Wiktor, J., Zajczkowski, M., Moskal, W., 2014. Large red cyanobacterial mats (*Spirulina subsalsa* Oersted ex Gomont) in the shallow sublittoral of the southern Baltic. *Oceanologia* 56 (3), 661–666, <http://dx.doi.org/10.5697/oc.55-3.661>.
- Yu, S., Kim, T., Yoo, K.H., Kang, K., 2017. The T47D cell line is an ideal experimental model to elucidate the progesterone-specific effects of a luminal subtype of breast cancer. *Biochem. Biophys. Res. Commun.* 486 (3), 752–758, <http://dx.doi.org/10.1016/j.bbrc.2017.03.114>.
- Zhang, Y., Sun, H., Zhu, H., Ruan, Y., Liu, F., Liu, X., 2014. Accumulation of hexabromocyclododecane diastereomers and enantiomers in two microalgae, *Spirulina subsalsa* and *Scenedesmus obliquus*. *Ecotoxicol. Environ. Saf.* 104, 136–142, <http://dx.doi.org/10.1016/j.ecoenv.2014.02.027>.
- Zhuhui, S., Guolan, H., 2000. Toxicity of triphenyltin to *Spirulina subsalsa*. *Bull. Environ. Contam. Toxicol.* 64 (5), 23–728, <http://dx.doi.org/10.1007/s001280000063>.

Available online at www.sciencedirect.com

ScienceDirect

journal homepage: www.journals.elsevier.com/oceanologia/

ORIGINAL RESEARCH ARTICLE

Budget of ^{90}Sr in the Gulf of Gdańsk (southern Baltic Sea)

Michał Saniewski*, Tamara Zalewska

Institute of Meteorology and Water Management, National Research Institute, Gdynia, Poland

Received 11 September 2017; accepted 17 November 2017

Available online 1 December 2017

KEYWORDS

^{90}Sr ;
Budget;
Gulf of Gdańsk

Summary In the period from 2005 to 2011 the major source of ^{90}Sr to the Gulf of Gdańsk was the Vistula river. Its contribution was 99.7% of the total load. The main processes responsible for the decrease in ^{90}Sr activity in the Gulf of Gdańsk were: radioactive decay (87%) and sediment deposition (13%). Average increase in the activity of ^{90}Sr in the Gulf of Gdańsk during the study period was 5.0% (114 GBq), which was almost 2 times higher than the loss of ^{90}Sr due to radioactive decay. In the years 1997–2015, the effective half-life of ^{137}Cs was 9.1 years and that of ^{90}Sr was 50.3 years. Assuming a further decrease in ^{137}Cs and maintaining ^{90}Sr concentrations at present level, it is expected that ^{90}Sr will become the major anthropogenic isotope having impact on the level of radioactivity in the Gulf of Gdańsk.

© 2017 Institute of Oceanology of the Polish Academy of Sciences. Production and hosting by Elsevier Sp. z o.o. This is an open access article under the CC BY-NC-ND license (<http://creativecommons.org/licenses/by-nc-nd/4.0/>).

1. Introduction

The Baltic Sea is an inland sea which is practically closed since the only connection with the North Sea and the Atlantic Ocean through the Danish Straits (Skagerrak and Kattegat between southern Sweden and the Danish islands) is relatively narrow. As a consequence, the water exchange between the Baltic Sea and North Sea is limited and amounts to 0.05% per year (Wängberg et al., 2001). This makes the Baltic Sea very sensitive to contamination with different pollutants (HELCOM, 2010), including radionuclides (IAEA, 2005). The Baltic Sea is still considered as one of the water bodies that is most polluted with ^{90}Sr and ^{137}Cs in the world

* Corresponding author at: Institute of Meteorology and Water Management, National Research Institute, Maritime Branch, Waszyngtona 42, 81-342 Gdynia, Poland. Tel.: +48 58 62 88 265; fax: +48 48 62 88 163.

E-mail address: michal.saniewski@imgw.pl (M. Saniewski).

Peer review under the responsibility of Institute of Oceanology of the Polish Academy of Sciences.



Production and hosting by Elsevier

<https://doi.org/10.1016/j.oceano.2017.11.002>

0078-3234/© 2017 Institute of Oceanology of the Polish Academy of Sciences. Production and hosting by Elsevier Sp. z o.o. This is an open access article under the CC BY-NC-ND license (<http://creativecommons.org/licenses/by-nc-nd/4.0/>).

(HELCOM, 2009; IAEA, 2005). The major sources of radionuclides inputs into the Baltic Sea were: atmospheric testing of nuclear weapons carried out during the late 1950s and early 1960s, the Chernobyl accident in 1986, discharges from nuclear reprocessing plants located outside the Baltic Sea (Sellafield and La Hague) and discharges from nuclear facilities in the Baltic Sea drainage area (Baklanov and Sorensen, 2001; HELCOM, 2009; Nielsen et al., 1999; Nies et al., 1995). It has been estimated that the total load of ^{90}Sr and ^{137}Cs introduced into the Baltic Sea from all sources amounts to 621 TBq and 5752 TBq, respectively.

Among many pollutants introduced into the Baltic Sea, the ^{90}Sr isotope is considered to be particularly dangerous, due to its specific nature and relatively long half-life (28.8 years) (Kryshev, 2006). Its chemical similarity to calcium is the reason why strontium is quite easily taken up and accumulated in a body, especially in bone tissues. However, data on the activity levels of ^{90}Sr in various compartments of the marine environment and biota is largely limited. At the same time knowledge on the ^{90}Sr levels in particular elements of the marine environment and knowledge on factors controlling its temporal and spatial distribution, are crucial for determining the degree of environmental contamination, especially in incidental situations. Information on the concentration factors in organisms is of special importance as allows to determine the exposure of organisms to the radioactivity related to ^{90}Sr presence.

Long-term observations of the variability in concentrations of ^{90}Sr and ^{137}Cs showed that the decrease of ^{90}Sr levels is not as significant as in the case of ^{137}Cs . Moreover, the decrease is smaller than expected from the radioactive decay. Therefore, based on the analysis of data on radionuclide concentrations in various components of the marine environment (abiotic – seawater and sediment, and biotic – fish and macrophytobenthic plants), obtained in the period of 2005–2011, the study, which results would become the basis for future scenarios concerning ^{90}Sr levels in the Baltic Sea, was undertaken. The assessment of the present level of ^{90}Sr pollution in the Baltic Sea was carried out in relation to current sources – riverine and atmospheric inputs of this isotope, based on the results of ^{90}Sr concentrations in the Vistula and atmospheric deposition, obtained for the same period as mentioned above. Finally, the main factors controlling distribution of the ^{90}Sr in the marine ecosystem were indicated, also in relation to long-term changes observed after potential introduction of significant ^{90}Sr loads into the Baltic Sea.

2. Material and methods

2.1. Study area

The Gulf of Gdańsk is located in the southeastern part of the Baltic Sea. Its northern boundary is the straight line connecting Cape Rozewie (54°50'N, 18°20'E) with Cape Taran (54°58'N, 19°59'E). The area of the Gulf of Gdańsk is 4940 km² (Lukawska-Matuszewska and Bolatek, 2008), while the volume of water is estimated at 291.2 km³ (Majewski, 1990). The Gulf of Gdańsk has an average depth of about 50 m, and a maximum of 118 m.

2.2. Methods of budget calculations

In order to balance the loads of ^{90}Sr in the Gulf of Gdańsk, it was assumed that the main sources of this isotope are: atmospheric deposition and Vistula river waters, while the factors having impact on the decrease of ^{90}Sr concentration in seawater are: radioactive decay, bioaccumulation and sedimentation processes (Fig. 1). The bioaccumulation took into account in the calculations was related only to marine plants and fish. The loads of ^{90}Sr were calculated based on literature data (mainly from own research) concerning concentrations of this isotope in particular components of the marine environment, measured in the period of 2005–2011, adopted for the estimation of the ^{90}Sr budget in the Gulf of Gdańsk.

Data on ^{90}Sr loads introduced into the Gulf of Gdańsk with atmospheric deposition and riverine runoff was obtained from the study by Saniewski and Zalewska (2016).

The concentrations of ^{90}Sr in seawater were measured in samples collected between 2005 and 2011 at five stations located in the Gulf of Gdańsk. The samples were obtained from the sea surface, from the bottom, and additionally along vertical profiles (every 20 m) at two stations (Fig. 1, Table 1). The analysis of ^{90}Sr distribution in seawater of the Gulf of Gdańsk, for the abovementioned study period, was presented in the work by Saniewski (2013).

Mean activity of ^{90}Sr in sediments was calculated based on literature data (Zalewska and Suplińska, 2013) and unpublished own data. The bottom areas with intensive sedimentation processes, associated with the transportation type of bottom (LOI – loss on ignition, values of 4–10%) and the accumulation bottom (with LOI values >10%) (Håkanson et al., 2003) account for respectively 1426 km² and 1840 km² of the Gulf of Gdańsk (Carman and Cederwall, 2001). Therefore, it was assumed that the ^{90}Sr deposition into sediments is most intensive in the area of 3266 km² (Fig. 1).

Since ^{90}Sr is bioaccumulated and biomagnified in the trophic chain, the concentrations of ^{90}Sr in macrophytobenthic plants and selected fish species specific to the Gulf of Gdańsk were taken into account in the budget calculations. To estimate the load of ^{90}Sr removed with the caught fish, the average activity values of ^{90}Sr in fish species (Zalewska et al., 2016) and the mass of fish caught in 2005–2011 in the study area (Szostak et al., 2006, 2007, 2008, 2009, 2010, 2011, 2012) were used.

The estimation of ^{90}Sr accumulated in marine plants was carried out using data on ^{90}Sr concentrations in selected species of macrophytobenthic plants (Zalewska, 2015). The amount of biomass having the potential for bioaccumulation was assessed on the basis of data collected during macrophytobenthos monitoring campaigns carried out in two locations: Orłowo Cliff and Kuźnica Hollow (Brzeska and Saniewski, 2012). The sampling for monitoring purposes took place in June, i.e. in the period of intensive primary production and rapid growth of both macroalgae and vascular plants. Samples were taken by a diver, along transects, from a depth of 1 m to a maximum depth of plant occurrence. The plant material was collected from the area determined by a randomly placed frame (0.5 m × 0.5 m). The frame was placed three times at each depth. The collected material was analyzed macroscopically and microscopically to sepa-

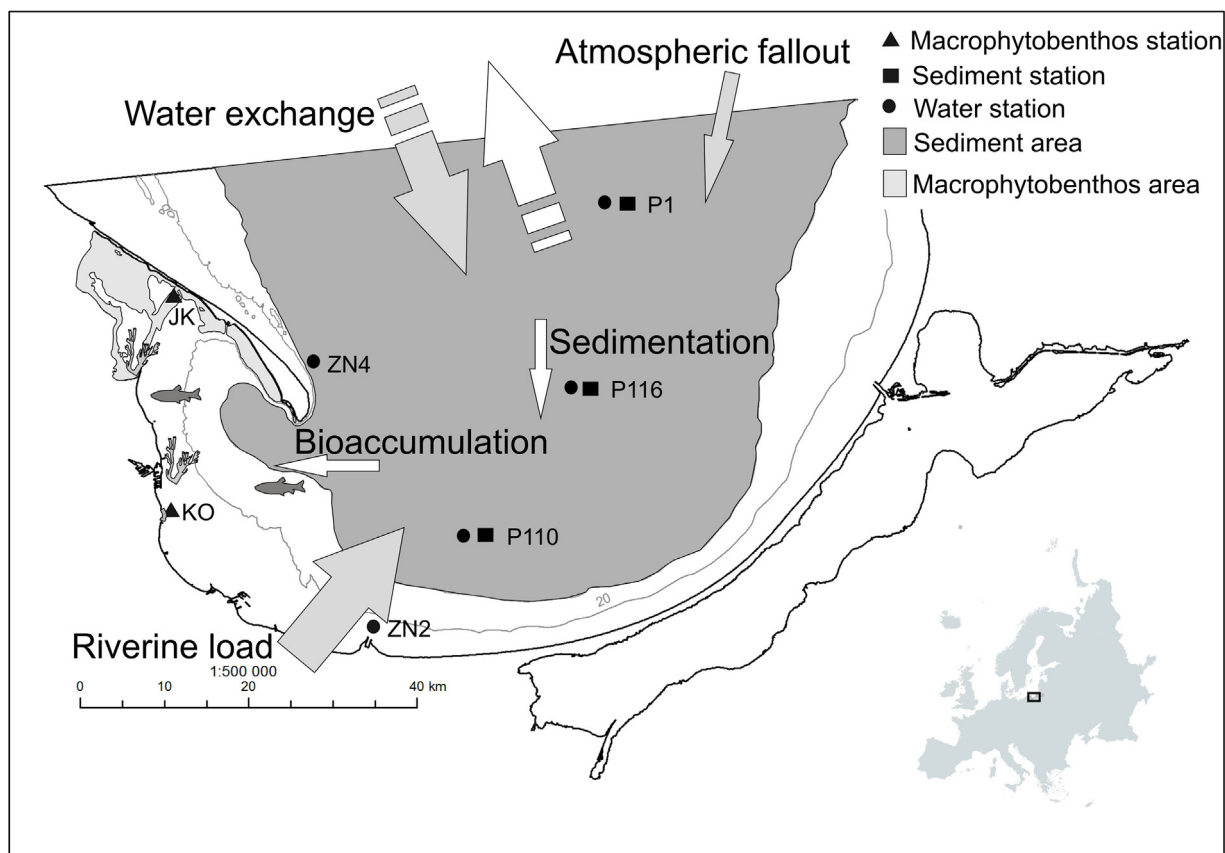


Figure 1 Location of sampling stations in the Gulf of Gdańsk.

Table 1 Activity concentrations of ^{90}Sr in seawater of the Gulf of Gdańsk in 2005–2011.

Station	Sampling depth [m]	Activity concentration of ^{90}Sr [Bq m^{-3}]						
		2005	2006	2007	2008	2009	2010	2011
ZN2	0	5.6 ± 0.5	9.2 ± 0.5	5.6 ± 0.5	4.2 ± 0.4	3.8 ± 0.4	6.4 ± 0.5	7.6 ± 0.5
	12	8.7 ± 0.6	8.8 ± 0.5	6.7 ± 0.5	5.4 ± 0.6	6.3 ± 0.4	9.8 ± 0.6	4.6 ± 0.4
P1	0	8.6 ± 0.5	9.9 ± 0.6	8.3 ± 0.5	7.6 ± 0.9	7.7 ± 0.6	8.8 ± 0.5	5.9 ± 0.5
	20	8.2 ± 0.5	9.8 ± 0.7	8.5 ± 0.6	7.9 ± 0.5	7.1 ± 0.4	8.4 ± 0.4	4.3 ± 0.6
	40	9.5 ± 0.6	8.8 ± 0.7	7.5 ± 0.4	7.8 ± 0.4	7.4 ± 0.4	7.6 ± 0.5	9.3 ± 0.9
	60	9.2 ± 0.6	6.9 ± 0.6	9.9 ± 0.5	7.2 ± 0.6	8.2 ± 0.4	8.1 ± 0.5	7.9 ± 0.5
	80	8.7 ± 0.6	8.6 ± 1.2	6.6 ± 0.6	8.2 ± 0.7	9.2 ± 0.4	8.0 ± 0.6	7.9 ± 0.4
P116	105	7.8 ± 0.5	9.8 ± 0.6	6.9 ± 0.4	5.4 ± 0.6	7.6 ± 0.4	6.9 ± 0.5	6.9 ± 0.4
	0	7.4 ± 0.6	8.9 ± 0.5	6.9 ± 0.5	7.6 ± 0.8	8.7 ± 0.4	8.6 ± 0.4	5.0 ± 0.4
P110	85	8.4 ± 0.5	10.0 ± 0.8	7.7 ± 0.5	6.4 ± 0.5	6.5 ± 0.4	8.2 ± 0.4	9.3 ± 0.5
	0	7.7 ± 0.7	8.1 ± 0.8	8.5 ± 0.4	6.5 ± 0.5	7.5 ± 0.5	7.0 ± 0.5	7.0 ± 0.5
ZN4	69	8.6 ± 0.6	9.4 ± 1.0	7.8 ± 0.4	4.5 ± 0.5	7.1 ± 0.5	8.6 ± 0.4	6.6 ± 0.5
	0	7.7 ± 0.5	9.9 ± 0.5	9.3 ± 1.1	5.9 ± 0.4	8.6 ± 0.4	6.7 ± 0.5	9.6 ± 0.5
ZN4	20	8.1 ± 0.8	10.1 ± 0.6	9.9 ± 0.8	6.4 ± 0.5	8.5 ± 0.6	6.5 ± 0.5	9.4 ± 0.5
	40	8.7 ± 0.8	10.6 ± 0.5	10.3 ± 0.8	5.5 ± 0.4	7.9 ± 0.6	9.5 ± 0.5	8.8 ± 0.5
	60	10.0 ± 0.7	8.9 ± 0.7	8.0 ± 0.7	5.2 ± 0.6	8.7 ± 0.5	8.9 ± 0.5	7.7 ± 0.5
	69	11.7 ± 0.7	9.0 ± 0.9	9.1 ± 0.8	4.4 ± 0.5	6.5 ± 0.6	8.1 ± 0.4	8.6 ± 0.5
Average concentration [Bq m^{-3}]		8.5	9.2	8.1	6.2	7.5	8.0	7.4

rate individual species which biomass was measured and converted into 1 m^2 of bottom area. In order to determine the biomass in the Gulf of Gdańsk, the total surface area of the occurrence of macrophytobenthic plants in the investi-

gated research areas was estimated and multiply by biomass specific to 1 m^2 (Fig. 1).

It was assumed that the exchange of ^{90}Sr in seawater at the northern boundary of the Gulf of Gdańsk is negligible as

^{90}Sr concentrations in seawater are uniform in different areas of the southern Baltic Sea.

The load of ^{90}Sr in seawater of the Gulf of Gdańsk determined for each year served as “a starting point” for calculations. The inflowing loads were given the positive values, while the loads removed from the environment as a result of the discussed processes were given the negative values.

3. Results and discussion

3.1. Load of ^{90}Sr in seawater

In the period from 2005 to 2011, the concentrations of ^{90}Sr in seawater of the Gulf of Gdańsk were at the similar levels (Table 1). The mean concentrations varied in a very narrow range, from 7.4 Bq m^{-3} in 2011 to 9.2 Bq m^{-3} in 2006. The exceptional year was 2008, when the average activity was 6.2 Bq m^{-3} , and this was due to the fact that concentrations in that year ranged from 4.2 Bq m^{-3} to 8.2 Bq m^{-3} . The lowest value was reported at the mouth of the Vistula. This is a common feature, also observed in other years, resulting from a slightly diluting influence of the Vistula waters. In 2009, the concentration at the mouth of the Vistula river was only 3.8 Bq m^{-3} , however, in 2006 the value in that area reached 9.2 Bq m^{-3} . Such variability can be associated with the wind pattern preceding the sampling period. During the study period, the maximum concentrations of ^{90}Sr , at the level of 10 Bq m^{-3} and higher were observed in the vicinity of the Hel Peninsula (Table 1). For the ^{90}Sr loads calculations in seawater, there were taken the average values of ^{90}Sr activities in seawater determined for particular years and the volume of seawater in the Gulf of Gdańsk. Calculated loads varied from 1817 GBq in 2008 to 2684 GBq in 2006 (Table 2). The standard deviation of the loads deposited in the Gulf of Gdańsk over the period of 2005–2011 did not exceed 15% (Saniewski, 2013).

3.2. Load of ^{90}Sr from atmospheric deposition and riverine input

The total loads of ^{90}Sr and ^{137}Cs from both sources: atmospheric deposition and riverine input, reaching the Gulf of Gdańsk between 2005 and 2011, were 1238 GBq and 450 GBq, respectively (Saniewski and Zalewska, 2016). The major source of both radionuclides to the Gulf of Gdańsk was the Vistula river; its contribution reached 99.7% in the case of ^{90}Sr and 95.8% as regarding ^{137}Cs . In the years 2006–2010, the riverine load of ^{137}Cs (431 GBq) was nearly three times smaller than that of ^{90}Sr (1234 GBq), although the average activity of ^{137}Cs in the surface soil layer in the Vistula river drainage area was about three times higher than the activity of ^{90}Sr (Solecki, 2006). The main reason for this fact was the migration of both isotopes in the terrestrial environment. The Sr^{2+} cations are mobile and more easily washed out by water to the rivers than the Cs^+ ions which are strongly absorbed on soil particles limiting its movement by chemical and biological processes (Ritchie and McHenry, 1990). The environmental mobility of ^{90}Sr is approximately one order of magnitude greater than that of ^{137}Cs and the runoff coefficient (transfer of radioactivity from catchments to the sea surface) for ^{90}Sr is much greater than that for ^{137}Cs (Cross et al., 2002). It was estimated that after the Chernobyl power plant disaster, the maximum deposition of ^{90}Sr in Poland was 1 kBq m^{-2} , and after the nuclear weapons testing it amounted to, on average, 3.2 kBq m^{-2} . As a result, in 1986 the deposition still remained at a level of approximately 1.5 kBq m^{-2} (UNSCEAR, 1982). In 1999, the average activity of ^{90}Sr in soil of the middle part of the Vistula drainage basin was 26.15 Bq kg^{-1} , the values ranged from 5.3 Bq kg^{-1} to 85.3 Bq kg^{-1} (Solecki and Chibowski, 2001). Taking into account published results (Solecki, 2006; Solecki and Chibowski, 2001) and the surface area of the Vistula drainage basin, it was calculated that in 1999 about 0.67 PBq of ^{90}Sr was deposited in the 0–10 cm soil layer, which could have

Table 2 Budget of ^{90}Sr in the Gulf of Gdańsk in years 2005–2011.

Years	2005	2006	2007	2008	2009	2010	2011
Total loads in seawater in the Gulf of Gdańsk [GBq]	2477	2684	2355	1817	2181	2331	2165
Loads from Vistula River [GBq]	+122	+137	+137	+118	+175	+316	+228
Loads from atmospheric deposition [GB]	+0.58	+0.53	+0.49	+0.64	+0.41	+0.49	+0.87
Radioactive decay [GBq]	−59	−64	−56	−43	−52	−55	−52
Loads deposited in sediments [GBq]	−7.45	−8.55	−7.48	−8.29	app.	app.	app.
Loads bioaccumulated in macrophytobentic plants [GBq]	app.	app.	app.	app.	app.	app.	−0.027
Loads in caught fish [GBq]	−0.0029	−0.0028	−0.0023	−0.0019	−0.0032	−0.0030	−0.0028
Increase of loads in seawater in the Gulf of Gdańsk [GBq]	56.4 (2.3%)	65.1 (2.4%)	74.3 (3.2%)	67.2 (3.7%)	115.1 (5.3%)	253.4 (10.9%)	169.7 (7.8%)

acted as a potential source of this isotope washed out by water to the river.

The lowest ^{90}Sr load of 118 GBq was introduced into the Gulf of Gdańsk with waters of the Vistula in 2008 (Table 2). In the period between 2005 and 2007, the load was in the range from 122 to 137 GBq, while in 2011 it reached 228 GBq. However, the highest load of 316 GBq was introduced in 2010, due to the flood event in the Vistula river drainage basin.

In the case of atmospheric deposition, the highest load of ^{90}Sr (0.87 GBq) was introduced to the Gulf of Gdańsk in 2011, as a result of the Fukushima Dai-ichi nuclear power plant disaster, which took place in March that year. The contaminated air masses were transported towards the area of Europe within about a month (Table 2). In other years, the loads remained in the range from 0.41 GBq in 2009 to 0.64 GBq in 2008. The total load of ^{90}Sr introduced to the Gulf of Gdańsk in the period of 2005–2011 amounted to 4 GBq, and was almost five times lower than the load of ^{137}Cs (Saniewski and Zalewska, 2016).

3.3. Radioactive decay

The correction for radioactive decay of ^{90}Sr was calculated based on the total load in seawater estimated for each year, taking into account the half-life value of 28.8 years. The obtained results ranged from 43 GBq in 2008 to 64 GBq in 2006 (Table 2).

3.4. Load of ^{90}Sr in sediments

The load of ^{90}Sr deposited in bottom sediments of the Gulf of Gdańsk between 2005 and 2008 was determined based on literature data concerning concentrations of ^{90}Sr in sediments (Zalewska and Suplińska, 2013; unpublished data) and taking into account the estimated area of sediments where undisturbed sedimentation occurs. Average concentrations of ^{90}Sr in 19-cm profiles of bottom sediments collected at stations P110, P116 and P1 varied in a relatively narrow range, from about 2–4 Bq kg⁻¹ d.w. The average values of ^{90}Sr concentration determined for each year (Table 3) were used to calculate the loads deposited in bottom sediments during one year. It was assumed that the average linear sedimentation rate specific to the Gulf of Gdańsk area is c.a. 2 mm per year (Zalewska et al., 2015). The average mass of a 1-cm thick sediment layer taken from the area of 19.63 cm² amounts to 7 g (unpublished data). The load of ^{90}Sr deposited every year in the topmost sediment

layer of the average thickness of 2 mm was determined on the basis of the following equation:

$$\text{TLS} = A * \text{LAR} * \frac{W}{S_N} * S,$$

where TLS – total load in sediment [Bq], A – mean activity of ^{90}Sr in sediments [Bq kg⁻¹], LAR – linear accumulation rate [cm], W – average mass of a single 1-cm sediment layer collected from the surface area determined by the Niemistö corer [kg], S_N – surface area determined by the Niemistö corer [m²], S – surface of sediment accumulation in the Gulf of Gdańsk [m²].

Since the concentrations of ^{90}Sr in sediment layers collected in 2005–2008 were very similar (range: 3.20–3.61 Bq kg⁻¹ d.w.), the values of ^{90}Sr loads were also comparable, from 7.45 GBq in 2005 to 8.55 in the following year (Table 2). Based on the results from the period of 2009–2011, the average value which we adopted for further calculations was 8 GBq.

3.5. Load of ^{90}Sr in macrophytobenthic plants

The calculations of ^{90}Sr loads accumulated in macrophytobenthic plants were carried out based on the research results from 2011 (Saniewski and Zalewska, 2017; Zalewska, 2015). Samples of macrophytobenthic plants were obtained from two locations. In the area of the Orłowo Cliff, 13 species were recognized, including 12 taxa of macroalgae and 1 species of a vascular plant (*Zostera marina*). Macroalgae were most commonly represented by green algae – 5 taxa, and red algae – 5 taxa; only 2 species were identified as brown algae. Along the transect in the Kuźnica Hollow, 14 species of macrophytobenthos were identified in 2011, including 4 taxa of green algae, 2 taxa of brown algae and also 2 taxa of red algae, as well as 6 species of vascular plants. Based on the analysis of ^{90}Sr in particular species, the average concentrations for individual groups collected in two investigated locations were determined. The lowest concentrations of ^{90}Sr were found in green algae (1.36 Bq kg⁻¹ d.w.), while the highest were measured in the case of red algae (6.58 Bq kg⁻¹ d.w.) (Table 4). For each group of the macrophytobenthic plants, the biomass per unit area (1 m²) was determined. Then, taking into account the bottom areas where macrophytobenthic plants commonly appear (Fig. 1), namely the Puck Bay within a depth range of 0–4 m (98.9541 km²) and the Orłowo Cliff area, depth range of 0–7 m (0.98 km²), the average biomass of macrophytobenthos in the Gulf of Gdańsk was estimated. On this basis, the load of ^{90}Sr bioaccumulated in plant tissues of the particular groups was calculated. The lowest ^{90}Sr load (7.5 e–07 GBq) was attributed to the vascular plants from the Orłowo Cliff, while the highest load (1.8 e–02 GBq) was calculated for the brown algae in the Kuźnica Hollow. The estimated total load of ^{90}Sr bioaccumulated in all the macrophytobenthic plants in 2011 amounted to 0.027 GBq.

3.6. Load of ^{90}Sr in caught fish

The average activity value of ^{90}Sr in fish caught in the southern Baltic did not reveal any decreasing trend over the study period, and remained at relatively similar level, from

Table 3 Average activity concentrations of ^{90}Sr in sediments in the Gulf of Gdańsk in years 2005–2008, based on Zalewska and Suplińska (2013).

Year	Activity of ^{90}Sr [Bq kg ⁻¹ d.w.]			Mean activity of ^{90}Sr [Bq kg ⁻¹ d.w.]
	P110	P116	P1	
2005	2.73	3.49	3.38	3.20
2006	2.4	4.25	4.36	3.67
2007	4.25	2.29	3.1	3.21
2008	3.49	4.03	3.16	3.56

Table 4 Average activity of ^{90}Sr and calculated loads accumulated in the macrophytobenthic plants based on data from 2011.

	Phylum	Biomass [kg m ²]	Average activity of ^{90}Sr [Bq kg ⁻¹]	Surface [km ²]	Total biomass [kg]	Load [GBq]
Puck Bay	Green algae (<i>Chlorophyta</i>)	0.000668	1.36	98.95	6.61 E+04	9.0 E–05
	Brown algae (<i>Phaeophyta</i>)	0.04186	4.37	98.95	4.14 E+06	1.8 E–02
	Red algae (<i>Rhodophyta</i>)	0.005391	5.47	98.95	5.33 E+05	2.9 E–03
	Vascular plant (<i>Spermatophyta</i>)	0.012497	4.56	98.95	1.24 E+06	5.6 E–03
Orłowo Cliff	Green algae (<i>Chlorophyta</i>)	0.03092	1.36	0.98	3.03 E+04	4.1 E–05
	Brown algae (<i>Phaeophyta</i>)	0.00769	6.58	0.98	7.54 E+03	5.0 E–05
	Red algae (<i>Rhodophyta</i>)	0.02156	5.32	0.98	2.11 E+04	1.1 E–04
	Vascular plant (<i>Spermatophyta</i>)	0.00019	4.06	0.98	1.86 E+02	7.6 E–07

Table 5 Average activity concentration of ^{90}Sr and load accumulated in caught fish in the Gulf of Gdańsk in 2005–2011, based on Zalewska et al. (2016).

	Average activity of ^{90}Sr [Bq kg ⁻¹ w.w.] ^a	Load [GBq]						
		2005	2006	2007	2008	2009	2010	2011
(<i>Clupea harengus</i>)	0.027 ± 0.004	1.2 E–04	8.3 E–05	1.3 E–04	1.2 E–04	1.5 E–04	1.8 E–04	2.1 E–04
Flounder (<i>Platichthys flesus</i>)	0.163 ± 0.017	2.9 E–04	2.7 E–04	3.0 E–04	2.4 E–04	2.4 E–04	2.8 E–04	2.4 E–04
Cod (<i>Gadus morhua</i>)	0.186 ± 0.020	7.5 E–04	1.0 E–03	5.2 E–04	6.5 E–04	7.5 E–04	9.6 E–04	8.8 E–04
Sprat (<i>Spratus spratus</i>)	0.037 ± 0.005	1.8 E–03	1.4 E–03	1.4 E–03	9.3 E–04	2.1 E–03	1.6 E–03	1.4 E–03

^a Data from Zalewska et al. (2016).

0.027 Bq kg⁻¹ w.w. for herring to 0.186 Bq kg⁻¹ w.w. in the case of cod (Table 5) (Zalewska et al., 2016). From among over 25 species of fish caught in the area of the Gulf of Gdańsk, the dominant in terms of quantity were: sprat, herring, cod and flounder. In the period between 2005 and 2011, the average contribution of these species was 98.1% of 52 796 tons of fish caught annually (Szostak et al., 2006, 2007, 2008, 2009, 2010, 2011, 2012). On average, in the years 2005–2011, the contribution of individual fish species was: 76.6% for the sprat, 10.0% for the herring, 8.2% for the cod and 3.2% for the flounder. On the basis of data on the mass of fish species caught in particular years and the values of ^{90}Sr concentrations in particular fish species, the total loads of the examined isotope removed from the Gulf of Gdańsk as a result of fishery activities were estimated. The total load of ^{90}Sr for all fish species ranged from 0.0019 GBq in 2008 to 0.0032 GBq in 2009 (Table 2).

3.7. Budget of ^{90}Sr in the Gulf of Gdańsk

The basis for the ^{90}Sr budget calculation was estimation of the loads of this isotope in seawater, for particular years in the period from 2005 to 2008. Then, the loads of ^{90}Sr related to atmospheric deposition and riverine input, responsible for the increase in the amount of this isotope in seawater were analyzed. Subsequently the loads accumulated in various elements of the marine environment were estimated (Table 2). During the entire study period, the processes such as radioactive decay of ^{90}Sr , sediment deposition, and bioaccumulation in macrophytobenthic plants and fish species, taking place in the Gulf of Gdańsk, were compensated by a significantly higher input of ^{90}Sr with the Vistula waters

(Table 2). Due to the fact that the load of ^{90}Sr bioaccumulated in fish and plant tissues is very small, and additionally some amount of this isotope may return from plant tissues to the environment as a consequence of plant decomposition (the scale of this process is unknown), and also having in mind the fact that in the case of fish, the removed load of ^{90}Sr only applied to the caught fish and not to the fish resources present in the Gulf of Gdańsk, it was decided to exclude these values from the budget.

In the period 2005–2011, a theoretical increase in the load of ^{90}Sr in seawater of the Gulf of Gdańsk was demonstrated. The smallest increase of 56.4 GBq, which accounted for 2.3%, was calculated for 2005. A comparable increase of approximately 2.4% (65.1 GBq) occurred in the following year. In the years 2007 and 2008, it remained at 74.3 GBq and 67.2 GBq, which accounted for 3.2% and 3.7%, respectively. The largest increase in the ^{90}Sr load, linked to the increased riverine water input caused by the flood event, was observed in 2010. It amounted to 253.4 GBq. The average increase in the activity of ^{90}Sr in the Gulf of Gdańsk in the period from 2005 to 2011 was 5.0% (114 GBq), which was almost 2 times higher than the loss of ^{90}Sr due to radioactive decay. In the forecasting of further variations in ^{90}Sr concentration in seawater of the Gulf of Gdańsk, the equalization of concentrations between the study area and open sea waters should be assumed.

The obtained results pointed to the cause of the lack of a clear decreasing trend related to ^{90}Sr concentration. Assuming that such a set of factors as discussed above, influencing the increase and decrease of ^{90}Sr concentrations in the Gulf of Gdańsk was maintained, it is expected that ^{90}Sr will become the major anthropogenic isotope determining the

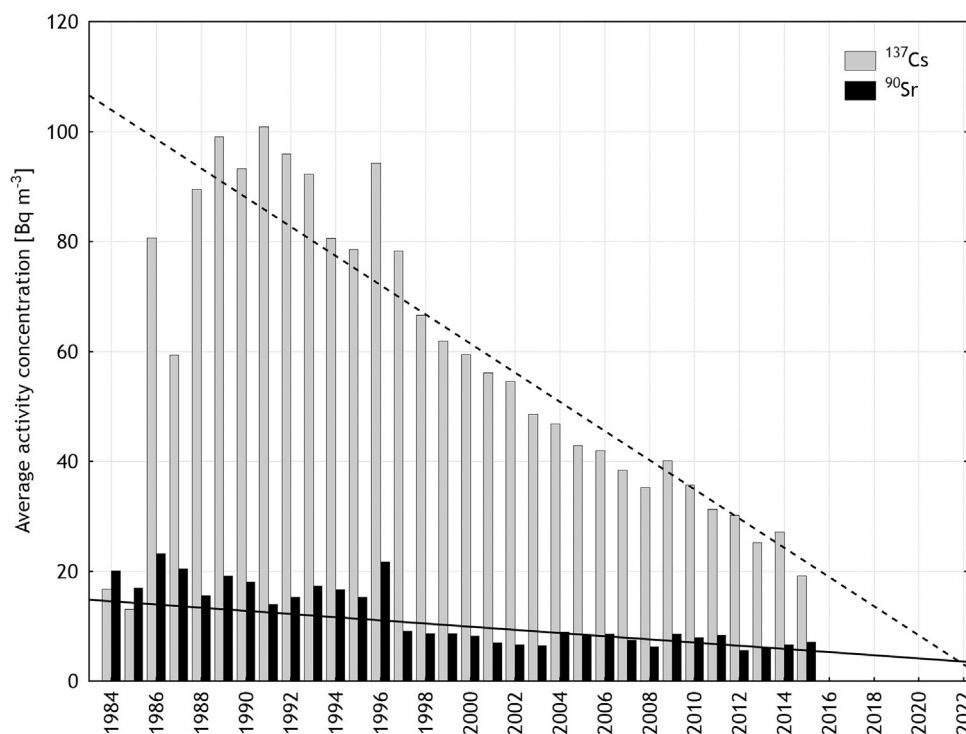


Figure 2 Average activity of ⁹⁰Sr and ¹³⁷Cs in the Gulf of Gdańsk in 1984–2015.

level of radioactivity. As observed based on the analysis of average ⁹⁰Sr concentration in seawater of the southern Baltic, the concentration of this isotope reached a maximum value of 23 Bq m⁻³ after the Chernobyl power plant accident (Fig. 2). In the period from 1988 to 1996 the concentration of ⁹⁰Sr ranged from 14.2 to 18.9 Bq m⁻³, whereas a significant decrease to the value of 9.2 Bq m⁻³ occurred in 1996 and 1997. Between 1998 and 2016 the concentration was stabilized, and varied within a range from 5.6 to 8.7 Bq m⁻³. In the similar period, since 1991 until now, there has been an apparent decrease in ¹³⁷Cs concentration. This direction of changes was also visible based on the ¹³⁷Cs to ⁹⁰Sr ratio in seawater of the Gulf of Gdańsk and the southern Baltic. Before the accident in the Chernobyl nuclear power plant in 1986, this ratio had been 0.8 (Majewski, 1990). Just after the accident it increased to 3.7 and further growth was observed in subsequent years (Majewski, 1990), mainly as a result of the increase in ¹³⁷Cs due to the inflow of more contaminated waters from the northern Baltic Sea and also due to a significant input with riverine waters. In 1991, the concentration of ¹³⁷Cs reached its maximum value of 101 Bq m⁻³, which was eight times higher than concentration of ⁹⁰Sr. In the period covered by this study, the abovementioned ratio of both isotopes decreased slightly from 5.1 to 3.7 and it is currently at a similar level. However, assuming a further decrease of ¹³⁷Cs and maintaining ⁹⁰Sr concentrations at present level, the alignment of activity levels is expected in 2022 (Fig. 2). In addition, there were determined the effective half-lives for these two isotopes in seawater of the southern Baltic Sea. Based on data from the period 1997–2015, they amounted to only 9.1 years in the case of ¹³⁷Cs and 50.3 years in the case of ⁹⁰Sr, which is almost twice longer than the theoretical half-life of ⁹⁰Sr. It could be assumed with high probability that approximately 35 years

after the Chernobyl disaster, the activity of ⁹⁰Sr will have exceeded that of ¹³⁷Cs, and the ⁹⁰Sr will have become the main isotope having substantial impact on the anthropogenic radioactivity in the southern part of the Baltic Sea.

References

- Baklanov, A., Sorensen, J.H., 2001. Parameterisation of radionuclide deposition in atmospheric long-range transport modelling. *Phys. Chem. Earth (B)* 26 (10), 787–799, [http://dx.doi.org/10.1016/S1464-1909\(01\)00087-9](http://dx.doi.org/10.1016/S1464-1909(01)00087-9).
- Brzeska, P., Saniewski, M., 2012. In: Zalewska, T., Jakusik, E., Łysiak-Pastuszak, E., Krzysiński, W. (Eds.), *Phytobentos in Southern Baltic in 2011 – Characteristics of Selected Elements of the Environment*, IMGW-PIB, Gdynia, 120–128, (in Polish).
- Carman, R., Cederwall, H., 2001. Sediments and macrofauna in the Baltic Sea – characteristics, nutrient contents and distribution. In: Wulff, F., Rahm, L., Larsson, P. (Eds.), *A System Analysis of the Baltic Sea*. Springer-Verlag, Berlin Heidelberg, 289–327.
- Cross, M.A., Smith, J.T., Saxen, R., Timms, D., 2002. An analysis of the environmental mobility of radiostromium from weapons testing and Chernobyl in Finnish river catchments. *J. Environ. Radioactiv.* 60, 149–163, [http://dx.doi.org/10.1016/S0265-931X\(01\)00101-1](http://dx.doi.org/10.1016/S0265-931X(01)00101-1).
- Håkanson, L., Lundin, L.-C., Savchuk, O., Ionov, V., Musielak, S., Furmanczyk, K., 2003. *The Baltic Sea*. In: Ryden, L., Migula, P., Andersson, M. (Eds.), *Environmental Science. 1 Baltic Univ. Press, Uppsala*, 20–147.
- HELCOM, 2009. *Radioactivity in the Baltic Sea 1999–2006*, *Baltic Sea Environ. Proc.* No. 117, 64 pp.
- HELCOM, 2010. *Hazardous substances in the Baltic Sea – an integrated thematic assessment of hazardous substances in the Baltic Sea*. In: *Baltic Sea Environ. Proc.* No. 120B. 119 pp.
- IAEA, 2005. *Worldwide marine radioactivity studies (WOMARS). Radionuclide levels in oceans and seas. Final report of a coordinated research project*. International Atomic Energy Agency, 197 pp.

- Kryshev, A.I., 2006. ^{90}Sr in fish: a review of data and possible model approach. *Sci. Total Environ.* 370, 182–189, <http://dx.doi.org/10.1016/j.scitotenv.2006.06.003>.
- Łukawska-Matuszewska, K., Bolatek, J., 2008. Spatial distribution of phosphorus forms in sediments in the Gulf of Gdańsk (southern Baltic Sea). *Cont. Shelf Res.* 28 (7), 977–990.
- Majewski, A., 1990. *Gulf of Gdańsk*. Geological Publ., Warszawa, 500 pp. (in Polish).
- Nielsen, S.P., Bengston, P., Bojanowski, R., Hagel, P., Herrmann, J., Illus, E., Jakobson, E., Motiejunas, S., Panteleev, Y., Skujina, A., Suplińska, M., 1999. The radiological exposure of man from radioactivity in the Baltic Sea. *Sci. Total Environ.* 237–238, 133–141, [http://dx.doi.org/10.1016/S0048-9697\(99\)00130-8](http://dx.doi.org/10.1016/S0048-9697(99)00130-8).
- Nies, H., Bojanowski, R., Karlberg, O., Nielsen, S.P., 1995. Sources of radioactivity in the Baltic Sea. *Baltic Sea Environ. Proc. No.* 61 6–18.
- Ritchie, J.C., McHenry, J.R., 1990. Application of radioactive fallout Cesium-137 for measuring soil erosion and sediment accumulation rates and patterns. *J. Environ. Qual.* 19 (2), 215–233, <http://dx.doi.org/10.2134/jeq1990.00472425001900020006x>.
- Saniewski, M., 2013. Spatiotemporal variations of the ^{90}Sr in the southern part of the Baltic Sea over the period of 2005–2010. *Sci. World J.* Article ID 276098.
- Saniewski, M., Zalewska, T., 2016. Atmospheric deposition and riverine load of ^{90}Sr and ^{137}Cs to the Gulf of Gdańsk (southern Baltic Sea) in the period 2005–2011. *J. Environ. Radioactiv.* 151, 1–11, <http://dx.doi.org/10.1016/j.jenvrad.2015.09.010>.
- Saniewski, M., Zalewska, T., 2017. ^{90}Sr in *Zostera marina* in Gulf of Gdańsk (southern Baltic Sea). *Oceanol. Hydrobiol. Stud.* 46 (1), 24–29, <http://dx.doi.org/10.1515/ohs-2017-0003>.
- Solecki, J., 2006. Studies of ^{90}Sr concentration and migration in the soils of the Łęczna–Włodawa Lake District. *J. Radioanal. Nucl. Chem.* 274 (1), 27–38, <http://dx.doi.org/10.1007/s10967-006-6889-x>.
- Solecki, J., Chibowski, S., 2001. Studies of soil samples mineralization conditions preceding the determination of ^{90}Sr . *J. Radioanal. Nucl. Chem.* 247, 165–169.
- Szostak, S., Kuzebski, E., Budny, T., 2006. *Maritime Fishing Industry in 2005*. *Nat. Mar. Fisheries Res. Inst.*, Gdynia, 34 pp. (in Polish).
- Szostak, S., Kuzebski, E., Budny, T., Rakowski, M., 2007. *Maritime Fishing Industry in 2006*. *Mar. Fisheries Res. Inst.*, Gdynia, 37 pp. (in Polish).
- Szostak, S., Kuzebski, E., Rakowski, M., Budny, T., 2008. *Maritime Fishing Industry in 2007*. *Mar. Fisheries Res. Inst.*, Gdynia, 38 pp. (in Polish).
- Szostak, S., Kuzebski, E., Rakowski, M., Budny, T., 2009. *Maritime Fishing Industry in 2008*. *Mar. Fisheries Res. Inst.*, Gdynia, 39 pp. (in Polish).
- Szostak, S., Rakowski, M., Budny, T., 2010. *Maritime Fishing Industry in 2009*. *National Mar. Fisheries Res. Inst.*, Gdynia, 35 pp. (in Polish).
- Szostak, S., Rakowski, M., Budny, T., 2011. *Maritime Fishing Industry in 2010*. *National Mar. Fisheries Res. Inst.*, Gdynia, 35 pp. (in Polish).
- Szostak, S., Rakowski, M., Budny, T., 2012. *Maritime Fishing Industry in 2011*. *National Mar. Fisheries Res. Inst.*, Gdynia, 34 pp. (in Polish).
- UNSCEAR, 1982. *Ionizing Radiation Sources and Biological Effects; Report to the General Assembly with annexes*. UN Publ., New York, 770 pp.
- Wängberg, I., Schmolke, S., Schager, P., Munthe, J., Ebinhaus, R., Iverfeldt, A., 2001. Estimates of air-sea exchange of mercury in the Baltic Sea. *Atmos. Environ.* 35, 5477–5484, [http://dx.doi.org/10.1016/S1352-2310\(01\)00246-1](http://dx.doi.org/10.1016/S1352-2310(01)00246-1).
- Zalewska, T., 2015. *Makrofitobentos Bioindicators in the Classification of the Marine Environment of the Southern Baltic Sea*. IMGW-PIB, Warszawa, (in Polish).
- Zalewska, T., Saniewski, M., Suplińska, M., Rubel, B., 2016. ^{90}Sr in fish from the southern Baltic Sea, coastal lagoons and freshwater lake. *J. Environ. Radioactiv.* 158–159, 38–46, <http://dx.doi.org/10.1016/j.jenvrad.2016.03.024>.
- Zalewska, T., Suplińska, M., 2013. Anthropogenic radionuclides ^{137}Cs and ^{90}Sr in the southern Baltic Sea ecosystem. *Oceanologia* 55 (3), 485–517, <http://dx.doi.org/10.5697/oc.55-3.485>.
- Zalewska, T., Woron, J., Danowska, B., Suplińska, M., 2015. Temporal changes in Hg, Pb, Cd and Zn environmental concentrations in the southern Baltic Sea sediments dated with ^{210}Pb method. *Oceanologia* 57 (1), 32–43, <http://dx.doi.org/10.1016/j.oceano.2014.06.003>.



ORIGINAL RESEARCH ARTICLE

Coastal hydrodynamics beyond the surf zone of the south Baltic Sea

Rafał Ostrowski ^{a,*}, Magdalena Stella ^a, Piotr Szmytkiewicz ^a,
Jarosław Kapiński ^b, Tomasz Marcinkowski ^b

^a *Institute of Hydro-Engineering, Polish Academy of Sciences, Gdańsk, Poland*

^b *Maritime Institute, Gdańsk, Poland*

Received 4 May 2017; accepted 30 November 2017

Available online 16 December 2017

KEYWORDS

Wind-driven current;
Wave-induced nearbed
oscillations;
Bed shear stresses;
Friction velocity;
Baltic Sea;
Moderate depths

Summary The paper presents experimental and theoretical investigations of hydrodynamic processes in a coastal region located close to the seaward boundary of the surf zone. The analysis is based on field data collected near Lubiatowo (Poland) by measuring equipment operated simultaneously by the Institute of Hydro-Engineering of the Polish Academy of Sciences (IBW PAN) and the Maritime Institute in Gdańsk (IMG). The data consist of wind velocity and direction measured at the IBW PAN Coastal Research Station (CRS) in Lubiatowo, deep-water wave buoy records, current profiles and sea bottom sediment parameters. Mean flow velocities measured in the entire water column have almost the same direction as wind. Nearbed flow velocities induced by waves and currents, as well as bed shear stresses, are modelled theoretically to determine sediment motion regimes in the area. It appears that the nonlinear wave–current interaction generates bed shear stresses greater than those that would result from the superposition of the impacts of waves and currents separately. The paper discusses the possibility of occasional intensive sediment transport and the occurrence of distinct seabed changes at greater coastal water depths adjacent to the surf zone. It was found that this can happen under the joint influence of waves and wind-driven currents.

© 2017 Institute of Oceanology of the Polish Academy of Sciences. Production and hosting by Elsevier Sp. z o.o. This is an open access article under the CC BY-NC-ND license (<http://creativecommons.org/licenses/by-nc-nd/4.0/>).

* Corresponding author at: IBW PAN, 7 Kościarska, 80-328 Gdańsk, Poland. Tel. +48 58 522 29 00. Fax. +48 58 552 42 11.

E-mail address: rafal.o@ibwpan.gda.pl (R. Ostrowski).

Peer review under the responsibility of Institute of Oceanology of the Polish Academy of Sciences.



Production and hosting by Elsevier

1. Introduction

At large water depths, the influence of wave-induced oscillatory flows and wave-driven currents on the sandy seabed is much less intensive than in the nearshore region. Sediment motion rates in the offshore areas are significantly smaller, and therefore seabed changes become less noticeable. At such locations, the motion of water (and consequently sediment movement) in the nearbed layer can be related to currents typically occurring in the open sea, for instance, drift currents. In tidal seas, such as the North Sea, the occurrence and movement of large sandy bed forms called sand waves or sand banks at depths of 20–30 m are closely associated with tidal phenomena, see [Carbajal and Montaño \(2001\)](#) and [Hulscher and van den Brink \(2001\)](#). However, [Belibassakis and Karathanasi \(2017\)](#) have recently shown that in a tidal basin (Saronic-Athens Gulf) a complex configuration of the coastline orientation, bathymetry, wave conditions and strong winds during extreme storms makes tidal currents less important to sediment transport. Similar large bed forms have also been observed, albeit sporadically, in a non-tidal environment, namely in the south Baltic coastal areas at depths of 15–30 m, see [Rudowski et al. \(2008\)](#). Moreover, it was observed that, in the south-eastern part of the Baltic Sea in the vicinity of Władysławowo (with water depths between 14 and 17.3 m), post-dredging pits, 11 months after sand extraction, were shallower by about 2–2.5 m, and traces left by a trailing suction hopper dredger disappeared completely. It is believed that the cause of this phenomenon was both slope slipping and the supply of deposits from the surrounding area. Another study in the southern Baltic Sea indicates that at depths of 15–20 m, a 0.4–0.8 m thick sand layer moves under storm conditions ([Uściniowicz et al., 2014](#)).

Open sea currents, such as gradient, geostrophic, inertial and gravitational currents or those arising as a result of seiches, are unlikely to generate intensive sediment transport at depths of less than 30 m. Recent research by [Ostrowski and Stella \(2016\)](#) shows that, aside from waves, wind-driven currents have the most important impact on hydrodynamic processes at a depth of ca. 20 m.

In the coastal zone (particularly in the surf zone), wind-driven flows are dominated by wave-driven currents. The role of wind-driven currents in marine hydrodynamics increases in regions more distant from the shoreline. On the other hand, the influence of wind-induced currents on bottom sediments decreases at bigger depths. Precise determination of the boundary between the zones of domination of wave-driven currents and wind-driven currents is difficult. This is mainly due to the fact that the parameters of both types of currents strongly depend on instantaneous local conditions: wind speed and direction, wave characteristics (height, period and direction of propagation) and the morphology of the coastal bottom. On the basis of field data collected at CRS Lubiawo and theoretical modelling with the commercial software MIKE 21, [Sokolov and Chubarenko \(2012\)](#) found the wind-induced component of currents in the surf zone to be quite high. It appears that wind can contribute almost 50% to the generation of the longshore current if it blows parallel to the shoreline and more than 20% if it blows at an angle of 45° to the shoreline. In all cases, however, the wave-driven longshore current is the predominant flow in the surf zone.

The situation seawards of the surf zone is most probably different.

In coastal areas of the Baltic Sea, the influence of the Coriolis effect may be neglected. A wind-driven current occurring in shallow basins has almost the same direction in the water column as the wind blowing over the water surface. Because the surface Ekman layer and the bottom Ekman layer overlap, the development of the Ekman spiral is hindered, and the wind-induced flow takes place in the wind direction ([Krauss, 2001](#); [Trzeciak, 2000](#); [Valle-Levinson, 2016](#)). The present paper deals with wind-driven currents occurring locally and temporarily. Hence, the wind-driven current velocity profile can be described by a directionally invariable distribution.

Wave-induced orbital nearbed velocities also have some impact on the sea bottom beyond the surf zone. The seaward boundary of this influence is conventionally related to the so-called depth of closure (h_c), at which even stormy waves do not cause intensive sediment transport (the so-called sheet flow). The corresponding extreme wave conditions are most often represented by the “effective” significant wave height (H_e), which is exceeded only 12 h per year, or 0.137% of the time. Simple formulas derived by [Birkemeier \(1985\)](#), or earlier by [Hallermeier \(1978, 1981\)](#), for the assessment of the depth of closure h_c from the effective significant wave height (H_e) and period (T_e), are discussed, for example, by [Dean \(2002\)](#). On a second front, the depth of closure h_c can be determined directly from bathymetric changes if only sufficient data are available.

For the multi-bar shore, characteristic of the south Baltic Sea, [Cerkowniak et al. \(2015a\)](#) obtained (from bathymetric surveys) actual values of the depth of closure $h_c = 6.0–7.7$ m, greater than the ones calculated using parameters of the effective significant wave height ($h_c = 4.9–6.5$ m). According to [Cerkowniak et al. \(2015b\)](#), wave-induced bed shear stresses during storms (with the deep water significant wave height H_s exceeding 3.5 m) cause intensive sediment transport (sheet flow) even at depths of 13–15 m. Such wave conditions, however, last no longer than 24 h per year, and it is interesting whether, by themselves, they cause distinct changes in the sea bottom, leading to the appearance and movement of large offshore bed forms. The research finding by [Cerkowniak et al. \(2015a\)](#) that direct bathymetric measurements of the shore yield larger values of the depth of closure than do theoretical calculations based on waves only, leads to the conclusion that another factor should be included. One should take into account that such forms at these depths can probably appear and evolve only if stormy waves are accompanied by strong sea currents.

The above considerations give rise to a hypothesis about an important role of currents typically occurring beyond the surf zone and interacting with wave-induced oscillatory flows. Under storm conditions, this interaction presumably generates bed shear stresses sufficient to cause intensive sediment transport and, consequently, distinct sea bottom evolution.

Verification of the above hypothesis requires a precise determination of the sediment driving forces (represented here by bed shear stresses) resulting from the interaction of nearbed wave-induced oscillations (orbital velocities) with steady currents occurring during severe storms at the seaward boundary of the surf zone and beyond the surf zone.

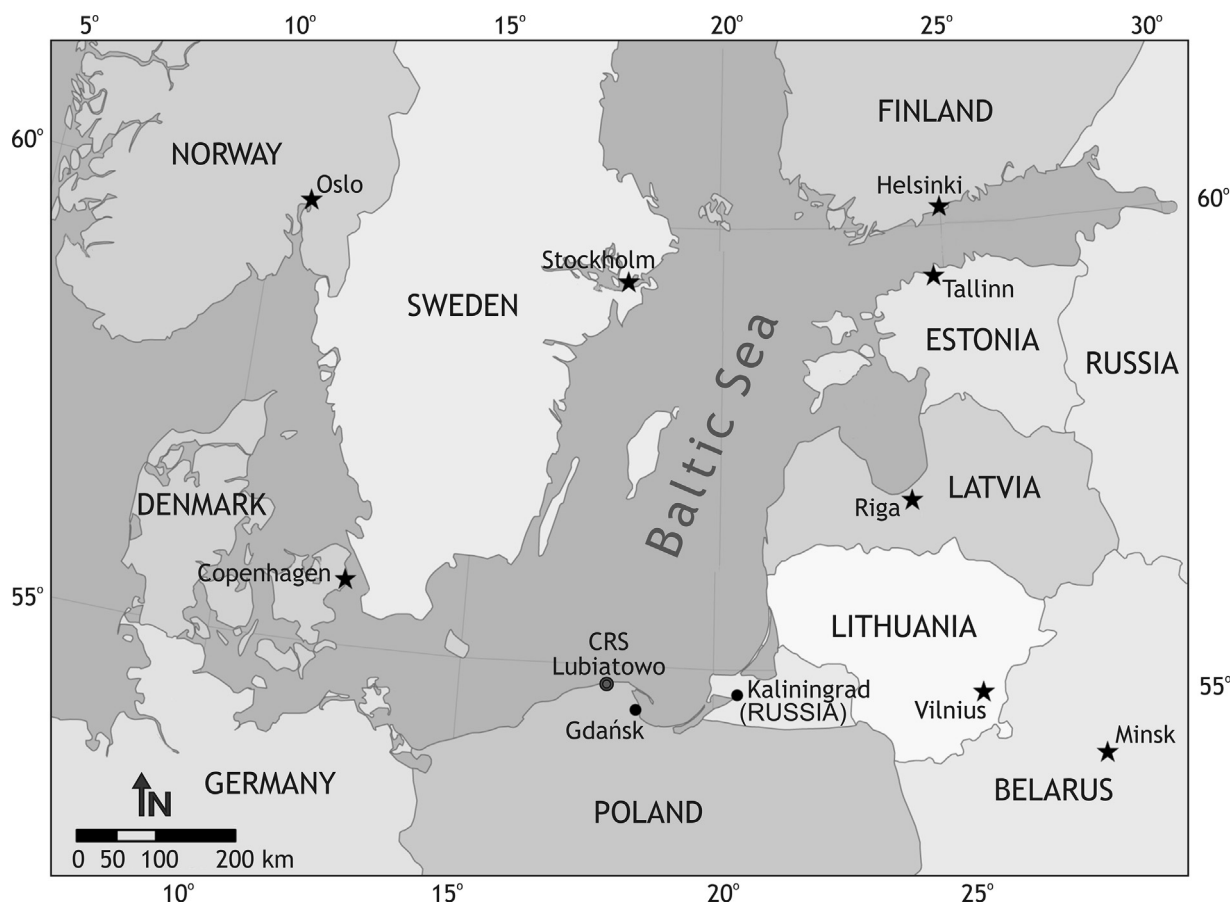


Figure 1 Location of CRS Lubiatowo on the Baltic coast.

The present study tackles this issue by analysing field data collected near Lubiatowo, Poland, as well as by mathematical modelling. Together with analysis of wave-current and wind data, an accurate theoretical description of the Shields parameter θ in the case of a synergic action of waves and the wind-driven current is the main purpose of this study.

2. Study site

The present study is based on the wind, wave and current data collected in the period from April 26, 2014 to June 30, 2014, as well as some other archival information and data, mainly concerning sediments.

The measurements were carried out by the Institute of Hydro-Engineering of the Polish Academy of Sciences (IBW PAN) and the Maritime Institute in Gdańsk (IMG) using scientific instruments located at the IBW PAN Coastal Research Station (CRS) in Lubiatowo and its vicinity. The study area of CRS Lubiatowo is situated about 70 km NW of Gdańsk (see Fig. 1). The hydrodynamics, lithodynamics and morphodynamics in the region of Lubiatowo are typical of the south Baltic sandy coast (see Cerkowniak et al., 2017; Ostrowski et al., 2015). For purposes of the present study, offshore wave buoy data and current profiles were used, as well as wind data collected on land at CRS Lubiatowo. In addition, results of sediment sampling and grain size analysis were taken into account.

The sea shore near Lubiatowo is mildly sloped (with an inclination of 1–2%) and consists of quartz sand having the median grain diameter d_{50} in the range from 0.1 to 0.4 mm (mostly 0.15–0.25 mm). The sediment density amounts to $\rho_s = 2650 \text{ kg m}^{-3}$. Cross-shore bathymetric profiles display 3–4 stable bars and an additional, ephemeral one occurring close to the shoreline. Such a multi-bar profile of the sea bottom is favourable to gradual wave energy dissipation, taking place by multiple wave breaking, see Pruszek et al. (2008).

3. Methods of field measurements

The offshore measurements near CRS Lubiatowo were carried out by means of an acoustic current profiler with an attached surface wave measurement module AWAC produced by Nortek and operating at 600 kHz transmission frequency. The device was installed with transducers facing up on a bottom-resting frame at a distance of about 1.47 Nm (i.e. 2.72 km) from the shoreline, where the mean water depth amounted to 17 m, at coordinates $54^{\circ}50.48'N$ and $17^{\circ}53.09'E$. Wave data were measured continuously once an hour for about 17 min (2048 samples recorded with a frequency of 2 Hz) and then averaged. Water flows were measured in 1 m thick layers once an hour, and they were averaged for 2-min recordings registered with 1 Hz frequency. The nearbed layer (about 1 m thick) was excluded from flow measurements for



Figure 2 Anemometer on top of a mast at CRS Lubiatowo.

technical reasons (the height of the frame on which the instrument was mounted and the so-called blanking distance, i.e. direct water body thickness to transducers, where the accuracy of measurements was not acceptable). Additionally, the results of flow measurements in the surface water layer (from 5 to 10% of the total depth) have limited reliability due to side-lobe interference. Therefore, this layer should be analysed with some care. Raw and processed wave data were collected in the internal memory of the instrument and delivered for analysis during maintenance cruises.

The wind data were collected by a cup anemometer SW-48 (produced by MORS, Poland) installed on a 22 m mast. The mast is located on land close to CRS Lubiatowo (54°48.70'N, 17°50.43'E), at a distance of about 150 m from the shoreline. The anemometer is installed a few metres above the upper branches of nearby trees (Fig. 2).

4. Wind records correction

The location of the anemometer does not satisfy standards of meteorological monitoring, and the measurements of wind parameters (particularly velocity) are biased. Although the mast is 12 m higher than indicated in the standards (10 m),

the increased terrain roughness, resulting from the presence of trees, makes that the recorded wind speed smaller than it would be over a flat ground, without trees or other obstacles, as required at state meteorological stations in Poland. It was necessary to investigate the differences between the wind speed measured at CRS Lubiatowo and the expected wind speed near the study site. Due to the lack of direct wind records from the time and place of the current measurements, it was necessary to obtain them in a different way. To do so, the authors compared measured data with values obtained from the ICM operating model (UM model) provided by SatBaltyk System (<http://satbaltyk.iopan.gda.pl>). These data were deemed reliable due to constant data assimilation and the calibration of the model with data measured at various meteorological stations. In addition, a visual analysis and comparison of ICM data with Lubiatowo measurements showed that wind directions were almost the same in both data series. Hourly time series of wind velocities were analysed for the coordinates 54°50'N, 17°50'E for the time period from May 08, 2016 to February 06, 2017, the only period for which data were available on the SatBaltyk System.

A rough analysis of wind data collected at CRS Lubiatowo and determined over the sea from ICM data shows that wind velocities measured in Lubiatowo are significantly lower than those obtained from ICM (Fig. 4). The maximum wind velocities recorded at CRS Lubiatowo slightly exceeded 10 m s⁻¹ on only two occasions, whereas ICM Model wind speeds exceeded 15 m s⁻¹ several times, reaching up to 20 m s⁻¹ under extreme conditions.

The present study includes, among others, investigations of wind-induced water flow at the location of the current profiler, beyond the surf zone, at a depth of 17 m. As mentioned above, wind measurements from CRS Lubiatowo are biased and should therefore be recalculated to become representative of the location considered. To this end, a joint analysis of wind parameters collected at CRS Lubiatowo and determined over the sea by the UM model (provided by the SatBaltyk System) was carried out. Statistical analysis of these two data series shows strong, positive correlation, with the correlation coefficient r of 0.78 (Fig. 3).

It was found that to obtain a reliable wind speed at the current monitoring point, wind velocities measured in Lubiatowo ought to be recalculated by the following regression equation:

$$y = 1.92 + 1.76x. \quad (1)$$

5. Measured results

Time series of selected parameters are shown in Figs. 4 and 6–8. The results of the wind speed recalculation are shown in Fig. 5, and the significant wave height record is plotted in Fig. 6. It can be seen in Fig. 6 that, for the period considered, the significant wave height amounts to 2–2.5 m during storms, and up to 2.76 m under extreme conditions. Figs. 7 and 8 suggest, as could be expected, that the currents near the surface are stronger than the nearbed currents, reaching maximum velocities of about 0.6 m s⁻¹ and 0.4 m s⁻¹, respectively.

Although the plots of wind speed and wave height look different, the extreme data occur at the same time. The wind

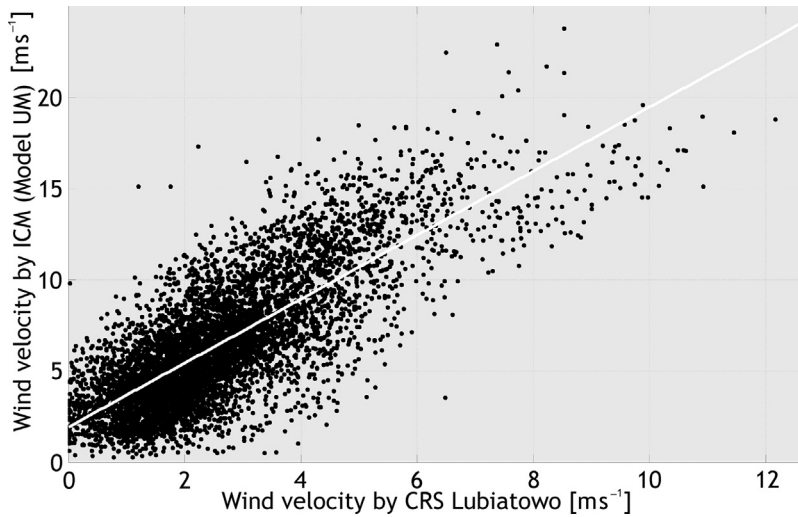


Figure 3 Scatterplot of wind measured at CRS Lubiatowo against ICM wind velocities for the period from May 08, 2016 to February 06, 2017.

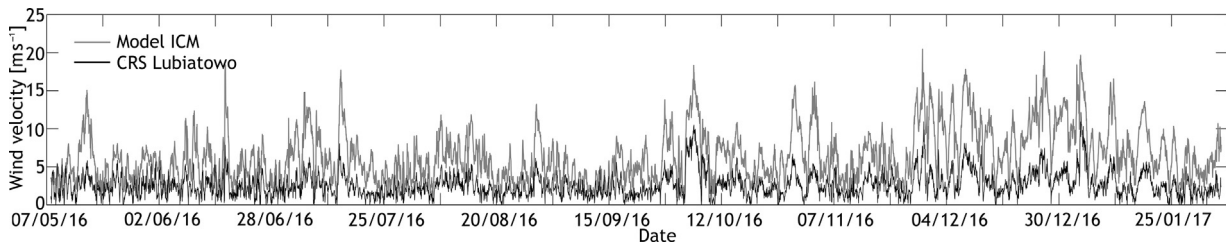


Figure 4 Time series of the mean hourly wind speed obtained from ICM (grey line) (data provided by SatBaltyk System) and measured at CRS Lubiatowo (black line) (both data sets from May 08, 2016 to February 06, 2017).

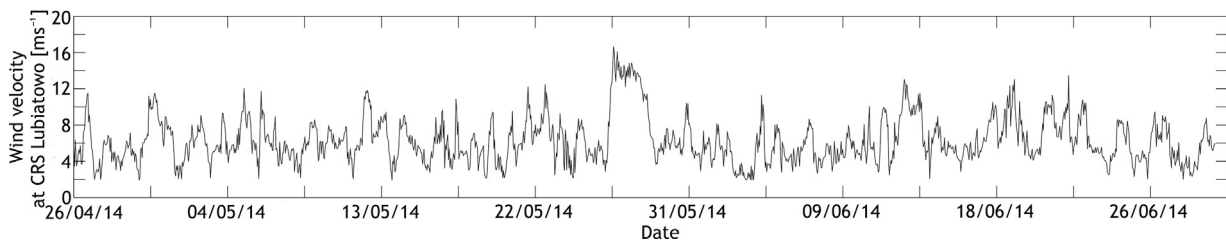


Figure 5 Wind speed measurements at CRS Lubiatowo recalculated by a regression equation for the time period from April 26, 2014 to June 30, 2014.

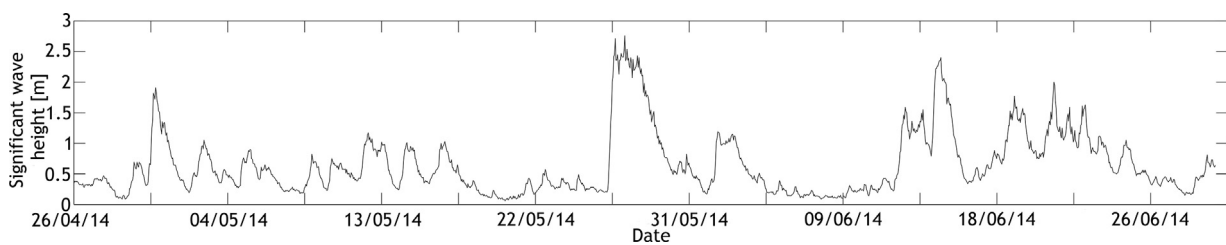


Figure 6 Hourly time series of the significant wave height in the vicinity of CRS Lubiatowo for the time period from April 26, 2014 to June 30, 2014.

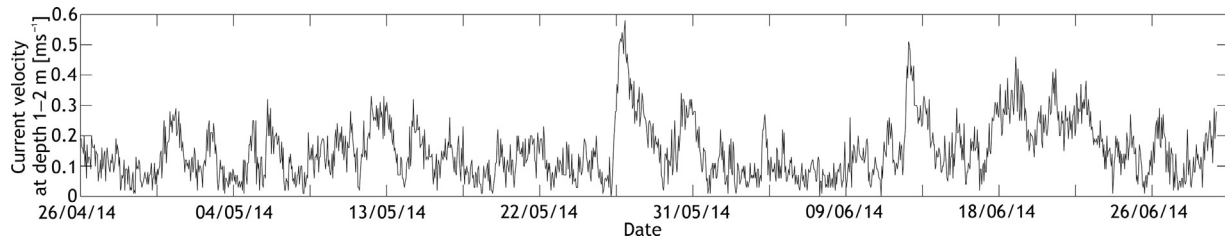


Figure 7 Time series of the mean hourly flow velocity in the subsurface layer (15–16 m above the bottom) for the time period from April 26, 2014 to June 30, 2014.

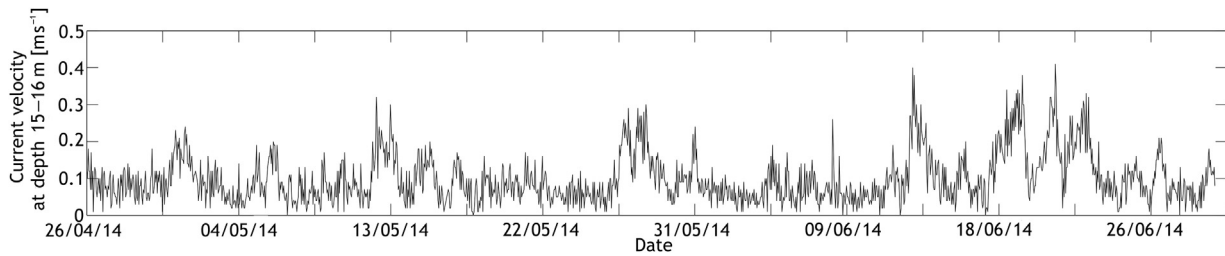


Figure 8 Time series of the mean hourly flow velocity in the nearbed layer (1–2 m above the bottom) for the time period from April 26, 2014 to June 30, 2014.

speed from Fig. 5 was used as an input in a theoretical model of wind-induced currents. The wave-induced current model is described below.

6. Methods of investigation

The investigations were focused on determining whether the motion of sediments beyond the surf zone is possible under storm conditions and how intensive it may be. In order to verify the possibility of sediment motion in the region where waves and currents had been measured, namely at a depth of 17 m, bed shear stresses were calculated for the following cases:

- wave-induced nearbed oscillatory flow with the overall bottom roughness (the so-called “equivalent” moveable bed roughness, as defined by Kaczmarek, 1995, 1999);
- nearbed stationary flow caused by the wind-driven current, with the bottom roughness of sand grains (the so-called “skin” bed roughness, as defined by Nielsen, 2009) and the roughness resulting from the presence of bed forms of various heights;
- nearbed flow caused by the wind-driven current superimposed on wave-induced nearbed oscillations, with the overall bottom roughness (“equivalent” moveable bed roughness).

Sediment transport intensity is conventionally estimated using the Shields parameter, which represents the dimensionless bed shear stress and is given by the following formula (see e.g. Nielsen, 2009):

$$\theta = \frac{u_f^2}{(s-1)gd}, \quad (2)$$

in which u_f is the friction velocity, s is the ratio of sediment density ρ_s to water density ρ ($s = \rho_s/\rho$; for quartz sand: about

2.65), g denotes acceleration due to gravity, and d stands for the seabed grain diameter.

6.1. Friction velocity

A reliable and precise determination of the friction velocity u_f is difficult, particularly for unsteady currents, e.g. wave-induced nearbed oscillatory flows. The friction velocity represents the bed shear stress τ (defined as $\tau = \rho u_f^2$), which is the main driving force for sediment transport. According to the basics of fluid mechanics, the bed shear stress τ depends on the water flow velocity and the sea bottom roughness. The seabed, if built of sandy sediments, becomes moveable under hydrodynamic impacts (resulting from turbulent water flow generated by waves and currents), which causes additional difficulties in a theoretical solution leading to the determination of the friction velocity u_f . In the present study, various theoretical approaches are applied to particular cases.

The dimensionless shear stress depends on the grain diameter d . Sediment sampling and analyses show that the sand occurring at the study site (water depth $h = 17$ m) is very fine. The present analysis was carried out for sand grain diameter $d_{50} = 0.00013$ m (based on sediment grain size analysis conducted at IBW PAN).

6.2. Wind-driven current

The shear stresses τ in the water column where the wind-driven current occurs are assumed to satisfy the Boussinesq hypothesis as follows:

$$\tau = \rho \nu_t \frac{du(z)}{dz}, \quad (3)$$

where ν_t is the kinematic turbulent viscosity in the vertical direction z , and $u(z)$ is the velocity of stationary water flow.

It is further assumed that the turbulent viscosity increases linearly from the bottom, being proportional to von Karman's constant κ and the friction velocity u_f , so that

$$\nu_t = \kappa u_f z. \quad (4)$$

Bearing in mind that the shear stress can be defined as $\tau = \rho u_f^2$, one obtains the logarithmic vertical distribution of velocity $u(z)$:

$$u(z) = \frac{u_f}{\kappa} \ln\left(\frac{z}{z_0}\right), \quad (5)$$

in which z_0 denotes the ordinate at which the velocity u equals zero.

The quantity z_0 can be regarded as a theoretical seabed level from which the logarithmic profile of the velocity $u(z)$ starts. Conventionally, this level is determined as $z_0 = k_N/30$, where k_N is the so-called Nikuradse roughness. The assumption of the bottom characterised by a “skin” roughness height of $2.5d$ (due to the presence of sand grains only) yields $z_0 = 2.5d/30$. If the sea bottom is covered by bed forms, the bottom roughness height will be $z_0 = k_f/30$, where k_f is the bed form height.

The wind-driven current speed in the surface layer equals 2–5% of the wind speed w at the 10 m height above the sea level (see e.g. Kim et al., 2010). In this study, the authors consider extreme cases of measured nearbed steady flows. The analysis of the wind data and surface current velocity measurements showed that for a wind speed averaged over 12 h exceeding 7 m s^{-1} the magnitude of the surface current (in a 1 m thick layer) is about 4% of the wind speed. Thus, the following formula is assumed:

$$u_{\text{surface}} = 0.04w. \quad (6)$$

The velocity calculated by Eq. (6) is assumed to satisfy the logarithmic distribution given by Eq. (5). With the assumed bed roughness and with the resulting value of z_0 , one can easily determine the friction velocity u_f from Eq. (5) if only the flow velocity u at any level z is known. The wind-driven flow velocity in the surface layer (from the mean water level to 1 m depth, namely for $z = 16.5 \text{ m}$) is calculated by Eq. (6).

If the mean flow velocity u_{mean} is available (averaged over the water column), it is necessary to take advantage of the logarithmic velocity distribution integrated over the water depth h , from the theoretical bed level z_0 to the water surface level. After integration of the logarithmic distribution of $u(z)$ given by Eq. (5), division by the water depth h and rearrangement, the following formula for the friction velocity u_f is obtained:

$$u_f = \frac{\kappa u_{\text{mean}}}{\ln\left(\frac{h}{z_0}\right) - 1 + \frac{z_0}{h}}. \quad (7)$$

It is visible from the form of Eqs. (3)–(5) that both the friction velocity u_f and the shear stress τ are constant in the entire water column (independent of the ordinate z).

6.3. “Equivalent” moveable bed roughness

In the case of shear stresses triggered over an arbitrarily shaped sea bottom by wave-induced oscillatory nearbed flows, the approach proposed by Kaczmarek (1995) was used.

The iterative procedure elaborated by Kaczmarek (1995) ensured the determination of the “equivalent” moveable bed roughness height k_e . This parameter comprises the overall roughness represented by the sand grains building the bottom and the effects of bedload. Further development of this concept by Kaczmarek (1999) led to the formulation of approximate equations describing the roughness height k_e as functions of the Shields parameter. The time-variable friction velocity $u_f(t)$ was determined by Fredsøe's integral momentum method (1984). This approach was adopted in the present study.

6.4. Waves and wind-driven current

Developed by Kaczmarek and Ostrowski (2002), the model of intensive near-bed sand transport under wave-current flow provided reliable values of sediment transport rates, successfully verified against laboratory and field data. In this model, as mentioned previously, the shear stress induced over the sea bottom characterised by the “equivalent” roughness of the moveable bed was the driving force of sediment movement. This approach was later applied by Ostrowski (2003) in the modelling of wave transformation, wave-driven currents, net sand transport and short-term morphodynamics of a multi-bar coastal zone.

For purposes of the present research, the abovementioned modelling framework was adapted to the case of the open sea (beyond the surf zone), where wave propagation under storm conditions is accompanied by the influence of a strong wind-driven current. To include this effect, the dispersion relationship for wave motion interacting with a steady flow, represented by the mean wind-driven current velocity u_{mean} , is used:

$$gk \tanh kh = (\omega - ku_{\text{mean}} \cos \alpha)^2, \quad (10)$$

where ω denotes angular frequency in the wave motion, $k = 2\pi/L$ is the wave number (L stands for the wave length), and α denotes the angle between the steady flow velocity u_{mean} and the wave propagation direction.

Similarly as in the case of wave-induced bed shear stresses, the time-variable friction velocity u_f for the bed shear stresses generated jointly by waves and the wind-driven current is determined using the theoretical concept of Kaczmarek and Ostrowski (2002).

The analysis of current data available for the period from April 26, 2014 to June 30, 2014 revealed extreme flow conditions (with the maximum measured velocity in the nearbed water layer) on June 12, 2014 and June 21, 2014.

As deduced by Kaczmarek and Ostrowski (1995, 1996), bed shear stresses and sediment transport rates under natural conditions (for irregular waves actually observed at sea) can be reliably modelled by the linear wave theory, using the root-mean-square wave height (H_{rms}) and the peak wave energy period (T_p) as inputs. Therefore, the bed shear stresses generated by waves and wave–current interactions were computed using the wave parameters H_{rms} and T_p . The values of H_{rms} and T_p corresponding to the extreme nearbed current velocities were obtained from the analysis of the wave data collected in the region considered (with water depth $h = 17 \text{ m}$). The wave parameters constituted a basis for the determination of wave-induced nearbed oscillatory

Table 4 Flow velocity frequency of occurrence in all measured layers for the time period from April 26, 2014 to June 30, 2014.

Frequency [%] Velocity [m s ⁻¹]	Distance from bottom [m]																	
	16–17	15–16	15–14	14–13	13–12	12–11	11–10	10–9	9–8	8–7	7–6	6–5	5–4	4–3	3–2	2–1		
0–0.05	0.0	0.2	0.1	0.2	0.3	0.1	0.2	0.3	0.5	0.5	0.4	0.4	0.4	0.1	0.3	0.5		
0.05–0.1	3.9	13.6	17.6	17.7	19.5	21.2	22.1	23.3	22.5	22.9	22.9	24.0	24.6	25.5	25.5	27.9		
0.1–0.15	9.2	23.8	28.1	28.0	28.7	29.8	28.6	28.1	28.1	30.3	31.8	31.0	31.5	33.4	36.1	35.6		
0.15–0.2	7.7	22.00	21.9	24.2	22.3	19.2	21.9	21.2	23.0	19.4	21.7	19.7	20.8	20.1	19.1	19.3		
0.2–0.25	9.0	17.2	14.8	12.2	12.2	14.1	11.4	11.4	10.8	11.6	10.6	12.2	10.7	10.6	10.0	9.1		
0.25–0.3	9.4	9.8	6.4	7.9	7.7	7.0	7.2	7.9	7.2	8.2	6.1	7.0	6.0	6.1	4.6	4.1		
0.3–0.35	13.9	7.6	6.3	5.3	5.1	4.7	4.9	3.5	4.5	3.8	3.5	3.1	3.3	2.0	2.9	2.5		
0.35–0.4	14.1	3.0	2.4	2.1	2.0	1.9	1.9	2.1	1.8	2.0	1.7	1.3	1.8	1.6	1.2	0.8		
0.4–0.45	9.8	1.2	0.7	1.2	0.8	0.7	0.7	1.1	0.7	0.9	1.1	0.8	0.4	0.4	0.3	0.1		
0.45–0.5	10.9	0.7	0.8	0.5	0.6	0.7	0.5	0.7	0.8	0.4	0.2	0.4	0.5	0.3	0.1	0.1		
>0.5	11.9	1.0	0.9	0.7	0.8	0.7	0.5	0.4	0.1	0.1	0.1	0.1	0.1	0.1	0.0	0.0		
Legend	[%]	0–1	2–3	4–5	6–7	8–9	10–11	12–13	14–15	16–17	18–19	20–21	22–23	24–25	26–27	28–29	30–31	32–33

Table 5 Input parameters for modelling the wind-driven current and bed shear stresses for two hydrodynamic impacts.

Parameters	Case 1	Case 2
Date	June 12, 2014	June 21, 2014
H_{rms}	0.76 m	1.41 m
T_p	5.85 s	6.42 s
w	11.16 m s ⁻¹	10.22 m s ⁻¹
α	10°	40°

8.1. Flow velocities

The results of flow measurements and computations are shown in Figs. 9–12.

It can be seen in Figs. 9 and 11 that agreement between the measured and modelled flow velocity profiles is reasonably good, irrespective of the assumed bottom roughness k_N .

The analysis of the field data showed that the measured mean flow velocities in the entire water column had almost the same direction as the wind. This is visible in Figs. 10 and 12.

8.2. Bed shear stresses

As already pointed out, the bed shear stress causes sediment transport, and the dimensionless shear stress θ is an indicator of the sediment motion intensity. Bed shear stresses were modelled for the hydrodynamic cases and with the input quantities described in Section 3. For the case of bed shear stresses (represented by the Shields parameter θ) induced solely by the wind-driven current, aside from the “skin” bed roughness ($k_N = 2.5d$), two values of the bed form roughness were assumed, namely $k_f = 0.05$ m and $k_f = 0.10$ m. For the cases of the wave-induced shear stress and the shear stress induced by waves and currents, the Shields parameter θ_{max} was calculated from the friction velocity $u_{fmax} = \max [(u_f(\omega t))]$. The results of modelling are given in Tables 6–8.

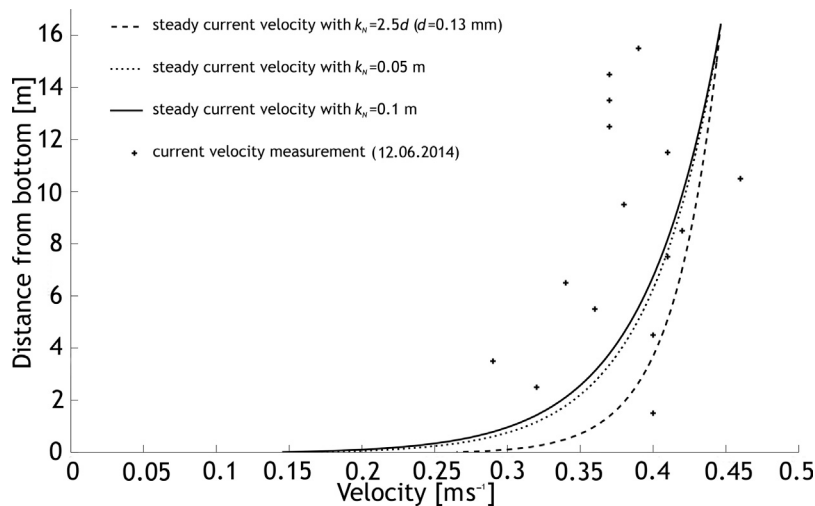


Figure 9 Velocity profiles of steady wind-driven current for different k_N and measured velocity on June 12, 2014 (case 1).

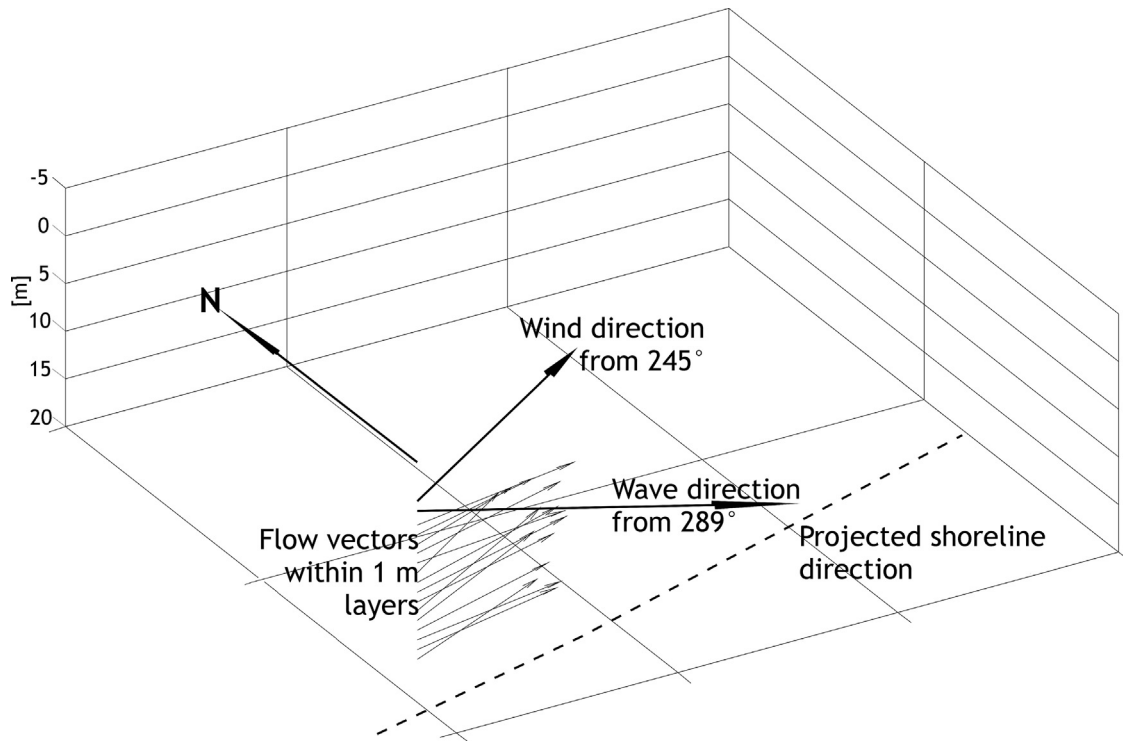


Figure 10 Scheme of measured current vectors together with wind and peak wave direction on June 12, 2014 (case 1).

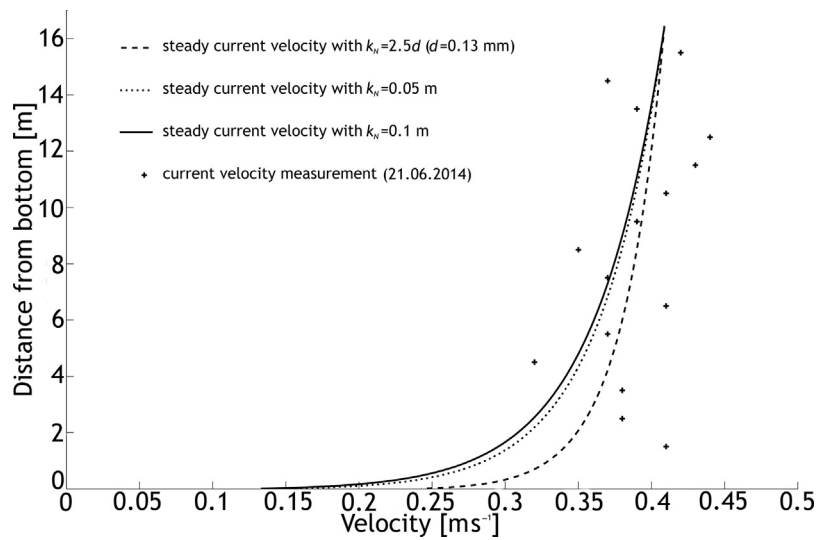


Figure 11 Velocity profiles of steady wind-driven current for different k_N and measured velocity on June 21, 2014 (case 2).

The quantity U_{1m} in Table 6 is the maximum nearbed wave-induced (free stream) oscillatory velocity (for sinusoidal waves, $U(\omega t) = U_{1m} \sin(\omega t)$).

In analysing the results of θ computations, the following regimes of sediment transport were assumed:

- $\theta \in <0; 0.05>$ no sediment motion;
- $\theta \in (0.05; 0.3>$ very weak sediment motion; ripples appear on the seabed;
- $\theta \in (0.3; 0.6>$ weak sediment motion; ripples develop;

- $\theta \in (0.6; 0.9>$ moderately intensive sediment motion; ripple height decreases;
- $\theta > 0.9$ intensive sediment motion (sheet flow), flat seabed.

The results of calculations shown in Table 6 (dimensionless maximum wave-induced bed shear stress θ_{max} with the “equivalent” bottom roughness) indicate that, under the wave conditions considered, seabed grains with a diameter of 0.13 mm move very little (case 1) or little (case 2). The corresponding values of θ_{max} amounting to 0.227 and

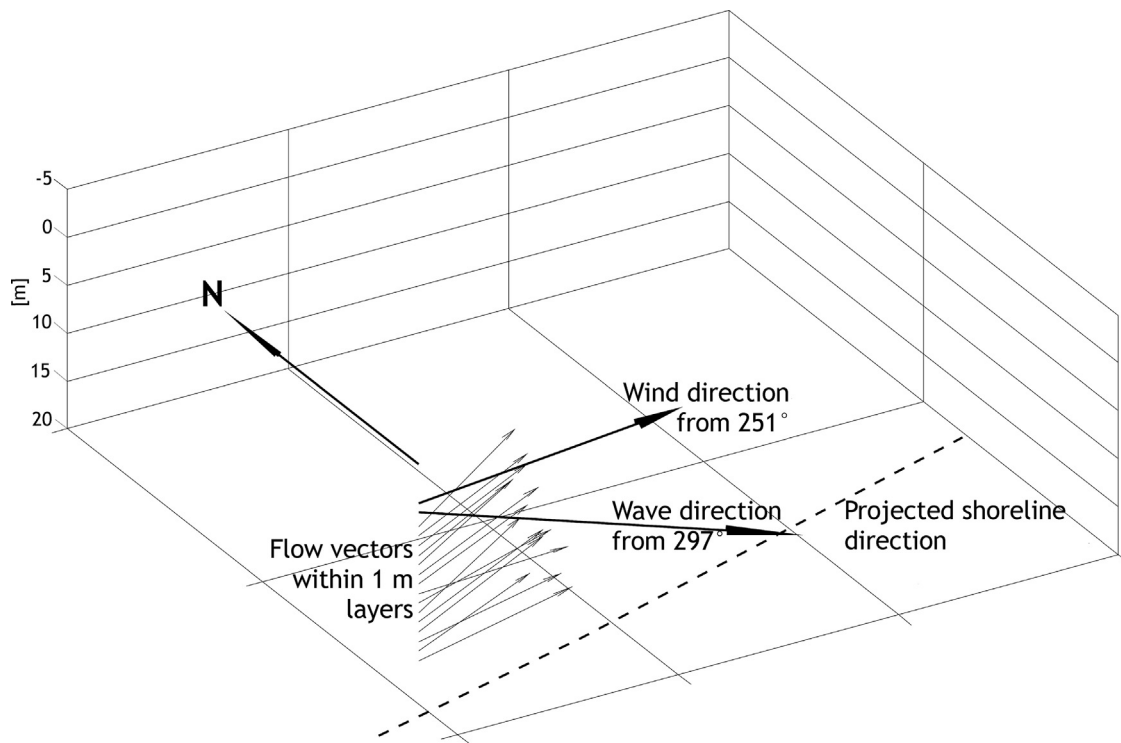


Figure 12 Scheme of measured current vectors together with wind and peak wave direction on June 21, 2014 (case 2).

Table 6 Wave-induced bed shear stress with “equivalent” bottom roughness.

	Case 1	Case 2
U_{1m}	0.105	0.245
U_{fmax}	0.008	0.033
θ_{max}	0.227	0.514

Table 7 Bed shear stress induced by wind-driven current.

	$k_N = 2.5d$	$k_N = k_f = 0.05 \text{ m}$	$k_N = k_f = 0.1 \text{ m}$
Case 1			
U_{mean}	0.420	0.399	0.395
U_f	0.013	0.019	0.021
θ	0.069	0.191	0.224
Case 2			
U_{mean}	0.380	0.365	0.361
U_f	0.012	0.018	0.019
θ	0.067	0.161	0.188

0.514 indicate development of ripple marks. Dimensionless bed shear stresses θ determined for the case of the sole wind-driven current under the conditions considered (Table 7), in comparison with wave-induced hydrodynamics and the “equivalent” bed roughness (Table 6), are distinctly smaller for all assumed bed roughness values, lying in the range from 0.067 to 0.224, which corresponds to very slight motion of grains.

The most interesting case is that of the nearbed wave–current interaction. Shown in Table 8, the results of the modelling of the dimensionless bed shear stresses θ_{max}

Table 8 Bed shear stress induced by nearbed wave–current interaction.

	$k_N = 2.5d$	$k_N = k_f = 0.05 \text{ m}$	$k_N = k_f = 0.1 \text{ m}$
Case 1			
U_{fmax}	0.035	0.034	0.033
θ_{max}	0.567	0.537	0.532
Case 2			
U_{fmax}	0.0401	0.0397	0.0397
θ_{max}	0.764	0.748	0.748

generated jointly by waves and the wind-driven current indicate that the sandy material under the conditions and at the site considered is subject to rather intense movement. Further, it appears that the values of θ_{max} given in Table 8 are higher than the sums of their counterparts (θ_{max} and θ) given in Tables 6 and 7. This nonlinear effect clearly implies a synergic character of wave–current interaction as a prime mover of marine lithodynamics.

It is worth noting that the values of U_{fmax} and θ_{max} shown in Table 8 are little dependent on the bed roughness k_N . This is typical of the wave-dominated bed boundary layer, which is weakly affected by the steady current. On the other hand, the steady current can be affected by the wave-dominated bed boundary layer constituting a larger apparent bottom roughness (see discussion by Ostrowski and Stella, 2016).

The values of bed shear stresses obtained for severe storm conditions occurring in the period considered are relatively high, exceeding the critical quantities for the motion of sand grains. Such results can explain sediment motion and the silting up of bottom excavations at significant depths, as well

as the appearance and migration of bed forms in a non-tidal sea (the south Baltic), observed by Rudowski et al. (2008) and Uścińowicz et al. (2014).

9. Final remarks and conclusions

According to Nielsen (2009), rapidly accelerated flows induced by waves have thinner bed boundary layers than longer period flows (such as tidal currents). Consequently, wave motions generate greater bed shear stresses for a given free stream velocity magnitude. This rule is confirmed by the results of the present study. The bed shear stresses determined for the wave-induced oscillatory flow are bigger than the ones determined for the wind-driven steady current although the wave-induced nearbed maximum velocity U_{1m} is smaller than the steady current velocity averaged over the water column (u_{mean}).

It was found that, for the cases considered, the measured mean flow velocities in the entire water column had almost the same direction as the wind. Hence, it appears that at the limited depths of the Baltic Sea the wind-driven current velocity profile can be described by a directionally invariable distribution.

For the site considered, the modelling of bed shear stresses for various extreme hydrodynamic impacts yields the highest values of the Shields parameter θ in the case of a joint action of waves and the wind-driven current. It appears that nonlinear wave–current interaction generates bed shear stresses bigger than would result from the superposition of results determined separately for the impacts of waves and currents. The calculated bed shear stresses are high enough to generate sediment transport.

The relatively intensive hydrodynamic conditions at a depth of 17 m, however, have an instantaneous character in the scale of a year. The question arises whether these conditions, given their relatively short duration, can explain the appearance and migration of bed forms, especially large forms, such as sand waves. It can be supposed that the significant seabed changes observed (Rudowski et al., 2008) result from extreme wave-current conditions occurring repeatedly in longer time scales, e.g. over a few years. Clarification of the above doubts requires a more detailed quantitative insight into sediment transport present beyond the surf zone. In particular, measurements of nearbed velocities combined with observations of seabed evolution at a depth of 15–25 m would shed new light on the hydrodynamic and lithodynamic processes taking place in this region.

Acknowledgements

The study was sponsored by the Ministry of Science and Higher Education, Poland, under mission-related programme No. 2 of IBW PAN and by the National Science Centre, Poland, under project No. PBS1/A6/8/2012.

References

- Belibassakis, K.A., Karathanasi, F.E., 2017. Modelling nearshore hydrodynamics and circulation under the impact of high waves at the coast of Varkiza in Saronic-Athens Gulf. *Oceanologia* 59 (3), 350–364, <http://dx.doi.org/10.1016/j.oceano.2017.04.001>.
- Birkemeier, W.A., 1985. Field data on seaward limit of profile change. *J. Waterway Port Coast. Ocean Eng.* 111 (3), 598–602, [http://dx.doi.org/10.1061/\(ASCE\)0733-950X\(1985\)111:3\(598\)](http://dx.doi.org/10.1061/(ASCE)0733-950X(1985)111:3(598)).
- Carbajal, N., Montaña, Y., 2001. Comparison between predicted and observed physical features of sandbanks. *Estuar. Coast. Shelf Sci.* 52 (14), 435–443, <http://dx.doi.org/10.1006/eccs.2000.0760>.
- Cerkowniak, G.R., Ostrowski, R., Stella, M., 2015a. Depth of closure in the multi-bar non-tidal nearshore zone of the Baltic Sea: Lubiatowo (Poland) case study. *Bull. Maritime Inst. Gdańsk.* 30 (1), 180–188, <http://dx.doi.org/10.5604/12307424.1185577>.
- Cerkowniak, G.R., Ostrowski, R., Stella, M., 2015b. Wave-induced sediment motion beyond the surf zone: case study of Lubiatowo (Poland). *Arch. Hydro-Eng. Environ. Mech.* 62 (1–2), 27–39, <http://dx.doi.org/10.1515/heelm-2015-0017>.
- Cerkowniak, G.R., Ostrowski, R., Pruszek, Z., 2017. Application of Dean's curve to investigation of a long-term evolution of the southern Baltic multi-bar shore profile. *Oceanologia* 59 (1), 18–27, <http://dx.doi.org/10.1016/j.oceano.2016.06.001>.
- Dean, R.G., 2002. *Beach Nourishment. Theory and Practice. Advanced Series on Ocean Engineering*, vol. 18. World Sci. Publ. Co. Pte. Ltd., 399 pp.
- Fredsøe, J., 1984. Turbulent boundary layer in combined wave-current motion. *J. Hydraul. Eng.* 110 (8), 1103–1120, [http://dx.doi.org/10.1061/\(ASCE\)0733-9429\(1984\)110:8\(1103\)](http://dx.doi.org/10.1061/(ASCE)0733-9429(1984)110:8(1103)).
- Hallermeier, R.J., 1978. Uses for a calculated limit depth to beach erosion. In: *Proceedings, 16th Coastal Engineering Conference. American Society of Civil Engineers*, 1493–1512.
- Hallermeier, R.J., 1981. A profile zonation for seasonal sand beaches from wave climate. *Coast. Eng.* 4 (3), 253–277.
- Hulscher, S.J.M.H., van den Brink, G.M., 2001. Comparison between predicted and observed sand waves and sand banks in the North Sea. *J. Geophys. Res.* 106 (C5), 9327–9338, <http://dx.doi.org/10.1029/2001JC900003>.
- Kaczmarek, L.M., 1995. Nonlinear effects of waves and currents on moveable bed roughness and friction. *Arch. Hydro-Eng. Environ. Mech.* 42 (1–2), 3–27.
- Kaczmarek, L.M., 1999. *Moveable Sea Bed Boundary Layer and Mechanics of Sediment Transport*. (D.Sc. thesis). IBW PAN, Gdańsk, 209 pp.
- Kaczmarek, L.M., Ostrowski, R., 1995. Modelling of bed shear stress under irregular waves. *Arch. Hydro-Eng. Environ. Mech.* 42 (1–2), 29–51.
- Kaczmarek, L.M., Ostrowski, R., 1996. Bedload under asymmetric and irregular waves: theory versus laboratory data. *Arch. Hydro-Eng. Environ. Mech.* 43 (1–4), 21–42.
- Kaczmarek, L.M., Ostrowski, R., 2002. Modelling intensive near-bed sand transport under wave-current flow versus laboratory and field data. *Coast. Eng.* 45 (1), 1–18, [http://dx.doi.org/10.1016/S0378-3839\(01\)00041-2](http://dx.doi.org/10.1016/S0378-3839(01)00041-2).
- Kim, S.Y., Cornuelle, B.D., Terrill, E.J., 2010. Decomposing observations of high-frequency radar derived surface currents by their forcing mechanisms: locally wind-driven surface currents. *J. Geophys. Res.* 115 (C12), <http://dx.doi.org/10.1029/2010JC006223>.
- Krauss, W., 2001. Chapter: Baltic sea circulation. In: Steele, J., Thorpe, S., Turekian, K. (Eds.), *Encyclopedia of Ocean Sciences*. Acad. Press, 236–244, <http://dx.doi.org/10.1006/rwos.2001.0381>.
- Nielsen, P., 2009. *Coastal and Estuarine Processes. Advanced Series on Ocean Engineering*, vol. 29. World Sci. Publ. Co. Pte. Ltd., 343 pp.
- Ostrowski, R., 2003. A quasi phase-resolving model of net sand transport and short-term cross-shore profile evolution. *Oceanologia* 45 (2), 261–282.
- Ostrowski, R., Schönhöfer, J., Szmytkiewicz, P., 2015. South Baltic representative coastal field surveys, including monitoring at the Coastal Research Station in Lubiatowo, Poland. *J. Mar. Syst.* 162, 89–97, <http://dx.doi.org/10.1016/j.jmarsys.2015.10.006>.

- Ostrowski, R., Stella, M., 2016. Sediment transport beyond the surf zone under waves and currents of the non-tidal sea: Lubiatowo (Poland) case study. *Arch. Hydro-Eng. Environ. Mech.* 63 (1), 63–77.
- Pruszek, Z., Szmytkiewicz, P., Ostrowski, R., Skaja, M., Szmytkiewicz, M., 2008. Shallow-water wave energy dissipation in a multi-bar coastal zone. *Oceanologia* 50 (1), 43–58.
- Rudowski, S., Łęczyński, L., Gajewski, Ł., 2008. Sand waves on the bottom of the deep nearshore and their role in shore formation. *Landf. Anal.* 9, 214–216, (in Polish).
- Sokolov, A., Chubarenko, B., 2012. Wind influence on the formation of nearshore currents in the southern Baltic: numerical modelling results. *Arch. Hydro-Eng. Environ. Mech.* 59 (1–2), 37–48.
- Trzeciak, S., 2000. *Marine Meteorology with Oceanography*. PWN, 249 pp., (in Polish).
- Uścińowicz, S., Jegliński, W., Miotk-Szpiganowicz, G., Nowak, J., Pączek, U., Przedziecki, P., Szeffler, K., Poręba, G., 2014. Impact of sand extraction from the bottom of the southern Baltic Sea on the relief and sediments of the seabed. *Oceanologia* 56 (4), 857–880, <http://dx.doi.org/10.5697/oc.56-4.857>.
- Valle-Levinson, A., 2016. Lecture 13. Equations of Motion, web location: http://www.essie.ufl.edu/~arnoldo/ocp6050/notes_pdf/ (31.05.16).



ORIGINAL RESEARCH ARTICLE

Parameters of wind seas and swell in the Black Sea based on numerical modeling

Boris Divinsky*, Ruben Kosyan

Shirshov Institute of Oceanology, Russian Academy of Sciences, Gelendzhik, Russia

Received 16 July 2017; accepted 30 November 2017

Available online 14 December 2017

KEYWORDS

Wind seas;
Swell;
Wave climate;
Black Sea;
Numerical modeling;
Separation of wave components

Summary The main objective of our work is to estimate the climatic peculiarities of the distribution of wind sea and swell in the Black Sea. The method of our research is numerical modeling. We tuned the spectral wave model DHI MIKE 21 SW for automatic separation of the components of surface waves. We estimated the peculiarities of the spatial distribution of the power of wind seas and swell in the basin of the Black Sea in the last 10 years (2007–2016). We determined the regions of domination of wind seas and swell in the field of mixed waves. © 2017 Institute of Oceanology of the Polish Academy of Sciences. Production and hosting by Elsevier Sp. z o.o. This is an open access article under the CC BY-NC-ND license (<http://creativecommons.org/licenses/by-nc-nd/4.0/>).

1. Introduction

1.1. General notes

Two main components can be usually distinguished in the structure of surface waves: wind seas and swell. The development of wind seas is immediately related to the local wind field. Swell is related to the waves propagating

beyond the zones of their generation, or the phase velocity of these waves exceeds the wind speed (for example, [US Army Corps of Engineers, 2002](#)). In the open ocean, swell can propagate over hundreds or even thousands of kilometers. The characteristics of swell in the Black Sea are limited by the geographical size and closeness of the sea basin.

Usually, the characteristics of wave field are presented as a set of integral parameters (significant wave height, mean

* Corresponding author at: Shirshov Institute of Oceanology, Russian Academy of Sciences, Oceanology, Prostornaya 1g, 353467 Gelendzhik, Krasnodar Region, Russia. Tel.: +7 918 4567922. Fax: +7 86141 28281.

E-mail address: divin@ocean.ru (B. Divinsky).

Peer review under the responsibility of Institute of Oceanology of the Polish Academy of Sciences.



period, general direction of propagation). Such an approach is justified in the case of one-dimensional wave field. If the wave spectrum is formed as a result of interaction between several wave systems it is reasonable to obtain separate wave characteristics for each of these systems.

Besides the fundamental scientific interest to the problem, separation of the wave field into individual components makes it possible to:

- more correctly describe the spatiotemporal structure of surface waves;
- efficiently calculate wave loads on the off- and onshore constructions and forecast hazardous phenomena in closed basins (low-frequency oscillations);
- clarify the schemes of redistribution and transport of bottom sediments;
- improve prognostic estimates of the wave situations for navigation at sea.

Currently, the information about the characteristics of mixed waves and swell is presented within a number of projects of the global reanalysis, for example, European Centre for Medium-Range Weather Forecasts ECMWF (Dee et al., 2011). The results of the recent researches performed on the basis of similar data sets made possible to estimate the climatic peculiarities of the distribution of swell on the oceanic scale (Bitner-Gregersen, 2015; Chong and Chong, 2017; Ewans et al., 2006; Kaiwen et al., 2015; Loffredo et al., 2009; Portilla et al., 2015; Semedo et al., 2011). Application of swell parameters from the database of reanalysis seems incorrect in the Black Sea because the time interval of such data is 3 h. A set of characteristics of storm activity in the Black Sea was investigated in Boukhanovsky and Lopatoukhin (2015). It was shown in particular, that the mean duration of storms is 14–25 h depending on the predefined threshold level. This is the cause that the time interval of the output fields of wind waves is obviously insufficient for the synoptic conditions of the Black Sea.

There are not so many publications on the separate description of surface wave components in the Black Sea. The authors of Boukhanovsky et al. (2000) made an attempt to construct climatic spectra for individual classes of waves in the northeastern part of the Black Sea. The analysis was based on the experimental data published in Kos'yan et al. (1998). The recurrences of climatic spectra for wind seas, swell, and mixed waves were estimated at 43%, 32%, and 25%, respectively. Characteristics of wind seas and swell based on the data of the ECMWF reanalysis in the southern part of the Black Sea in the period from October 1, 2000 to February 28, 2006 with an interval of 12 h were analyzed in the dissertation by Berkün (2007). Such an analysis can be considered only as an estimate due to the cause mentioned above. One of the recent publications is Van Vledder and Akpınar (2016). Unfortunately, by the time our paper has been prepared, this manuscript was available only in the form of a thesis. Therefore it is difficult to make comments.

1.2. Methods of separating of wave components

Calculation of integral wave characteristics with the account for the mixed waves is usually related to the analysis of the

power spectra of surface waves or physical conditions of wave propagation.

Several approaches are applied depending on the available data:

- Analysis of one-dimensional frequency spectrum.

Separation frequency f_{sep} is selected in the wave spectrum; it is assumed that the interval of the power spectrum below this frequency corresponds to swell, and the interval of higher frequencies corresponds to wind seas. Then, the curve of spectral density $S(f)$ is integrated and, for example, significant heights of wind seas and swell are determined:

$$H_{s,swell} = 4 \sqrt{\int_{f_l}^{f_{sep}} S(f) df}, \quad H_{s,wind} = 4 \sqrt{\int_{f_{sep}}^{f_u} S(f) df},$$

where f_l, f_u are the lower and upper integration frequencies.

Frequency f_{sep} can be specified as a constant or function $f_{sep} = 0.8f_{PM}$, where f_{PM} is the frequency of the Pierson–Moskowitz spectrum peak corresponding to the full developed waves (Pierson and Moskowitz, 1964). Frequency f_{PM} is determined by relation $f_{PM} = 0.14g/U_{10}$, where U_{10} is wind velocity at a height of 10 m, g is the acceleration due to gravity. The separation frequency can be also determined from the analysis of wave steepness (Wang and Hwang, 2001) on the basis of the fact that wind seas are steeper than swell and that the maximum steepness is observed in the vicinity of the spectrum maximum.

- Application of the criterion that takes into account the wave age.

The wave component is considered swell if the following condition is satisfied (Bidlot, 2001):

$$\frac{U_{10}}{c} \cos(\theta - \theta_w) < 0.83,$$

where c is the phase velocity of waves, θ, θ_w are the directions of waves and wind, respectively.

- Analysis of two-dimensional frequency-directional spectrum.

The frequency-directional spectrum contains full information about the structure of surface waves. Determination of the main characteristics is performed by integration of individual parts of the two-dimensional spectrum corresponding to the wave systems. We focus attention on publication by Portilla et al. (2009), in which the authors suggested an automatic method of wave separation considering a two-dimensional spectrum as a watershed chart, which makes possible detection of the entire set of the wave systems.

A brief conclusion. If the frequencies of swell and wind seas are quite close, the efficiency of separation using only the frequency spectrum is extremely low. These approaches operate in the case of distinct separation of wave components. Analysis of the frequency-directional spectrum due to its completeness seems a more correct method of separation.

1.3. Goals of our research

The main goal of our research is the assessment of climatic peculiarities of the distribution of wind seas and swell over the Black Sea basin. Let us formulate the main objectives:

- analyze the capabilities of the MIKE SW model to automatically separate wind seas and swell;
- determine optimal tuning of the spectral wave model for automatic separation of wave components;
- obtain separate integral characteristics of the components of surface waves based on the experimental data;
- investigate the features of spatial distribution of the power of wind seas and swell in the basin of the Black Sea during the last 10 years (2007–2016).

2. Separation methodology

In this section, we shall briefly describe the model we used, as well as the experimental data, and physical aspects of modeling. It is noteworthy that absolute separation of the experimental wave field into individual components can be done very rarely. More frequently we deal with mixed waves formed under the influence of numerous external and internal factors. Unambiguous interpretation of the frequency-directional spectrum is hardly possible in such situations; therefore, one would not avoid subjectivity in conclusions.

2.1. Numerical model

In this work, we use the MIKE 21 SW spectral wave model developed at the Danish Hydraulic Institute (DHI, 2007). The

model reproduces the main physical mechanisms of generation, transformation, and decay of wind waves. A description of the model and stages of its verification are described in detail in Divinsky and Kosyan (2017). Here, we present only the main features of the model:

- irregular grid for calculations covers the entire Black Sea basin; it consists of 20,000 elements of calculation (Fig. 1);
- the model uses the data of the global atmospheric reanalysis ERA-Interim as the initial wave field; the data are presented by the European Centre for Medium-Range Weather Forecasts (<http://apps.ecmwf.int>). The domain is limited by coordinates 40°N and 47°N, 27°E and 42°E. The spatial resolution of wind fields is the same by latitude and longitude, it is equal to 0.25°, the time step is 3 h.

We used the experimental data measured using various devices (Datawell buoys, ADCP, string wave recorders, satellite observations) to verify the model. The problem of surface waves separation into components requires initial experimental data that make possible calculation of frequency-directional spectra. The authors possess initial data of the wave experiment near Gelendzhik in 1996–2003 obtained using the Datawell Waverider instrument (Kosyan et al., 1998). The coordinates of its location are: 44°30'40N, 37°58'70E (Fig. 1); the depth of the sea at the location is 85 m.

2.2. Separation of wave components based on experimental data

Two-dimensional spectrum of wind waves gives us a possibility to study the peculiarities of the wave energy distribution

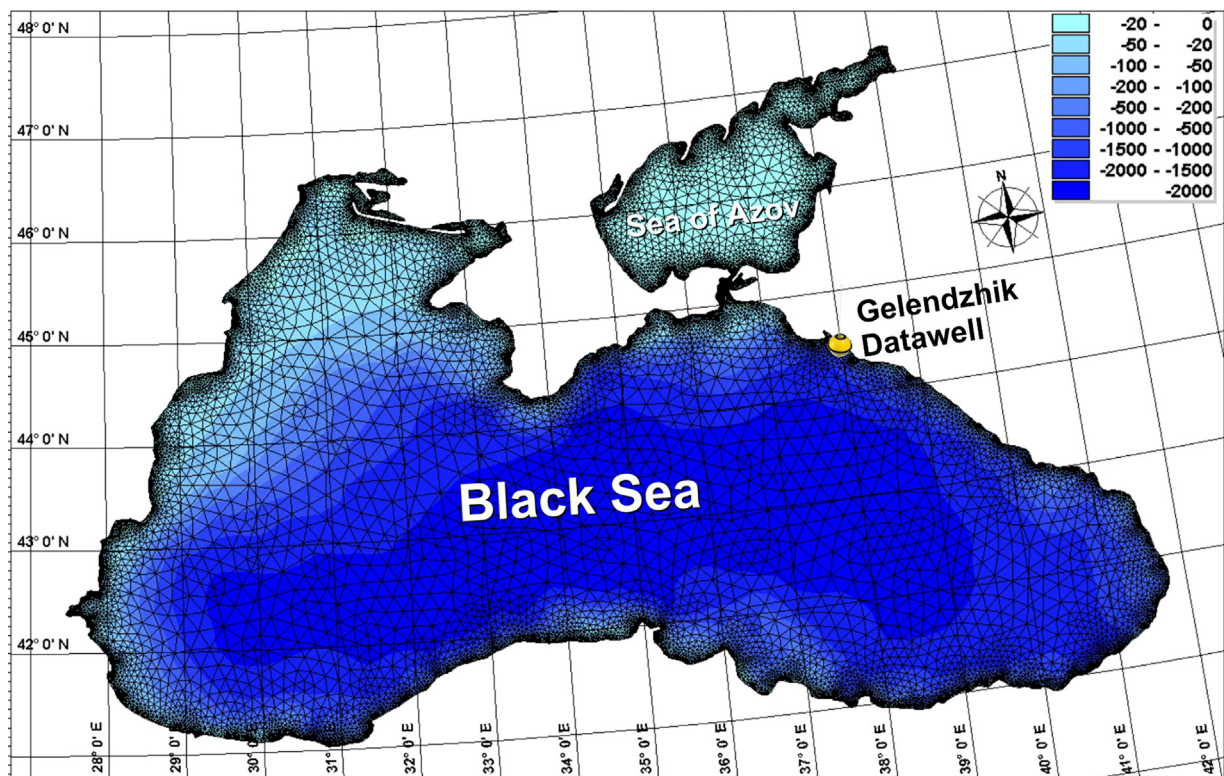


Figure 1 Calculation grid and bathymetric chart of the Black and Azov Sea (m).

both in the frequency range and by the direction of waves; hence it is possible to distinguish the wave systems.

We emphasize several important issues:

- location of the peaks of two-dimensional spectral density relative to the direction of the dominating wind is the determining issue of the analysis;
- when the atmospheric conditions change, the frequency-directional spectrum may contain several swell systems (in addition to the wind sea components). We do not put forward a goal of detailed description, thus, the concept of swell includes the entire surface waves whose direction does not match the general wind direction;
- the frequency maximum of the spectral density corresponding to swell is greater than the peaks frequencies of wind seas.

An example of separation of wind sea components and swell based on the analysis of two-dimensional experimental spectrum is shown in Fig. 2.

In this example, the frequency for separating the wave components is 0.16 Hz. Significant wave heights are found by integration of the corresponding intervals of two-dimensional spectrum $F(f, \theta)$:

$$H_{s,swell} = 4 \sqrt{\int_{f_l}^{f_{sep}} \int_0^{2\pi} F(f, \theta) df d\theta},$$

$$H_{s,wind} = 4 \sqrt{\int_{f_{sep}}^{f_u} \int_0^{2\pi} F(f, \theta) df d\theta}.$$

Under the conditions of the change in the wind direction, the main part of the power spectrum belongs to the wind seas propagating from the south with a significant wave height of 1.42 m. The swell with a significant wave height of 1.11 m conserved its western direction. Integration of the entire spectrum results in the significant wave height of mixed waves equal to 1.80 m.

Fig. 3 gives an idea about the transformation of the two-dimensional spectrum during the propagation of an atmospheric cyclone and a sharp change in the wind direction. Under such conditions, the prevailing wind seas change to the domination of swell.

It follows from Fig. 3 that after the change in the wind direction from the southwestern to the northern, the resulting wave field consists of two swell systems

(south-southeastern and western-southwestern) and northern wind seas. The estimates of significant wave heights of individual wave systems obtained by integration of the frequency-directional spectra are also shown in Fig. 3.

If we apply a similar procedure to the two-dimensional experimental spectra we can get the integral parameters of wind seas and swell over the time period we are interested in. The power spectra are calculated from 20-min time series that recorded the displacement of the buoys along three coordinates with a frequency of 1.28 Hz. The records in the experiment were collected with an interval of 3 h. When the significant wave height exceeded a threshold of 1.5 m, the records were registered every hour.

2.3. Tuning of the wave model

Spectral wave model MIKE 21 SW makes possible automatic separation of the model field of wind waves into individual components. The quality and physical background of this separation depend on the parameters specified by the user. We emphasize several important issues.

The MIKE 21 SW model is based on the solution of the equation of wave energy balance. The main physical processes (wind pumping, wave breaking, energy dissipation caused by bottom friction and wave breaking) are described with semi-empirical functions. We assume that in the conditions of our measurements the effects related to the bottom friction and wave breaking over shallow depths have a local character; therefore, the parameters describing these effects do not participate in the tuning of the model. The main calibration parameters are two coefficients, C_{dis} and δ_{dis} , which determine the numerical interpretation of the energy losses due to wave breaking (in other words, wave breaking over deep water):

- coefficient C_{dis} determines the general level of dissipation and, first of all, influences the wave heights;
- parameter δ_{dis} is an analog of the wave function; it controls the dissipation of individual components, thus influencing the wave periods. Variation of δ_{dis} from 0 to 1 allows us either to increase or decrease the dissipation level at low or high frequencies.

Strictly saying, it is not possible to interpret both coefficients independently: for example, the choice of coefficient

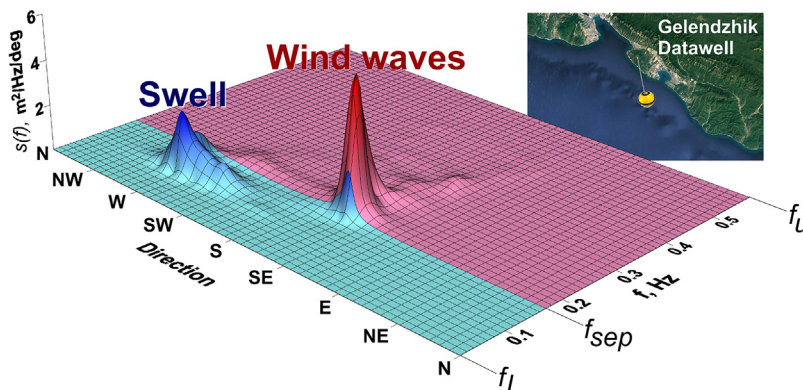


Figure 2 Separation of the components of wind waves (December 21, 1997; 20:00).

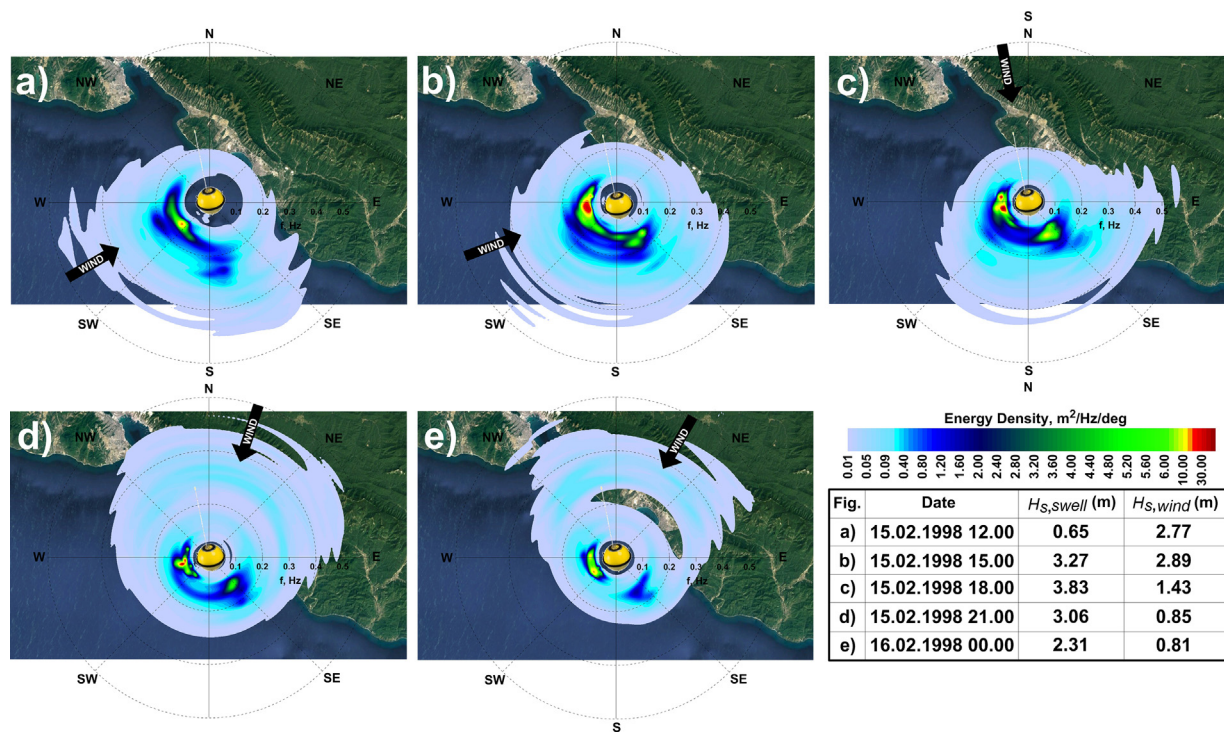


Figure 3 Experimental frequency-directional spectra of surface waves and significant wave heights of the corresponding components of swell and wind seas.

C_{dis} depends on the specified value of δ_{dis} . In addition, the optimum tuning of parameters C_{dis} and δ_{dis} is strongly determined by the physical conditions of generation and propagation of surface waves (Christie et al., 2014; Siadatmousavi et al., 2011).

We think that correct tuning of the spectral model under the conditions of automatic separation of the model field into individual components should provide the following:

- consistency between the model and experimental integral characteristic and the two-dimensional wave energy spectra both for the entire wave field and its components (swell and wind seas);
- physically justified statistical estimates of the parameters of swell and wind seas.

The numerical experiments allowed us to determine the optimum configuration of the spectral model:

- fifty spectral frequencies are distributed in the range of periods from 1.6 to 17.3 s based on the relation $f_n = f_0 C^n$ ($f_0 = 0.055$ Hz, $C = 1.05$, $n = 1, 2, \dots, 50$);
- the amount of discrete directions is 32 so that the model resolution with respect to the directions is 11.25° ;
- the values of coefficients determining energy dissipation due to wave breaking are: $C_{dis} = 5.5$, $\delta_{dis} = 0.15$;
- separation of wave components is performed using the criterion of wave age.

We give an example of the results of automatic separation of surface wave components in December 1997 (Fig. 4).

It follows from Fig. 4 that the spectral model quite reliably separates the components of swell and wind seas. A limited number of experimental time periods, for which we performed separation, is related to the fact that one of the goals of this research is a demonstration of the capabilities of the DHI spectral model to separate the components. We did not use the existing algorithms for separation of experimental spectra, which are applied to large datasets because the approaches to identify the spectral peaks realized in these approaches (relative heights, distances between peaks etc.) are not universal and require verification. Selected analysis of two-dimensional experimental spectra was performed manually with the account for wind characteristics.

Let us consider modeling results in more detail (Fig. 5).

We clarify that total significant wave height in Fig. 5 is determined as $\sqrt{H_{s,swell}^2 + H_{s,wind}^2}$. The atmospheric circulation over the time period February 19–21, 1998 changed strongly several times. The conditions of swell formation were different. On February 15–16, a change of the strong southwestern wind to the northeastern direction caused generation of swell with significant wave heights comparable with the heights of wind seas (the transformation of experimental two-dimensional spectrum is shown in Fig. 3). There was no strong wind change on February 17–18; therefore, the waves from the east dominated in the storm conditions. On February 19–20, the stably directed southwestern wind gradually increased and decreased. This change generally did not cause the development of swell. The calculated two-dimensional wave energy spectra for the selected time periods on February 15–16 are shown in Fig. 6.

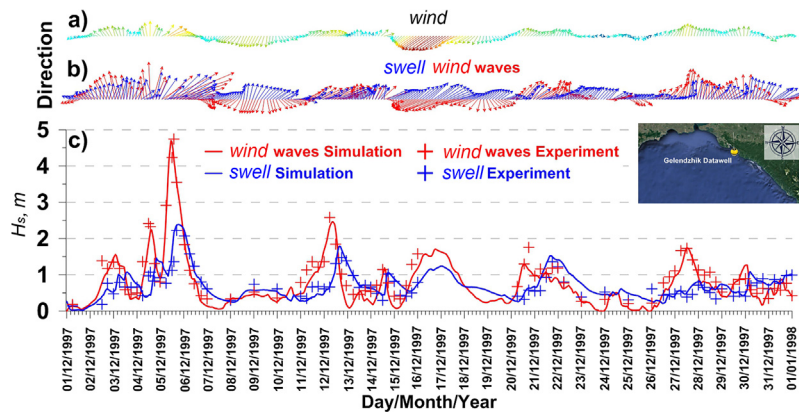


Figure 4 Comparison of the model and experimental parameters of surface wave components in December 1997 at the location of buoy Gelendzhik Datawell. (a) General direction of the wind; (b) mean direction of the swell (blue vectors) and wind seas (red vectors); (c) simulated and experimental significant wave heights of wave components.

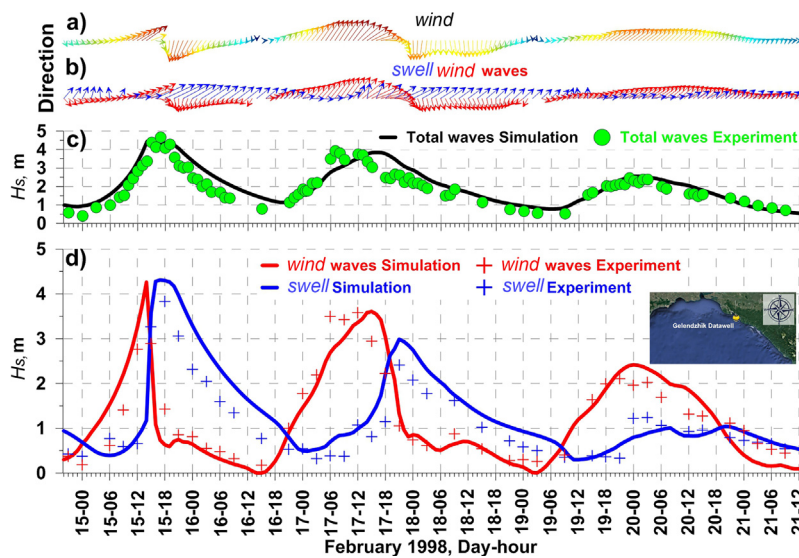


Figure 5 Comparison of the model and experimental parameters of surface waves on February 15–21, 1998 at the location of buoy Gelendzhik Datawell. (a) General direction of the wind; (b) mean direction of the swell (blue vectors) and wind seas (red vectors); (c) simulated and experimental total significant wave heights; (d) simulated and experiments significant wave heights of wave components.

It follows from Fig. 6 that model spectra adequately reflect the physical mechanism of the development of wind seas related to the sharp change in the wind direction. They generally correspond to the experimental spectra during the same time period (Fig. 3). Some distortions are related to the localization of secondary southwestern swell.

Fig. 7 shows the histograms of surface wave parameters in the winter period from December 1, 1997 to March 31, 1998. Here: (a)–(c) are model data with separated wave components; (d)–(f) are modeling results related to the total wave field.

Let us summarize the results shown in Fig. 7:

- significant swell heights (Fig. 7a) are on the average 0.5–1.0 m; the distribution of swell periods has two peaks (Fig. 7b); the peaks correspond to periods of 4 and 7 s; the direction of swell (Fig. 7c) is limited by sector 170–270°;
- the spectral model generally correctly reproduces the main statistical properties of the total wave field including significant wave heights (Fig. 7d) and mean periods (Fig. 7e);
- the recurrence frequency of the southwestern wave direction exceeds the other directions (Fig. 7f). This is caused by the underestimation of the northeastern winds. Strong northeastern winds (katabatic winds, bora) are characteristic of the coastal zone studied here. These winds are not adequately represented by the ERA-Interim global reanalysis.

2.4. Brief notes and conclusions

Thus, we performed tuning of the spectral model, which adequately separates the wave field into individual

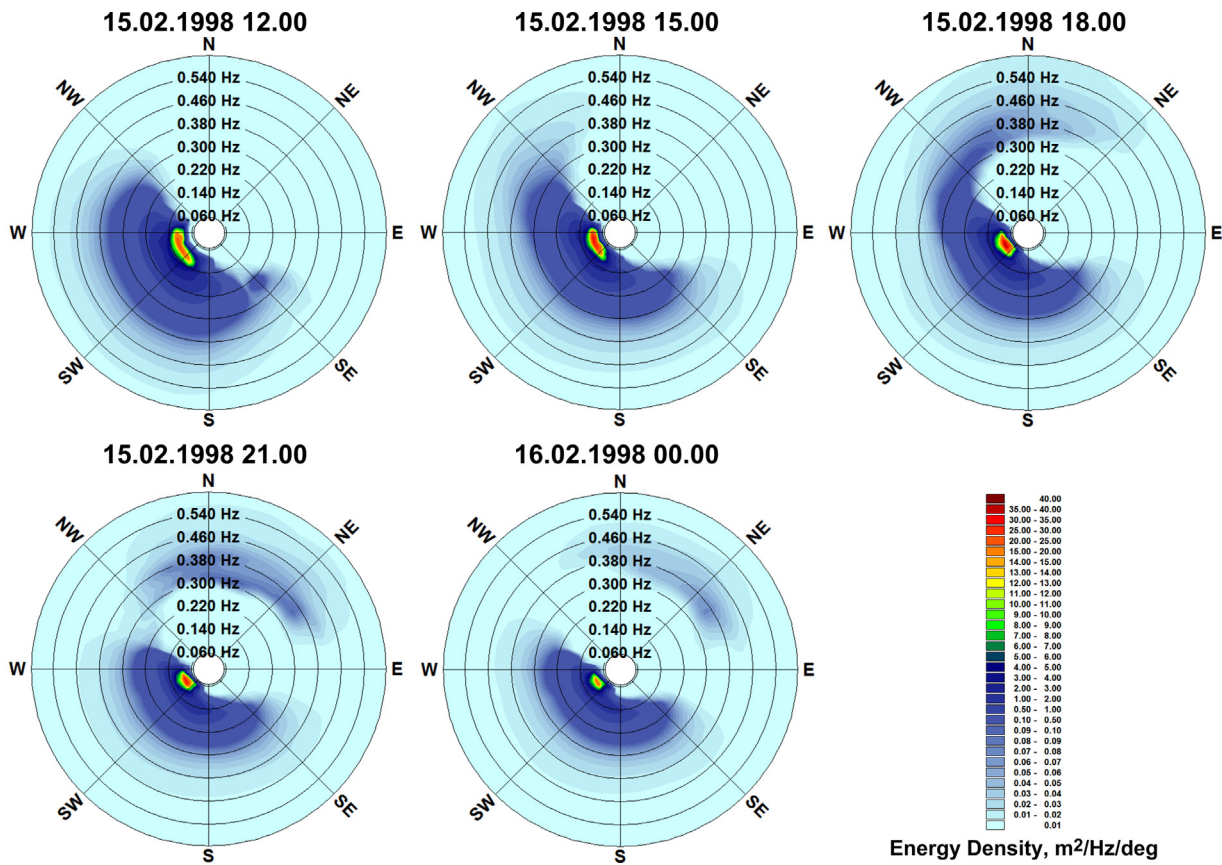


Figure 6 Model frequency-directional spectra of surface waves on February 15–18, 1998.

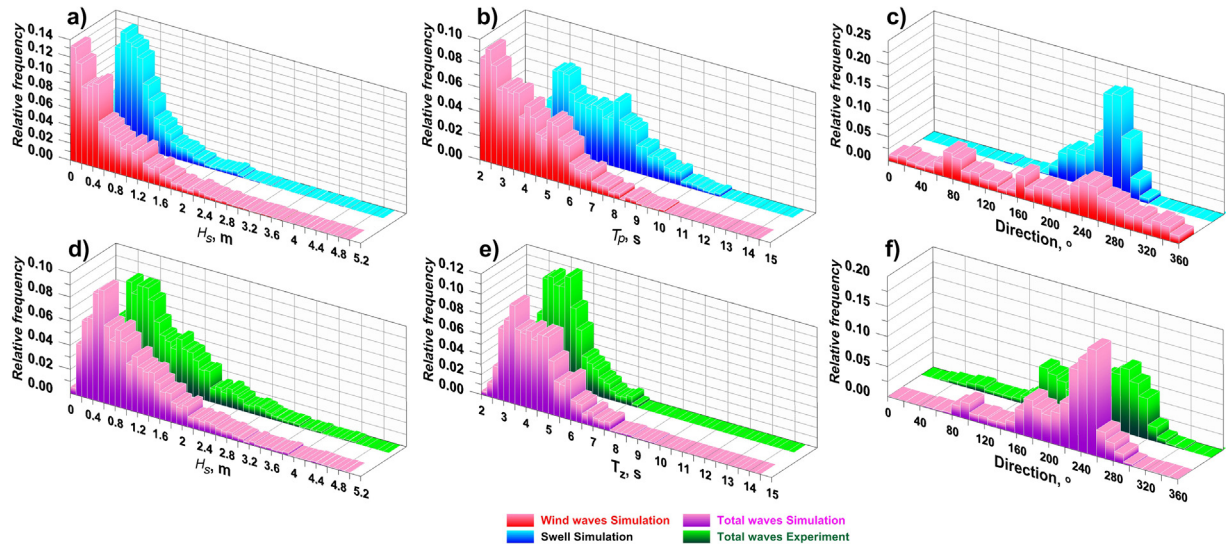


Figure 7 Statistical distribution of parameters of wind waves from December 1, 1997 to March 31, 1998 (a)–(c) show wave components; (d)–(f) show total wave field.

components. The model frequency-directional wave spectra generally correspond to the two-dimensional experimental spectra. Statistical peculiarities of integral parameters of swell and wind seas are physically justified (Fig. 7). Over-estimation of the swell contribution to the total wave field under the conditions of sharp wind change is a disadvantage of the model.

We emphasize an important fact. The tuning parameters used in the description of wave energy dissipation due to white-capping were obtained from the analysis of the experimental data in the northeastern part of the Black Sea. It is difficult to say whether they are valid for the entire sea basin. Weak coverage of the Black Sea with experimental wave stations, which make possible to get the main wave

characteristic: two-dimensional wave energy spectra, is an obstacle to solve this problem. We understand the role of these restrictions and will make an attempt to estimate in the first approximation the peculiarities of the propagation of surface wave components in the Black Sea.

3. Results and discussion

We constructed a dataset consisting of the fields of calculated parameters of wind wave components in the Black Sea with a time step of 1 h, which covers a period of 10 years (2007–2016). The dataset of calculated characteristics includes the following (separately for swell, wind seas, and total wave field):

- spatial distributions of significant and maximum wave heights, mean periods, periods of spectral maximum, wave directions;
- frequency-directional spectra;
- power of waves.

The power of irregular wind waves can be determined as a function of the squared significant wave heights and energetic period (Boyle, 2004). The unit of measurements is kilowatt per meter of the wave front. Estimates of wind wave power completely depend on the correctness and adequacy of the spectral model during reproduction of all stages of wave development. Let us discuss the wind wave power because power is a function of two main integral parameters of wind waves (height and period); thus, it characterizes the energetic importance of storms.

Figs. 8 and 9 present spatial distribution of mean power of wind seas and swell over a period from 2007 to 2016. Averaging was performed over a rectangular grid with sides 12.5×11.5 km.

The maximum power of wind seas is recorded in the western part of the sea, which results in a clearly manifested maximum of the spatial distribution (Fig. 8). The region of high wave power spreads in the meridional direction from west to east turning around Crimea. The mean power of swell is distributed more uniformly (Fig. 9). The local power peaks are observed in the southwestern and southern parts of the Black Sea. In general, the swell is spread everywhere excluding shallow bays in the northern part of the sea.

Let us estimate the contribution of swell to the total power of surface waves. With this in mind, we plot a chart of the ratio of swell power P_{swell} to the power of the total wave field P_{total} , $(P_{swell}/P_{total}) \times 100\%$, Fig. 10.

Fig. 10 clearly demonstrates the domination of contribution of wind seas to the total power of wind waves in the Black Sea ($P_{swell}/P_{total} < 0.5$). Swell dominates in the shelf zone of the southern and eastern parts of the sea. The wave climate in the narrow coastal zone of these regions is almost completely determined by the swell fields ($P_{swell}/P_{total} > 0.8$). The recurrence of swell by directions has its specific peculiarities in different regions of the sea (Fig. 11).

Swell from the western-northwestern direction dominates in the deep-water part of the Black Sea. The southwestern and central regions of the sea are influenced by the swell from the northeast. Swell from the southeast is manifested in the northwestern part, while the southwestern swell dominates in the northeastern part of the sea. The strongest swell with a power exceeding 20 kW m^{-1} develops in the southwestern, northeastern, and southwestern regions of the sea.

It was discussed above that climatic estimates of the distribution of surface wave components were summarized over a period of 10 years (2007–2016). These estimates need much computational resources. We hope that further research would allow us to widen the database of wave parameters and clarify the results presented here.

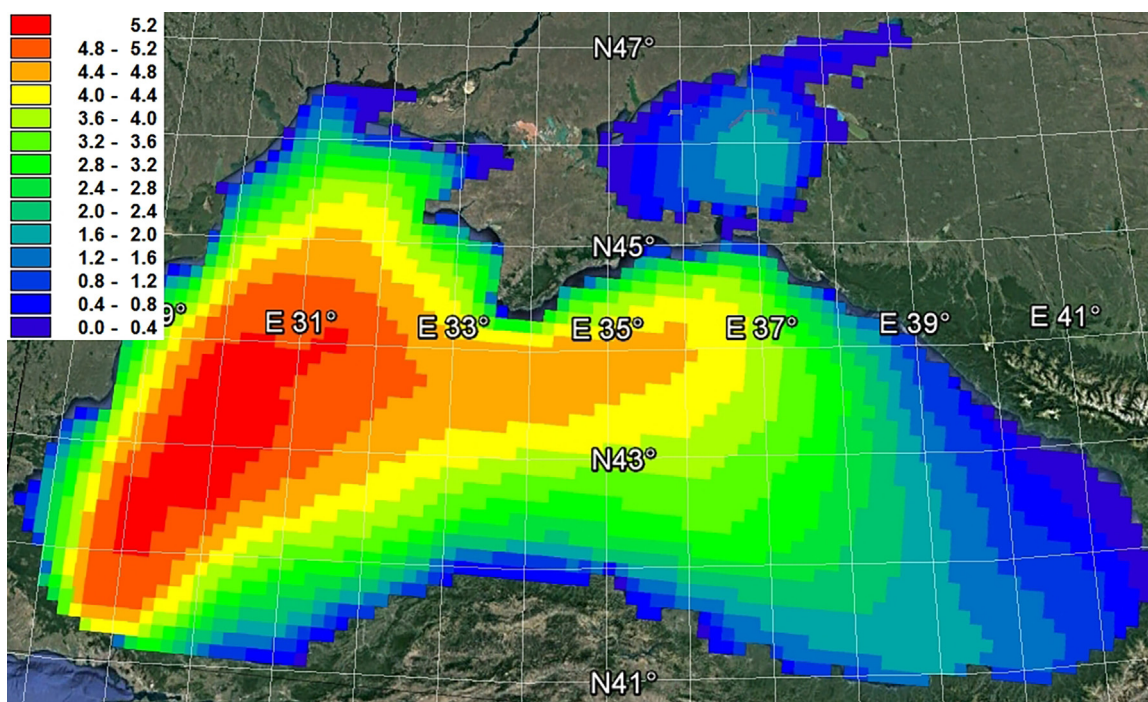


Figure 8 Mean power of wind seas over 2007–2016 (kW m^{-1}).

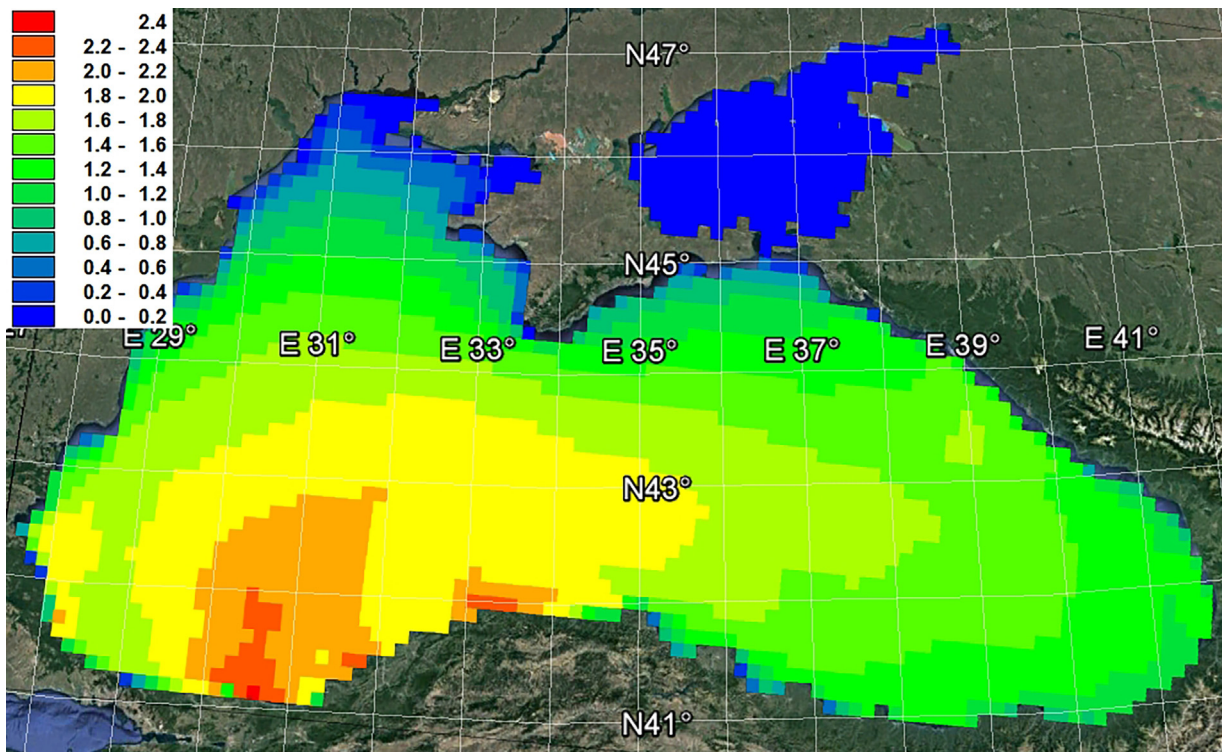


Figure 9 Mean swell power over 2007–2016 (kW m^{-1}).

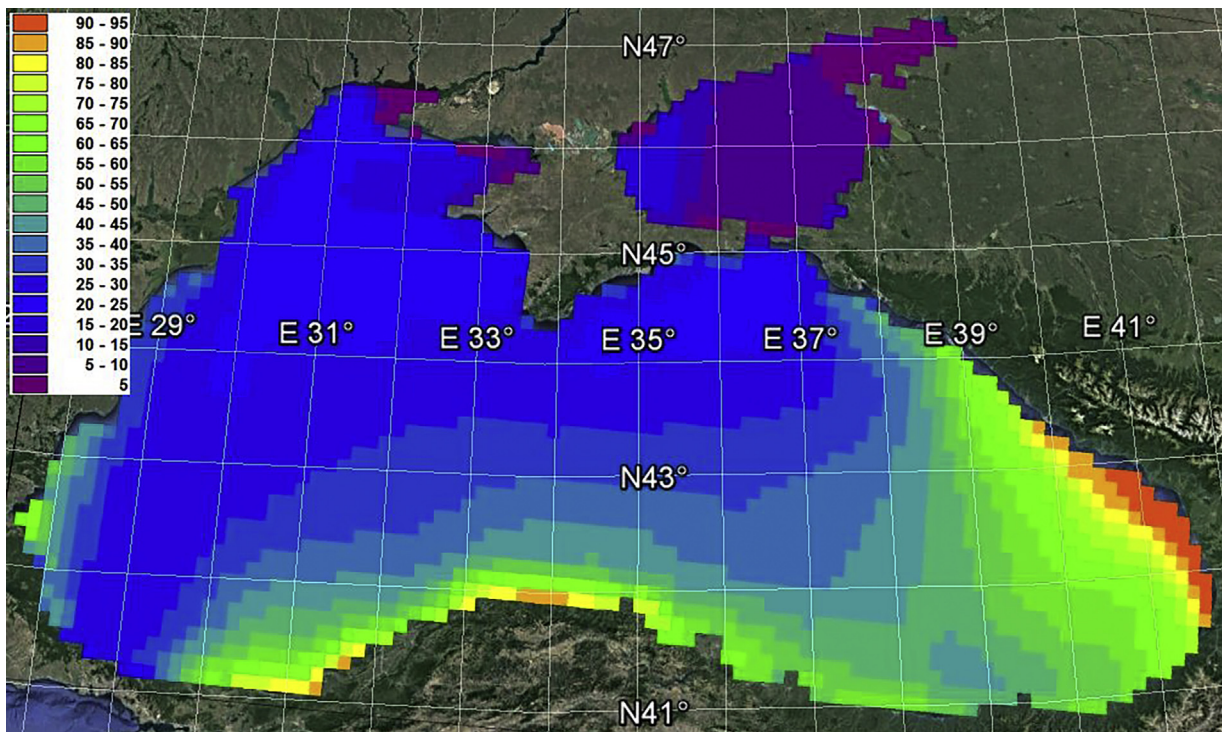


Figure 10 Ratio of the mean swell power to the power of the total wave field in 2007–2016 (%).

4. Conclusions

The main goal of the study presented here is an assessment of climatic peculiarities in the distribution of wind seas and swell

in the Black Sea. The analysis is based on numerical modeling using the DHI MIKE 21 SW spectral wave model. Previously, the model was verified on the basis of numerous instrumental observations of wind waves in the Black and Azov Sea.

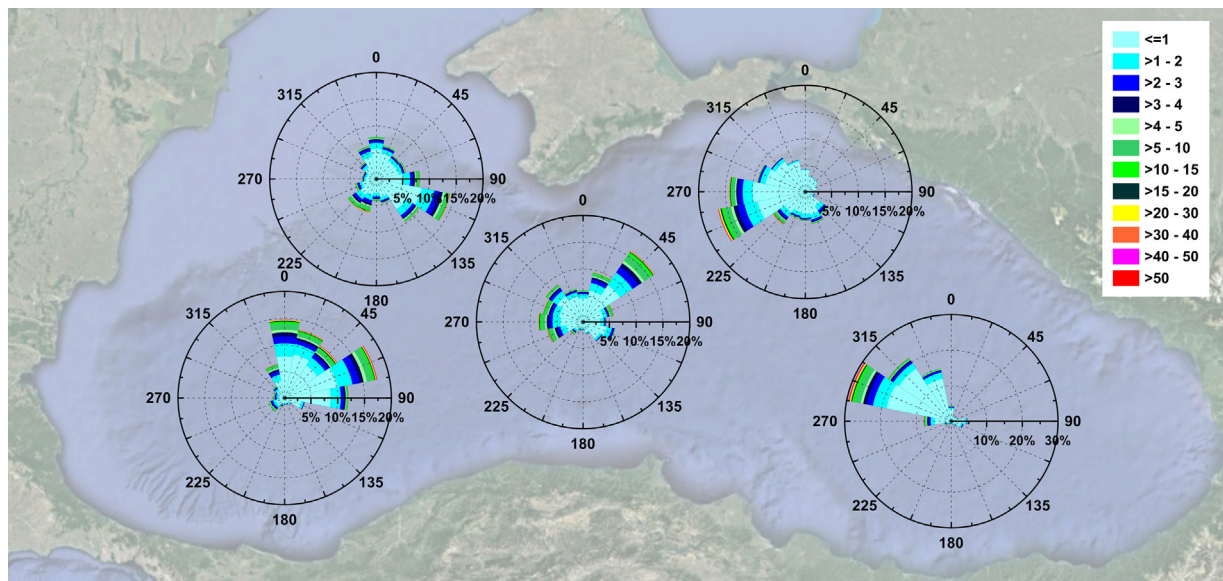


Figure 11 Rose graphs of swell power (kW m^{-1}) in the Black Sea in 2007–2016.

The main results of our research are as follows:

- we studied the peculiarities of the spatial distribution of wind sea and swell power in the Black Sea over the last 10 years (2007–2016);
- we determined the regions, in which wind seas and swell dominate on the basis of their contribution to the total wave field of mixed waves;
- auxiliary numerical experiments allowed us to determine the optimal tuning and adjustments of the spectral wave model for automatic separation of wave components;
- the model correctly reproduces the main integral characteristics of mixed wave;
- the model frequency-directional wave spectra generally correspond to the experimental two-dimensional spectra;
- statistical peculiarities of integral parameters of swell and wind seas are physically justified.

We emphasize some important details. Two coefficients C_{dis} and δ_{dis} , which determine the numerical interpretation of the energy losses due to wave overturning, are the main calibration parameters of the MIKE SW model in the problem of automatic separation of wave components. The values of these coefficients were determined at the stage of the model verification using the experimental wave data in the north-eastern part of the Black Sea. Of course, without the corresponding experimental verification we cannot consider that these coefficients are universal for the entire basin. Insufficient coverage of the Black Sea with the direct instrumental observations is a problem of any research. Satellite altimetry provides mean data and cannot be used as the basis of the special analysis. These restrictions are the natural disadvantages of our investigations.

The last comment. The existing methods of separating the components of sea waves are based not on the experimental data but on the materials from the global wave models (WAM, WAVEWATCH). It is clear that the global models do not reflect the specific regional features of waves. Hence, the errors in the estimates of two-dimensional model spectra are added to

the indefiniteness, which is characteristic of the separation of wind seas and swell. In other words, we think that analysis of the consistency between the two-dimensional model and experimental spectra should become one of the initial stages of the investigation, which would later make possible to get correct wave statistics.

Acknowledgments

This work was initiated by the Russian Science Foundation, project no. 14-17-00547. The processing of experimental data, used for this paper was supported by the Russian Science Foundation, Project no. 14-50-00095. The computer calculations were supported by the Russian Foundation for Basic Research (Projects 16-45-230781 and 17-05-00183). Analysis of the results was carried out within the framework of the program 0149-2018-0013.

References

- Berkün, U., 2007. *Wind and swell wave climate for the Southern Part of Black Sea*. (Thesis). Graduate School of Natural and Applied Sciences of Middle East Technical University, Ankara, Turkey, 141 pp.
- Bidlot, J.-R., 2001. *ECMWF wave model products*. In: *ECMWF Newsletter*, No. 91, ECMWF, Reading, United Kingdom, 9–15.
- Bitner-Gregersen, E.M., 2015. Joint met-ocean description for design and operations of marine structures. *Appl. Ocean Res.* 51, 279–292, <http://dx.doi.org/10.1016/j.apor.2015.01.007>.
- Boukhanovsky, A.V., Lopatoukhin, L.I., 2015. *Storms statistics at sea (alternative approach)*. *Fundamentalnaya i prikladnaya gidrofizika* 8 (4), 86–94, (in Russian).
- Boyle, G., 2004. *Renewable Energy: Power for a Sustainable Future*, 2nd ed. Oxford Univ. Press, 464 pp.
- Bukhanovsky, A.V., Lopatukhin, L.I., Rozhkov, V.A., Divinsky, B.V., Kos'yan, R.D., 2000. *Typification of instrumentally measured wind waves in the Black Sea*. *Oceanology (Engl. Transl.)* 40 (2), 267–275.
- Chong, W.Z., Chong, Y.L., 2017. Analysis of temporal and spatial characteristics of waves in the Indian Ocean based on ERA-40

- wave reanalysis. *Appl. Ocean Res.* 63, 217–228, <http://dx.doi.org/10.1016/j.apor.2017.01.014>.
- Christie, D., Vögler, A., Morrison, J., Greenwood, C., Venugopal, V., Topper, M., 2014. The Hebridean wave model. In: *Proc. of the 2nd International Conference on Environmental Interactions of Marine Renewable Energy Technologies (EIMR2014)*, 28 April–02 May, Stornoway, Isle of Lewis, Outer Hebrides, Scotland.
- Dee, D., Uppala, S., Simmons, A., Berrisford, P., Poli, P., Kobayashi, S., et al., 2011. The ERA Interim reanalysis: configuration and performance of the data assimilation system. *Q.J.R. Meteorol. Soc.* 137 (656), 553–597, <http://dx.doi.org/10.1002/qj.828>.
- Divinsky, B., Kosyan, R., 2017. Spatiotemporal variability of the Black Sea wave climate in the last 37 years. *Cont. Shelf Res.* 136, 1–19, <http://dx.doi.org/10.1016/j.csr.2017.01.008>.
- Ewans, K.C., Bitner-Gregersen, E.M., Guedes Soares, C., 2006. Estimation of wind-sea and swell components in a bimodal sea state. *J. Offshore Mech. Arctic Eng.* 128 (4), 265–270, <http://dx.doi.org/10.1115/1.2166655>.
- Kaiwen, Z., Jian, S., Changlong, G., Weizeng, S., 2015. Analysis of the global swell and wind sea energy distribution using WAVE-WATCH III. *Adv. Meteorol.* 2016, <http://dx.doi.org/10.1155/2016/8419580> 8419580, 9 pp.
- Kos'yan, R.D., Divinsky, B.V., Pushkarev, O.V., 1998. Measurements of parameters of wave processes in the open sea near Gelendzhik. In: *The Eighth Workshop of NATO TU-WAVES/Black Sea*, METU, Ankara, Turkey, 5–6.
- Loffredo, L., Monbaliu, J., Bitner-Gregersen, E., Toffoli, A., 2009. The role of spectral multimodality in wave climate design. In: *11th International Workshop on Wave Hindcasting and Forecasting and Coastal Hazard Symposium*, Halifax, Canada, October 18–23, 2009, 18–23.
- Pierson Jr., W.J., Moskowitz, L., 1964. A proposed spectral form for fully developed wind seas based on the similarity theory of S. A. Kitaigorodskii. *J. Geophys. Res.* 69 (24), 5181–5190.
- Portilla, J., Ocampo-Torres, F., Monbaliu, J., 2009. Spectral partitioning and identification of wind sea and swell. *J. Atmos. Ocean. Technol.* 26, 107–122, <http://dx.doi.org/10.1175/2008JTECHO609.1>.
- Portilla, J., Caicedo, A., Padilla-Hernández, R., Cavalerie, L., 2015. Spectral wave conditions in the Colombian Pacific Ocean. *Ocean Model.* 92, 149–168, <http://dx.doi.org/10.1016/j.oceanmod.2015.06.005>.
- Semedo, A., Suselj, K., Rutgersson, A., Sterl, A., 2011. A global view on the wind sea and swell climate and variability from ERA-40. *J. Climate* 24 (5), 1461–1479, <http://dx.doi.org/10.1175/2010JCLI3718.1>.
- Siadatmousavi, S., Jose, F., Stone, G., 2011. Evaluation of two WAM white capping parameterizations using parallel unstructured SWAN with application to the Northern 42 Gulf of Mexico, USA. *Appl. Ocean Res.* 33 (1), 23–30, <http://dx.doi.org/10.1016/j.apor.2010.12.002>.
- US Army Corps of Engineers, 2002. *Coastal Engineering Manual. Engineer Manual 1110-2-1100*, vol. 6. U.S. Army Corps of Engineers, Washington, D.C..
- Van Vledder, G., Akpinar, A., 2016. The swell climate in the black sea. In: *The 35th International Conference on Coastal Engineering, ICCE*, Antalya, Turkey, 17–20 November, 2016.
- Wang, D., Hwang, P., 2001. An operational method for separating wind sea and swell from ocean wave spectra. *J. Atmos. Ocean. Technol.* 18 (12), 2052–2062.



ORIGINAL RESEARCH ARTICLE

Spatio-temporal variability of the size-fractionated primary production and chlorophyll in the Levantine Basin (northeastern Mediterranean)

Nebil Yucel ^{a,b,*}^a Faculty of Marine Sciences & Technology, Iskenderun Technical University, Hatay, Turkey^b Institute of Marine Sciences, Middle East Technical University, Erdemli, Mersin, Turkey

Received 1 June 2017; accepted 22 December 2017

Available online 9 January 2018

KEYWORDS

Primary production;
Chlorophyll;
Picoplankton;
Rhodes Gyre;
Cilician Basin;
Levantine Basin

Summary Spatial and temporal variations in size-fractionated primary production (PP) and chl *a*, in relation to ambient physicochemical parameters, were studied in the three distinct ecosystems of northeastern Levantine Basin namely eutrophic Mersin Bay, mesotrophic Rhodes Gyre, and oligotrophic offshore waters. These ecosystems were visited in July and September 2012 and March and May 2013. Total primary production (TPP) rates ranged between 0.22 and 17.8 mg C m⁻³ h⁻¹ within the euphotic zone, whereas depth-integrated TPP rates were in the range 21.5–348.8 mg C m⁻² h⁻¹ (mean: 105.5 ± 88 mg C m⁻² h⁻¹), with the lowest rates recorded for offshore waters. Similar spatio-temporal variations were observed in chl *a* concentrations, ranging from 2.3 to 117.9 mg m⁻² (mean: 28.9 ± 24.9 mg m⁻²) in the study area. The Mersin Bay TPP rates have exceeded almost 8–12 times those measured in the offshore waters and the Rhodes Gyre; however, the chl *a* concentrations measured in coastal waters (0.343 mg m⁻³) and the Rhodes Gyre (0.308 mg m⁻³) were only threefold larger than the offshore values. PP and chl *a* were dominated by picoplankton in the study area whereas small nanoplankton, being the most active, displayed the highest assimilation ratio in offshore waters (6.8) and the Rhodes Gyre (2.8). In the upper-layer waters depleted of P (0.02–0.03 μM) of the northeastern Mediterranean, a positive correlation was observed between NO₃ + NO₂ and PP (and thus, chl *a*), which strongly suggests that reactive P and inorganic nitrogen are co-limiting factors in the production and biomass distribution of the phytoplankton community in both shelf and offshore waters.

© 2018 Institute of Oceanology of the Polish Academy of Sciences. Production and hosting by Elsevier Sp. z o.o. This is an open access article under the CC BY-NC-ND license (<http://creativecommons.org/licenses/by-nc-nd/4.0/>).

* Correspondence to: Iskenderun Technical University, Faculty of Marine Sciences & Technology, Department of Water Resources Management and Organization, Meydan Mah. 512 Sk, 31320 Iskenderun, Hatay, Turkey. Tel.: +90 326 614 1693x3720; fax: +90 326 614 1877.

E-mail address: nebiyucel@gmail.com.

Peer review under the responsibility of Institute of Oceanology of the Polish Academy of Sciences.



Production and hosting by Elsevier

<https://doi.org/10.1016/j.oceano.2017.12.003>

0078-3234/© 2018 Institute of Oceanology of the Polish Academy of Sciences. Production and hosting by Elsevier Sp. z o.o. This is an open access article under the CC BY-NC-ND license (<http://creativecommons.org/licenses/by-nc-nd/4.0/>).

1. Introduction

The eastern Mediterranean Sea is one of the world's least productive regions, with low nutrient and chlorophyll concentration (Ediger and Yılmaz, 1996; Krom et al., 1991; Psarra et al., 2005; Yucel, 2013). In general, primary production (PP) rate and chlorophyll concentration tends to decrease from west to east and north to south in the Mediterranean (Siokou-Frangou et al., 2010). Increasing oligotrophy toward the east can mainly be attributed to increasing phosphorus limitation (N/P ratio increase from 20 to 29) in the northeastern Levantine waters due to limited inputs of nutrients from external sources and the fact that its deep waters have high N/P (25–26) ratios (Krom et al., 1991, 2010; Thingstad et al., 2005; Yılmaz and Tugrul, 1998; Yucel, 2013). Atmospheric depositions supply a considerable amount of nutrients to the oligotrophic offshore waters (Guerzoni et al., 1999; Koçak et al., 2010; Krom et al., 2004). This atmospheric dry and wet deposition support new production during spring and autumn in the offshore eastern Mediterranean (Herut et al., 2005; Markaki et al., 2003). Primary production in the eastern Mediterranean is principally dominated by eddies and currents that control the distribution of nutrients in the upper-layer waters (Ediger and Yılmaz, 1996). Annual PP is estimated to vary regionally and seasonally between 20.3 and 151.2 g C m⁻² y⁻¹ (Siokou-Frangou et al., 2010 and references there in; Yucel, 2013). The lowest chlorophyll concentrations were recorded in the anticyclonic regions of the Levantine Basin during the dry period, reaching as low as 0.01–0.23 mg m⁻³ (Ediger and Yılmaz, 1996). However, concentrations reach high levels ranging 2.49–3.1 mg m⁻³ in the Rhodes gyre and in the coastal waters enriched by terrestrial inputs (Ediger and Yılmaz, 1996; Yucel, 2013). In the basin, phytoplankton blooms are generally observed in late winter and spring, following the winter convectonal mixing (Siokou-Frangou et al., 2010). Up till now, only a few PP rate estimations have been conducted for the Cilician Basin (northeastern Mediterranean) (Ediger et al., 2005; Yayla, 1999; Yılmaz, 2006; Yucel, 2013), all of which highlighted apparent major differences between coastal and offshore waters. Offshore waters are commonly known as oligotrophic (Ediger et al., 2005; Ediger and Yılmaz, 1996; Yucel, 2013). Coastal waters (Mersin and Iskenderun Bays) display a high production capacity (Tugrul et al., 2016; Yılmaz, 2006; Yucel, 2013) due to the input of nutrients from natural and anthropogenic sources (through contaminated rivers and direct discharge of partially treated domestic and industrial wastewaters). Cyclonic systems in the open Levantine Basin differ in terms of their biological, chemical, and physical properties from the surrounding waters owing to the rising of nutrient-rich deep waters toward the base of the euphotic zone (EZ) for most of the year, sometimes reaching the surface during severe winters (Ediger and Yılmaz, 1996; Ediger et al., 2005). Chlorophyll concentrations and PP rates varied between 0.02 and 1.0 mg m⁻³ and 38.5 and 268 mg C m⁻² day⁻¹ in the Rhodes Gyre (Ediger et al., 2005). In severe winter-spring periods, the highest rates of PP and Chl-*a* were recorded in the peripheries of the Rhodes Gyre (Ediger et al., 2005). The coastal waters of the northeastern Cilician Basin are fed by perennial rivers, namely Goksu, Tarsus, Seyhan, Ceyhan, and some other smaller rivers, with associated chemical properties (high

NO₃ + NO₂/PO₄ ratios and Si/NO₃ + NO₂ ratio mostly <1 in the last 2 decades) (Uysal et al., 2008). In the coastal zone, atmospheric and river inputs, winter convectonal mixing, and summer upwelling events determine the surface nutrient concentrations and rates of the new and regenerated PP (Ediger et al., 2005; Uysal, 2006; Uysal and Köksalan, 2010; Uysal et al., 2008).

Phytoplankton composition and abundance in the sea are determined by the physicochemical characteristics of upper-water masses, rates of nutrient inputs, and also by the changes in N/P/Si ratios within the euphotic zone. Diatoms have been reported as the most abundant group in the Cilician Basin shelf waters (Eker and Kideyş, 2000; Eker-Develi et al., 2003; Kideyş et al., 1989; Polat et al., 2000; Uysal et al., 2003; Uysal et al., 2008). However, in the Levantine offshore waters, small phytoplankton dominate the total biomass and abundance (Li et al., 1993; Siokou-Frangou et al., 2010; Uysal et al., 2004; Uysal, 2006; Yucel, 2013). Recent studies pertaining to flow cytometry and high-performance liquid chromatography have also revealed that in the oligotrophic Levantine open sea, small-sized phytoplankton is the major contributor to the total phytoplankton biomass (Li et al., 1993; Yucel, 2008, 2013). It appears that PP rate data from the Levantine shelf and open sea waters are very limited for the assessment of spatio-temporal variability in the northeastern Mediterranean (Ediger et al., 2005; Yılmaz, 2006; Yucel, 2013). This study aims to enhance the existing knowledge pertaining to PP and size-based standing biomass potential of the basin by comparing and contrasting ecosystems that extend from highly oligotrophic to eutrophic, in relation to ambient physicochemical parameters, on a seasonal basis.

2. Material and methods

2.1. Sample collection and methodology

In this study, five stations were visited for measuring chemical (phosphate, nitrite + nitrate, silicate), biological (size-fractionated chlorophyll and primary production experiments), and physical (salinity, temperature, depth, photosynthetically active radiation (PAR), fluorescence, secchi disc depth [SDD]) parameters of the water column along a transect extending from Mersin Bay to Rhodes Gyre representing the coastal, offshore, and cyclonic areas of the northern Levantine Basin (Fig. 1, Table 1) during July and September 2012 and March and May 2013. Water samples from pre-defined depths (1, 2, 5, 13, 25 and 39 m for coastal waters and 1, 4, 8, 20, 50, 75, 100, 150 and 200 m for offshore and Rhodes Gyre) were collected on board the *r/v Bilim-2* of the Institute of Marine Sciences (METU) using Niskin bottles fitted onto a rosette sampler, coupled with Sea-Bird Electronics-911 plus CTD (conductivity, temperature, depth) probe. Profiles of temperature, salinity, PAR and fluorescence were obtained using the standard Sea-Bird data processing software.

2.1.1. Nutrient analysis

Nutrient (nitrate + nitrite, phosphate, silicate) samples from the bottle casts were collected into 100 ml high-density polyethylene bottles that were pre-cleaned with

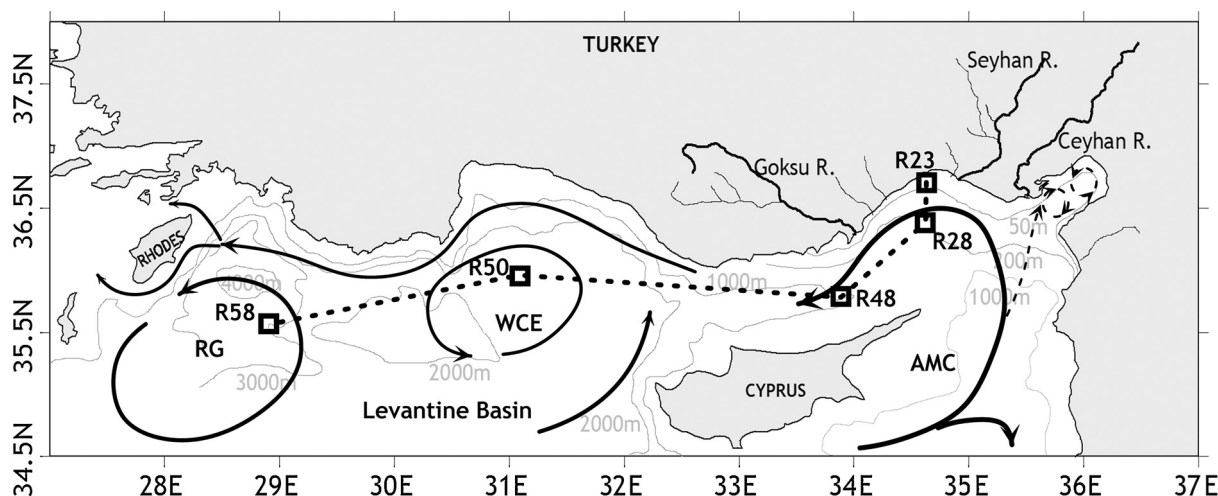


Figure 1 Location of sampling stations in the northeastern Mediterranean including rivers, bathymetry and main currents (AMC: Asia Minor Current, WCE: West Cyprus Eddy, RG: Rhodes Gyre). Modified from Siokou-Frangou et al. (2010).

Table 1 List of sampling stations.

Area	Stations	Position	Sampling depth [m]	Total depth [m]	Sampling date
Coastal	R23	N36.700 E34.700	39	40	
Offshore	R28	N36.300 E34.700	200	223	July 3–8, 2012
	R48	N35.871 E33.981	200	1006	September 20–25, 2012
	R50	N35.750 E31.000	200	2320	March 12–21, 2013
Rhodes Gyre	R58	N35.500 E29.000	200	2800	May 6–12, 2013

10% HCl. Bottles for nitrate + nitrite and phosphate analysis were kept frozen (-20°C), whereas those for silicate were kept cool ($+4^{\circ}\text{C}$) in the dark until the analysis. Nutrient measurements were carried out using a Bran + Luebbe model four-channel auto-analyzer, employing the standard methods described in Grasshoff et al. (1983) and Strickland and Parsons (1972). Detection limits for nitrate + nitrite, phosphate, and silicate were 0.05, 0.02, and $0.3\ \mu\text{M}$, respectively.

2.1.2. Chlorophyll-*a*

Seawater samples (2 l) collected at selected depths (including deep chlorophyll maximum) within the euphotic zone (EZ:1% of surface light depth – Table 2) were then filtered onto Whatman nucleopore polycarbonate filters for size fractionation (0.2, 2.0, and $5.0\ \mu\text{m}$ pore sizes and 47 mm diameter) at a low vacuum. Organic particles collected on the filters were then extracted with the help of 5 ml 90% acetone solution through the use of an ultrasonicator (60 Hz for 1 min). The final volumes of the extracts were then adjusted to 10 ml. The homogenized samples were kept in the dark at $+4^{\circ}\text{C}$ overnight and then centrifuged at 3500 rpm for 10 min in order to remove cellular debris. Chl-*a* concentrations of the centrifuged samples were determined through the fluorometric method, using a Hitachi F-2500 type fluorescence spectrophotometer. The Chl-*a* concentration of each sample was calculated according to the formula given by Strickland and Parsons (1972).

2.1.3. Primary production

Samples for primary production (PP) experiments were taken from surface and the lower depths within the euphotic layer, taking into account the incident PAR levels (at depths where 75, 50, 25, 10, 1, and 0.1% of surface PAR levels were achieved) and additionally from the deep chlorophyll maximum depth. *In situ* incubation experiments were consistently carried out around noon by following the methodology forwarded by Steemann Nielsen (1952). For the determination of PP, acid-cleaned transparent polycarbonate bottles (75 ml light and dark bottles for each depth) were filled with seawater samples taken from the selected depths, and $2\ \mu\text{Ci}\ ^{14}\text{C-NaHCO}_3$ solution were added to each bottle, and then the closed bottles were incubated for three hours. After incubation, the contents of each pair of light bottles were filtered using nucleopore polycarbonate filters (0.2, 2.0 and $5.0\ \mu\text{m}$ pore sizes and 25 mm diameter) at a low vacuum pressure. The contents of the dark bottles were also filtered with the use of $0.2\ \mu\text{m}$ pore size filters as blank. In this work, three different pore size filters were used for fractionated PP experiments in order to determine the contribution of picoplankton (Pico) ($0.2\text{--}2\ \mu\text{m}$); small nanoplankton (Nano) ($2\text{--}5\ \mu\text{m}$) and microplankton (larger nanoplankton and microplankton as Micro) ($>5\ \mu\text{m}$) to the total production at each depth. Filters were then transferred to scintillation vials and acidified with 1 ml 0.5 N HCl. Scintillation cocktail was added to the vials after 24 h. Radioactivity of each solution was measured using a Perkin Elmer

Table 2 Range of bio-physico-chemical variables (mean, minimum and maximum values) in the study area.

Parameters	R23	R28	R48	R50	R58	
Temperature [°C]	23.00 (16.34–29.13)	18.34 (16.00–29.03)	17.73 (15.98–28.71)	17.14 (15.34–27.66)	15.91 (14.30–25.34)	
Salinity	39.03 (37.95–39.45)	39.10 (38.87–39.49)	39.09 (38.82–39.59)	39.07 (38.87–39.51)	39.06 (38.84–39.50)	
Secchi Disc Depth [m]	11.5 (8–16)	24.3 (19–27)	27.3 (22–31)	27.5 (26–31)	27.5 (24–30)	
Depth of the Euphotic Zone (EZ; 1% light depth)	37 (26–bottom)	78 (61–86)	87 (70–100)	88 (83–100)	88 (77–96)	
NO ₃ +NO ₂ [μM]	0.45 (0.05–2.66)	0.39 (0.05–2.48)	0.39 (0.05–2.41)	0.60 (0.05–3.82)	1.18 (0.05–5.51)	
PO ₄ [μM]	0.03 (0.02–0.07)	0.03 (0.02–0.07)	0.03 (0.02–0.08)	0.04 (0.02–0.13)	0.04 (0.02–0.17)	
Si [μM]	1.76 (0.20–4.48)	0.90 (0.42–2.34)	0.83 (0.32–1.96)	0.98 (0.44–3.17)	2.21 (0.74–6.80)	
N/P (in EZ)	4.4 (exclude March 2013)(1.7–88.7)	5.2 (2.3–17.5)	6.9 (2.5–24.5)	5.8 (1.4–29.5)	13.7 (1.7–85.7)	
N/Si (in EZ)	0.31 (0.06–0.92)	0.18 (0.07–0.79)	0.21 (0.07–0.63)	0.20 (0.07–1.02)	0.24 (0.05–1.34)	
Total Chl [mg m ⁻³]	0.381 (0.024–1.365)	0.157 (0.022–1.203)	0.162 (0.011–0.569)	0.087 (0.012–0.563)	0.229 (0.016–1.257)	
Depth Integrated Chl [mg m ⁻²]	13.2 (2.3–25.8)	21.9 (14.9–27.1)	25.9 (6.5–53.5)	17.1 (4.1–32.1)	46.2 (8.4–118)	
Mean Chl (Depth Integrated/Depth) [mg m ⁻²]	0.343 (0.06–0.66)	0.146 (0.10–0.18)	0.17 (0.04–0.36)	0.11 (0.03–0.21)	0.308 (0.05–0.78)	
Total Primary Production [mg C m ⁻³ h ⁻¹]	5.48 (0.23–17.80)	0.76 (0.01–2.46)	0.63 (0.08–1.58)	0.72 (0.03–2.26)	0.42 (0.01–1.15)	
Depth Integrated Prim. Production [mg C m ⁻² h ⁻¹]	193.3 (30.1–348.8)	88.2 (21.54–188.5)	83.1 (29.9–142.9)	103 (33.9–222.8)	60 (21.9–91.7)	
Mean PP (Depth Integrated/Depth) [mg C m ⁻² h ⁻¹]	4.95 (0.77–8.94)	0.59 (0.14–1.26)	0.55 (0.19–0.95)	0.69 (0.22–1.48)	0.40 (0.14–0.61)	
% Contribution of groups to TCHL	Pico	36 (17–55)	73 (58–79)	67 (47–85)	59 (35–79)	70 (59–78)
	Nano	31 (26–37)	9 (4–15)	10 (8–16)	10 (4–19)	9 (2–14)
	Micro	34 (23–48)	17 (12–26)	22 (7–37)	31 (13–45)	21 (12–27)
% Contribution of groups to TPP	Pico	42 (26–54)	62 (48–77)	61 (38–78)	73 (64–86)	70 (51–86)
	Nano	24 (21–27)	19 (16–29)	20 (11–41)	11 (6–19)	16 (6–43)
	Micro	34 (21–47)	18 (7–27)	18 (11–27)	15 (6–24)	14 (8–24)

Tri-Carb 2810 TR Scintillation Counter. Hourly rates of production were calculated from the measurements, and then these rates were converted to depth-integrated production rates [$\text{mg C m}^{-2} \text{h}^{-1}$] using the trapezoidal method (O'reilly and Zetlin, 1998).

2.1.4. Statistical methods

Principal component analysis (PCA) was used to summarize environmental variable inter-correlations and their potential underlying environmental factor patterns/gradients. For these analyses, log transformation was first applied to all variables and then all the variables were standardized to zero mean and unit variance prior to PCA on the correlation matrix, using the *r* (R Core Team, 2012) package *vegan*'s (Oksanen et al., 2012) RDA (Redundancy analysis) function.

3. Results

3.1. Hydrographic properties

Temperature and salinity profiles for each station and sampling period are presented in Fig. 2. Surface temperature ranged between 15.92 and 29.13°C in the area (Fig. 2), where relatively much cooler waters were recorded near Rhodes cyclonic Gyre. The water column was almost well mixed due to the strong winter convective mixing as observed in March 2013 (Fig. 2). Thermal stratification in the upper layer becomes apparent after March; the warmer-surface mixed layer was observed to deepen by 60 m in September 2012 (Fig. 2). The seasonal thermocline is consistently steeper and shallower in the cyclonic Rhodes Gyre due to the upwelling of cooler deep waters (Fig. 2).

Fig. 2 clearly shows that the upper layer T and S profiles are influenced by the river inflow, especially during winter–spring. In the open sea, surface salinity decreased from 39.13 to a level of about 38.0 psu in March 2013 (Fig. 2). As expected, surface salinity increased to 39.51 psu during summer–early autumn (Fig. 2) due to excess evaporation and limited freshwater input. It should be noted that less saline (≤ 38.87 psu) Atlantic waters were detected between 45 and 70 m below the seasonal halocline (20–40 m) in September 2012 at the offshore stations (St. 28-R48-R50) and Rhodes Gyre (St. R58), flowing westward in the northern Levantine sea (Fig. 2). Euphotic zone was thicker (≈ 90 m) in offshore waters and Rhodes Gyre compared to the coastal sector where light can reach the bottom (Table 2).

3.2. Nutrients

Typical nutrient profiles from the stations are presented in Fig. 3, which clearly indicate that the offshore surface waters were depleted in dissolved inorganic nutrients. Although the surface phosphate values were very low (0.02–0.04 μM) both in the coastal and offshore areas, concentrations of silicate and $\text{NO}_3 + \text{NO}_2$ were significantly higher in coastal waters of the Cilician Basin fed by $\text{NO}_3 + \text{NO}_2^-$ and Si-laden, but P-depleted river waters (Fig. 3). Thus, concentrations for $\text{NO}_3 + \text{NO}_2$ and silicate ranged from 0.05 to 5.5 μM and 0.2 to 6.8 μM , in the offshore and coastal waters, respectively. Spatio-temporal variations of the physicochemical and biological parameters that were measured in this study are summarized in Table 2. Nutrient concentrations of the EZ waters were very low in the offshore waters, and concentrations began to increase and reached the highest value at

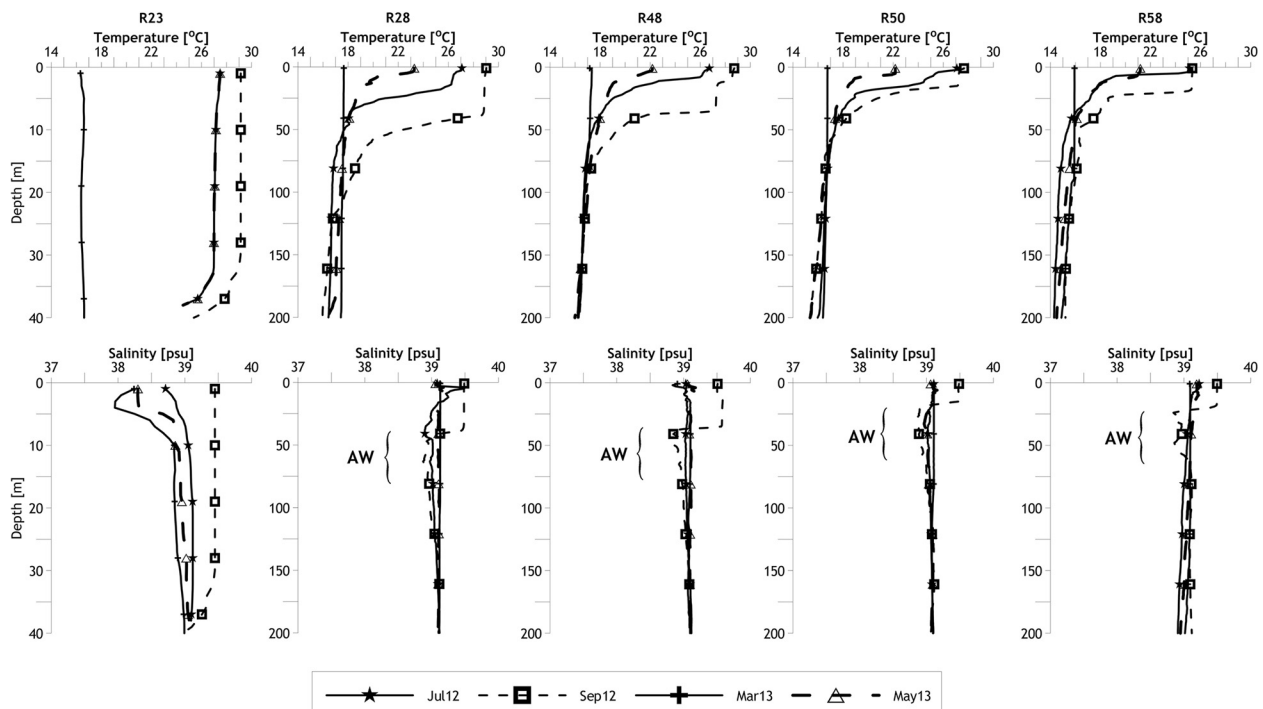


Figure 2 Temperature and salinity profiles at stations visited in the Levantine basin (AW: Atlantic Water salinity signature detected at stations R28 to R58). Modified from Yucel (2017).

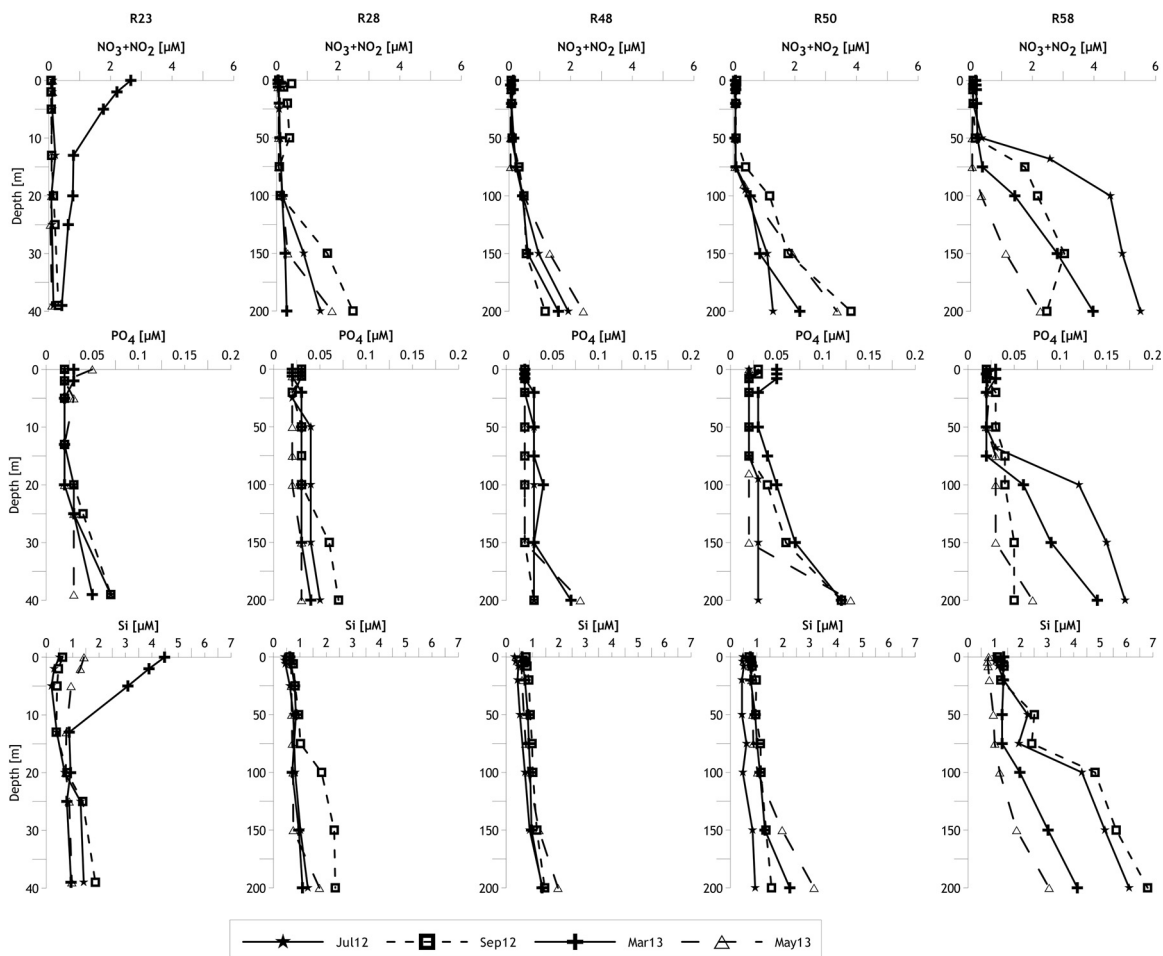


Figure 3 Vertical distributions of dissolved nutrients at the stations visited in the Levantine basin. Modified from Yucel (2017).

200 m depth, below the EZ in the Levantine offshore waters and Rhodes Gyre; the nutricline was markedly sharp in the Rhodes Gyre and formed at shallower depths (between 50 and 75 m) (Fig. 3). An increase was observed in phosphate concentrations, following winter convective mixing (March 2013) in the offshore waters. The highest seasonal variations were seen in the EZ of the Rhodes Gyre, where nutrient concentrations were measured over a wide range (Table 2, Fig. 3).

Very low N/P (4.4–13.7) and N/Si (0.2–0.3) ratios were observed in EZ waters of the study area (Table 2). Higher values were found for the deeper parts of the EZ (≈ 80 –100 m) in offshore waters and Rhodes Gyre. N/P values reached peak levels in the surface coastal waters in March 2013 (88.7) and at 68 m near Rhodes Gyre in September 2012 (85.7).

3.3. Size-based chlorophyll-a

Changes in chlorophyll concentration with respect to depth for all the stations visited are presented in Fig. 4. Overall, total Chl-*a* concentration varied regionally and seasonally from 0.011 to 1.365 mg m⁻³ in the study area (Table 2). Surface- and layer-averaged concentrations increased in rainy seasons (March 2013) in river-fed coastal waters while concentrations inversely increased with depth in the dry

season (July and September 2012) (Fig. 4). Generally, total Chl-*a* concentrations at offshore surface waters (St. R28, R48, and R50) remained very low, but reached elevated maxima in stations R48 (0.569 mg m⁻³, July 2012) and R28 (1.2 mg m⁻³, in September 2012) during the stratification period. Additionally, higher values were measured near and at the bottom of the EZ during the stratification period (July and September 2012), as the deep chlorophyll maximum (DCM), a typical feature of the eastern Mediterranean (Ediger and Yılmaz, 1996; Kress and Herut, 2001; Siokou-Frangou et al., 2010), was formed between 75 and 100 m throughout the study period. However, this feature can weaken or totally disappear in winter due to the intensive vertical mixing, as was the case in March 2013, during which Chl-*a* was distributed homogeneously within the entire EZ (variations were observed ± 0.02 –0.04 mg m⁻³ in water column). In July 2012, higher Chl-*a* concentrations (0.514–0.569 mg m⁻³) were recorded in the much warmer upper layer of EZ (4–50 m) at St. R48, although concentrations have not generally exceeded 0.2 mg m⁻³ in the upper layer of EZ in the offshore waters of the northern Levantine Basin. Very low layer-averaged concentrations were observed in May 2013 following the spring bloom (Fig. 4). Average Chl-*a* concentration for the upper 10 m of Rhodes Gyre was calculated as low as 0.06 mg m⁻³ for the study period. While DCM was found in July 2012 (1.26 mg m⁻³) and May 2013 (0.52 mg m⁻³) within

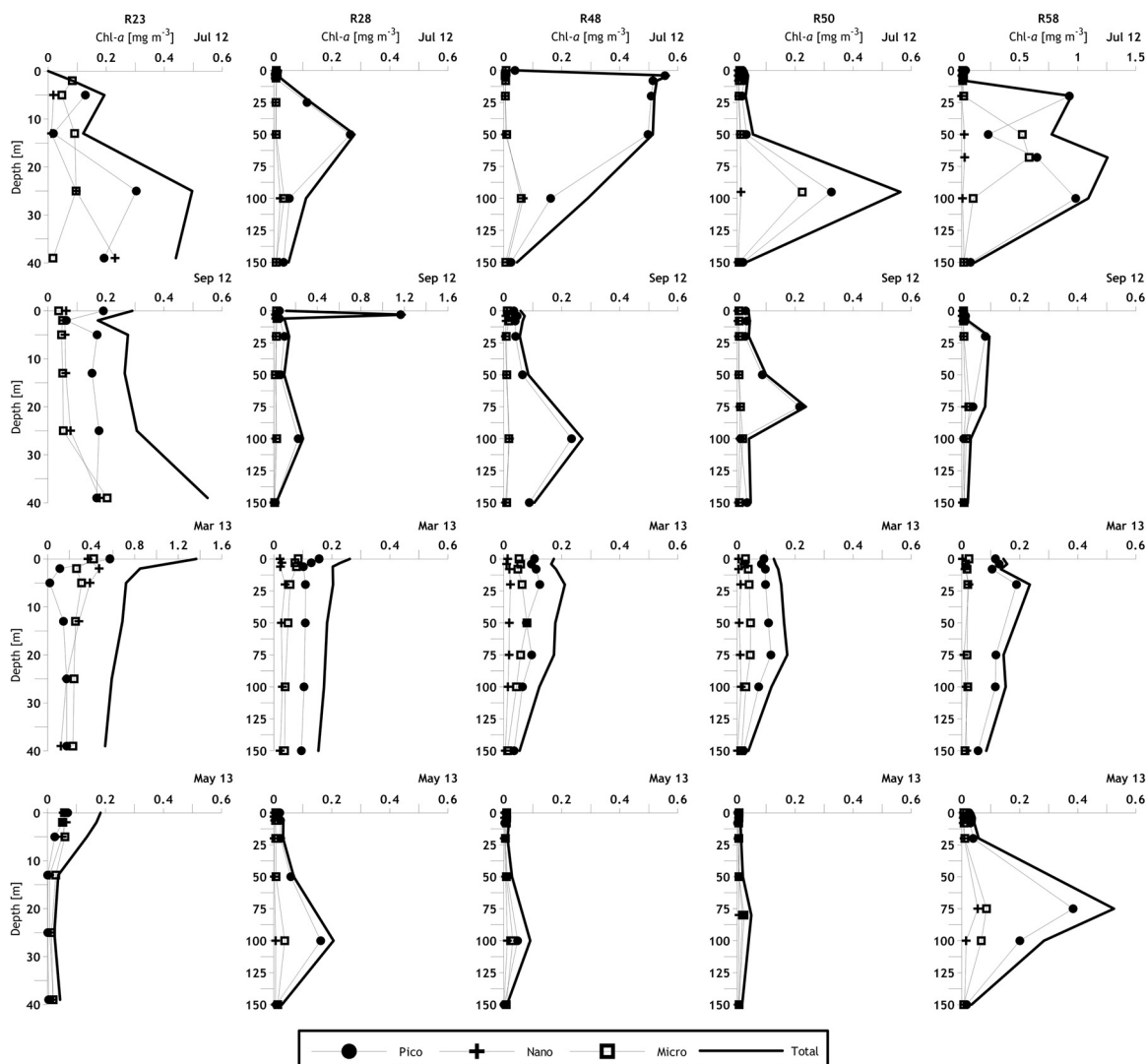


Figure 4 Changes in size fractionated and total chlorophyll *a* concentrations with depth at selected stations in the Levantine basin (Note: the different depth scales for the coastal st. R23; and different scale at R23 for March 2013 and R58 for July 2012 (x and y axes)).

the nutricline ($\approx 75\text{--}100\text{ m}$), it disappeared in September 2012 and March 2013 in EZ of the cyclonic Rhodes Gyre.

Size-fractionated Chl-*a* profiles indicate picoplankton ($61 \pm 19\%$) to be the major contributor in the EZ of the study area (Fig. 4). Contribution of small nanoplankton and microplankton to the bulk Chl-*a* were calculated as $14 \pm 10\%$ and $25 \pm 12\%$, respectively. Small nanoplankton contribution increased for the total Chl-*a* in nutrient-rich upper layer of coastal waters, while the contribution was negligible for offshore waters and the Rhodes Gyre. Microplankton including larger nanoplankton formed the second dominant group in the coastal waters, DCM, and near the nutricline (50 m) in Rhodes Gyre (Fig. 4). Contribution of picoplankton increased in summer and early autumn (hot and dry season) and decreased during the rainy and cold period (March 2013) in coastal waters, except in the surface waters.

3.4. Size-based primary production

Depth distributions of size-fractionated and total primary production (TPP) rates are presented in Fig. 5. TPP displayed

a remarkable seasonal and regional variability between the sampling sites. TPP rates were discovered to be apparently high ($1.42\text{--}17.80\text{ mg C m}^{-3}\text{ h}^{-1}$) in March 2013 (representing late winter–early spring conditions) at all the stations, and the productive layer was rather broad, extending down to the 0.1% light depth. The TPP rate over the basin decreased markedly to the levels of $0.13\text{--}3.32\text{ mg C m}^{-3}\text{ h}^{-1}$ in the upper EZ (down to 25% light depth) in May 2013, when the upper layer was stratified and the available nutrients were already consumed during the spring bloom period. Principally, the TPP displayed an increasing trend in the upper layer of the EZ (10% light depth) and then decreased steadily toward the base of the EZ, which varied from 61 m (1% light depth) to 100 m in the oligotrophic open sea for the summer–autumn period (Table 2).

In the coastal waters of the Mersin Bay (St. R23), TPP rates were maximal in March, followed by July and September, whereas the least levels were observed in May. Rates peaked at the surface during spring (March 2013) and dropped to its lowest levels (layer-averaged rate: $1.5\text{ mg C m}^{-3}\text{ h}^{-1}$), following the major spring bloom in May 2013.

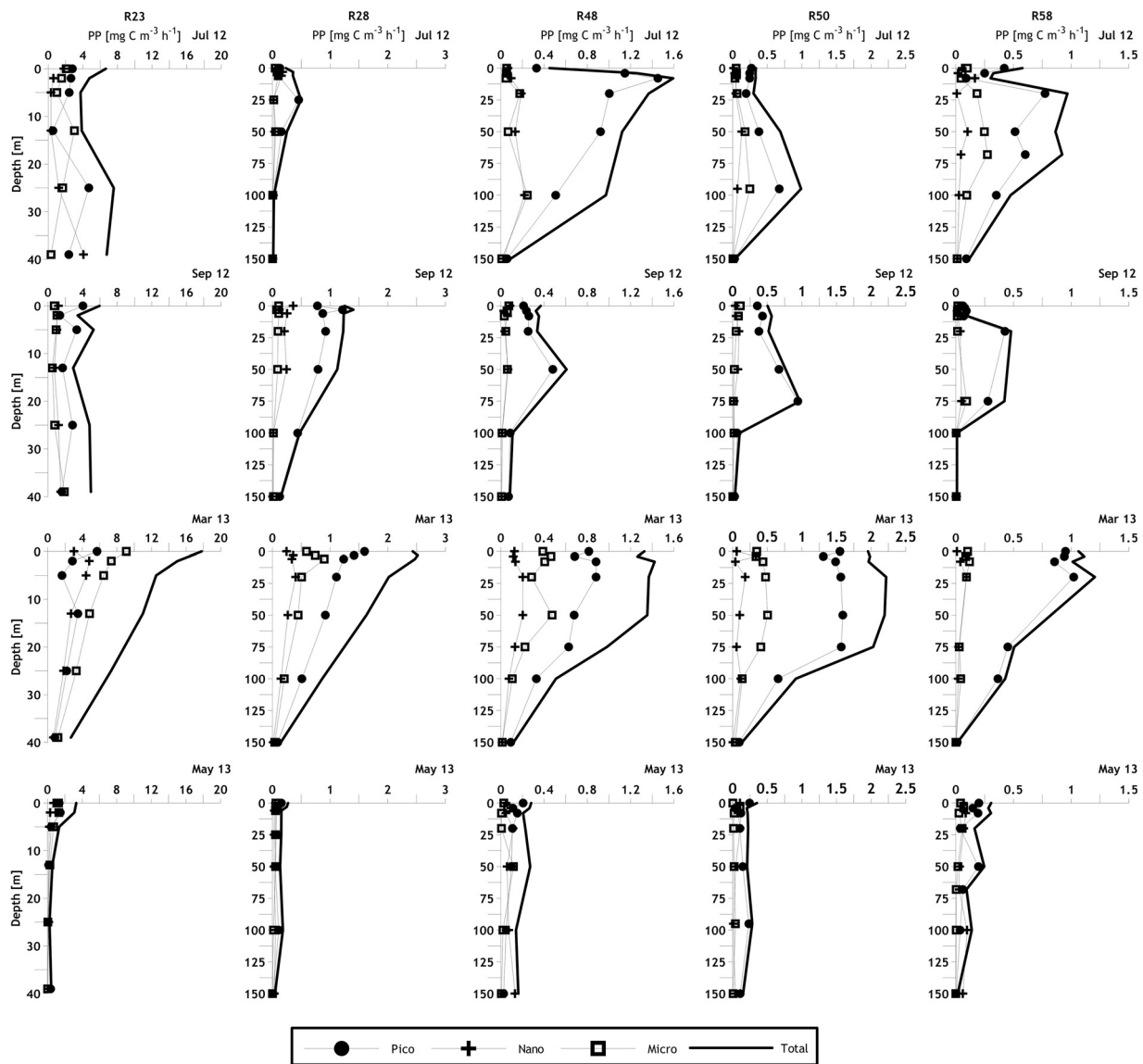


Figure 5 Changes in size fractionated and total primary production rates with depth at selected stations in the Levantine basin (Note: the different depth scales for the coastal st. R23; and different scale for all station).

In the offshore waters of the northern Levantine Basin (St. R28, R48, and R50), rates decreased to low levels of 0.71–0.84 mg C m⁻³ h⁻¹ (EZ layer-averaged values), which are 6.7 times lower than those found for the coastal region influenced by river inputs. It should be noted that enhanced TPP rates were observed in the subsurface waters between 8 and 100 m in July and September, reaching the maximal rate upper layer of the EZ (8 m in July).

In the Rhodes Gyre (St. R58), TPP rate was found high at the depths between thermocline (10–20 m) and the base of the EZ (≈100 m) and low in highly illuminated surface waters during summer–autumn. After the winter convective mixing (March 2013), TPP increased at the surface waters (top 25 m), in comparison with dry and hot seasons (July and September 2012) and decreased slightly toward the lower end of the EZ. Very low (0.219 ± 0.09 mg C m⁻³ h⁻¹) TPP rates were measured in the water column in May 2013 in Rhodes Gyre.

Size-fractionated PP profiles indicate picoplankton to be the major contributor (62 ± 17%) at all sites throughout the study period. Contribution of picoplankton to TPP reached up to 86% in offshore waters (St. R50, September 2012) and Rhodes Gyre (March 2013), and TPP in DCM was also markedly dominated by picoplankton. Microplankton including larger nanoplankton was the second dominant group (20 ± 11%) followed by small nanoplankton (18 ± 11%) in the northern Levantine Sea, while shifting with each other in the different depth layers within EZ in the offshore waters (July and September 2012 and May 2013). EZ averages indicate small nanoplankton to be more productive than microplankton at St. R28, R48, and R58 (Rhodes Gyre). Microplankton production exceeded that of small nanoplankton only in coastal waters (47%) and made a major contribution to offshore waters, following winter convective mixing in March 2013.

3.5. Principal component analysis (PCA)

Environmental variables were analyzed using the principal component analysis. First, 5 components were selected from Table 3 and accounted for 95% of the total variation. The loading plot of PCA of abiotic and biotic parameters is presented in Fig. 6. Component 1 (PC1) can explain 63% of

Table 3 Eigen values and corresponding values of percentage of variance for each component.

Component	Eigen value	% of variance	Cumulative %
1	12.34	63.0	63.0
2	3.08	15.7	78.7
3	1.76	9.0	87.7
4	0.92	4.7	92.4
5	0.56	2.8	95.3
6	0.30	1.5	96.8
7	0.24	1.2	98.1
8	0.14	0.7	98.8
9	0.12	0.6	99.4
10	0.05	0.3	99.7
11	0.02	0.1	99.9
12	0.01	0.0	100

Extraction method: principal component analysis.

the total variance and component 2 (PC2) can explain 15% of the total variance. In two dimensional space, given by F1 vs F2, variables were separated into three groups (i.e., one including NPP: nanoplanktonic PP, MPP: microplanktonic PP, TPP: total PP and PPP: picoplanktonic PP). Correlations are present between NPP, MPP, TPP, and PPP (Supplementary Fig. S1). Additionally, PO₄, silicate, and NO₃ + NO₂ have similar trends. According to the distribution of the stations, R23 differed from other stations with high production.

4. Discussion

4.1. Seasonal variability in size-fractionated primary production and chlorophyll in coastal waters

In the northeastern Mediterranean Sea, regional rivers, upwelling events, and atmospheric (wet + dry) depositions are regarded as the main sources of nutrients (Koçak et al., 2010; Uysal, 2006; Uysal and Köksalan, 2010, 2017). Though the eastern Mediterranean is commonly reported to be one of the least productive basins in the world (Siokou-Frangou et al., 2010), the coastal waters of Mersin Bay display a high primary production (PP) capacity (Yılmaz, 2006; Yucel, 2013) due to high concentration of nutrients (especially silicate and

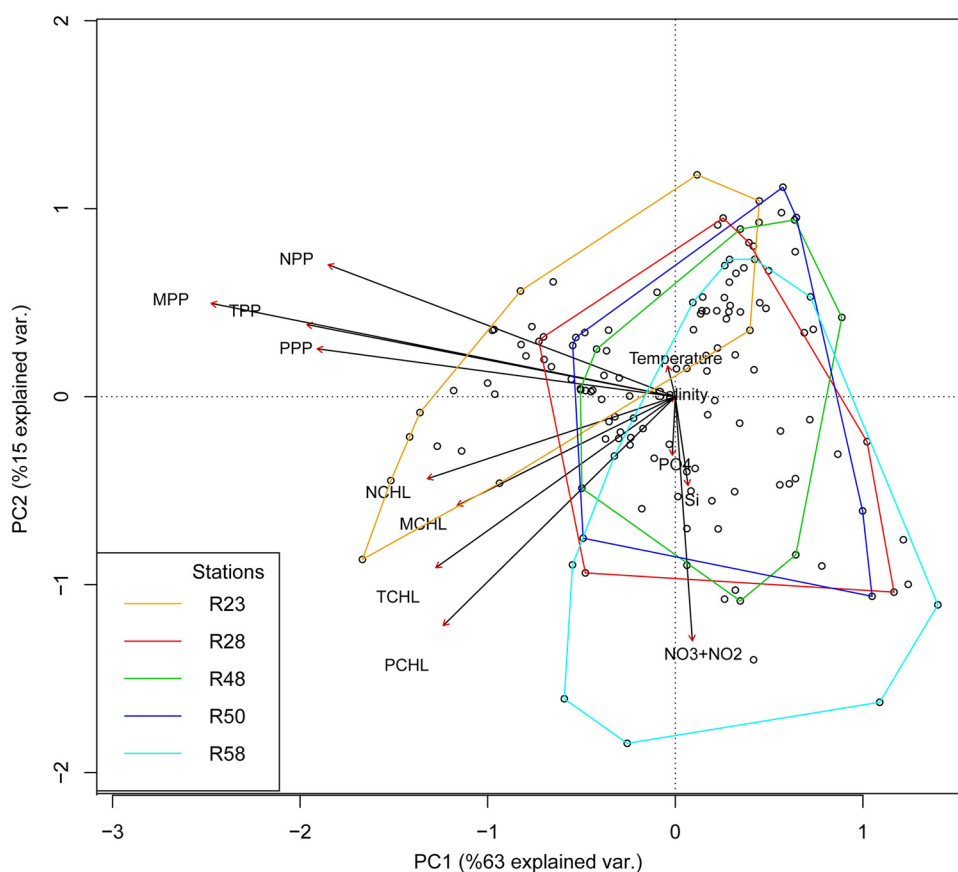


Figure 6 Results of principal components analysis of production, chlorophyll and environmental parameters (NPP: nanoplanktonic PP, MPP: microplanktonic PP, TPP: total PP and PPP: picoplanktonic PP, NCHL: nanoplanktonic Chl, MCHL: microplanktonic Chl, TPP: total Chl and PCHL: picoplanktonic Chl).

$\text{NO}_3 + \text{NO}_2$) introduced by local rivers (Seyhan, Lamas, Tarsus, and some smaller brooks) (Koçak et al., 2010). Elevated surface nutrient concentrations in less saline coastal waters of Mersin Bay lead to the enhancement of dissolved inorganic and organic nutrients, total PP, algal biomass, as well as changes in algal composition as compared to the nutrient-poor Levantine offshore waters.

The total PP in the coastal waters of northern Levantine Sea was as high as $193 \text{ mg C m}^{-2} \text{ h}^{-1}$, exceeding most of the PP rates to date reported for different sub-regions of the Mediterranean (Siokou-Frangou et al., 2010; Yucel, 2013). Exchange of productive and nutrient-rich coastal Mersin Bay waters with oligotrophic offshore waters is limited due to the blockage of westward flowing of the Asia Minor Current (AMC) present in the northeastern Levantine deep Basin. This mechanism creates highly contrasting water masses with very low and very high production capacities within the wide shelf basin of Mersin Bay on the NE Levantine basin (Yucel, 2008).

TPP rate and chlorophyll concentrations of Mersin Bay coastal waters (St. R23) have increased markedly in March 2013, when the surface salinity was measured below 38 psu and the concentrations of silicate and $\text{NO}_3 + \text{NO}_2$ at the surface were maximal, following the winter convective mixing and pronounced river runoff (Fig. 3). Such optimum conditions have stimulated PP in coastal waters favoring microplankton + larger nanoplankton (47% of total primary production: $162.8 \text{ mg C m}^{-2} \text{ h}^{-1}$) as the dominant group. Additionally, Yucel (2013) measured the microplankton + larger nanoplankton-dominated high primary production rates in summer and autumn (October 2010, July and August, 2011) in coastal waters that were affected partially by the local river run off. Microplankton is composed mainly of diatoms that consume the majority of available nutrients in the coastal waters, compared to smaller cells. Moreover, higher silicate concentrations favor diatoms in coastal waters at concentrations above $2 \mu\text{M}$ (Egge and Asknes, 1992; Fogg, 1991). Therefore, in the present study significant positive correlations were obtained between nutrients ($\text{NO}_3 + \text{NO}_2$ and silicate) and microplankton production and chlorophyll in coastal waters (Supplementary Fig. S1). Conversely, picoplankton was generally observed to be the dominant contributor to the bulk flora in summer and autumn, when the nutrient concentrations were relatively low in coastal waters during the course of this study (Table 2, Fig. 4). However, contrary to the dominance of diatoms in the phytoplankton composition of coastal waters that was reported in previous studies (Eker and Kideys, 2000; Eker-Develi et al., 2003; Kideys et al., 1989; Polat et al., 2000; Uysal et al., 2003) where picoplankton was missed or not studied along with large phytoplankton groups, except some ataxonomic phytoplankton studies, recent studies indicate that phytoplankton composition was generally dominated by picoplankton (Yilmaz, 2006; Yucel, 2008; Yucel, 2013; Yucel et al., 2017). Picoplankton is a better competitor with the lower energy requirements and higher production efficiency than microplankton in nutrient-poor waters during summer and autumn in coastal waters (Finkel et al., 2005; Moutin et al., 2002). Moreover, picoplankton, the major contributor in hot and dry seasons, is more tolerant of warmer waters than microplankton, which cannot tolerate higher temperatures (Supplementary Fig. S1) (Yucel, 2013). Small nanoplankton was the least

contributing group in coastal waters, where their remarkably increased contribution to TPP was only observed in very favorable environmental conditions (March 2013).

Based on very low N/P and N/Si ratios, nitrogen was suggested to be the limiting nutrient during July and September 2012 and May 2013 in coastal waters. Despite the high levels of phosphate and silicate, the lower nitrogen concentration of the water column delimited phytoplankton growth significantly during May 2013. These low $\text{NO}_3 + \text{NO}_2$ concentrations have limited the growth and shaped the phytoplankton composition in coastal waters (Yucel, 2013). Actually, changes in size groups of the phytoplankton is highly dynamic in coastal waters and may change at short time intervals, depending on the changes in ambient physicochemical conditions, river regime, nutrient concentrations and composition, activity of cells, predation and competition (Romero et al., 2013).

4.2. Seasonal variability of size-fractionated primary production and chlorophyll in offshore waters

In offshore waters of the northern Levantine Basin, nutrient concentrations were observed to be low and distributed homogeneously at the top 100 m of the water column, and then increasing with the increasing depth down to the nutricline, which occurs between 300 and 500 m (Yilmaz and Tugrul, 1998; Yucel, 2013). Besides, small-scale upwelling events and atmospheric deposition offer a certain amount of nutrients to the oligotrophic offshore waters. Goksu River also supplies nutrients to the south and the southwestern offshore surface waters. The direct (increasing nutrients)/indirect (increasing chlorophyll) effects of the Goksu River can reach Cyprus via currents (Fig. 1) (Uysal et al., 2008; Yilmaz and Tugrul, 1998; Yucel, 2008).

Nutrient concentrations were very low in the upper layer, covering the euphotic (EZ) (75 m) and exhibiting typical characteristics of oligotrophic environments in the northern Levantine Sea throughout the year (Ediger et al., 2005). Phosphorus was near the detection limit ($0.02 \mu\text{M}$) and $\text{NO}_3 + \text{NO}_2$ was also very low within the EZ (Table 2); the nutrient profiles displayed a gradual increasing trend below the EZ. Phosphorus is utilized faster than nitrate and silicate in the oligotrophic eastern Mediterranean (Krom et al., 2005). Although it is widely accepted that phosphorus is the limiting nutrient for primary production, low N/P (6 ± 0.8) and N/Si (0.195 ± 0.015) ratios also indicated nitrogen limitation or nitrogen + phosphorus co-limitation in the offshore waters (Yucel, 2013). Since phosphorus concentration of the upper layer of EZ was at very low levels (Table 2), no clear relationship appeared between the biological parameters and the phosphorus concentration throughout the study period in the offshore waters of northern Levantine Sea (Supplementary Fig. S1). Phosphorus supplied from the P-limited Levantine intermediate depths is utilized rapidly and phosphorus concentration declines below $0.03 \mu\text{M}$ (undetectable by conventional colorimetric method) in the offshore EZ as the inorganic N ($\text{NO}_3 + \text{NO}_2 + \text{NH}_4$) enters the system with higher N/P ratio. Therefore, inorganic N can be measured at background levels ($0.1\text{--}0.2 \mu\text{M}$) in the EZ in summer-autumn period. Following intense winter convective mixing, higher PP levels were observed all over the northern Levantine

offshore waters (top 75 m), due to nutrient supply from the intermediate depths.

In the early spring period, the surface $\text{NO}_3 + \text{NO}_2$ was observed to as low as levels of $0.05\text{--}0.23\ \mu\text{M}$ whilst phosphorus was at hardly detectable (detection limit) levels of $0.02\text{--}0.04\ \mu\text{M}$ due to consumption of nutrients supplied from deep waters by photosynthesis in the EZ internal sources (Ediger and Yilmaz, 1996; Krom et al., 1991). Thus, the low concentrations of $\text{NO}_3 + \text{NO}_2$, PO_4 and the low N/P ratio (<15) strongly suggest that N and P co-limited production during the post-bloom period in the Levantine basin.

In the offshore waters where the seasonal thermocline was located at shallow depths (about 10–50 m) 10–25 m in July 2012, higher concentrations of chlorophyll and PP values displayed broad vertical distribution, vanishing at the base of the thermocline. In the more productive thermocline zone, PP was dominated by picoplankton (Fig. 5) and nutrient concentrations were low, ranging between 0.07 and $0.08\ \mu\text{M}$ for $\text{NO}_3 + \text{NO}_2$ and $0.02\text{--}0.03\ \mu\text{M}$ for PO_4 (St. R48, Fig. 3). Picoplankton dominated PP and low nutrient concentrations in the thermocline depth range of EZ indicate that the PP was stimulated by nutrients mainly generated from small-size detritus accumulated with the thermocline zone (Ediger et al., 2005) and also labile forms of the colloidal and dissolved organic nutrients in the oligotrophic and mesotrophic marine environments (Berman and Bronk, 2003; Bronk et al., 2007; Roussenov et al., 2006; Torres-Valdes et al., 2009).

In the 2013 late spring, when there was no apparent seasonal thermocline formation in the upper layer, nutrients available in the EZ were almost consumed by phytoplankton; the $\text{NO}_3 + \text{NO}_2$ and PO_4 were very low ($0.05\text{--}0.07\ \mu\text{M}$ and $0.02\text{--}0.02\ \mu\text{M}$, respectively). Low Chl-*a* and PP values measured in the spring indicate that the majority of nutrients supplied to the EZ during the winter mixing period have been consumed and the system had the background nutrient levels of the Levantine EZ waters.

No close relationship was observed between the water column PP and the chlorophyll concentration. Chlorophyll peaks (DCM) were observed below the high PP zone at the same station (Figs. 4 and 5). The formation of DCM is well known to develop in the light-limited depths of the offshore EZ extending the seasonal thermocline, depending on the depths of the seasonal thermohaline feature, limited nutrient supply from the EZ boundary and rate of nutrients regenerated in the thermohaline feature near the base of the EZ where the DCM was formed during summer–early autumn period (Fig. 4). High light condition could stimulate primary productivity in the upper layer of EZ (10–75 m), far above the nutricline in offshore waters. In addition, intrusion of nutrients into the base of EZ may provoke low light adapted phytoplankton (Ediger et al., 2005) in DCM, which was dominated by picoplankton consisting mainly of *Synechococcus* and *Prochlorococcus* in the eastern Mediterranean. Although phytoplankton composition was not available for this study, Li et al. (1993) found *Prochlorococcus* to be more abundant than *Synechococcus* in the water column of offshore waters in the eastern Mediterranean. Ghiglione et al. (2008) also observed high concentration of *Prochlorococcus* at the base of the DCM, while *Synechococcus* was observed in the upper 40 m in the Gulf of Lions. Furthermore, Yucel (2013) found that contribution of *Prochlorococcus* to

total picoplankton increase was below 30–40 m in eastern Mediterranean offshore waters.

Picoplanktonic primary production (65%) and bulk chlorophyll (66%) dominated phytoplankton composition in offshore waters of the northern Mediterranean (Table 2).

Microplankton + larger nanoplankton formed the second dominant group in the nutrient-depleted offshore waters. All previous studies indicated that phytoplankton composition shifted from microplankton to picoplankton with increasing oligotrophy and picoplankton has been considered to dominate the phytoplankton in the oligotrophic offshore waters of the eastern Mediterranean (Li et al., 1993; Siokou-Frangou et al., 2010; Uysal, 2006; Uysal and Köksalan, 2010; Yucel, 2013). The contribution of picoplankton to the total primary production exceeded 70% in Levantine offshore waters (Yucel, 2013). Low N/P ratios can be ascribed to rapid utilization of available nitrogen by picoplankton (cyanobacteria and prochlorophytes), which have high affinity to nitrogen species in offshore waters. Cyanobacterial production can be satisfied significantly by the scarce amount of nitrogen sources (Karl et al., 1997; Moore et al., 2002; Pantoja et al., 2002). Moreover, picoplankton has more advantages, with the high surface to volume ratio to reaching low concentrations of nutrients and photoprotectant pigments to survive excess light conditions, compared to microplankton (Finkel et al., 2009; Yucel, 2013). Excess input of phosphate in early spring also provoked micro- and nanoplanktonic production and biomass in offshore waters (Figs. 3–5).

4.3. Seasonal variability of size-fractionated primary production and chlorophyll in Rhodes Gyre

In Rhodes Gyre, nutrient concentrations started to increase rapidly in the base of the EZ in this study (Fig. 3). Since the nutricline was located just above the EZ seasonally variable amounts of nutrients have been pumped by upwelling processes from the nutricline depths to the lower depths of the EZ (Ediger and Yilmaz, 1996). This phenomenon stimulates primary productivity in the EZ (1% light depth: 59–80 m) throughout the year. In the Levantine Basin, nitracline was formed at shallower depths than phosphocline, even in Rhodes Gyre; for example, $\text{NO}_3 + \text{NO}_2$ gradient started at 50 m whereas the PO_4 gradient was observed at 75 m in the Rhodes Gyre because of either the selective accumulation of labile $\text{NO}_3 + \text{NO}_2$ or the selective removal of reactive phosphate by sinking particle (Yilmaz and Tugrul, 1998).

In the gyre the upper layer is thermally stratified during late spring–autumn period. Therefore, limited nutrients are supplied from the nutricline depths to the upper mixed depths of EZ (50 m), which leads to consumption of available nutrients via photosynthesis and thus low nutrient ($\text{NO}_3 + \text{NO}_2$, PO_4) concentrations with low N/P (≈ 5), as observed in the Levantine offshore waters during the study period (Table 2). However, chlorophyll concentrations measured in the upper layer of cyclonic Rhodes Gyre in July 2012 and May 2013 have exceeded those observed in both coastal (salinity: 37.9–39.4 psu) and offshore waters (salinity: 38.9–39.59 psu) (Fig. 4). In the Gyre waters, chlorophyll profiles were broader (25–100 m) in July 2012, reaching higher concentrations at the EZ base (75 and 100 m) in May

2013, which indicates the role of nutrient inputs from the shallower nutricline (50–75 m), keeping chlorophyll concentrations at the levels of coastal waters partly fueled by terrestrial inputs during dry period. Consequently, low nutrient high chlorophyll (LNHC) condition was observed in the upper part of the EZ during the summer (July 2012). High nutrient low chlorophyll (HNLC) condition could develop in the core of the Rhodes Gyre, as observed in March 1992 (Ediger et al., 2005), due to the dilution of organic matter produced in the upper layer by upwelling water masses. However, such a condition was as not observed in March 2013, as the less saline deep water could not replace the more saline, warmer surface layer within the Gyre (Fig. 2). Therefore, very low phosphate ($0.04 \mu\text{M}$), $\text{NO}_3 + \text{NO}_2$ ($0.69 \mu\text{M}$), and chlorophyll ($<0.23 \text{ mg m}^{-3}$) concentrations were measured at top 150 m in March 2013, following the winter convectonal mixing. The March 2013 data strongly suggest that low PP rates may represent post-bloom phase in the surface waters of the region, with low nutrient concentrations. However, the chlorophyll was higher in the Rhodes Gyre than in the Cilician basin waters, due presumably limited nutrient inputs from the density gradient zone situated at the base of the EZ and regenerated of nutrients in the light-limited zone of the EZ. High levels of POC/Chl-*a* ratio in

the EZ determined by Ediger et al. (2005) was attributed to detritus and heterotrophic activity-dominated in the EZ during nutrient depleted spring-autumn periods over the Levantine basin. In addition, lowest nutrient concentrations and low PP rates were observed in top 50 m at the end of spring (May 2013), while total chlorophyll reached 0.525 mg m^{-3} at the DCM formed at 75 m (Fig. 4). In summer (July 2012), the DCM formed was broader, extending down to 100 m, with slightly higher nutrient concentrations than in May 2013.

Picoplankton was the major contributor (65%) to total PP within EZ, including DCM, as observed in offshore waters, followed by microplankton + larger nanoplankton. Total chlorophyll was also dominated by picoplankton (70%) in the Rhodes Gyre (Table 2). The contribution of larger cells ($>5 \mu\text{m}$) was maximal (0.581 mg m^{-3} and $0.274 \text{ mg C m}^{-3} \text{ h}^{-1}$) in July 2012 at the 50–75 m depth range at nutricline, with high phosphate, $\text{NO}_3 + \text{NO}_2$, and Si concentrations being pumped from the lower layer of the EZ. It seems that microplankton cannot compete with picoplankton in Rhodes Gyre under low nutrient conditions, as it was seen in coastal and offshore waters, but an increase was seen in their contribution in high nutrient conditions (in July 2012 in coastal waters and March 2013 in Rhodes Gyre), which provoke microplanktonic growth (Egge and Asknes, 1992; Fogg, 1991).

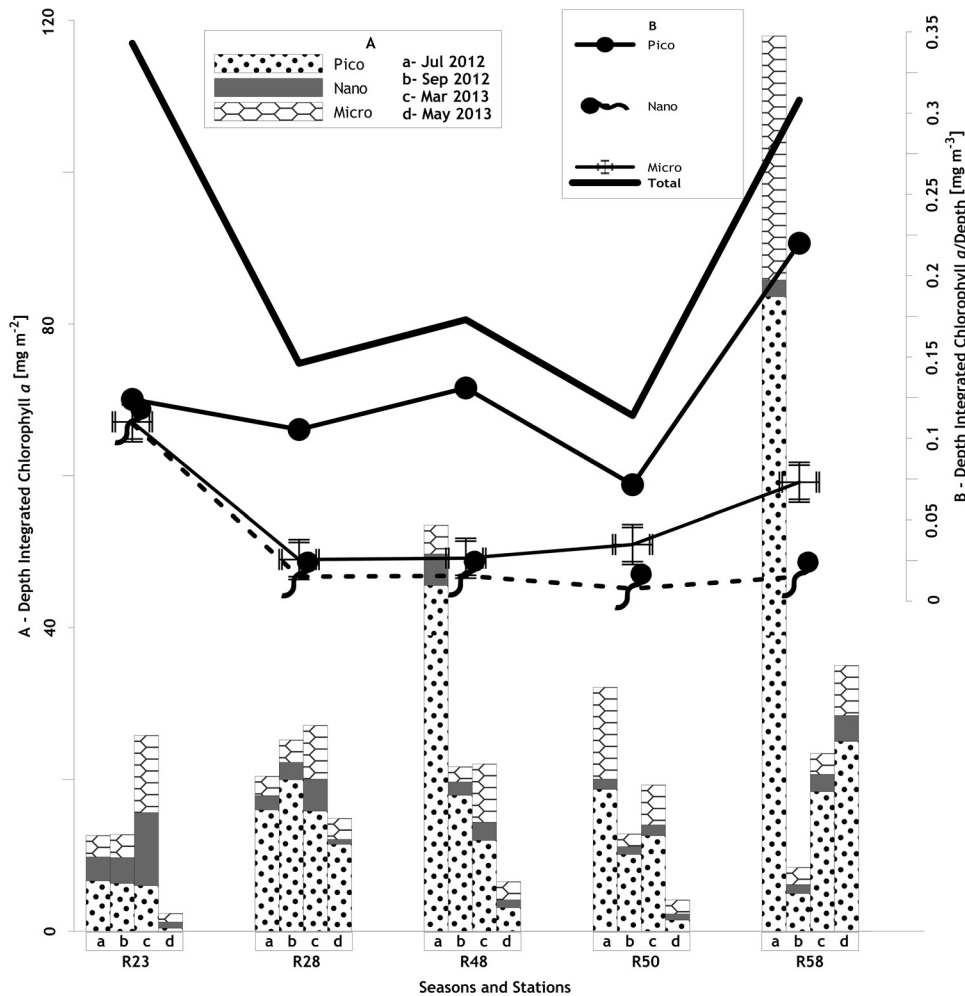


Figure 7 Depth integrated (A) and mean (B) chlorophyll *a* values calculated for all stations and sampling periods. (Note: the different integration depth for the coastal st. R23).

4.4. Longitudinal variability of size-fractionated primary production, chlorophyll, and assimilation ratio

Along the east-west transect (from St. R28 to R58), PP showed a gradual decrease from $0.588 \text{ mg C m}^{-3} \text{ h}^{-1}$ to $0.402 \text{ mg C m}^{-3} \text{ h}^{-1}$ in the area (Fig. 8B). In addition, depth-integrated PP (DIPP) also decreased from $193.3 \text{ mg C m}^{-2} \text{ h}^{-1}$ in coastal waters to $60 \text{ mg C m}^{-2} \text{ h}^{-1}$ in Rhodes Gyre. In contrast to the east-west decreasing trend in PP, concentration of chlorophyll increased toward Rhodes Gyre (from 0.146 mg m^{-3} in St. R28 to 0.308 mg m^{-3}) and DICHL (depth-integrated chlorophyll) fluctuated between 13.2 and 46.2 mg C m^{-2} in the study area. The PP rate and the chlorophyll concentration were not in accordance in the northern Levantine Sea during the study period which was discussed above (Figs. 7 and 8). Studied areas of northern Levantine Basin are well known to have different bio-physicochemical characteristics and dynamics (Ediger and Yilmaz, 1996; Ediger et al., 2005; Yilmaz and Tugrul, 1998). Chlorophyll concentrations in the Rhodes Gyre were close to those of the coastal waters (0.343 mg m^{-3}), where riverine nutrient inputs feed the coastal ecosystem. As usual, very high primary production rates were recorded for whole study area after the intense winter convectonal mixing, which

determines the nutrient budget of the EZ in March 2013 (Fig. 8A). After the bloom period in late spring (May 2013), very low PP rates and chlorophyll were measured when phosphate and $\text{NO}_3 + \text{NO}_2$ were almost depleted in the area.

The coastal waters of the northern Levantine Sea had different characteristics and were separated statistically from the other stations with high production capacity ($4.955 \text{ mg C m}^{-3} \text{ h}^{-1}$) (Fig. 6). Although Rhodes Gyre and offshore waters had some similar features, Rhodes Gyre was also separated from others due to its distinct-high nutrient (below 50 m) and chlorophyll concentrations in the euphotic layer (below 50 m). All results showed that coastal waters were affected by river input, while offshore waters and cyclonic Rhodes Gyre were influenced by convective winter mixing and continual upwelling events, respectively.

Contribution of all groups to TPP slightly decreased toward the west, while all groups increased their contribution to total chlorophyll from R28-the most eastern part of offshore waters to R58-Rhodes Gyre. While contribution of smaller cells ($<2 \mu\text{m}$) to DICHL increased from the east to the west in the northern Levantine Basin, DIPP rates decreased throughout the transect. Conversely, the opposite trend (low chlorophyll and high PP of picoplankton) was observed in the cyclonic West Cyprus Eddy (WCE) (St. R50), with small scale

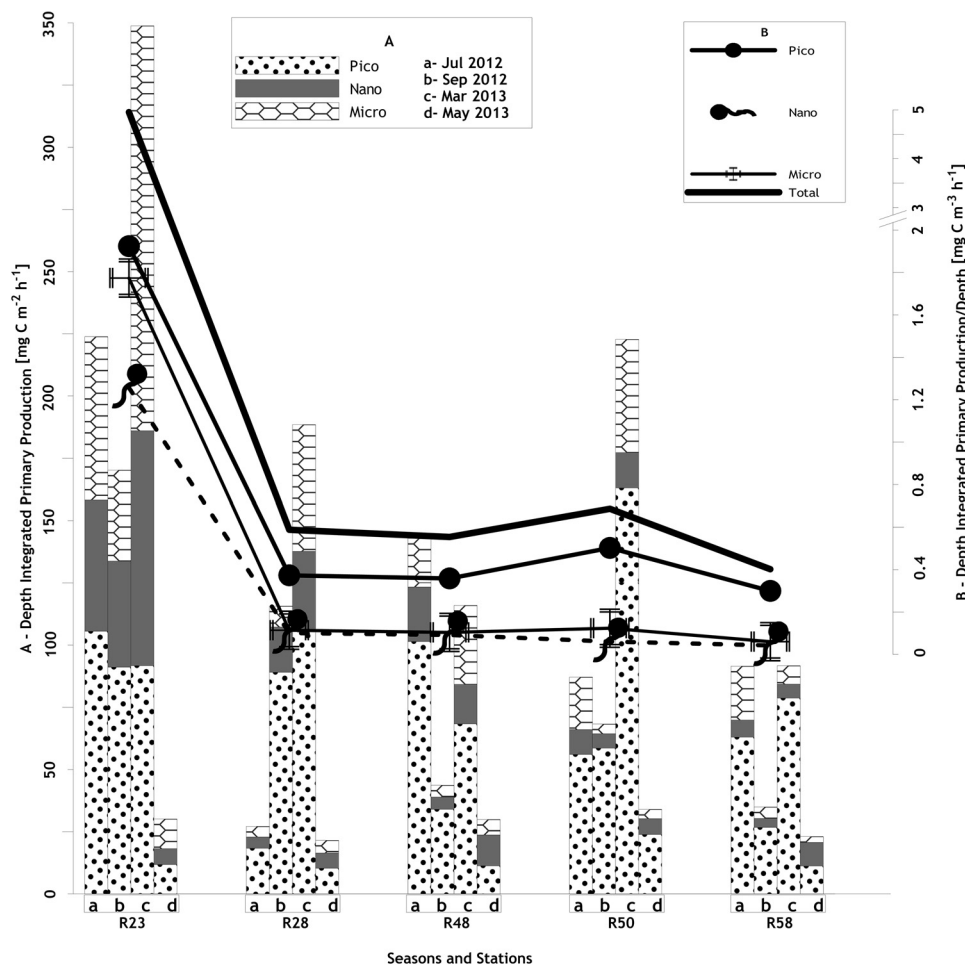


Figure 8 Depth integrated (A) and mean (B) primary production values in the five stations and four seasons studied (Note: the different integration depth for the coastal st. R23 and “break” line of B axis at 2–3).

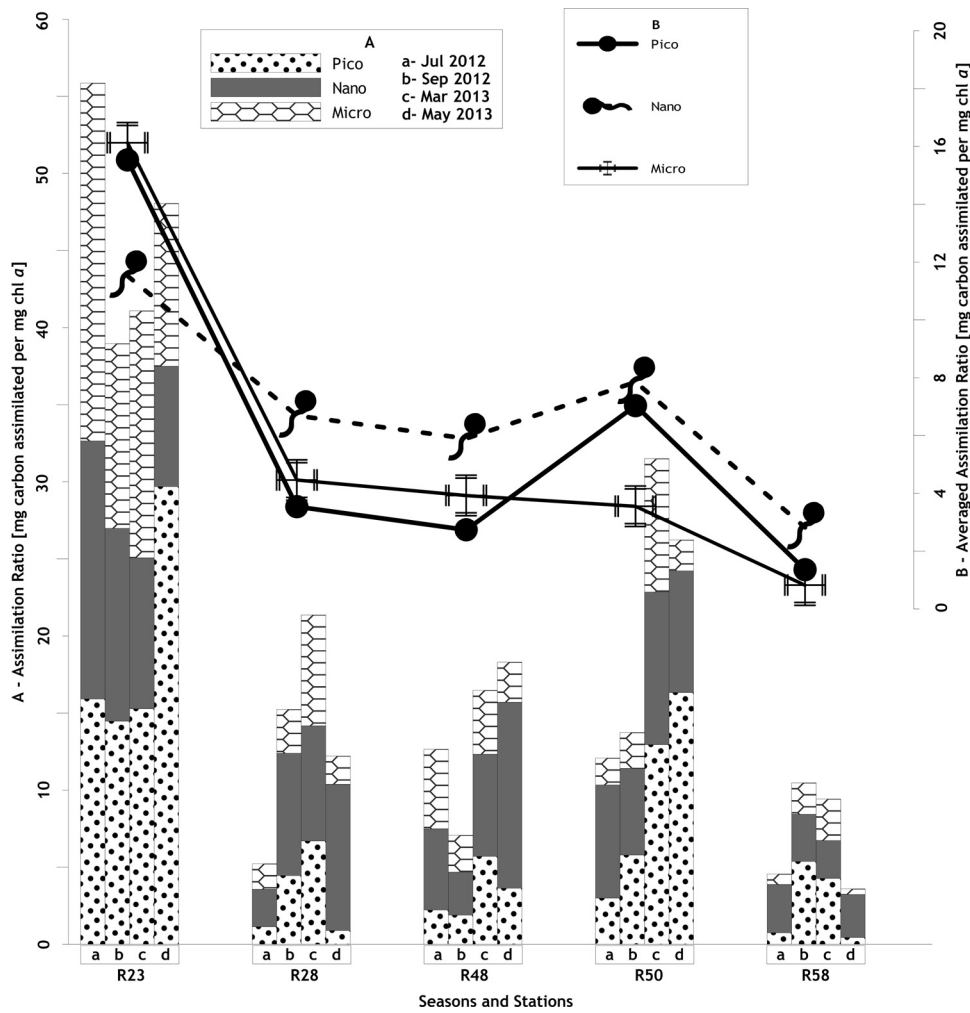


Figure 9 Distribution of seasonal (A) and mean (B) assimilation ratios at the stations.

nutrient intrusions below the EZ (less than Rhodes Gyre). Moreover, the contribution of microplankton to DICHL increased from eastern part of the offshore waters to the WCE and Rhodes Gyre, where EZ layer-averaged nutrient concentration increased along the transect, while it was not observed in DIPP. Small nanoplankton was the least contributor in DICHL and DIPP in the northern Levantine Sea during the study period.

The physiological state of an individual cell can be different according to the stages of a bloom in different marine ecosystems (Falkowski and Raven, 2007). Although chlorophyll defines the size of the standing stock, PP just indicates the carbon assimilation capacity of the flora. High level of chlorophyll does not necessarily correspond to high PP or physiological activity, as it is dependent on the stage of the bloom. Moreover, there is no linear relationship between chlorophyll and carbon assimilation capacity due to the complex effects of light, temperature and nutrient on phytoplankton physiology (Wang et al., 2009).

In the northern Levantine Sea, assimilation ratio (AR: mg carbon assimilated per mg chl a) was calculated at the lowest (1.3) for Rhodes Gyre (St. R58) and the highest (14.6) for coastal waters (St. R23) (Fig. 9). Assimilation ratio (6) was found higher than other offshore stations at St. R50, which also had higher production capacity due to the relatively

higher nutrient concentrations in comparison with other offshore stations. St. R50 was in the center of the cyclonic West Cyprus eddy, which transfers nutrients from the aphotic layer to the EZ and may stimulate productivity. Phytoplankton in the Rhodes Gyre were found to be the least active (low PP, low nutrient concentrations and high chlorophyll [LNHC] in the periphery of the gyre where the nutrients were quickly utilized and converted to biomass by phytoplankton) compared to other stations. As expected, assimilation ratios of picoplankton were not found to be the highest, as it was seen in DICHL and DIPP at all the stations (Fig. 9). Although picoplankton assimilate carbon more efficiently than nanoplankton and microplankton (Finkel et al., 2005), their lifespan may be shorter than the decomposition duration of chlorophyll content. Though the contribution of small nanoplankton to PP ($<0.024 \text{ mg C m}^{-3} \text{ h}^{-1}$) and chlorophyll ($<0.055 \text{ mg m}^{-3}$) was minor, they were observed to be the most active group in the northern Levantine Sea. Nanoplankton comprises different trophic types of groups (mixotrophic, heterotrophic, and phototrophic) in the aquatic ecosystem (Riemann et al., 1995). A mixotrophic nanoplankton may have a better carbon assimilation ratio with low chlorophyll high production capacity in the eastern Mediterranean. This could be one way of expressing their high assimilation ratio in the oligotrophic offshore waters and cyclonic Rhodes Gyre.

5. Conclusions

In the northern Levantine Sea, the rate of primary production and phytoplankton species composition in the coastal and open sea are determined by the seasonally varying rates of river inflows, availability and inputs rates of nutrients by dry + wet atmospheric depositions, upwelling events and regenerated from slowly sinking detritus of nano + picoplankton produced in the EZ. Temperature varying seasonally between 16 and 29°C is also another important factor that regulates the success and composition of the pelagic flora. Picoplankton was the most dominant phytoplankton group in the northern Levantine Sea. High nutrient concentrations (nitrogen and silicate) trigger productivity of microplankton in the river-fed (with $\text{Si}/\text{NO}_3 + \text{NO}_2 < 1.0$) coastal waters during the rainy season (March) and in cyclonic Rhodes Gyre during the summer. Low N/P in the nutrient-depleted ($\text{NO}_3 + \text{NO}_2 < 0.15 \mu\text{M}$; $\text{PO}_4 < 0.03 \mu\text{M}$) euphotic zone indicated nitrogen and possibly P co-limitation in the northern Levantine Basin in July and September 2012 and May 2013. The seasonal averaged total primary production rates observed in coastal waters was 8–12 times higher than those observed in offshore waters and the Rhodes Gyre, respectively. However, the mean total Chl-*a* values display less spatial variability, ranging from 0.14 mg m^{-3} in the offshore waters to the levels of 0.34 mg m^{-3} in the more productive Levantine coastal waters and 0.31 mg m^{-3} in Rhodes Gyre.

Acknowledgements

I am grateful to Prof. Süleyman Tuğrul for providing Chl-*a* and nutrient data and Prof. Zahit Uysal and Dr. Valeria Ibellio for their suggestions and comments. I acknowledge Prof. Mehmet Cenk Haytaç for his help in English and Dr. Sedat Gündoğdu for his comments and help in statistical analysis. I would also like to thank Dr. Georgia Assimakopoulou for her corrections and crew of the RV *Bilim-2*. Financial support was provided by The Scientific and Technological Research Council of Turkey (TUBITAK) in framework of the 111Y023 project (Dynamics and bacterial and primary production potential of distinct ecosystems composed of upwelling regions, shelf and offshore waters in the eastern Mediterranean, reflections on higher trophic levels).

Appendix A. Supplementary data

Supplementary data associated with this article can be found, in the online version, at [doi:10.1016/j.oceano.2017.12.003](https://doi.org/10.1016/j.oceano.2017.12.003).

References

- Berman, T., Bronk, D.A., 2003. Dissolved organic nitrogen: a dynamic participant in aquatic ecosystems. *Aquat. Microb. Ecol.* 31, 279–305, <http://dx.doi.org/10.3354/ame031279>.
- Bronk, D.A., See, J.H., Bradley, P., Killberg, L., 2007. DON as a source of bioavailable nitrogen for phytoplankton. *Biogeosciences* 4, 283–296, <http://dx.doi.org/10.5194/bg-4-283-2007>.
- Ediger, D., Tuğrul, S., Yılmaz, A., 2005. Vertical profiles of particulate organic matter and its relationship with chlorophyll-*a* in the upper layer of northeastern Mediterranean. *J. Mar. Syst.* 55 (3–4), 311–326, <http://dx.doi.org/10.1016/j.jmarsys.2004.09.003>.
- Ediger, D., Yılmaz, A., 1996. Characteristics of deep chlorophyll maximum in the North-eastern Mediterranean with respect to environmental conditions. *J. Mar. Syst.* 9 (3–4), 291–303, [http://dx.doi.org/10.1016/S0924-7963\(96\)00044-9](http://dx.doi.org/10.1016/S0924-7963(96)00044-9).
- Egge, J.K., Asknes, D.L., 1992. Silicate as regulating nutrient in phytoplankton competition. *Mar. Ecol. -Prog. Ser.* 83, 281–289, <http://dx.doi.org/10.3354/meps083281>.
- Eker, E., Kideys, A.E., 2000. Weekly variations in phytoplankton community structure of a harbour in Mersin Bay (north-eastern Mediterranean). *Turk. J. Bot.* 24, 13–24.
- Eker-Develi, E., Kideys, A.E., Tuğrul, S., Yılmaz, D., Ediger, D., 2003. Phytoplankton dynamics in the Northeastern Mediterranean with respect to relative dust deposition. In: Yılmaz, A. (Ed.), *Proceedings of the Second International Conference on "Oceanography of the Eastern Mediterranean and Black Sea: Similarities and Differences of Two Interconnected Basins"*, 14–18 October 2002. METU Cultural and Convention Center, Tubitak Publ., Ankara, Turkey, 686–694, (in Turkish).
- Falkowski, P., Raven, J.A., 2007. *Aquatic Photosynthesis*, 2nd ed. Princeton Univ. Press, ISBN-13: 978-0691115511, 500 pp.
- Finkel, Z.V., Katz, M.E., Wright, J.D., Schofield, O.M.E., Falkowski, P.G., 2005. Climatically driven microevolutionary patterns in the size of marine diatoms over the Cenozoic. *Proc. Natl. Acad. Sci. U.S.A.* 102 (25), 8927–8932, <http://dx.doi.org/10.1073/pnas.0409907102>.
- Finkel, Z.V., Beardall, J., Flynn, K.J., Quigg, A., Rees, T.A.V., Raven, J.A., 2009. Phytoplankton in a changing world: cell size and elemental stoichiometry. *J. Plankton Res.* 32 (1), 119–137, <http://dx.doi.org/10.1093/plankt/fbp098>.
- Fogg, G.E., 1991. The phytoplanktonic ways of life. *New Phytol.* 118 (2), 191–232, <http://dx.doi.org/10.1111/j.1469-8137.1991.tb00974.x>.
- Ghiglione, J.F., Larcher, M., Lebaron, P., 2008. Spatial and temporal scales of variation in bacterioplankton community structure in the NW Mediterranean Sea. *Aquat. Microb. Ecol.* 40 (3), 229–240, <http://dx.doi.org/10.3354/ame040229>.
- Grasshoff, K., Ehrhardt, M., Kremling, K., 1983. *Methods of Seawater Analysis*. Verlag Chemie, Weinheim, 237 pp.
- Guerzoni, S., Chester, R., Dulac, F., Herut, B., Loye-Pilot, M.D., Measures, C., Migon, C., Molinaroli, E., Moulin, C., Rossini, P., Saydam, C., Soudine, A., Ziveri, P., 1999. The role of atmospheric deposition in the biogeochemistry of the Mediterranean Sea. *Prog. Oceanogr.* 44 (1–3), 147–190, [http://dx.doi.org/10.1016/S0079-6611\(99\)00024-5](http://dx.doi.org/10.1016/S0079-6611(99)00024-5).
- Herut, B., Zohary, T., Krom, M.D., Mantoura, R.F.C., Pitta, P., Psarra, S., Rassoulzadegan, F., Tanaka, T., Thingstad, T.F., 2005. Response of East Mediterranean surface water to Saharan dust: on-board microcosm experiment and field observations. *Deep-Sea Res. Pt. II* 52 (22–23), 3024–3040, <http://dx.doi.org/10.1016/j.dsr2.2005.09.003>.
- Karl, D., Letelier, R., Tupas, L., Dore, J., Christian, J., Hebel, D., 1997. The role of nitrogen fixation in biogeochemical cycling in the subtropical North Pacific Ocean. *Nature* 388 (6642), 533–538, <http://dx.doi.org/10.1038/41474>.
- Kideys, A.E., Ünsal, M., Bingel, F., 1989. Seasonal changes in net phytoplankton off Erdemli, northeastern Mediterranean, DOĞA. *Turk. J. Bot.* 13 (1), 45–54.
- Koçak, M., Kubilay, N., Tuğrul, S., Mihalopoulos, N., 2010. Atmospheric nutrient inputs to the northern Levantine basin from a long-term observation: sources and comparison with riverine inputs. *Biogeosciences* 7 (12), 4037–4050, <http://dx.doi.org/10.5194/bg-7-4037-2010>.
- Kress, N., Herut, B., 2001. Spatial and seasonal evolution of dissolved oxygen and nutrients in the Southern Levantine Basin (Eastern Mediterranean Sea): chemical characterisation of the water

- masses and inferences on the N:P ratios. *Deep-Sea Res. Pt. I* 48 (11), 2347–2372, [http://dx.doi.org/10.1016/S0967-0637\(01\)00022-X](http://dx.doi.org/10.1016/S0967-0637(01)00022-X).
- Krom, M.D., Emeis, K.C., Van Cappellen, P., 2010. Why is the Eastern Mediterranean phosphorus limited? *Prog. Oceanogr.* 85 (3–4), 236–244, <http://dx.doi.org/10.1016/j.pocean.2010.03.003>.
- Krom, M.D., Kress, N., Brenner, S., Gordon, L.I., 1991. Phosphorus limitation of primary productivity in the eastern Mediterranean. *Limnol. Oceanogr.* 36 (3), 424–432, <http://dx.doi.org/10.4319/lo.1991.36.3.0424>.
- Krom, M.D., Herut, B., Mantoura, R.F.C., 2004. Nutrient budget for the Eastern Mediterranean: implications for P limitation. *Limnol. Oceanogr.* 49 (5), 1582–1592, <http://dx.doi.org/10.4319/lo.2004.49.5.1582>.
- Krom, M.D., Woodward, E.M.S., Herut, B., Kress, N., Carbo, P., Mantoura, R.F.C., et al., 2005. Nutrient cycling in the south east Levantine basin of the Eastern Mediterranean: results from a phosphate starved system. *Deep-Sea Res. Pt. II* 52 (22–23), 2879–2896, <http://dx.doi.org/10.1016/j.dsr2.2005.08.009>.
- Li, W.K.W., Zohary, T., Yacobi, Y.Z., Wood, A.M., 1993. Ultraphytoplankton in the eastern Mediterranean Sea: towards deriving phytoplankton biomass from flow cytometric measurements of abundance, fluorescence and light scatter. *Mar. Ecol. -Prog. Ser.* 102, 79–87, <http://dx.doi.org/10.3354/meps102079>.
- Markaki, Z., Oikonomou, K., Kocak, M., Kouvarakis, G., Chaniotaki, A., Kubilay, N., Mihalopoulos, N., 2003. Atmospheric deposition of inorganic phosphorus in the Levantine Basin, eastern Mediterranean: spatial and temporal variability and its role in seawater productivity. *Limnol. Oceanogr.* 48 (4), 1557–1568, <http://dx.doi.org/10.4319/lo.2003.48.4.1557>.
- Moore, L.R., Post, A.E., Rocap, G., Chisholm, S.W., 2002. Utilization of different nitrogen sources by the marine cyanobacteria *Prochlorococcus* and *Synechococcus*. *Limnol. Oceanogr.* 47 (4), 989–996, <http://dx.doi.org/10.4319/lo.2002.47.4.0989>.
- Moutin, T., Thingstad, T.F., Wambeke, F.V., Marie, D., Raimbault, P., Slawyk, G., Claustre, H., 2002. Does competition for nanomolar phosphate supply explain the predominance of the cyanobacterium *Synechococcus*? *Limnol. Oceanogr.* 47 (5), 1562–1567, <http://dx.doi.org/10.4319/lo.2002.47.5.1562>.
- Oksanen, J., Blanchet, F.G., Kindt, R., Legendre, P., Minchin, P.R., O'Hara, R.B., Simpson, G.L., Solymos, P., Stevens, M.H.H., Wagner, H., 2012. *Vegan: Community Ecology Package*, Version 2.0-4, <http://cran.r-project.org/web/packages/vegan/index.html>.
- O'Reilly, E.J., Zetlin, C., 1998. *Seasonal, horizontal and vertical distribution of phytoplankton chlorophyll Northeast US continental shelf ecosystems*. Report NMFS 139. A Tech. Rep. the Fishery Bulletin. U.S. Department of Commerce, Seattle, WA, 126 pp.
- Pantoja, S., Repeta, D.J., Sachs, J.P., Sigman, D.M., 2002. Stable isotope constraints on the nitrogen cycle of the Mediterranean Sea water column. *Deep Sea Res. Pt. I* 49 (9), 1609–1621, [http://dx.doi.org/10.1016/S0967-0637\(02\)00066-3](http://dx.doi.org/10.1016/S0967-0637(02)00066-3).
- Polat, S., Avcı, D., Işık, O., Çiçek, E., 2000. Interrelationships between phytoplankton abundance and physico-chemical parameters in Yumurtalık Bight, northeastern Mediterranean. *J. Fish. Aquat. Sci.* 17 (3–4), 129–142, <http://www.egejfas.org/download/article-file/57255>.
- Psarra, S., Zohary, T., Krom, M.D., Mantoura, R.F.C., Polychronaki, T., Stambler, N., Tanaka, T., et al., 2005. Phytoplankton response to a Lagrangian phosphate addition in the Levantine Sea (Eastern Mediterranean). *Deep Sea Res. Pt. II* 52 (22–23), 2944–2960, <http://dx.doi.org/10.1016/j.dsr2.2005.08.015>.
- R Core Team, 2012. *R: A Language and Environment for Statistical Computing*. R Foundation for Statistical Computing, Vienna, <https://www.gbif.org/tool/81287/r-a-language-and-environment-for-statistical-computing>.
- Riemann, B., Havskum, H., Thingstad, F., Bernard, C., 1995. The role of mixotrophy in pelagic environments. In: Joint, I. (Ed.), *NATO AS1 Series, Molecular Ecology of Aquatic Microbes*, vol. 38. Springer-Verlag, Berlin, 87–114, http://dx.doi.org/10.1007/978-3-642-79923-5_6.
- Romero, E., Peters, F., Guadayol, Ò., 2013. The interplay between mild physicochemical forcing and plankton dynamics in a coastal area. *Limnol. Oceanogr.* 58 (3), 903–920, <http://dx.doi.org/10.4319/lo.2013.58.3.0903>.
- Roussenov, V., Williams, R.G., Mahaffey, C., Wolff, G.A., 2006. Does the transport of dissolved organic nutrients affect export production in the Atlantic Ocean? *Glob. Biogeochem. Cy.* 20, GB3002, <http://dx.doi.org/10.1029/2005GB002510>.
- Siokou-Frangou, I., Christaki, U., Mazzocchi, M.G., Montresor, M., Ribera d'Alcalá, M., Vaqué, D., Zingone, A., 2010. Plankton in the open Mediterranean Sea: a review. *Biogeosciences* 7 (5), 1543–1586, <http://dx.doi.org/10.5194/bg-7-1543-2010>.
- Stemann Nielsen, E., 1952. The use of radioactive carbon (C14) for measuring organic production in the sea. *ICES J. Mar. Sci.* 18 (2), 117–140, <http://dx.doi.org/10.1093/icesjms/18.2.117>.
- Strickland, J.D.H., Parsons, T.R., 1972. *A practical handbook of seawater analysis*. *Bull. Fish. Res. Board. Can.* 167, 1–130.
- Thingstad, T.F., Krom, M.D., Mantoura, R.F.C., Flaten, G.A.F., Groom, S., Herut, B., Kress, N., Law, S.C., Pasternak, A., Pitta, P., Psarra, S., Rassoulzadegan, F., Tanaka, T., Tselipides, A., Wassmann, P., Woodward, E.M.S., Wexels Riser, C., Zodiatis, G., Zohary, T., 2005. Nature of phosphorus limitation in the ultraoligotrophic eastern Mediterranean. *Science* 309 (5737), 1068–1071, <http://dx.doi.org/10.1126/science.1112632>.
- Tugrul, S., Yucel, N., Akçay, I., 2016. Chemical oceanography of the northeastern Mediterranean. In: Turan, C., Salihoğlu, B., Özgür-Özbek, E., Öztürk, B. (Eds.), *The Turkish Part of Mediterranean Sea Marine Biodiversity, Fisheries Conservation and Governance*. Turkish Marine Research Foundation (TUDAV), Istanbul, 15–29. http://www.tudav.org/images/2016/documents/MEDITERRANEAN_SEA_2016.pdf.
- Torres-Valdes, S., Roussenov, V.M., Sanders, R., Reynolds, S., Pan, S., Mather, R., Landolfi, A., Wolff, G.A., Achterberg, E.P., Williams, R.G., 2009. Distribution of dissolved organic nutrients and their effect on export production over the Atlantic Ocean. *Glob. Biogeochem. Cycles* 23 (4), GB4019, <http://dx.doi.org/10.1029/2008GB003389>.
- Uysal, Z., Senichkina, L., Kuzmenko, L., Georgieva, L., Altukhov, D., 2003. *Weekly changes in phytoplankton species composition, diversity, abundance, and biomass across the northern Levantine basin shelf waters*. In: Yılmaz, A. (Ed.), *Proceedings of the Second International Conference on "Oceanography of the Eastern Mediterranean and Black Sea: Similarities and Differences of Two Interconnected Basins, 14–18 October 2002*. METU Cultural and Convention Center, Tubitak Publ, Ankara, 680–686, (in Turkish).
- Uysal, Z., Yıldız, Y.Ç., Tuğrul, S., 2004. *Levantine baseni pikoplankton (heterotrofik bakteri ve cyanobakteri) içerik ve dinamikleri*. Tubitak Publ, Ankara, 67 pp.
- Uysal, Z., 2006. Vertical distribution of marine cyanobacteria *Synechococcus* spp. in the Black, Marmara, Aegean, and eastern Mediterranean seas. *Deep Sea Res. 2 Top. Stud. Oceanogr.* 53 (17–19), 1976–1987, <http://dx.doi.org/10.1016/j.dsr2.2006.03.016>.
- Uysal, Z., Latif, M.A., Özsoy, E., Tuğrul, S., Kubilay, N., Beşiktepe, Ş. T., Yemenicioğlu, S., Mutlu, E., Ediger, D., Beşiktepe, Ş., Ediger, V., Ak Örek, Y., Örek, H., Demirel, M., Tunç, Ş.Ç., Terbiyik, T., 2008. *Kilikya Baseni Kıyosal Ekosisteminde Dolaşım. Taşınım ve Ötrofikasyon Araştırmaları Projesi No: 104Y277*. Erdemli-Mersin.
- Uysal, Z., Köksalan, İ., 2010. *Synechococcus* dynamics in the Levantine basin shelf waters (northeastern Mediterranean). *Mediterr. Mar. Sci.* 11 (2), 277–294, <http://dx.doi.org/10.12681/mms.77>.
- Uysal, Z., Köksalan, İ., 2017. Short term temporal and spatial fluctuations in marine cyanobacterium *Synechococcus* abundance in oligotrophic deep shelf water (northeastern Mediterranean). *Fresenius Environ. Bull.* 26 (8), 5115–5124.
- Wang, X.J., Behrenfeld, M., Le Borgne, R., Murtugudde, R., Boss, E., 2009. Regulation of phytoplankton carbon to chlorophyll ratio by

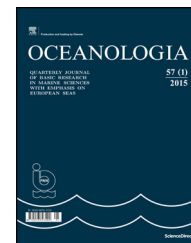
- light, nutrients and temperature in the Equatorial Pacific Ocean: a basin-scale model. *Biogeosciences* 6, 391–404, <http://dx.doi.org/10.5194/bg-6-391-2009>.
- Yayla, M.K., 1999. Primary Production, Availability and Uptake of Nutrients and Photo-Adaptation of Phytoplankton in The Black Sea, The Sea of Marmara and the Eastern Mediterranean. (M.Sc. thesis). Institute of Marine Science, Middle East Technical Univ, Mersin, Turkey, 128 pp.
- Yılmaz, A., Tugrul, S., 1998. The effect of cold- and warm-core eddies on the distribution and stoichiometry of dissolved nutrients in the Northeastern Mediterranean. *J. Mar. Syst.* 16 (3–4), 253–268, [http://dx.doi.org/10.1016/s0924-7963\(97\)00022-5](http://dx.doi.org/10.1016/s0924-7963(97)00022-5).
- Yılmaz, D., 2006. Temporal Variation of Phytoplankton in the North-eastern Shelf of Mediterranean Sea: Composition, Pigment Signature and Production. (Ph.D. thesis). Institute of Marine Science, Middle East Technical Univ, Mersin, Turkey, 165 pp.
- Yucel, N., 2008. Phytoplankton Pigment Distribution in the Cilician Basin (Northeastern Mediterranean). (M.Sc. thesis). Institute of Marine Science, Middle East Tech. Univ, Mersin, Turkey, 175 pp.
- Yucel, N., 2013. Monthly Changes in Primary and Bacterial Productivity in the North-Eastern Mediterranean Shelf Waters. (Ph.D. thesis). Institute of Marine Science, Middle East Tech. Univ, Mersin, Turkey, 179 pp., <http://etd.lib.metu.edu.tr/upload/12616125/index.pdf>.
- Yucel, N., 2017. Seasonal and spatial variation of bacterial production and abundance in the northern Levantine Sea. *Mediterr. Mar. Sci.* 18 (1), 97–106, <http://dx.doi.org/10.12681/mms.1627>.
- Yucel, N., Uysal, Z., Tugrul, S., 2017. Variability in phytoplankton pigment composition in Mersin Bay. *Turk. J. Aquat. Sci.* 32 (1), 49–70, <http://dx.doi.org/10.18864/tjas201705>.



Available online at www.sciencedirect.com

ScienceDirect

journal homepage: www.journals.elsevier.com/oceanologia/



ORIGINAL RESEARCH ARTICLE

Stokes transport in layers in the water column based on long-term wind statistics

Dag Myrhaug*, Hong Wang, Lars Erik Holmedal

Norwegian University of Science and Technology (NTNU) Trondheim, Norway

Received 6 October 2017; accepted 19 December 2017

Available online 3 February 2018

KEYWORDS

Marine litter;
Random surface gravity waves;
Stokes transport velocity;
Wind statistics

Summary This paper addresses the Stokes transport velocity for deep water random waves in given layers in the water column based on wind statistics, which can be estimated by the simple analytical tool provided here. Results are exemplified by using the Phillips and Pierson-Moskowitz model wave spectra together with long-term wind statistics from one location in the northern North Sea and from four locations in the North Atlantic. The results are relevant for e.g. assessing the drift of marine litter in the ocean based on, for example, global wind statistics.

© 2018 Institute of Oceanology of the Polish Academy of Sciences. Production and hosting by Elsevier Sp. z o.o. This is an open access article under the CC BY-NC-ND license (<http://creativecommons.org/licenses/by-nc-nd/4.0/>).

1. Introduction

There has recently been much focus on the environmental issues related to plastic litter in the oceans; see e.g. [van Sebille et al. \(2015\)](#), [Sherman and van Sebille \(2016\)](#), [Keswani et al. \(2016\)](#), [Brennecke et al. \(2016\)](#), [Avio et al. \(2017\)](#); also documenting that plastic litter occurs in different layers in the water column beneath the ocean surface. One impor-

tant constituent of ocean circulation models is the Stokes drift which contributes to the transport of plastic as well as microplastic located in different layers in the water column. The wave-average of the water particle trajectory in the wave propagation direction gives the Lagrangian velocity referred to as the Stokes drift, while the volume Stokes transport is obtained as the integral over the water depth of the Stokes drift ([Raschle et al., 2008](#)). The general background and further details of the Stokes drift are given in e.g. [Dean and Dalrymple \(1984\)](#). [Myrhaug et al. \(2016\)](#) gives a brief review of the literature up to that date (see the references therein). More recent works include those of [Brevik et al. \(2016\)](#), [Li et al. \(2017\)](#) and [Myrhaug \(2017\)](#).

The purpose of the present analytical study is to provide a simple analytical tool which yields estimates of the Stokes transport velocity for deep water random waves in given layers in the water column based on wind statistics. The Stokes transport velocity is obtained by integrating the Stokes drift between two elevations in the water column

* Corresponding author at: Department of Marine Technology, Otto Nielsens vei 10, NO-7491 Trondheim, Norway. Tel.: +47 73 59 55 27; fax: +47 73 59 55 28.

E-mail address: dag.myrhaug@ntnu.no (D. Myrhaug).

Peer review under the responsibility of Institute of Oceanology of the Polish Academy of Sciences.



and dividing by the distance between these two elevations. Results are exemplified by using the two model wave spectra by Phillips and Pierson-Moskowitz together with long-term wind statistics from one location in the northern North Sea and from four locations in the North Atlantic. The present results are relevant for estimating the drift of e.g. marine litter in the ocean based on global wind statistics.

2. Theoretical background

Based on classical potential wave theory the time-averaged Lagrangian drift at a z -level in the water column in a water depth d is (Dean and Dalrymple, 1984):

$$\bar{u}_L(z) = \frac{ga^2k^2}{\omega} \frac{\cosh 2k(z+d)}{\sinh 2kd}, \quad (1)$$

where g is the acceleration of gravity, a is the linear wave amplitude, and k is the wave number related to the cyclic wave frequency ω by the dispersion relationship

$$\omega^2 = gk \tanh kd. \quad (2)$$

According to Eq. (1) the drift of the water particles is in the direction of the wave propagation; the maximum is at the mean free surface $z = 0$, and decreases rapidly towards the sea bed as $z \rightarrow -d$ (z is positive upwards). This drift velocity is commonly referred to as Stokes drift.

When assessing the transport of material in the water column the drift velocity associated with the Stokes transport in different layers of the water column is a quantity of interest. This drift velocity is obtained by integrating Eq. (1) between two levels $z = -h_2$ and $z = -h_1$ in the water column and divided by the distance between these two levels $\Delta h = h_2 - h_1$, given as

$$v = \frac{1}{\Delta h} \int_{-h_2}^{-h_1} \bar{u}_L(z) dz = \frac{ga^2k}{2\omega} \times \frac{\sinh[2kd(1-h_1/d)] - \sinh[2kd(1-h_2/d)]}{\Delta h \cdot \sinh(2kd)}. \quad (3)$$

In deep water (i.e. for large kd and thus $\omega^2 = gk$ from Eq. (2)) the Stokes transport velocity in Eq. (3) reduces to

$$v = \frac{a^2\omega}{2\Delta h} \left(e^{-2(\omega^2/g)h_1} - e^{-2(\omega^2/g)h_2} \right). \quad (4)$$

If an individual random wave with amplitude a_n and cyclic wave frequency ω_n is considered, then the Stokes transport velocity for individual random waves in deep water is given as

$$v_n = \frac{1}{2} a_n^2 \omega_n \frac{1}{\Delta h} \left(e^{-2(\omega_n^2/g)h_1} - e^{-2(\omega_n^2/g)h_2} \right). \quad (5)$$

The wave amplitude is obtained from the wave spectrum $S(\omega)$ as $a_n^2 = 2S(\omega_n)\Delta\omega$ where $\Delta\omega$ is a constant separation between frequencies. By substituting this in Eq. (5) and considering an infinite number of wave components, the total Stokes transport velocity within a sea state of random waves is obtained as

$$V = \frac{1}{\Delta h} \int_0^\infty \omega S(\omega) \left(e^{-2(\omega^2/g)h_1} - e^{-2(\omega^2/g)h_2} \right) d\omega. \quad (6)$$

The two terms in the parenthesis of Eq. (6) represent the attenuation of the wave motion in the water column, which here is approximated by taking ω as the spectral peak frequency ω_p . As a result Eq. (6) becomes

$$V = \frac{1}{\Delta h} \left(e^{-2(\omega_p^2/g)h_1} - e^{-2(\omega_p^2/g)h_2} \right) m_1, \quad (7)$$

where m_1 is the first spectral moment obtained from the definition of the n th spectral moment

$$m_n = \int_0^\infty \omega^n S(\omega) d\omega; \quad n = 0, 1, 2, \dots \quad (8)$$

By combining Eq. (7) with the spectral mean period $T_1 = 2\pi m_0/m_1$, the significant wave height $H_s = 4\sqrt{m_0}$, and that there is a relationship between T_1 and the spectral peak period $T_p = 2\pi/\omega_p$, i.e. $T_1 = \gamma_1 T_p$, Eq. (7) is rearranged to

$$V = \frac{1}{\Delta h} \left(e^{-2(\omega_p^2/g)h_1} - e^{-2(\omega_p^2/g)h_2} \right) \frac{\pi H_s^2}{8\gamma_1 T_p}. \quad (9)$$

Thus, V is defined in terms of the sea state parameters H_s and T_p in deep water.

3. Example of results for two standard wave spectra and long-term wind statistics

Two standard deep water wave spectra are chosen; the Phillips and the Pierson-Moskowitz spectra, which both have been used frequently in contexts discussing the Stokes drift, e.g. see Li et al. (2017) and the references therein. The Phillips spectrum was also used by exemplifying results in Myrhaug et al. (2014, 2016) and in Myrhaug (2017), where the latter reference presented the surface Stokes drift and the Stokes transport using long-term wind statistics from the northern North Sea location used here, and from one location on the northwest Shelf of Australia.

3.1. Phillips and Pierson-Moskowitz spectra

The Phillips spectrum is (Tucker and Pitt, 2001)

$$S(\omega) = \alpha \frac{g^2}{\omega^5}, \quad \omega \geq \omega_p = \frac{g}{U_{10}}, \quad (10)$$

where $\alpha = 0.0081$ is the Phillips constant, and U_{10} is the mean wind speed at the 10 m elevation above the sea surface. By using the definition of the spectral moments in Eq. (8), it follows that

$$H_s = 4\sqrt{m_0} = \frac{2\sqrt{\alpha}}{g} U_{10}^2, \quad (11)$$

$$\gamma_1 = \frac{T_1}{T_p} = \frac{2\pi m_0}{T_p m_1} = \frac{3}{4}, \quad (12)$$

$$T_p = \frac{2\pi}{\omega_p} = \frac{2\pi}{g} U_{10}. \quad (13)$$

Furthermore, the wave length corresponding to the spectral peak period, $\lambda_p = 2\pi/k_p$, is obtained from $\omega_p^2 = gk_p$ as

$$\lambda_p = \frac{g}{2\pi} T_p^2 = \frac{2\pi}{g} U_{10}^2. \quad (14)$$

The results in the following are given for $h_1 = 0$ and $h_2 = \lambda_p/s$ where $s \geq 2$, i.e. the Stokes transport velocity corresponds to the mean drift velocity over a fraction of the wave length beneath the surface downwards in the water column. For $s = 2$ the result represents the mean drift velocity over the whole water column since the wave motion in deep water penetrates down to about half the wave length. Thus, by taking $h_1 = 0$, $h_2 = \lambda_p/s$ and substituting Eqs. (11)–(14) in Eq. (9), Eq. (9) is given in terms of U_{10} as

$$V_{Ph} = \frac{S\alpha}{6\pi} (1 - e^{-4\pi/s}) U_{10} = 0.000430s(1 - e^{-4\pi/s}) U_{10}; s \geq 2. \quad (15)$$

The Pierson-Moskowitz (PM) spectrum with U_{10} as the parameter is (Tucker and Pitt, 2001)

$$S(\omega) = \alpha \frac{g^2}{\omega^5} \exp\left(-1.25 \frac{\omega_p^4}{\omega^4}\right), \quad (16)$$

where

$$\omega_p = \frac{2\pi}{T_p}; T_p = 0.785U_{10}, \quad (17)$$

$$H_s = 0.0246U_{10}^2, \quad (18)$$

$$T_1 = 0.606U_{10}, \quad (19)$$

$$\gamma_1 = \frac{T_1}{T_p} = 0.772, \quad (20)$$

$$\lambda_p = \frac{g}{2\pi} T_p^2 = 0.962U_{10}^2. \quad (21)$$

It should be noted that the PM spectrum was originally given with the mean wind speed at the 19.5 m elevation above the sea surface as the parameter, while the present formulation is based on taking $U_{10} = 0.93U_{19.5}$ (Tucker and Pitt, 2001). Then, by substituting these relationships in Eq. (9) the result is

$$V_{PM} = 0.000407s(1 - e^{-4\pi/s}) U_{10}; s \geq 2. \quad (22)$$

Thus it appears that V_{PM} is slightly smaller than V_{Ph} , i.e. the ratio is

$$\frac{V_{PM}}{V_{Ph}} = 0.947. \quad (23)$$

Fig. 1 shows examples of the Phillips and PM spectra for $U_{10} = 10 \text{ m s}^{-1}$ and Fig. 2 shows V/U_{10} versus s for s in the range 2–32 for the two spectra. For both spectra it appears that the ratio increases as s increases, i.e. the mean transport increases as the thickness of the layer decreases, giving ratios in the range 0.1 to about 0.5 percent. For $U_{10} = 10 \text{ m s}^{-1}$ this gives $\lambda_p = 64.0 \text{ m}$ (Eq. (14)) for the Phillips spectrum and $\lambda_p = 96.2 \text{ m}$ (Eq. (21)) for the PM spectrum. Thus, for s in the range 2–32, the Stokes transport velocity corresponds to the mean values over intervals from 32 m down to 2 m, respectively, for the Phillips spectrum, and over intervals from 48 m down to 3 m, respectively, for the PM spectrum.

Fig. 3 shows the corresponding results as those in Fig. 2 for the volume Stokes transport per crest length over different heights in the water column, i.e. $M = V\lambda_p/s$ versus s . For both spectra it appears that M decreases as s increases, i.e. the mean transport over a height in the water column beneath the surface decreases as the thickness of the layer decreases. As for the example discussed in Fig. 2, this means that for s in the range 2–32 the values

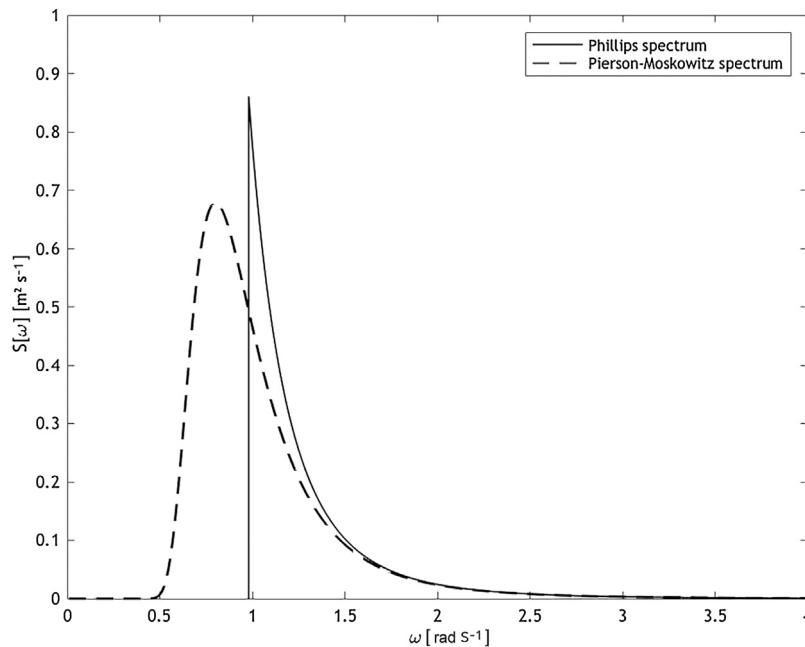


Figure 1 Phillips spectrum and Pierson-Moskowitz spectrum for $U_{10} = 10 \text{ m s}^{-1}$.

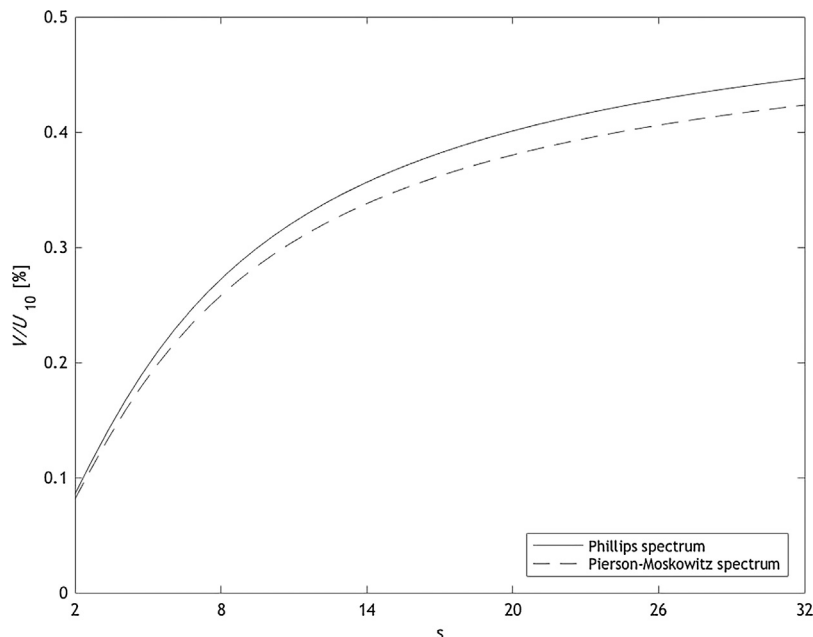


Figure 2 V/U_{10} versus s : Phillips spectrum, Eq. (15); Pierson-Moskowitz spectrum, Eq. (22).

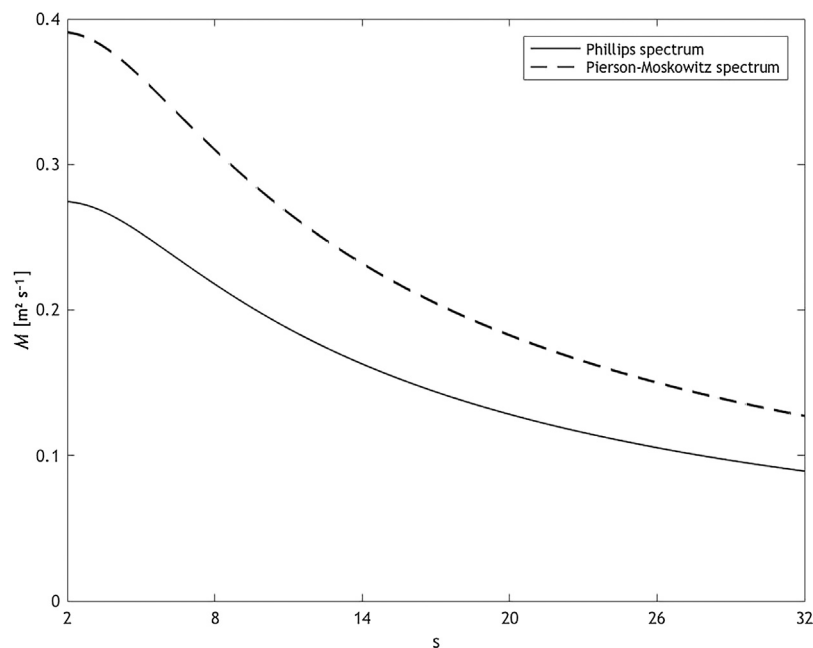


Figure 3 $M = V\lambda_p/s$ versus s corresponding to the results in Fig. 2 for the Phillips spectrum and the Pierson-Moskowitz spectrum.

of M correspond to the values over heights in the water column from 32 m below the surface to 2 m below the surface, respectively, taking the values from $0.27 \text{ m}^2 \text{ s}^{-1}$ to $0.09 \text{ m}^2 \text{ s}^{-1}$, respectively, for the Phillips spectrum. For the PM spectrum the M values are a factor 1.422 larger than those for the Phillips spectrum, taking the values $0.38\text{--}0.13 \text{ m}^2 \text{ s}^{-1}$ corresponding to the heights in the water column from 48 m below the surface to 3 m below the

surface, respectively. The reason for these larger PM spectrum values is that the value of λ_p for PM is a factor 1.502 larger than that for the Phillips spectrum, i.e. due to the lower frequencies present in the PM spectrum (see Fig. 1). By considering e.g. near neutrally buoyant litter, this means that M is the volume transport (of the litter) per crest length over the given height in the water column beneath the surface due to the wave-induced drift.

3.2. Long-term wind statistics

Results for V can be obtained from available wind statistics for an ocean area, e.g. from a long-term distribution of U_{10} (see Bitner-Gregersen (2015) for a review of different parametric models for the cumulative distribution function (*cdf*) or the probability density function (*pdf*) of U_{10}). In the present examples the long-term statistics of V are exemplified by using five *cdfs* of U_{10} . First, the *cdf* of U_{10} given by Johannessen et al. (2001) is used; based on 1 hourly values of U_{10} from wind measurements covering the years (1973–1999) from the northern North Sea (NNS). Second, four *cdfs* of U_{10} given by Mao and Rychlik (2017) are used, based on estimation of Weibull *cdfs* for wind speeds along ship routes in the North Atlantic (NA) fitted to 10 years of wind speed data. The results are given for the following four locations in the North Atlantic; 20°W 60°N, 10°W 40°N, 40°W 50°N, 20°W 45°N. All these *cdfs* of U_{10} are described by the two-parameter Weibull model

$$P(U_{10}) = 1 - \exp\left[-\left(\frac{U_{10}}{\theta}\right)^\beta\right]; \quad U_{10} \geq 0, \quad (24)$$

with the Weibull parameters given in Table 1.

3.3. Statistical properties of Stokes transport velocity

Now the long-term statistics of V can be derived by using the distribution of U_{10} given in Eq. (24) and Table 1. Statistical quantities of interest are e.g. the expected (mean) value of V , $E[V]$, and the variance of V , $Var[V]$, which are proportional to $E[U_{10}]$ and $Var[U_{10}]$, respectively. This requires calculation of $E[U_{10}^n]$, which for a two-parameter Weibull distributed quantity is given by (Bury, 1975)

$$E[U_{10}^n] = \theta^n \Gamma\left(1 + \frac{n}{\beta}\right), \quad (25)$$

where Γ is the gamma function. Furthermore (Bury, 1975)

$$Var[U_{10}^n] = E[U_{10}^{2n}] - (E[U_{10}^n])^2. \quad (26)$$

The results for $E[V]$ and the ratio between the standard deviation of $V (= \sqrt{Var[V]})$ and $E[V]$ (std.dev./m.v.) are given in Table 2. It should be noted that this standard deviation to mean value ratios are the same as for U_{10} . For the Phillips spectrum it appears that $E[V]$ is 0.00645 m s^{-1} (NNS) and in the range 0.00540 m s^{-1} to 0.00840 m s^{-1} (NA), where the latter value refers to the location 40°W 50°N. The values corresponding to the PM spectrum are also given, i.e. obtained by multiplying the Phillips spectrum values by a factor 0.947 (see Eq. (23)). It is also noted that the standard deviation to mean value ratios are large, i.e. in the range 43–60%.

Similarly, a characteristic value of λ_p , i.e. $E[\lambda_p]$ for the Phillips spectrum is obtained from Eq. (14) as

$$E[\lambda_p] = \frac{2\pi}{g} E[U_{10}^2], \quad (27)$$

and for the PM spectrum from Eq. (21) as

$$E[\lambda_p] = 0.962 E[U_{10}^2]. \quad (28)$$

The results are given in Table 2, showing that $E[\lambda_p]$ is in the range from about 31 m to about 73 m for the Phillips spectrum, and in the range from about 46 m to about 109 m for the PM spectrum.

A quantity of interest is the volume Stokes transport per crest length. Table 2 gives the values of $M = E[V] \cdot E[\lambda_p]/2$, i.e. the volume Stokes transport per crest length over the whole water column where there is wave activity, since the wave motion goes down to about half the wave length. For the Phillips spectrum it appears that M is $0.159 \text{ m}^2 \text{ s}^{-1}$ (NNS)

Table 1 Weibull parameters for U_{10} (see Eq. (24)) and results for $E[U_{10}]$.

North Atlantic (NA) location	θ [m s^{-1}]	β	$E[U_{10}]$ [m s^{-1}]
20°W 60°N	10.99	2.46	9.75
10°W 40°N	7.11	2.30	6.30
40°W 50°N	11.04	2.48	9.79
20°W 45°N	9.32	2.47	8.27
Northern North Sea (NNS)	8.426	1.708	7.52

Table 2 Example of results using wind statistics from the Northern North Sea (NNS) and the North Atlantic (NA), see Table 1. Results corresponding to Ph = Phillips spectrum; PM = Pierson-Moskowitz spectrum.

Distribution	$E[V]$ [m s^{-1}] Ph/PM	St.dev/m.v.	$E[\lambda_p]$ [m] Ph/PM	$M = E[V] \times E[\lambda_p]/2$ [$\text{m}^2 \text{ s}^{-1}$] Ph/PM
NA, location				
20°W 60°N	0.00836/0.00792	0.43	72.3/108.6	0.302/0.430
10°W 40°N	0.00540/0.00511	0.46	30.8/46.3	0.083/0.118
40°W 50°N	0.00840/0.00795	0.43	72.8/109.3	0.306/0.436
20°W 45°N	0.00709/0.00671	0.43	51.9/78.0	0.184/0.262
NNS	0.00645/0.00611	0.60	49.3/74.0	0.159/0.226

and in the range $0.083 \text{ m}^2 \text{ s}^{-1}$ to $0.306 \text{ m}^2 \text{ s}^{-1}$ (NA), where the latter value refers to the location $40^\circ\text{W } 50^\circ\text{N}$; for the PM spectrum the values are a factor 1.422 larger. Thus, these example calculations show that the mean value of the Stokes transport in the North Atlantic is up to a factor of about two larger than that in the northern North Sea. Furthermore, by taking the Phillips spectrum result for $M = 0.306 \text{ m}^2 \text{ s}^{-1}$ (NA) as an example, the mean volume Stokes transport \pm one standard deviation is 0.18 and $0.44 \text{ m}^2 \text{ s}^{-1}$, respectively, in the water column from the surface down to about 36 m. The corresponding intervals (i.e. the mean value \pm one standard deviation) of the volume Stokes transport for the water columns from the surface ($z = 0 \text{ m}$) to about $z = -18 \text{ m}$, $z = -9 \text{ m}$, $z = -4.5 \text{ m}$, $z = -2.3 \text{ m}$ are $(0.090, 0.22) \text{ m}^2 \text{ s}^{-1}$, $(0.045, 0.11) \text{ m}^2 \text{ s}^{-1}$, $(0.023, 0.055) \text{ m}^2 \text{ s}^{-1}$, $(0.011, 0.028) \text{ m}^2 \text{ s}^{-1}$, respectively. This is of direct relevance e.g. to the volume transport of near neutrally buoyant litter as discussed in Fig. 3.

To the authors' knowledge there are limited results from observations and models to compare with. However, according to Rasclé et al. (2008, Fig. 8) the surface Stokes drift U_S is about 1.3% of U_{10} in the open ocean. More specifically, in their Fig. 8 they also illustrated the variability of U_S/U_{10} , i.e. being in the range 0.4% to 1.7% for U_{10} in the range 6–10 m s^{-1} , i.e. corresponding to the range of $E[U_{10}]$ for the present data, see Table 1.

Following Webb and Fox-Kemper (2011), the unidirectional surface Stokes drift velocity within a sea state for random waves in deep water is given by

$$U_S = \frac{\pi^3 H_s^2}{g T_3^3}, \quad (29)$$

where $T_3 = 2\pi (m_0/m_3)^{1/3}$ is the wave period related to the surface Stokes drift velocity.

For the Phillips spectrum it follows that

$$T_3 = \frac{2^{1/3} \pi}{g} U_{10} = 0.403 U_{10}, \quad (30)$$

$$U_{Sph} = 2\alpha U_{10} = 0.0162 U_{10}. \quad (31)$$

For the PM spectrum (Tucker and Pitt, 2001)

$$m_n = \frac{1}{4} \alpha g^2 (1.25 \omega_p)^{n/4-1} \Gamma\left(1 - \frac{n}{4}\right). \quad (32)$$

Eq. (32) is valid for n smaller than 4, yielding $m_3 = 0.0835 U_{10}$, and thus

$$T_3 = 0.483 U_{10}, \quad (33)$$

$$U_{SPM} = 0.0170 U_{10}. \quad (34)$$

Then it follows that the ratio $E[U_S]/E[U_{10}] = U_S/U_{10}$ for both the Phillips spectrum (Eq. (31)) and the PM spectrum (Eq. (34)) is in the upper range of the results given in Rasclé et al. (2008, Fig. 8) referred to, i.e. in the range 0.4–1.7%. However, e.g. by taking into account the standard deviation of the results (see Table 2), $E[U_S]$ minus one standard deviation divided by $E[U_{10}]$ will be within a wider range of these values. Although this comparison only covers the surface Stokes drift velocity it should give some confidence to the

present results. However, further comparisons with observations or models for the Stokes drift in layers in the water column are also required to make firm conclusions regarding the validity of the results.

4. Conclusions

The main conclusions from this work are as follows:

1. By using the Phillips and Pierson-Moskowitz model wave spectra together with long-term wind statistics from one location in the northern North Sea and from four locations in the North Atlantic, example calculations show that the mean value of the Stokes transport in the North Atlantic is up to a factor of about two larger than that in the northern North Sea; the standard deviation to the mean value ratios are in the range 43–46% in the North Atlantic and 60% in the northern North Sea.
2. Agreement is also found between the present results and those by Rasclé et al. (2008) for the surface Stokes drift velocity.

Overall, the present method can be used to assess the Stokes transport velocity for deep water random waves within sea states based on global wind statistics, which is important to estimate further the drift of e.g. near neutrally buoyant marine litter in the oceans.

Acknowledgements

This work was carried out as part of the project “Air-Sea Interaction and Transport Mechanisms in the Ocean” funded by the Norwegian Research Council (221988). This support is gratefully acknowledged.

References

- Avio, C.G., Gorki, S., Regoli, F., 2017. Plastics and microplastics in the oceans: from engineering pollutants to emerged threat. *Mar. Environ. Res.* 128, 2–11, <http://dx.doi.org/10.1016/j.marenvres.2016.05.012>.
- Bitner-Gregersen, E.M., 2015. Joint met-ocean description for design and operations of marine structures. *Appl. Ocean Res.* 51, 279–292, <http://dx.doi.org/10.1016/j.apor.2015.01.007>.
- Breivik, Ø., Bidlot, J.-R., Janssen, A.E.M., 2016. A Stokes drift approximation based on the Phillips spectrum. *Ocean Model* 100, 49–56, <http://dx.doi.org/10.1016/j.ocemod.2016.01.005>.
- Brennecke, D., Duarte, B., Paiva, F., Cacador, I., Canning-Clode, J., 2016. Microplastics as vector for heavy metal contamination from the marine environment. *Estuar. Coast. Shelf Sci.* 178, 189–195, <http://dx.doi.org/10.1016/j.ecss.2015.12.003>.
- Bury, K.V., 1975. *Statistical Models in Applied Science*. John Wiley & Sons, New York, 646 pp.
- Dean, R.G., Dalrymple, R.A., 1984. *Water Wave Mechanics for Engineers and Scientists*. Prentice-Hall, Inc., New Jersey, USA, 353 pp.
- Johannessen, K., Meling, T.S., Haver, S., 2001. Joint distribution for wind and waves in the Northern North Sea. In: *Proc. 11th Int. Offshore and Polar Engineering Conf.*, vol. III, Stavanger, Norway, 19–28.
- Keswani, A., Oliver, D.M., Gutierrez, T., Quilliam, R.S., 2016. Microbial hitchhikers on marine plastic debris: human exposure risks at bathing water and beach environments. *Mar. Environ. Res.* 118, 10–19, <http://dx.doi.org/10.1016/j.marenvres.2016.04.006>.

- Li, Q., Fox-Kemper, B., Breivik, Ø., Webb, A., 2017. Statistical models of global Langmuir mixing. *Ocean Model* 113, 95–114, <http://dx.doi.org/10.1016/j.ocemod.2017.03.016>.
- Mao, W., Rychlik, I., 2017. Estimation of Weibull distribution for wind speeds along ship routes. *Proc. IMechE Pt. M: J. Eng. Maritime Environ.* 231 (2), 464–480, <http://dx.doi.org/10.1177/1475090216653495>.
- Myrhaug, D., 2017. Stokes drift estimation for sea states based on long-term variation of wind statistics. *Coast. Eng. J.* 59 (1), 175008, <http://dx.doi.org/10.1142/S0578563417500085>.
- Myrhaug, D., Wang, H., Holmedal, L.E., 2014. Stokes drift estimation for deep water waves based on short-term variation of wave conditions. *Coastal Eng.* 88, 27–32, <http://dx.doi.org/10.1016/j.coastaleng.2014.01.014>.
- Myrhaug, D., Wang, H., Holmedal, L.E., Leira, B.J., 2016. Effects of water depth and spectral bandwidth on Stokes drift estimation based on short-term variation of wave conditions. *Coastal Eng.* 114, 169–176, <http://dx.doi.org/10.1016/j.coastaleng.2016.04.001>.
- Rasclé, N., Ardhuin, F., Queffelec, P., Croizé-Fillon, D., 2008. A global wave parameter database for geophysical applications. Part 1: Wave-current-turbulence interaction parameters for the open ocean based on traditional parameterizations. *Ocean Model.* 25 (3–4), 154–171, <http://dx.doi.org/10.1016/j.ocemod.2008.07.006>.
- Sherman, P., van Sebille, E., 2016. Modelling marine surface microplastic transport to assess optimal removal locations. *Environ. Res. Lett.* 11 (1), 014006, <http://dx.doi.org/10.1088/1748-9326/11/1/014006>.
- Tucker, M.J., Pitt, E.G., 2001. *Waves in Ocean Engineering*. Elsevier, Amsterdam, 548 pp.
- van Sebille, E., Wilcox, Ch., Lebreton, L., Maximenko, N., Hardesty, B.D., van Franeker, J.A., Eriksen, M., Siegel, D., Galgani, F., Law, K.L., 2015. A global inventory of small floating plastic debris. *Environ. Res. Lett.* 10 (12), 124006, <http://dx.doi.org/10.1088/1748-9326/10/12/124006>.
- Webb, A., Fox-Kemper, B., 2011. Wave spectral moments and Stokes drift estimation. *Ocean Model.* 40, 273–288, <http://dx.doi.org/10.1016/j.ocemod.2011.08.007>.



Available online at www.sciencedirect.com

ScienceDirect

journal homepage: www.journals.elsevier.com/oceanologia/



ORIGINAL RESEARCH ARTICLE

Microbial enzymatic activity and its relation to organic matter abundance on sheltered and exposed beaches on the Polish coast

Aleksander M. Astel*, Katarzyna Bigus, Marcin Stec

Faculty of Mathematics and Natural Sciences, Pomeranian University, Słupsk, Poland

Received 30 June 2017; accepted 15 January 2018

Available online 3 February 2018

KEYWORDS

The Baltic Sea;
Coastal sediments;
Vertical depth;
The distance from the water line;
Nutrients;
Principal component analysis

Summary The activity of lipase, aminopeptidase, α -glucosidase, β -glucosidase was correlated and assessed according to an abundance of organic matter and total forms of nutrients in beach sediments characterized by different strength of anthropopressure and degree of sheltering. 76% of the data variance was explained by six factors identified by the use of principal component analysis: (1) anthropogenic rich in N, (2) microbial enzymatic activity, (3) labile organic matter, (4) bacterial growth, (5) anthropogenic rich in P and (6) hydrolytic. Differences in secondary bacterial production according to the distance from the water line, vertical cores and seasonality are limited by the accessibility of biochemical compounds (lipids, proteins, carbohydrates, total organic carbon), total phosphorus and nitrogen. Sediments collected in exposed beaches were not as rich in organic matter as these collected in sheltered ones due to the impact of sea waves of higher energy and backward current facilitating cleaning. The highest microbial enzymatic activity was observed in the beach infilled prior to the tourist season with well-aerated sand mined from the main harbor canal. Microorganisms induce α -glucosidase synthesis to decompose hardly assimilable COM during deficit of easily assimilable PRT and CHO. The lack of easily assimilable matter activates stronger hydrolytic activity in lower layers of core sediments.

© 2018 Institute of Oceanology of the Polish Academy of Sciences. Production and hosting by Elsevier Sp. z o.o. This is an open access article under the CC BY-NC-ND license (<http://creativecommons.org/licenses/by-nc-nd/4.0/>).

* Corresponding author at: Pomeranian University in Słupsk, Faculty of Mathematics and Natural Sciences, Institute of Biology and Environmental Protection, Department of Environmental Chemistry, 22b Arciszewskiego Str., 76-200 Słupsk, Poland. Tel.: +48 59 8045 423; Fax.: +48 59 84 05 337.

E-mail addresses: aleksander.astel@apsl.edu.pl, AliAst@poczta.fm (A.M. Astel).

Peer review under the responsibility of Institute of Oceanology of the Polish Academy of Sciences.



Production and hosting by Elsevier

<https://doi.org/10.1016/j.oceano.2018.01.001>

0078-3234/© 2018 Institute of Oceanology of the Polish Academy of Sciences. Production and hosting by Elsevier Sp. z o.o. This is an open access article under the CC BY-NC-ND license (<http://creativecommons.org/licenses/by-nc-nd/4.0/>).

1. Introduction

Sea coasts are contact zones between the land and the sea or the ocean. One of the few possible types of coasts are beaches, which are the most common form of littoral accumulation. Sandy beaches being a buffer zone between the land and the sea are characterized by wide spectrum of sizes, morphologies and ranges of exposure to oceanographic conditions (Mudryk et al., 2011; Novitsky and MacSween, 1989; Rodil and Lastra, 2004). Those environments are very dynamic, as they are shaped by wind, sand and water remaining in constant motion (Germán Rodríguez et al., 2003; McLachlan et al., 1996; Rodil and Lastra, 2004; Schoeman et al., 2000). Marine beaches, sandy ones in particular, are often subjected to considerable anthropogenic pressure due to recreational and economic functions (Antonowicz et al., 2015; Węśławski et al., 2000). Diverse forms of organic matter including variety of its constituents (lipids, proteins, carbohydrates, total organic carbon, total phosphorus and total nitrogen) transform beaches into specific ecosystems inhabited by microorganisms which participate in the transformation and mineralization of the matter (Koop and Griffiths, 1982; Phillips et al., 2011), and hence sandy beaches play an important role in energy flow and organic matter turnover. Being considered an important component of sandy beach community, bacteria mineralize about 70% of organic matter. Beaches can also be considered huge water filters (approximately $10\text{--}70\text{ m}^3\text{ m}^{-1}\text{ d}^{-1}$) (Brown and McLachlan, 1990; Heymans and McLachlan, 1996; Nair and Loka Bharathi, 1980). During water permeation, a large amount of organic matter is adsorbed by the sand grain surface as particulate (POM) and dissolved (DOM) organic matter (Mudryk and Podgórska, 2006).

Productivity of sandy beaches is ultimately limited by the nutrient load (Khiyama and Makemson, 1973). The rate of DOM and POM decomposition depends on the availability of nutrient, physiological properties and bacteria metabolic activity. According to Boetius (1995), production and activity of bacterial hydrolytic enzymes depend on availability, distribution and concentration of organic substrates. Therefore, the activity of enzymes in vertical profiles reflects the distribution of organic matter in water basin sediments. Organic matter accumulated in sediments is further utilized by interstitial organisms and returns to the sea in the form of nutrients. Therefore, on most beaches an interstitial system acts as a biological filter that enhances the mineralization of organic matter and purifies water. Heterotrophic bacteria inhabiting coastal ecosystems are not a homogeneous group of organisms. They represent the population of various physiological groups which is characterized by the ability to carry out the processes of depolymerization of a wide spectrum of macromolecular compounds (Krstulović and Solić, 1988; Mudryk et al., 1999, 2011).

Quality and quantity of organic matter in surface sediments have been considered a major factor in determining the amounts of material potentially available to consumer organisms, thus affecting community structure and benthic metabolism (Buchanan and Longbottom, 1970; Graf et al., 1983; Graf, 1989; Grant and Hargrave, 1987; Thompson and Nichols, 1988). Organic matter (OM) in the marine environment consists of labile and refractory compounds whose

relative importance may have profound implications for OM diagenesis and organic carbon turnover (Danovaro et al., 1993; Daumas et al., 1983; Fabiano et al., 1995; Fichez, 1991a; Rowe and Deming, 1985). The labile portion contains mainly simple sugars, fatty acids and proteins that are rapidly mineralized. On the contrary, the refractory matter, which consists of substances like humic and fulvic acids and complex carbohydrates, is characterized by lower degradation rates (Biddanda and Riemann, 1992; Buscaill et al., 1990; Danovaro et al., 1999a; Fabiano and Danovaro, 1994; Handa et al., 1972; Robinson et al., 1982; Sargent et al., 1983; Wilson et al., 1986). Sandy beaches usually receive large input of organic matter, which comprises an important source of nutrients for offshore production (Brown and McLachlan, 1990; Jędrzejczak, 1999). Local changes of sedimentary organic matter in the marine environment affect spatial distribution, metabolism and dynamics of all benthic components, from bacteria to macrofauna (Cividanes et al., 2002). Quantitative information on vertical fluxes of particulate proteins, carbohydrates and lipids is extremely rare (Danovaro et al., 1999b). In general, it is expected that labile carbon flux is coupled with surface productivity and decreases with depth (Carney, 1989).

Despite the fact that a range of studies have been conducted worldwide on microbial enzymatic activity on various beaches (Cividanes et al., 2002; Danovaro et al., 1993, 1999a,b; Danovaro, 1996; Dell'Anno et al., 2002; Fabiano et al., 1995, 2004; Fernandes et al., 2012; Fichez, 1991a,b; Graf and Meyer-Reil, 1985; Khripounoff et al., 1985; Meyer-Reil, 1983), only a few of them were focused on the comparison of microbial enzymatic activity. Few papers have attempted to analyze microbial enzymatic activity comprehensively according to biochemical composition of the sedimentary organic matter and specific characteristic of the beach. Moreover, to the best of our knowledge, in the case of the Polish coast only two scientific papers concern microbial enzymatic activity on sandy beaches (Mudryk and Podgórska, 2006; Perliński and Mudryk, 2016). Therefore, the aims of this study were to investigate: (1) the biochemical composition variability of the sedimentary organic matter and microbial enzymatic activity on 3 beaches subjected to a different degree of exposure and anthropopression, (2) the temporal changes in the quantity of sedimentary organic matter composition and microbial enzymatic activity in sheltered and exposed beaches, and (3) the variation of the above mentioned parameters according to the distance from the water line and vertical core depth.

2. Material and methods

2.1. Study area and sampling sites description

The study was carried out in three spots on 130 km long section of the Polish coast, between 232nd and 102nd km of the Polish sea border where the widest, the most beautiful and attractive, according to touristic activity, sandy beaches are located (Fig. 1).

Samples were collected in Ustka ($54^{\circ}34'N/16^{\circ}51'E$) on the eastern side of the mouth of the Słupia river, in Człopino ($54^{\circ}43'N/17^{\circ}14'E$) and in Puck ($54^{\circ}44'N/18^{\circ}24'E$). Ustka, Człopino and Puck are situated in northern Poland. They

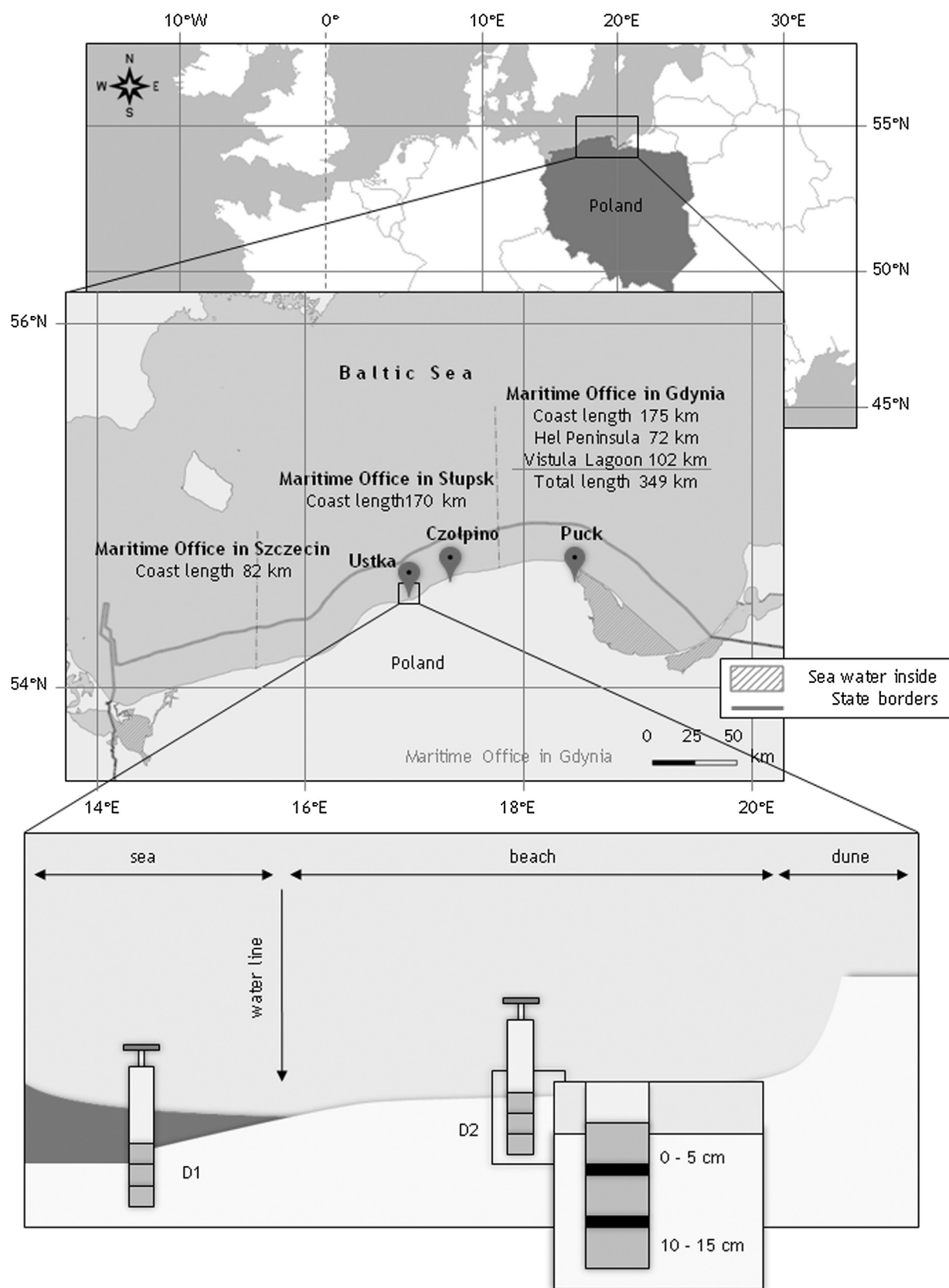


Figure 1 Location of sampling sites and presentation of the horizontal profile of one of the beaches.

differ in terms of degrees of anthropogenic impact and exposition. To avoid repetition, readers are kindly referred to our previous paper presenting very detailed description of the locations according to geomorphology of deposits and anthropogenic impact (Bigus et al., 2016). The only information worth emphasizing here is that beaches located in Ustka and Czolpino are exposed, while the beach located in Puck is a sheltered one. Moreover, the strength of anthropogenic impact decreases in the following order: Puck (heavy) > Ustka (moderate) > Czolpino (light) since the beach located in Czolpino is the part of the Słowiński National Park which is registered on the World List of Biosphere Reserves, the beach in Ustka is located close to the mouth of the slightly polluted Słupia River and the harbor used mainly by fishing and tourist boats while the beach located in Puck belongs to the Gdańsk Bay which is one of the 27 ecologically endangered areas in Poland and one of 132 pollution “hot spots” in the Baltic (Szefer, 2002).

2.2. Sampling and analytical methods

Sand samples were collected seasonally (winter (W), spring (S), summer (Su) and autumn (Au)) in 2011 and 2012 from two sites different in terms of environmental parameters on each beach. Site D1 (sea) – was located approximately 3 m offshore, at a depth of about 1 m underwater while site D2 (beach) – was around halfway up the beach, 30 m from the water line.

Sand cores were taken with a hand-operated Morduchaj-Boltowski sampler (length – 30 cm, inner diameter – 15 cm). 15 cm long sand cores were collected in three replicates and divided into 2 terminal sections in the field (0–5 cm and 10–15 cm). An intermediate section was skipped since previous studies showed that the highest differences in microbiological parameters could be observed between surface and subsurface layers of the marine beach (Mudryk and Podgórska, 2007; Ołańczuk-Neyman and Jankowska, 1998; Perliński and Mudryk, 2016). Sand samples were placed in polyethylene bags and put in a special container of temperature not exceeding 8°C and then transported to the laboratory. Since the accomplishment of full microbiological analysis was not possible in a relatively short period of time, samples were frozen to –60°C, however, just before analysis, the batch of samples subjected for treatment was defrosted. Several microbiological and chemical parameters were determined in sand sediments: lipase, aminopeptidase, α -glucosidase, β -glucosidase, secondary bacterial production (SBP), total bacteria number (TBN), lipids (LIP), proteins (PRT), carbohydrates (CHO), organic matter (OM), total organic carbon (TOC), total phosphorus (TP), total nitrogen (TN), biopolymeric carbon (BPC) and complex organic matter (COM). Sand samples were only mixed prior to the chemical analysis, while they were diluted tenfold in a sterile water buffer (pH = 7.2) and sonicated (Ellery and Schleyer, 1984) to separate bacteria from sediment prior to the microbiological analysis. Sonication was done using ultrasonic sonicator Bandelin SONOPLUS HD 2070 (Bandelin, Germany) for 1 min at the frequency of 20 kHz. Methodological details of the above-mentioned settings are depicted in Table 1. Measurements of absorption for LIP, PRT and CHO were done using Hitachi U-5100 (Hitachi, Japan) against deionized water produced by

HLP 10 (HydroLab, Poland), while spectrofluorimetric measures for lipase, aminopeptidase, α -glucosidase and β -glucosidase were done using Hitachi F-2500 (Hitachi, Japan). Enzyme activities in core sediments were determined using substrate proxies: MUF (4-methylumbelliferone) and MCA (L-leucine-4-methyl-coumarinyl-7-amide) for lipase/ α -glucosidase/ β -glucosidase and aminopeptidase, respectively.

2.3. Statistical methods

Two types of statistical procedures were applied in this study. Differences in median values of microbiological and chemical parameters determined in the sand cores collected on three different beaches were analyzed by the use of nonparametric *H* Kruskal–Wallis's and *U* Mann–Whitney's tests, while in order to discover seasonal differences as well as vertical and horizontal variation of microbiological and chemical parameters of dredge material collected in Ustka, Czolpino and Puck, including their mutual relations, factor analysis was applied along with the method of Principal Component Analysis (PCA) (Massart and Kaufman, 1997; Vandeginste et al., 1997). PCA enables reduction of the dimensionality of the space of the variables in the direction of the highest variance of the system. New variables, called principal components being linear combinations of the previous variables, replace the old coordinates of the factor space. Very often primary PCA solution is additionally rotated using one of the possible strategies (orthogonal rotations: varimax, biqurtimax, quartimax, equamax; skewed rotations: oblimix, promax, etc.). Rotation strategy simplifies the structure of factors and therefore makes its interpretation easier and more reliable since it strengthens the role of the latent factors with a higher impact on the variation explanation and diminishes the role of PCs with a lower impact (Cattell, 1978; Thurstone, 1947). Prior to running PCA, Spearman's correlation matrix was calculated while Bartlett's test (Bartlett, 1951) was applied to check if the correlation matrix is an identity matrix (null hypothesis). An identity matrix is a matrix in which all of the diagonal elements are 1 (correlation of a given parameter with itself) and all of the diagonal elements are 0 (all parameters are orthogonal). Basing on Bartlett's test results, the null hypothesis was rejected and hence the use of PCA was validated. All calculations were performed by the use of the software package STATISTICA 12.0 (Statsoft Inc., USA).

3. Results

Seasonal, horizontal and vertical variations were not considered in the initial stage of data analysis since it was the target planned for multidimensional analysis. This is why the overall basic statistics concerning microbiological and chemical parameters measured in the beach sediments are shown in Table 2.

The average concentration of PRT decreases in the following order: Ustka ($453 \mu\text{g g}^{-1}$) > Puck ($372 \mu\text{g g}^{-1}$) > Czolpino ($268 \mu\text{g g}^{-1}$). Whereas beach sediments collected in Puck were the most abundant with LIP ($250 \mu\text{g g}^{-1}$) overtaking Ustka ($176 \mu\text{g g}^{-1}$) and Czolpino ($112 \mu\text{g g}^{-1}$). Similar order was observed for CHO: Puck ($582 \mu\text{g g}^{-1}$) > Ustka ($509 \mu\text{g g}^{-1}$) > Czolpino ($338 \mu\text{g g}^{-1}$) and for OM: Puck

Table 1 The list of microbiological and chemical parameters determined in sand samples collected from three Polish beaches.

Parameter	Method	Details	Reference
Lipase Aminopeptidase α -Glucosidase β -Glucosidase	Hopp's	MUF and MCA being derivatives of coumarin are fluorescent markers used to determine enzyme activity. These markers attach to an appropriate substrate and remain fluorescently inactive at this moment. Enzymatic action causes the release of markers and increase of fluorescence. The higher fluorescence the higher enzymatic activity.	Hoppe (1984), Misis and Fabiano (2005)
SBP	Modified Fuhrman's and Azam's	Determination of tritium tagged thymidine incorporated to bacterial DNA using liquid scintillation counter Canberra Packard Tri-Carb 2100TR	Allen et al. (2002), Fuhrman and Azam (1982), Jugnia et al. (2000)
TBN	DAPI	Using epifluorescence microscope Olympus BX41 equipped with excitation-barrier cube UV-2A (excitation $\lambda = 365$ nm, emission $\lambda = 420$ nm)	Porter and Feig (1980)
LIP	Zöllner's and Kirsch's	Extraction fatty compounds using chloroform-methanol mixture, absorption measure using wave length 530 nm	Zöllner and Kirsch (1962)
PRT CHO	Markwell's Dubois's	Absorption measure using wave length 480 nm Absorption measure using wave length 480 nm for hexose and 490 for pentose	Markwell et al. (1978) DuBois et al. (1956)
OM	By weight	Comparison of sample mass before and after roasting	Januszkiewicz (1978)
TOC	Tiurin's	Combustion with H_2SO_4 and $K_2Cr_2O_7$ and titration using $Fe(NH_2)SO_4 \cdot 6H_2O$	Myślińska (2001)
TP	Molybdate method	After preliminary mineralization using concentrated H_2SO_4 and 30% H_2O_2 , ascorbic acid as a reducer	Bednarek et al. (2005)
TN	Kjeldahl's	After preliminary mineralization using concentrated H_2SO_4 and 30% H_2O_2 using Büchi Distillation Unit K – 350	Bednarek et al. (2005)
BPC	Computational	As the sum of organic carbon present in lipids, proteins and carbohydrates	Fabiano et al. (2004)
COM	Computational	TOC-BPC	Cividanes et al. (2002)

(42 mg g^{-1}) > Ustka (19 mg g^{-1}) > Czołpino (11 mg g^{-1}). In all presented orders core sediments from Czołpino were least abundant with OM proving that increasing anthropopression is positively correlated with an increase of OM abundance.

To evaluate the differences in values of microbiological and biochemical parameters in the sand cores collected in three different beaches results were statistically assessed by the use of nonparametric *H* Kruskal–Wallis (K–W) test (Table 3).

Data listed in Table 3 indicate that statistically significant differences in median values of chemical parameters as LIP, CHO, OM, TOC, TP, TN, BPC and COM prevail over microbiological ones. In the group of microbiological parameters, the only difference was found for α -glucosidase in Czołpino and Ustka. Secondary bacterial production and total bacteria number are comparable in core sediments of all the beaches. This is because of the similarity of the geomorphology of sediments and seawater chemistry. The highest number of differences was found between Czołpino and Puck. They concern median values of LIP, CHO, OM, TOC, TP, TN, BPC and COM and all values were much higher in Puck than in Czołpino (from 71% for BPC to 403% in the case of TN).

As mentioned above, Spearman's correlation matrix was calculated prior to running PCA (Table 4).

An analysis of correlations among microbiological and chemical parameters revealed that 28 out of 105 correlation coefficients were statistically significant at $p = 0.01$. Only 2 out of 28 coefficients were negative. Negative coefficients were found between CHO, TP and the activity of α -glucosidase (respectively $r_s = -0.37$ and $r_s = -0.38$). The activity of lipase was positively correlated with SBP ($r_s = 0.30$) and activity of aminopeptidase ($r_s = 0.49$). Single positive correlation ($r_s = 0.33$) between the activity of aminopeptidase and SBP was found. α -glucosidase activity was positively correlated with OM ($r_s = 0.38$), TOC ($r_s = 0.39$) and COM ($r_s = 0.39$). The highest number of positive coefficients ranging between 0.32 and 1.00 was found for LIP, CHO, OM, TOC, TN, BPC and COM.

The consecutive step consisted in a multidimensional analysis since the correlation matrix was not an identity one. Six independent factors, obtained as an effect of a varimax rotated solution of PCA explaining almost 76% of the variance of the entire data set, were distinguished (Table 5).

Factor 1 explaining nearly 25% of the total variance indicates strong positive correlation between OM, TOC, TN and COM. Positive correlation between OM, TOC and TN is not surprising and rather evident since total organic carbon is

Table 2 Basic statistics of microbiological and chemical parameters in the beach sediments from three Polish beaches (northern Poland) (S.D. – standard deviation).

	Location	N	Mean	Median	Minimum	Maximum	S.D.
Lipase [nM MUF g ⁻¹ h ⁻¹]	Ustka	32	230	143	19	951	227
Aminopeptidase [nM MCA g ⁻¹ h ⁻¹]			60	37	2	300	64
α-Glucosidase [nM MUF g ⁻¹ h ⁻¹]			51	24	2	237	61
β-Glucosidase [nM MUF g ⁻¹ h ⁻¹]			27	21	2	99	24
SBP [μg C g ⁻¹ h ⁻¹]			70	41	4	257	69
TBN [cell g ⁻¹]			6,421,421	6,400,096	1,509,553	12,019,297	2,207,518
LIP [μg g ⁻¹]			176	149	51	542	115
PRT [μg g ⁻¹]			453	269	78	1782	404
CHO [μg g ⁻¹]			509	387	121	2985	493
OM [mg g ⁻¹]			19	18	5	34	10
TOC [mg g ⁻¹]			11	11	3	20	6
TP [μg g ⁻¹]			70	57	8	226	54
TN [μg g ⁻¹]			251	251	88	469	71
BPC [μg g ⁻¹]	549	410	251	1749	322		
COM [mg g ⁻¹]	11	10	3	20	6		
Lipase [nM MUF g ⁻¹ h ⁻¹]	Czotpino	32	138	112	2	715	133
Aminopeptidase [nM MCA g ⁻¹ h ⁻¹]			39	25	3	273	52
α-Glucosidase [nM MUF g ⁻¹ h ⁻¹]			26	10	1	145	37
β-Glucosidase [nM MUF g ⁻¹ h ⁻¹]			18	11	1	59	17
SBP [μg C g ⁻¹ h ⁻¹]			41	27	2	219	50
TBN [cell g ⁻¹]			5,768,562	5,553,173	1,913,988	14,236,203	2,687,490
LIP [μg g ⁻¹]			112	95	6	324	80
PRT [μg g ⁻¹]			268	218	86	804	181
CHO [μg g ⁻¹]			338	335	53	650	134
OM [mg g ⁻¹]			11	9	5	21	5
TOC [mg g ⁻¹]			9	6	1	20	5
TP [μg g ⁻¹]			99	64	8	232	72
TN [μg g ⁻¹]			95	94	49	208	32
BPC [μg g ⁻¹]	345	313	222	595	97		
COM [mg g ⁻¹]	8	6	1	19	5		
Lipase [nM MUF g ⁻¹ h ⁻¹]	Puck	32	119	104	4	416	88
Aminopeptidase [nM MCA g ⁻¹ h ⁻¹]			42	35	1	108	33
α-Glucosidase [nM MUF g ⁻¹ h ⁻¹]			37	17	1	165	48
β-Glucosidase [nM MUF g ⁻¹ h ⁻¹]			38	9	1	252	62
SBP [μg C g ⁻¹ h ⁻¹]			52	31	2	421	77
TBN [cell g ⁻¹]			5,820,068	5,416,809	2,903,134	16,147,673	2,458,823
LIP [μg g ⁻¹]			250	190	41	1428	264
PRT [μg g ⁻¹]			372	224	92	3862	656
CHO [μg g ⁻¹]			582	531	177	1864	305
OM [mg g ⁻¹]			42	30	5	183	39
TOC [mg g ⁻¹]			30	21	2	139	30
TP [μg g ⁻¹]			260	152	63	855	205
TN [μg g ⁻¹]			478	329	177	1739	378
BPC [μg g ⁻¹]	590	476	278	2688	433		
COM [mg g ⁻¹]	30	21	2	136	30		

usually the carbon stored in soil organic matter, while nitrogen is one of the major components of OM. Similar mutual increase of TOC, COM and TN was observed before by others (Cividanes et al., 2002; Fabiano et al., 1995; Rodil et al., 2008). Because of this, based on source oriented interpretation of the factor, its meaning reflects communal wastes discharged by high-rate (with elevated removal of nutrients) wastewater treatment plants (as is in the case of Słupsk and Ustka wastewater treatment plants) and surface run-off from

agriculture. This is why it could be conditionally named as “anthropogenic rich in N”.

Factor 2 explains a lesser part of the total variance (about 10%) and shows a directly proportional correlation between lipase, aminopeptidase and SBP. It could be accepted as “microbial enzymatic activity” and informs about the activity of microorganisms toward oil spills (Ziervogel et al., 2012, 2016).

Factor 3 indicates a strong positive correlation between PRT, CHO and BPC. It explains about 14% of the total variance

Table 3 Statistical assessment of the differences of median values of microbiological parameters, enzymatic activity and concentration of total forms of elements according to the location of the beach by the use of multiple Kruskal–Wallis test ($p = 0.05$).

Parameter	<i>H</i> value of K–W test (insignificant <i>p</i> value)	<i>H</i> value of multiple K–W's test (insignificant <i>p</i> value)		
		Czotpino vs Ustka	Czotpino vs Puck	Ustka vs Puck
Lipase	4.71 ($p = 0.0948$)	–	–	–
Aminopeptidase	3.48 ($p = 0.1747$)	–	–	–
α -Glucosidase	8.21	2.83	1.03 ($p = 0.9061$)	1.78 ($p = 0.2159$)
β -Glucosidase	2.57 ($p = 0.2759$)	–	–	–
SBP	4.62 ($p = 0.0989$)	–	–	–
TBN	3.28 ($p = 0.1939$)	–	–	–
LIP	12.35	2.37 ($p = 0.0535$)	3.43	1.06 (0.8627)
PRT	2.63 ($p = 0.2679$)	–	–	–
CHO	20.29	2.00 ($p = 0.1346$)	4.50	2.49
OM	25.64	2.82	5.05	2.23 ($p = 0.0772$)
TOC	17.73	1.77 ($p = 0.2300$)	4.19	2.42
TP	30.84	1.68 ($p = 0.2773$)	3.74	5.42
TN	65.52	5.52	7.87	2.36 ($p = 0.0541$)
BPC	21.81	3.45	4.45	1.00 ($p = 0.9510$)
COM	17.32	1.68 ($p = 0.2799$)	4.14	2.46

Table 4 Spearman's correlation coefficients ($p = 0.01$) between microbiological and chemical parameters determined in core sediments collected in three Polish beaches.

	Lipase	Amino-peptidase	α -Glucosidase	β -Glucosidase	SBP	GA	LIP	PRT	CHO	OM	TOC	TP	TN	BPC	COM
Lipase	1.00														
Aminopeptidase	0.49	1.00													
α -Glucosidase	0.12	0.20	1.00												
β -Glucosidase	0.11	0.08	–0.12	1.00											
SBP	0.30	0.33	0.17	–0.01	1.00										
GA	0.17	0.11	0.08	–0.22	0.09	1.00									
LIP	0.12	0.00	0.11	0.06	–0.09	0.21	1.00								
PRT	0.03	0.07	0.16	–0.01	0.00	–0.16	–0.17	1.00							
CHO	–0.04	0.04	–0.37	0.18	–0.12	0.00	0.00	0.10	1.00						
OM	–0.05	0.11	0.38	0.07	–0.15	0.03	0.32	0.15	0.10	1.00					
TOC	–0.03	0.08	0.39	0.05	–0.21	–0.00	0.33	0.17	0.06	0.96	1.00				
TP	0.05	0.10	–0.38	–0.05	0.16	–0.06	0.01	–0.23	0.32	–0.06	–0.08	1.00			
TN	0.05	0.11	0.08	0.12	0.09	0.08	0.38	–0.06	0.40	0.41	0.32	0.34	1.00		
BPC	0.03	0.07	0.02	0.16	–0.12	0.01	0.39	0.59	0.57	0.39	0.38	–0.02	0.37	1.00	
COM	–0.03	0.08	0.39	0.04	–0.21	–0.00	0.32	0.15	0.04	0.96	1.00	–0.08	0.32	0.36	1.00

Bold values are statistically significant on $p = 0.01$.

and, being a reflection of mutual relations between proteins and carbohydrates, can be conditionally named as “labile organic matter”. Strong contribution of biopolymeric carbon within factor 3 is in agreement with expectations since BPC is the sum of lipid, protein and carbohydrate carbon.

Factor 4 (8% of the variance) indicates the proportional relation between TBN and LIP. It is evident that moist and warm environment of beaches abounding with lipids from many sources (UV filters, tanning oils and lotions, fat from wastewater treatment plants, etc.) makes a favorable habitat for bacteria growth. This is why the fourth factor could be accepted as “bacterial growth”.

Factor 5 accounts for 9% of the total variance and contains only one parameter – TP. Since it suggests an impact of phosphates from raw domestic wastes or dumps from

low-rate (without increased removal of nutrients) wastewater treatment plants, it was called “an anthropogenic rich in P”.

Factor 6 accounts for 8% of the total variance and contains inversely correlated α -glucosidase and β -glucosidase. Similarly as in the case of factor 2 it reflects microbial enzymatic activity, however to distinguish it from factor 2, it was called “hydrolytic”. α -glucosidase breaks down starch and disaccharides to glucose and is located in the brush border of the small intestine that acts upon 1,4-alpha bonds. This is in contrast to β -glucosidase which catalyzes the hydrolysis of the glycosidic bonds to terminal non-reducing residues in beta-D-glucosides and oligosaccharides, with the release of glucose. An inversely proportional correlation between α - and β -glucosidase refers to the ability of microorganisms to

Table 5 Factor analysis solution after normalized varimax rotation.

	Factor 1	Factor 2	Factor 3	Factor 4	Factor 5	Factor 6
Lipase	−0.07	0.72	0.01	0.20	−0.18	0.19
Aminopeptidase	0.01	0.70	−0.08	−0.07	0.08	0.12
α-Glucosidase	0.27	0.03	−0.30	−0.06	−0.45	−0.52
β-Glucosidase	0.19	0.09	−0.09	−0.15	−0.07	0.81
SBP	−0.16	0.70	−0.01	−0.13	0.26	−0.21
TBN	−0.09	0.13	−0.03	0.75	−0.00	−0.29
LIP	0.38	−0.15	0.09	0.69	0.11	0.10
PRT	0.41	0.09	0.73	−0.11	−0.28	−0.16
CHO	0.04	−0.09	0.78	−0.07	0.23	0.12
OM	0.96	−0.04	0.18	0.03	0.04	0.03
TOC	0.96	−0.05	0.18	0.04	0.04	0.04
TP	0.18	0.07	−0.08	0.04	0.83	−0.03
TN	0.59	0.01	0.06	0.07	0.48	−0.02
BPC	0.44	−0.04	0.86	0.16	−0.05	−0.02
COM	0.96	−0.05	0.17	0.03	0.04	0.04
Eigenvalue	3.80	1.57	2.09	1.18	1.39	1.16
% of the explained variance	25%	10%	14%	8%	9%	8%
% of the cumulated variance	25%	35%	49%	57%	68%	76%

Note: Values in bold are the factor loadings higher than 0.5 and those, which were further interpreted; varimax rotation was applied as indubitably the most popular rotation method by far (Hervé, 2010).

decompose OM. When easily assimilable matter (i.e. proteins, monosaccharide) is present in the environment, a growth of microorganisms synthesizing β-glucosidase and hence an increase of its activity is observed. In the meantime an activity of α-glucosidase decreases. After the source of easily assimilable matter is exhausted or when fresh and hardly assimilable matter appears in the environment, mutual dependence between both forms of glucosidase switches in the direction of α-glucosidase activity increase (to decompose hardly assimilable matter). This is why the activity of both forms of glucosidase can not increase or decrease simultaneously. Higher activity of α-glucosidase or β-glucosidase is conditioned by the kind of OM present in the environment (Zeng et al., 2010).

To verify and evaluate the differences in median values of microbiological parameters, enzymatic activity and a concentration of total forms of elements according to a location of the sampling point, core depth and seasonality, the U Mann–Whitney test was applied and its results are depicted in Table 6.

As ensues from data presented in Table 6 CHO, PRT and BPC abundance differs seasonally in Ustka and Czolpino, while in Puck CHO and BPC abundance differs only according to the distance from the water line. Besides the winter period, an increase in the concentration of all labile forms of organic matter is observed in Ustka (winter: PRT – 291.99 μg g^{−1}; CHO – 456.27 μg g^{−1}; BPC – 502.06 μg g^{−1}; spring: PRT – 232.76.99 μg g^{−1}; CHO – 273.44 μg g^{−1}; BPC – 344.74 μg g^{−1}; summer: PRT – 569.87 μg g^{−1}; CHO – 403.19 μg g^{−1}; BPC – 530.24 μg g^{−1}; autumn: PRT – 716.19 μg g^{−1}; CHO – 902.99 μg g^{−1}; BPC – 817.47 μg g^{−1}) and Czolpino (winter: PRT – 138.34 μg g^{−1}; CHO – 364.70 μg g^{−1}; BPC – 299.48 μg g^{−1}; spring: PRT – 290.70 μg g^{−1}; CHO – 256.39 μg g^{−1}; BPC – 353.35 μg g^{−1}; summer: PRT – 287.96 μg g^{−1}; CHO – 365.98 μg g^{−1}; BPC – 365.80 μg g^{−1}; autumn: PRT – 356.87 μg g^{−1}; CHO –

363.96 μg g^{−1}; BPC – 361.07 μg g^{−1}). The observed increase of labile organic matter abundance in spring, summer and autumn matches the increase of biological activity in the corresponding seasons in the coastal zone of the southern Baltic Sea (Håkanson and Bryhn, 2008; Smayda, 1997; Vu, 2016). In Puck significant seasonal changes of PRT, CHO and BPC are not observed while sediments dredged from location D1 are at least two and a half times more abundant with CHO (691.51 μg g^{−1}) and BPC (732.32 μg g^{−1}) than these dredged from D2 (CHO – 472.96 μg g^{−1}; BPC – 447.80 μg g^{−1}). The lack of seasonal changes in this case is probably caused by the stability of sea water characteristics (temperature, aeration, etc.) in Puck Bay while variation along a horizontal transect of the beach is caused by analogical reasons as were presented for F1 interpretation (sheltered beach, low slope, energy of waves and hydrodynamics, etc.).

4. Discussion

The concentration of OM found on exposed locations in Ustka (19 mg g^{−1}) and Czolpino (11 mg g^{−1}) is similar to OM concentration found on exposed beaches in Germany: 5.9 mg g^{−1} (Meyer-Reil et al., 1980), 16.80 mg g^{−1} (Meyer-Reil, 1983) and on the Ligurian coast: 19.25 mg g^{−1} (Fabiano et al., 1995). A comprehensive comparison of dredge material collected in various world-wide spread locations according to the abundance of proteins, carbohydrates and lipids is presented in Fig. 2.

Human activity, emission of pollutants in particular, increases the total budget of labile and refractory OM in the environment (Dell'Anno et al., 2002). However, it must be recalled that a simple division into anthropogenic and natural origin of OM according to its labile or refractory characteristic is not an easy task. As an example, easily mineralized PRT, LIP and CHO are components of the majority of living organisms. They can be both of “marine” and “terrestrial”

Table 6 Statistical assessment of the differences of median values of microbiological parameters, enzymatic activity and concentration of total forms of elements according to sampling points' location along the beach, depth of the core and seasonality by the use of Mann–Whitney's and multiple Kruskal–Walli's tests ($p = 0.05$).

Parameter	<i>U</i> value of Mann–Whitney test (according to location and depth) and <i>H</i> value of multiple K–W's test (according to seasons) (insignificant <i>p</i> value)		
	Ustka	Czołpino	Puck
Lipase	99 ($p = 0.2828$) ^l 108 ($p = 0.4624$) ^d 3.32 ($p = 0.3439$) ^s	86 ($p = 0.1178$) ^l 87 ($p = 0.1269$) ^d 1.90 ($p = 0.5921$) ^s	103 ($p = 0.3558$) ^l 77 ($p = 0.0570$) ^d 0.56 ($p = 0.9043$) ^s
Aminopeptidase	60 ^l 102 ($p = 0.3365$) ^d 2.20 ($p = 0.5316$) ^s	91 ($p = 0.1689$) ^l 123 ($p = 0.8653$) ^d 8.80 ^s	97 ($p = 0.2503$) ^l 64 ^d 4.30 ($p = 0.2299$) ^s
α -Glucosidase	90 ($p = 0.1575$) ^l 92 ($p = 0.1809$) ^d 4.06 ($p = 0.2551$) ^s	85 ($p = 0.1092$) ^l 122 ($p = 0.8358$) ^d 3.46 ($p = 0.3278$) ^s	107 ($p = 0.4397$) ^l 59 ^d 1.03 ($p = 0.7937$) ^s
β -Glucosidase	124 ($p = 0.8950$) ^l 107 ($p = 0.4397$) ^d 5.38 ($p = 0.1461$) ^s	109 ($p = 0.4856$) ^l 97 ($p = 0.2503$) ^d 12.29 ^s	126 ($p = 0.9549$) ^l 97 ($p = 0.2503$) ^d 3.32 ($p = 0.3443$) ^s
SBP	55 ^l 105 ($p = 0.3964$) ^d 4.86 ($p = 0.1823$) ^s	74 ^l 95 ($p = 0.2206$) ^d 9.99 ^s	49 ^l 64 ^d 0.07 ($p = 0.9954$) ^s
TBN	127 ($p = 0.9849$) ^l 108 ($p = 0.4624$) ^d 9.11 ^s	97 ($p = 0.2503$) ^l 103 ($p = 0.3558$) ^d 10.80 ^s	91 ($p = 0.1689$) ^l 123 ($p = 0.8653$) ^d 11.26 ^s
LIP	117 ($p = 0.6923$) ^l 118 ($p = 0.7203$) ^d 4.39 ($p = 0.2219$) ^s	115 ($p = 0.6375$) ^l 102 ($p = 0.3365$) ^d 8.62 ^s	101 ($p = 0.3179$) ^l 124 ($p = 0.8950$) ^d 7.07 ($p = 0.0697$) ^s
PRT	115 ($p = 0.6375$) ^l 109 ($p = 0.4856$) ^d 8.28 ^s	114 ($p = 0.6109$) ^l 125 ($p = 0.9249$) ^d 9.05 ^s	94 ($p = 0.2067$) ^l 100 ($p = 0.3000$) ^d 7.13 ($p = 0.0679$) ^s
CHO	86 ($p = 0.1178$) ^l 119 ($p = 0.7487$) ^d 9.32 ^s	65 ^l 96 ($p = 0.2351$) ^d 3.36 ^s	70 ^l 82 ($p = 0.08663$) ^d 3.01 ($p = 0.3903$) ^s
OM	111 ($p = 0.5340$) ^l 115 ($p = 0.6375$) ^d 3.20 ($p = 0.3624$) ^s	104 ($p = 0.3758$) ^l 120 ($p = 0.7774$) ^d 3.74 ($p = 0.2908$) ^s	0 ^l 109 ($p = 0.4856$) ^d 1.85 ($p = 0.6042$) ^s
TOC	113 ($p = 0.5847$) ^l 118 ($p = 0.7203$) ^d 3.14 ($p = 0.3707$) ^s	117 ($p = 0.6923$) ^l 126 ($p = 0.9549$) ^d 4.41 ($p = 0.2200$) ^s	0 ^l 111 ($p = 0.5340$) ^d 1.71 ($p = 0.6353$) ^s
TP	107 ($p = 0.4397$) ^l 124 ($p = 0.8950$) ^d 1.86 ($p = 0.6012$) ^s	116 ($p = 0.6647$) ^l 126 ($p = 0.9549$) ^d 2.04 ($p = 0.5636$) ^s	112 ($p = 0.5591$) ^l 114 ($p = 0.6109$) ^d 13.01 ^s
TN	121 ($p = 0.8210$) ^l 98 ($p = 0.2660$) ^d 4.16 ($p = 0.2451$) ^s	99.5 ($p = 0.2913$) ^l 123.5 ($p = 0.8801$) ^d 6.25 ($p = 0.1001$) ^s	46 ^l 113 ($p = 0.5847$) ^d 1.21 ($p = 0.7499$) ^s
BPC	113 ($p = 0.5847$) ^l 120 ($p = 0.7774$) ^d 10.96 ^s	81 ($p = 0.0796$) ^l 88 ($p = 0.1365$) ^d 3.89 ($p = 0.2737$) ^s	73 ^l 102 ($p = 0.3365$) ^d 0.85 ($p = 0.8376$) ^s
COM	109 ($p = 0.4856$) ^l 117 ($p = 0.6923$) ^d 3.02 ($p = 0.3877$) ^s	119 ($p = 0.7487$) ^l 128 ($p = 0.9849$) ^d 4.62 ($p = 0.2017$) ^s	0 ^l 110 ($p = 0.5095$) ^d 1.71 ($p = 0.6353$) ^s

l – location (sea vs beach), d – depth (0–5 cm vs 10–15 cm), s – season (winter, spring, summer, autumn).

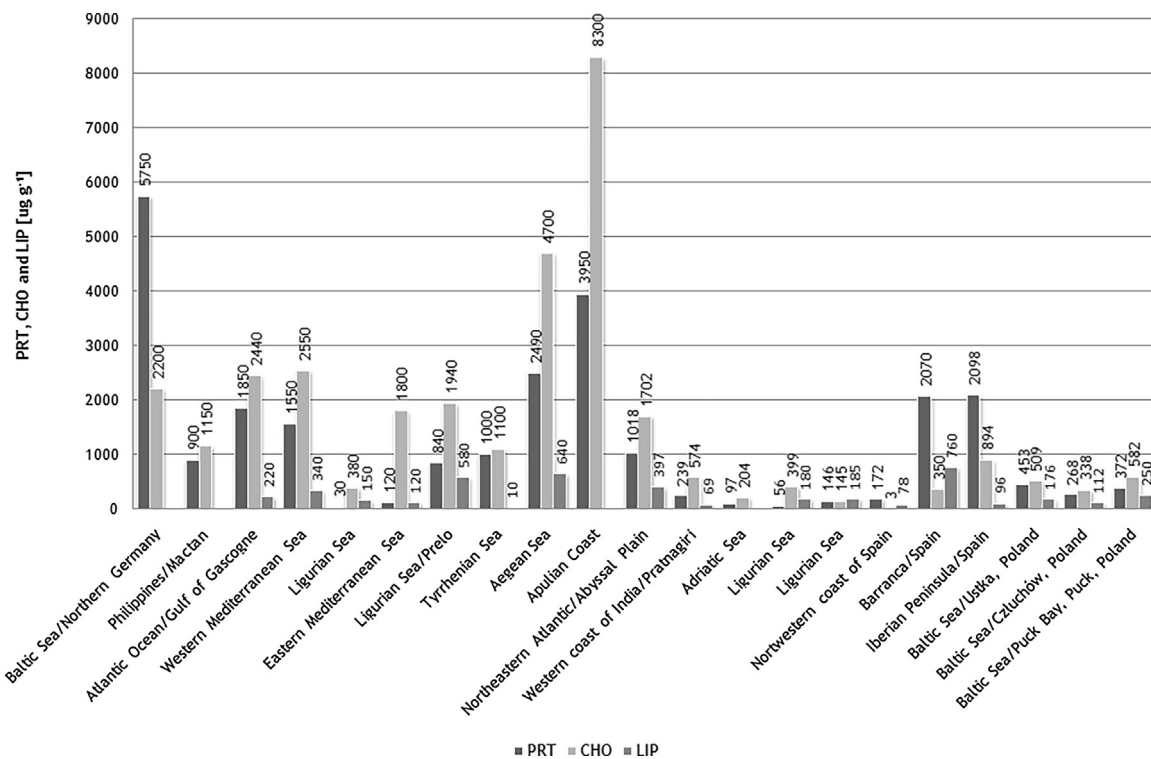


Figure 2 Comprehensive comparison of dredge material collected in various world-wide spread locations according to abundance of labile forms of organic matter (proteins, carbohydrates and lipids).

origin, since i.e. CHO can be photosynthesized by producers in the sea or be a product of decomposition of organic matter present in the debris of animals and plants (Penna et al., 2009). On the other hand, humic and fulvic acids and lignin are of natural origin despite the fact that they belong to refractory OM. Having in mind the facts mentioned above, it could be generalized that OM present in beach sediments can be both of natural or anthropogenic origin with a different contribution of labile or refractory forms, however the higher labile form contribution, the higher the naturalness of OM.

Anthropogenic domination of sources of OM in Puck and Ustka was positively verified by a calculation of contribution of labile forms of OM in the total OM budget. For Ustka and Puck it was 6% and 3%, respectively, while for Człuchów it was 65%. For Puck there are two simultaneous factors causing higher accumulation of organic matter. As mentioned above, one of them is anthropoppression while the other concerns the degree of sheltering. Grain size should not be considered a differentiating factor since sediment from the beaches in Ustka, Człuchów and Puck indicates a predominance of fine-grained sands with little variation in all the locations (Bigus et al., 2016). Sheltered (covered) beaches like in Puck, characterized by fine-grained sediments, have a much higher capacity of pollutant accumulation (McLachlan et al., 1996) than exposed beaches characterized by similarly grained sediments due to poorer oxygenation and lower drainage. Limited hydrodynamics of the sheltered beach favors the accumulation of sedimentary organic matter due to a limited renewal of interstitial water (Incera et al., 2003). In addition, low energy of the surge permits the formation of fine and stable sediments that allowed the settlement of a higher amount of fauna (Nordstrom, 1992). On the contrary,

stronger hydrodynamics of the exposed beaches permits deposition of coarser sediments through which water runs easily, preventing the accumulation of organic matter while hydrodynamic stress concerning the impact of waves limits biological richness (McLachlan et al., 1996).

As is shown in Fig. 2, dredged material collected on the Polish coast is characterized by a similar concentration of proteins, carbohydrates and lipids to those collected on the Ligurian coast (Danovaro et al., 1993; Fabiano et al., 1995, 2004), Adriatic beaches (Danovaro et al., 2001), northwestern coast of Spain (Rodil et al., 2007) as well as on the western coast of India (Fernandes et al., 2012). Beach sediments collected in Ria de Arousa (Cividanes et al., 2002), in the northwestern part of the Iberian Peninsula (Incera et al., 2003), in the Gulf of Gascogne (Khrpounoff et al., 1985), in the area of the Porcupine Abyssal Plain (Danovaro et al., 2001), in the Philippines (Graf and Meyer-Reil, 1985) and on the Tyrrhenian (Fabiano and Danovaro, 1994) and the Ligurian coasts close to Prelo Bay (Danovaro et al., 1999b) as well as in the western (Fichez, 1991a) and eastern (Danovaro et al., 1993) parts of the Mediterranean Sea were at least four to five times more abundant with PRT, CHO and LIP. Concentrations of labile forms of organic matter were significantly higher (more than tenfold) in dredge material collected in the Aegean Sea (Danovaro et al., 1999a), on the Apulian coast (Dell'Anno et al., 2002) and in northern Germany (Meyer-Reil, 1983) than in the samples collected in Poland.

Comprehensive comparison of microbial enzymatic activity on the Polish coast with other locations is enigmatic due to the limited number of papers dealing with this topic (Danovaro et al., 2001; Misic and Fabiano, 2005), however activity of aminopeptidase did not exceed 6.65 and

3.7 nM MCA g⁻¹ h⁻¹ in beach sediments collected in the Ligurian Sea (Misić and Fabiano, 2005) and the Adriatic Sea (Danovaro et al., 2001), which is almost tenfold lower than in dredge sediments collected in Ustka, Czluchów and Puck. Similarly, tenfold lower activities of α-glucosidase and β-glucosidase were found in the warmer ecosystem of the Mediterranean beaches (Danovaro et al., 2001; Misić and Fabiano, 2005). Other results concerning microbial enzymatic activity in core sediments of Polish beaches indicate comparable results for lipase (183.75 nM MUF g⁻¹ h⁻¹), aminopeptidase (94.38 nM MCA g⁻¹ h⁻¹), α-glucosidase (24.40 nM MUF g⁻¹ h⁻¹) and β-glucosidase (28.10 nM MUF g⁻¹ h⁻¹) activities (Perliński and Mudryk, 2016).

Basing on results depicted in Table 3 it could be unequivocally concluded that beach sheltering joined with strong anthropogenic impact results in huge deposition of both labile and refractory organic matter, particularly those rich in nutrients. As presented in Fig. 1, the beach in Puck is sheltered from large and long period waves by the Hel Peninsula, which separates the land from the Baltic Sea almost precluding an exchange of water. Moreover, the Vistula River flowing through Żuławy Wiślane, being the most important agricultural area in northern Poland, discharges huge loads of N and P to the Baltic Sea, causing significant pollution in the entire region of Puck Bay. According to recent environmental reports in 2009, the Vistula River discharged 92.1 kt of N and 6.44 kt of P (Report, 2010) to the Baltic Sea. In 2011, the total load of N and P increased to 102.1 kt and 7.0 kt, respectively (Report, 2012). The other important source of OM in the vicinity of Puck beach, LIP and CHO in particular, is wastewater from treatment plants located close to the coastline in Puck Bay and the marina located in Puck. Vessels and yachts docking in harbors and marinas are a common source of many organic substances such as fuel, paints, anti-fouling agents, oils and soaps. Communal wastes are the dominant source of phosphorus compounds in Puck Bay, and hence in core sediments collected in Puck. Such an explanation seems logical since significant differences between median values of CHO, TOC, TP and COM were found for Ustka and Puck. In Puck an increase ranging from 14% (CHO) to 271% (TP) in comparison with Ustka was observed. Apart from α-glucosidase statistically different median of concentrations between core sediments collected in Ustka and Czołpino was found for OM, TN and BPC. An increased abundance of nitrogen-rich compounds in core sediments collected in Ustka can be explained by the load of the Stupia River which flows through the agricultural areas in the middle Pomeranian Voivodship, while an increase of OM and BPC abundance can be explained by the impact of two wastewater treatment plants for Słupsk and Ustka located close to the mouth of the Stupia River. According to recent environmental reports, coastal rivers (including the Vistula River) in the Pomeranian region in Poland in 2011 discharged 105.35 kt of N and 7.16 kt of P, however, the contribution of the Stupia and Łeba rivers were much lower. In 2009 the Stupia River discharged 0.812 kt of N and only 0.05 kt of P (Report, 2010) to the Baltic Sea while the Łeba River discharged 0.739 kt of N and 0.046 kt of P. In 2011 the total load of N and P compounds due to the Stupia and Łeba rivers was as follows: Stupia – 1.231 kt N and 0.068 kt P; Łeba – 0.936 kt N and 0.044 kt P (Report, 2010, 2012).

The relation between the above characterized factors and locations (including the distance from the water line and vertical core depth) of the particular beach as well as seasonality were identified by the visualization of factor score values. The unanimous sign of factor scores and factor loadings corresponds to a high influence of a given factor (and hence high concentration of an analyte or high value of the measured parameter) on core sediment sample, while reverse sign corresponds to low influence. Moreover, the higher factor score value, the higher the influence. The plot of scores for the first factor visualized according to the location of the beach is presented in Fig. 3.

It could be easily observed that core sediments collected in Ustka and Czołpino create relatively homogenous groups, while those collected in Puck are spread. The location of samples along F1 axis (OM, TOC, TN, COM) proves that dredge material collected in Ustka and Czołpino is not as rich in organic matter and its constituents as those collected in Puck. This phenomenon reflects a mutual impact of two factors. On the one hand, the beach in Puck is sheltered by the Hel Peninsula and impacted by low energy waves in comparison to exposed locations in Ustka and Czołpino. On the other hand, Puck Bay consists of waters which are highly polluted with organic matter and nutrients due to load discharged by the Vistula River and three wastewater treatment plants located on the coast (Dębogórze, Wschód, Swarzewo). According to Incera et al. (2003), low hydrodynamics of sheltered beaches favors the accumulation of sedimentary organic matter due to a scarce renewal of interstitial water. Additionally, low energy surge permits formation of stable sediments which allow settlement of large amounts of fauna (Nordstrom, 1992). The beaches in Ustka and Czołpino are exposed and endangered by high energy and long period waves. Stronger hydrodynamics and reverse current facilitate mixing of water column and hence limit OM deposition on the beach (McLachlan et al., 1996), however slightly higher factor scores in Ustka compared with Czołpino confirm differences in median concentration values for OM and TN (Table 3) indicating a stronger impact of anthropogenic sources poor in P (the load carried out by the Stupia River waters).

Dispersion for a point set for Puck and compact form of a point sets for Ustka and Czołpino suggests different variability according to seasonal changes, the distance from the water line and vertical core depth. For Puck, much higher factor 1 scores were obtained for samples collected approximately 3 m offshore. Hence, they are richer in OM, TOC, TN and COM than these collected halfway up the beach.

It was statistically proved that only for Puck, location plays an important role and differentiates core sediments collected in the sea from these collected in the middle of the beach according to OM and its constituents. Because of high energy waves, core sediments in Ustka and Czołpino are seasonally stable and homogeneous along the beach as well as along vertical depth. Contrarily, the concentration of OM, TOC, TN and COM in dredge material collected 3 m offshore in Puck is higher (68 mg g⁻¹, 51 mg g⁻¹, 656 μg g⁻¹ and 50 μg g⁻¹, respectively) than in the middle of the beach (15 mg g⁻¹, 9 mg g⁻¹, 299 μg g⁻¹ and 9 μg g⁻¹, respectively). Again, such dependence can be explained by the impact of waves of low hydrodynamics observed in Puck. In locations with a low slope (i.e. sheltered beaches), low wave action

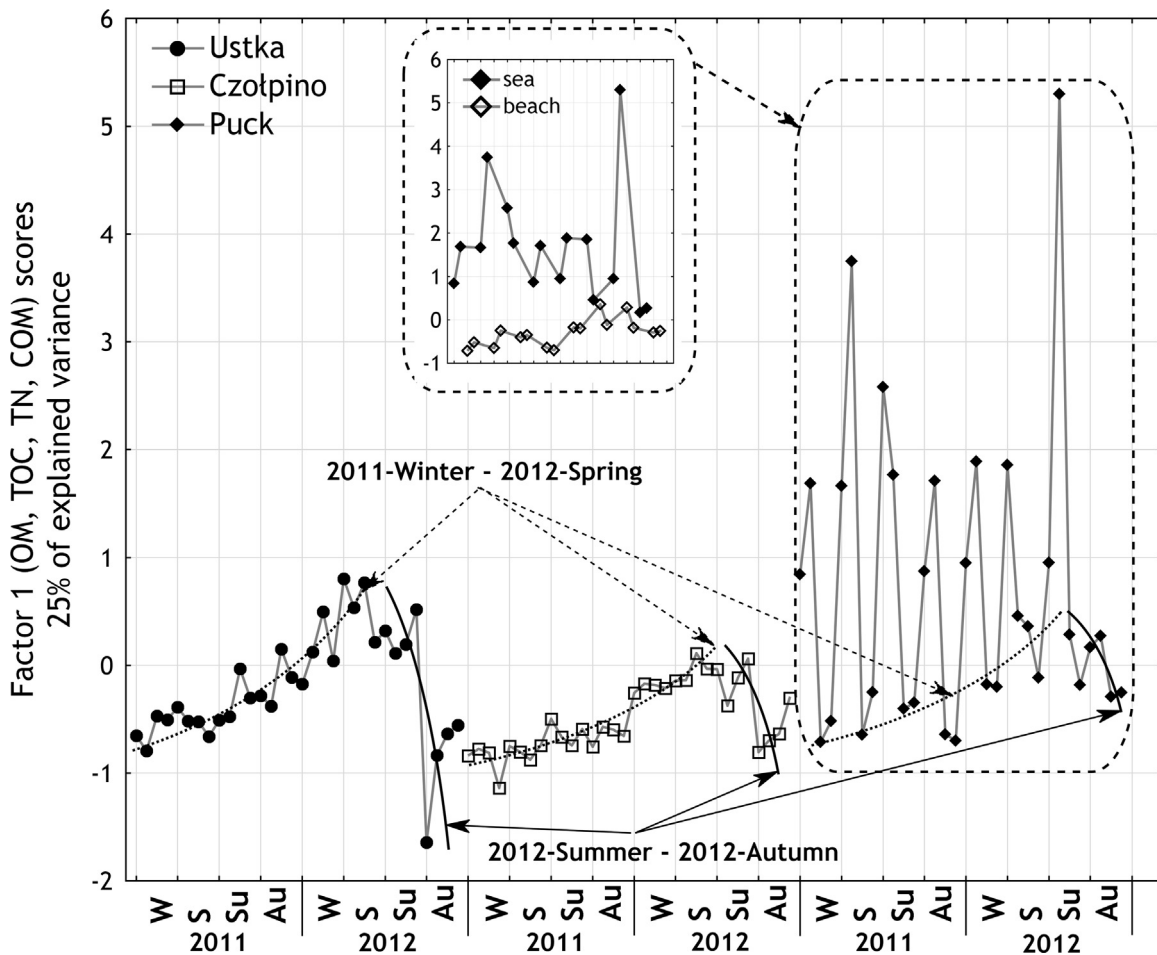


Figure 3 Factor 1 (anthropogenic rich in N) scores according to the location of the beach and horizontal transect in Puck (on x axis W, S, Su and Au states for winter, spring, summer and autumn, respectively).

facilitates OM enrichment and deposition within the narrow belt of shallow water since waves do not have enough energy to transport OM along a vertical transect of the beach (Incera et al., 2003).

As could be seen in Fig. 3, time series revealed another unique pattern confirmed by statistical testing (Table 5). Although there is a lack of seasonality in the period between winter 2011 and autumn 2012, a clear exponential increase of the concentration of OM, TOC, TN and COM in core sediments collected in all Polish beaches can be observed. This occurs even in Puck for samples collected in the middle of the beach. However, it breaks down during the last two seasons: summer 2012 and autumn 2012. Since the mentioned observation concerned the entire Polish coast (Ustka, Czołpino and Puck), it was assumed that accidental changes in OM, TOC, TN and COM abundance were caused by a sudden and extensive phenomenon related to biological activity. In the southern Baltic Sea two algae blooms are usually observed. The first of them caused by algae takes place in spring, while the other of much less intensity caused by cyanobacteria takes place in the summer season. The spring bloom is due to an increase of temperature after the winter period and intensive runoff discharge of nutrients (mainly N and P) from farmlands. Algae bloom usually finishes prior to the highest peak of touristic season when the temperature rises, oxygen

deficiency appears and an abundance of nutrients has been depleted (Forsberg, 1991). Such explanation fits with a sudden drop of the concentration of OM, TOC, TN and COM observed at the turn of the spring 2012 and summer 2012 seasons, however as ensues from Fig. 3, corresponding algae bloom did not take place in 2011.

The plot of scores for the factor presenting “microbial enzymatic activity” is shown in Fig. 4.

All core sediments create spread groups indicating substantial variation. Basing on factor 2 scores, the highest microbial enzymatic activity (lipase, aminopeptidase and SBP) was observed in core sediments collected in Ustka (Table 2). However, an existence of extreme values in all locations caused the disappearance of statistically significant differences (Table 3) in the activity of lipase, aminopeptidase and secondary bacterial production between the beaches. Despite this, a careful inspection of the data presented in Table 5 revealed the distance from the water line as a factor which differentiates microbial enzymatic activity in Ustka, and vertical core depth in Puck. An average concentration of aminopeptidase and SBP in samples from location D1 (sea) was $36 \text{ nM MCA g}^{-1} \text{ h}^{-1}$ and $54 \mu\text{g C g}^{-1} \text{ h}^{-1}$, respectively, while in samples collected in D2 (beach) it was $84 \text{ nM MCA g}^{-1} \text{ h}^{-1}$ and $87 \mu\text{g C g}^{-1} \text{ h}^{-1}$, respectively. The highest microbial enzymatic activity in Ustka is probably

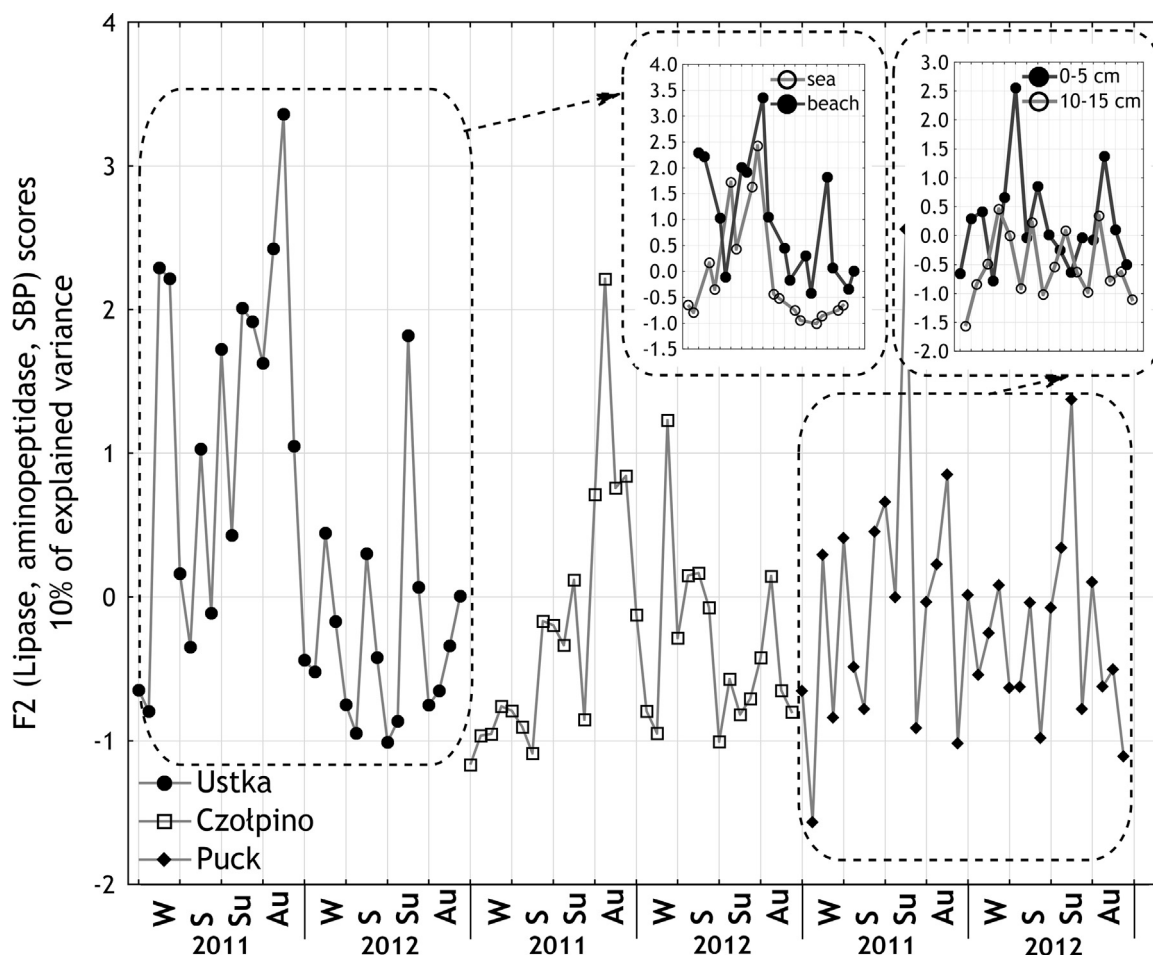


Figure 4 Factor 2 (microbial enzymatic activity) scores according to the location of the beach as well as horizontal transect in Ustka and vertical core depth in Puck (on x axis W, S, Su and Au states for winter, spring, summer and autumn, respectively).

caused by infilling with well-aerated sand mined from the main harbor canal carried out to protect unique ecosystem of dunes against substantial abrasion of the coast as well as to assure extraordinary touristic features of this health resort (Bigus et al., 2016). Statistically higher secondary bacterial production observed on the beach ($82 \mu\text{g C g}^{-1} \text{h}^{-1}$) in comparison with the sea ($23 \mu\text{g C g}^{-1} \text{h}^{-1}$) in Ustka confirms that infilling campaigns increase mixing and aeration, and hence facilitate the enzymatic activity of microorganisms in the middle of the beach in comparison with location D1. Due to the lack of seasonal and even annual stability of beach sediments in Ustka caused by infilling actions, the depth-dependent variation of microbial enzymatic activity was not observed. Contrarily, in the case of beach characterized by low slope, low hydrodynamic sand seasonal stability depth-dependent variation in microbial enzymatic activity could be noticed. In the upper layer of beach sediments dredged in Puck the activity of lipase, aminopeptidase, as well as, SBP was almost twice as high ($147 \text{ nM MUF g}^{-1} \text{h}^{-1}$, $55 \text{ nM MCA g}^{-1} \text{h}^{-1}$ and $75 \mu\text{g C g}^{-1} \text{h}^{-1}$, respectively) as in the lower layer ($90 \text{ nM MUF g}^{-1} \text{h}^{-1}$, $29 \text{ nM MCA g}^{-1} \text{h}^{-1}$ and $30 \mu\text{g C g}^{-1} \text{h}^{-1}$, respectively). An increased microbial enzymatic activity in the upper layer of the beach sediments reflects a higher total bacteria number in it, and hence higher SBP. In general, better mixing (also caused by tourist

movement), aeration and higher temperature observed in the upper layer of beach sediments facilitate microbial enzymatic activity (Halliday and Gast, 2011; Piggot et al., 2012). However, it should be noticed that organic matter mineralization is not only caused by psammon organisms. The other important factor which facilitates high molecular compounds degradation is photodegradation dependent on insolation. Photodegradation is the most intensive on beaches strongly exposed to sunlight and this is why mineralization of organic matter runs fastest in sediments at a depth of 0–5 cm (Kaiser and Herndl, 1997).

Inverse time variation, in comparison with “anthropogenic rich in N” factor, was observed for an abundance of the labile organic matter. A plot of scores for the third factor visualized according to the location of the beach is presented in Fig. 5.

Similarly, as it was reported by Incera et al. (2003), BPC was dominated by PRT and followed by CHO on all Polish beaches. Starting from winter 2011 to spring 2012, a slight decrease of the abundance of a labile organic matter was observed in all the locations, with the highest variation in Puck. However, statistical assessment (Table 3) proved that only in the case of CHO and BPC some significant differences appeared in the pairwise arrangement of the beaches (Czotpino vs Puck and Ustka vs Puck). Concentrations of carbohydrates were the highest in Puck ($582 \mu\text{g g}^{-1}$), moderate in

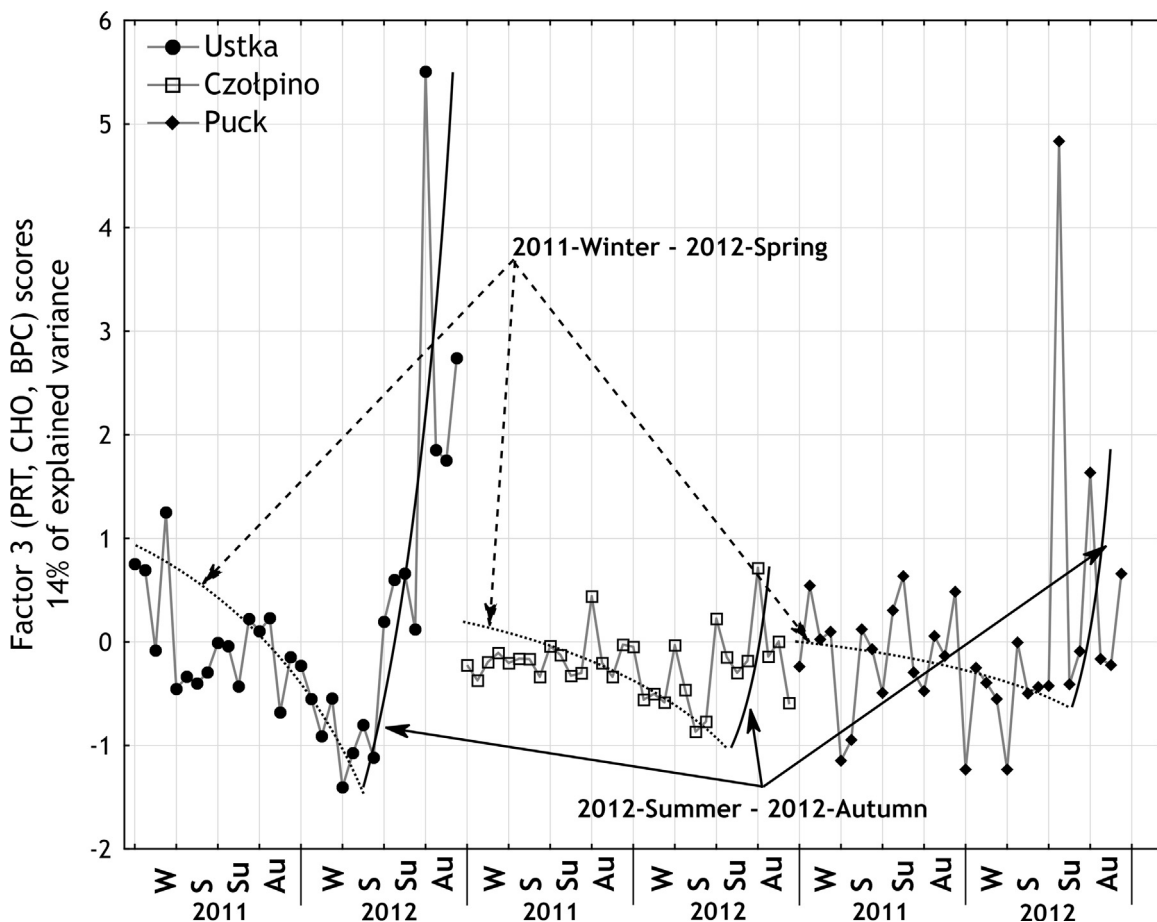


Figure 5 Factor 3 (labile organic matter) scores according to the location of the beach (on x axis W, S, Su and Au states for winter, spring, summer and autumn, respectively).

Ustka ($509 \mu\text{g g}^{-1}$) and the lowest in Czołpino ($338 \mu\text{g g}^{-1}$). The lack of statistically significant differences in average CHO concentration in core sediments was found between Ustka and Czołpino. The similar sequence of the concentration of BPC was found for the three investigated locations: Puck ($590 \mu\text{g g}^{-1}$) > Ustka ($549 \mu\text{g g}^{-1}$) > Czołpino ($345 \mu\text{g g}^{-1}$), however in this case the lack of statistically important differences was related to Ustka and Puck. Observed differences in abundance of labile organic matter seem to be a mixed effect of two factors: anthropogenic pressure and degree of sheltering and generally decrease in the following order: highly polluted and sheltered > moderately polluted and exposed > lightly polluted and exposed being in agreement with the results presented before by [Incera et al. \(2003\)](#).

As mentioned above, the time-dependent phenomenon of the inverse characteristic in comparison with factor 1 scores was observed for an abundance of labile forms of organic matter in the entire belt of the Polish coast. In Ustka, Czołpino and Puck a sudden and unexpected increase of abundance of CHO, PRT and BPC was observed in summer 2012 and autumn 2012. Increasing concentration of labile forms of OM correlated with decreasing concentration of nutrients (mainly N and P) could be associated with the algae blooms mentioned above usually taking place in Spring in the zone of the southern Baltic Sea. Due to carbohydrate and protein production potential, many microalgae significantly

increase their cellular neutral biochemical form content when present in an environment rich in nutrients as is typical in coastal zones ([Håkanson and Bryhn, 2008](#); [Smayda, 1997](#); [Vu, 2016](#)).

Total bacteria number and concentration of lipids are almost independent of the degree of beach sheltering or anthropogenic pressure on the Polish coast. Such conclusion arises from the analysis of [Fig. 6](#) where spread and range of factor 4 scores in Ustka, Czołpino and Puck are comparable.

An application of multiple K–W's test ([Table 3](#)) confirmed the lack of statistically significant differences in TBN in cores dredged in Ustka, Czołpino and Puck and indicated only one pairwise difference between Czołpino ($112 \mu\text{g g}^{-1}$) and Puck ($250 \mu\text{g g}^{-1}$) concerning LIP concentration. The overlapping pattern of points presented in [Fig. 6A](#) and [B](#) interpreted together with K–W's test results ([Table 5](#)) suggests that neither location of the sampling point in a vertical transect of the beach nor vertical core depth discriminates sediment samples according to bacterial growth. The only difference refers to the seasonal variation of TBN. During winter TBN is almost twice as high (around 7mln cell g^{-1}) as during summer (around 4mln cell g^{-1}), while during autumn and spring it is comparable (around 6mln cell g^{-1}). Such phenomenon could be easily explained by beach freezing during winter season. When the external temperature drops down, the upper layer of the beach as well as the shallow part of the coast freeze creating a tight ice cover which usually reaches

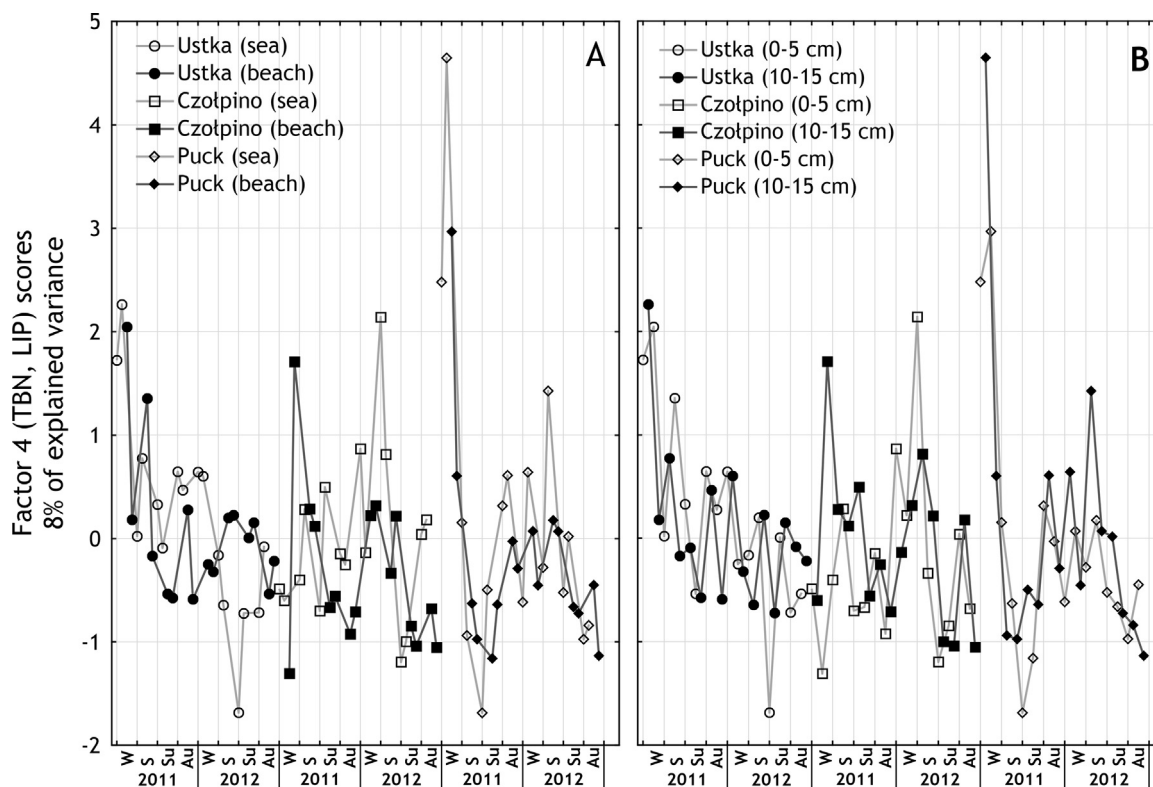


Figure 6 Factor 4 (bacterial growth) scores according to the location of the beach as well as (A) the distance from the water line and (B) vertical core depths (on x axis W, S, Su and Au states for winter, spring, summer and autumn, respectively).

the end of the breakwater (up to several dozens of meters). Below the frost zone, the processes of bacterial multiplication still take place, however their intensity is much lower than during summer time and limited by periodic defrosting caused by occasional temperature increase during sunny days. Limited access of sea water to the beach due to elongated ice cover makes removal of organic matter and bacteria difficult and results in bacteria accumulation (Węstawski et al., 2005).

Terrestrial and even more precisely anthropogenic origin is evident when one analyzes factor 5 scores presented in Fig. 7.

A huge load of phosphorus carried out by the Vistula River through Żuławy Wiślane as well as the impact of local low-rate wastewater treatment plants reflect higher factor 5 scores in Puck. High factor 5 scores correspond with statistical difference of TP concentration median values (Table 3) and refer to the highest concentration of TP ($260 \mu\text{g g}^{-1}$) in comparison with the respective value in Ustka ($70 \mu\text{g g}^{-1}$) and Czołpino ($99 \mu\text{g g}^{-1}$). Simple comparison proves that the middle Pomeranian region is relatively slightly impacted by phosphorus compounds carried out by surface flow. Moreover, the impact of the open sea, and waves of high energy in particular, facilitate the cleaning effect as well as the biodegradation of phosphorus compounds (HELCOM, 2009). Nevertheless, it seems that in the period of one year (winter, 2011–winter, 2012) slightly increasing trend is observed for TP concentration in Ustka and Czołpino. Due to the lack of huge variation in Ustka and Czołpino an additional interesting phenomenon was discovered. As can be seen in Fig. 7, an increasing trend of TP

changes in Ustka has a zigzag form and all minimal values concern the upper layer (0–5 cm) of sediments collected in the middle of the beach. It suggests that phosphorus in the lower layers of beach sediments could be immobilized in the form of calcium or aluminum phosphates, and hence become inactivated and not easily accessible (Forsberg, 1991; HELCOM, 2009).

Similarly as in the case of factor 1 (“anthropogenic rich in N”) and factor 3 (“labile organic matter”), some interesting although unexpected time-dependent change (possibly caused by algae bloom) was observed in the period between spring 2012 and autumn 2012. In all the locations, a huge drop in the load of TP was observed with minimal values in spring and summer 2012. It corresponds proportionally with a drop of OM, TOC, TN and COM which was discussed above. After the end of summer 2012 the concentration of TP dynamically increased once more, reaching the pre-drop level of concentration similarly as in the case of factor 3 (“labile organic matter”). As mentioned above, algae bloom usually ceases prior to the highest peak of touristic season when the temperature rises, oxygen deficiency appears and the abundance of nutrients has been exhausted (Forsberg, 1991). Exhaustion of easily accessible N source causes termination of algae blooms in this case, while anthropogenic P load carried out constantly by coastal rivers causes its dynamic increase prior to the winter season. The last factor analyzed was “hydrolytic” one and its factor scores are presented in Fig. 8.

As ensues from Fig. 8, a majority of factor scores for all investigated Polish beaches range between -1 to $+1$, indicating similar variation. The lack of statistically important

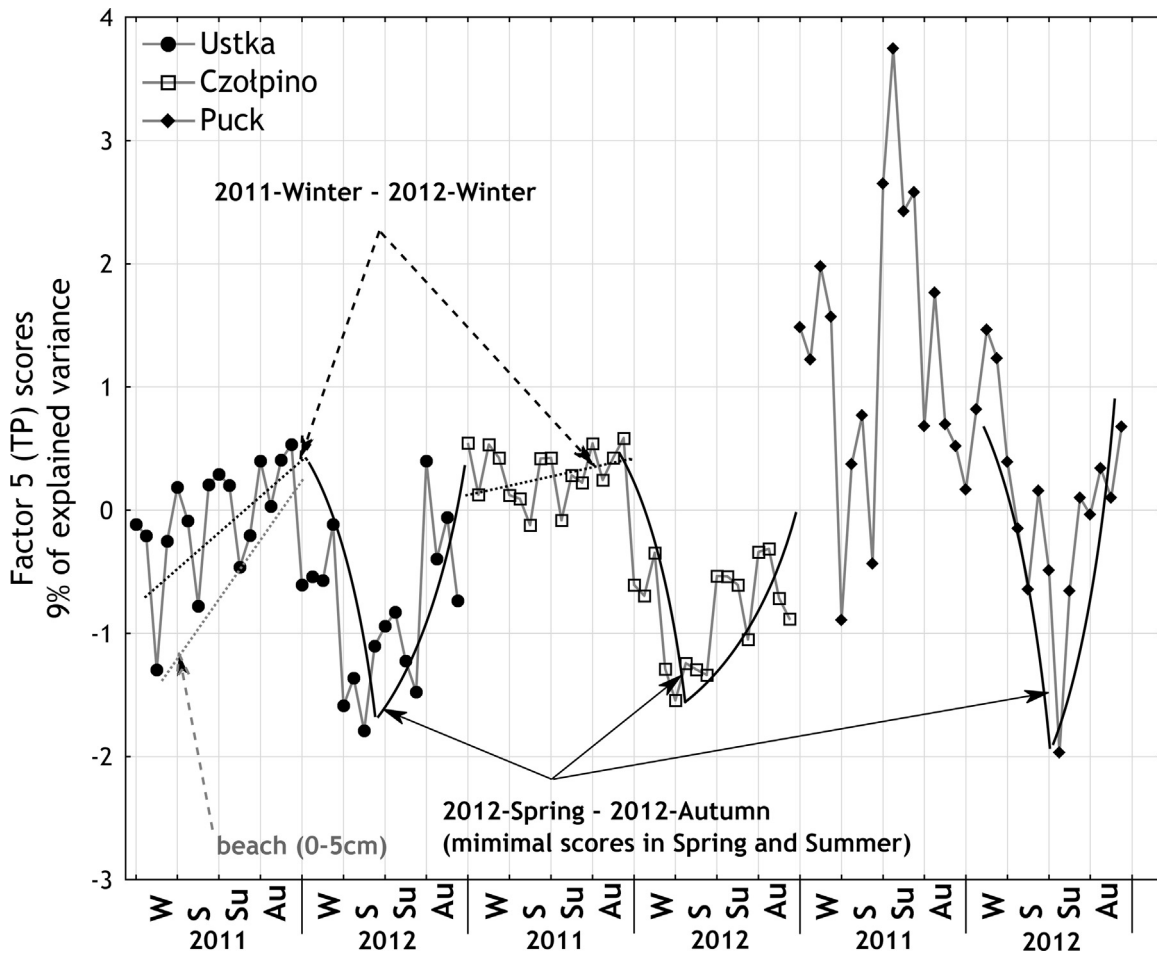


Figure 7 Factor 5 (anthropogenic rich in P) scores according to the location of the beach (on x axis W, S, Su and Au states for winter, spring, summer and autumn, respectively).

differences between the median activity of α -glucosidase and β -glucosidase was confirmed in pairs: Czotpino-Puck and Ustka-Puck. The only difference appeared between α -glucosidase activity in Ustka and Czotpino (Table 3). It appears that in Ustka twice as high activity of α -glucosidase is observed which is confirmed by corresponding mean and median values (Table 2) as well as a slightly higher spread of extreme factor 6 scores. As mentioned above, the activity of α -glucosidase increases when hardly assimilable matter appears in the environment, which is much more predictable in a location of moderate anthropogenic impact (Ustka) than in a clean area (Czotpino). A careful inspection of Fig. 8 revealed some other interesting details. During Spring 2012 some significant drop of factor 6 scores is observed in Ustka and Czotpino. For the “hydrolytic” factor, the observed drop relates to an increase of α -glucosidase activity (due to a negative factor score value, Table 4). Increased α -glucosidase activity in Ustka and Czotpino fits with maximal factor 1 scores (Fig. 3) and minimal factor 3 scores (Fig. 5) in these locations. Such simultaneous assessment proves that microorganisms induce α -glucosidase synthesis to decompose hardly assimilable COM during deficit of easily assimilable PRT and CHO. Moreover, in both locations (Ustka, Czotpino) the mentioned drop consists of two pairs of scores. Among them, lower and upper scores correspond with lower and upper layer of

sediment cores respectively. It suggests that the lack of easily assimilable matter activates stronger hydrolytic activity in the lower layers of core sediments.

5. Conclusions

The microbial enzymatic activity and its relation to various forms of organic matter abundance in beach sediments still remain an underdeveloped field of research. The results of the presented research prove the occurrence of essential changes in microbial enzymatic activity in sediments dredged from beaches diversified according to the anthropogenic impact and the degree of sheltering. The dredged material collected on the Polish coast is generally characterized by lower concentrations of PRT, CHO and LIP, as well as higher microbial enzymatic activity as compared to other coasts spread in southern Europe. Biochemical analysis of sediments derived from three different locations enables identification of various factors (anthropogenic rich in N, microbial enzymatic activity, labile organic matter, bacterial growth, anthropogenic rich in P and hydrolytic) impacting their microbial activity according to seasonality as well as horizontal and vertical profiles of the beach. Therefore, it can be concluded from the present study that anthropogenically originated OM dominates over natural

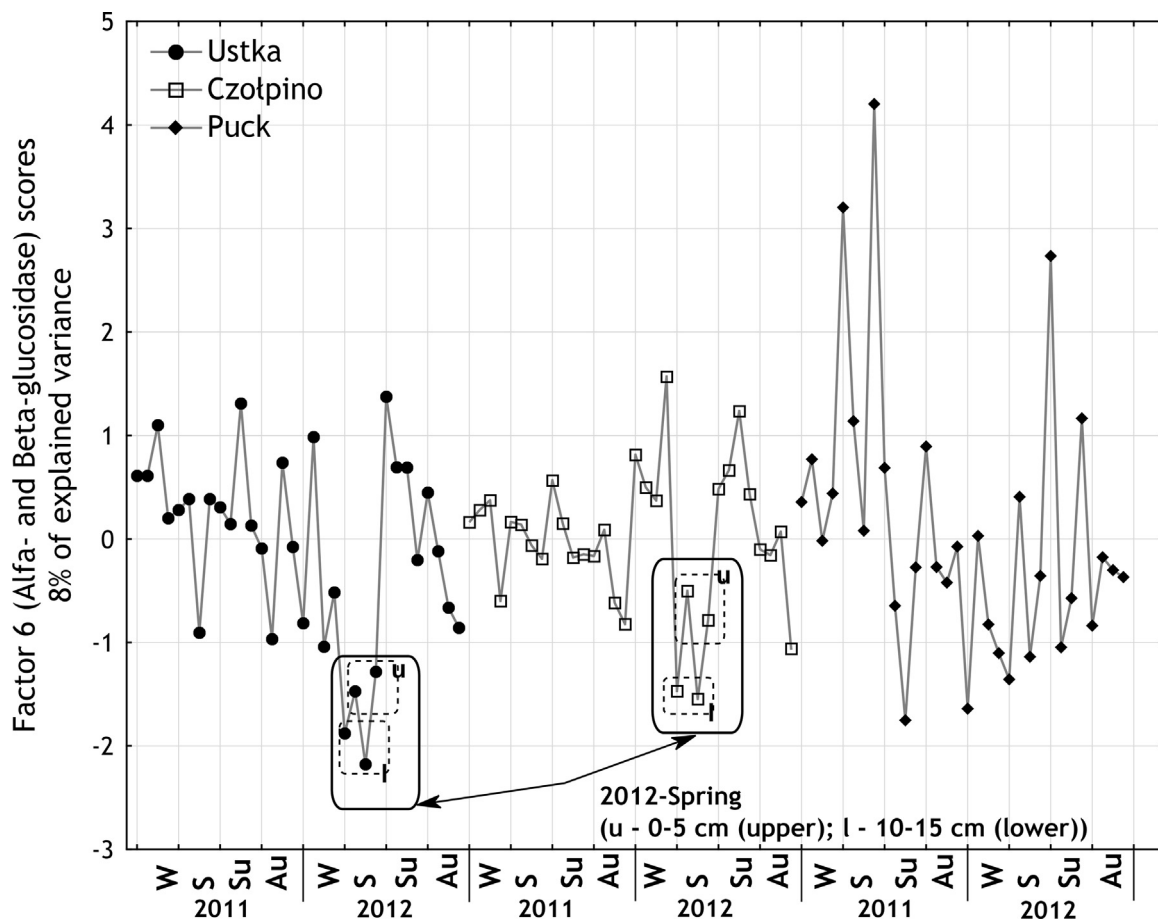


Figure 8 Factor 6 (hydrolytic) scores according to the location of the beach (on x axis W, S, Su and Au states for winter, spring, summer and autumn, respectively).

one on the Polish coast. The highest impact of artificial pollution takes place in Puck Bay, where several factors related to pollution sources as well as hydrodynamics of the sea create negative interactions for the environment. Microbial enzymatic activity depends on beach management, while hydrolytic activity varies according to the accessibility of hardly or easily assimilable forms of organic matter.

References

- Allen, J.I., Somerfield, P.J., Siddorn, J., 2002. Primary and bacterial production in the Mediterranean Sea: a modeling study. *J. Mar. Syst.* 33–34, 473–495.
- Antonowicz, J.P., Mudryk, Z., Zdanowicz, M., 2015. A relationship between accumulation of heavy metals and microbiological parameters in the surface microlayer and subsurface water of a coastal Baltic lake. *Hydrobiologia* 762, 65–80.
- Bartlett, M.S., 1951. The effect of standardization on a chi square approximation in factor analysis. *Biometrika* 38, 337–344.
- Bednarek, R., Dziadowiec, H., Pokojka, U., Prusinkiewicz, Z., 2005. *Research Concerning Ecology and Soil*. 344 pp.. PWN, Warsaw, (in Polish).
- Biddanda, B., Riemann, F., 1992. Detrital carbon and nitrogen relations, examined with degrading cellulose. *Mar. Ecol.* 13 (3), 271–283.
- Bigus, K., Astel, A.M., Niedzielski, P., 2016. Seasonal distribution of metals in vertical and horizontal profiles of sheltered and exposed beaches on Polish coast. *Mar. Pollut. Bull.* 106 (1–2), 347–359.
- Boetius, A., 1995. Microbial hydrolytic enzyme activities in deep-sea sediments. *Helgoländer Meeresuntersuchungen* 49, 177–187.
- Brown, A.C., McLachlan, A., 1990. *Ecology of Sandy Shores*. Elsevier, Amsterdam, 392 pp.
- Buchanan, J.B., Longbottom, M.R., 1970. The determination of organic matter in marine muds: the effect of the presence of coal and the routine determination of proteins. *J. Exp. Mar. Biol. Ecol.* 5, 158–169.
- Buscail, R., Pocklington, R., Daumas, R., Guidi, L., 1990. Fluxes and budget of organic matter in the benthic boundary layer over the northwestern Mediterranean margin. *Cont. Shelf Res.* 10, 1089–1122.
- Carney, R.S., 1989. Examining relationship between organic carbon flux and deep-sea deposit feeding. In: *Ecology of marine deposit feeders*, Lopez, G., Taghon, G., Levinton, J. (Eds.), *Lecture Notes on Coastal and Estuarine Studies*, vol. 31. Springer, New York, pp. 24–58.
- Cattell, R.B., 1978. *The Scientific Use of Factor Analysis in Behavioral and Life Sciences*. Plenum Press, New York, 618 pp.
- Cividanes, S., Incera, M., López, J., 2002. Temporal variability in the biochemical composition of sedimentary organic matter in an intertidal flat of the Galician coast (NW Spain). *Oceanol. Acta* 25, 1–12.
- Danovaro, R., 1996. Detritus-bacteria-miоfauna interactions in a seagrass bed (*Posidonia oceanica*) of the NW Mediterranean. *Mar. Biol.* 127, 1–13.

- Danovaro, R., Fabiano, M., Della Croce, N., 1993. Labile organic matter and microbial biomasses in deep-sea sediments (Eastern Mediterranean Sea). *Deep-Sea Res.* 1 40 (5), 953–965.
- Danovaro, R., Marralle, D., Della Croce, N., Parodi, P., Fabiano, M., 1999a. Biochemical composition of sedimentary organic matter and bacterial distribution in the Aegean Sea: trophic state and pelagic–benthic coupling. *J. Sea Res.* 42, 117–129.
- Danovaro, R., Dinet, A., Duineveld, G., Tselepidis, A., 1999b. Benthic response to particulate fluxes in different trophic environments: a comparison between the Gulf of Lions–Catalan sea (W Mediterranean) and the Cretan Sea (E-Mediterranean). *Prog. Oceanogr.* 44 (1), 287–312.
- Danovaro, R., Dell'Anno, A., Trucco, A., Serresi, M., Vanucci, S., 2001. Determination of virus abundance in marine sediments. *Appl. Environ. Microbiol.* 67, 1384–1387.
- Daumas, R., Sautriot, D., Calmet, D., 1983. Evolution de constituants labiles de la matière organique dans les sédiments profonds de diverses marges continentales. In: D'Orgon à Misedor (Eds.), *Géochimie organique des sédiments marins*. C.N.R.S., Paris, 99–150.
- Dell'Anno, A., Mei, M.L., Pusceddu, A., Danovaro, R., 2002. Assessing the trophic state and eutrophication of coastal marine systems: a new approach based on the biochemical composition of sediment organic matter. *Mar. Pollut. Bull.* 44, 611–622.
- DuBois, M., Gilles, K.A., Hamilton, J.K., Rebers, P.A., Smith, F., 1956. Colorimetric method for determination of sugars and related substances. *Anal. Biochem.* 28 (3), 350–356.
- Ellery, W.N., Schleyer, M.H., 1984. Comparison of homogenization and ultrasonication as techniques in extracting attached sedimentary bacteria. *Mar. Ecol.-Prog. Ser.* 15 (3), 247–250.
- Fabiano, M., Danovaro, R., 1994. Composition of organic matter in sediments facing a river estuary (Tyrrhenian Sea): relationships with bacteria and microphytobenthic biomass. *Hydrobiologia* 277, 71–84.
- Fabiano, M., Danovaro, R., Frascchetti, S., 1995. A three-year time series of elemental and biochemical composition of organic matter in subtidal sediments of the Ligurian Sea (northwestern Mediterranean). *Cont. Shelf Res.* 15 (11–12), 1453–1469.
- Fabiano, M., Marin, V., Misic, C., Moreno, M., Salvo, V.S., Vezzulli, L., 2004. Sedimentary organic matter and bacterial community in microtidal mixed beaches of the Ligurian sea (NW Mediterranean). *Chem. Ecol.* 20 (6), 423–435.
- Fernandes, C.E., Das, A., Nath, B.N., Faria, D.G., LokaBharathi, P.A., 2012. Mixed response in bacterial and biochemical variables to simulated sand mining in placer-rich beach sediments, Ratnagiri, West coast of India. *Environ. Monit. Assess.* 184 (5), 2677–2689.
- Fichez, R., 1991a. Suspended particulate organic matter in a Mediterranean submarine cave. *Mar. Biol.* 108, 167–174.
- Fichez, R., 1991b. Composition and fate of organic matter in submarine cave sediments; implications for the biogeochemical cycle of organic carbon. *Oceanol. Acta* 14 (4), 369–377.
- Forsberg, C., 1991. Eutrophication of the Baltic Sea. Uppsala Univ. Press, Uppsala, 32 pp.
- Fuhrman, J.A., Azam, F., 1982. Thymidine incorporation as a measure of heterotrophic bacterioplankton production in marine surface waters: evaluation and field results. *Mar. Biol.* 66 (2), 109–120.
- Germán Rodríguez, J.G., Lastra, M., López, J., 2003. Meiofauna distribution along a gradient of sandy beaches in northern Spain. *Estuar. Coast. Shelf Sci.* 58, 63–69.
- Graf, G., 1989. Pelagic–benthic coupling in a deep-sea benthic community. *Nature* 341, 437–439.
- Graf, T.R., Meyer-Reil, L.A., 1985. Remineralization of organic substances on benthic surfaces in the intertidal reef off Mactan, Cebu, Philippines. *Philippine Sci.* 22, 42–46.
- Graf, G., Shulz, T., Peinert, R., Meyer-Reil, L.A., 1983. Benthic response to sedimentation events during autumn to spring at a shallow water station in the Western Kiel Bight. I. Analysis of processes on a community level. *Mar. Biol.* 77 (3), 235–246.
- Grant, J., Hargrave, B.T., 1987. Benthic metabolism and the quality of sediment organic carbon. *Biol. Oceanogr.* 4 (3), 243–264.
- Håkanson, L., Bryhn, A.C., 2008. Eutrophication in the Baltic Sea: Present Situation, Nutrient Transport Processes, Remedial Strategies. Springer-Verlag, Berlin, 300 pp.
- Halliday, E., Gast, R.J., 2011. Bacteria in beach sands: an emerging challenge in protecting coastal water quality and bather health. *Environ. Sci. Technol.* 45 (2), 370–379.
- Handa, N., Yanagi, K., Matsunaga, K., 1972. Distribution of detrital material in the Western Ocean and their biochemical nature. *Memorie dell'Istituto Italiano di Idrobiologia* 29, 53–71.
- Hervé, A., 2010. Factor Rotations in Factor Analyses, <http://www.utd.edu/~herve/Abdi-rotations-pretty.pdf> (accessed 17.01.10).
- HELCOM, 2009. Eutrophication in the Baltic Sea – an integrated thematic assessment of the effects of nutrient enrichment and eutrophication in the Baltic Sea region. In: *Baltic Sea Environment Proceedings No. 115B*, Helsinki Commission. Helsinki 148 pp.
- Heymans, J.J., McLachlan, A., 1996. Carbon budget and network analysis of a high-energy beach/surf-zone ecosystem. *Estuar. Coast. Shelf Sci.* 43 (4), 485–505.
- Hoppe, H.G., 1984. Relations between bacterial extracellular enzyme activities and heterotrophic substrate uptake in a brackish-water environment. 2. In: *Colloque International de Bacteriologie Marine*, Brest, France, 1–5.
- Incera, M., Cividanes, M., Lastra, M., López, J., 2003. Temporal and spatial variability of sedimentary organic matter in sandy beaches on the northwest coast of the Iberian Peninsula. *Estuar. Coast. Shelf Sci.* 58, 55–61.
- Januszkiewicz, T., 1978. Study on methods of chemical analyses of the composition of contemporary bottom sediments in lakes. *Olsztyn, Szesty Naukowe ART* 8, 3–30, (in Polish).
- Jędrzejczak, M.F., 1999. The degradation of stranded carrion on a Baltic Sea sandy beach. *Oceanol. Stud.* 28 (3–4), 109–141.
- Jugnia, L.B., Tadonlélé, R.D., Sime-Ngando, T., Devaux, J., 2000. The microbial food web in the recently flooded Sep Reservoir: diel fluctuations in bacterial biomass and metabolic activity in relation to phytoplankton and flagellate grazers. *Microb. Ecol.* 40 (4), 317–329.
- Kaiser, E., Herndl, G.J., 1997. Rapid recovery of marine bacterioplankton activity after inhibition by UV radiation in coastal waters. *Appl. Environ. Microbiol.* 63 (10), 4026–4031.
- Khiyama, H.M., Makemson, J.C., 1973. Sand beach bacteria: enumeration and characterization. *Appl. Microbiol.* 26 (3), 293–297.
- Khripounoff, A., Crassous, P., Desbrynyères, D., Le Cox, J.R., 1985. Le flux organique particulaire et ses transformations à l'interface eau-sédiment. *Oceanol. Acta* 8 (3), 293–301.
- Koop, K., Griffiths, C.L., 1982. The relative significance of bacteria, meio- and macrofauna on an exposed sandy beach. *Mar. Biol.* 66 (3), 295–300.
- Krstulović, N., Solić, M., 1988. Distribution of proteolytic, amyolytic and lipolytic bacteria in the Kastela Bay. *Acta Adriat.* 29, 75–82.
- Markwell, M.A.K., Hass, S.M., Bieber, L.L., Tolbert, M.E., 1978. A modification of the Lowry procedure to simplify protein determination in membrane and lipoprotein samples. *Anal. Biochem.* 87 (1), 206–210.
- Massart, D.L., Kaufman, L., 1997. *The Interpretation of Analytical Chemical Data by the Use of Cluster Analysis*. Wiley-Interscience, New York, 237 pp.
- McLachlan, A., De Ruyck, A., Hacking, N., 1996. Community structure on sandy beaches: patterns of richness and zonation in relation to tide range and latitude. *Revista Chilena de Historia Natural* 69, 451–467.
- Meyer-Reil, L.A., 1983. Benthic response to sedimentation events during autumn to spring at a shallow-water station in the Western Kiel Bight. II. Analysis of benthic bacterial populations. *Mar. Biol.* 77 (3), 247–256.
- Meyer-Reil, L.A., Bölter, M., Dawson, R., Liebezeit, G., Szweringi, H., Wolter, K., 1980. Interrelationships between microbiological

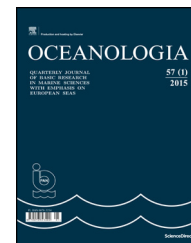
- and chemical parameters of sandy beach sediments, a summer aspect. *Appl. Environ. Microbiol.* 39 (4), 797–802.
- Misic, C., Fabiano, M., 2005. Enzymatic activity on sandy beaches of the Ligurian Sea (NW Mediterranean). *Microb. Ecol.* 49 (4), 513–522.
- Mudryk, Z., Podgórska, B., 2006. Enzymatic activity bacterial strains isolated from marine beach. *Pol. J. Environ. Stud.* 15, 441–448.
- Mudryk, Z., Podgórska, B., 2007. Culturable microorganisms in sandy beaches in the south Baltic Sea. *Pol. J. Ecol.* 55, 221–231.
- Mudryk, Z., Donderski, W., Skórczewski, P., Walczak, M., 1999. Neustonic and planktonic bacteria isolated from a brackish lake Gardno. *Pol. Arch. Hydrobiol.* 46, 121–129.
- Mudryk, Z., Skórczewski, P., Perliński, P., Wielgat, M., 2011. Studies concerning heterotrophic bacteria decomposing macromolecular compounds at two marine beaches. *Oceanol. Hydrobiol. Stud.* 40, 74–83.
- Myślińska, E., 2001. *Laboratory Studies of Soils*. PWN, Warsaw, 277 pp., (in Polish).
- Nair, S., Loka Bharathi, P.A., 1980. Heterotrophic bacterial population in tropical sandy beaches. *Mahasagar* 13 (3), 261–267.
- Nordstrom, K.F., 1992. *Estuarine Beaches*. Elsevier, London/New York, 226 pp.
- Novitsky, J.A., MacSween, M.C., 1989. Microbiology of a high energy beach sediment: evidence for an active and growing community. *Mar. Ecol.-Prog. Ser.* 52, 71–75.
- Olańczuk-Neyman, K., Jankowska, K., 1998. Bacteriological investigations of the sandy beach ecosystem in Sopot. *Oceanologia* 40, 137–151.
- Penna, N., Kovač, N., Ricci, F., Penna, A., Capellacci, S., Faganeli, J., 2009. The role of dissolved carbohydrates in the Northern Adriatic macroaggregate formation. *Acta Chim. Slov.* 56, 305–314.
- Perliński, P., Mudryk, Z.J., 2016. Activity of extracellular enzymes on the marine beach differing in the level of antropopressure. *Environ. Monit. Assess.* 188 (3), 188–200.
- Phillips, M.C., Solo-Gabriele, H.M., Reniers, A.J.H.M., Wang, J.D., Kiger, R.T., Abdel-Mottaleb, N., 2011. Pore water transport of enterococci out of beach sediments. *Mar. Pollut. Bull.* 62 (11), 2293–2298.
- Piggot, A.M., Klaus, J.S., Johnson, S., Phillips, M.C., Solo-Gabriele, H.M., 2012. Relationship between enterococcal levels and sediment biofilms at recreational beaches in South Florida. *Appl. Environ. Microbiol.* 78 (17), 5973–5982.
- Porter, K.G., Feig, Y.S., 1980. The use of DAPI for identifying and counting aquatic microflora. *Limnol. Oceanogr.* 25 (5), 943–948.
- Report, 2010. The Report on the State of the Environment in the Pomeranian Province in 2010. Biblioteka Monitoringu Środowiska, Gdańsk 169 pp., <https://www.gdansk.wios.gov.pl/monitoring/282-raporty-o-stanie-srodowiska-w-województwie-pomorskim.html> (accessed 14.04.16).
- Report, 2012. The Report on the State of the Environment in the Pomeranian Province in 2012. 180 pp.. Biblioteka Monitoringu Środowiska, Gdańsk <http://www.gdansk.wios.gov.pl/monitoring/282-raporty-o-stanie-srodowiska-w-województwie-pomorskim.html> (accessed 14.04.16).
- Robinson, J.D., Mann, K.H., Novitsky, J.A., 1982. Conversion of the particulate fraction of seaweed detritus to bacterial biomass. *Limnol. Oceanogr.* 27 (6), 1072–1079.
- Rodil, I.F., Lastra, M., 2004. Environmental factors affecting benthic macrofauna along a gradient of intermediate sandy beaches in northern Spain. *Estuar. Coast. Shelf Sci.* 61 (1), 37–44.
- Rodil, L.F., Lastra, M., López, J., 2007. Macroinfauna community structure and biochemical composition of sedimentary organic matter along a gradient of wave exposure in sandy beaches (NW Spain). *Hydrobiologia* 579 (1), 301–316.
- Rodil, I.F., Cividanes, S., Lastra, M., López, J., 2008. Seasonal variability in the vertical distribution of benthic macrofauna and sedimentary organic matter in an estuarine beach (NW Spain). *Estuar. Coasts* 31 (2), 382–395.
- Rowe, G.T., Deming, J., 1985. The role of bacteria in the turnover of organic carbon in deep-sea sediments. *J. Mar. Res.* 43 (4), 925–950.
- Sargent, J.R., Hopkins, C.C.E., Seiring, J.V., Youngson, A., 1983. Partial characterization of organic material in surface sediments from Balsfjorden, northern Norway, in relation to its origin and nutritional value for sediment-ingesting animals. *Mar. Biol.* 76 (1), 87–94.
- Schoeman, D.S., McLachlan, A., Dugan, J.E., 2000. Lessons from a disturbance experiment in the intertidal zone of an exposed sandy beach. *Estuar. Coast. Shelf Sci.* 50 (6), 869–884.
- Smayda, T.J., 1997. Harmful algal blooms: Their ecophysiology and general relevance to phytoplankton blooms in the sea. *Limnol. Oceanogr.* 42 (5 Part 2), 1137–1153.
- Szefer, P., 2002. *Metals, Metalloids and Radionuclides in the Baltic Sea Ecosystem*. Elsevier Science, Amsterdam, 766 pp.
- Thompson, J.K., Nichols, F.H., 1988. Food availability controls seasonal cycle of growth in *Macomabalthica* (L.) in San Francisco Bay, California. *J. Exp. Mar. Biol. Ecol.* 116 (1), 43–61.
- Thurstone, L.L., 1947. *Multiple Factor Analysis: A Development and Expansion of Vectors of the Mind*. University of Chicago Press, Chicago, 535 pp.
- Vandeginste, B.G.M., Massart, D.L., Buydens, L.M.C., De Jong, S., Lewi, P.J., Smeyers-Verbeke, J., 1997. *Handbook of Chemometrics and Qualimetrics; Data Handling in Science and Technology, Parts A and B*. Elsevier, Amsterdam, 886 pp., 876 pp.
- Vu, N.T., 2016. *Algae Biology*, https://www.academia.edu/1741106/ALGAE_BIOLOGY (accessed 27.07.16).
- Węstawski, M., Urban-Malinga, B., Kotwicki, L., Opaliński, K.W., Szymelfenig, M., Dutkowski, M., 2000. Sandy coastlines – are there conflicts between recreation and natural values? *Oceanol. Stud.* 2, 5–18.
- Węstawski, J.M., Szymelfenig, M., Urbański, J., 2005. *The Beach: User's Manual*. Centre of Excellence for Shelf Seas Science. IO PAN Press, Sopot, 112 pp.
- Wilson, J.O., Buchsbaum, R., Valiela, I., Swain, T., 1986. Decomposition in salt marsh ecosystems: phenolic dynamics during decay of litter of *Spartina alterniflora*. *Mar. Ecol. Progr. Ser.* 29 (2), 177–187.
- Zeng, X., Xiao, X., Wang, F., 2010. Response of bacteria in the deep-sea sediments and the Antarctic soils to carbohydrates: effects on ectoenzyme activity and bacterial community. *J. Environ. Sci. (China)* 22 (11), 1779–1785.
- Ziervogel, K., McKay, L., Rhodes, B., Osburn, C.L., Dickson-Brown, J., Arnosti, C., Teske, A., 2012. Microbial enzymatic activity and secondary production in sediments affected by the sedimentation pulse following the Deepwater Horizon oil spill. *PLoS ONE* 7 (4), 34816.
- Ziervogel, K., Joye, S.B., Arnosti, C., 2016. Microbial enzymatic activity and secondary production in sediments affected by the sedimentation pulse following the Deepwater Horizon oil spill. *Deep-Sea Res. II* 129, 241–248.
- Zöllner, K., Kirsch, A., 1962. Über die quantitative Bestimmung von Lipiden (Mikromethode) mittels der vielen natürlichen Lipiden (allen bekannten Plasmalipiden) gemeinsamen Sulfophosphovanillin-Reaktion. *Zeitschrift für die Gesamte Experimentelle Medizin* 135, 545–561.



Available online at www.sciencedirect.com

ScienceDirect

journal homepage: www.journals.elsevier.com/oceanologia/



ORIGINAL RESEARCH ARTICLE

Wind wave climate of west Spitsbergen: seasonal variability and extreme events

Kacper Wojtysiak ^{a,*}, Agnieszka Herman ^b, Mateusz Moskalik ^a

^a *Institute of Geophysics, Polish Academy of Sciences, Warszawa, Poland*

^b *Institute of Oceanography, University of Gdańsk, Gdynia, Poland*

Received 28 August 2017; accepted 18 January 2018

Available online 6 February 2018

KEYWORDS

Arctic;
Wave climate;
Hindcast;
Reanalysis;
Svalbard

Summary Waves are the key phenomenon directly influencing coastal morphodynamics. Facing insufficient observations, wind wave climate of the west coast of Spitsbergen can be characterized on the basis of the modelled data. Here we have used the results of spectral wave models: Wave Watch III (WW3) hindcast and WAM in ERA-interim (ERAi) reanalysis. We have observed the presence of seasonal cycle with difference of up to 1 m between significant wave heights in summer and winter. In wave-direction analysis we have noticed the southwestern swell component of remarkably narrow width, thus we expect unidirectional swell impact on the coastline. Extreme events analysis revealed that storms occur mainly in winter, but the most energetic ones (significant wave height of up to 9.5 m) occur in spring and autumn. We have identified positive trends in storms' frequency (2 storms per decade) and storms' total duration (4 days per decade) on the south of the study area. More storms can result in the increase of erosion rate on the southwestern coasts of Spitsbergen, but this change may be highly dependent on the sea ice characteristics. Wave heights of wind sea and swell are correlated with the relevant atmospheric circulation indices, especially the North Atlantic Oscillation. In the recent decade, the correlation is stronger with WW3 than with ERAi data, at some locations explaining over 50% (over 30%) of the total variance of wind sea (swell) wave heights. In ERAi data, the relationship with circulation indices seems sensitive to the length of the analysis period.

© 2018 Institute of Oceanology of the Polish Academy of Sciences. Production and hosting by Elsevier Sp. z o.o. This is an open access article under the CC BY-NC-ND license (<http://creativecommons.org/licenses/by-nc-nd/4.0/>).

* Corresponding author: Institute of Geophysics PAS, ul. Księcia Janusza 64, PL-01-452 Warszawa, Poland. Tel.: +48 601807333.

E-mail addresses: kwojtys@igf.edu.pl (K. Wojtysiak), oceagah@gmail.com (A. Herman), m Mosk@igf.edu.pl (M. Moskalik).

Peer review under the responsibility of Institute of Oceanology of the Polish Academy of Sciences.



Production and hosting by Elsevier

<https://doi.org/10.1016/j.oceano.2018.01.002>

0078-3234/© 2018 Institute of Oceanology of the Polish Academy of Sciences. Production and hosting by Elsevier Sp. z o.o. This is an open access article under the CC BY-NC-ND license (<http://creativecommons.org/licenses/by-nc-nd/4.0/>).

1. Introduction

Wind wave conditions are an important feature in variety of coast-related processes (Semedo et al., 2015; Wang and Swail, 2001; Zacharioudaki et al., 2015). Instrumental monitoring of waves is usually restricted to single points (buoys, ships, oil platforms) or relatively narrow areas via remote sensing (regarding small time scales). The downside of those techniques is usually insufficient temporal and/or spatial extent and/or resolution. Recent development of numerical methods (Thomas and Dwarakish, 2015 and the references therein) resulted in the gain of scientific acclaim of modelled data due to its increasing precision. Simulations, unlike measurements, are free from the limitations of purely observational approach.

In this study, we are using model-based hindcast/reanalysis to describe wind-wave characteristics of the north-eastern Greenland Sea shelf area, west of Svalbard Archipelago. In situ wave monitoring is rare in the offshore areas of the Arctic. Several buoys are deployed only in the area of Chukchi Sea and the ones in Atlantic Ocean are located in the area of the western Iceland shelf and north-east of Shetland Islands, several hundreds of kilometres from the area of interest of the present study. Although some observations of the waves are being conducted, location of buoys is restricted to in-shore areas in fjords, in shallow (order of 10–30 m) water, which puts the validation of the model data from off-shore locations in question.

Few papers describe wind waves in regions that contain this study's domain (Reistad et al., 2011; Semedo et al., 2015; Stopa et al., 2016). Moreover, they have larger-scale, regional character, as opposed to this paper, which aims to characterize a relatively small part of the Arctic Ocean's coastal zone.

Wave climate in the study area consists of swell from the North Atlantic and locally generated wind waves, and is influenced by a number of factors including the sea ice coverage, bathymetry, tidal currents. Wave climate of the Nordic-Greenland Seas is characterized by well-marked seasonality of significant wave height (H_s), with stormy period in December through February, followed by a decrease in spring and a calm period in June to mid-August (Stopa et al., 2016).

Apart from seasonal variability, the wave climate undergoes long-term changes. Many studies (e.g. Bertin et al., 2013; Kushnir et al., 1997; Young et al., 2011) indicate the presence of a positive trend in wave heights for the Northern Hemisphere with the emphasis on the North Atlantic. Stopa et al. (2016) conclude that wind speeds and wave heights on Nordic-Greenland Seas have been increasing within the last 20 years, and mention the role of atmospheric indices (e.g., North Atlantic Oscillation) in the process. They also indicate the prevalence of swell in the total wave energy, but the role of sea-ice interactions with waves is unclear. Semedo et al. (2015) also notice a significant share (not less than 50%) of swell in the total significant wave height, and their results indicate prevailing directions of waves origin to be south-west for swell, and east for wind sea, regardless of the season.

This paper focuses on characterizing the west Spitsbergen wave climate on the basis of hindcasted and reanalyzed wave parameters which are: significant wave height (H_s), peak

period (T_p), –1st moment mean period (T_m), and incoming wave direction (Θ). The goal is to describe typical wave conditions and to extract information about occurrence, frequency and duration of extreme events. Our main motivation for conducting this study is that there are, to our knowledge, no similar research studies conducted for this area so far, despite its importance in, e.g., impact on coastal erosion rates. In the study by Zagórski et al. (2015), it is clearly pointed out that wave activity and storm occurrence strongly contribute to erosion rates of the coast of Isbjornhamna, one of the Hornsund fjord's bays, posing a threat to the infrastructure of the Polish Polar Station located there. In other research, Sessford et al. (2015), analyzed data from field sites located in the inner parts of Isfjorden and Van Mijenfjorden and concluded that the influence of waves on the coasts was minimal. The two examples with seemingly contradictory conclusions actually suggest significant differences in wave influence on individual parts of the coast. Results from local studies cannot be extrapolated to the coasts of the west Spitsbergen in general.

Details on the area of interest, data sources and used methods are described in the next section of this paper, which is followed by the results and discussion on seasonality, wave directions, wind wave extreme events and possible correlations with chosen atmospheric indices. Conclusions and remarks about the future goals are presented in the last section.

2. Data and methods

2.1. Study area

Svalbard is an isolated archipelago influenced climatically by two substantially different water bodies – the Arctic and Atlantic oceans. Spitsbergen, the biggest island of the archipelago, is a vivid example of the above. Its east coast remains under a cold regime of Arctic waters, while the climate of the western shores is significantly altered by the warm North Atlantic Current originating in the Gulfstream (Drange et al., 2005; Przybylak, 2003). Przybylak (2003) points out that the Atlantic region of the Arctic – defined as the combined areas of Greenland Sea, Barents Sea and Svalbard – stands out from its remaining parts, as it is significantly warmer (up to 20°C higher monthly mean air temperature, compared to other regions of the same latitude). Wind speeds in this area are also of the highest in the entire Arctic. Since prevailing winds in the region are Polar Easterlies, main wind directions are from the east and north east, with speeds up to 8–10 m s⁻¹ (monthly average) and directional distribution narrow during winter, while summer months are characterized by wind speeds of ca. 5 m s⁻¹ and the directional distribution is considerably wider.

The seas to the west of Spitsbergen are, in general, free of multiyear ice (Johannessen et al., 2004; Onarheim et al., 2014). In the past 3 decades, first year sea ice developed only in the Sorkapp area in the far south and close to the Albert I Land in the far north. As Onarheim et al. (2014) describe, sea ice extent north of Svalbard gradually decreased in last decades. What has to be mentioned to complete the description of the ice conditions is the

phenomenon of sea ice clusters of considerable ice concentration (>30%), which are episodically observed along the west coast of Spitsbergen. These events are of variable duration (days to months long) and scale. They may occur in late winter throughout spring, up until late autumn, and are very well visible in remote sensing data (<http://polarview.met.no/>). Styszynska and Buchert (2004) have described one of the most prominent events of this kind that took place from May to July 2004, when closed drift ice formed a 50-km-wide stream along the west coast of Spitsbergen, significantly disturbing marine traffic in the area. The scale of the event was explained by a shift of the West Spitsbergen Current (WSC) to the west. This shift, combined with atmospheric circulation at that time, created favourable conditions to move substantial ice masses from the south-east part of the Island to the south-west and further north-west. A similar event of a smaller scale occurred from May to June 2011, and was briefly mentioned by Kruszewski (2012). This kind of sea ice behaviour is observable in the ice coverage data sets used in this paper and may have significant influence on wave propagation from the open ocean to the coasts.

For our study we have chosen the north-eastern part of the Greenland Sea, bordering with the west coast of Spitsbergen. The latitudes of the domain of study span the range between 76 and 80°N, while longitudes are contained within 5 and 20°E (Fig. 1a). For a detailed analysis we selected 9 points along a line that follows the general, approximate shape of the Spitsbergen coastline and its shelf (Fig. 1b), with the purpose to analyze spatial variability of the wave environment in different parts of the domain of interest. All points are located within the shelf area, 15–55 km from the coast and the ocean depth varies between 155 and 380 m with exception of point 3 (80 m) and 9 (490 m).

2.2. The datasets

As a source of wind wave data, two datasets were used. The National Oceanic and Atmospheric Administration's (NOAA) WaveWatch III (WW3) hindcast was obtained from the archive located on public NOAA's Environmental Modeling Center/Marine Modeling & Analysis Branch ftp server (<ftp://polar.ncep.noaa.gov/pub/history/waves>). The second source was the European Centre for Medium-Range Weather Forecasts' ERA-Interim (ERAi) reanalysis (Dee et al., 2011). Both datasets are open-access databases. We decided to use two independent sources based on two different models with some differences in algorithms describing the physical processes, in numerical methods, as well as configuration, particularly in terms of wave frequency cut-off and treatment of the sea ice influence (Dee et al., 2011; Tolman, 2014). WW3 data offers higher spatial and temporal resolution, as well as better performance in terms of swell propagation, while ERAi delivers longer time series which is necessary for an analysis of long-term variability. For the comparison of both datasets' selected characteristics see Table 1.

2.3. WW3

We have acquired nearly ten-year time series (February 2005–March 2015) of H_s , T_p and θ with temporal resolution of 8 measurements a day, and grid cell size of $0.5 \times 0.5^\circ$. WW3 hindcast, apart from bulk parameters characterizing whole wave energy spectra, contains also data derived from 2-dimensional energy spectra separated into variable number of partitions, which enables analysis of separate wave systems aside from their superposition. These data were used in the analysis of wave directions. Full documentation of the WW3 model can be found in WaveWatch 3 manual by Tolman (2014). As an additional variable, sea ice concentration

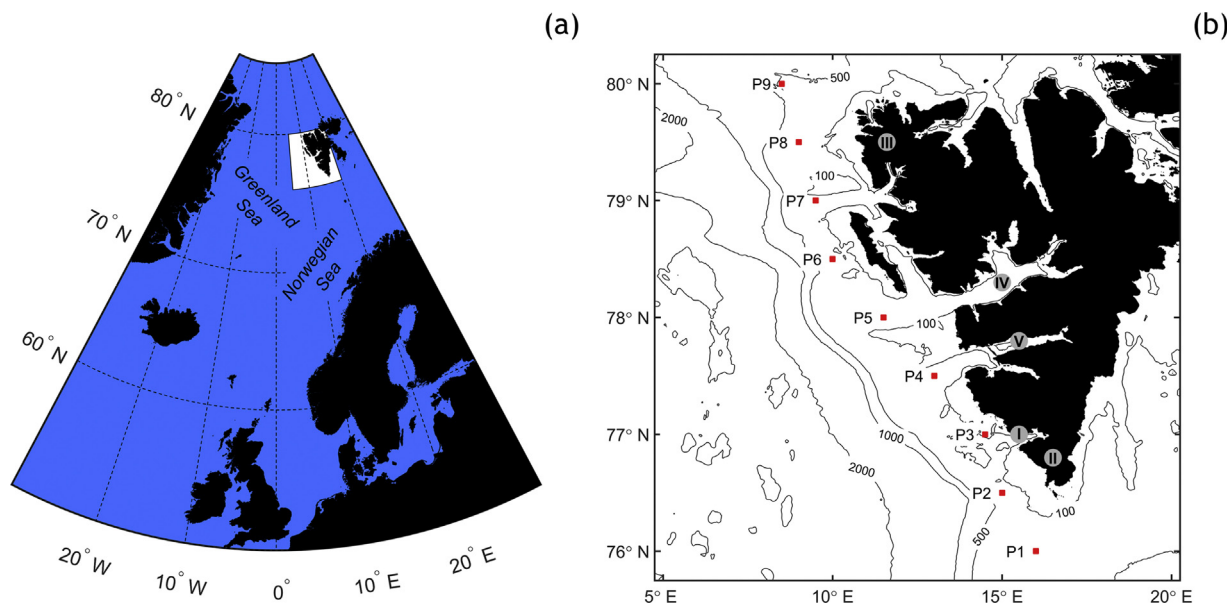


Figure 1 (a) Map of North Atlantic with the study area shown as white field. (b) Grid limits of the study area with points of analysis marked red and numbered from P1 to P9. Grey circles mark the locations as follows: I – Polish Polar Station in Hornsund, II – Sorkapp, III – Albert I Land, IV – Isfjorden, V – Van Mijenfjorden.

Table 1 Comparison of the datasets used in the analysis.

	WW3	ERAi
Spectral wave model used	WaveWatch III	WAM
Partitioning of energy spectra	Bulk, wind sea, up to 9 swells	Bulk, wind sea, total swell
Dataset time range used	Feb 2005–Apr 2015	Jan 1979–Dec 2015
Native spatial resolution [°]	0.5 × 0.5	1 × 1
Temporal resolution (values per 24 h)	8	4
Spectral resolution	36 directions 50 frequencies	24 directions 30 frequencies

values were obtained from the NCEP/NCAR Climate Data Assimilation System (<ftp://polar.ncep.noaa.gov/pub/cdas/>). Ice concentration data is available in the same spatial resolution, but calculated once per day.

2.4. ERAi

ERAi wind wave data is based on the modified WAM model, improved in terms of parameterization of physical processes important for long-term, climate simulations. The model is two-way coupled to the atmospheric model and its operational resolution is $1 \times 1^\circ$. Time series of H_s , T_m and Θ were extracted for period from January 1979 to December 2015 with temporal resolution of 4 measurements per day. The data was retrieved as bulk, and also as two separate partitions of wind sea and total swell. ECMWF database offers the option to linearly interpolate grid data for selected parameters. Option $0.5 \times 0.5^\circ$ was chosen to obtain data at the same locations as the WW3 hindcast. No temporal interpolation was applied to the timeseries. ERAi archive delivers also sea ice concentration data, which were, additionally, extracted in the same spatial and temporal resolution as the wave data. For further information about ERAi reanalysis and WAM model configuration, see [Dee et al. \(2011\)](#) and references therein.

2.5. Data processing

The time series extracted from both data sets were inspected for continuity, and multiple fragments containing 'not-a-number' values (NaNs) in the ERAi and WW3 data were found. These NaNs are related to the models' configuration: wave energy is set to zero in grid points in which sea ice concentration exceeds a limiting value, equal to 0.30 in ERAi and 0.67 in WW3 (for ice concentrations between 0.33 and 0.67, WW3 uses a parameterization of wave propagation and attenuation in ice). The amount of NaNs in ERAi time series is therefore significantly higher than in WW3. To summarize, in majority of cases 'NaNs' in the data represent grid masking related to the presence of sea ice. All analyses in this study are performed using the standard type I (Ice time included) strategy that is thoroughly explained by [Tuomi et al. \(2011\)](#).

Before proceeding with further analysis, we compared the modelled H_s values with the available observation data ([Fig. 2a, b](#)). Additionally, a comparison of the WW3 and ERAi datasets was performed (see below and Supplementary Note S1). The next step was calculating seasonal variability of significant wave height for both sets in their full time range.

Here, apart from calculating the daily mean H_s values, LOESS model was applied to generate smoothed curves for both mean and 99th percentile values. Next, diagrams of daily mean H_s values were created for each point.

Due to the fact that initial study of period time series did not show clear seasonal pattern, and that both datasets contain different type of wave period data (peak period in WW3 and mean period in ERAi); period related analysis was not included in the main text. Instead, it is illustrated in the supplementary material (see Supplementary Note S1 and Supplementary Fig. S5).

For visualization of incoming wave directions, the partitioned WW3 data were used, with separated wind wave and a number of swell fractions. WW3 data are divided into partitions corresponding to modelled wave systems. Each partition is assigned a wind fraction parameter, ranging from 0 (swell wave) to 1 (wind sea). In order to eliminate from further analysis partitions of uncertain type, entries with wind fraction values between 0.3 and 0.7, which make circa 5% of the data, were not considered in calculations. For details on WW3 partitioning scheme and wind fraction calculation see [Tolman \(2014\)](#), section 3.9.

For analysis of extreme events we applied automated approach to obtain local H_s maximum values. Matlab function – *findpeaks* was used to extract the subset of peak values (H_s) with their location (in time) and width (duration) in the timeseries. In order to configure the function properly, we used elements of Peaks Over Threshold method – a statistical approach that involves the analysis of the sample of independent extreme values over a certain threshold ([Teena et al., 2012](#)). The function was given the following arguments:

- Minimum peak height (h_{mp}), restricting the algorithm to ignore peaks lower than the given value, expressed in metres; an analogue of the threshold value in the POT method,
- Minimum peak prominence (p_{mp}), a difference between considered peak and the local minima with relation to the peaks in the neighbourhood, expressed in metres; *findpeaks* will ignore small peaks on the slopes of the tall ranges of major peaks, but will preserve isolated peaks of given prominence, if all other conditions are met,
- Minimum distance between peaks (d_{mp}), expressed in hours, forces the algorithm to find peaks outside the specified range of each other; a declustering routine to prevent identifying groups of clustered peaks as separate events.

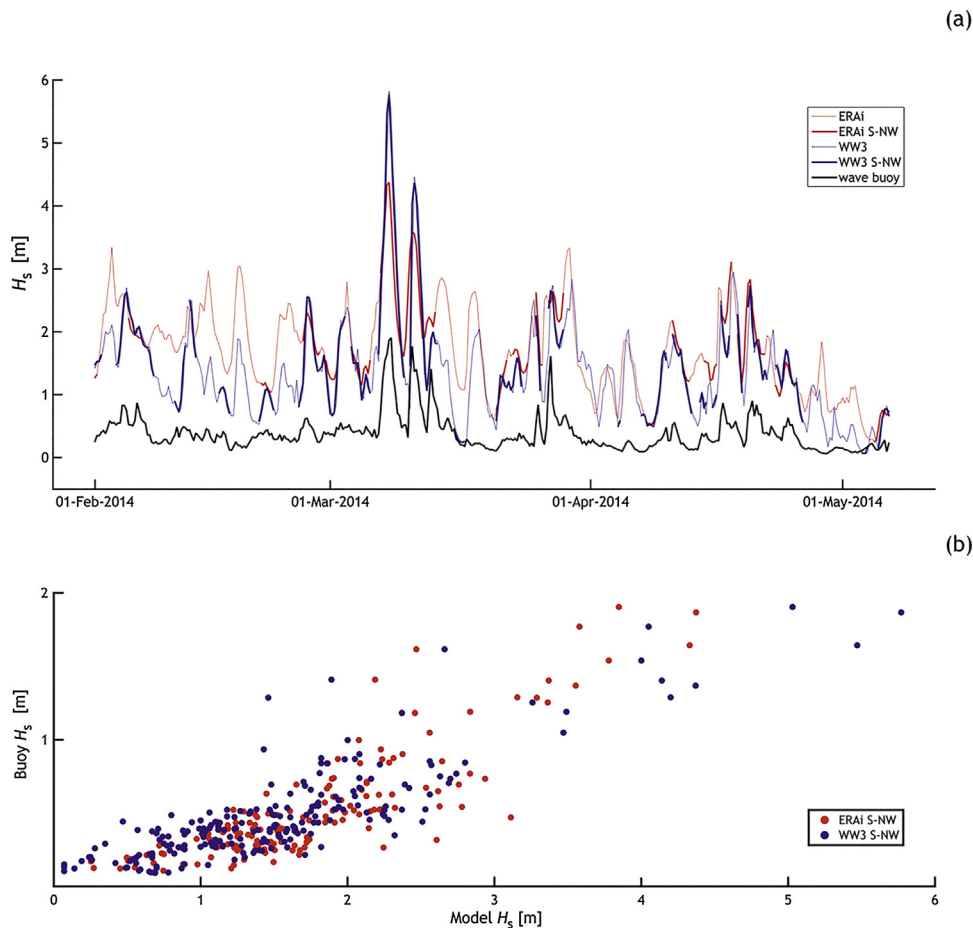


Figure 2 (a) Comparison of H_s time series from wave products used in this study (point P3 in Fig. 1b) with the wave buoy data from in-shore location in Hornsund fjord (marked “1” in Fig. 1b). The sections of the modelled time series with wave directions propagating from the directions (θ) between 180° (South) and 300° (North-West) are marked with thick lines. (b) Scatterplot of modelled H_s associated with θ in range of $180\text{--}300^\circ$ against the wave buoy data.

With the above arguments introduced, the algorithm scans the time series finding the highest peak, discards all peaks in range of d_{mp} , then repeats until there are no more peaks to consider.

The h_{mp} argument was initially set to 2.5 m – a value that corresponds to the 90th percentile of all WW3 and ERAI H_s values from all points combined. This approach enabled the analysis of extremes with the reference of the entire study area. After visual inspection of H_s time series, by the method of trial and error the p_{mp} value was set to 1 m to prevent finding low and/or short peaks. The d_{mp} value was deduced from iterative test, when the argument was inputted in range from 6 to 360 h and compared against the resulting number of peaks found by the function. After exceeding 24 h the number of peaks retrieved decreases rapidly while the mean time between two consecutive peaks started to increase from the base level of approximately 48 h. Regarding the fact that the average storm duration is shorter than the average time between the two consecutive storms, we set the d_{mp} to 72 h which is a sum of the average storm duration and the shortest period of silence directly after it. We have found this value high enough to consider all resulting peaks independent, but low enough to avoid sacrificing

the size of the final subset by excluding consecutive yet independent events.

In order to elucidate the influence of the large-scale atmospheric forcing on wave conditions in the region of interest, we analyzed linear correlation coefficients between the wave height (for wind sea and swell separately) and atmospheric circulation indices associated with those Northern Hemisphere teleconnection patterns that exhibit strong activity over the North Atlantic and parts of the Arctic surrounding the Svalbard Archipelago. The climate teleconnection data are available from the [Climate Prediction Center of the U.S. National Weather Service \(http://www.cpc.ncep.noaa.gov/data/teledoc/telecontents.shtml\)](http://www.cpc.ncep.noaa.gov/data/teledoc/telecontents.shtml). The patterns and their associated indices are obtained with a Rotated Principal Component Analysis (RPCA) applied to standardized (by monthly means and standard deviations) height anomalies of the 500 hPa isobaric surface heights north of 20°N , starting from January 1950. In our analysis, we use monthly indices of the following five patterns: North Atlantic Oscillation (NAO), East Atlantic (EA), East Atlantic/Western Russia (EAWR), Polar/Eurasia (POLEUR) and Scandinavia (SCAND). Due to their calculation procedure, the indices are linearly uncorrelated (e.g., in the subset of the

whole dataset corresponding to the WW3 time frame, i.e. 2005–2015, all absolute values of the pairwise correlation coefficients are lower than 0.08, see Suppl. Fig. S1). Additionally, we use time series of the monthly Arctic Oscillation (AO), the leading mode of variability of the anomalies of the 1000 hPa isobaric surface heights poleward of 20°N, as AO is routinely used in climate studies in the Arctic. Because the 500 and 1000 hPa anomalies are not independent (especially over the North Atlantic, where both are dominated by the Icelandic low and the Azores high), there is a strong correlation between the leading modes of their variability. In the period 2005–2015, the correlation coefficient between AO and NAO equals 0.63; AO is also significantly correlated with SCAND (−0.24) and POLEUR (0.24), see Suppl. Fig. S1. For ERAi data, the correlation coefficients with the atmospheric circulation indices were calculated for two time periods: 2005–2015 (to compare with analogous values for WW3 data) and 1979–2015.

2.6. Data reliability and consistency

Both data sources used in this study have certain limitations regarding the expected accuracy of the data. Firstly, the spatial resolution of both models was too low to depict the study area's shoreline and bottom topography with sufficient detail. Secondly, the spatial resolution of the wind data used to force the wave models was too low to describe details of Svalbard's landscape. Therefore, it is reasonable to expect lower accuracy of the wave products for short-fetched waves generated locally by easterly winds (which is the dominating wind direction in the analyzed region).

As already mentioned in the introduction, all available in situ wave measurements in the area of study are from shallow, in-shore locations, and using these measurements for direct validation of the modelled data from WW3 or ERAi cannot be considered without some important remarks. Fig. 2a illustrates the comparison of the WW3 and ERAi H_s values from point P3 of the analysis to the time series from a pressure sensor based on a wave buoy that was deployed for 100 days in Hansbukta, a bay near the Polish Polar Station in Hornsund, at the depth of 25 m. The location of peaks and the general shape of the curves represent surprisingly good level of similarity (Pearsons' correlation coefficients are 0.75 for WW3 and 0.67 for ERAi), particularly when one considers landward wave propagation directions (coeff. of 0.89 for WW3 and 0.86 for ERAi), it is not the case for the rest of the plot. Clearly, both models generate peaks that are absent in the buoy's log; presumably due to the coastline's shape preventing waves of certain directions from propagating into the buoy's location, or due to the increased fetch for seaward winds. The scatterplot of modelled H_s associated with the landward θ values against the H_s from observations (Fig. 2b) reveals strong linear relationships between the models and the buoy. The last remark is that the H_s values from the buoy are significantly lower than the modelled H_s . Considering the distance and significant decrease in water depth between modelled and monitored location, which results in the transformation of waves entering the fjord, the accuracy of modelled H_s can be described as sufficient for the purpose of this study, with all the remarks mentioned.

Both WW3 and WAM have been evaluated in other studies. Chawla et al. (2013) have validated WW3 model for quality and precision, and concluded that the model performs accurately in the case of the offshore areas, and that there is some decrease in level of agreement for coastal areas, caused by unresolved bathymetric features, and problems with quality of wind input at land margins. Kumar and Naseef (2015) assessed the performance of ERAi wave data in India's nearshore waters and came to similar conclusions; they also found a tendency to overestimate low, and underestimate high H_s values. Stopa and Cheung (2014) have compared wind and wave data from ERAi dataset with NCEP Climate Forecast System Reanalysis (CFSR-W which is based on WW3 model) validating both reanalyses with the same set of altimeter and buoy data, and found that while CFSR-W offers better quality of upper percentile waves, ERAi is more reliable for modelling long-term variability, due to the better temporal homogeneity.

In order to better investigate the quality of the WW3 and ERAi data sets in our area of study, we performed a comparative analysis of these data, complemented with a comparison to a third, local wave product available only within a short period of time. Details of this analysis and its results are presented in the Supplementary Note S1. As can be seen, the overall agreement between the data sets considered is satisfactory, with high correlation coefficients between the respective variables, no significant bias, but relatively high standard deviation of differences (especially in the case of wave directions). Notably, the differences between the models are higher for swell waves (in particular, very-low-frequency swell) than for wind sea. Importantly, even considering errors that inevitably are present in the data, our analyses indicate that the conclusions formulated further in this study are not substantially affected by these errors.

3. Results and discussion

3.1. Seasonality

Most apparent feature of the analyzed data is clear seasonality present in both datasets (Fig. 3). For WW3 the maxima of the mean H_s and the 99th percentile occur between December and January. Their values are 2.6 m and 5.4 m, respectively. For ERAi the general patterns are similar, but the values are higher, with the respective maxima of 2.8 and 6.3 m. This result is consistent with previous studies (Atkinson, 2005; Semedo et al., 2015; Stopa et al., 2016). Additionally, 99th percentile curves modelled with LOESS are less symmetric than the mean H_s , as the descending slopes are steeper than the increasing ones, which implies difference in duration of the transition periods. Moreover, the smoothed curves do not reflect some details that are visible in the daily 99th percentile data (Fig. 3, dotted lines), where maximum values occur in March and therefore the 'high-energy period' ends abruptly in the spring, while the summer–autumn transition is more gradual. Going further, the highest spike of the 99th percentile H_s in the spring corresponds to the vernal equinox (March 20–21st), while the autumn maximum is located near October 30th which is the beginning of polar night for the latitudes considered. In Fig. 4, an approach to visualize inter-annual variability of H_s was made. Seasons are

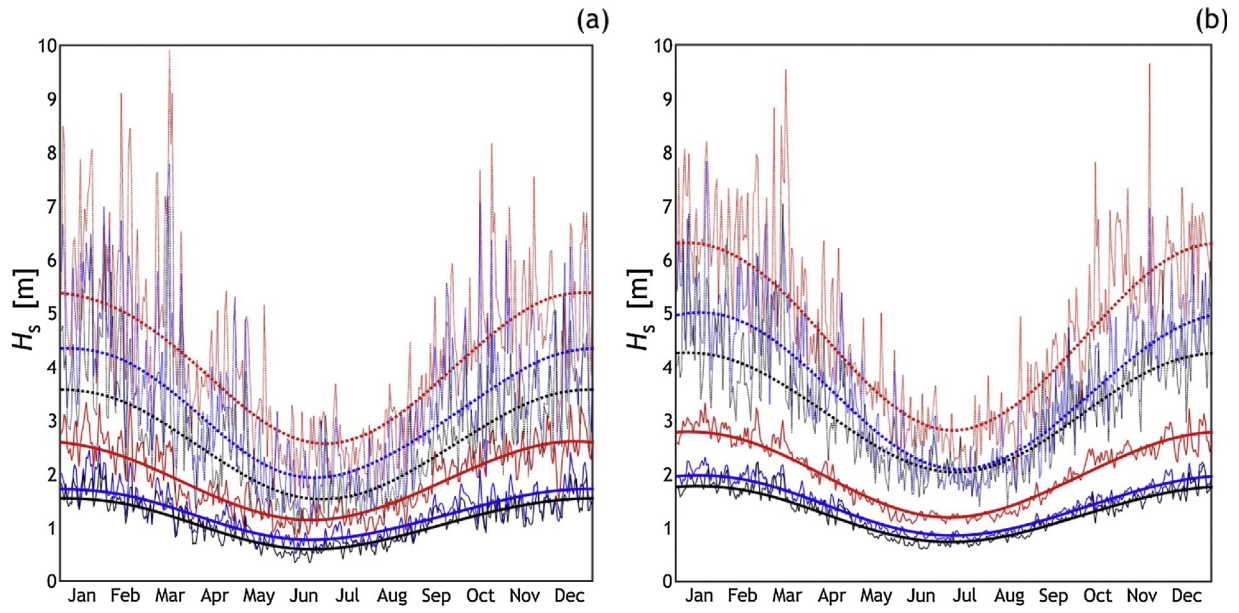


Figure 3 Seasonal variability of H_s in points 1 (red), 5 (blue) and 9 (black) for (a) 10 year period (WW3) and (b) 37 year period (ERAi). Daily means (solid) and 99th percentile (dotted) values are shown. Smoothed lines represent wrapped robust LOESS model.

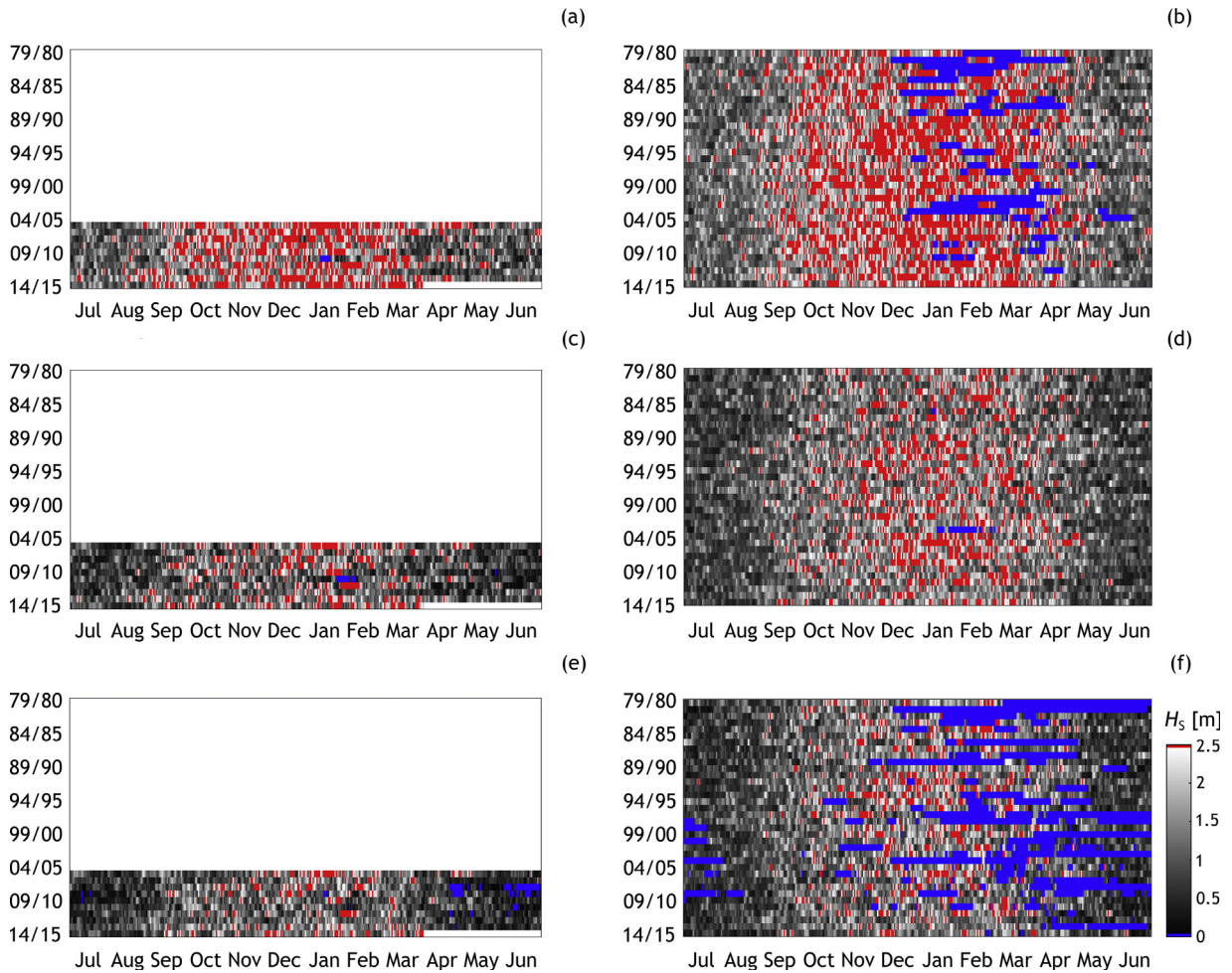


Figure 4 Inter-annual H_s changes in points P1 (a, b), P5 (c, d), P9 (e, f) for WW3 (a, c, e) and ERAi (b, d, f). Each row in the graphic represents single winter-centred season. Blue colour marks the lack of data (sea ice present).

displayed in a 'winter-centred' manner, as it is the part of the year that is most active in terms of wave heights. The graphic confirms seasonal pattern of H_s changes from Fig. 3, but it also shows the extreme event frequency changes during the analyzed periods (red pixels) which is helpful in further analysis of extremes. Also, the sea ice presence can be observed only on southern and northern points of study area.

3.2. Wave directions

It has been recognized that separate analysis of wind sea and swell provides better insight into wave characteristics (Guedes Soares, 1984; Portilla et al., 2009). The visualization of the incoming wave directions (Fig. 5) has been generated from WW3 partitioned data, as we have chosen independent wave systems analysis, where partition-corresponding directions are present instead of mean values calculated from total energy spectra (see Tolman, 2014). These data are not available in ERAi dataset, which offers the data divided to wind sea and swell partitions only. We believe that WW3 approach presents better resemblance to the real-life

situation, than analysing bulk, or separated wind sea and total swell components. Data is presented in form of wave roses with 36 directional bins of 10° width. The results reveal that substantial amount of swell arrives from the south-west with a gradual shift to the south with increasing latitude. Wind sea behaviour is more complex, and prevailing directions, usually two or three, change significantly depending on the analyzed location. At the southern points (P1, P2), the prevailing directions are E and NW. In the middle zone (points P3–P7) waves come mostly from NW, SW and NE, and in the north (points P8, P9) waves from N and NE are the most frequent. These wave directions are in accordance with the wind pattern characterizing the study area presented by Cisek et al. (2017). As mentioned in 'Data reliability and consistency' subsection, wind sea parameters for waves coming from the land directions may be inaccurate, but this is not the case for swell, where incoming directions indicate origin of the majority of waves to be the Norwegian Sea. Point data analysis also suggests that wave activity is more intense in the southern part of the study area which could be related to increase of sea ice concentration while heading north, but in fact, observations of sea ice presence (Norwegian Ice Service – MET Norway: <http://polarview.met.no/>) in the study area show that the problem is more complex, as ice is usually absent in the middle part of the coastline (points P4 to P7) and is mostly present in points P1 to P3 and P9 (see Fig. 4). Therefore we infer that distance from swell generation area is responsible for average swell state, and ice presence distorts this pattern to some degree. Directions of waves and spatial distribution of wave height indicate that the northern parts of the fjords' shorelines, especially in the south of Spitsbergen, are more exposed to wave-driven erosion, which is in accordance to the study of Zagórski et al. (2015). In the case of the west coast of Spitsbergen outside of fjords and bays, effects of sheltering can be omitted as there are no major obstacles for waves further offshore. Bottom morphology influence, on the other hand, is hard to estimate, and demands small scale, local studies.

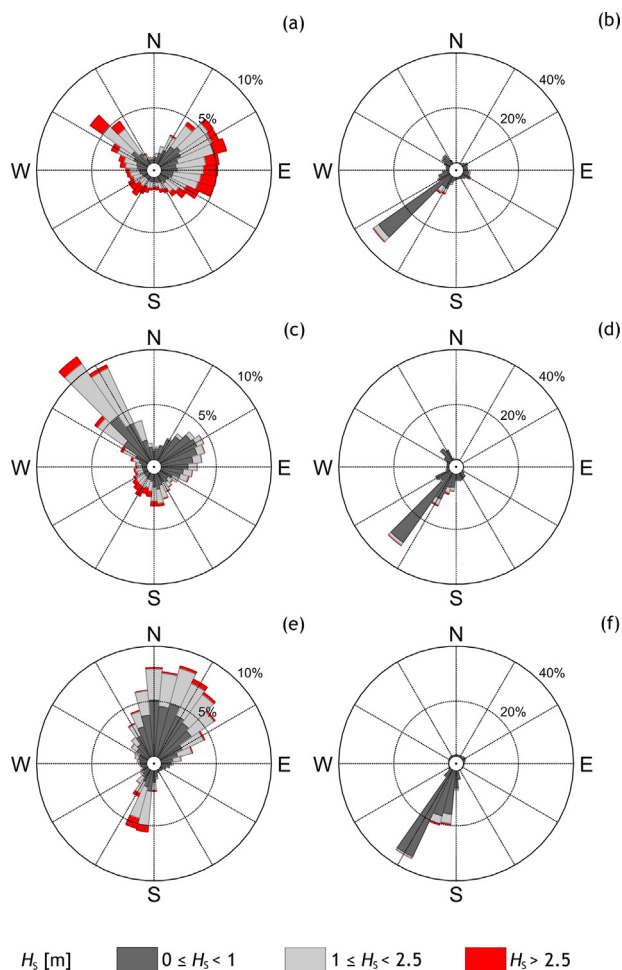


Figure 5 WW3 incoming directions of wind sea (a, c, e) and swell (b, d, f) partitioned components for points P1 (a, b), P5 (c, d) and P9 (e, f). Please note that the scale varies between the wind sea and swell. All directions are presented in meteorological convention. Generated with WindRose code (Pereira, 2014).

3.3. Extreme events

Characteristics of extreme events are shown in form of multiplots containing 3 computed variables averaged annually (Fig. 6a, c, e), and seasonally for winter (December, January, February – DJF, Fig. 6b, d, f). Those variables are: annual or seasonal mean of maximum H_s in individual extreme events, denoted with $H_{s,max}$; extreme events count; and extreme events total duration expressed in days. Analogous plots for spring (March, April, May – MAM), summer (June, July, August – JJA), and autumn (September, October, November – SON), as well as those for WW3 data are available in the Supplementary Material (Suppl. Figs. S9 and S10). For an additional analysis, a parameter describing the number of days with sea ice concentration exceeding 25% has been added. $H_{s,max}$ values oscillate around 3.5–4 m and lower values are observed in northern locations regardless of the analyzed period. In both datasets the number of extreme events ranges from less than 10 to over 40 annually. Events' total duration spans from 20 to over 80 days per year. In the same time, 25% ice concentration days vary greatly from 0 to 100, and even exceeding 250 in point 9 for ERAi

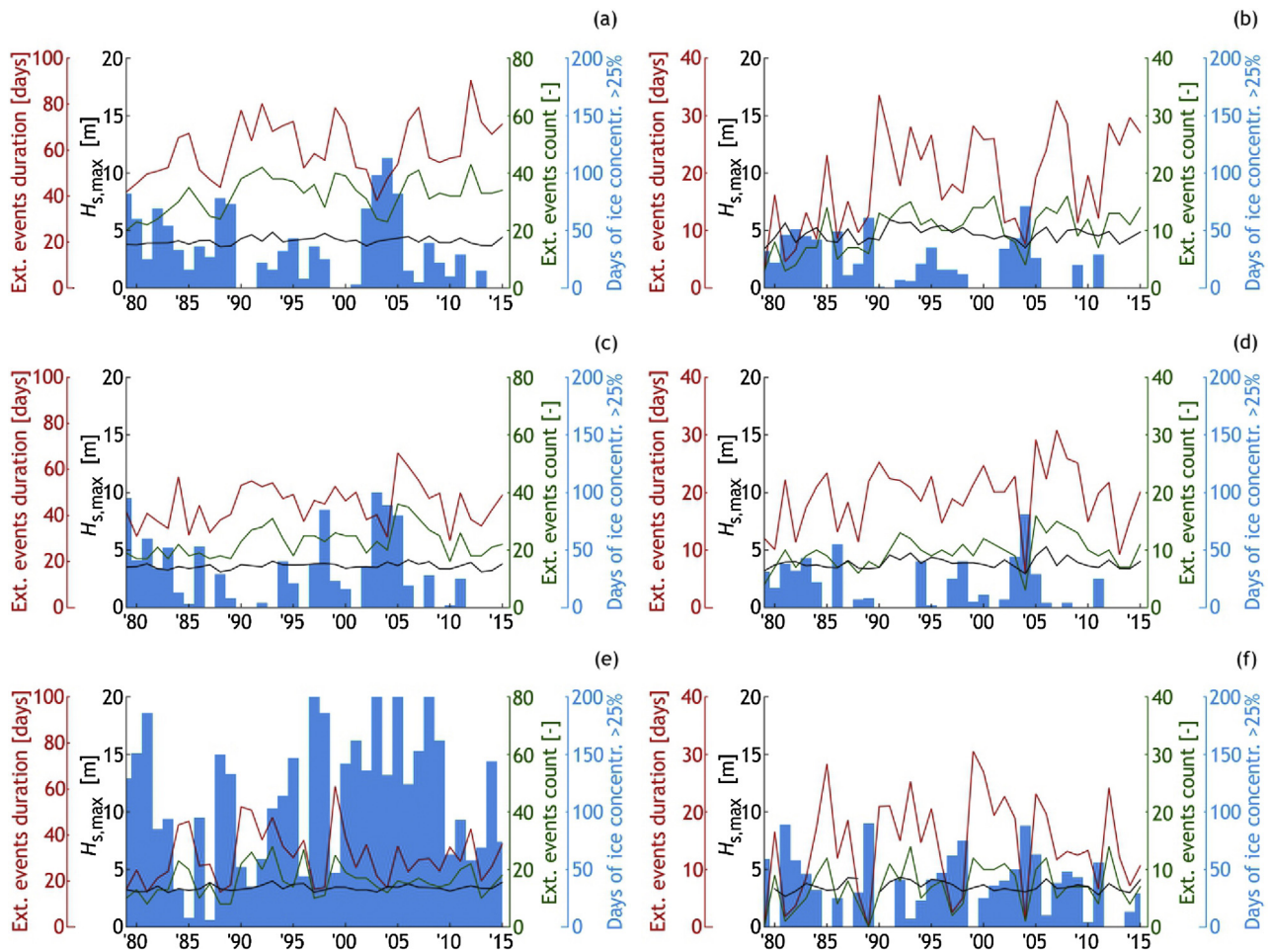


Figure 6 Extreme event parameters calculated from ERAi dataset for annual (a, c, e) and DJF (b, d, f) for points P1 (a, b), P5 (c, d) and P9 (e, f). For practical reasons, instead of being normalized, individual variables have separate y-axes to enable easy absolute value readout. Please note that the scales differ between annual and DJF charts. Generated with addaxis code (Lee, 2005).

dataset. Examination of $H_{s,max}$ reveals no significant trend, which can indicate that average extreme events' H_s does not change noticeably in the given time period. This is expected, as $H_{s,max}$ represents only the scale of the events occurring in given environment, and does not provide the complete information about the events. Information about extreme event count and duration provides a valuable insight about the change of how frequently high sea state occurs in the area and how long it typically lasts. These values vary annually and the WW3 dataset (see Suppl. Fig. S9) is not long enough to observe any trends. However, in 37-year period (Suppl. Fig. S10), the trend in events duration is clear for points 1 and 2. To approximate the trend values, linear regression was performed with a bootstrap method (number of repetitions: 1000), and corresponding values of the mean trend at points 1 and 2 are 0.39 and 0.41 days per year with standard deviation of 0.16 and 0.13, respectively (see Table 2), which gives roughly 9–10 h more of high sea per year. Event count trends (0.23 and 0.20 events per year, both with standard deviation of 0.08) reflect the trend pattern of events duration described above. We infer that the observed trends are not driven by temporal inhomogeneity in the data, as they do not occur uniformly in space, but are restricted to the southern part of the study area only. It seems reasonable to assume

that any temporal inhomogeneities in the data related, e.g., to changes of the model configuration or input data sources would manifest themselves consistently at all analyzed locations instead of producing a spurious signal at some points without affecting neighbouring ones. After analysing the relation between the events count and duration it becomes evident that event count is the key variable, and its increase in time determines the trend of the events' total duration. Remarkably, almost all statistically significant trend values are contained in DJF period. The described differences in wave climate between south and north of the study area correspond to the conclusions by Cisek et al. (2017), who found evidence for southern Spitsbergen being under stronger ocean influence than the north-west.

Ice concentration bar graph was added to extreme event parameters plot to show the substantial influence of sea ice in ERAi data, as drops in the number and duration of extreme events overlap with spikes of the number of >25% ice concentration days. The scale of influence of the short-lived sea ice patches on waves is not well known, but its existence is unquestionable. Its magnitude is determined not only by spatial characteristics of the ice patch itself (its spatial extent, ice type, etc.), but also by wave parameters, as wind sea's expected response will be more

Table 2 Mean slope coefficients and standard deviations of bootstrapped linear trends calculated for annual and seasonal extreme event duration. Significant trends (positive with more than 95% probability) are shown in bold.

Point no.	Annual		DJF		MAM		JJA		SON	
	Trend [d y ⁻¹]	Std. dev.	Trend [d y ⁻¹]	Std. dev.	Trend [d y ⁻¹]	Std. dev.	Trend [d y ⁻¹]	Std. dev.	Trend [d y ⁻¹]	Std. dev.
1	0.39	0.16	0.38	0.11	0.05	0.11	-0.04	0.06	0.03	0.04
2	0.41	0.13	0.37	0.10	0.06	0.09	-0.04	0.04	0.06	0.06
3	0.07	0.17	0.11	0.12	-0.04	0.08	-0.02	0.03	0.06	0.05
4	0.10	0.16	0.13	0.12	-0.07	0.07	-0.02	0.02	0.11	0.07
5	0.16	0.14	0.10	0.09	-0.01	0.06	0.00	0.02	0.10	0.07
6	0.11	0.16	0.08	0.10	0.00	0.08	0.01	0.04	0.06	0.05
7	0.23	0.15	0.16	0.10	0.03	0.07	-0.01	0.02	0.07	0.07
8	0.12	0.15	0.13	0.10	-0.02	0.06	-0.01	0.02	0.04	0.05
9	0.04	0.16	0.08	0.12	0.03	0.06	-0.02	0.02	-0.05	0.04

noticeable than the response of swell, which can propagate within the ice over great distances (Ardhuin et al., 2016; Zhao et al., 2015).

3.4. Correlation with atmospheric indices

The correlation coefficients between the atmospheric circulation indices and significant wave height of wind sea and swell at points 1–9 are shown in Fig. 7. For the ERAi data, they are calculated in two versions, for the “WW3 time period” 2005–2015 and for the whole period 1979–2015.

In the 2005–2015 decade, the overall pattern of the values of the correlation coefficients is relatively uniform along the whole west coast of Spitsbergen, especially in the case of swell (Fig. 7b, d), which predominantly travels from the open ocean and is not sensitive to local conditions at individual points. As expected, the point-to-point variability is higher in the case of wind sea, strongly affected by the neighbouring coastline. This is the case especially for the WW3 data (Fig. 7a).

At all points, the highest positive correlation is obtained for NAO, in the case of WW3 exceeding 0.4 for H_s of swell and at some points reaching 0.5 for H_s of wind sea. This significant correlation with NAO is not surprising, as a number of earlier studies demonstrated significant influence of this pattern on various local atmospheric, oceanic and glacial processes in Svalbard, including the length of the melting season (Kvamstø et al., 2011), hydrography of the West Spitsbergen Current (Saloranta and Haugan, 2001), or changes in air temperature and precipitation (Osuch and Wawrzyniak, 2016). As the archipelago is located to the north-east of the centre of the Icelandic low, it experiences stronger than usual winds from the southerly sector during positive phases of NAO, i.e., from directions favourable to wave development. The same is true for AO, itself related to NAO (see section on data processing), although the respective correlations are weaker. In the case of wind sea, comparable correlations are observed at central points (No. 3–5) for the POLEUR pattern, in its positive phase associated with negative pressure anomalies over the central Arctic, and with a strong circumpolar vortex. Correlation of similar strength to that with NAO, but opposite in sign, occurs between wind sea and EA, the second most prominent pattern over the North Atlantic region, associated with an extensive

low-pressure system south of Island and north of the Azores (a so-called “southern-shifted NAO”). In the analysis period 2005–2015, EA stayed almost exclusively in its positive phase; in particular, it never dropped below zero after February 2012. Due to the above-mentioned southerly shift of the EA centre relative to the centre of NAO, EA tends to be associated with easterly rather than southerly winds, which explains the negative correlation with wind sea west of Svalbard and very low (0.1–0.2) correlation coefficients with swell. The relationships of wave heights with the remaining indices are lower, although in the case of WW3 data many are statistically significant. Overall, the five uncorrelated indices together explain 30–35% of the total variance of H_s of swell (except at point 9) and between 9 and 68% of variance of H_s of wind sea at the analyzed locations (Fig. 8). Remarkably, whereas the correlation coefficients for swell in the period 2005–2015 are almost the same in ERAi and WW3 (red and blue curves in Fig. 8b), this is not the case for wind sea, where correlations with WW3 are significantly higher, with higher point-to-point variability (Fig. 8a). This may be a consequence of higher spatial resolution of WW3 data that enables better representation of locally generated wind waves. The values of the correlation coefficients with ERAi data are not only lower and more spatially uniform – they are also substantially lower for the period 1979–2015 than for 2005–2015 (Figs. 7e, f and 8). A possible explanation is that either the ERAi data or the atmospheric data used to calculate the atmospheric circulation indices (or both datasets) are non-uniform within the years 1979–2015. Another one is that, at least for some circulation patterns, the period 2005–2015 is too short to cover their whole range of variability (see, e.g., the comment on the EA pattern above, that hardly went into its negative phase since 2012), which may lead to some spurious correlations not present when longer time periods are considered. The above explanations are not mutually exclusive, and their relevance is impossible to determine based on the information available.

4. Conclusions

This study described wind wave climate of West Spitsbergen based on two independent model datasets covering 10 and

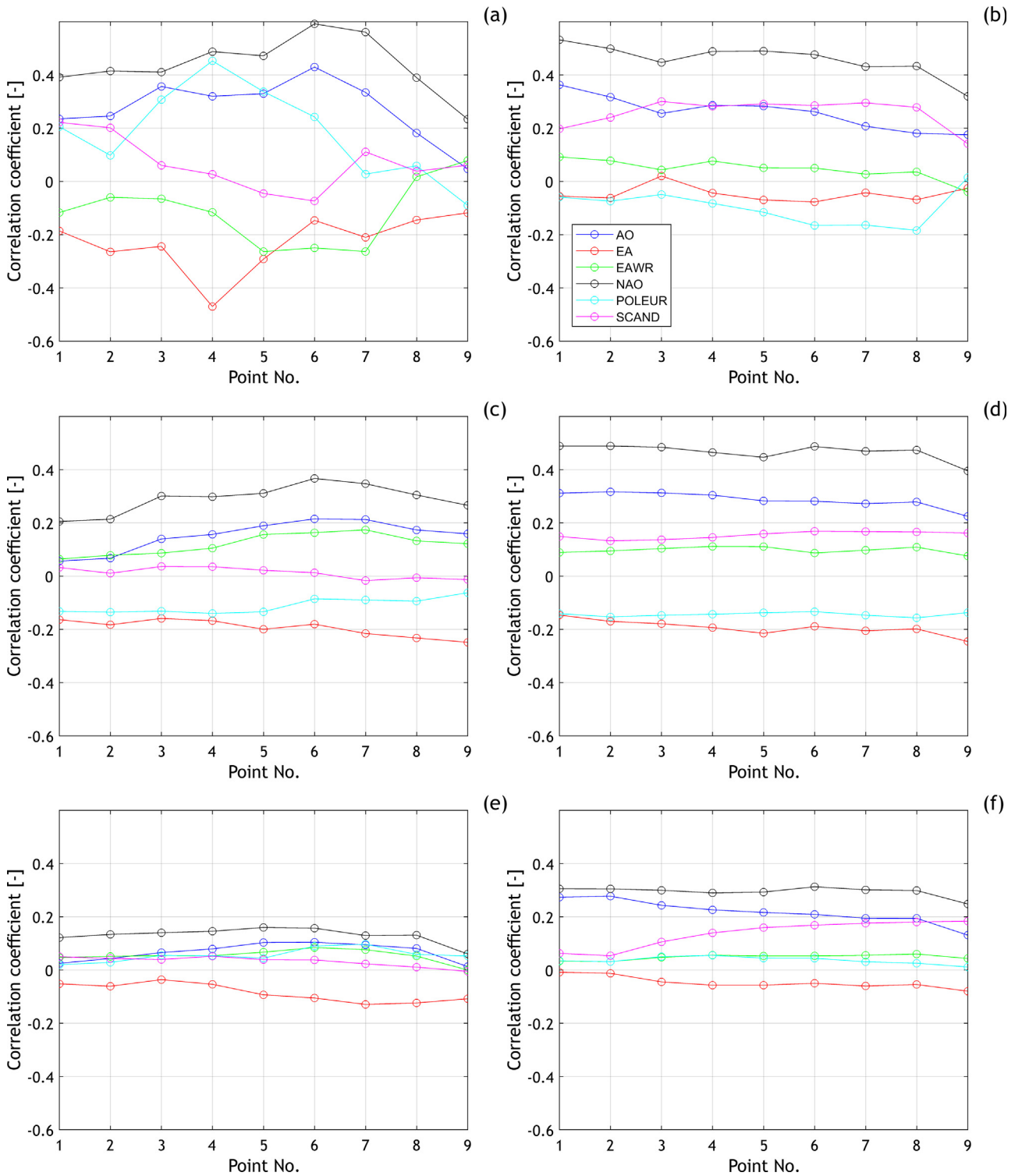


Figure 7 Correlation coefficients between the atmospheric circulation indices and the significant wave height of wind sea (a, c, e) and swell (b, d, f) in the nine analyzed points, calculated for the WW3 data in the period 2005–2015 (a, b), and for the ERAi data in the period 2005–2015 (c, d) and 1979–2015 (e, f).

37-year time period, respectively. Wave data from 9 offshore locations were analyzed to establish short and long-term characteristics of the wave environment at its typical and extreme states.

Seasonal pattern of wave heights in the investigated area resembles the North Atlantic annual cycle, with northward-decreasing differences between winter and summer. As expected, high-sea-states are most frequent in winter, but

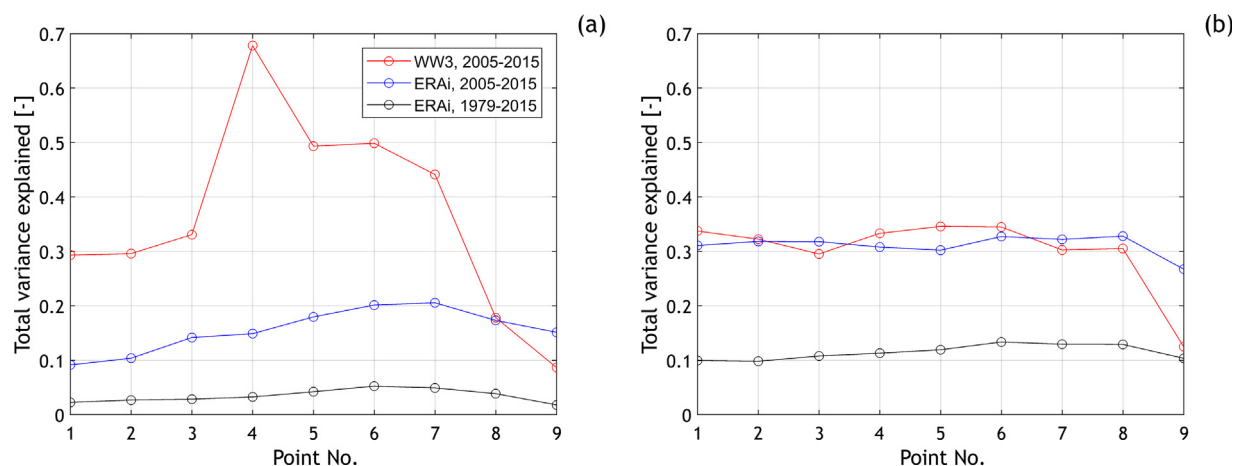


Figure 8 Fraction of the total variance of the WW3 and ERAi wind wave (a) and swell (b) wave height explained by the 5 independent atmospheric circulation indices (EA, EAWR, NAO, POLEUR and SCAND) at points P1–P9.

the highest 99th percentile wave height values coincide with the early spring and late autumn.

Wave direction characteristics have been based on WW3 multi-partitioned data. The general wind sea direction is from the north-west, with exception of points located farthest to the south and farthest to the north, where, respectively, easterly and northerly waves are significant part of the spectrum. The pattern of swell component is unequivocal with over 60% of swell direction values in the data is south-west. This pattern clearly indicates unidirectional swell conditions on entrances to all West Spitsbergen fjords, which may result in easily predictable swell component influence on coastal morphodynamics.

On the basis of extreme event analysis conducted in this study we conclude that among the components constituting extreme events, frequency is the key variable that visibly increased for the last four decades, which is expressed in the positive trends of extreme events count and their total duration. Positive trends have been found to be of the most statistical significance in the south part of the study area, and exclusively during the winter. Interestingly, ice conditions in the southern part of study area are more stable than in the north, which would suggest, that ice regime is not connected to the extreme events frequency trend by means of local influence, however we cannot exclude diminishing sea ice as an indirect cause affecting the waves through impacting atmospheric circulation on regional scale. Nevertheless, it has to be stressed that the sea ice impacts wave climate, and the topic of sea-ice and waves' mutual dependencies demands further investigation.

Association of NAO index to H_z values on West Spitsbergen is significant, but somewhat problematic, as it varies in time and is much stronger for the period of last 10 years, than for the period 1979–2015. There are at least two possible reasons to explain this result, but despite the fact, that ERAi database is generally acclaimed for good quality in terms of data integrity, further study on this issue is necessary to properly address it.

Acknowledgements

This work has been financed by National Science Centre project no. 2013/09/B/ST10/04141. This work was also

partially supported within statutory activities no. 3841/E-41/S/2016, 3841/E-41/S/2017 of the Ministry of Science and Higher Education of Poland, and from the funds of the Leading National Research Centre (KNOW) received by the Centre for Polar Studies for the period 2014–2018.

We would like to thank the two Anonymous Reviewers for their helpful remarks. We would also like to thank Brandy Bell for her swift and selfless input in the language proofreading.

All wind wave products used in this paper were provided by National Oceanic and Atmospheric Administration (NOAA) and European Centre for Medium-Range Weather Forecasts (ECMWF), and are publicly available.

Appendix A. Supplementary data

Supplementary data associated with this article can be found, in the online version, at [doi:10.1016/j.oceano.2018.01.002](https://doi.org/10.1016/j.oceano.2018.01.002).

References

- Ardhuin, F., Sutherland, P., Doble, M., Wadhams, P., 2016. Ocean waves across the Arctic: attenuation due to dissipation dominates over scattering for periods longer than 19 s: observed ocean wave attenuation across the arctic. *Geophys. Res. Lett.* 43 (11), 5775–5783, <http://dx.doi.org/10.1002/2016GL068204>.
- Atkinson, D.E., 2005. Observed storminess patterns and trends in the circum-Arctic coastal regime. *Geo-Mar. Lett.* 25 (2–3), 98–109, <http://dx.doi.org/10.1007/s00367-004-0191-0>.
- Bertin, X., Prouteau, E., Letetrel, C., 2013. A significant increase in wave height in the North Atlantic Ocean over the 20th century. *Glob. Planet. Change* 106, 77–83, <http://dx.doi.org/10.1016/j.gloplacha.2013.03.009>.
- Chawla, A., Spindler, D.M., Tolman, H.L., 2013. Validation of a thirty year wave hindcast using the Climate Forecast System Reanalysis winds. *Ocean Model.* 70, 189–206, <http://dx.doi.org/10.1016/j.ocemod.2012.07.005>.
- Cisek, M., Makuch, P., Petelski, T., 2017. Comparison of meteorological conditions in Svalbard fjords: Hornsund and Kongsfjorden. *Oceanologia* 59 (4), 413–421, <http://dx.doi.org/10.1016/j.oceano.2017.06.004>.

- Dee, D.P., Uppala, S.M., Simmons, A.J., Berrisford, P., Poli, P., Kobayashi, S., Andrae, U., Balmaseda, M.A., Balsamo, G., Bauer, P., Bechtold, P., Beljaars, A.C.M., van de Berg, L., Bidlot, J., Bormann, N., Delsol, C., Dragani, R., Fuentes, M., Geer, A.J., Haimberger, L., Healy, S.B., Hersbach, H., Hólm, E.V., Isaksen, I., Kållberg, P., Köhler, M., Matricardi, M., McNally, A.P., Monge-Sanz, B.M., Morcrette, J.-J., Park, B.-K., Peubey, C., de Rosnay, P., Tavolato, C., Thépaut, J.-N., Vitart, F., 2011. The ERA-Interim reanalysis: configuration and performance of the data assimilation system. *Q. J. R. Meteorol. Soc.* 137 (656), 553–597, <http://dx.doi.org/10.1002/qj.828>.
- Drange, H., Dokken, T., Furevik, T., Gerdes, R., Berger, W. (Eds.), 2005. *The Nordic Seas: An Integrated Perspective Oceanography, Climatology, Biogeochemistry, and Modeling*, Geophysical Monograph Series. American Geophys. Union, Washington, D.C., 365 pp.
- Environmental Modeling Center/Marine Modeling and Analysis Branch, 2016. WW3 hindcast archive [WWW Document], <ftp://polar.ncep.noaa.gov/pub/history/waves>.
- Guedes Soares, C., 1984. Representation of double-peaked sea wave spectra. *Ocean Eng.* 11 (2), 185–207, [http://dx.doi.org/10.1016/0029-8018\(84\)90019-2](http://dx.doi.org/10.1016/0029-8018(84)90019-2).
- Johannessen, O.M., Bengtsson, L., Miles, M.W., Kuzmina, S.I., Semenov, V.A., Alekseev, G.V., Nagurnyi, A.P., Zakharov, V.F., Bobylev, L.P., Pettersson, L.H., Hasselmann, K., Cattle, H.P., 2004. Arctic climate change: observed and modelled temperature and sea-ice variability. *Tellus A* 56 (4), 328–341, <http://dx.doi.org/10.1111/j.1600-0870.2004.00060.x>.
- Kruszewski, G., 2012. Ice conditions in Hornsund and adjacent waters (Spitsbergen) during winter season 2010–2011. *Probl. Klimatol. Polar.* 22, 69–82.
- Kumar, S.V., Naseef, M.T., 2015. Performance of ERA-Interim wave data in the nearshore waters around India. *J. Atmos. Oceanic Technol.* 32 (6), 1257–1269, <http://dx.doi.org/10.1175/JTECH-D-14-00153.1>.
- Kushnir, Y., Cardone, V.J., Greenwood, J.G., Cane, M.A., 1997. The recent increase in North Atlantic wave heights. *J. Climate* 10 (8), 2107–2113, [http://dx.doi.org/10.1175/1520-0442\(1997\)010<2107:TRIINA>2.0.CO;2](http://dx.doi.org/10.1175/1520-0442(1997)010<2107:TRIINA>2.0.CO;2).
- Kvamstø, N.G., Steinskog, D.J., Stephenson, D.B., Tjøstheim, D.B., 2011. Estimation of trends in extreme melt-season duration at Svalbard. *Int. J. Climatol.* 32 (14), 2227–2239, <http://dx.doi.org/10.1002/joc.3395>.
- Lee, H., 2005. addaxis [WWW Document], <http://www.mathworks.com/matlabcentral/fileexchange/9016-addaxis> (accessed 14.10.16).
- National Center for Environmental Prediction, 2016. Northern Hemisphere Teleconnection Patterns [WWW Document], <http://www.cpc.ncep.noaa.gov/data/teledoc/telecontents.shtml>.
- National Center for Environmental Prediction, 2016. Climate Data Assimilation System Sea Ice Concentrations, January 1, 1979 to Present [WWW Document], <ftp://polar.ncep.noaa.gov/pub/cdas/>.
- Norwegian Meteorological Institute, 2016. Ice Information Portal [WWW Document], <http://polarview.met.no/> (accessed 9.6.16).
- Onarheim, I.H., Smedsrud, L.H., Ingvaldsen, R.B., Nilsen, F., 2014. Loss of sea ice during winter north of Svalbard. *Tellus A* 66 (1), 23933, <http://dx.doi.org/10.3402/tellusa.v66.23933>.
- Osuch, M., Wawrzyniak, T., 2016. Inter- and intra-annual changes in air temperature and precipitation in western Spitsbergen. *Int. J. Climatol.* 37 (7), 3082–3097, <http://dx.doi.org/10.1002/joc.4901>.
- Pereira, D., 2014. Wind Rose [WWW Document], <http://www.mathworks.com/matlabcentral/fileexchange/47248-wind-rose> (accessed 14.10.16).
- Portilla, J., Ocampo-Torres, F.J., Monbaliu, J., 2009. Spectral partitioning and identification of wind sea and swell. *J. Atmos. Oceanic Technol.* 26 (1), 107–122, <http://dx.doi.org/10.1175/2008JTECH-O609.1>.
- Przybylak, R., 2003. *The Climate of the Arctic, Atmospheric and Oceanographic Sciences Library*. Kluwer Acad. Publ., Dordrecht, Boston, 270 pp.
- Reistad, M., Breivik, Ø., Haakenstad, H., Aarnes, O.J., Furevik, B.R., Bidlot, J.-R., 2011. A high-resolution hindcast of wind and waves for the North Sea, the Norwegian Sea, and the Barents Sea. *J. Geophys. Res.* 116 (C5), C05019, <http://dx.doi.org/10.1029/2010JC006402>.
- Saloranta, T.M., Haugan, P.M., 2001. Interannual variability in the hydrography of Atlantic water northwest of Svalbard. *J. Geophys. Res.* 106 (C7), 13931–13943, <http://dx.doi.org/10.1029/2000JC000478>.
- Semedo, A., Vettor, R., Breivik, Ø., Sterl, A., Reistad, M., Guedes Soares, C., Lima, D., 2015. The wind sea and swell waves climate in the Nordic seas. *Ocean Dyn.* 65 (2), 223–240, <http://dx.doi.org/10.1007/s10236-014-0788-4>.
- Sessford, E.G., Gøril Bæverfjord, M., Hormes, A., 2015. Terrestrial processes affecting un lithified coastal erosion disparities in central fjords of Svalbard. *Polar Res.* 34 (1), 24122, <http://dx.doi.org/10.3402/polar.v34.24122>.
- Stopa, J.E., Cheung, K.F., 2014. Intercomparison of wind and wave data from the ECMWF Reanalysis Interim and the NCEP Climate Forecast System Reanalysis. *Ocean Model.* 75, 65–83, <http://dx.doi.org/10.1016/j.ocemod.2013.12.006>.
- Stopa, J.E., Ardhuin, F., Girard-Ardhuin, F., 2016. Wave climate in the Arctic 1992–2014: seasonality and trends. *Cryosphere* 10 (4), 1605–1629, <http://dx.doi.org/10.5194/tc-10-1605-2016>.
- Styszynska, A., Buchert, L., 2004. The sea ice cover in Hornsund Fjord and its foreshore (SW Spitsbergen) during winter season 2003/2004. In: Styszynska, A., Marsz, A.A. (Eds.), *Polish Polar Studies: 30th International Polar Symposium*, Gdynia, 2004. Maritime Univ., Gdynia, 369–376.
- Teena, N.V., Sanil Kumar, V., Sudheesh, K., Sajeev, R., 2012. Statistical analysis on extreme wave height. *Nat. Hazards* 64 (1), 223–236, <http://dx.doi.org/10.1007/s11069-012-0229-y>.
- Thomas, T.J., Dwarakish, G.S., 2015. Numerical wave modelling – a review. *Aquatic Proc.* 4, 443–448, <http://dx.doi.org/10.1016/j.aqpro.2015.02.059>.
- Tolman, H.L., 2014. User Manual and System Documentation of WAVEWATCH III(R) VERSION 4.18 [WWW Document], <http://polar.ncep.noaa.gov/waves/wavewatch/manual.v4.18.pdf> (accessed 9.5.16).
- Tuomi, L., Kahma, K.K., Pettersson, H., 2011. Wave hindcast statistics in the seasonally ice-covered Baltic Sea. *Boreal Environ. Res.* 16 (6), 451–472.
- Wang, X.L., Swail, V.R., 2001. Changes of extreme wave heights in northern hemisphere oceans and related atmospheric circulation regimes. *J. Climate* 14 (10), 2204–2221, [http://dx.doi.org/10.1175/1520-0442\(2001\)014<2204:COEWHL>2.0.CO;2](http://dx.doi.org/10.1175/1520-0442(2001)014<2204:COEWHL>2.0.CO;2).
- Young, I.R., Zieger, S., Babanin, A.V., 2011. Global trends in wind speed and wave height. *Science* 332 (6028), 451–455, <http://dx.doi.org/10.1126/science.1197219>.
- Zacharioudaki, A., Korres, G., Perivoliotis, L., 2015. Wave climate of the Hellenic Seas obtained from a wave hindcast for the period 1960–2001. *Ocean Dyn.* 65 (6), 795–816, <http://dx.doi.org/10.1007/s10236-015-0840-z>.
- Zagórski, P., Rodzik, J., Moskalić, M., Strzelecki, M.C., Lim, M., Błaszczak, M., Promińska, A., Kruszewski, G., Styszynska, A., Malczewski, A., 2015. Multidecadal (1960–2011) shoreline changes in Isbjørnhamna (Hornsund, Svalbard). *Pol. Polar Res.* 36 (4), 369–390, <http://dx.doi.org/10.1515/popore-2015-0019>.
- Zhao, X., Shen, H.H., Cheng, S., 2015. Modeling ocean wave propagation under sea ice covers. *Acta Mech. Sin.* Xuebao 31 (1), 1–15, <http://dx.doi.org/10.1007/s10409-015-0017-5>.

Available online at www.sciencedirect.com

ScienceDirect

journal homepage: www.journals.elsevier.com/oceanologia/

ORIGINAL RESEARCH ARTICLE

Climate-related trends and meteorological conditions in the Porsanger fjord, Norway

Agata Cieszyńska^{a,b,*}, Małgorzata Stramska^{b,a}

^aDepartment of Earth Sciences, Szczecin University, Szczecin, Poland

^bInstitute of Oceanology, Polish Academy of Sciences, Sopot, Poland

Received 25 July 2017; accepted 22 January 2018

Available online 10 February 2018

KEYWORDS

Arctic;
Norwegian fjord;
Marine meteorology;
Climate change;
Seasonal variability

Summary Climate-related trends and meteorological conditions in the Porsanger fjord, in the vicinity of the Barents Sea, have been analyzed. Meteorological data include wind speed and direction, air temperature (AT) and precipitation from Era-Interim reanalysis (1986–2015) as well as local observations (2006–2015) from Honningsvaag and Lakselv. Statistically significant trends in annual AT means are $0.0485^{\circ}\text{C year}^{-1}$ near the fjord mouth and $0.0416^{\circ}\text{C year}^{-1}$ near the fjord head. Wind speed and precipitation data do not reveal any definite trends. Statistical analysis confirms the significant spatial variability of meteorological conditions in the fjord. For example, there are large differences in the annual AT cycle, with respective monthly means for January and July of -8.4 and 12.6°C at Lakselv (fjord head) and -2.5 and 10.1°C at Honningsvaag (fjord mouth). Strong wind events ($>12\text{ m s}^{-1}$) are more frequent at Honningsvaag than at Lakselv. The annual cycle is characterized by stronger winds in winter and seasonality of wind direction. At Lakselv, the dominant wind directions in summer are: N, NNW and S and in winter: S and SSE. At Honningsvaag, the wind directions in summer present strong variability, no fixed pattern being pronounced, whilst the dominant sectors in winter are: S and SSW. Daily cycles in AT and wind speed are also observed. Precipitation at a given location can change by about 30% year-on-year and varies spatially. Estimates of terrigenous water discharge (derived from the E-HYPE model) reveal a seasonal cycle with the maximum discharge in late spring/early summer.

© 2018 Institute of Oceanology of the Polish Academy of Sciences. Production and hosting by Elsevier Sp. z o.o. This is an open access article under the CC BY-NC-ND license (<http://creativecommons.org/licenses/by-nc-nd/4.0/>).

* Corresponding author at: The Institute of Oceanology of the Polish Academy of Sciences, Department of Marine Physics, Marine Biophysics Laboratory, Powstancow Warszawy 55, 81-712 Sopot, Poland. Tel.: +48 (58) 7311806.

E-mail addresses: cieszynska.agata@gmail.com, acieszynska@iopan.gda.pl (A. Cieszyńska), mstramska@wp.pl (M. Stramska).

Peer review under the responsibility of Institute of Oceanology of the Polish Academy of Sciences.



Production and hosting by Elsevier

<https://doi.org/10.1016/j.oceano.2018.01.003>

0078-3234/© 2018 Institute of Oceanology of the Polish Academy of Sciences. Production and hosting by Elsevier Sp. z o.o. This is an open access article under the CC BY-NC-ND license (<http://creativecommons.org/licenses/by-nc-nd/4.0/>).

1. Introduction

The Arctic is playing a key role in global climate change. An earlier analysis has shown that positive linkage to global warming will dominate in the Arctic for the next 50–100 years (McGuire et al., 2006). The Barents Sea (BS) is a region of great importance for climate change in the Arctic because it lies on the main heat transport pathway in the Equator–Poleward direction (Ådlandsvik and Loeng, 1991; Piechura et al., 2001; Schauer et al., 2002; Smedsrud et al., 2010, 2013). Surface inflows of Atlantic water into the Barents Sea have warmed during the last 30 years by about 0.3°C (Levitus et al., 2009). Russian scientists have documented positive Atlantic Water temperature anomalies (advected through BS) during 2000–2009 with temperatures warmer by $0.5\text{--}1.2^{\circ}\text{C}$ than the mean value based on data from 1951 to 2000 (Boitsov et al., 2012). Moreover, model results point to the significance of sea ice and atmospheric fields in the Barents Sea as possible climate change amplifiers (Goosse and Holland, 2005; Semenov et al., 2009). Rising air and water temperatures are intimately associated with the continuously diminishing sea ice cover (Döscher et al., 2014). The linear trend in ice extent in the Arctic has been estimated at $-4 \pm 0.2\%$ decade $^{-1}$ for 1978–2010, and $-8.3 \pm 0.6\%$ decade $^{-1}$ for 1996–2010 (Comiso, 2012). Since 1996 the Arctic sea ice cover has thus diminished about twice as rapidly as

the global rate during 1978–2010. According to Årthun et al. (2012), sea ice reduction in the Barents Sea has been even more significant (about 50% between 1998 and 2008) and has occurred concurrently with the increase in Atlantic heat transport due to both strengthening and warming of the water inflow. Observation-based heat budget calculations (Årthun et al., 2012) show that the heat content, ocean-atmosphere heat fluxes and sea ice cover in the Barents Sea respond to increased heat transport from the Norwegian Sea on a monthly to annual timescale. Another quantity useful in climate change studies is the sea surface temperature (SST). On the basis of the 32-year (1982–2013) National Oceanic and Atmospheric Administration (NOAA) data set, it has been shown that the regionally averaged SST trend in the BS (about $0.03^{\circ}\text{C year}^{-1}$) is greater than the global trend. This trend is different at different locations, the highest values (about $0.06^{\circ}\text{C year}^{-1}$) being recorded off Svalbard and in coastal regions of the White Sea (Jakowczyk and Stramska, 2014). Trends in coastal regions have not been adequately described, however, even if such regions are of special interest because of increased human activity and important land-ocean interactions.

The present study focuses on one of the largest fjords in Norway, the Porsanger fjord (Fig. 1), which lies in the north of the country, in the coastal zone of the Barents Sea. The main objective was to investigate recent climate-related trends

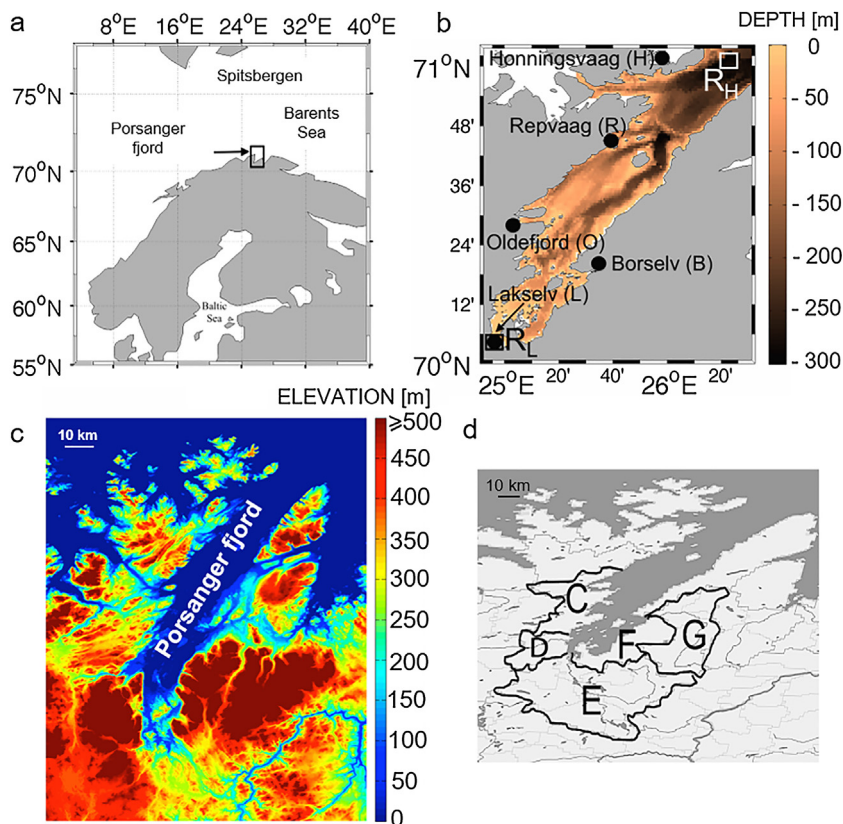


Figure 1 (a) Position of the Porsanger fjord in northern Europe; (b) the fjord's bathymetry showing the Norwegian Meteorological Institute's stations (black dots) and pixels, where data from the Era-Interim reanalysis were extracted (the white square at the fjord mouth – R_H and the black square at the fjord head – R_L); (c) terrain elevation based on the U.S. Geological Survey data (USGS – lta.cr.usgs.gov/GMTED2010); (d) catchment areas (denoted from C to G), where water runoff was estimated using the E-HYPE model data (Swedish Meteorological and Hydrographical Institute, <http://hypeweb.smhi.se/europehype/time-series/>).

and to describe the meteorological conditions and their variability inside the fjord. This information will expand knowledge of basic physical processes shaping the fjord's environment. Meteorological conditions can influence oceanographic conditions inside fjords, as has been shown by previous results from numerical modelling and field studies (e.g. Asplin et al., 1999; Cottier et al., 2010; Leth, 1995; Myksovoll et al., 2011, 2012; Svendsen and Thompson, 1978; Svendsen, 1991, 1995). This study is a component of the NORDFLUX (Application of in situ observations, high frequency radars and ocean colour to study suspended matter, particulate carbon and dissolved organic carbon fluxes in coastal waters of the Barents Sea) interdisciplinary oceanographic project. The project was motivated by the desire to improve understanding of the role of fjords in the transport of terrigenous material to the ocean. This paper provides a meteorological context for the interpretation of the hydrographic results from NORDFLUX experiment discussed in other papers (Białogrodzka et al., 2017; Stramska et al., 2016, 2018).

The IPCC Fifth Assessment Report (Stocker et al., 2013) states that the Arctic region will continue to warm more rapidly than the global mean rate until the end of the century. The projected changes in air temperature and precipitation are unevenly distributed over the Arctic (Koenigk et al., 2015), so local studies are needed for a better understanding of spatial variability of climate and meteorological conditions. Such studies are necessary means for ground-truthing large-scale climate change scenarios and enable local factors and vulnerability to different environmental conditions to be identified. Spatial variability of past and future changes of air temperature and precipitation at Svalbard have been discussed by Førland et al. (2011) and Osuch and Wawrzyniak (2016). Other environmental changes associated with climate trends have also been investigated in Norway (Kaste et al., 2006). Apart from the increase in air temperature, these changes include higher amounts and variations in the timing of precipitation, changes in seasonal weather patterns (milder winters, earlier springs, wetter autumns) and occurrence of extreme weather events. Although the Porsanger and some other Fennoscandian fjords have already been studied in the general context of climate and meteorological conditions (Eilertsen and Skarðhamar, 2006; Syvitski et al., 2012), the present study is according to the authors' knowledge the first one describing these aspects in detail with respect to the Porsanger fjord.

The paper is organized in the following way. First, basic information about the study region is provided. Next, data sets and methods are described. The results section documents climate-related changes and analyses average meteorological conditions in the Porsanger fjord on the basis of long-term observations. Finally, meteorological conditions in 2014 and 2015 are compared with their long-term counterparts in order to assess whether the conditions in the years when the NORDFLUX experiments were carried out can be described as typical or not.

2. Study region

A very specific region was selected for this study, namely, the Porsanger fjord (about 25.0–26.5°E and 70.0–71.0°N) in northern Norway, adjacent to the Barents Sea (Fig. 1). Some

geographers consider this region to be a transition zone between sub-arctic and high-arctic regions (Linell and Tedrow, 1981; Mills and Speak, 1998; Niedźwiedź, 1997; Stonehouse, 1989; Woo and Gregor, 1992). However, other scientists define the boundary of the Arctic by the Polar Circle (see for example <http://www.nationalgeographic.org/encyclopedia/arctic/>), so by this criterion the Porsanger fjord is a part of the Arctic region. Also, according to various criteria used by the Arctic Monitoring and Assessment Programme (<http://www.amap.no>; Arctic Pollution Issues 1998) the Porsanger fjord, or at least its northern part, is classified as a part of the European Arctic. However, even if the exact borderline of the Arctic is debatable, it seems natural to expect that the environmental conditions inside the fjord are closely linked to the climate-induced changes observed in the Arctic region generally and in the neighbouring Barents Sea in particular.

The Porsanger fjord is approximately 100 km in length, 15–20 km in width and has a maximum depth of more than 230 m. According to its bathymetry (Fig. 1b), the fjord can be divided into three different zones: 0–30 km – inner zone, 30–70 km – middle zone and 70–100 km – outer zone. The inner zone is separated from the rest of the fjord by a sill (60 m) some 30 km from the fjord head. The middle part starts outside the sill. The borderline between the middle and the outer zone of the fjord lies near the island of Tamsøya, some 70 km from the fjord head. The outer zone ends in a deep sill (180 m), so it is well connected with the coastal waters of the Barents Sea. This is in contrast to the inner part, where the environment is very different from the rest of the fjord and maintains a unique arctic ecosystem (Eilertsen and Frantzen, 2007). Tides in the Porsanger fjord are considerable, with a range of the order of about 3 m. The M2 component is the most important tidal component influencing sea level and surface currents (Stramska et al., 2016). The Porsanger fjord is surrounded by mountainous terrain (Fig. 1c), the highest peaks being situated to the south-west and south-east of the fjord. The land on either side of the middle part of the fjord is not very high (no higher than 300 m above sea level) but undulating, although there are some narrow valleys between higher elevations on both its eastern and western sides. There is a similar but wider valley at the head of the fjord, along which southerly winds can freely blow. The relief is also relatively low on the western side of the fjord, near its mouth on the Barents Sea. Generally speaking, the Porsanger fjord lies in a mountainous region with medium and high elevations. These tend to prevent the free flow of the wind, especially in the inner part of the fjord. Due to land topography, wind direction above fjord waters can differ from the large scale patterns above the land. Wind patterns along the fjord affect in turn sea surface currents. According to Stramska et al. (2016) only about 10–30% of the variance in surface currents in the study area can be attributed to tidal currents; the influence of winds is therefore significant.

3. Data sets and methods

The analyses in this paper are based on data obtained from several sources. The basic information about the data sets used is provided below.

3.1. ERA-Interim meteorological data

Unfortunately, long-term, high-quality consistent meteorological observations from conventional sources are not available for the study region. Thirty-year-long (1986–2015) wind, air temperature (AT) and precipitation reanalysis data have therefore been used to determine climate-related trends (obtained from the European Centre for Medium-Range Weather Forecasts (ECMWF) through the ERA-Interim reanalysis service (<http://apps.ecmwf.int/datasets/data/interim-full-daily/>). In such a reanalysis, models and observations are combined in an optimal way to derive consistent, global estimates of various atmospheric and oceanographic parameters. The ERA-Interim reanalysis has been carried out with a sequential data assimilation scheme, advancing forward in time. In each cycle, all available observations from in situ and satellite observations are combined with a forecast model to estimate the evolving state of the global atmosphere and its underlying surface. Daily data with 0.125° spatial resolution are used in the present work. Two grid points have been selected, one near the fjord mouth at 71.0°N, 26.375°E (R_H), the other near the fjord head at 70°N, 25°E (R_L) (Fig. 1b). Since these data originate from reanalysis, they represent large-scale (interpolated) conditions, in contrast to the local data described below. On the other hand, since ERA-Interim data have been reanalyzed using consistent methods, they seem to be well suited to the documentation of long-term, climate-related trends. Here, precipitation data represent daily-accumulated values, but all other data reflect average conditions on specific days. For an in-depth description of ERA-Interim reanalysis data, the reader is referred to [Dee et al. \(2011\)](#).

3.2. Local meteorological data

Air temperature, wind and precipitation records for the 10-year period from 2006 to 2015 (from the eKlima service (www.eklima.met.no), Norwegian Meteorological Institute) were used to describe the average meteorological conditions in the study area. The data have been quality controlled and used in many studies (e.g. [Aalto et al., 2014](#); [Bienau et al., 2014](#)). In contrast to the ERA-Interim data, eKlima data provide information at a local scale. AT and wind data with hourly resolution are available for two stations in the Porsanger fjord – Honningsvaag (71.60°N, 25.59°E; altitude above mean sea level (alt.) 14 m) and Lakselv (70.40°N, 24.59°E; alt. 5 m). These stations are marked in Fig. 1b by the letters H and L, respectively. The precipitation data provide information on daily totals [mm day^{-1}] and are available for 4 stations (Fig. 1b) – Lakselv (L) (details given above), Børselv (B) (70.31°N, 25.56°E, alt. 23 m; 70.32°N, 25.55°E, alt. 13 m), Oldefjord (O) (70.47°N, 25.08°E, alt. 50 m) and Repvaag (R) (70.75°N, 25.67°E, alt. 3 m) – but these data do not always cover the same time intervals. Station L data are available for 2006–2015, but station O data from September 15, 2009 to the present. Since the data for September 2009 are incomplete, the analysis for O begins here from October 2009. For station B, the data are available from 2006 to 2015, but the geographical position of the station was changed in February 2015 from 70.32°N, 25.55°E to 70.31°N, 25.54°E. The distance between these two locations is about 1.1 km. For the present discussion of

interannual variability, the data from both Børselv locations have been merged into one set and are denoted as a single point (B). Nevertheless, the data for January, February and March 2015 are missing and historical data for station R for 2006–2013 are often missing or invalid. The complete data sets from two years (2014 and 2015) from station R have thus been used in this analysis.

3.3. Water runoff data

Estimates of terrigenous water discharge into the fjord are based on data from the E-HYPE model, version 3.11 (obtained from the Swedish Meteorological and Hydrographical Institute service, <http://hypeweb.smhi.se/eurohype/time-series/>). Data from 1980 to 2015 (36 years) have been used to investigate long-term trends. Water runoff estimates derived from the E-HYPE reflect daily average volumetric flows of terrigenous water from a given sub-basin into the sea and are expressed in $\text{m}^3 \text{s}^{-1}$. The model has been extensively validated with in situ data. A full description of the E-HYPE model and the results of its validation are given in [Arheimer \(2011\)](#) and [Donnelly et al. \(2016\)](#). According to the information provided on the E-HYPE home website, the model development procedure involves a stepwise, simultaneous calibration being applied to 116 representative upstream sites with river discharge observations, manual and remote sensing snow observations, evapotranspiration, as well as annual glacier mass balance observations for the period 1980–2000. The system has been evaluated using data from all available river discharge stations (1347) in 1979–2009. This paper discusses data from the sub-regions marked in Fig. 1d by the letters C, D, E, F, G, respectively corresponding to the E-HYPE model sub-regions 8209557, 8209627, 8000709, 8200458 and 8210123; only regions delivering 100% of the runoff water to the fjord are discussed.

3.4. Terrain elevation data

Global Multi-resolution Terrain Elevation Data 2010 with 7.5 arc second resolution provided by the U.S. Geological Survey (USGS – lta.cr.usgs.gov/GMTED2010) ([Danielson and Gesh, 2011](#)) are used to visualize the topography of the land surrounding the Porsanger fjord (Fig. 1c). Figure 1c is a general visualization of the terrain elevation around the fjord. The relief has been depicted in constrained scale (up to 500 m above sea level) to enable differences in elevation to be distinguished. The highest terrain elevations are located at south-western and south-eastern sides of the basin. These are areas where the relief significantly exceeds 500 and reaches 1000 m.

3.5. Methods

The data processing steps include calculations of daily data from hourly air temperature and wind eKlima data. The AT and wind speed ERA-Interim data were downloaded as four values per day, from which daily fields were calculated (the values from 0:00, 6:00, 12:00 and 18:00) and precipitation was downloaded as 12 h accumulations twice a day. The water runoff data were provided as daily estimates of volumetric flow.

Table 1 Air temperature (AT), wind speed and precipitation trends at Lakselv and Honningsvaag on the basis of the 30-year time series of ERA-Interim reanalysis data. 'X' means trends are not statistically significant. Trends are also not statistically significant in the months not shown in the Table 1.

Trends – Lakselv/Honningsvaag			
Period	AT [°C]	Wind speed [m s ⁻¹]	Precipitation [mm]
Annual averages	0.0416/0.0485	X/X	X/X
January	X/X	X/X	X/–0.9616
April	X/X	–0.0891/–0.0585	X/X
May	X/0.0592	0.0702/0.0720	X/X
September	0.0760/0.0707	0.1022/0.0985	X/X
November	X/0.1007	–0.1215/–0.1194	X/X
December	X/0.1267	X/–0.1731	X/X

Table 2 Air temperature statistics at Lakselv (L) and Honningsvaag (H) on the basis of local meteorological data from 2006 to 2015 with hourly resolution.

Air temperature [°C]				
2006–2015	Mean/median	10th percentile/90th percentile	Min/max	Standard deviation
<i>Lakselv (L)</i>				
Full years	2.0/2.6	–10.3/12.8	–31.2/32.6	9.0
January	–8.4/–7.7	–17/–0.2	–30/8.8	6.6
February	–8.9/–8.2	–18.9/0.1	–31.2/8.7	7.4
March	–4.3/–3.4	–12.6/2.4	–28.8/10.9	5.9
April	0.8/1.2	–4.7/5.8	–21.5/12.4	4.3
May	6.2/5.7	1.1/11.9	–6.9/25	4.4
June	9.6/9	5.4/14.7	0.2/25.1	3.8
July	12.6/12	8/18.2	2.2/32.6	4.0
August	11.7/11.4	7/17.2	–2.9/27	4.0
September	8.3/8.3	3.5/13.3	–3.4/22.5	3.8
October	2.2/2.5	–3.1/7.4	–18.8/14.4	4.4
November	–2.6/–1.8	–9.3/2.9	–25.7/10.4	4.9
December	–5.2/–4.3	–13.4/1.6	–23.1/9.8	5.6
<i>Honningsvaag (H)</i>				
Full years	3.3/3.1	–3.9/10.4	–17.1/25.8	5.6
January	–2.5/–2.3	–6.9/1.8	–14.9/6.6	3.5
February	–3.5/–3.3	–8.7/1.3	–17.1/7.5	3.9
March	–1.6/–1.7	–5.6/2.4	–10.4/7.5	3.2
April	0.9/1.2	–2.9/4.3	–8.8/9.5	2.8
May	4.7/4.4	1.1/8.4	–2.6/19.4	3.0
June	7.4/6.9	4.3/10.9	0.3/22.8	3.0
July	10.1/9.5	6.9/14.5	3.3/25.8	3.1
August	10.4/10	6.9/14.1	3.7/22.2	2.8
September	8.2/8.2	4.9/11.6	0.2/17.8	2.6
October	4.1/3.9	0.6/8.0	–5.3/12.1	2.9
November	0.9/1	–2.6/4.3	–7.6/9.0	2.7
December	–0.4/–0.2	–4.3/3.1	–11.5/8.2	3.0

The monthly, annual and multi-year averages were calculated from daily eKlima data. Standard statistical methods were used for the data analysis (Sheskin, 2000). Using these methods, trends, standard deviations and the 10th and 90th percentiles (Tables 1–3) were calculated. The average, median, minimum (min) and maximum (max) were also calculated for full years and months for 2006–2015.

The assumption underlying the analysis of Era-Interim data and water runoff data (E-HYPE) was that simple linear regression can describe climate-related trends. The linear trends were fitted to each time series record by the least squares method and tested for statistical significance. The trends presented here were calculated on annually averaged data in order to filter out the annual cycle, which is sig-

Table 3 Wind speed statistics at Lakselv (L) and Honningsvaag (H) on the basis of local meteorological data from 2006 to 2015 with hourly resolution.

Wind speed [m s^{-1}]				
2006–2015	Mean/median	10th percentile/90th percentile	Min/max	Standard deviation
<i>Lakselv (L)</i>				
Full years	5.4/4.9	1.3/10.1	0.1/25.7	3.5
January	6.7/6.6	1.4/12	0.1/24.3	4.1
February	6.5/6.4	1.2/11.8	0.1/22.4	4.0
March	6.1/5.9	1.2/11.4	0.1/25.4	4.0
April	5.3/4.8	1.2/9.9	0.1/21.6	3.4
May	4.9/4.5	1.3/8.8	0.1/25.5	3.1
June	4.9/4.7	1.6/8.5	0.2/20.0	2.8
July	4.5/4.3	1.4/7.7	0.1/18.8	2.6
August	3.9/3.6	1/7.3	0.1/16.7	2.4
September	4.5/4.1	1.1/8.3	0.1/20.0	2.9
October	5.3/4.9	1.4/9.8	0.1/23.5	3.3
November	6.1/5.8	1.6/10.9	0.2/21.9	3.6
December	6.4/6.1	1.6/11.5	0.1/25.7	3.9
<i>Honningsvaag (H)</i>				
Full years	6.2/5.7	1.7/11.2	0.1/28	3.7
January	8.0/7.9	2.6/13.2	0.1/23.6	4.0
February	7.9/7.6	2.9/13.1	0.2/26.2	4.0
March	7.6/7.4	3/12.4	0.1/24.6	3.7
April	6.0/5.5	1.9/10.8	0.1/26.4	3.5
May	5.2/4.8	1.4/9.6	0.1/20.2	3.2
June	4.9/4.6	1.5/8.8	0.1/20.6	2.9
July	4.4/4.1	0.9/8.2	0.3/20.0	2.9
August	4.2/3.8	0.8/7.8	0.3/18.0	2.8
September	5.3/4.9	1.4/9.4	0.3/21.0	3.3
October	6.1/5.7	1.9/10.7	0.3/20.2	3.3
November	7.0/6.7	2.5/11.5	0.3/23.4	3.5
December	7.6/7.2	2.7/12.7	0.3/28	4.0

nificant in all data sets. The 30-year and 36-year trends were also calculated for monthly Era-Interim and E-HYPE model data, respectively.

As regards wind characteristics, the standard meteorological convention was followed. Accordingly, North (N) indicates winds blowing from the North (346° to 15°), South (S) is for winds blowing from 166° to 195° , East (E) is for winds blowing from 76° to 105° , and West (W) is for winds blowing from 256° to 285° . Intercardinal sectors are defined as NE (46 – 75°), SE (106 – 135°), NW (286 – 315°) and SW (226 – 255°). Finally, the secondary intercardinal sectors are NNE (16 – 45°), SSE (136 – 165°), NNW (316 – 345°), and SSW (196 – 225°).

To discuss the daily scale of variability, time series were analyzed using algorithms described by Bendat and Piersol (2011). The power spectra of the AT and wind speed were obtained from data with hourly resolution using a Fourier transform of the autocovariance function, to which the Parzen weighting function was applied. In all the cases considered here, the time series record consisted of a total of $N = 2048$ data points, representing about 85 days. The autocovariance functions were calculated with a maximum time lag $M = 220$. The standard error was about $\sim 30\%$ in the power spectral estimates.

4. Results

4.1. Long-term trends

Time series of annually averaged ERA-Interim air temperatures at locations R_H and R_L are presented in Fig. 2. These data show that annually averaged ATs were always greater at the fjord mouth (R_H). Long-term trends are similar at both locations, the trend at R_H being slightly higher ($0.0485^\circ\text{C year}^{-1}$) than at R_L ($0.0416^\circ\text{C year}^{-1}$). The trends are statistically significant at confidence level 95% ($\alpha = 95\%$). Patterns in interannual variability are well correlated, the correlation coefficient R between annually averaged data is 0.9851.

In order to investigate whether temperature trends vary seasonally, 30-year trends in the monthly AT data were estimated – see Table 1. This shows that AT trends are statistically significant and positive at R_L in September and at R_H in May, September, November and December.

Time series of ERA-Interim annual averages of wind speed (Fig. 2c and d) show a pattern of interannual variability, but long-term trends are not statistically significant. Mean annual wind speed was on average greater at R_H , reflecting

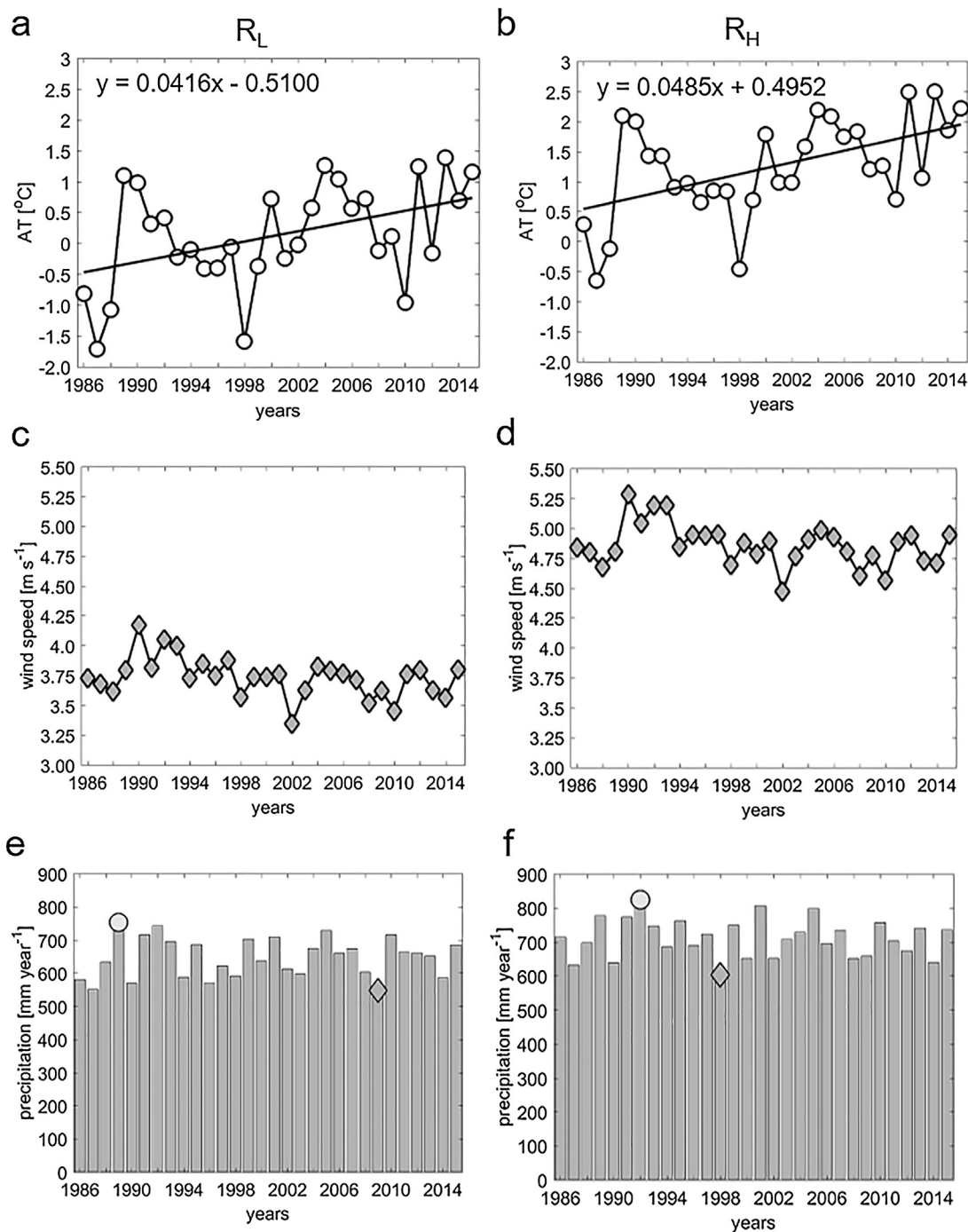


Figure 2 Time series of (a, b) annual mean air temperature (AT), (c, d) wind speed, and (e, f) total annual precipitation. The left-hand panel (R_L) shows data for the location near the fjord head (Lakselv) and the right-hand panel (R_H) for the location near the fjord mouth (Honningsvaag). (e and f) Grey circles – maximum annual precipitation totals; dark grey diamonds – minimum precipitation totals. Based on ERA-Interim reanalysis data.

the stronger influence of oceanic storms at this location than at R_L . The differences between the maximum and minimum annual wind speeds are 0.83 and 0.82 m s^{-1} at R_L and R_H , respectively. The trend in the monthly wind speed was significant in April, May, September, November at both locations (R_H and R_L) and in December at R_H (see Table 1). Standard

deviations were estimated using daily wind speed data for every year (1986–2015). The standard deviation was the greatest in 1995 at both R_L and R_H and reached 1.86 m s^{-1} and 2.32 m s^{-1} , respectively; it was the lowest in 1998 at both R_L (1.40 m s^{-1}) and R_H (1.85 m s^{-1}). Present results show that there is no statistically significant trend in wind speed

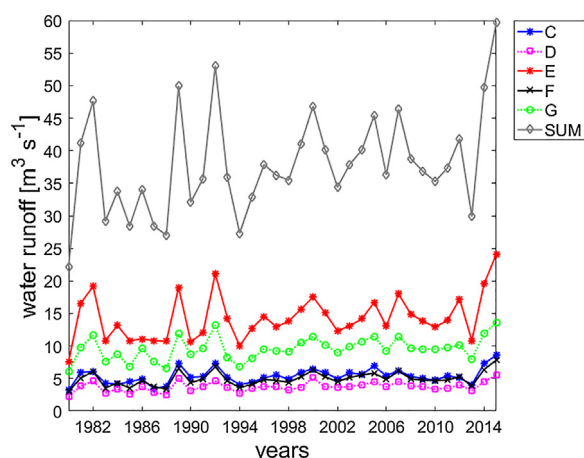


Figure 3 Time series (1980–2015) of annual mean water runoff for different catchment areas (C–G) and their sum (denoted by SUM). Based on the E-HYPE model data.

standard deviations at either station. Summarizing, wind speed was on average significantly higher and its variability stronger at the station located near the fjord mouth than in its inner part.

Annual precipitation totals are shown in Fig. 2e and f. These data do not manifest a statistically significant trend at either location in annual precipitation totals. Regarding monthly accumulations, the trend was estimated only for January at R_H (Table 1). Maximum annually accumulated precipitation was recorded in 1989 at R_L and in 1992 at R_H . Minimum values were observed in 2009 at R_L and in 1998 at R_H . The difference between the maximum and minimum annual precipitation was about $204.8 \text{ mm year}^{-1}$ near the fjord head and $221.1 \text{ mm year}^{-1}$ near the fjord mouth. This is about 31.7% and 31.1% of the multiyear average at R_L and R_H , respectively. The interannual variability in precipitation is thus significant.

Time series of water runoff in 1980–2015 are displayed in Fig. 3 for each of the sub-catchment regions and as the total runoff from all regions. The figure shows that water runoff into the fjord was the largest in region E (southern part of the fjord, see Fig. 1d), through which the Lakselva river flows. Long-term trends in annually averaged water runoff were small but positive and statistically significant for each catchment area and for the total runoff. The trends for the total runoff and for the sub-catchment E (the one with the greatest water discharge) are $0.3012 \text{ m}^3 \text{ s}^{-1}$ and $0.1205 \text{ m}^3 \text{ s}^{-1}$, respectively. Water runoff peaked in region G in 1992 while in all catchment areas and for the total runoff (SUM) in 2015. Minimum values were recorded in all catchments in 1980.

To summarize, long-term trends in the Porsanger fjord are statistically significant for air temperatures and terrigenous water runoff, but not for wind speed or precipitation. Based on ERA-Interim data it is clear that the differences between the outer and inner parts of the fjord are of great importance: the outer part of the fjord has slightly higher mean annual AT and stronger winds than its inner part.

4.2. Annual cycles

This section describes the main features of the annual cycles in the data sets and shows how the in situ experiments,

carried out from June 1 to July 1, 2014 and from May 24 to June 24, 2015, were timed with respect to the local annual cycle. All the relevant meteorological data are from local stations of the Norwegian Meteorological Institute (eKlima): local data should provide a better picture of the variability inside the fjord than the large-scale Era-Interim data.

Mean monthly AT data estimated for Lakselv and Honningsvaag from the 10-year (2006–2015) time series, as well as for 2014 and 2015, are compared in Fig. 4a and b. At Lakselv, the lowest 10-year mean monthly AT of -8.9°C was recorded in February, and its highest value of 12.6°C in July. Monthly mean ATs at this station in 2015 were higher than the 10-year average, except in January, May, June and July. Unusually high temperatures were also measured in February and July 2014. At Honningsvaag, the lowest 10-year mean monthly AT was calculated for February (-3.5°C) and the highest for July (10.1°C) and August (10.4°C). The differences between the 10-year mean monthly AT and the mean monthly AT for 2014 and 2015 at Honningsvaag resemble the pattern at Lakselv. The mean monthly temperatures at Lakselv and Honningsvaag in June 2014 and 2015 were similar to the 10-year means at each location.

The difference between the maximum and minimum mean monthly AT was 21.6°C at Lakselv and 13.9°C at Honningsvaag. The amplitude of the annual AT cycle is significantly larger at Lakselv than at Honningsvaag. This can be attributed to the fact that climate at Honningsvaag (near the open Barents Sea) is strongly influenced by maritime air masses. In contrast, Lakselv (situated in the inner part of the fjord though only $\sim 100 \text{ km}$ from Honningsvaag) is influenced by a continental climate, with higher summer temperatures and lower winter temperatures than in the oceanic regions.

Mean monthly wind speed estimates at Lakselv and Honningsvaag from the 2006–2015 time series are compared in Fig. 4c and d. There is a clear annual cycle in wind speed at both locations, with a larger mean value in winter and late autumn and a lower mean in summer. At Lakselv, the minimum 10-year monthly mean wind speed is in August (3.9 m s^{-1}) and the maximum (6.7 m s^{-1}) in January. At Honningsvaag, the lowest 10-year monthly mean wind speed is also in August (4.1 m s^{-1}) and the highest in January (8.0 m s^{-1}). Thus, the seasonal pattern of the 10-year mean annual wind speed is similar at both locations, but the mean wind speed and the amplitude of the annual cycle are larger at Honningsvaag than at Lakselv (amplitude of 3.9 m s^{-1} and 2.8 m s^{-1} , respectively). This is most likely a result of the geographical positions of these meteorological stations: Lakselv is situated in the inner part of the fjord, where the terrain is higher than around Honningsvaag. The land elevation sets up a barrier to winds. Comparison of 2014 and 2015 with the 10-year means shows that winds were stronger than average in June 2014 and in May/June 2015, but relatively weak in May 2014. In winter 2015 (February and March) winds were stronger than the multi-year monthly means for this time of the year.

Wind roses were plotted (Fig. 5) to illustrate the 10-year and annual (2014 and 2015) statistics of wind characteristics (speed and direction). Data with hourly resolution were used to draw these plots, as wind speed and direction are highly variable in the Porsanger fjord region.

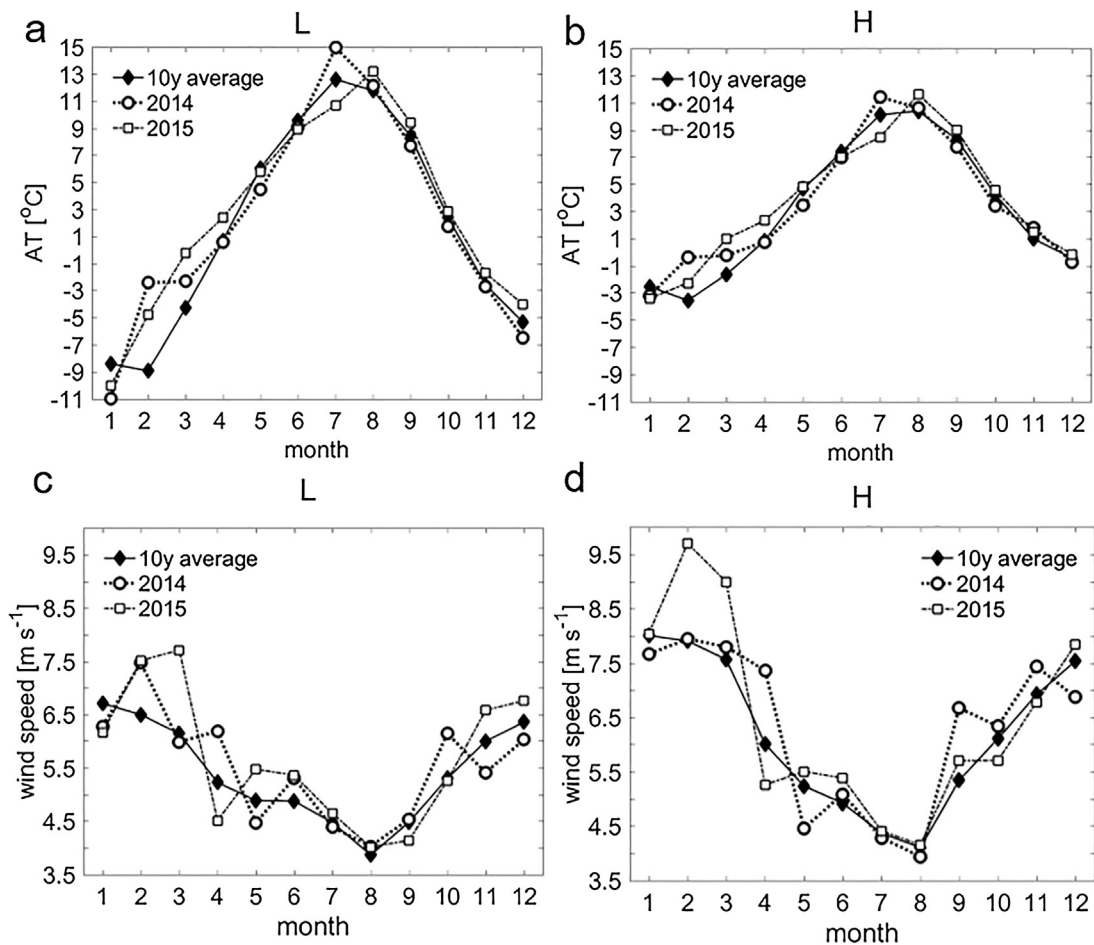


Figure 4 Annual cycle of (a, b) monthly mean air temperature (AT) and (c, d) wind speed. The left-hand panel is for Lakselv (L), the right-hand one for Honningsvaag (H). Each figure compares the 10-year averages with 2014 and 2015 monthly means. Based on data from the Norwegian Meteorological Institute, www.eklima.met.no.

Figure 5 shows that S winds prevailed at both stations, Lakselv and Honningsvaag. Winds from the E were the least frequent at both locations. There are, however, significant differences between these two locations. At Lakselv the second most frequent sector was SSE, whereas at Honningsvaag it was SSW. This was observed in the 10-year data set (Fig. 5a, b) as well as in 2014 (Fig. 5c, d) and 2015 (Fig. 5e, f). Moreover, NNW winds at Honningsvaag were relatively rare, whereas in Lakselv they blew with a frequency of between 13 and 15%. In contrast, winds from NW to SSW were seldom recorded at Lakselv, whereas at Honningsvaag these wind directions were quite common and included wind speeds even exceeding 16 m s^{-1} . These differences in winds are most likely due to the topography of land, sheltering the stations and fjord to some degree (Fig. 1c). The main difference between the 10-year mean and the 2014 and 2015 wind roses at Lakselv is that in 2014 and 2015 there were more SSE winds than in the 10-year time series. At Honningsvaag in 2014 and 2015 SSW winds were less frequent than in the 10-year time series. This was compensated by winds from the S and SW sectors. Nevertheless, it seems that the differences in wind directions between the two locations are more significant than the differences in the statistics for the 10-year and 2014 and 2015 data sets at one station.

The annual pattern of precipitation is shown in Fig. 6 as a multi-year mean and 2014 and 2015 monthly accumulated values recorded at 4 stations. The positions of these stations are marked in Fig. 1b. Figure 6 shows that precipitation was the highest at Repvaag, especially in 2015. Note that the plot displaying the precipitation at Repvaag (Fig. 6d) has a different vertical scale from all the other sub-plots in Fig. 6; this was done to make the other sub-plots more readable. Figure 6 underlines the fact that precipitation is a local phenomenon and that there are large differences between the values recorded at the various stations. The annual patterns of monthly means are different at each station, and the annual cycle is not as well pronounced and regular as in the case of air temperature or winds.

At Lakselv, the multiyear mean monthly precipitation fell to a minimum in January, but rose to a maximum in July. On the basis of monthly means, rainfall in June 2014 (the month of the NORDFLUX experiment) was more abundant than in any of the other months of June in 2006–2015 for that station. At Oldefjord (O), the lowest multiyear mean monthly total precipitation was in May and the highest in October. May as the month with minimum precipitation is an exception here compared with the other locations. At this station, 2015 was a year with high precipitation, including June,

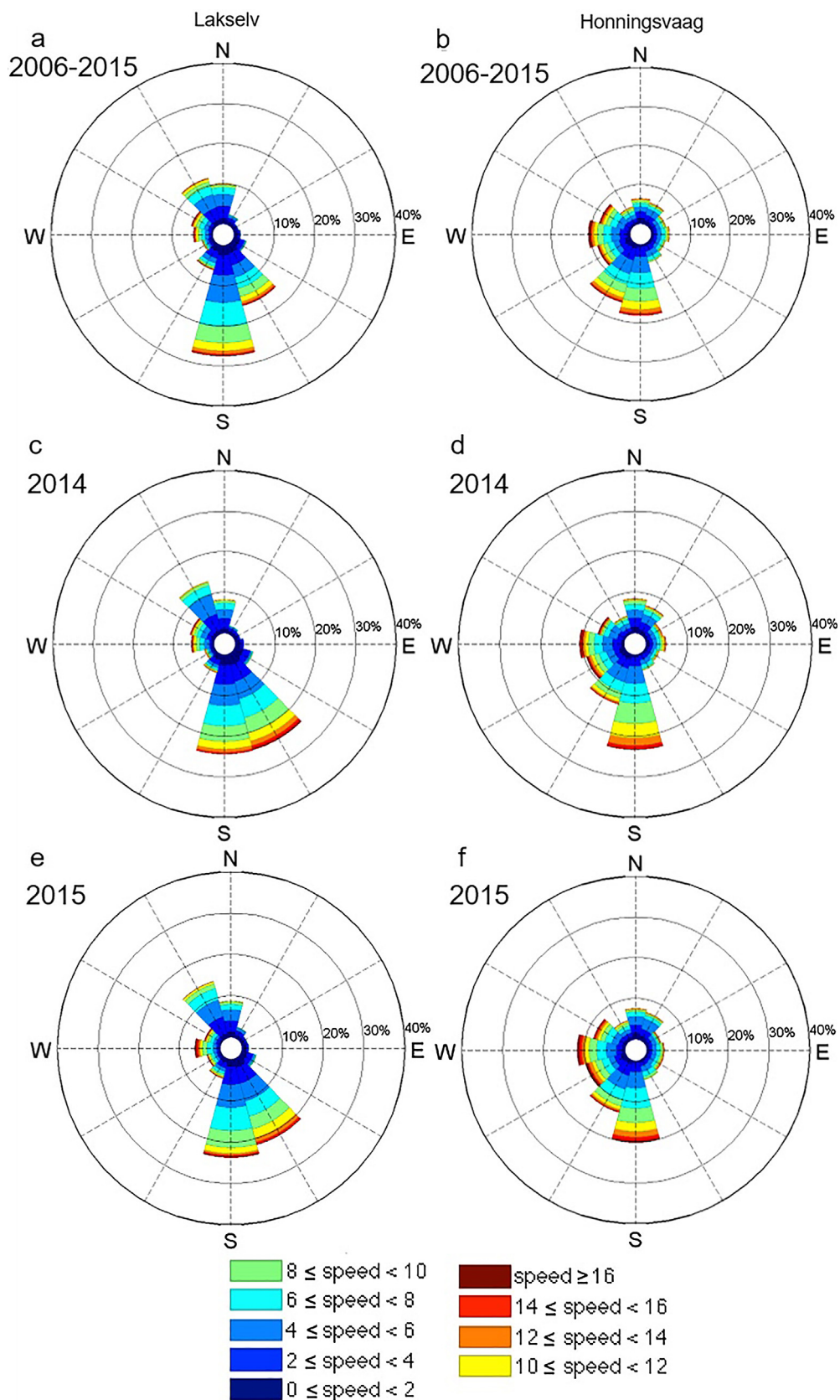


Figure 5 Wind roses summarizing wind conditions: (a) and (b) data from 2006 to 2015, (c) and (d) data from 2014, (e) and (f) data from 2015. The left-hand panel is for Lakselv (L), the right-hand one for Honningsvaag (H). Each wind rose shows the frequencies (in %) of different wind directions (according to the meteorological convention) and the frequencies of wind speeds for a given direction. The solid black circles inside the wind roses indicate 10, 20, 30 and 40%. Based on data from the Norwegian Meteorological Institute, www.eklima.met.no.

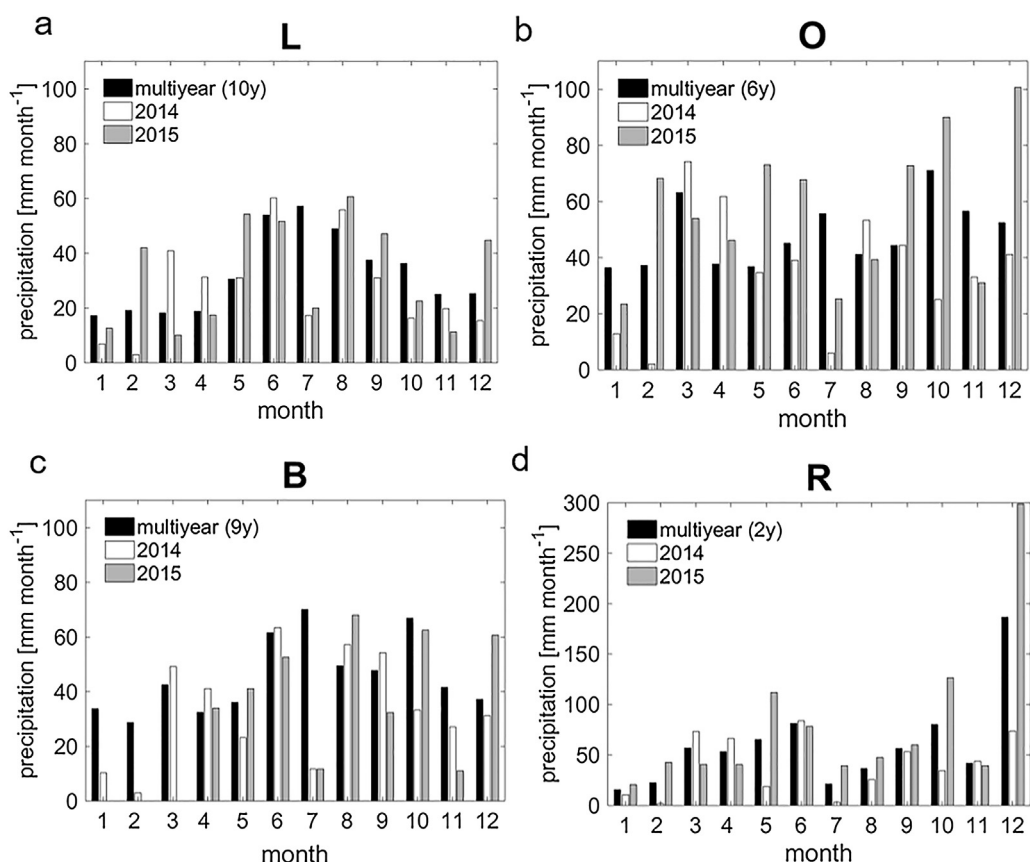


Figure 6 Monthly accumulated precipitation for four stations: (a) Lakselv (L), multiyear mean based on data from 2006 to 2015; (b) Oldefjord (O), multiyear mean for 2010–2015; (c) Børselv (B), multiyear mean for 2006–2015; (d) Repvaag (R), multiyear mean for 2014–2015. Each figure shows the multiyear average and estimates for 2014 and 2015. Based on data from the Norwegian Meteorological Institute, www.eklima.met.no.

the month of the NORDFLUX experiment. At Børselv, the multiyear mean monthly precipitation dropped to a minimum in February and rose to a maximum in October. The results of the NORDFLUX experiment indicate that June 2015 was a month with relatively high precipitation compared to other Junes in 2006–2015. Note that at Børselv, no data were available for February and March 2015, and the data for January were incomplete. At Repvaag, the multiyear mean monthly precipitation was the lowest in January, and the highest in December. In both 2014 and 2015 there was intense precipitation at Repvaag in June (NORDFLUX experiment).

To recapitulate: regarding the conditions during the NORDFLUX experiments, rainfall was heavier at all locations in May 2015 and less intense at almost all locations in May 2014 than the respective 10-year mean. In addition, there was more precipitation at three stations (O, B, R) in June 2015 than the 10-year mean and the same was true for Lakselv and Repvaag in June 2014.

The annual water runoff cycle in the Porsanger fjord is more pronounced than the annual precipitation cycle. This is illustrated in Fig. 7, which compares the 36-year (1980–2015) daily water discharge estimates for 5 sub-regions. In addition, the total runoff from all 5 regions (SUM) is displayed in Fig. 7f and g. These show that water runoff is extremely low in the winter months (December–March). The 36-year monthly mean water discharge reaches its maximum in May (regions C, E and F) or in June (regions D, G and the SUM). This

is because snowmelt in late spring/early summer contributes to the total discharge. There is, however, a significant inter-annual variability during the summer months, as indicated by the grey lines in Fig. 7f. Regionally, runoff is estimated to be the largest in the biggest catchment region E. This is where the Lakselva river delivers water from the mountains. The second most important region is G, with the Børselva river. According to this analysis, precipitation is quite heavy in these areas (see Fig. 6a, c): the weather stations at L and B are respectively situated in catchments E and G.

4.3. Short-term variability

Short-term fluctuations contribute significantly to the overall variability of weather conditions in the Porsanger region at synoptic and daily time scales. In order to illustrate the intensity of this variability, AT time series at Honningsvaag and Lakselv for 2014 and 2015 have been plotted in Fig. 8a with full (hourly) resolution. Figure 8b shows similar time series for wind speed. For comparison, each figure includes the 10-year average daily data. There is a well-pronounced annual cycle in the 10-year average daily time series of AT and wind speed. The annual cycle is also evident in the standard deviation for wind speed. The figures show that short-term fluctuations include changes in AT of the order of a few °C (up to ~20°C in extreme situations), whereas changes in wind

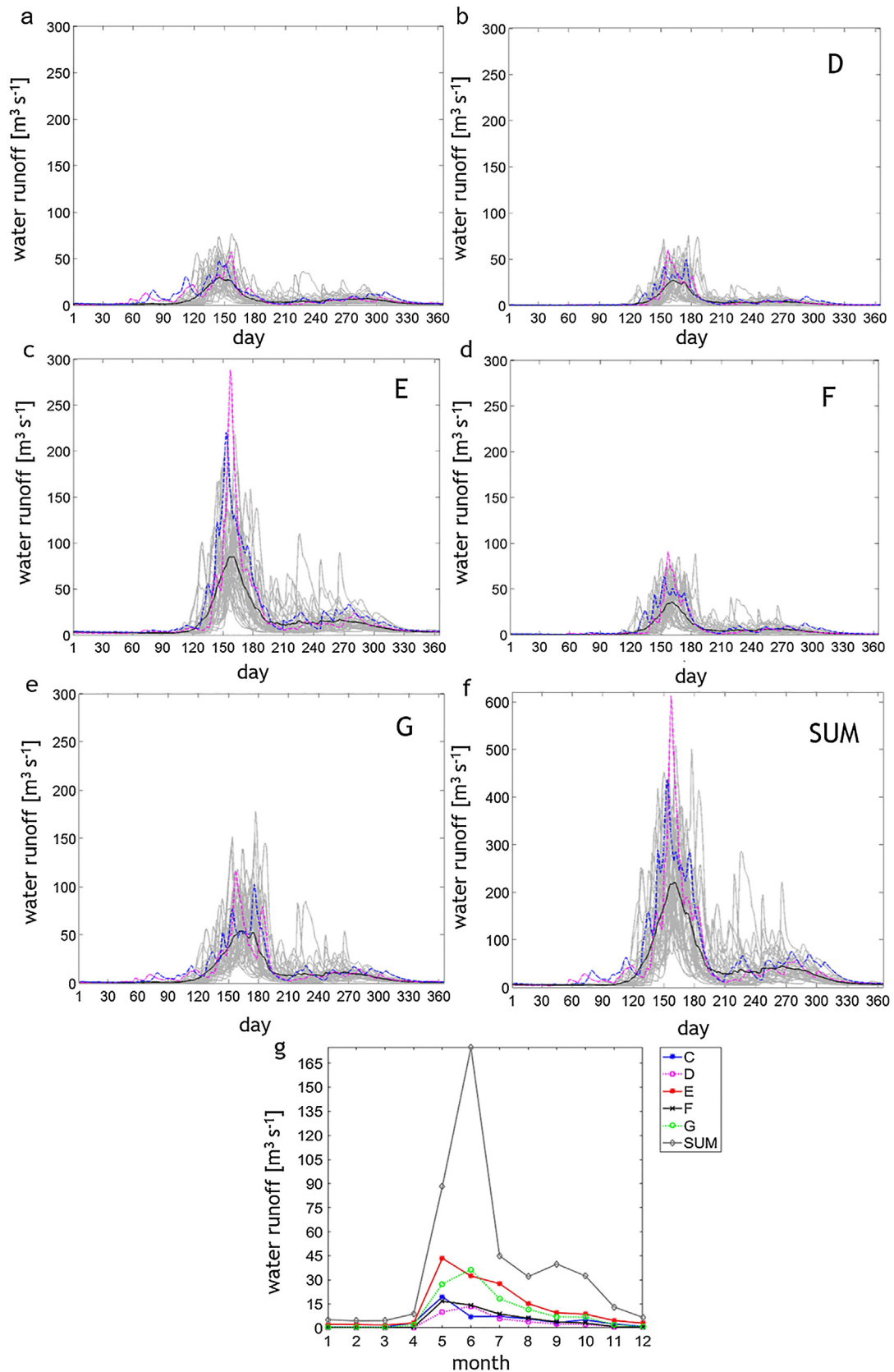


Figure 7 Annual cycle of (a–e) daily water runoff for different sub-regions (C–G) and (f) the total runoff (SUM). The solid fair grey lines in figures a–f display data for 1980–2013, the dashed dark grey lines are for 2014, the solid dark grey lines are for 2015, the solid black lines are for 36-year average. (Online: The solid grey lines in figures a–f display data for 1980–2013, the dashed pink lines are for 2014 and the dashed blue lines are for 2015, the solid black lines are for 36-year average.) (g) Compares monthly mean water runoff in different catchment sub-regions (C–G) and their sum (SUM), as denoted in the legend. Based on the E-HYPE model data.

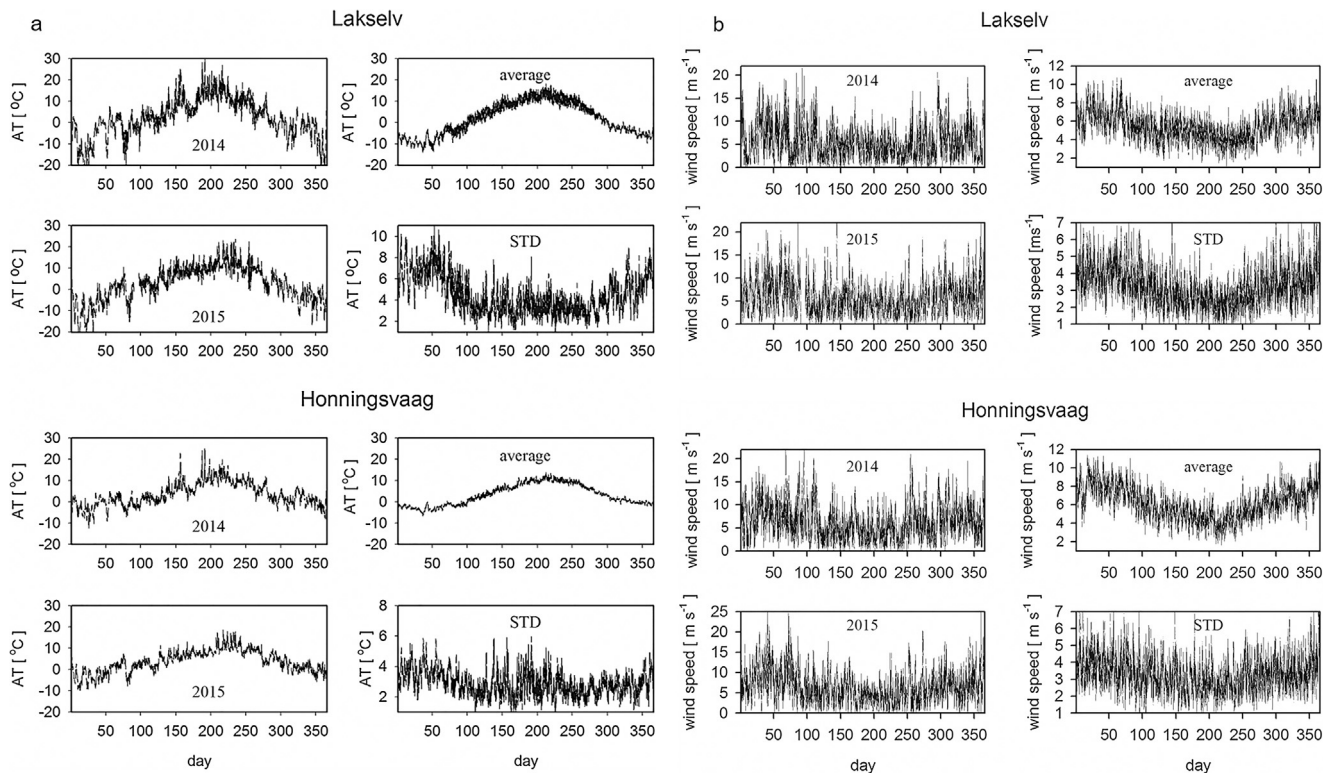


Figure 8 Annual cycle of (a) air temperature (AT), and (b) wind speed at Lakselv and Honningsvaag. Each figure presents the 10-year average daily time series (labelled 'average') in comparison to 2014 (labelled '2014') and 2015 (labelled '2015') hourly data. The standard deviation is also depicted (labelled 'STD'). Based on data from the Norwegian Meteorological Institute, www.eklima.met.no.

speed were as much as 20 m s^{-1} . Short-term wind events reached their greatest speeds in the winter months. For the period of the bio-optical NORDFLUX experiment in 2014 (year days 152–182, i.e. June 1–July 1) there were observed air temperature events significantly higher than the 10-year average data, whereas in 2015 (year days 144–175, i.e. May 24–June 24) air temperatures were similar to the 10-year average AT records (Fig. 8a).

The overall range of variability and frequency distributions of specific ATs and wind speeds are illustrated in Fig. 9a and b as annual and monthly information for selected months (April, May and June). The results for all months are summarized in Tables 2 and 3. Figure 9 shows that the respective AT frequency distributions were broader for Lakselv than for Honningsvaag. The range of ATs was about 20°C for the monthly distributions at each location in summer (June). It can be seen from Table 2 that average and median ATs at Lakselv were greater in summer but smaller in winter in comparison to Honningsvaag. The differences were quite large. For February, for instance, the average and median ATs at Lakselv were -8.9°C and -8.2°C , respectively; the corresponding values for Honningsvaag were -2.5°C and -2.3°C . In summer (July), the average and median ATs at Lakselv were 12.6°C and 12°C , respectively, while at Honningsvaag they were 10.1°C and 9.5°C . Annual average and median ATs were lower at Lakselv (2.0 and 2.6°C , respectively) than at Honningsvaag (3.3 and 3.1°C , respectively) and the annual AT amplitude was larger at Lakselv than at Honningsvaag. This is consistent with the fact that Lakselv is

situated in the inner part of the fjord, under the influence of continental air masses.

This statistical analysis of AT data shows clearly that despite the relatively short distance between them (approximately 100 km), the outer and inner parts of the fjord differ dramatically as far as the thermal characteristics of air masses are concerned. The frequency distributions of wind speed (Fig. 9b) show that low wind speeds were more frequent at Lakselv than at Honningsvaag. Table 3, summarizing the statistics, shows that in the full year analysis, the average and median wind speeds were lower at Lakselv (5.4 and 4.9 m s^{-1}) than at Honningsvaag (6.2 and 5.7 m s^{-1}). For the specific month analysis, means and medians were always higher at H than at L, except in May, when those values were similar.

Wind roses illustrating wind speed and directions in different months are shown in Figs. 10 and 11 for Lakselv and Honningsvaag, respectively. These wind roses are based on the data series for 2006–2015 with hourly resolution (eklima data). At Lakselv (Fig. 10) there was a strong prevalence of S winds during winter (December, January, February), in early spring (March) and in autumn (October, November). Furthermore, strong wind events were more frequent during these months than during the rest of the year. Figure 10 highlights the seasonal variability of wind characteristics at Lakselv. From wind roses one can see that during summer the prevailing direction of winds was opposite to prevailing direction of winds in winter. Additionally, it is noticeable that the month of May can be considered as a transition period

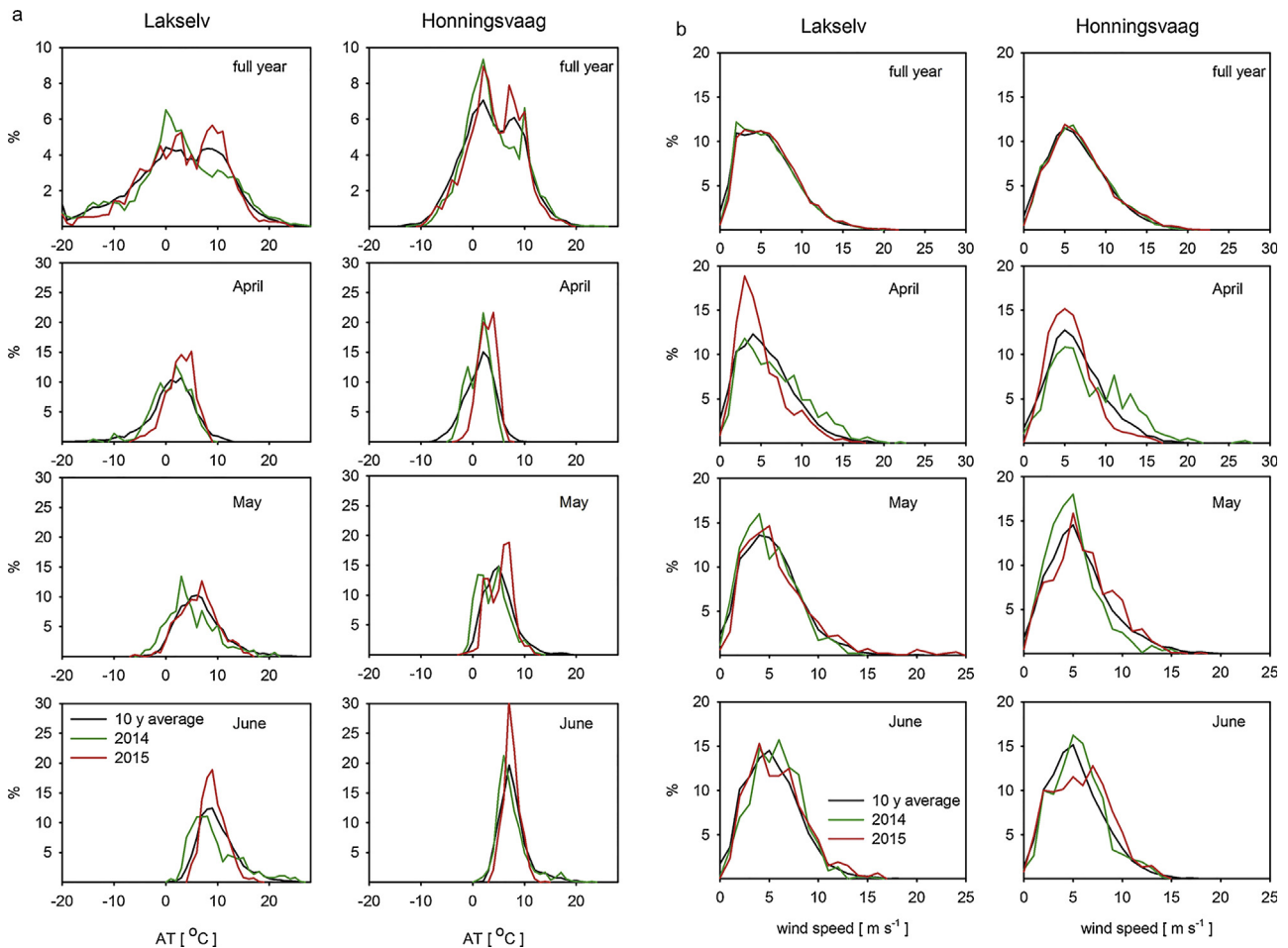


Figure 9 Frequency distribution of (a) air temperature (AT), and (b) wind speed at Lakselv (left-hand panel) and Honningsvaag (right-hand panel). The 10-year average is shown in black, and the data for 2014 and 2015 are plotted as grey lines, dashed and solid, respectively. (Online: The data for 2014 and 2015 are plotted as green and red lines, respectively.) Both figures (a and b) show plots summarizing the conditions over the whole year, and in the months of April, May and June. Based on data from the Norwegian Meteorological Institute, www.eklima.met.no.

between spring and summer wind conditions, since it presented a combination of wind characteristics typical for April and June. The wind roses for Honningsvaag (Fig. 11) indicate a variability of wind directions even greater than that at Lakselv. As at L, direction from S prevailed at H in winter (December, January, February), in early spring (March) and in autumn (October, November). However, the second most frequent wind direction was SSW (in contrast to Lakselv). As at L, strong wind events were more frequent at H in autumn and winter. The S and SSW sectors were dominant in the 10-year April wind rose for H. SW, W and NW winds were not so frequent, even though the strongest wind speed events (even exceeding 16 m s^{-1}) were from these directions. All sectors except SSE, SE, NE and NNW were frequent in the 10-year May wind rose (Fig. 11 May), but westerlies and easterlies dominated. The N, NE, W and NW sectors prevailed in the 10-year June wind rose (Fig. 11 Jun), and the highest wind speeds were also recorded in this month. Summarizing, one can say that in spring and summer the wind direction distribution in H is very variable, any fixed pattern not being observed that time. On the contrary, in L the pattern is plainly pronounced and shows strong seasonal variability in

wind directions between summer and winter months. Comparing these seasons, it is clear that they are characterized by the dominance of completely opposed wind directions with S and SSE winds blowing in winter and N and NNW in summer.

The wind patterns at Lakselv and Honningsvaag for the months of April, May and June of 2014 and 2015 are additionally analyzed (Fig. 12). Attention is intentionally drawn here to the period when winds could have affected hydrological conditions in the fjord during NORDFLUX experiments. A seasonal wind pattern is discernible from these characteristics, albeit with some year-to-year fluctuations. There were more strong wind events in April 2014 than in April 2015 at both stations (Fig. 12 Aprils). What is more, N winds were recorded at Lakselv in April 2015, but were not observed so frequently in April 2014. At Honningsvaag in April 2015 winds blew from the NNE, NE, E, SE and SSE sectors, whereas in April 2014 there were hardly any winds from these directions. At both locations, May 2014 was a relatively calm month, with only S and SSE winds sometimes exceeding 12 m s^{-1} at Lakselv and SW and NNE winds exceeding 14 m s^{-1} at Honningsvaag. The wind conditions at Lakselv in June 2014 and

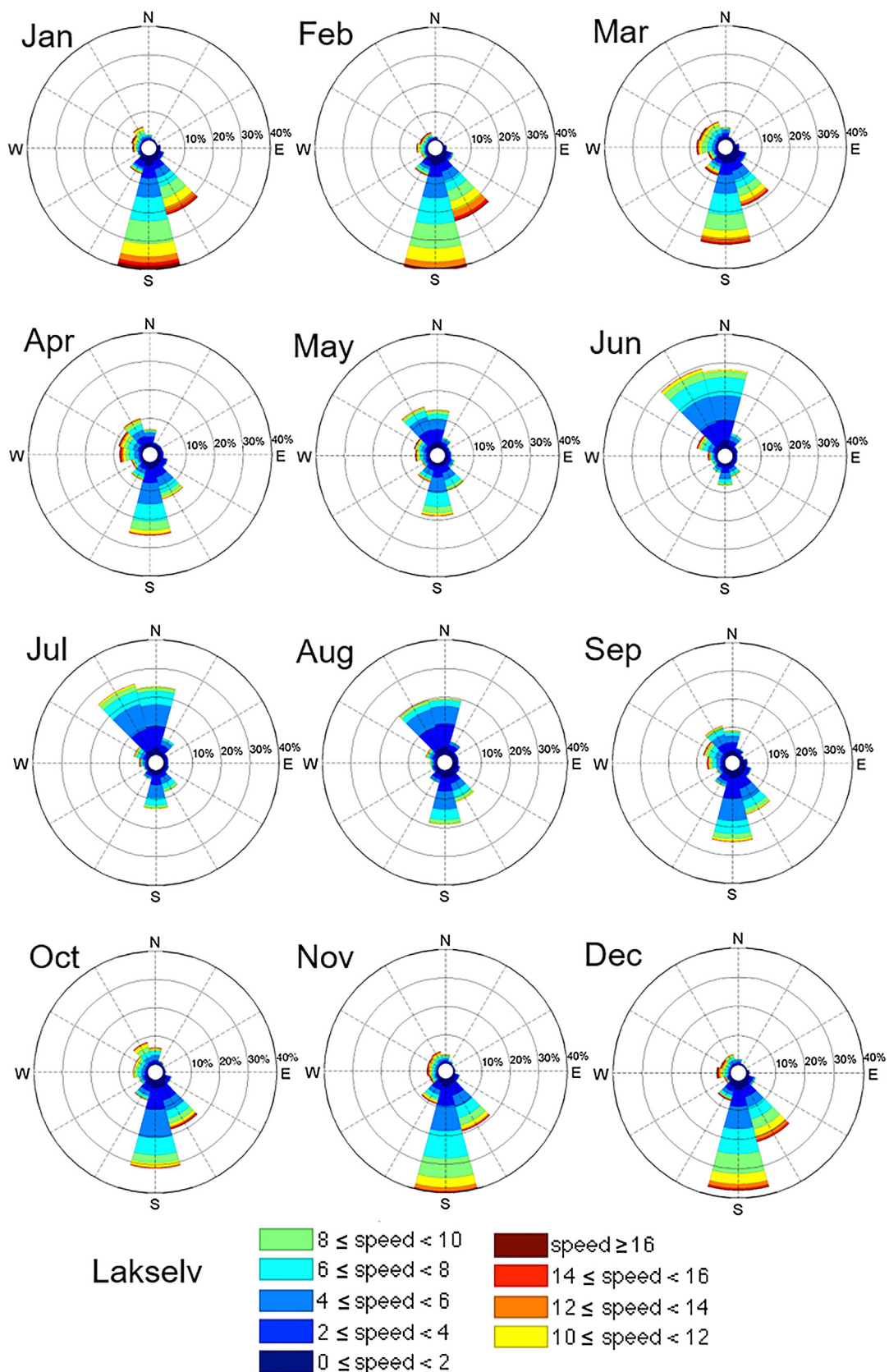


Figure 10 Wind roses comparing wind conditions in different months at Lakselv for 2006–2015. Wind roses for specific months are labelled with their abbreviations. Based on data from the Norwegian Meteorological Institute, www.eklima.met.no.

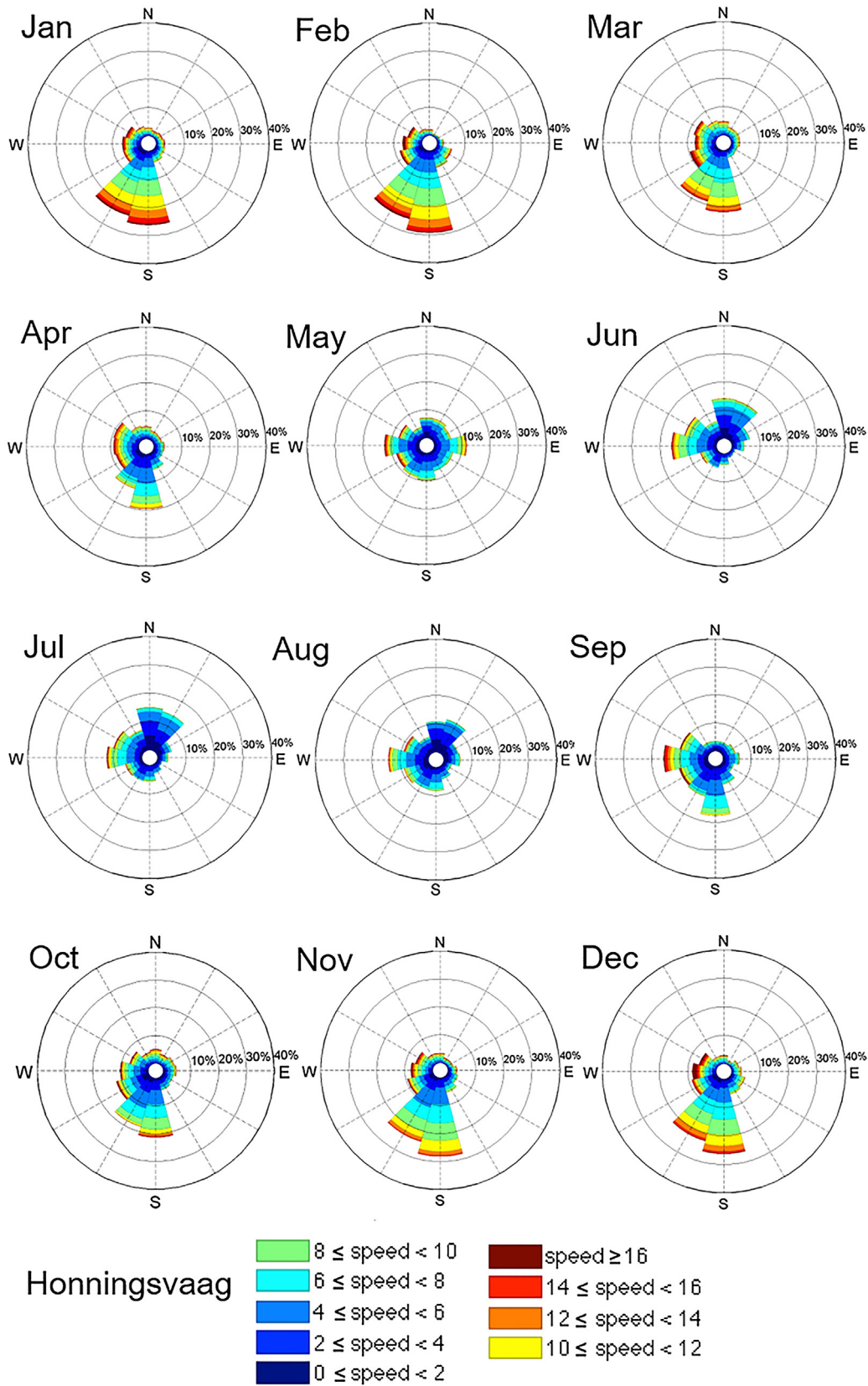


Figure 11 Wind roses comparing wind conditions in different months at Honningsvaag for 2006–2015. Wind roses for specific months are labelled with their abbreviations. Based on data from the Norwegian Meteorological Institute, www.eklima.met.no.

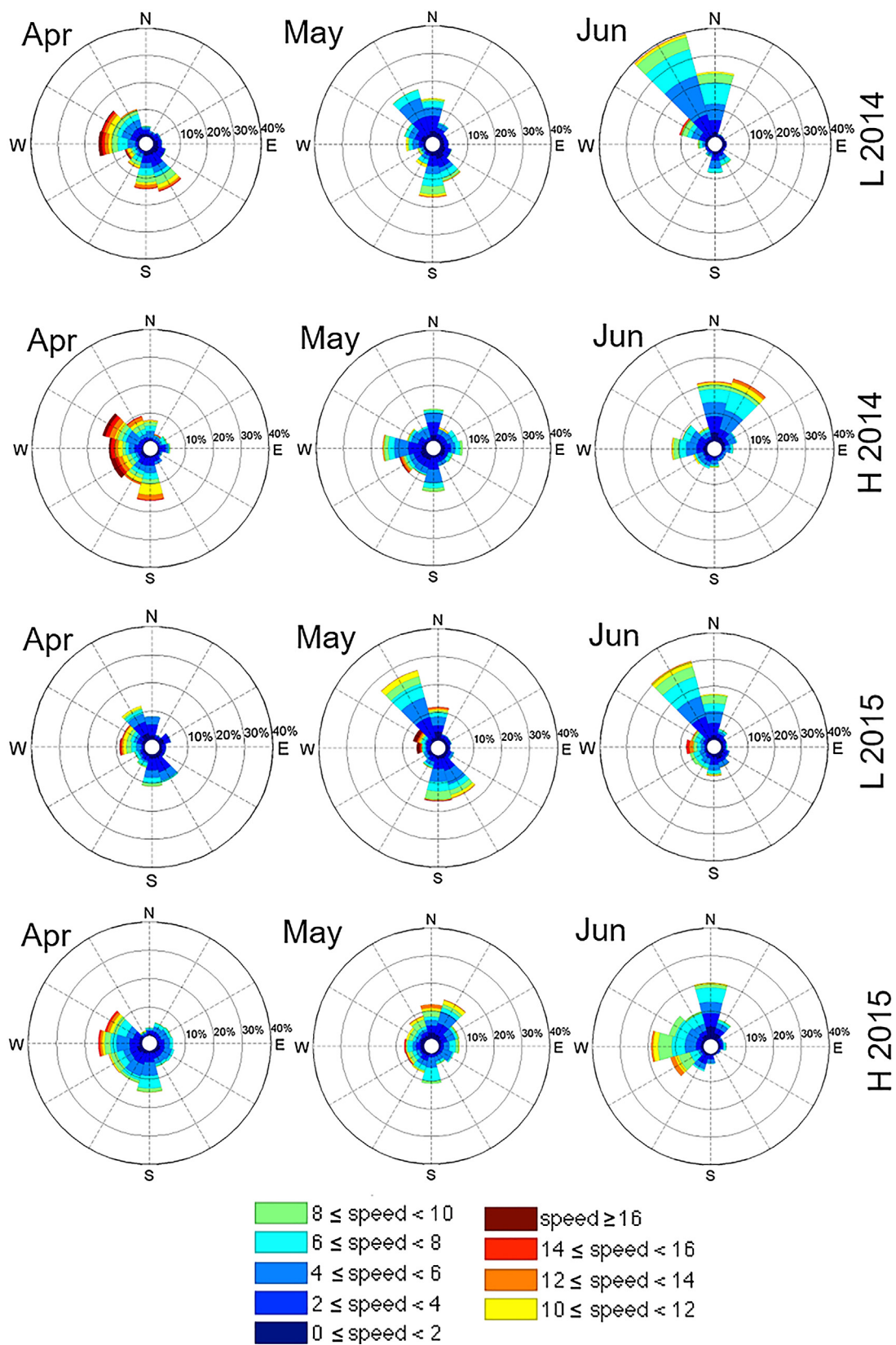


Figure 12 Wind roses comparing wind conditions in the months of April, May and June in 2014 and 2015. The first and the third rows are for Lakselv (L), the second and the fourth rows are for Honningsvaag (H). Wind roses for specific months are labelled with their abbreviations. Based on data from the Norwegian Meteorological Institute, www.eklima.met.no.

June 2015 were almost the same, but there were some differences. For example, we noted the occurrence of high ($\sim 10 \text{ m s}^{-1}$) winds from the S, SSW and SW sectors in June 2015, high westerly wind speed episodes in June 2015 and rare, strong wind speed events in the NW sector in June 2014. At Honningsvaag, June 2014 was different in the context of wind characteristics from June 2015. In June 2014 NNE winds dominated, whereas in June 2015 there were scarcely any winds from that direction. In addition, westerlies were often registered in June 2015, whereas in June 2014 they were not so frequent and significantly weaker. With regard to the spring and early summer wind patterns along the fjord, strong wind events were less frequent in the months of June than in the Aprils and Mays. Compared with the other two months, the months of May still seemed to exhibit transitional features. The spring/early summer wind characteristics in Porsanger do display seasonality but there are some year-to-year differences.

Summarizing, there are large differences in the wind directions at L and H. The variability is greater at Honningsvaag, which is a result of different geographical conditions: H

is situated near the ocean and surrounded by small hills, whereas L lies inland and is sheltered by higher mountains (see Fig. 1b, c). The wind direction at Lakselv seems to be more influenced by the fjord's topography than the wind in H.

Short-term variability includes periodic changes occurring on a daily time scale. Figure 13a exemplifies an AT data subset showing in better focus the within-day AT variability at Lakselv and Honningsvaag. First of all, the daily changes in air temperature are significant. They are associated with the variable shortwave radiation flux resulting from the daily cycle of the solar zenith angle. Interestingly, the spatial variability of the daily AT cycle also leads to a pronounced daily cycle of the difference between ATs at Lakselv and Honningsvaag (Fig. 13b). This is because Lakselv is more under the influence of vast land areas. Because of the difference in specific heat capacity, the land surface warms up more efficiently during the day than the ocean surface. Heat fluxes warm the air above the land surface, so there is a faster increase in air temperature during the day at Lakselv than at Honningsvaag, which lies near the ocean. Wind speeds are also influenced by this process, since air expands

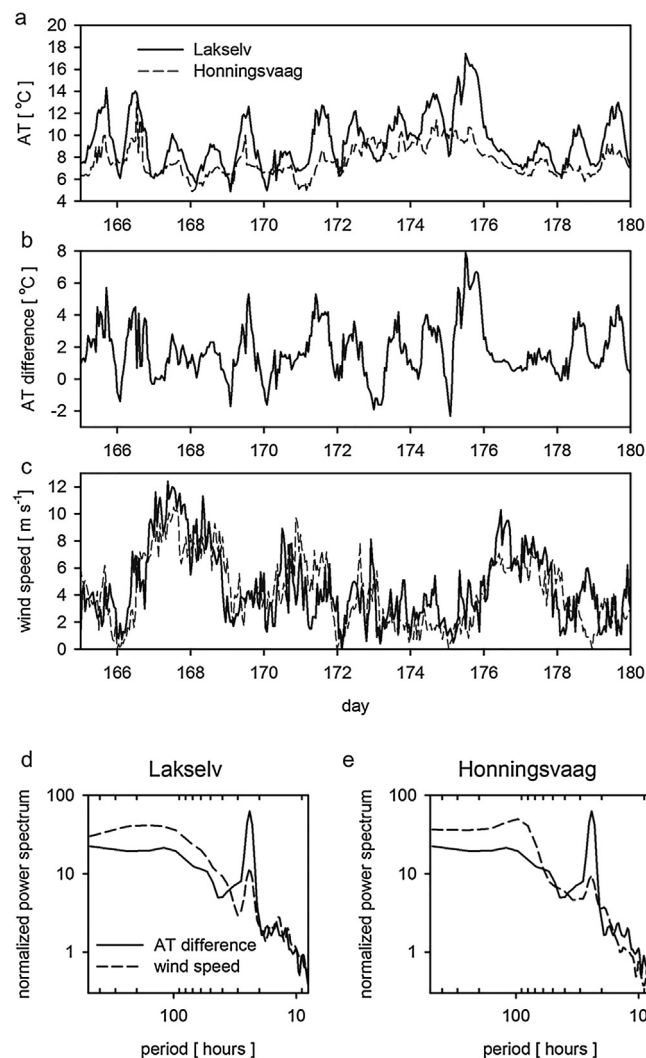


Figure 13 Example time series of (a) air temperature (AT) at Lakselv and Honningsvaag, (b) the AT difference between Lakselv and Honningsvaag, (c) wind speed in the summer of 2014. (d and e) Power spectra of AT difference (solid black line) and wind speed (dashed black line) at Lakselv and Honningsvaag. Based on data from the Norwegian Meteorological Institute, www.eklima.met.no.

on warming up. During the day, therefore, the air pressure is lower over the land than over the ocean. The within-day variabilities of wind speed at Lakselv and Honningsvaag are displayed in Fig. 13c. Clearly, the daily wind speed cycle is not as obvious as the daily cycle in air temperature difference. In order to illustrate the importance of the daily cycles, power spectra were calculated from the 2014 summer data. The normalized power spectra are similar at L and H. There is a significant peak on the diurnal time scale for the AT difference (Fig. 13d and e). The 24-h wind speed peak is more pronounced at Lakselv than at Honningsvaag. These daily cycles were not observed in winter (not shown here). The daily patterns in the AT and wind speed differences between H and L are an interesting feature of the meteorological situation shaping the fjord environment during the spring and summer months.

5. Discussion

Climate change is having a significant effect on the Arctic environment, where global trends are being amplified (Screen and Simonds, 2010; Serreze and Barry, 2011). Most research in the European Arctic focuses on very specific regions such as Svalbard, where intense interdisciplinary research regarding many aspects of climate related changes has been carried on for many years (Cisek et al., 2010, 2017; Głowacki and Niedźwiedź, 1997; Gluchowska et al., 2016; Haarpaintner et al., 2001; Kędra et al., 2013; Marsz and Styszyńska, 2013; Piechura and Walczowski, 2009; Putkonen, 1998; Strzelecki et al., 2015; Svendsen et al., 2002; Zagórski et al., 2015). In contrast, there is less information in the literature for some other regions, such as the coastal regions of the Barents Sea. For a full understanding of how a spatially variable environment like the Arctic functions, research needs to embrace different locations in order to acquire information on a range of different local environments. This will enable knowledge to be extrapolated to a larger scale with better precision.

This paper focuses on the Porsanger fjord, which is situated in the coastal region of the Barents Sea. Even though the Barents Sea is known to play an important role in the entire Arctic context (Döscher et al., 2014; Inoue et al., 2012; Mastowski et al., 2004), coastal processes in the Barents Sea have not received enough attention in the literature, so far. This work analyses meteorological and water runoff data for the fjord in order to better characterize the conditions shaping its environment. The results confirm that this region is undergoing warming related to climate change: this is indicated by rising air temperatures. The estimated trend for AT in the Porsanger fjord is $0.0485^{\circ}\text{C year}^{-1}$ at the fjord mouth (R_H) and $0.0416^{\circ}\text{C year}^{-1}$ at the fjord head (R_L). For comparison, global linear trends in air temperature have been estimated at $0.007^{\circ}\text{C year}^{-1}$ based on data for 1901–2010 and $0.017^{\circ}\text{C year}^{-1}$ based on 1979–2010 temperatures (Morice et al., 2012). Trends in the Arctic are larger than global average (Serreze and Francis, 2006). In the open Barents Sea, such trends are even stronger than in other Arctic regions (Koenigk et al., 2015); based on data for 1982–2013 they have been estimated at $\sim 0.2^{\circ}\text{C year}^{-1}$ (Jakowczyk and Stramska, 2014). The AT trends derived in this work for the Porsanger fjord are thus higher than the global average,

but lower than those in the open Barents Sea. Moreover, presented results point to AT monthly trends being statistically significant and positive at R_L in September and at R_H in May, September, November and December (Table 1). Hence, the increase in AT is more evident in the spring and autumn. This may imply that the spring/summer season in the Porsanger fjord region is becoming longer, as has been observed in other Arctic fjords (Gjelten et al., 2016).

There were also annual trends in land-originated water discharges in all analyzed sub-regions. In contrast to AT and freshwater runoff, the results shows that climate change does not seem to have had a significant effect on long-term changes in either wind speed or precipitation in this region. At a first glance, it can be somewhat puzzling that statistically significant trends were detected in land-originated water runoff estimates, whilst trends in precipitation were not statistically significant. This can be partly explained by the fact that accurate precipitation representation in reanalysis is of a special difficulty and that generally precipitation is the most uncertain quantity provided by ERA-Interim. This is because precipitation is highly variable in space but there are not enough in situ data collected for assimilation in data reanalysis (Dee et al., 2011). In addition, the water runoff depends not only on precipitation, but also on evaporation and other processes. According to authors' supplementary calculations (based on ERA-Interim data not shown here), there was no statistically significant trend in the precipitation minus evaporation ($P - E$) in the study region, except for the month of June in Lakselv. However water runoff depends also on other factors, such as snow melt and efficiency of water transport on land from other regions. For example, significant precipitation can occur far away from the fjord and amplify the land-originated water inflow into the basin independently on precipitation rates in the vicinity of the fjord.

One of the most noticeable observation from this research is that the Porsanger fjord is a region with significant spatial variability. Thermal and wind conditions are quite different in its inner and outer parts, even if the distance between the sites is only around 100 km. The inner part is strongly affected by aspects of continental climate; the outer part, in contrast, is governed by maritime influences. This leads to large differences in ATs recorded at the two stations. On average, the difference in mean monthly ATs at Lakselv and Honningsvaag is about 5.9°C in winter (January) and 2.5°C in summer (July). There are also significant differences in other statistical quantities, such as median, 10th and 90th percentiles and standard deviations, showing that air temperatures are more variable at Lakselv than at Honningsvaag. Average and median wind speeds are significantly lower at Lakselv (5.4 and 4.9 m s^{-1}) than at Honningsvaag (6.2 and 5.7 m s^{-1}). The annual amplitude of wind speed, as well as the standard deviation of the time series, is higher at Honningsvaag than at Lakselv. This shows that wind conditions are more variable at the former than at the latter station.

There is also noticeable spatial variability of wind directions. Winds at Lakselv are more influenced by the surrounding topography (mountains) than at Honningsvaag, where the land is lower. Moreover, strong wind events (above 12 m s^{-1}) are more frequent at Honningsvaag than at Lakselv. The steep longshore gradients in meteorological parameters such as wind, AT and precipitation presented in this study have been

also observed for other Fennoscandian fjords (Wassmann et al., 1996).

The Porsanger fjord is characterized by a strong annual cycle in AT and wind data (speed and direction), as this is a region where the polar night (from the last week in November to the third week in January) and polar day (mid-May to the end of July) occur. Based on monthly means, the multiyear average annual AT amplitude is 21.5°C at Lakselv and 13.9°C at Honningsvaag. In the annual wind speed cycle there are more variable winds and higher average wind speeds in winter than in summer. There is a well pronounced seasonal shift in wind direction. In summer (June), NNW and N winds are more frequent at Lakselv, whereas N and W winds prevail at Honningsvaag. In winter (January), S and SE winds prevail at Lakselv, whilst winds from the S and SW sectors are the most frequent at Honningsvaag. The annual precipitation cycle is not so well pronounced, and the precipitation records at these two stations display different patterns. Generally, for all stations where precipitation totals were analyzed, the annual patterns of monthly means are different at each location, and the annual cycle is not as well noticeable as in the case of AT or winds. The results also reveal differences between the monthly precipitation totals in 2014 and 2015, and the 10-year mean monthly totals. This implies significant inter-annual variability in precipitation in specific months (Fig. 6). In contrast to precipitation, the annual cycle of water runoff is very clear. Terrigenous water discharge is extremely low in the winter months but high in the late spring and summer. This is because seasonal patterns in snow melt significantly affect water runoff. Water runoffs are the largest in the innermost region E, where the Lakselva supplies the river water. The second most important region is the eastern catchment G, with the Børselva river.

Synoptic-scale and within-day variability is also intense in the Porsanger fjord. Wind patterns and air temperatures can change dramatically within hours. In addition, there are evidently regular patterns in the AT daily cycle in the time series records, but they are of different intensities at L and H. Interestingly, the daily cycle of air temperature difference between Lakselv and Honningsvaag is also strong and has an influence on winds. This has been confirmed by the power spectra of air temperature and wind speed in spring/summer with statistically significant peaks indicating diel variability. Similar peaks are absent from the time series from late autumn and winter.

Climate and weather change issues in the Arctic region require further studies. Information from in situ observations, confirming model conclusions and predictions, needs continuous updating. The broad range of data analyzed in this paper shows that the Porsanger fjord is a region sensitive to climate change. Since certain meteorological and climatic parameters of Fennoscandian fjords are correlated (Eilertsen and Skarðhamar, 2006), the main features of climate-related trends and the effects of oceanic/continental interactions shaping the Porsanger fjord environment may be similar in other fjords in comparable geographical locations.

6. Conclusions

One of the main conclusions of this study is the amplification of global warming being observed in Porsanger fjord. Positive

air temperature annual trends were estimated at both examined locations, fjord head – R_L and fjord mouth – R_H . These trends are higher than the global AT trend but lower than the annual AT trend calculated for the open Barents Sea. Based on monthly trends it seems that warming is more evident in the spring and autumn months. Positive annual trends were calculated also in land-originated water discharge for all catchments delivering 100% of their runoff water to the fjord. In contrast, no significant trends were noted in precipitation and wind speed time series.

Additionally, well pronounced annual cycle was observed in AT and wind speed data at both investigated stations, Lakselv and Honningsvaag. This includes a marked seasonal shift in wind direction. In summer (June), NNW and N winds were more frequent at Lakselv, whereas N and W winds dominated at Honningsvaag. In winter (January), S and SE winds prevailed at Lakselv whilst winds from the S and SW sectors were dominant at Honningsvaag. The annual cycle in precipitation was not as obvious as for AT and wind speed, but freshwater runoff was also displaying seasonal variability, with maximum runoff observed in June.

Temporal variability at shorter time scales (synoptic, daily) was also substantial. Short-term fluctuations include changes in AT of the order of a few °C (up to ~20°C in extreme situations), whereas changes in wind speed were up to 20 m s⁻¹. In addition, considerable interannual variability was observed. Finally, there were remarkable discrepancies in ATs and winds recorded at the same time at different locations within the fjord, underlining the significance of spatial variability. These can be explained by the fact that in spite of the relatively short distance between the stations (~100 km) the influence of continental and maritime weather patterns is different at both ends of the fjord. Furthermore, wind patterns are influenced by varying land topography.

The results presented in this manuscript emphasize the fact that arctic fjords are very complex systems. Due to intense temporal and spatial variability, research in such regions requires long-term high-temporal resolution data and sufficient spatial coverage, if one wants to develop a good understanding of air–water–land interactions taking place in the fjords. If these requirements are not satisfied, it is likely that experimental data will not reveal the true status of environmental interactions and changes taking place in such regions.

Acknowledgements

The authors are grateful to all the people involved in the programmes providing free access to the data sets used in the study.

Long-term analysis was based on ERA-Interim reanalysis data (European Centre for Medium-Range Weather Forecasts (ECMWF) ERA-Interim reanalysis service, http://apps.ecmwf.int/datasets/data/interim-full-daily/levtype=sfc/?date_date_range=2010-01-01). Local observational data were derived via the eKlima website (www.eklima.met.no), a product of the Norwegian Meteorological Institute.

The terrigenous water discharge data used in this research were obtained from the E-HYPE model. This set had to be purchased because there were no post-2010 data available in

free access (Swedish Meteorological and Hydrographical Institute, <http://hypeweb.smhi.se/europehype/time-series/>).

The terrain elevation data used to illustrate Porsanger fjord nearby land elevation were obtained from the U.S. Geological Survey (USGS – lta.cr.usgs.gov/GMTED2010).

The wind rose depiction technique was based on the Daniel Pereira free access Matlab code. The script was modified by the authors of this paper.

The authors would also like to thank Mr. Peter Senn for English language support.

This work was funded by the Norway Grants through the Polish-Norwegian Research Programme operated by the National Centre for Research and Development (NCBR contract No. 201985 entitled 'Application of in situ observations, high frequency radars, and ocean colour, to study suspended matter, particulate carbon, and dissolved organic carbon fluxes in coastal waters of the Barents Sea'). Partial funding for MS and AC comes from the statutory funds at IO PAN.

References

- Aalto, J., le Roux, P.C., Luoto, M., 2014. The meso-scale drivers of temperature extremes in high-latitude Fennoscandia. *Clim. Dyn.* 42 (1–2), 237–252, <http://dx.doi.org/10.1007/s00382-012-1590-y>.
- Ådlandsvik, B., Loeng, H., 1991. A study of the climatic system in the Barents Sea. *Polar Res.* 10 (1), 45–50, <http://dx.doi.org/10.1111/j.1751-8369.1991.tb00633.x>.
- AMAP, 1998. Assessment Report: Arctic Pollution Issues. Chapter 2: Physical/Geographical Characteristics of the Arctic, 9–24, Available from: <https://www.amap.no/documents/doc/amap-assessment-report-arctic-pollution-issues/68> (accessed 16.12.17).
- Arheimer, B., 2011. E-HypeWeb: service for water and climate information – and future hydrological collaboration across Europe. In: Hřebíček, J., Schimak, G., Denzer, R. (Eds.), *Environmental Software Systems. Frameworks of Environment, IFIP Advances in Information and Communication Technology*. Springer, Berlin, 657–666.
- Årthun, M., Eldevik, T., Smedsrud, L.H., Skagseth, Ø., Ingvaldsen, R. B., 2012. Quantifying the influence of Atlantic heat on Barents Sea ice variability and retreat. *J. Climate* 25, 4736–4743, <http://dx.doi.org/10.1175/JCLI-D-11-00466.1>.
- Asplin, L., Salvanes, A.G.V., Kristoffersen, J.B., 1999. Nonlocal wind-driven fjord-coast advection and its potential effect on plankton and fish recruitment. *Fish. Oceanogr.* 8 (4), 255–263, <http://dx.doi.org/10.1046/j.1365-2419.1999.00109.x>.
- Bendat, J.S., Piersol, A.G., 2011. *Random Data: Analysis and Measurement Procedures, Fourth Edition*, Wiley Series in Probability and Statistics. John Wiley and Sons, Inc., Hoboken, NJ, 640 pp.
- Białogrodzka, J., Stramska, M., Ficek, D., Wereszka, M., 2017. Total suspended particulate matter in the Porsanger fjord (Norway) in the summer of 2014 and 2015. *Oceanologia* 60 (1), 1–16, <http://dx.doi.org/10.1016/j.oceano.2017.06.002>.
- Bienau, M.J., Hattermann, D., Kröncke, M., Kretz, L., Otte, A., Eiserhardt, W.L., Milbau, A., Graae, B.J., Durka, W., Eckstein, R.L., 2014. Snow cover consistently affects growth and reproduction of *Empetrum hermaphroditum* across latitudinal and local climatic gradients. *Alpine Bot.* 124 (2), 115–129, <http://dx.doi.org/10.1007/s00035-014-0137-8>.
- Boitsov, V.D., Karsakov, A.L., Trofimov, A.G., 2012. Atlantic water temperature and climate in the Barents Sea, 2000–2009. *ICES J. Mar. Sci.* 69 (5), 833–840.
- Cisek, M., Colao, F., Demetrio, E., 2010. Remote and local monitoring of dissolved and suspended fluorescent organic matter off the Svalbard. *J. Optoelectron. Adv. Mater.* 12 (7), 1604–1618.
- Cisek, M., Makuch, P., Petelski, T., 2017. Comparison of meteorological conditions in Svalbard fjords: Hornsund and Kongsfjorden. *Oceanologia* 59 (4), 413–421, <http://dx.doi.org/10.1016/j.oceano.2017.06.004>.
- Comiso, J.C., 2012. Large decadal decline of the arctic multiyear ice cover. *J. Climate* 25 (4), 1176–1193, <http://dx.doi.org/10.1175/JCLI-D-11-00113.1>.
- Cottier, F.R., Nilsen, F., Skogseth, R., Tverberg, V., Skardhamar, J., Svendsen, H., 2010. Arctic Fjords: A Review of the Oceanographic Environment and Dominant Physical Processes, vol. 344(1). Geol. Soc., London, Special Publications, pp. 35–50, <http://dx.doi.org/10.1144/SP344.4>.
- Danielson, J.J., Gesh, D.B., 2011. Global Multi-resolution Terrain Elevation Data 2010 [GMTED 2010]. U.S. Geologic Survey Open-File Report 2011-1073, 26 pp., <https://pubs.usgs.gov/of/2011/1073/pdf/of2011-1073.pdf>.
- Dee, D.P., Uppala, S.M., Simmons, A.J., Berrisford, P., Poli, P., Kobayashi, S., Andrae, U., Balmaseda, M.A., Balsamo, G., Bauer, P., Bechtold, P., Beljaars, A.C.M., Van De Berg, L., Bidlot, J., Bormann, N., Delsol, C., Dragani, R., Fuentes, M., Geer, A.J., Haimberger, L., Healy, S.B., Hersbach, H., Hólm, E.V., Isaksen, I., Kållberg, P., Köhler, M., Matricardi, M., McNally, A.P., Monge-Sanz, B.M., Morcrette, J.-J., Park, B.-K., Peubey, C., De Rosnay, P., Tavolato, C., Thépaut, J.-N., Vitart, F., 2011. The ERA-Interim reanalysis: configuration and performance of the data assimilation system. *Q. J. R. Meteor. Soc.* 137 (656), 533–597, <http://dx.doi.org/10.1002/qj.828>.
- Donnelly, Ch., Andersson, J.C.M., Arheimer, B., 2016. Using flow signatures and catchment similarities to evaluate the E-HYPE multi-basin model across Europe. *Hydrol. Sci. J.* 61 (2), 255–273, <http://dx.doi.org/10.1080/02626667.2015.1027710>.
- Döscher, R., Vihma, T., Maksimovich, E., 2014. Recent advances in understanding the Arctic climate system state and change from a sea ice perspective: a review. *Atmos. Chem. Phys.* 14 (24), 13571–13600, <http://dx.doi.org/10.5194/acp-14-13571-2014>.
- Eilertsen, H.Ch., Frantzen, S., 2007. Phytoplankton from two sub-Arctic fjords in northern Norway 2002–2004: I. Seasonal variations in chlorophyll *a* and bloom dynamics. *Mar. Biol. Res.* 3 (5), 319–332, <http://dx.doi.org/10.1080/17451000701632877>.
- Eilertsen, H.Ch., Skardhamar, J., 2006. Temperatures of north Norwegian fjords and coastal waters: variability, significance of local processes and air–sea heat exchange. *Estuar. Coast. Shelf Sci.* 67 (3), 530–538, <http://dx.doi.org/10.1016/j.ecss.2005.12.006>.
- Førland, E.J., Benestad, R., Hanssen-Bauer, I., Haugen, J.E., Skaugen, T.E., 2011. Temperature and precipitation development at Svalbard 1900–2100. *Adv. Meteorol.* 1–14, <http://dx.doi.org/10.1155/2011/893790>.
- Gjelten, H.M., Nordii, Ø., Isaksen, K., Førland, E.J., Sviashchennikov, P.N., Wyszynski, P., Prokhorova, U.V., Przybylak, R., Ivanov, B.V., Urazgildeeva, A.V., 2016. Air temperature variations and gradients along the coast and fjords of western Spitsbergen. *Polar Res.* 35 (1), 1–13, <http://dx.doi.org/10.3402/polar.v35.29878>.
- Głowacki, P., Niedźwiedz, T., 1997. Climatological conditions in Hornsund (Spitsbergen) during succeeding Polish Polar Expeditions. In: Głowacki, P. (Ed.), *Polish Polar Studies, 24th Polar Symposium*. Warsaw. Inst. Geophys. PAN, Warszawa, 81–94.
- Gluchowska, M., Kwaśniewski, S., Promińska, A., Olszewska, A., Goszczko, I., Falk-Petersen, S., Hop, H., Węstawski, J.M., 2016. Zooplankton in Svalbard fjords on the Atlantic–Arctic boundary. *Polar Biol.* 39 (10), 1785–1802, <http://dx.doi.org/10.1007/s00300-016-1991-1>.
- Goosse, H., Holland, M.M., 2005. Mechanisms of decadal arctic climate variability in the community climate system model, version 2 (CCSM2). *J. Climate* 18, 3552–3570.
- Haarpaintner, J., Gascard, J.-C., Haugan, P.M., 2001. Ice production and brine formation in Storfjorden, Svalbard. *J. Geophys. Res.* 106 (C7), 14001–14013.

- Inoue, J., Masatake, E.H., Takaya, K., 2012. The role of Barents Sea ice in the wintertime cyclone track and emergence of a warm-arctic cold-Siberian anomaly. *J. Climate* 25 (7), 2561–2568, <http://dx.doi.org/10.1175/JCLI-D-11-00449.1>.
- Jakowczyk, M., Stramska, M., 2014. Spatial and temporal variability of satellite-derived sea surface temperature in the Barents Sea. *Int. J. Remote Sens.* 35 (17), 6545–6560, <http://dx.doi.org/10.1080/01431161.2014.958247>.
- Kaste, Ø., Wright, R.F., Barkved, L.J., Bjerkeng, B., Engen-Skaugen, T., Magnusson, J., Sælthun, N.R., 2006. Linked models to assess the impacts of climate change on nitrogen in a Norwegian river basin and fjord system. *Sci. Total Environ.* 365 (1–3), 200–222, <http://dx.doi.org/10.1016/j.scitotenv.2006.02.035>.
- Kędra, M., Renaud, P.E., Andrade, H., Goszczko, I., Ambrose Jr., W. G., 2013. Benthic community structure, diversity, and productivity in the shallow Barents Sea bank (Svalbard Bank). *Mar. Biol.* 160 (4), 805–819, <http://dx.doi.org/10.1007/s00227-012-2135-y>.
- Koenigk, T., Berg, P., Döscher, R., 2015. Arctic climate change in an ensemble of regional CORDEX simulations. *Polar Res.* 34 (1), <http://dx.doi.org/10.3402/polar.v34.24603>.
- Leth, O.K., 1995. A study on the effect of local wind on the dynamics of the upper layer in the inner part of Malangen. In: Skjoldal, H. R., Hopkins, C., Erikstad, K.E., Leinaas, H.P. (Eds.), *Ecology of Fjords and Coastal Waters*. Elsevier, Amsterdam, 185–194.
- Levitov, S., Antonov, J., Boyer, L., Locamini, T.P., Garcia, H.E., Mishonov, A.V., 2009. Global Ocean heat content 1955–2008 in light of recently revealed instrumentation problems. *Geophys. Res. Lett.* 36 (7), L070608, <http://dx.doi.org/10.1029/2008GL037155>.
- Linell, K.A., Tedrow, J.C.F., 1981. *Soil and Permafrost Surveys in the Arctic*, 1st ed. Clarendon Press, Oxford, 279 pp.
- Marsz, A.A., Styszyńska, A. (Eds.), 2013. *Climate and Climate Change at Hornsund, Svalbard*. Gdynia Maritime Univ. Publ., Gdynia, 402 pp.
- Mastowski, W., Marble, D., Walczowski, W., Schauer, U., Clement, J. L., Semtner, A.J., 2004. On climatological mass, heat, and salt transports through the Barents Sea and Fram Strait from a pan-Arctic coupled ice-ocean model simulation. *J. Geophys. Res.* 19, C03032, <http://dx.doi.org/10.1029/2001JC001039>.
- McGuire, A.D., Chapin III, F.S., Walsh, J.E., Wirth, Ch., 2006. Integrated regional changes in arctic climate feedbacks: implications for the global climate system. *Annu. Rev. Environ. Resour.* 31, 61–91, <http://dx.doi.org/10.1146/annurev.energy.31.020105.100253>.
- Mills, W., Speak, P., 1998. *Keyguide to Information Sources on the Polar and Cold Regions*, 1st ed. Mansell, London and Washington, 330 pp.
- Morice, C.P., Kennedy, J.J., Rayner, N.A., Jones, P.D., 2012. Quantifying uncertainties in global and regional temperature change using an ensemble of observational estimates: The HadCRUT4 data set. *J. Geophys. Res.* 117, D08101, <http://dx.doi.org/10.1029/2011JD017187>.
- Myksovoll, M.S., Sundby, S., Ådlandsvik, B., Vikebø, F.B., 2011. Retention of coastal cod eggs in a fjord caused by interactions between egg buoyancy and circulation pattern. *Mar. Coast. Fisher.* 3 (1), 279–294, <http://dx.doi.org/10.1080/19425120.2011.595258>.
- Myksovoll, M.S., Sandvik, A.D., Skarøhamar, J., Sundby, S., 2012. Importance of high resolution wind forcing on eddy activity and particle dispersion in a Norwegian fjord. *Estuar. Coast. Shelf Sci.* 113, 293–304, <http://dx.doi.org/10.1016/j.ecss.2012.08.019>.
- Niedźwiedz, T., 1997. The climates of the “Polar regions”. In: Yoshino, M., Douguedroit, A., Paszyński, J., Nkemdirim, L. (Eds.), *Climates and Societies—A Climatological Perspective*. The GeoJournal Library, vol. 36. Springer, Dordrecht, 309–324, http://dx.doi.org/10.1007/978-94-017-1055-8_14.
- Osuch, M., Wawrzyniak, T., 2016. Climate projections in the Hornsund area, Southern Spitsbergen. *Polish Pol. Res.* 37 (3), 379–402, <http://dx.doi.org/10.1515/popore-2016-0020>.
- Piechura, J., Walczowski, W., 2009. Warming of the West Spitsbergen Current and sea ice north of Svalbard. *Oceanologia* 51 (2), 147–164, <http://dx.doi.org/10.5697/oc.51.2.147>.
- Piechura, J., Beszczyńska-Möller, A., Osiński, R., 2001. Volume, heat and salt transport by the West Spitsbergen Current. *Polar Res.* 20 (2), 125–248, <http://dx.doi.org/10.1111/j.1751-8369.2001.tb00061.x>.
- Putkonen, J., 1998. Soil thermal properties and heat transfer processes near Ny-Alesund, northwestern Spitsbergen, Svalbard. *Polar Res.* 17 (2), 165–179, <http://dx.doi.org/10.1111/j.1751-8369.1998.tb00270.x>.
- Schauer, U., Loeng, H., Rudels, B., Ozhigin, V., Dieck, W., 2002. Atlantic water flow through the Barents and Kara Sea. *Deep Sea Res.* 49 (12), 2281–2296.
- Screen, J.A., Simonds, I., 2010. The central role of diminishing sea ice in recent Arctic temperature amplification. *Nature* 464, 1334–1337, <http://dx.doi.org/10.1038/nature09051>.
- Semenov, V.A., Park, V., Latif, M., 2009. Barents Sea inflow shutdown: a new mechanism for rapid climate changes. *Geophys. Res. Lett.* 36 (14), L14709, <http://dx.doi.org/10.1029/2009GL038911>.
- Serreze, M.C., Barry, R.G., 2011. Processes and impacts of Arctic amplification: a research synthesis. *Glob. Planet. Change* 77 (1–2), 85–96, <http://dx.doi.org/10.1016/j.gloplacha.2011.03.004>.
- Serreze, M.C., Francis, J.A., 2006. The Arctic amplification debate. *Climate Change* 76 (3–4), 241–264, <http://dx.doi.org/10.1007/s10584-005-9017-y>.
- Sheskin, D.J., 2000. *Handbook of Parametric and Nonparametric Statistical Procedures*, 3rd ed. CRC Press, London and New York, 1185 pp.
- Smedsrud, L.H., Ingvaldsen, R., Nilsen, J.E.Ø., Skagseth, Ø., 2010. Heat in the Barents Sea: transport, storage and surface fluxes. *Ocean Sci.* 6, 219–234, <http://dx.doi.org/10.5194/os-6-219-2010>.
- Smedsrud, L.H., Esau, I., Ingvaldsen, R.B., Eldevik, T., Haugan, P.M., Li, C., Lien, V.S., Olsen, A., Omar, A.B., Otterå, O.H., Risebrobakken, B., Sandø, A.B., Semenov, V., Sorokina, S.A., 2013. The role of the Barents Sea in the Arctic climate system. *Rev. Geophys.* 51 (3), 415–449, <http://dx.doi.org/10.1002/rog.20017>.
- Stocker, T.F., Qin, D., Plattner, G.-K., Tignor, M., Allen, S.K., Boschung, J., Nauels, A., Xia, Y., Bex, V., Midgley, P.M., 2013. *Climate Change 2013: The Physical Science Basis. Contribution of Working Group I to the Fifth Assessment Report of the Intergovernmental Panel on Climate Change*. Cambridge University Press, Cambridge, United Kingdom/New York, NY, USA, 1535 pp.
- Stonehouse, B., 1989. *Polar Ecology*, 1st ed. Blackie, London, 222 pp.
- Stramska, M., Jankowski, A., Cieszyńska, A., 2016. Surface currents in the Porsanger fjord in northern Norway. *Pol. Polar Res.* 37 (3), 337–360, <http://dx.doi.org/10.1515/popore-2016-0018>.
- Stramska, M., Børsheim, K.Y., Jankowski, A., Søiland, H., Cieszyńska, A., 2018. Observations of ocean currents in the Porsanger fjord in the coastal region of the Barents Sea in the summer of 2014 and 2015. *Estuar. Coast. Shelf Sci.* (submitted for publication).
- Strzelecki, M.C., Malecki, J., Zagórski, P., 2015. The influence of recent deglaciation and associated sediment flux on the functioning of polar coastal zone – Northern Petuniabukta, Svalbard. In: Maanan, M., Robin, M. (Eds.), *Sediment Fluxes in Coastal Areas*. Coastal Research Library, vol. 10. Springer, Dordrecht, pp. 23–45, http://dx.doi.org/10.1007/978-94-017-9260-8_2.
- Svendsen, H., 1991. Preliminary Results from a Hydrographical Investigation of Porsangerfjord, Altafjord and Adjacent Coastal Waters, June–August 1990. *Rep. Geophys. Inst. Univ. Bergen, Norway*, p. 28.
- Svendsen, H., 1995. Physical oceanography of coupled fjord-coast systems in northern Norway with special focus on frontal dynamics and tides. In: Skjoldal, H.R., Hopkins, C., Erikstad, K.E., Leinaas, H.P. (Eds.), *Ecology of Fjords and Coastal Waters*. Elsevier Science, Amsterdam, 149–164.

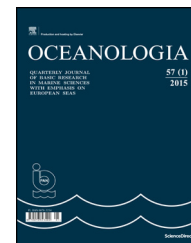
- Svendsen, H., Thompson, R.O.R.Y., 1978. Wind-driven circulation in a fjord. *J. Phys. Oceanogr.* 8, 703–712, [http://dx.doi.org/10.1175/1520-0485\(1978\)008<0703:WDCIAF>2.0.CO;2](http://dx.doi.org/10.1175/1520-0485(1978)008<0703:WDCIAF>2.0.CO;2).
- Svendsen, H., Beszczynska-Moller, A., Hagen, J.O., Lefauconnier, B., Tverberg, V., Gerland, S., Orbeak, J.B., Bischof, K., Papucci, K., Zajaczkowski, M., Azzolini, R., Bruland, O., Wiencke, Ch., Winther, J.G., Dallmann, W., 2002. The physical environment of Kongsfjorden-Krossfjorden, an Arctic Fjord system in Svalbard. *Polar Res.* 21 (1), 133–166, <http://dx.doi.org/10.1111/j.1751-8369.2002.tb00072.x>.
- Syvitski, J.P.M., Burrell, D.C., Skei, J.M., 2012. *Fjords: Processes and Products*, 1st ed. Springer Science & Business Media, New York, 215 pp.
- Wassmann, P., Svendsen, H., Keck, A., Reigstad, M., 1996. Selected aspects of the physical oceanography and particle fluxes in fjords of northern Norway. *J. Mar. Syst.* 8, 53–57, [http://dx.doi.org/10.1016/0924-7963\(95\)00037-2](http://dx.doi.org/10.1016/0924-7963(95)00037-2).
- Woo, M.K., Gregor, D.J., 1992. *Arctic Environment: Past, Present and Future*. McMaster University Department of Geography, Hamilton, 164 pp.
- Zagórski, P., Rodzik, J., Moskalik, M., Strzelecki, M.C., Lim, M., Błaszczuk, M., Promińska, A., Kruszewski, G., Styszyńska, A., Malczewski, A., 2015. Multidecadal (1960–2011) shoreline changes in Isbjørnhamna (Hornsund, Svalbard). *Pol. Polar Res.* 36 (4), 369–390, <http://dx.doi.org/10.1515/popore-2015-0019>.



Available online at www.sciencedirect.com

ScienceDirect

journal homepage: www.journals.elsevier.com/oceanologia/



ORIGINAL RESEARCH ARTICLE

The effects of cyanobacterial blooms on MODIS-L2 data products in the southern Caspian Sea

Karim Naghdi ^{a,*}, Masoud Moradi ^a, Keivan Kabiri ^a, Majid Rahimzadegan ^b

^a Department of Marine Remote Sensing, Iranian National Institute for Oceanography and Atmospheric Science, Tehran, Iran

^b Department of Water Resources, Civil Eng. Faculty, K. N. Toosi University of Technology, Tehran, Iran

Received 25 July 2017; accepted 9 February 2018

Available online 6 March 2018

KEYWORDS

Remote sensing;
Cyanobacterial index;
Floating algae index;
Chlorophyll-*a*;
Fluorescence line
height

Summary MODIS satellite imageries with minimal cloud cover (<25%) were used to extract cyanobacteria index, floating algae index, fluorescence line height, chlorophyll-*a* and sea surface temperature products, for seven days concurrent with blooms. The results showed a positive correlation between cyanobacteria index and chlorophyll-*a* ($R = 0.74$, $p \leq 0.05$ and $R = 0.75$, $p \leq 0.05$ for 2005 and 2010 respectively), and a negative correlation between the cyanobacteria index and fluorescence line height ($R = -0.74$, $p \leq 0.05$ and $R = -0.93$, $p \leq 0.005$ for 2005 and 2010 respectively). Further analysis showed that considering Fluorescence Line Height is not sufficient to detect the cyanobacterial blooms in the offshore area. However, the results indicated a weak correlation between cyanobacteria index and floating algae index ($R = -0.42$, $p = 0.34$ and $R = -0.47$, $p = 0.29$ for 2005 and 2010 respectively). The results also indicated that the irregular increases in the cyanobacteria index and chlorophyll-*a* in the study region was an operational index for the incidence of cyanobacterial bloom, where the surface wind speed and temperature conditions were $<4 \text{ m s}^{-1}$ and $\geq 30^\circ\text{C}$, respectively. Finally, a linear model was defined for monitoring, which determines occurrence or non-occurrence of cyanobacteria bloom based on daily monitoring of the changes of products. In order to evaluate the proposed model, its efficiency was tested on datasets at different times and locations, and the results were consistent with field reports, as expected.

© 2018 Institute of Oceanology of the Polish Academy of Sciences. Production and hosting by Elsevier Sp. z o.o. This is an open access article under the CC BY-NC-ND license (<http://creativecommons.org/licenses/by-nc-nd/4.0/>).

* Corresponding author. Department of Marine Remote Sensing, Iranian National Institute for Oceanography and Atmospheric Science (INIOAS), No. 3, Etemadzadeh St., Fatemi Ave., Tehran, Iran. Tel.: +98 9122254009.

E-mail address: k_naghdi2002@yahoo.com (K. Naghdi).

Peer review under the responsibility of Institute of Oceanology of the Polish Academy of Sciences.



Production and hosting by Elsevier

<https://doi.org/10.1016/j.oceano.2018.02.002>

0078-3234/© 2018 Institute of Oceanology of the Polish Academy of Sciences. Production and hosting by Elsevier Sp. z o.o. This is an open access article under the CC BY-NC-ND license (<http://creativecommons.org/licenses/by-nc-nd/4.0/>).

1. Introduction

Algal blooms occur naturally in both fresh and marine waters throughout the world (Codd et al., 2005; Oyama et al., 2016). Under favorable conditions, high nutrient concentrations, suitable water temperature and adequate light energy, algae species can rapidly grow and cause “blooms”. The Caspian Sea is the largest enclosed inland water body on Earth, and has frequently experienced harmful algal blooms over the past decade (Moradi, 2014). The reported bloom-producing algae in the southern Caspian Sea are members of Cyanobacteria Blue-Green Algae (Nasrollahzadeh et al., 2008). The cyanobacteria are a species of algae that can produce potent toxins, which may cause adverse health effects on wildlife and ecosystems or potentially affect human health (Oyama et al., 2016). Along the southern Caspian Sea, harmful cyanobacterial blooms (CBs) have caused losses to natural resources and coastal economies over the past decade (Moradi, 2014). Potentially toxic CBs occur in the Southern Caspian Sea in mid-summer. A monstrous algal bloom in the southern Caspian Sea occurred in August 2005, which affected an area of 20,000 km² (Moradi, 2014; Nasrollahzadeh et al., 2011; Tahami, 2013). Furthermore, small scales of algal bloom were observed in Iranian coastal waters frequently in 2006–2010 (Nasrollahzadeh et al., 2008).

One of the applications of satellite remote sensing images is synoptic monitoring of CB events, which can help in quantifying the CB dynamics, growth, and senescence (Riha and Krawczyk, 2011; Sayers et al., 2016). Cyanobacteria monitoring is done from satellite data, which are dominantly calculated based on chlorophyll concentrations over bloom surfaces. Phycocyanin (PC) is a marker pigment of cyanobacteria blooms, and has been used as an indicator in satellite monitoring during the study of these blooms (Kahru et al., 2000, 2007; Kutser, 2004, 2009; Sayers et al., 2016; Simis et al., 2005).

Vincent et al. (2004) developed algorithms to detect PC from Landsat TM data for mapping CBs in Lake Erie and improved our understanding of the temporal and spatial dynamics of CBs formation in such systems. Ruiz-Verdú et al. (2008) has evaluated the three remote sensing methods (single reflectance ratio algorithm, semi-empirical baseline algorithm, and nested semi-empirical band ratio algorithm) for PC concentrations with field data in the Spain and Netherlands within the period 2001–2005. The three methods and their maximum errors were shown for waters with either low or very high PC ($PC < 50 \text{ mg m}^{-3}$ or $PC > 200 \text{ mg m}^{-3}$), and their best results are moderate to high PC concentrations ($50\text{--}200 \text{ mg m}^{-3}$). Han et al. (2008) developed a Cyanobacteria index model using 3, 4 and 1 bands of Moderate Resolution Imaging Spectroradiometer (MODIS) data in Taihu Lake (southern China). Wynne et al. (2010) proposed the cyanobacteria index (CI) for MODIS satellite imagery and then analyzed it in western Lake Erie. Hu (2009) developed the floating algae index (FAI) using the medium-resolution (250 and 500 m) data from MODIS satellite imagery, and utilized it to detect the floating algae in the Open Ocean, however, it may be a useful index for deriving bloom patterns in the lakes. Maximum Chlorophyll Index (MCI) computed from bands 8, 9 and 10 of Medium

Resolution Imaging Spectrometer (MERIS) FR level 1 data form an important tool for detection of intense plankton blooms (Gower et al., 2005). Wynne et al. (2008) developed an algorithm based on the Fluorescence Line Height (FLH), which exploits the spectral shape of cyanobacteria absorption features in the red and 'red edge' parts of the electromagnetic spectrum using MERIS satellite. Hu and Feng, 2016 developed a new algal bloom index using the nFLH data product of MODIS satellite imagery. It has shown improved performance over the original nFLH. Moradi (2014) has used FAI, FLH, Chlorophyll-*a* (Chl-*a*) concentrations and CI to compare of the efficacy of MODIS and MERIS data for detecting CBs in the southern Caspian Sea. Wynne et al. (2013) compared MODIS and MERIS spectral shapes for CB detection in Lake Erie and indicated that MODIS can provide a substitute for the MERIS for CB detection.

The current research focuses on studying CB and its effects on MODIS-L2 data products in the southern Caspian Sea. FAI, CI, FLH, Chl-*a*, and SST products of MODIS satellite image and wind stress were selected according to previous research and characteristics of different species of cyanobacteria. Among the most important studies it can be referred to (El Hourany et al., 2017; Hu, 2009; Jafar-Sidik et al., 2017; Moradi, 2014; Stramska and Bialogrodzka, 2016; Webster, 1990). Table 1 shows the list of definitions and acronyms used throughout the text. Since CB occurs in the absence of surface wind and on calm water levels, maximum concentrations of CB as determined from wind speed were observed on 16th and 19th of August 2005, when the wind speed ranged from 0 to $<4 \text{ m s}^{-1}$. This trend has also happened during the development of the bloom process in August 2010. SST has been hypothesized as a key force in the growth of CBs (El Hourany et al., 2017; Paerl, 1988). On the other hand, the lack of wind (less turbulence) increases the water temperature. The cyanobacteria can come closer to the surface (because many cyanobacteria species can regulate their buoyancy) if wind interference is smaller than their swimming capability. In a calm weather condition, the cyanobacteria blooms lose their buoyancy and create surface scum. Strong wind may also mix the scum in the water column, where cyanobacteria biomass is not changed, but only the optical properties of the biomass are changed.

Table 1 List of acronyms and parameters.

Symbol	Definition
Chl- <i>a</i>	Chlorophyll- <i>a</i> concentration [mg m^{-3}]
CI	Cyanobacteria index [mg m^{-3}]
SST	Sea surface temperature [$^{\circ}\text{C}$]
FAI	Floating algae index
FLH	Fluorescence line height [$\text{mW cm}^{-2} \mu\text{m}^{-1} \text{sr}^{-1}$]
PC	Phycocyanin
CB	Cyanobacterial bloom
R_{rc}	Rayleigh-corrected reflectance [dimensionless]
u	10 m U wind component [m s^{-1}]
v	10 m V wind component [m s^{-1}]
τ	Wind stress [$\text{kg m}^{-1} \text{s}^{-2}$ (N m^{-2})]
C_d	Surface drag coefficient [dimensionless]

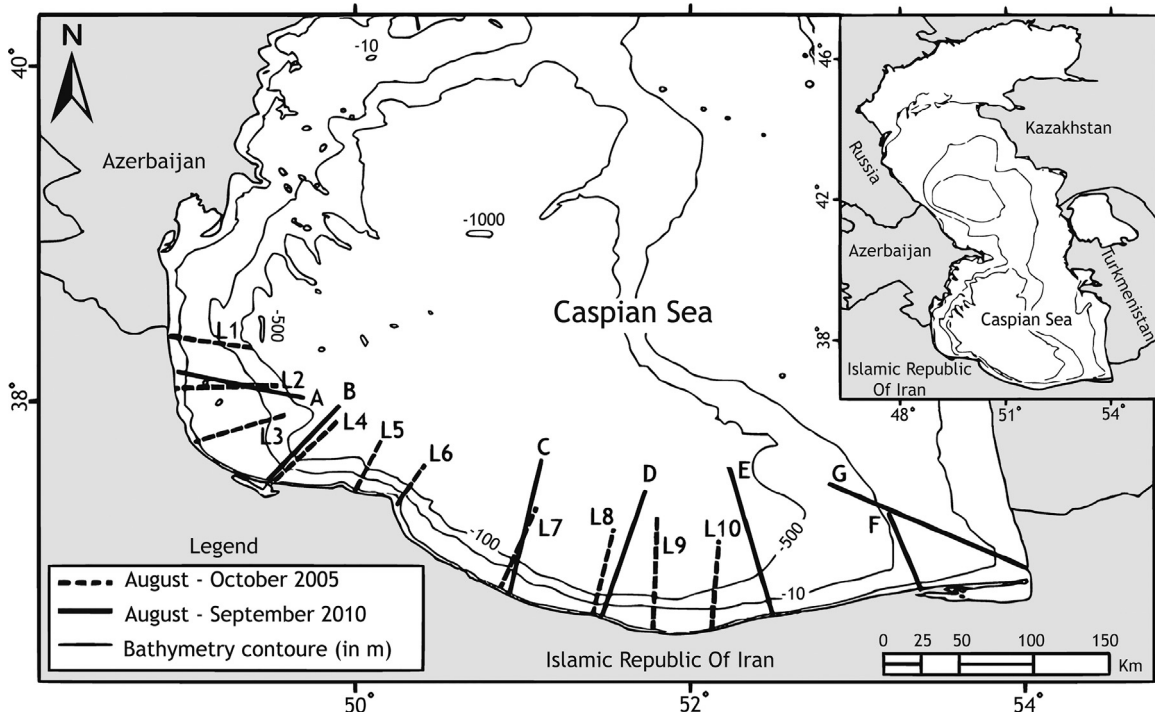


Figure 1 The study area and sampling transects conducted in the southern Caspian Sea (L1: 15/09/2005, L2: 10/09/2005, L3: 8/09/2005, L4: 5/09/2005, L5: 1/09/2005, L6: 10/10/2005, L7: 24/08/2005, L8: 20/08/2005, L9: 18/08/2005, L10: 16/08/2005, A: 1/08/2010, B: 5/08/2010, C: 7/08/2010, D: 10/08/2010, E: 12/08/2010, F: 14/08/2010, G: 15/08/2010) (Moradi, 2014).

2. Material and methods

2.1. Study area

The Caspian Sea is the largest lake in the world with a surface area of $\sim 386,400$ and ~ 7250 km of coastline (Kostianoy and Kosarev, 2005). It extends for almost 1200 km from north to south, with an average width of 320 km and a maximum depth of ~ 1000 m. The physical and biological characteristics of the Caspian Sea are common to both seas and lakes. The Caspian Sea is not a freshwater lake but is often named as the largest lake in the world (Ghafouri, 2008). Currently, the average salinity of the Caspian Sea is 12.3 g kg^{-1} (Peeters et al., 2000). The Caspian Sea is shared between five countries including Iran, Russia, Kazakhstan, Turkmenistan and Azerbaijan (Fig. 1). It is under severe environmental impact such as the water level fluctuations, toxic algal blooms, overfishing, industrial and urban pollutions.

Roohi et al. (2009) reported that a total of 226 phytoplankton species in five phytoplankton groups (diatoms, chlorophytes, cyanophytes, dinoflagellates and euglenophytes) were identified in the Caspian Sea and that a number of species in summer (101 species) was higher than in other seasons. According to the field data in September 2005, average biomass and cyanophyte abundance at 7 and 20 m depths were 1.655 mg m^{-3} and $582 \times 10^6 \text{ cells m}^{-3}$.

Naturally, all cyanobacteria species contain a low concentration of the accessory photosynthetic phycobilin pigment PC. The amount of it depends on species and environmental conditions. PC pigment is the main diagnostic for the presence of cyanobacteria. Usually, researchers use Chl-*a* to assess a total algal biomass and PC is used as an index

or indicator of cyanobacteria biomass (Robertson, 2009). Optical properties of PC in the visible wavelength range can be a useful method to detect and quantify cyanobacterial biomass in remotely sensed data when the suitable spectral resolution is available. When cyanobacteria blooms dominate the water body, the reflectance spectrum shows a local minimum between 600 and 625 nm caused by a maximum of PC absorption around that wavelength and a reflectance maximum around 650 nm caused by a minimum of PC absorption around that wavelength (Ruiz-Verdú et al., 2008). Although, in the presence of other phytoplankton groups, the absorption features of Chl-*a* (shoulder centered around 623 nm), Chlorophyll-*b* (around 600 nm and 650 nm), and Chlorophylls-*c1* and *c2* (around 590 nm and 640 nm) overlap with PC absorption (Ficek et al., 2004; Ruiz-Verdú et al., 2008). The effect of these pigments, water itself, and other water constituents (such as colored dissolved organic matter (CDOM), detritus, and suspended non-algal particles) in the PC absorption region cannot be ignored, when interpreting absorption with the aim to quantify PC (Dekker, 1993).

2.2. Field data

Field data were collected by the Iranian Fisheries Research Organization (IFRO) in the southern Caspian Sea in August and October 2005, and August and September 2010 (Moradi, 2014). The surface water samples were collected at a depth of 1 m in transects perpendicular to the coastlines of western, central and eastern regions (Fig. 1). The analysis of PC for this study was reported in detail by Moradi (2014). The southern Caspian Sea had CBs that started in August 2005 (Nasrollahzadeh et al., 2011). Then again in 2007, 2009, and 2010.

2.3. Satellite data

As CB in the Caspian Sea has occurred often in August and September months, all images related to August and September of the years 2005 and 2007, 2009 and 2010 were investigated to examine this phenomenon. Given the cloud status and the dates reported for CB in different areas of the southern Caspian Sea, MODIS imageries without clouds cover or at least with cloud cover of seven consecutive days for the years 2005 and 2010 were selected.

The daytime MODIS Aqua Level-1A data at 1 km spatial resolution from the 14th to 20th of August 2005 and the 3rd to 9th of August 2010 were downloaded from NASA GODARD Space data archive (<http://ladsweb.nascom.nasa.gov/data>). MODIS level 1A data were processed to level 2 (L2) data using the software package SeaDAS (version 6.4) (FU, 1998). Cloudy pixels were detected using the Wang and Shi (2006) cloud-masking method and MODIS-L2 products were presented for the pixels, which are without cloud cover. This method uses the MODIS short wave infrared (SWIR) reflectance threshold at either 1240 or 1640 nm to identify clear sky from clouds for MODIS data processing (Moradi, 2014; Wang and Shi, 2006).

Given that the remote sensing from the satellite to land or sea surface in the visible and near infrared is strongly affected by the presence of the atmosphere on the Sun-target-Sensor path, atmospheric correction of the MODIS image was performed using the iterative approach for sediment-rich waters that includes a correction for water-leaving radiance caused by sediment and a correction for absorbing aerosols. The spectral bands of MODIS were corrected for atmospheric absorption and Rayleigh scattering using a computer software provided by the MODIS Rapid Response Team, based on the Second Simulation of a Satellite Signal in the Solar Spectrum (6S) radiative transfer calculations code. The 6S is a basic radiative transfer code that enables simulates the signal observed by a satellite sensor at the sea surface. The 6S code needs a set of input parameters such as the spectral characteristics of sensor, latitude of the target, the ground reflectance of a target, azimuth and zenith angles of the Sun and the sensor, an atmospheric model for gaseous components, an aerosol model type and the aerosol concentration (Vermote et al., 1997). It is useful for calculation of lookup tables in the Ocean Color Sensor atmospheric correction algorithm such as MODIS, and has been used successfully in the numerous marine remote sensing studies (Levy et al., 2005; Loeb and Kato, 2002; Matarrese et al., 2004; Potes et al., 2011; Thieuleux et al., 2005).

The MODIS Level 2 products that were obtained from SeaDAS 6.4 software included SST, Chl-*a*, FLH and Rayleigh-corrected reflectance (R_{rc}), and the R_{rc} were used in the calculation of CI and FAI. R_{rc} (dimensionless) is a quasi-surface reflectance that provides correction for Rayleigh reflectance, various gaseous transmittances, glint and white-caps. The Ocean Biology Processing Group (OBPG) generates the Level-2 SST products by MODIS bands 31 and 32 in thermal-infrared using the Multi-Sensor Level-1 to Level-2 software (msl12). NASA's Ocean Color Group generates standard Chl-*a* concentration produced using MODIS imagery based on the OC3M algorithm. The FLH approach was used to detect areas affected by harmful algal boom based on MODIS bands:

band 13 (667 nm), 14 (678 nm) and 15 (748 nm). The maximum chlorophyll fluorescence is measured at band 14. Bands 13 and 15 are used for back-scattering correction (Hu et al., 2005).

2.4. Methodology

The satellite images of seven consecutive days (14th to 20th August 2005 and 3rd to 9th August 2010) were prepared and FAI, CI, FLH, Chl-*a*, and SST products were calculated on a daily basis, so that any correlation between the CI (as an indicator of CB) and other products were revealed. As shown in Figs. 3 and 4, three regions (A, B, and C) were considered for analyzing the correlation among the studied parameters, each of these regions includes 360 pixels (12×30 pixels). In order to reduce the possible errors, the mean values of 360 pixels were calculated for each of the parameters (FAI, CI, FLH, Chl-*a*, and SST). The mean value was considered as its daily value of the parameter. For simplifying the process of determining the trend of daily variations in the parameters, the mean value was used, but the analyses were performed based on more than 2500 data ($12^{\text{pixels}} \times 30^{\text{pixels}} \times 7^{\text{day}} = 2520$) in each region. According to field reports, the status of CB is clear in three regions (A, B and C). The mean values of the pixels of three regions (A, B and C) for each product (including FAI, CI, FLH, Chl-*a*, and SST) were calculated on a daily basis to investigate the time-series data. In order to make possible a comparison between all the parameters, the values have been standardized based on the average and standard deviation (Eq. (1)):

$$Z = \frac{(X - \mu)}{\sigma}, \quad (1)$$

where Z is the standardized value, X is the parameters value, μ is the arithmetic mean of the distribution, and σ is the standard deviation of the distribution.

In the study area, there are various species of cyanobacteria and phytoplankton that have some similarities in the structure and spectral reflectance. These similarities may cause some uncertainties in the results of each of the CI, Chl-*a* or FLH indices. Then, simultaneous application of these indices as a combined model and assessment of the obtained results using field data will reduce the uncertainties and increase the accuracy and certainty of the final results. For this purpose, a binary vector (01) corresponding to the datasets of 16 and 19 August 2005 was defined, which reported that CB was equal to 1 and the remaining days were considered to be zero. Therefore, the relationship between this vector and the parameters influenced by CB was defined as a linear model and its coefficients were calculated. In this algorithm, values less than zero indicate a non-occurrence of the CB phenomenon and values between zero and 0.5 indicate the CB phenomenon in a low concentration and values equal to or greater than 0.5 indicate the occurrence of CB. Values greater than one indicate high concentration of CB and the saturation of the MODIS sensor bands, replaced by one in this algorithm (Fig. 2).

All of the implementations of this research were performed in the SeaDAS 6.4 software and the final maps were produced using ArcGIS 10.2.2 software. The proposed index in the current research has been developed based on two CBs

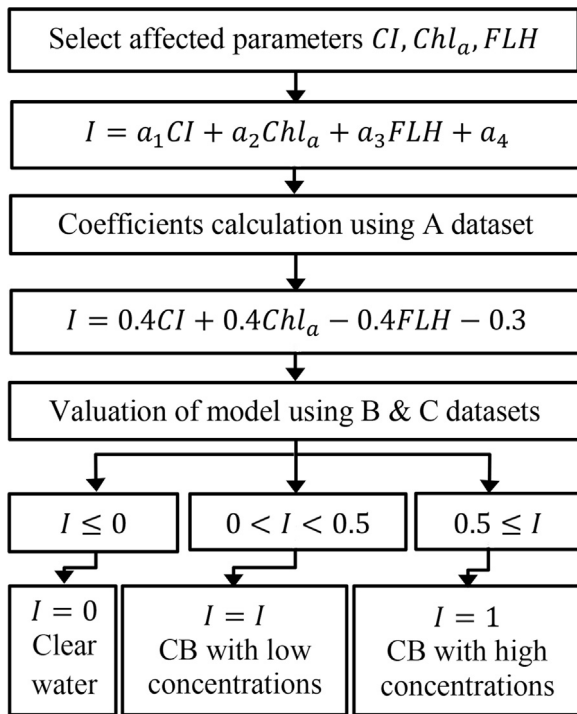


Figure 2 CB detection algorithm based on impact on MODIS-L2 products.

in years 2005 and 2010 and in three regions of A, B, C. The proposed index has been defined based on the data of two regions of A and B and evaluated by CB of 2010. It is noteworthy that CB occurs every few years and it has occurred in years 2005, 2007, 2009, and 2010 over the past decade. The current paper has been presented based on the data of 2005 and 2010, since due to the cloudiness of some days in the years 2007 and 2009, it was impossible to provide at least 7-day time series of the images simultaneous with CB occurrence.

2.4.1. MODIS floating algae index (FAI)

We selected the FAI for detecting CBs from the MODIS images. Floating algae on the water surface have higher reflectance in the NIR than in other wavelengths; hence can be distinguished from surrounding waters (Hu, 2009). The FAI was developed by Hu (2009) for MODIS images, and it is less sensitive to changes in observational conditions such as solar/viewing geometry, and sun glint and environmental parameters than the other indexes such as NDVI or EVI (Hu, 2009). It was calculated using the following equation:

$$FAI = R_{rc,859} - R_{rc,645} + (R_{rc,1240} - R_{rc,645}) \times \left(\frac{859 - 645}{1240 - 645} \right), \quad (2)$$

where R_{rc} is the corrected reflectance, and the number in the equation are the numeric values of the center wavelength of the MODIS band ($\lambda_{RED} = 645$ nm, $\lambda_{NIR} = 859$ nm, $\lambda_{SWIR} = 1240$ nm).

2.4.2. Cyanobacteria index (CI)

The CI uses the spectral curvature to detect cyanobacteria, so that a stronger curvature indicates higher concentrations of cyanobacteria (Wynne et al., 2008). The CI is defined as:

$$CI_{MODIS} = - \left[\rho_s(678) - \rho_s(667) - \{ \rho_s(748) - \rho_s(667) \} \left(\frac{678 - 667}{748 - 667} \right) \right]. \quad (3)$$

ρ_s is the irradiance reflectance (reflectance (in sr^{-1}) multiplied by π sr). Therefore, CI_{MODIS} is dimensionless. The numbers in the equations are numeric values of the utilized wavelengths in nanometers.

2.4.3. Wind stress

Wind speed hourly data were downloaded from the European Center for Medium range Weather Forecasting (ECMWF) website (<http://www.ecmwf.int/>), and daily wind stress were calculated on a daily basis. Wind stress (τ) was calculated using (Wynne et al., 2010):

$$\tau = \rho C_d (u^2 + v^2), \quad (4)$$

where ρ is the density of air, estimated to be 1.223 kg m^{-3} , u is the 10 m U wind component, v is the 10 m V wind component and C_d is the surface drag coefficient determined by:

$$C_d = 0.001 \times (0.69 + 0.081 \times \sqrt{u^2 + v^2}). \quad (5)$$

3. Results and discussion

Regions A and B were determined in different locations across images taken in 2005 and the region C was located on images taken in 2010. Considering the field reports, the status of cyanobacteria bloom is clear in three regions (A, B and C). In region A, CBs occurred on 16th and 19th of August 2005 and in region C CBs occurred on 5th and 7th of August 2010. In a calm weather condition, the cyanobacteria blooms lose their buoyancy and create surface scum. Strong wind may also mix the scum in the water column. Region A was defined within the realm of CB. Region B was defined outside the realm of CB, but close to the region A, to take into consideration the same environmental and climatic conditions and so that their only major difference would be the CB occurrence (Fig. 3). Likewise, the region C was defined within the realm of CB (Fig. 4).

Figs. 4 and 3 display the spatial distribution of Chl-*a* in the southern Caspian Sea over the period of 14th August 2005 to 20th August 2005 as well as 3rd August 2010 to August 2010. As it can be seen in Fig. 4, regions A and C are under the influence of CB throughout the study time period. However, fluctuations of the environmental factors, such as intensity of blooms, are not similar in various days and areas. For example, the intensity and extent of the bloom peaks on 16th and 19th August 2005, to the extent that saturation can be observed in some areas of the sensing bands (white spots around area A) (Moradi, 2014). On the other hand, in region B, no bloom is observed in different days. Of course, care must be taken that the chlorophylls observed in these images are not necessarily associated with various species of cyanobacteria and some of them might be associated with other species of phytoplankton. Therefore, observation of chlorophyll concentrations in the satellite images is not a sufficient evidence for proving CB and other PC-sensitive indexes, that are specific characteristics of various species of cyanobacteria, must also be investigated.

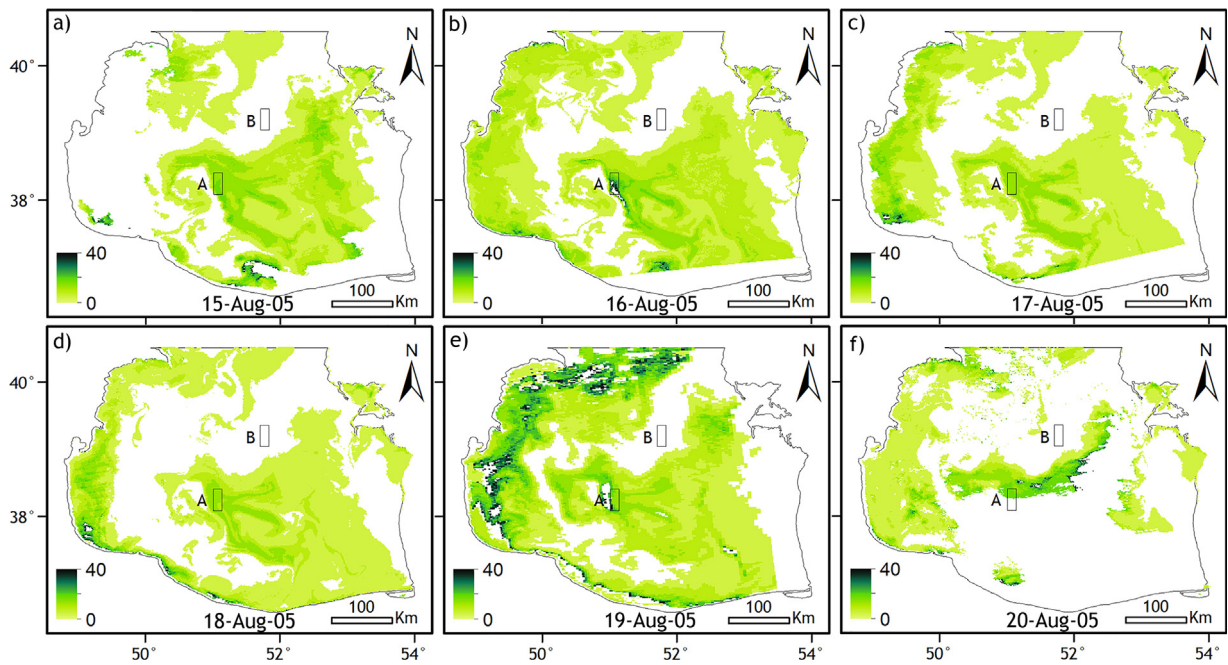


Figure 3 The Chl-*a* maps for study area (15th to 20th August 2005).

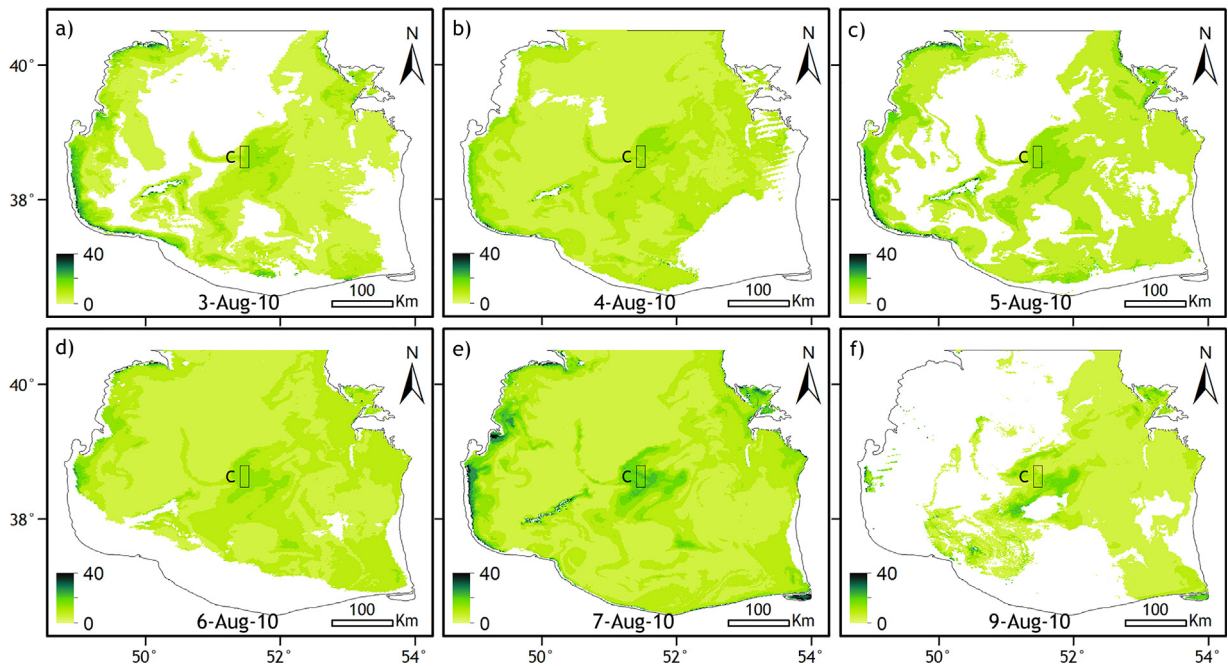


Figure 4 The Chl-*a* maps for study area (and 3rd to 9th August 2010).

Fig. 5 shows the variations of CI, FAI, FLH, Chl-*a*, and SST products for three regions (A, B and C). Fig. 6 shows the correlation between components of Fig. 3.

Fig. 5a shows the variations of CI, FAI, FLH, Chl-*a*, and SST products for region A. Fig. 6 (squares) shows the correlation between components of Fig. 5a. Therein Fig. 6, the positive

correlation between CI and Chl-*a* ($R = 0.74$, $p \leq 0.05$) is clear, and indicated that all indices had some Chl-*a* as photosynthetic pigment and that their accumulation in CB occurrence made them more visible on satellite images (Simis et al., 2005). Although the cell contents of cyanobacteria were different in diverse environmental and biological conditions,

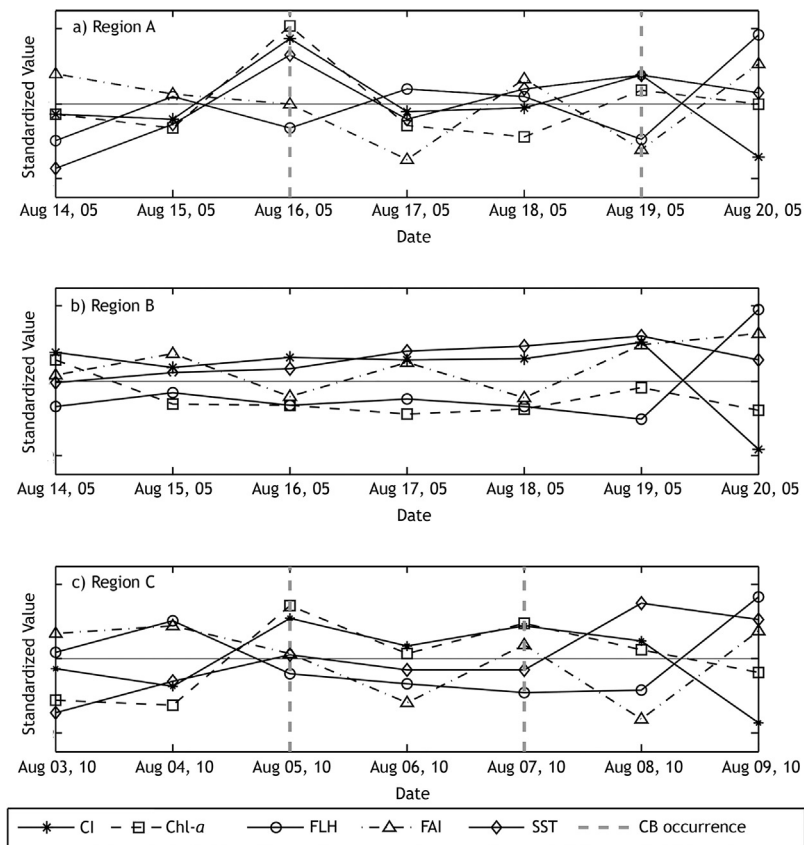


Figure 5 The CI, FAI, FLH, Chl-*a*, SST standardize value for region A, B, and C, from top to bottom, respectively.

increasing the value of these indices could be a clue to detect CB on satellite images. Correlation between CI and FAI in region A is low ($R = -0.42$, $p = 0.34$), indicating that the FAI index has been inefficient in the Caspian Sea. As noted above, FAI has been defined for Open Ocean and it is not suitable for enclosed lakes such as Caspian Sea (Hu, 2009). Fig. 6 (squares) shows that there is a negative correlation between the CI and FLH ($R = -0.74$, $p \leq 0.05$).

Temporal changes of CI, FAI, FLH, Chl-*a* and SST products were also investigated from 3rd to 9th of August 2010 for region C. The results have been shown in Figs. 5c and 6 (circles). The results show that region C is similar to region A, which confirms the relationship between the changes in these indicators and the incidence of CB phenomenon. Fig. 5b together with R and p values in Fig. 6 (triangles) shows that there is no significant relationship between changes in CI, FAI, and Chl-*a* in region B and confirms that the observed changes in three indicators of CI, FAI, and Chl-*a* for region A are after the occurrence of CB phenomenon. The weak correlation between CI and Chl-*a* in region B suggests that the low Chl-*a* value in this region is related to other phytoplankton species and it is not due to cyanobacterial growth. On the other hand, high correlation coefficient between CI and Chl-*a* in the A and C regions suggests that Chl-*a* index is affected by cyanobacteria and confirms that cyanobacteria have the greatest share in the Chl-*a* identified in these regions. As it was shown in the results, there was high inverse correlation between CI and FLH in the regions A, B, and C, but the correlation value between FLH and CI in the region B is not at 95% confidence level, so it is not

acceptable. Further analysis showed that considering FLH is not sufficient to detect the CBs in the offshore area, because it has been defined for coastal water based on MODIS imagery and it is not suitable for offshore water (Hu et al., 2005). The FLH performance may be affected by atmospheric scattering/absorption, sun radiations, and the physiological properties of algal species (Letelier and Abbott, 1996). However, FLH is affected by CB phenomenon well and then it has been used in the proposed index.

Fig. 7 shows that rapid expansion and intensification of the bloom occurred during a period with $SST \geq 30^\circ\text{C}$. It is important to mention that the mean SST of the southern Caspian Sea in August 2002–2013 was 25.5°C . El Hourany et al. (2017) stated that the SST is inversely correlated to Chl-*a*, but the results of this study did not show this correlation. Such result can be related to several reasons such as the optimum temperature of the blooming phytoplankton species and water stratification (Xing et al., 2014).

SST spatial variations in Fig. 7 can be due to water depth and local variations in atmospheric conditions. As water depth is high in the southern Caspian Sea, the effect of depth will not be significant, and atmospheric conditions have the greatest effect in SST spatial variations, which its reason is surface wind. As shown in Fig. 8, the wind stress value in the studied area was not the same in various days. Spatial variations in wind intensity value have caused spatial variations in SST. In other words, wind intensity reduced the SST value in areas where the surface wind intensity was high, while the SST value increased in areas where the wind

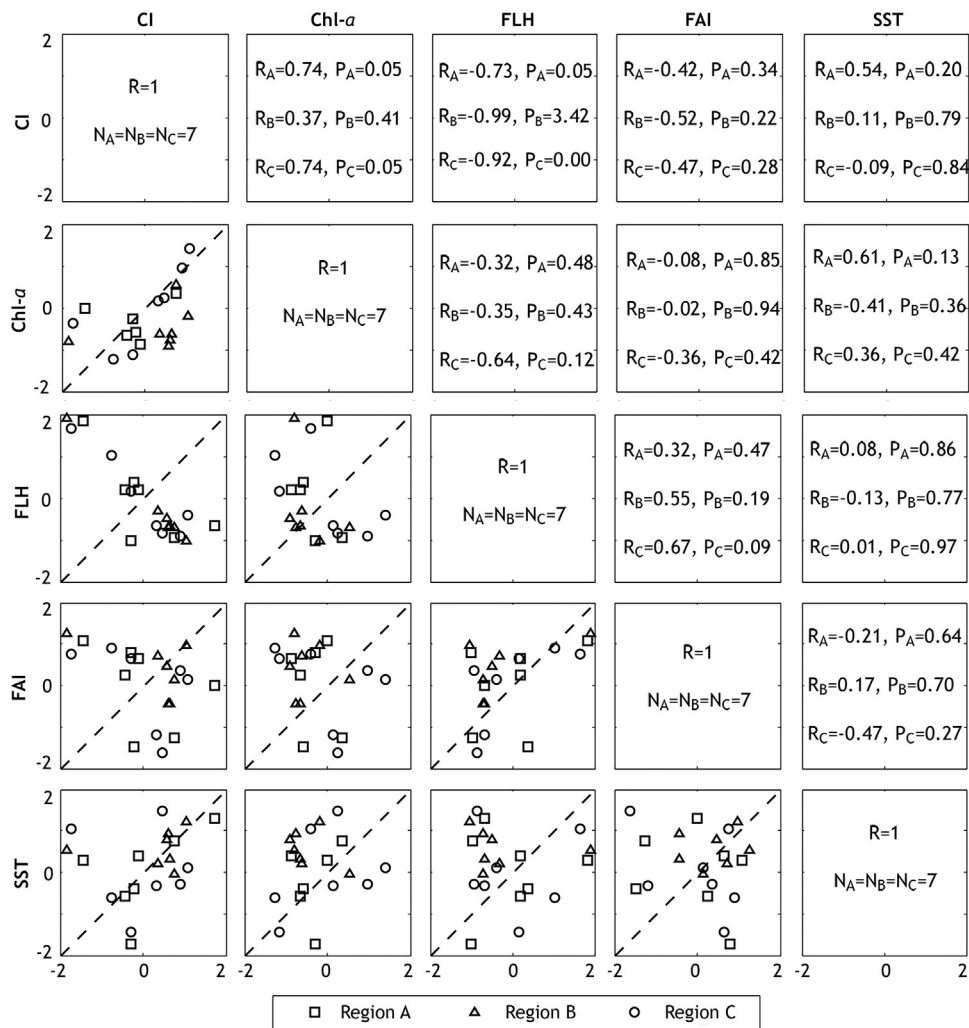


Figure 6 Correlation matrix for region A, B, and C. Biplots are shown under the diagonal and correlation coefficients are shown over the diagonal (Black: region A, Blue; region B, and Red: region C).

intensity was less. The results show that in the absence of surface wind and appropriate temperature condition, a sudden increase in the daily values of CI and Chl- α in the southern Caspian Sea could be an index for the incidence of the CB phenomenon (Webster, 1990).

Fig. 8 shows that the decreases in bloom area and intensity occurred after a daily increase in wind stress. Generally, in shallow waters, the increase in the wind speed to an excess of 4 m s^{-1} was sufficient to cause buoyant cyanobacteria to be submerged below the surface (George and Edwards, 1976). It must be noted that the strong wind stress ($>4 \text{ m s}^{-1}$) required mixing the CB through the water column because of the depth $<100 \text{ m}$ in the southern Caspian Sea, since generally, deeper water will be more stratified and require a greater stress for mixing (Wynne et al., 2010).

In the previous sections, the correlation between CB phenomenon and MODIS-L2 products was investigated and the results showed that there was a significant correlation between the occurrence of the CB phenomenon and the changes in CI, FLH, and Chl- α products, while there was no correlation between FAI, SST and this phenomenon. In order

to evaluate the proposed model, its function has been tested on the B and C region datasets. The results of the model's evaluation detected CB in C region on 5th and 7th of August 2010 and none was detected in the B region, which is consistent with field reports.

In Fig. 9, the triangles indicate the occurrence of the CB phenomenon ($I \geq 0.5$) and the squares indicate the CB phenomenon with low concentrations ($0 < I \leq 0.5$), and zero values (circles) indicate the non-occurrence of the CB phenomenon.

4. Conclusion

In this study the application of MODIS-L2 products was analyzed as a potential tool for monitoring cyanobacterial blooms (CBs). Toxic CBs are a growing environmental problem in the Caspian Sea waters and usually occur in the middle of summer. Detecting and monitoring CBs outbreaks are facing significant challenges at both local and regional scales. The effects of CBs on MODIS-L2 products: Chl- α , FLH, FAI, SST, and CI in the southern Caspian Sea have been analyzed. The

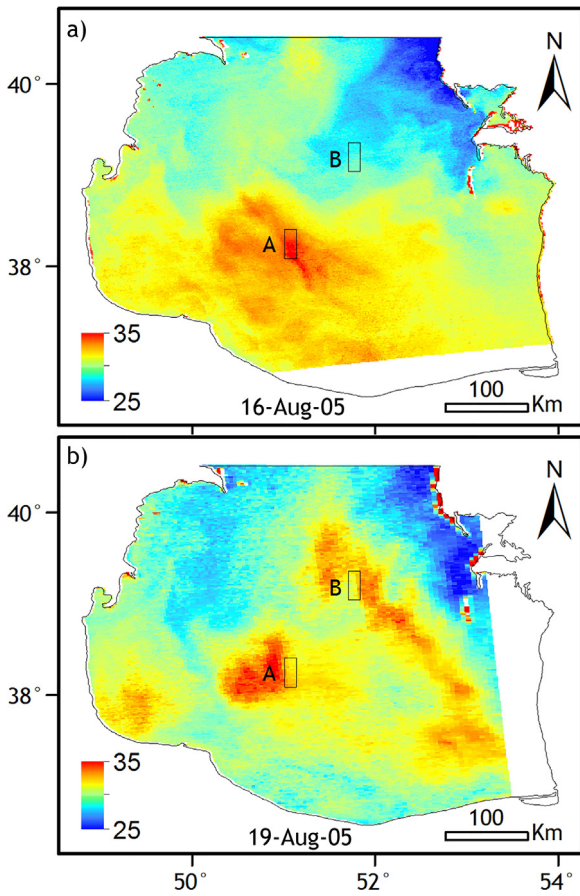


Figure 7 The SST value for 16th and 19th August 2005 simultaneous with CB occurrence.

results revealed a positive high correlation between CI and Chl-*a*, and a negative high correlation between the CI and FLH in the three studied regions. However, results showed that considering FLH is not sufficient to detect the CB in the offshore area, because the FLH performance is affected by atmospheric scattering/absorption, sun radiations, and the physiological properties of algal species. However, CB is affected by FLH well and hence it was used in the proposed index. Also, the results indicate a weak correlation between CI and FAI. In the absence of surface wind, and suitable temperature condition ($SST \geq 30^{\circ}C$), a sudden increase in the daily values of CI and Chl-*a* in the southern Caspian Sea could be operational indexes of incidence of the CB phenomenon. After examining, a linear model was run on MODIS Level-2 data products to evaluate the correlation and impact of CB phenomenon on these data sets. The output of this model shows the occurrence or absence of CB. The model was evaluated on the datasets of B and C regions. The results were consistent with the field reports of CB occurrence in the studied region. The advantage of daily access to MODIS-L2 products caused correlation and solidity, and the impact of CB phenomenon on these products to be a base for defining a linear relationship between the changes in these products and the occurrence of CB phenomenon, which can be used to monitor the CB phenomenon in studied regions. To define more complex and accurate models, more data of CB occurrence in the last decade are required, but there are limitations in this regard as a result of the frequent cloudy conditions of the Caspian Sea and lack of field data that is simultaneous with the occurrence of CB phenomenon. The models and results obtained in the current research can be used for level 2 products obtained from other Ocean Color satellites, such as MERIS and Sentinel 3.

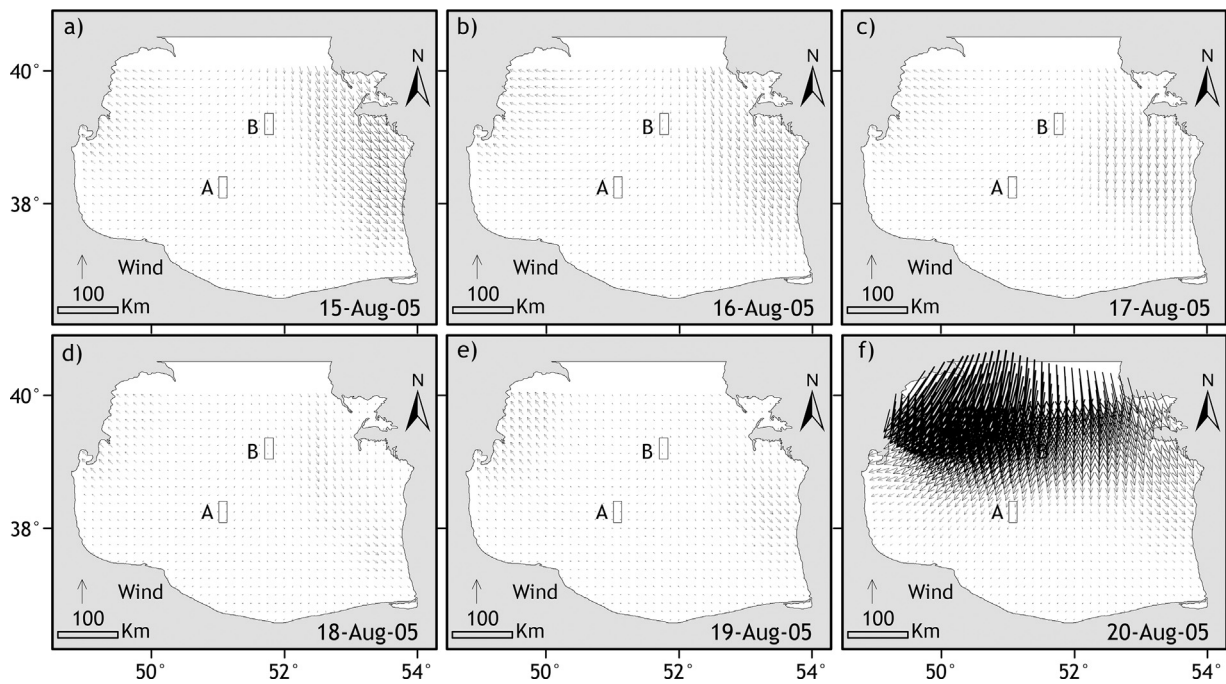


Figure 8 Wind stress vector (15th to 20th August 2005).

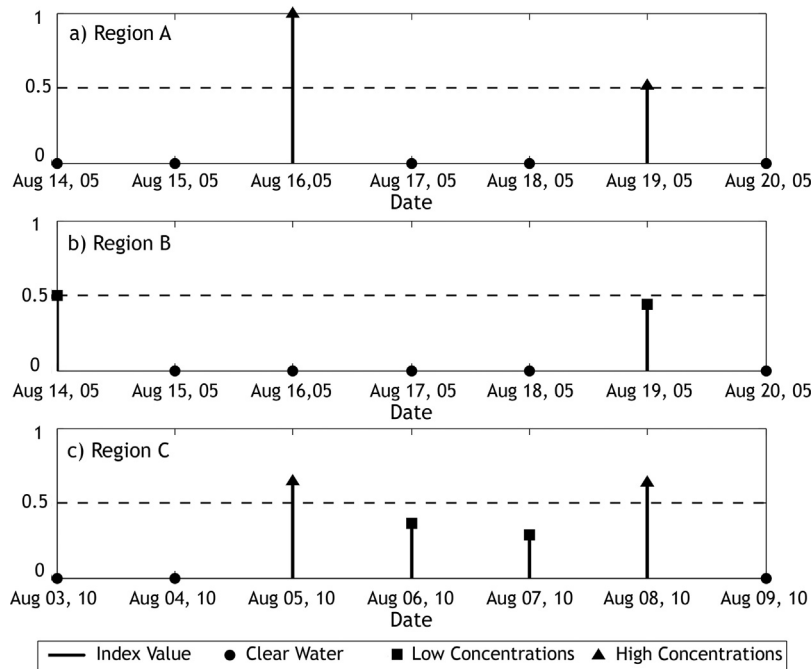


Figure 9 The evaluation of the proposed algorithm.

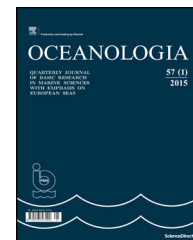
Acknowledgements

We express our gratitude to NASA Goddard Space Flight Center for providing MODIS data and SeaDAS software package and also, we deeply appreciate IFRO for providing us with data of field measurements. We would also like to acknowledge the reviewers of the manuscript for their good comments which have helped to improve the quality of this manuscript.

References

- Codd, G.A., Morrison, L.F., Metcalf, J.S., 2005. Cyanobacterial toxins: risk management for health protection. *Toxicol. Appl. Pharmacol.* 203 (3), 264–272, <http://dx.doi.org/10.1016/j.taap.2004.02.016>.
- Dekker, A.G., 1993. *Detection of optical water quality parameters for eutrophic waters by high resolution remote sensing*. (Ph.D. thesis). Vrije University, The Netherlands, Amsterdam.
- El Hourany, R., Fadel, A., Gemayel, E., Abboud-Abi Saab, M., Faour, G., 2017. Spatio-temporal variability of the phytoplankton biomass in the Levantine basin between 2002 and 2015 using MODIS products. *Oceanologia* 59 (2), 153–165, <http://dx.doi.org/10.1016/j.oceano.2016.12.002>.
- Ficek, D., Kaczmarek, S., Ston-Egiert, J., Wozniak, B., Majchrowski, R., Dera, J., 2004. Spectra of light absorption by phytoplankton pigments in the Baltic; conclusions to be drawn from a Gaussian analysis of empirical data. *Oceanologia* 46 (4), 533–555.
- FU, G., 1998. SeaDAS: the SeaWiFS data analysis system. In: *Proc PORSEC98 Qingdao China*. 73–79.
- George, D.G., Edwards, R.W., 1976. The effect of wind on the distribution of chlorophyll *a* and crustacean plankton in a shallow eutrophic reservoir. *J. Appl. Ecol.* 13 (3), 667–690, <http://dx.doi.org/10.2307/2402246>.
- Ghafouri, M., 2008. The caspian sea: rivalry and cooperation. *Middle East Policy* 15 (2), 81–96, <http://dx.doi.org/10.1111/j.1475-4967.2008.00351.x>.
- Gower, J., King, S., Borstad, G., Brown, L., 2005. Detection of intense plankton blooms using the 709 nm band of the MERIS imaging spectrometer. *Int. J. Remote Sens.* 26 (9), 2005–2012, <http://dx.doi.org/10.1080/01431160500075857>.
- Han, X., Cong, P., Qin, Y., Zhu, X., 2008. Retrieval of cyanobacteria in Taihu based on MODIS data. *Int. Soc. Opt. Photonics 71230Y*, <http://dx.doi.org/10.1117/12.816195>.
- Hu, C., 2009. A novel ocean color index to detect floating algae in the global oceans. *Remote Sens. Environ.* 113 (10), 2118–2129, <http://dx.doi.org/10.1016/j.rse.2009.05.012>.
- Hu, C., Feng, L., 2016. Modified MODIS fluorescence line height data product to improve image interpretation for red tide monitoring in the eastern Gulf of Mexico. *J. Appl. Remote Sens.* 11, 012003, <http://dx.doi.org/10.1117/1.JRS.11.012003>.
- Hu, C., Muller-Karger, F.E., Taylor, C. (Judd), Carder, K.L., Kelble, C., Johns, E., Heil, C.A., 2005. Red tide detection and tracing using MODIS fluorescence data: a regional example in SW Florida coastal waters. *Remote Sens. Environ.* 97 (3), 311–321, <http://dx.doi.org/10.1016/j.rse.2005.05.013>.
- Jafar-Sidik, M., Gohin, F., Bowers, D., Howarth, J., Hull, T., 2017. The relationship between Suspended Particulate Matter and Turbidity at a mooring station in a coastal environment: consequences for satellite-derived products. *Oceanologia* 59 (3), 365–378, <http://dx.doi.org/10.1016/j.oceano.2017.04.003>.
- Kahru, M., Leppänen, J.M., Rud, O., Savchuk, O.P., 2000. Cyanobacteria blooms in the Gulf of Finland triggered by saltwater inflow into the Baltic Sea. *Mar. Ecol. Prog. Ser.* 207, 13–18.
- Kahru, M., Savchuk, O.P., Elmgren, R., 2007. Satellite measurements of cyanobacterial bloom frequency in the Baltic Sea: interannual and spatial variability. *Mar. Ecol. Prog. Ser.* 343, 15–23, <http://dx.doi.org/10.3354/meps06943>.
- Kostianoy, A.G., Kosarev, A.N., 2005. *The Caspian Sea Environment*. Springer Science & Business Media, Berlin Heidelberg, p. 272 pp.
- Kutser, T., 2004. Quantitative detection of chlorophyll in cyanobacterial blooms by satellite remote sensing. *Limnol. Oceanogr.* 49, 2179–2189.
- Kutser, T., 2009. Passive optical remote sensing of cyanobacteria and other intense phytoplankton blooms in coastal and inland

- waters. *Int. J. Remote Sens.* 30 (17), 4401–4425, <http://dx.doi.org/10.1080/01431160802562305>.
- Letelier, R.M., Abbott, M.R., 1996. An analysis of chlorophyll fluorescence algorithms for the moderate resolution imaging spectrometer (MODIS). *Remote Sens. Environ.* 58 (2), 215–223, [http://dx.doi.org/10.1016/S0034-4257\(96\)00073-9](http://dx.doi.org/10.1016/S0034-4257(96)00073-9).
- Levy, R.C., Remer, L.A., Martins, J.V., Kaufman, Y.J., Plana-Fattori, A., Redemann, J., Wenny, B., 2005. Evaluation of the MODIS aerosol retrievals over ocean and land during CLAMS. *J. Atmos. Sci.* 62, 974–992, <http://dx.doi.org/10.1175/JAS3391.1>.
- Loeb, N.G., Kato, S., 2002. Top-of-atmosphere direct radiative effect of aerosols over the tropical oceans from the clouds and the earth's radiant energy system (CERES) satellite instrument. *J. Clim.* 15, 1474–1484, [http://dx.doi.org/10.1175/1520-0442\(2002\)015<1474:TOADRE>2.0.CO;2](http://dx.doi.org/10.1175/1520-0442(2002)015<1474:TOADRE>2.0.CO;2).
- Matarrese, R., Chiaradia, M.T., Pasquale, V.D., Pasquariello, G., 2004. Chlorophyll-*a* concentration measure in coastal waters using MERIS and MODIS data. In: *IGARSS 2004. 2004 IEEE International Geoscience and Remote Sensing Symposium*. Presented at the IGARSS 2004. 2004 IEEE International Geoscience and Remote Sensing Symposium, vol. 6. 3639–3641, <http://dx.doi.org/10.1109/IGARSS.2004.1369907>.
- Moradi, M., 2014. Comparison of MODIS and MERIS data in detecting cyanobacterial bloom events in the Southern Caspian Sea. *IJRS*, <http://dx.doi.org/10.1016/j.marpolbul.2014.06.053>.
- Nasrollahzadeh, H.S., Din, Z.B., Foong, S.Y., Makhloogh, A., 2008. Spatial and temporal distribution of macronutrients and phytoplankton before and after the invasion of the ctenophore, *Mnemiopsis leidyi*, in the Southern Caspian Sea. *Chem. Ecol.* 24 (4), 233–246, <http://dx.doi.org/10.1080/02757540802310967>.
- Nasrollahzadeh, H.S., Makhloogh, A., Pourgholam, R., Vahedi, F., Qanqermeh, A., Foong, S.Y., 2011. The study of nodularia spumigena bloom event in the southern Caspian Sea. *Appl. Ecol. Environ. Res.* 9, 141–155.
- Oyama, Y., Matsushita, B., Fukushima, T., 2016. Cyanobacterial blooms as an indicator of environmental degradation in waters and their monitoring using satellite remote sensing. In: Nakano, S., Yahara, T., Nakashizuka, T. (Eds.), *Aquatic Biodiversity Conservation and Ecosystem Services, Ecological Research Monographs*. Springer, Singapore, 1–85.
- Paerl, H.W., 1988. Nuisance phytoplankton blooms in coastal, estuarine, and inland waters. *Limnol. Oceanogr.* 33, 823–843.
- Peeters, F., Kipfer, R., Achermann, D., Hofer, M., Aeschbach-Hertig, W., Beyerle, U., Imboden, D.M., Rozanski, K., Fröhlich, K., 2000. Analysis of deep-water exchange in the Caspian Sea based on environmental tracers. *Deep Sea Res. Part Oceanogr. Res. Pap.* 47 (4), 621–654, [http://dx.doi.org/10.1016/S0967-0637\(99\)00066-7](http://dx.doi.org/10.1016/S0967-0637(99)00066-7).
- Potes, M., Costa, M.J., Silva, J.C.B., da Silva, A.M., Morais, M., 2011. Remote sensing of water quality parameters over Alqueva Reservoir in the south of Portugal. *Int. J. Remote Sens.* 32 (12), 3373–3388, <http://dx.doi.org/10.1080/01431161003747513>.
- Riha, S., Krawczyk, H., 2011. Development of a remote sensing algorithm for cyanobacterial phycocyanin pigment in the Baltic Sea using neural network approach. In: *Proc. SPIE 8175*. Presented at the Remote Sensing of the Ocean, Sea Ice, Coastal Waters, and Large Water Regions 2011, 817504, 7 pp., <http://dx.doi.org/10.1117/12.898081>.
- Robertson, A.L., 2009. Using band ratio, semi-empirical, curve fitting, and partial least squares (PLS) models to estimate cyanobacterial pigment concentration from hyperspectral reflectance. (MSc Thesis). Indiana University, Indianapolis.
- Roohi, A., Kideys, A.E., Sajjadi, A., Hashemian, A., Pourgholam, R., Fazli, H., Khanari, A.G., Eker-Develi, E., 2009. Changes in biodiversity of phytoplankton, zooplankton, fishes and macrobenthos in the Southern Caspian Sea after the invasion of the ctenophore *Mnemiopsis leidyi*. *Biol. Invas.* 12 (17), 2343–2361, <http://dx.doi.org/10.1007/s10530-009-9648-4>.
- Ruiz-Verdú, A., Simis, S.G., de Hoyos, C., Gons, H.J., Peña-Martínez, R., 2008. An evaluation of algorithms for the remote sensing of cyanobacterial biomass. *Remote Sens. Environ.* 112 (11), 3996–4008, <http://dx.doi.org/10.1016/j.rse.2007.11.019>.
- Sayers, M., Fahnenstiel, G.L., Shuchman, R.A., Whitley, M., 2016. Cyanobacteria blooms in three eutrophic basins of the Great Lakes: a comparative analysis using satellite remote sensing. *Int. J. Remote Sens.* 37 (17), 4148–4171, <http://dx.doi.org/10.1080/01431161.2016.1207265>.
- Simis, S.G., Peters, S.W., Gons, H.J., 2005. Remote sensing of the cyanobacterial pigment phycocyanin in turbid inland water. *Limnol. Oceanogr.* 50, 237–245.
- Stramska, M., Bialogrodzka, J., 2016. Satellite observations of seasonal and regional variability of particulate organic carbon concentration in the Barents Sea. *Oceanologia* 58 (4), 249–263, <http://dx.doi.org/10.1016/j.oceano.2016.04.004>.
- Tahami, F.S., 2013. Study on cyanobacteria in different years and seasons in southern Caspian Sea. *J. Nov. Appl. Sci.* 2, 1102–1109.
- Thieuleux, F., Moulin, C., Bréon, F.M., Maignan, F., Poitou, J., Tanré, D., 2005. Remote sensing of aerosols over the oceans using MSG/SEVIRI imagery. *Ann. Geophys.* 23, 3561–3568.
- Vermote, E.F., Tanré, D., Deuze, J.L., Herman, M., Morcrette, J.-J., 1997. Second simulation of the satellite signal in the solar spectrum, 6S: an overview. *IEEE Trans. Geosci. Remote Sens.* 35, 675–686.
- Vincent, R.K., Qin, X., McKay, R.M.L., Miner, J., Czajkowski, K., Savino, J., Bridgeman, T., 2004. Phycocyanin detection from LANDSAT TM data for mapping cyanobacterial blooms in Lake Erie. *Remote Sens. Environ.* 89, 381–392, <http://dx.doi.org/10.1016/j.rse.2003.10.014>.
- Wang, M., Shi, W., 2006. Cloud masking for ocean color data processing in the coastal regions. *IEEE Trans. Geosci. Remote Sens.* 44 (11), 3105–3196, <http://dx.doi.org/10.1109/TGRS.2006.876293>.
- Webster, I.T., 1990. Effect of wind on the distribution of phytoplankton cells in lakes. *Limnol. Oceanogr.* 35 (5), 989–1001, <http://dx.doi.org/10.4319/lo.1990.35.5.0989>.
- Wynne, T.T., Stumpf, R.P., Tomlinson, M.C., Warner, R.A., Tester, P. A., Dyble, J., Fahnenstiel, G.L., 2008. Relating spectral shape to cyanobacterial blooms in the Laurentian Great Lakes. *Int. J. Remote Sens.* 29 (12), 3665–3672, <http://dx.doi.org/10.1080/01431160802007640>.
- Wynne, T.T., Stumpf, R.P., Tomlinson, M.C., Dyble, J., 2010. Characterizing a cyanobacterial bloom in western Lake Erie using satellite imagery and meteorological data. *Limnol. Oceanogr.* 55 (5), 2025–2036, <http://dx.doi.org/10.4319/lo.2010.55.5.2025>.
- Wynne, T.T., Stumpf, R.P., Briggs, T.O., 2013. Comparing MODIS and MERIS spectral shapes for cyanobacterial bloom detection. *Int. J. Remote Sens.* 34, 6668–6678, <http://dx.doi.org/10.1080/01431161.2013.804228>.
- Xing, X., Claustre, H., Wang, H., Poteau, A., D'Ortenzio, F., 2014. Seasonal dynamics in colored dissolved organic matter in the Mediterranean Sea: Patterns and drivers. *Deep Sea Res. I* 83, 93–101, <http://dx.doi.org/10.1016/j.dsr.2013.09.008>.



ORIGINAL RESEARCH ARTICLE

Impact of climate change on the Curonian Lagoon water balance components, salinity and water temperature in the 21st century

Darius Jakimavičius*, Jūratė Kriaučiūnienė, Diana Šarauskienė

Laboratory of Hydrology, Lithuanian Energy Institute, Kaunas, Lithuania

Received 6 July 2017; accepted 14 February 2018

Available online 1 March 2018

KEYWORDS

Curonian Lagoon;
RCP scenarios;
HBV modelling software;
Water salinity;
Water temperature

Summary The Curonian Lagoon is a shallow water body connected to the Baltic Sea by a narrow navigable strait, which enables an exchange of water of different salinity. The projected climate change together with the peculiarities of mixing water will undoubtedly alter hydrological regime of this lagoon. The study uses three climate model outputs under four RCP scenarios, four sea level rise scenarios and hydrological modelling in order to project the extent to which water balance components, salinity and temperature may change in the future. In order to simulate river inflow, the Nemunas River hydrological model was created using HBV software. In general, the changes of the lagoon water balance components, salinity and temperature are expected to be more significant in 2081–2100 than in 2016–2035. It was estimated that in the reference period (1986–2005) the river inflow was 22.1 km³, inflow from the sea was 6.8 km³, salinity (at Juodkrantė) was 1.2 ppt and average water temperature of the lagoon was 9.2°C. It was projected that in 2081–2100 the river inflow may change from 22.1 km³ (RCP2.6) to 15.9 km³ (RCP8.5), whereas inflow from the sea is expected to vary from 8.5 km³ (RCP2.6) to 11.0 km³ (RCP8.5). The lagoon salinity at Juodkrantė is likely to grow from 1.4 ppt (RCP2.6) to 2.6 ppt (RCP8.5) by the end of the century due to global sea level rise and river inflow decrease. The lagoon water temperature is projected to increase by 2–6°C by the year 2100.

© 2018 Institute of Oceanology of the Polish Academy of Sciences. Production and hosting by Elsevier Sp. z o.o. This is an open access article under the CC BY-NC-ND license (<http://creativecommons.org/licenses/by-nc-nd/4.0/>).

* Corresponding author at: Laboratory of Hydrology, Lithuanian Energy Institute, Breslaujos st. 3, LT444003 Kaunas, Lithuania. Tel.: +370 8 37 401801; fax: +370 37 351271.

E-mail address: darius.jakimavicius@lei.lt (D. Jakimavičius).

Peer review under the responsibility of Institute of Oceanology of the Polish Academy of Sciences.



Production and hosting by Elsevier

<https://doi.org/10.1016/j.oceano.2018.02.003>

0078-3234/© 2018 Institute of Oceanology of the Polish Academy of Sciences. Production and hosting by Elsevier Sp. z o.o. This is an open access article under the CC BY-NC-ND license (<http://creativecommons.org/licenses/by-nc-nd/4.0/>).

1. Introduction

Lagoons represent a complex and unique coastal environment which requires special attention in the context of climate change (Lillebo et al., 2015). These water bodies are especially sensitive to any environmental changes. Water temperature and sea level rise that in turn leads to an increase in water salinity are fundamental environmental descriptors that play a vital role in sustainability of lagoon ecosystems. Both of them are projected to change in the future (Anthony et al., 2009).

The rise of sea surface temperature (SST) is tightly connected with the effects of climate change. According to observation data beginning in 1880, the global ocean warms by $0.005^{\circ}\text{C year}^{-1}$ (Huang et al., 2014; Liu et al., 2014). Considerably stronger growth tendencies of SST were estimated in 1986–2005: $0.02^{\circ}\text{C year}^{-1}$ (Huang et al., 2015a). SST in European seas is increasing more rapidly than in the global oceans. The rate of increase is higher in the northern European seas and lower in the Mediterranean Sea (Coppini et al., 2007). The results obtained by Stramska and Białogrodzka (2015) also revealed that this process takes place slightly faster in inner and relatively close seas, e.g. according to the data of 1982–2013, SST increased from 0.03 to $0.06^{\circ}\text{C year}^{-1}$ in the Baltic Sea (depending on location). In the 21st century, the generally expected warming of the annual Mediterranean SST ranges from 0.45°C in the RCP2.6 scenario, through 1.15°C in the RCP4.5 scenario and 1.42°C in the RCP6.0 scenario, to 2.56°C in the RCP8.5 scenario (Shaltout and Omstedt, 2014). The rises of global surface temperature by the year 2100 projected by the IPCC should range from about 1.3°C for RCP 2.6 to 4.4°C for RCP 8.5 (IPCC, 2013).

According to the data of 1880–2009, the global mean sea level rise (SLR) was 1.6 mm year^{-1} (Church and White, 2011). As reported by Navrotskaya and Chubarenko (2013), over the past 150 years, the rate of SLR in the lagoons and coastal areas of the Southeast Baltic Sea ($1.7\text{--}1.8 \text{ mm year}^{-1}$) is close to the SLR rate in the World Ocean. In the second half of the 20th century, the rate of SLR in the lagoons and marine areas became stronger: up to 3.6 mm year^{-1} in the Vistula Lagoon and in 1959–2006 in the Baltic Sea, exceeding the rate of the global ocean SLR. Similar tendencies of water level changes are identified for the Curonian Lagoon, but they depend on the length of available data series. For example, in the period of 1986–2005 (the reference period), the Curonian Lagoon water level grew $1.64 \text{ mm year}^{-1}$. If other data series are used (e.g. 1961–1990), the rate of this growth may reach 4 mm year^{-1} (Dailidienė et al., 2011; Jakimavičius and Kriauciūnienė, 2013). Projections of relative SLR indicate a statistically significant increase in mean sea level along the entire European coastline: by around 21 and 24 cm by the 2050s under RCP4.5 and RCP8.5 respectively to reach 53 and 74 cm by the end of the century (Vousdoukas et al., 2017). However, according to Grinsted et al. (2015), SLR is not uniform globally but is affected by a range of regional factors: the median 21st century relative SLR projection is 80 cm near London and Hamburg, with a relative sea level drop of 0.1 m in the Bay of Bothnia (near Oulu, Finland).

As a consequence of sea level rise, the increase of sea-water intrusion to transitional water bodies (lagoons and

estuaries) is supposed to occur (Chen et al., 2016; Liu and Liu, 2014; Vargas et al., 2017). Less fresh water might also reach such water bodies due to reduced river inflow (Dailidienė and Davulienė, 2008; Jakimavičius and Kovalenkoviene, 2010; Vargas et al., 2017). Water salinity of the Curonian Lagoon also mainly depends on fresh (inflowing from rivers) and brackish (entering from the Baltic Sea) water exchange, which is a complex process with many driving factors. Zemlys et al. (2013) developed a 3D model to reveal characteristic features of water exchange between these two water bodies and related vertical and horizontal salinity distributions. The later study (Umgiesser et al., 2016) showed that the most important physical force that influences the water renewal time in the Curonian Lagoon is the Nemunas River discharge. The investigation by Dailidienė and Davulienė (2008) proved that the mean water salinity in the Klaipėda Strait and in the northern part of the Curonian Lagoon in 1984–2005 was increasing, but whether it is going to increase in the future has not yet been assessed.

Sea surface temperature, level rise and salinity are closely related with each other and with water balance elements. All of these variables are changing and are expected to change in the future as direct or indirect consequences of global climate warming. SST and salinity have a considerable importance for marine organisms, may directly affect the state of ecosystem, limit the number of species, and are very important for juveniles' incubation period. Surveys, such as the ones conducted by Gasiūnaitė (2000), Gasiūnaitė and Razinkovas (2002), have shown that zooplankton in the northern part of the Curonian Lagoon is very sensitive to salinity variation. Effects of different salinity conditions on the abundance and community composition of some aquatic macrophytes and microorganisms in the Curonian Lagoon were assessed by Kataržytė et al. (2017). Increased summer water temperature causes ongoing eutrophication and algae blooms in the Curonian Lagoon. Harmful algal blooms in July–October result in the deterioration of water chemical parameters, death of fish in the coastal zone and pollution with toxins (Aleksandrov et al., 2015).

The Curonian Lagoon is regarded as a water body abundant with fish, temporarily or permanently inhabited by around 50 fish species. This unique and valuable lagoon ecosystem is going to experience the impact of climate change due to increased water salinity and higher water temperature. There is an increasing concern that this ecosystem may be strongly modified or destroyed in the future by the projected changes.

This study intends to use climate model outputs under RCP scenarios and hydrological modelling in order to project the extent to which water balance components, salinity and temperature of the Curonian Lagoon will change in two future periods: 2016–2035 and 2081–2100.

The expected future changes were projected according to a new set of scenarios (called the Representative Concentration Pathways (RCPs)) presented in the Intergovernmental Panel on Climate Change Fifth Assessment Report (IPCC, 2013). When climate model outputs of the new generation (Representative Concentration Pathways – RCP) scenarios are used, hydrological modelling may be applied to assess the future environmental changes that are likely to happen in case any scenario occurs.

2. Material and methods

2.1. Study area

The Curonian Lagoon is a shallow water body that is separated from the Baltic Sea by a narrow, dune-covered sand spit (the Curonian Spit) (Fig. 1). At its north end, the lagoon is connected to the Baltic Sea by the navigable Klaipėda Strait. The east coast of the lagoon is low, forested wetland, part of which forms the Nemunas River delta.

The Curonian Lagoon is a territory of high international environmental value. The Nemunas delta has a regional park status and belongs to the Ramsar Convention sites. The lagoon meets the requirements of the Bonn Convention and is one of the most valuable and important bird areas in Lithuania. In 1929, in a headland of the Nemunas delta – Ventė Cape, a famous Lithuanian ornithologist professor T. Ivanauskas opened an ornithology station, where each year about 60–80 thousand birds are ringed. The Curonian Lagoon is famous for its abundance of fish as well. The Curonian Spit is declared a national park and is included in the UNESCO World Heritage List.

The whole surface area of the lagoon is 1584 km² (Červinskas, 1972). Lithuania owns only 381.6 km² of its northern part (Žilinskas and Petrokas, 1998). The average depth of this shallow lagoon is 3.8 m. The greatest depth is in the northern part, where the Klaipėda Seaport is located and the water territory is dredged up to 16 m. The total volume of the lagoon is 6.2 km³ (Gailiušis et al., 2001). The residence time of lagoon water in the northern basin is about 77 days, while the average for the southern basin is nearly 200 days (Umgieser et al., 2016).

On average, the Nemunas discharged 22.1 km³ year⁻¹ of fresh water to the eastern part of the lagoon in the period of 1986–2005. Depending on the ratio of brackish water inflow from the Baltic Sea through the Klaipėda Strait and fresh

water coming from the Nemunas River, salinity of the entire Curonian Lagoon changes. According to the data of 1986–2005, salinity in the Curonian Lagoon is 2.5 ppt at Klaipėda, 1.2 ppt at Juodkrantė, and less than 0.1 ppt at Ventė and Nida.

2.2. Methodology and data

Water balance of the Curonian Lagoon consists of the following components: river inflow (Q_R), precipitation on the surface of the lagoon (P), evaporation from the lagoon (E), inflow from the sea (Q_{BS}) and outflow from the lagoon (Q_{CL}). The main steps for evaluation of projections of water balance components, salinity and water temperature of the Curonian Lagoon in the 21st century were (Fig. 2): 1. Adaptation of climate scenarios for Lithuanian territory according to three climate models and 4 scenarios; 2. Evaluation of projections of water balance components of the Curonian Lagoon according to climate scenarios for near (2016–2035) and far (2081–2100) future periods; 3. Evaluation of projections of water temperature and salinity in the 21st century.

The data outputs of projected precipitation and air temperature were acquired from global climate models presented in the Intergovernmental Panel on Climate Change Fifth Assessment Report (IPCC, 2013) according to a new set of RCP (Representative Concentration Pathways) scenarios (Moss et al., 2010; van Vuuren et al., 2011). Values of the daily mean air temperature T (°C) and daily amount of precipitation P (mm) in the near-future (2016–2035) and far-future (2081–2100) periods were estimated according to three climate models (GFDL-CM3, HadGEM2-ES, NorESM1-M) and four RCP scenarios (RCP2.6, RCP4.5, RCP6.0 and RCP8.5). The climate model cells are large (up to $2.5 \times 1.895^\circ$). Since Lithuanian territory falls into 5 climate model cells, P and T values derived from the climate models were recalculated for 16 meteorological stations using the quantile mapping

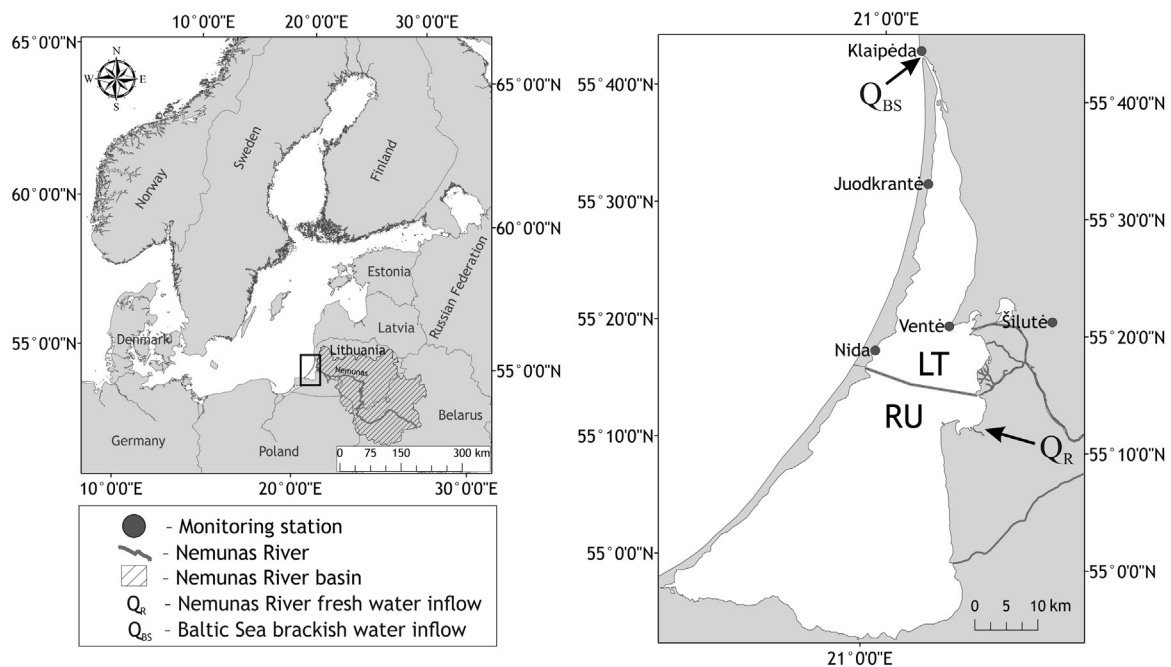


Figure 1 Location of the Curonian Lagoon and measurement stations.

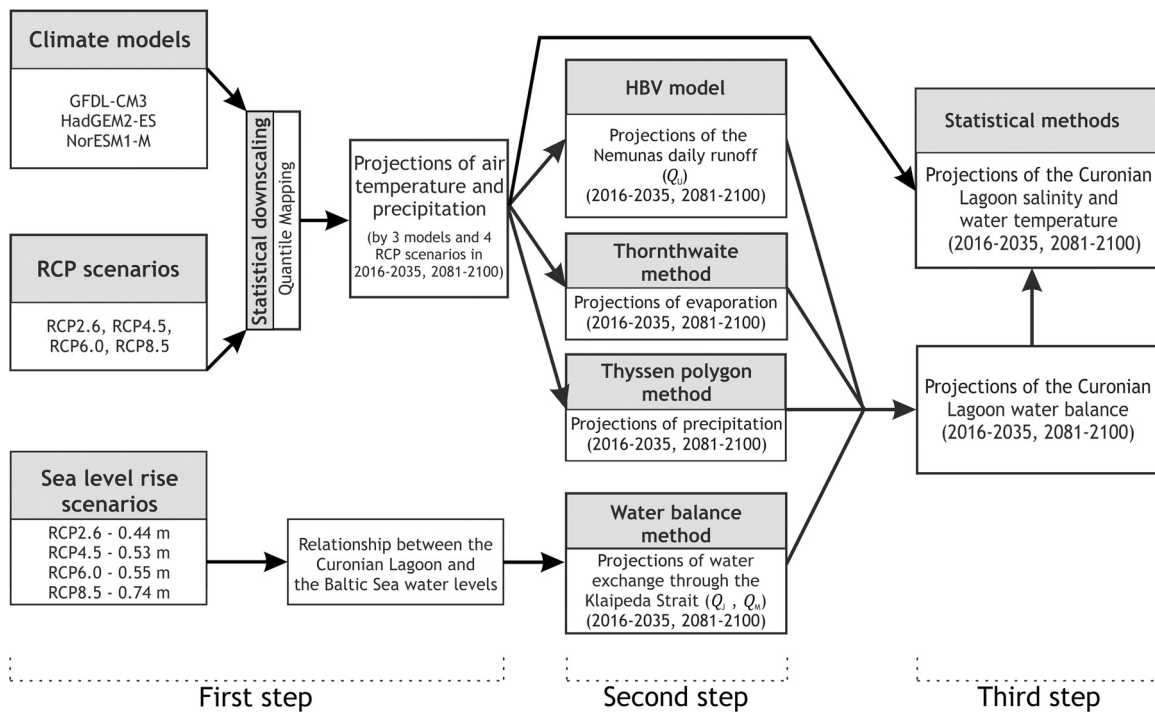


Figure 2 The principal scheme of the study.

statistical downscaling method (Teutschbein and Seibert, 2013).

The nonparametric empirical quantile method is based on the concept that there is a transformation h , which can be described by the following equation (Gudmundsson et al., 2012; Sunyer et al., 2015):

$$St^{Obs} = h(St^{CMRP}) = ECDF^{Obs-1}(ECDF^{CMRP}(St^{CMFut})), \quad (1)$$

where St^{Obs} is an observed meteorological parameter, St^{CMRP} is the climate model output for the reference period, $ECDF^{Obs}$ is an empirical cumulative distribution function for the observed period, $ECDF^{CMRP}$ is an empirical cumulative distribution function for the climate model reference period, St^{CMFut} is a meteorological parameter which is modelled by the climate model for the future period. All estimated results are compared with the values of the reference period (1986–2005).

Estimation of the Curonian Lagoon's future water level was performed according to 4 sea water level rise scenarios which project a water level rise of 0.44 m (RCP2.6), 0.53 m (RCP4.5), 0.55 m (RCP6.0) and 0.74 m (RCP8.5) from 2005 to 2100. Projections of the Curonian Lagoon's water level for the periods of 2016–2035 and 2081–2100 were accomplished using the lagoon level data (1986–2005) at Juodkrantė and considering the water level rising tendencies described by the scenarios.

In order to simulate river inflow to the lagoon, the Nemunas River hydrological model was created using the HBV modelling software (Integrated ..., 2005) based on the following water balance equation:

$$P - E - Q = \frac{d}{dt}[SP + SM + UZ + LZ + V], \quad (2)$$

where P is the precipitation, E is an evaporation, Q is the runoff, SM is the soil moisture, SP is the snow pack, UZ is an upper groundwater zone, LZ is the lower groundwater zone, V is the lake or dam volume.

The daily values of river discharges (Q) in the Nemunas catchment from 10 water gauging stations (WGS) as well as T and P from 14 meteorological stations (MS) (Fig. 3) were necessary for model creation. Information about the modelled catchment area, the presence of lakes and forests, mean elevation (above sea level) of the area, WGS and MS was required as well. The created hydrological model was calibrated according to the data of 1986–1995 and validated using the data of 1996–2005. The projection of the Nemunas runoff at its mouth was estimated in daily steps for 2016–2035 and 2081–2100 using the calibrated model as well as the output data from the selected climate models and RCP scenarios.

The amount of evaporation and precipitation was calculated using the data of Klaipėda, Nida and Šilutė MS. Input of each MS was evaluated according to the Thiessen polygon method (Balany, 2011). The Thornthwaite equation was used to calculate the amount of evaporation (Thornthwaite, 1948):

$$E = 16 \times \left(\frac{10 \times T}{I} \right)^a \times \frac{\mu \times N}{360}, \quad (3)$$

where E is the evaporation per month, (mm month^{-1}), T is the mean monthly air temperature ($^{\circ}\text{C}$), I is an empirical annual heat index, a is an empirical I exponent, μ is the number of days in a particular month, N is the mean number of sunny hours per month (depends on a latitude). This equation was introduced quite a long time ago, but recent comprehensive scientific studies (Jakimavičius et al., 2013;

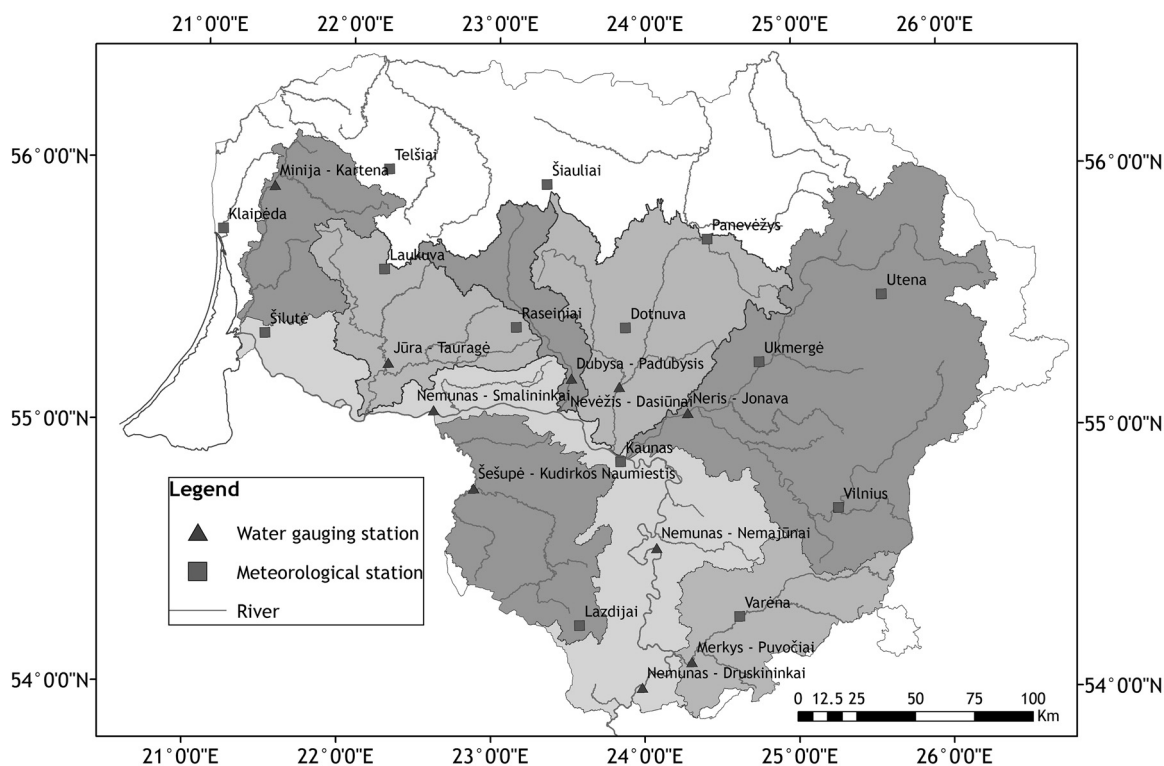


Figure 3 Location of water gauging and meteorological stations in the investigated territory of the Nemunas River catchment.

Lu et al., 2005) showed that it can still be successfully applied to estimate the evaporation rate.

Water exchange through the Klaipėda Strait was calculated using a water balance method. A modified equation of water balance created by Gailiušis et al. (1992) was applied:

$$(Q_R + P - E) + Q_{\text{exch}} = \Delta V, \quad (4)$$

$$\text{if } Q_{\text{exch}} > 0, Q_{\text{exch}} = Q_{\text{BS}}, \quad (5)$$

$$\text{if } Q_{\text{exch}} < 0, Q_{\text{exch}} = Q_{\text{CL}}, \quad (6)$$

where Q_R is the river inflow, km^3 , P is the precipitation on the surface of the lagoon, km^3 , E is an evaporation from the lagoon, km^3 , Q_{exch} is the water exchange between the Curonian Lagoon and the Baltic Sea, km^3 , Q_{BS} is an inflow from the sea, km^3 , Q_{CL} is an outflow from the lagoon, km^3 , ΔV is the change in the volume of the lagoon, km^3 .

Change of the Curonian Lagoon volume was estimated according to the water level projection. Daily volume changes and modelled river inflow were used to estimate flow discharges between the sea and the lagoon. Values of Q_{BS} and Q_{CL} were assessed as a difference between the volume change in the Curonian Lagoon and the sum of river inflow. The negative discharge indicated a flow from the Curonian Lagoon to the Baltic Sea, while the positive discharge showed a flow of the opposite direction.

Projections of the Curonian Lagoon salinity were performed using statistical relations between water salinity at Juodkrantė (S_J) and the ratio of inflow from the sea (Q_{BS}) and

the river inflow (Q_R). Monthly values of Q_{BS} and Q_R were estimated according to the multiannual water balance of the lagoon (1986–2005). Such structure of Eq. (7) was selected deliberately. Large inflow from the Baltic Sea (Q_{BS}) increases the salinity of the Curonian Lagoon, while significant inflow from the Nemunas River (Q_R) has an opposite effect. That is why the ratio of these two variables was chosen. A constant of 0.036 was selected in case if there is no inflow from the sea in a particular (modelled) month, i.e. $Q_{\text{BS}} = 0$. Such cases may occur in the presence of the significant discharge from the Nemunas (e.g. during floods). These phenomena are very rare: there were only 3 of them observed in 1986–2005. The constant value of 0.036 is the least monthly salinity value (ppt) in the lagoon at Juodkrantė in 1986–2005. The rest of constants (0.066, 0.635, 0.025 and 1.062) were generated using the statistical software package Statistica 10.

$$S_J = 0.036 + \left(\frac{0.066 \times Q_{\text{BS}}^{0.635}}{0.025 \times Q_R^{1.062}} \right), \quad (7)$$

where S_J is the monthly water salinity at Juodkrantė, ppt; Q_{BS} is the monthly inflow from the sea, km^3 ; Q_R is the monthly river inflow, km^3 .

The estimated correlation coefficient between the measured salinity values and the calculated ones according to Eq. (7) was equal to 0.75. This coefficient is statistically significant when $p < 0.05$.

To project the mean monthly water temperatures of the Curonian Lagoon, statistical relations between water and air temperatures were created using the data of 1986–2005. Water temperatures at Klaipėda, Juodkrantė, Nida and Ventė were calculated using the following equations:

$$T_{KW} = (0.95 \times T_{KA}) + 1.02, \quad (8)$$

$$T_{JW} = (1.10 \times T_{NA}) - 0.31, \quad (9)$$

$$T_{NW} = (1.13 \times T_{NA}) - 0.45, \quad (10)$$

$$T_{VW} = \left(1.12 \times T_{iSA} \right) + 0.29, \quad (11)$$

where T_{KW} , T_{JW} , T_{NW} , T_{VW} is the water temperature at Klaipėda, Juodkrantė, Nida and Ventė, °C, T_{KA} , T_{NA} , T_{SA} is an air temperature at Klaipėda, Nida and Šilutė, °C.

Eqs. (8)–(11) are valid only for the positive air temperature. When air temperature reaches 0°C, it is assumed that in a given territory water temperature reaches 0.2°C and stabilizes. This threshold water temperature (0.2°C) was estimated as an average of minimal monthly temperatures at Klaipėda, Juodkrantė, Ventė and Nida in 1986–2005.

Correlation between the values of air and water temperatures was very high: from 0.98 (Eq. (8)) to 0.99 (Eq. (10)). These coefficients are statistically significant when $p < 0.05$.

Weighted coefficients for each WGS were estimated using the Thiessen polygon method. The mean water temperature of the Curonian Lagoon was projected according to the created statistical relations as well as air temperature projections under three climate models and four RCP scenarios for the periods of 2016–2035 and 2081–2100:

$$T_{CLW} = (0.006 \times T_{KW}) + (0.066 \times T_{JW}) + (0.160 \times T_{VW}) + (0.768 \times T_{NW}), \quad (12)$$

where T_{CLW} is the mean water temperature of the Curonian Lagoon, °C.

3. Results

3.1. Calibration and validation of the Nemunas River runoff model

When creating the Nemunas catchment hydrological model, the Nemunas River from the selected starting point (Druskininkai) to the mouth (the Curonian Lagoon) was divided into separate parts sequentially attaching the catchments of: Nemunas to Druskininkai, Merkys, Nemunas from Druskininkai to Nemajūnai, Neris, Nevėžis, Dubysa, Nemunas from Nemajūnai to Smalininkai, Jūra, Miniija, Nemunas from Smalininkai to Lagoon, Šešupė.

Nemajūnai to Smalininkai, Šešupė, Jūra, Miniija and Nemunas from Smalininkai to the Curonian Lagoon (Fig. 4).

The separate subbasins were merged together into a single Nemunas River runoff model. Each subbasin was calibrated separately, using the main sixteen calibration parameters which were adapted to each subbasin. The calibration parameters were divided into four groups and calibration was started from the first group parameters (volume changes). The entire process of calibration is described in more detail in (Integrated ..., 2005; Kriaučiūnienė et al., 2013). The model calibration was performed in the period of 1986–1995 (correlation coefficient (R) – 0.88, Nash–Sutcliffe efficiency (NSE) – 0.78, accumulated difference between the calculated and the observed discharge (Accdiff) – 7.4%), while the model validation was carried out in the period of 1996–2005 (R – 0.75, NSE – 0.62, Accdiff – 5.7%) (Fig. 5). The created hydrological model was calibrated (1986–1995) and validated (1996–2005) according to the observed hydrological and meteorological data. Meteorological and water gauging station network, which data are used to develop the hydrological model, are presented in Fig. 3.

The calibrated model was then used to simulate the Nemunas inflow to the Curonian Lagoon in a historical period. In Fig. 6, the observed runoff values are compared to the simulated ones (the outputs of three climate models (average of GFDL-CM3, HadGEM2-ES and NorESM1-M) for the period of 1986–2005). This modelling is necessary to perform in order to find out how precisely the selected models reflect the historical climate conditions. Since the hydrographs of the observed and simulated historical runoff were very similar (the mean annual discharges were $700 \text{ m}^3 \text{ s}^{-1}$ and $696 \text{ m}^3 \text{ s}^{-1}$), the selected climate models can be used for future runoff simulation.

3.2. Changes of water balance components of the Curonian Lagoon

The water balance components of the reference period are analyzed in Table 1. The water balance income consists of the following components: river inflow (Q_R) – $22.1 \text{ km}^3 \text{ year}^{-1}$ (from 15.4 to $30.0 \text{ km}^3 \text{ year}^{-1}$), inflow from the sea (Q_{BS}) – $6.8 \text{ km}^3 \text{ year}^{-1}$ (from 5.4 to $9.0 \text{ km}^3 \text{ year}^{-1}$) and precipitation (P) – $1.3 \text{ km}^3 \text{ year}^{-1}$ (from 0.9 to $1.7 \text{ km}^3 \text{ year}^{-1}$). The balance losses include outflow from the lagoon (Q_{CL}) – $28.6 \text{ km}^3 \text{ year}^{-1}$ (from 20.9 to $36.8 \text{ km}^3 \text{ year}^{-1}$) and evaporation (E) – $1.0 \text{ km}^3 \text{ year}^{-1}$ (from 0.9 to $1.1 \text{ km}^3 \text{ year}^{-1}$). All of these components have seasonal variation. The greatest values of Q_R and Q_{CL} are characteristic for spring (April),

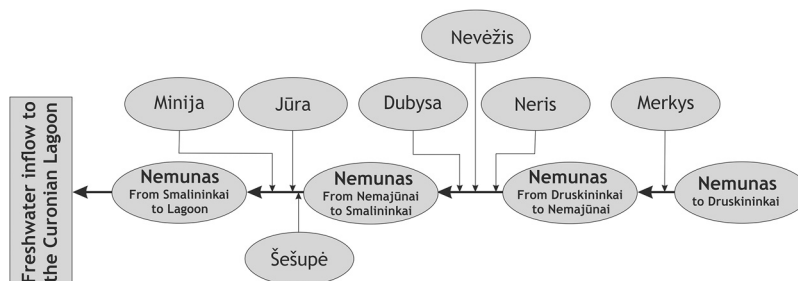


Figure 4 The scheme of the Nemunas River hydrological model.

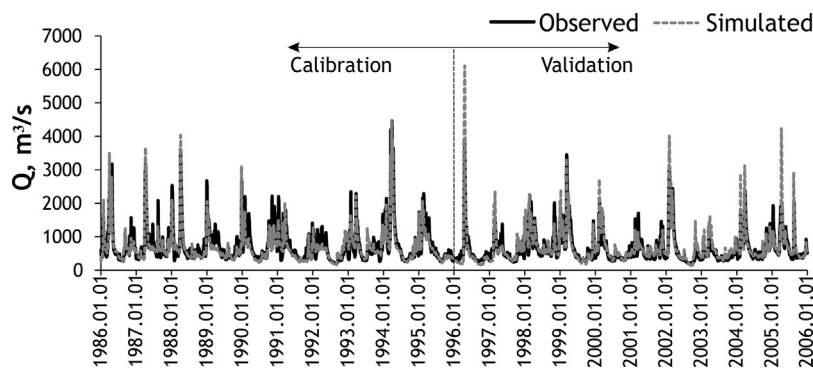


Figure 5 Comparison of observed and simulated runoff of the Nemunas River in the periods of calibration (1986–1995) and validation (1996–2005).

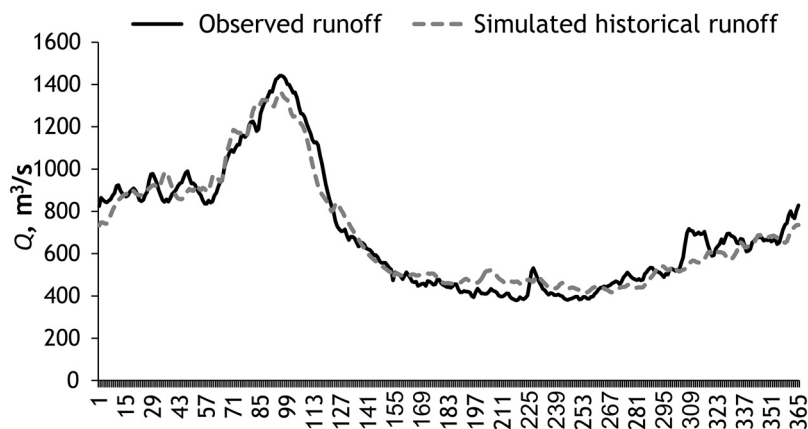


Figure 6 Comparison of observed average runoff at the mouth of the Nemunas River in historical period (1986–2005) with simulated historical runoff according to average data of three climate models (GFDL–CM3, HadGEM2–ES and NorESM1–M).

while the smallest ones are observed in summer (July). On the contrary, Q_{BS} is the smallest in spring (April) and the largest at the end of autumn (November). E increases in summer (July) and decreases in winter months, whereas P decreases in spring and is the most intensive in the autumn season.

Fig. 7 outlines that under four RCP scenarios, the components of the lagoon water balance are not expected to change significantly in the nearest future (2016–2035). The analysis indicated that in this period, Q_R and Q_{CL} averaged by all RCPs should decrease by 6.8% and 2.1% respectively, whereas Q_{BS} , E and P should increase by 13.9%, 10.8%, 6.1% respectively in relation to the reference period (1986–2005).

Considerably larger changes are projected in the far-future period (2081–2100). Q_R is going to decrease from 0.1% (RCP2.6) to 28.2% (RCP8.5), and will on average be 13.4% smaller than in the reference period. Q_R values should redistribute among the seasons. The greatest annual inflow changes are projected in winter and spring. Q_R in winter is expected to be greater from 1.9% (RCP2.6) to 10.3% (RCP8.5), while Q_R in the spring season should get smaller from 5.0% (RCP2.6) to 9.7% (RCP8.5) in comparison with the reference period. Because of rising global sea level and decreasing river inflow, the water exchange through the Klaipėda Strait (Q_{CL} and Q_{BS}) is expected to change. Q_{CL} should decline from 30.2 km³ (RCP2.6) to 26.5 km³

(RCP8.5), which, according to all four RCPs, constitutes an average decrease of only 0.7% if compared to the reference value of 1986–2005. Inflow from the sea (Q_{BS}) is projected to increase quite significantly (i.e. from 24.8% to 61.3%) due to several reasons, including decreased river inflow (projected to shrink from 0.1 to 28.2% according to different scenarios) and rising sea level (expected to grow by 0.44–0.74 m from 2005). Inflow from the sea has seasonal patterns. The projections indicate that it will get smaller by 3.4% in winter and greater by 4.5% in spring, on average, whereas in other seasons it will remain almost the same. Depending on the scenario, precipitation is expected to grow by 8.7–15.1%, while evaporation is expected to increase by 14.9–41.1% in comparison with the reference period amounts.

3.3. Changes of the Curonian Lagoon salinity

In the reference period, the average salinity of the Curonian Lagoon at Juodkrantė (S_J) was 1.2 ppt. Its smallest values were observed in spring (0.5 ppt), while the largest ones were detected in autumn (1.9 ppt). The average annual salinity data at Juodkrantė demonstrates an upward trend equal to 0.08 ppt over a decade. The comparison of S_J values and both Q_R and Q_{BS} values presented in Table 1 indicated that S_J at Juodkrantė is directly proportional to inflow from the sea and inversely proportional to river inflow. Based on

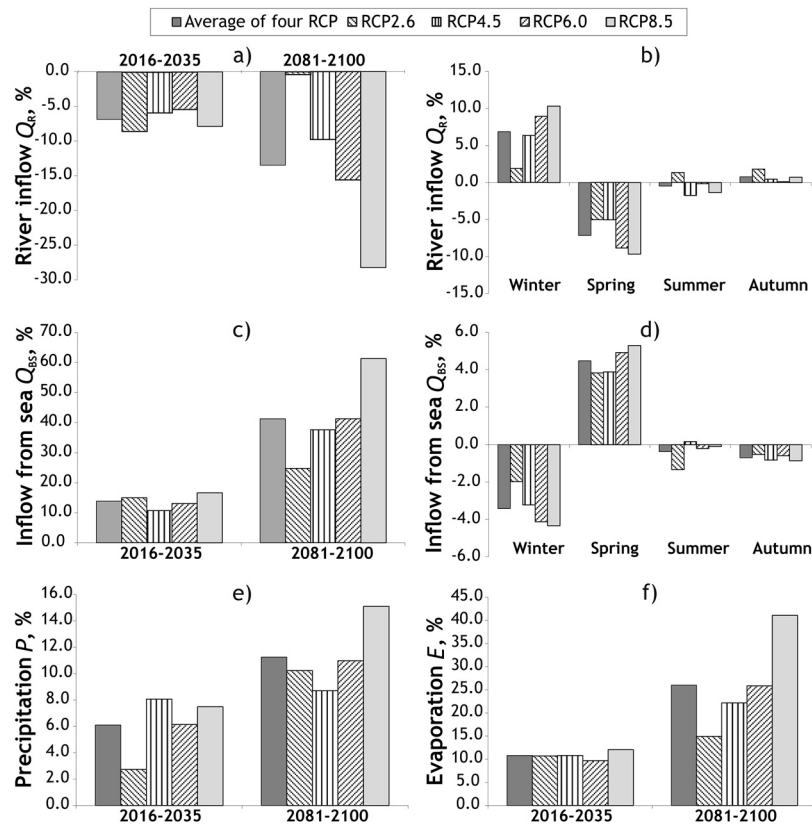


Figure 7 Changes of the components of the Curonian Lagoon water balance (in % comparing projections of 2016–2035 and 2081–2100 with average values of 1986–2005): (a) river inflow, (b) seasonal river runoff in 2081–2100, (c) inflow from the sea, (d) seasonal inflow from the sea in 2081–2100, (e) precipitation on the surface of the lagoon, (f) evaporation from the lagoon.

Table 1 The water balance of the Curonian Lagoon in the reference period (1986–2005) ($\text{km}^3 \text{ year}^{-1}$).

Balance component	Month												Annual
	I	II	III	IV	V	VI	VII	VIII	IX	X	XI	XII	
Q_R	2.4	2.2	3.0	3.2	1.8	1.2	1.1	1.1	1.1	1.4	1.7	1.9	22.1
Q_{BS}	0.6	0.4	0.4	0.2	0.4	0.6	0.5	0.6	0.6	0.8	0.9	0.9	6.8
P	0.1	0.1	0.1	0.1	0.1	0.1	0.1	0.1	0.1	0.2	0.1	0.1	1.3
Income	3.0	2.7	3.5	3.5	2.3	1.9	1.7	1.9	1.9	2.3	2.8	2.9	30.2
Q_{CL}	2.8	2.7	3.5	3.8	2.2	1.6	1.6	1.7	1.7	2.1	2.5	2.5	28.6
E	0.0	0.0	0.0	0.1	0.1	0.2	0.2	0.2	0.1	0.1	0.0	0.0	1.0
Losses	2.8	2.7	3.5	3.8	2.3	1.8	1.8	1.9	1.9	2.2	2.5	2.5	29.6
ΔV	0.0	0.0	0.0	0.0	0.1	0.0	0.0	0.0	0.0	0.0	0.0	0.1	0.1
Error	0.3	0.0	0.0	-0.3	-0.1	0.1	-0.1	0.1	0.0	0.1	0.3	0.3	0.5

this dependence, Eq. (7) was created and used to estimate S_j in the selected future twenty-year period (2016–2035 and 2081–2100).

The projections revealed an increase of the lagoon water salinity at Juodkrantė (Fig. 8) which can be attributed to changes of water exchange through the Klaipėda Strait and the Nemunas inflow. In the nearest future, the projected changes will probably be insignificant (up to 1.3 ppt, i.e. by 0.1 ppt larger than in the reference period) according to RCP4.5 and RCP6.0 scenarios, whereas other scenarios indicate a slightly greater increase of the average salinity values

(1.5 ppt), i.e. by 0.3 ppt larger than in 1986–2005. Fig. 8a presents that a greater variation is possible in summer and autumn. During these seasons, salinity is projected to be larger than in the reference period, while a smaller variation is expected during the rest of the seasons. In winter and spring, salinity values will likely be similar to or somewhat less than those in the past. At the end of the 21st century, salinity changes are projected to be more significant and grow depending on scenario severity (they can reach as much as 2.6 ppt according to RCP8.5) (Fig. 8b). It is important to mention that these changes would occur in case of a

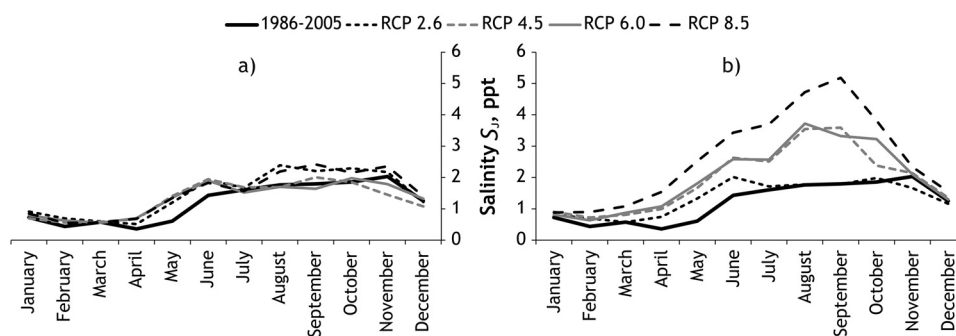


Figure 8 Projections of the Curonian Lagoon salinity (at Juodkrantė) in: (a) 2016–2035, (b) 2081–2100.

considerable decrease of the Nemunas inflow and rising sea level.

3.4. Changes of water temperature of the Curonian Lagoon

Fig. 9 outlines the water temperature of the Curonian Lagoon. Its annual variation at Klaipėda differs from the one at Juodkrantė, Nida or Ventė. The reason for such phenomenon is the position of Klaipėda, i.e. it is located at the junction of the sea and the lagoon. Since the volume of the Baltic Sea is many times greater than the Curonian Lagoon, its water warms up more gradually and cools down slower. In the reference period, the average annual water temperature was 8.8°C at Klaipėda, 9.1°C at Juodkrantė, 9.2°C at Nida and 9.3°C at Ventė. The average water temperature of the entire Curonian Lagoon, calculated according to Eq. (12) was 9.2°C, which is very similar to the measured one at Nida. This variable had an upward trend in the period of 1986–2005: it rose up by 0.7°C at Klaipėda, by 0.8°C at Nida, by 0.9°C at Juodkrantė and by 1.0°C at Ventė. It was estimated that the average annual water temperature of the Curonian Lagoon rose at an average rate of 0.04 degrees per year.

Projections of water temperature of the Curonian Lagoon were performed using Eqs. (8)–(12) of four WGS and for two selected future periods (Fig. 10). In the nearest future, considerable differences among the projected water

temperature values according to the selected scenarios were not identified; this variable is expected to grow by 1.7°C on average (Fig. 10a). As usual, in the far-future period, the projected changes are going to be more significant: the mean annual water temperature may grow by at least 2.3°C (according to RCP2.6) or even by 6.3°C (according to the most severe RCP8.5 scenario) compared to the reference period values. On average, the annual water temperature is projected to be higher by 4.1°C than in the reference period: it will rise by 2.3°C in winter, 4.2°C in spring, 5.0°C in summer and 4.3°C in autumn. The warmer lagoon water is likely to create unfavourable conditions for forming a permanent ice cover in winter.

4. Discussion and conclusions

The performed analysis presented in this paper attempted to cover the full complexity of the potential impact of climate change on the Curonian Lagoon water balance components, salinity and temperature. Projections were performed using three global climate models and four RCP scenarios. Values of the projected variables were compared with the ones in the reference period of 1986–2005. The estimated water balance of the Curonian Lagoon (in 1986–2005) and projections of the Nemunas inflow revealed that considerable variations should be expected in the future. In all cases, the projected changes are going to be much more significant in the second period (2081–2100) than in the first one (2016–2035). In the

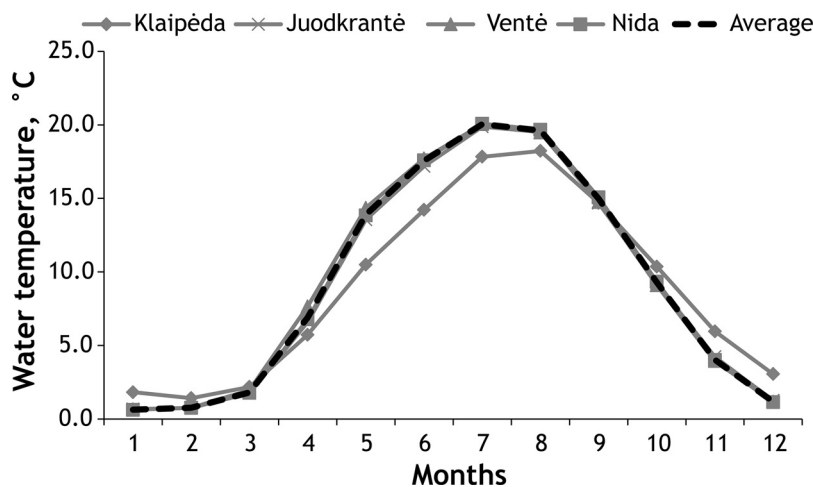


Figure 9 Water temperature of the Curonian Lagoon in the reference period (1986–2005).

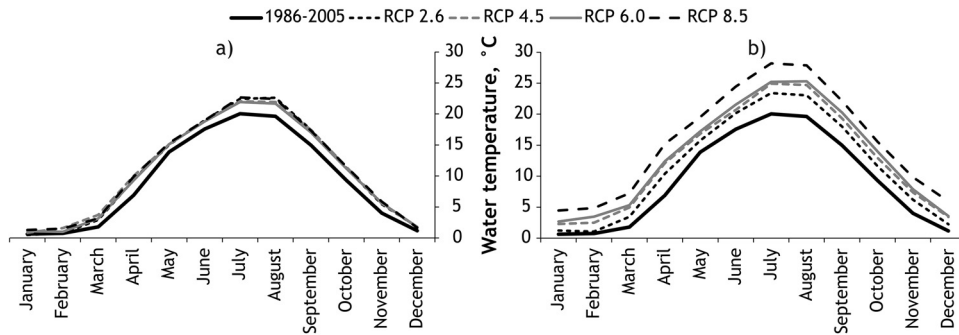


Figure 10 Projections of water temperature of the Curonian Lagoon in: (a) 2016–2035, (b) 2081–2100.

nearest future, the Nemunas annual inflow may decline to 20.3 km³ (RCP2.6). In the far-future period, it is expected to decrease to 15.9 km³ (RCP8.5), while in the reference period it was 22.1 km³. In the period of 2081–2100, considerable seasonal redistribution of the Nemunas annual inflow is expected. According to climate scenarios, the river inflow will increase by an average of 6.9% in winter and 0.8% in autumn, whereas it is expected to decrease by 7.1% in spring and 0.5% in summer. Due to rising sea water level and smaller amounts of river inflow, inflow from the sea annual input is expected to increase up to 8.0 km³ in the nearest future and up to 11.0 km³ in the far future according to RCP8.5 (the scenario which projects the most drastic changes), while in the past (1986–2005) it was 6.8 km³. According to RCP8.5, the major changes of annual precipitation and evaporation are likely to occur in the far-future period as well: evaporation should intensify by 41.1%, while precipitation should increase by 15.1%.

As inflow from the sea is expected to increase, the same will happen to salinity values. In the nearest future, salinity at Juodkrantė is projected to reach 1.4 ppt on average (from 1.3 ppt by RCP2.6 to 1.5 ppt by RCP8.5). At the end of the century, salinity will gain significantly higher values: from 1.4 ppt (RCP2.6) to 2.6 ppt (RCP8.5). On average, it is projected to reach 2.0 ppt, whereas the reference period value was 1.2 ppt. If future changes projected by RCP8.5 scenario come true, salinity would reach the reference values (2.6 ppt according to Dailidienė and Davulienė, 2008) of the Curonian Lagoon at Klaipėda (i.e. very close to the Baltic Sea). This outcome is contrary to that of Vuorinen et al. (2015) who found that unchanged salinity conditions at the end of the 21st century are possible as well.

In the reference period (1986–2005), water temperature of the Curonian Lagoon grew by 0.04°C year⁻¹. These results are in line with those of previous studies, indicating that the warming trend of the mean surface water temperature in the Curonian lagoons was 0.03°C year⁻¹ in the period of 1961–2008 (Dailidienė et al., 2011). Similar temperature growth tendencies were determined for the Baltic Sea as well. SST averaged over the entire Baltic Sea increased at the rate of 0.05°C year⁻¹ (Stramska and Białogrodzka, 2015). Smaller seas and especially shallow lagoons are getting warmer much faster than the global ocean temperature (0.02°C year⁻¹ over the reference period) (Huang et al., 2015b).

This study shows that in the nearest future, the inflow from the sea, evaporation, water temperature and salinity are projected to increase more under the RCP2.6 scenario

than the rest of scenarios. These findings are in agreement with other results (Westervelt et al., 2015). The most likely explanation of this is the increase of meteorological parameters, such as air temperature and precipitation projected according to the RCP2.6 scenario until the middle of the 21st century, as well as the decrease of these variables that is expected to occur in the second half of the century. In the far-future period, the most significant changes of all investigated variables are expected according to the RCP 8.5 scenario.

This study does not rule out the presence of other factors that may have an influence on the state of the Curonian Lagoon in the future. It is difficult to project anthropogenic activities, such as land use changes in river catchments, Klaipėda Strait permeability changes, etc., that may alter the results of this study, creating a degree of additional uncertainty. However, there is a strong possibility that in the long term period (the end of 21st century), the projected changes will have the estimated tendencies.

Acknowledgments

The authors are grateful to the Marine Research Department under the Environmental Protection Agency of Lithuania, which so kindly facilitated the salinity and water level observation data necessary for this study.

This research is a part of a scientific study 'Impact Assessment of Climate Change and Other Abiotic Environmental Factors on Aquatic Ecosystems' (project no. SIT-11/2015) funded under the National Research Programme 'Sustainability of agro-, forest and water ecosystems (2015–2021)'.

References

- Aleksandrov, S., Gorbunova, J., Rudinskaya, L., 2015. Effect of climate change and mollusc invasion on eutrophication and algae blooms in the lagoon ecosystems of the Baltic Sea. *Geophys. Res. Abstr.* 17 EGU2015-5846.
- Anthony, A., Atwood, J., August, P., Byron, C., Cobb, S., Foster, C., Fry, C., Gold, A., Hagos, K., Heffner, L., Kellogg, D.Q., Lellis-Dibble, K., Opaluch, J.J., Oviatt, C., Pfeiffer-Herbert, A., Rohr, N., Smith, L., Smythe, T., Swift, J., Vinhateiro, N., 2009. Coastal lagoons and climate change: ecological and social ramifications in U.S. Atlantic and Gulf coast ecosystems. *Ecol. Soc.* 14 (1), 8, 29 pp.
- Balany, F., 2011. Different ways of calculating catchment rainfall: case in Indonesia. *J. Civil Eng. Forum* XX (1), 1175–1182, <http://dx.doi.org/10.22146/jcef.18944>.

- Červinskas, E., 1972. *New measurements of the Curonian Lagoon area*. Works Lithuanian Acad. Sci. Geogr. Geol. 9, 45–49, (in Lithuanian).
- Chen, Y., Zuo, J., Zou, H., Zhang, M., Zhang, K., 2016. Responses of estuarine salinity and transport processes to sea level rise in the Zhujiang (Pearl River) Estuary. *Acta Oceanol. Sin.* 35 (5), 38–48, <http://dx.doi.org/10.1007/s13131-016-0857-2>.
- Church, J.A., White, N.J., 2011. Sea-level rise from the late 19th to the early 21st century. *Surv. Geophys.* 32 (4), 585–602, <http://dx.doi.org/10.1007/s10712-011-9119-1>.
- Coppini, G., Pinardi, N., Marullo, S., Loewe, P., 2007. Compiled for EEA by the Istituto Nazionale di Geofisica e Vulcanologia (INGV) based on Datasets Made Available by the Hadley Center. HADISST1: <http://hadobs.metoffice.com/hadisst/data/download.html>. ENEA within Mediterranean Operational Oceanography Network (MOON), and Bundesamt für Seeschifffahrt und Hydrographie (BSH) within the Baltic Operational Oceanography System (BOOS).
- Dailidienė, I., Davulienė, L., 2008. Salinity trend and variation in the Baltic Sea near the Lithuanian coast and in the Curonian Lagoon in 1984–2005. *J. Marine Syst.* 74, S20–S29, <http://dx.doi.org/10.1016/j.jmarsys.2008.01.014>.
- Dailidienė, I., Baudler, H., Chubarenko, B., Navrotskaya, S., 2011. Long term water level and surface temperature changes in the lagoons of the southern and eastern Baltic. *Oceanologia* 53 (1), 293–308, <http://dx.doi.org/10.5697/oc.53-1-TI.293>.
- Gailiūšis, B., Kovalenkoviėnė, M., Jurgelėnaitė, A., 1992. *Water balance of the Curonian Lagoon*. *Power Eng.* 2, 67–73.
- Gailiūšis, B., Jablonskis, J., Kovalenkoviėnė, M., 2001. *The Lithuanian Rivers. Hydrography and Runoff*. Lithuanian Energy Institute, Kaunas, 792 pp.
- Gasiūnaitė, Z.R., 2000. *Coupling of the limnetic and brackishwater plankton crustaceans in the Curonian Lagoon (Baltic Sea)*. *Int. Rev. Hydrobiol.* 85, 649–657, [https://doi.org/10.1002/1522-2632\(200011\)85:5/6<653::AID-IROH653>3.0.CO;2-W](https://doi.org/10.1002/1522-2632(200011)85:5/6<653::AID-IROH653>3.0.CO;2-W).
- Gasiūnaitė, Z., Razinkovas, A., 2002. *The salinity tolerance of two cladoceran species from the Curonian Lagoon: an experimental study*. *Sea Environ.* 2 (7), 28–32.
- Grinsted, A., Jevrejeva, S., Riva, R.E.M., Dahl-Jensen, D., 2015. Sea level rise projections for northern Europe under RCP8.5. *Clim. Res.* 64, 15–23, <http://dx.doi.org/10.3354/cr01309>.
- Gudmundsson, L., Bremnes, J.B., Haugen, J.E., Engen-Skaugen, T., 2012. Technical Note: downscaling RCM precipitation to the station scale using statistical transformations – a comparison of methods. *Hydrol. Earth Syst. Sci.* 16, 3383–3390, <http://dx.doi.org/10.5194/hessd-9-6185-2012>.
- Huang, B., Banzon, V.F., Freeman, E., Lawrimore, J., Liu, W., Peterson, T.C., Smith, T.M., Thorne, P.W., Woodruff, S.D., Zhang, H.M., 2014. Extended reconstructed sea surface temperature version 4 (ERSST.v4): Part I. Upgrades and intercomparisons. *J. Climate* 28, 911–930, <http://dx.doi.org/10.1175/JCLI-D-14-00006.1>.
- Huang, B., Thorne, P., Smith, T., Liu, W., Lawrimore, J., Banzon, V., Zhang, H., Peterson, T., Menne, M., 2015a. Further exploring and quantifying uncertainties for extended reconstructed sea surface temperature (ERSST) version 4 (v4). *J. Climate* 29, 3119–3142, <http://dx.doi.org/10.1175/JCLI-D-15-0430.1>.
- Huang, B., Banzon, V.F., Freeman, E., Lawrimore, J., Liu, W., Peterson, T.C., Smith, T.M., Thorne, P.W., Woodruff, S.D., Zhang, H.M., 2015b. Extended Reconstructed Sea Surface Temperature (ERSST), Version 4. [Sea Surface Temperature]. NOAA National Centers for Environmental Information, <http://dx.doi.org/10.7289/V5KD1VVF> (accessed 23.05.17).
- Integrated Hydrological Modelling System, 2005. *Manual. Version 5.8. Swedish Meteorological and Hydrological Institute*, 115 pp.
- IPCC, 2013. *Climate change 2013: the physical science basis*. In: Stocker, T.F., Qin, D., Plattner, G.-K., Tignor, M., Allen, S.K., Boschung, J., Nauels, A., Xia, Y., Bex, V., Midgley, P.M. (Eds.), Contribution of Working Group I to the Fifth Assessment Report of the Intergovernmental Panel on Climate Change. Cambridge University Press, Cambridge, United Kingdom/New York, NY, USA, p. 1535, <http://dx.doi.org/10.1017/CBO9781107415324>.
- Jakimavičius, D., Kovalenkoviėnė, M., 2010. *Long-term water balance of the Curonian Lagoon in the context of anthropogenic factors and climate change*. *Baltica* 23 (1), 33–46.
- Jakimavičius, D., Kriaučiūnienė, J., 2013. The climate change impact on the water balance of the Curonian Lagoon. *Water Resour.* 40 (2), 120–132, <http://dx.doi.org/10.1134/S0097807813020097>.
- Jakimavičius, D., Kriaučiūnienė, J., Gailiūšis, B., Šarauskiėnė, D., 2013. Assessment of uncertainty in estimating the evaporation from the Curonian Lagoon. *Baltica* 26 (2), 177–186, <http://dx.doi.org/10.5200/baltica.2013.26.18>.
- Kataržytė, M., Vaičiūtė, D., Bučas, M., Gyraitė, G., Petkuvienė, J., 2017. Microorganisms associated with charophytes under different salinity conditions. *Oceanologia* 59 (2), 177–186, <http://dx.doi.org/10.1016/j.oceano.2016.10.002>.
- Kriaučiūnienė, J., Jakimavičius, D., Šarauskiėnė, D., Kaliaška, T., 2013. Estimation of uncertainty sources in the projections of Lithuanian river runoff. *Stochast. Environ. Res. Risk Assess.* 27 (4), 769–784, <http://dx.doi.org/10.1007/s00477-012-0608-7>.
- Lillebo, A., Staltnacke, P., Gooch, G.D., 2015. *Coastal Lagoons in Europe – Integrated Water Resource Strategies*. IWA Publishing, 250 pp.
- Liu, W.C., Liu, H.M., 2014. Assessing the impacts of sea level rise on salinity intrusion and transport time scales in a tidal estuary, Taiwan. *Water* 6, 324–344, <http://dx.doi.org/10.3390/w6020324>.
- Liu, W., Huang, B., Thorne, P.W., Banzon, V.F., Zhang, H.M., Freeman, E., Lawrimore, J., Peterson, T.C., Smith, T.M., Woodruff, S.D., 2014. Extended Reconstructed Sea Surface Temperature version 4 (ERSST.v4): Part II. Parametric and structural uncertainty estimations. *J. Climate* 28, 931–951, <http://dx.doi.org/10.1175/JCLI-D-14-00007.1>.
- Lu, J., Sun, G., McNulty, S.G., Amaty, D.M., 2005. A comparison of six potential evapotranspiration methods for regional use in the Southeastern United States. *J. Am. Water Resour. Assoc.* 31 (6), 612–633, <http://dx.doi.org/10.1111/j.1752-1688.2005.tb03759.x>.
- Moss, R.H., Edmonds, J.A., Hibbard, K.A., Manning, M.R., Rose, S.K., van Vuuren, D.P., Carter, T.R., Emori, S., Kainuma, M., Kram, T., Meehl, G.A., Mitchell, J.F., Nakicenovic, N., Riahi, K., Smith, S.J., Stouffer, R.J., Thomson, A.M., Weyant, J.P., Wilbanks, T.J., 2010. The next generation of scenarios for climate change research and assessment. *Nature* 463 (7282), 747–756, <http://dx.doi.org/10.1038/nature08823>.
- Navrotskaya, S.E., Chubarenko, B.V., 2013. Trends in the variation of the sea level in the lagoons of the Southeastern Baltic. *Oceanologia* 53 (1), 13–23, <http://dx.doi.org/10.1134/S0001437012050128>.
- Shaltout, M., Omstedt, A., 2014. Recent sea surface temperature trends and future scenarios for the Mediterranean Sea. *Oceanologia* 56 (3), 411–443, <http://dx.doi.org/10.5697/oc.56-3.411>.
- Stramska, M., Białogrodzka, J., 2015. Spatial and temporal variability of sea surface temperature in the Baltic Sea based on 32-years (1982–2013) of satellite data. *Oceanologia* 57 (3), 223–235, <http://dx.doi.org/10.1016/j.oceano.2015.04.004>.
- Sunyer, M.A., Hundedcha, Y., Lawrence, D., Madsen, H., Willems, P., Martinkova, M., Vormoor, K., Burger, G., Hanel, M., Kriaučiūnienė, J., Loukas, A., Osuch, M., Yucel, I., 2015. Inter-comparison of statistical downscaling methods for projection of extreme precipitation in Europe. *Hydrol. Earth Syst. Sci.* 19, 1827–1847, <http://dx.doi.org/10.5194/hess-19-1827-2015>.
- Teutschbein, C., Seibert, J., 2013. Is bias correction of regional climate model (RCM) simulations possible for non-stationary conditions? *Hydrol. Earth Syst. Sci.* 17, 5061–5077, <http://dx.doi.org/10.5194/hess-17-5061-2013>.

- Thornthwaite, C.W., 1948. An approach toward a rational classification of climate. *Geogr. Rev.* 38 (1), 55–94.
- Umgiesser, G., Zemlys, P., Erturk, A., Razinkova-Baziukas, A., Méziné, J., Ferrarin, C., 2016. Seasonal renewal time variability in the Curonian Lagoon caused by atmospheric and hydrographical forcing. *Ocean Sci.* 12, 391–402, <http://dx.doi.org/10.5194/os-12-391-2016>.
- vanVuuren, D.P., Edmonds, J., Kainuma, M., Riahi, K., Thomson, A., Hibbard, K., Hurtt, G.C., Kram, T., Krey, V., Lamarque, J.F., Masui, T., Meinshausen, M., Nakicenovic, N., Smith, S.J., Rose, S.K., 2011. The representative concentration pathways: an overview. *Climatic Change* 109, 5–31, <http://dx.doi.org/10.1007/s10584-011-0148-z>.
- Vargas, C.I.C., Vaz, N., Dias, J.M., 2017. An evaluation of climate change effects in estuarine salinity patterns: application to Ria de Aveiro shallow water system. *Estuar. Coast. Shelf Sci.* 189, 33–45.
- Vousdoukas, M.I., Mentaschi, L., Youkouvalas, E., Verlaan, M., Feyen, L., 2017. Extreme sea levels on the rise along Europe's coasts. *Earths Future* 5, 304–323, <http://dx.doi.org/10.1002/2016EF000505>.
- Vuorinen, I., Hänninen, J., Rajasilta, M., Laine, P., Eklund, J., Montesino-Pouzols, F., Corona, F., Junker, K., Markus Meier, H. E., Dippner, J.W., 2015. Scenario simulations of future salinity and ecological consequences in the Baltic Sea and adjacent North Sea areas – implications for environmental monitoring. *Ecol. Indic.* 50, 196–205, <http://dx.doi.org/10.1016/j.ecolind.2014.10.019>.
- Westervelt, D.M., Horowitz, L.W., Naik, V., Golaz, J.C., Mauzerall, D. L., 2015. Radiative forcing and climate response to projected 21st century aerosol decreases. *Atmos. Chem. Phys.* 15 (22), 12681–12703, <http://dx.doi.org/10.5194/acp-15-12681-2015>.
- Zemlys, P., Ferrarin, C., Umgiesser, G., Gulbinskas, S., Bellafore, D., 2013. Investigation of saline water intrusions into the Curonian Lagoon (Lithuania) and two-layer flow in the Klaipėda Strait using finite element hydrodynamic model. *Ocean Sci.* 9, 573–584, <http://dx.doi.org/10.5194/os-9-573-2013>.
- Žilinskas, G., Petrokas, T., 1998. The cartometric characteristics of the northern part of Curonian Lagoon and problems of their determination. *Ann. Geograph.* 31, 110–122.



Available online at www.sciencedirect.com

ScienceDirect

journal homepage: www.journals.elsevier.com/oceanologia/



ORIGINAL RESEARCH ARTICLE

Ecosystem of the Polish part of the Vistula Lagoon from the perspective of alternative stable states concept, with implications for management issues

Ryszard Kornijów*

Department of Fisheries Oceanography and Marine Ecology, National Marine Fisheries Research Institute, Gdynia, Poland

Received 21 November 2017; accepted 21 February 2018

Available online 7 March 2018

KEYWORDS

Baltic Sea;
Coastal management;
Regime shift;
Food-web interactions;
Drivers

Summary The alternative stable states concept finds broad application in reference to both terrestrial and aquatic ecosystems. For some reason, attempts to implement the concept to explain processes observed in estuaries and Baltic lagoons are very rare. Based on information included in publications issued over the last 60 years, three co-existing states were designated within the strongly elongated basin the Vistula Lagoon, namely: phytoplankton-dominated (Middle Basin), macrophyte-dominated (Elbląg Bay), and transition state balancing between the two former ones (West Basin). Regions of the lagoon representing such states are similar in terms of nutrient concentrations, but they considerably differ in terms of: exposure to wind and wave action, salinity, anthropogenic impact, and multi-level top-down regulations. The paper discusses the role of such drivers, responsible for both the maintenance of a given state, and the past transition into the present alternative state. Moreover, it presents chances for the improvement of the situation, as well as threats which can undermine them.

© 2018 Institute of Oceanology of the Polish Academy of Sciences. Production and hosting by Elsevier Sp. z o.o. This is an open access article under the CC BY-NC-ND license (<http://creativecommons.org/licenses/by-nc-nd/4.0/>).

* Correspondence to: Department of Fisheries Oceanography and Marine Ecology, National Marine Fisheries Research Institute, Kotłątąja 1, 81-332 Gdynia, Poland. Tel. +48 58 73 56 340, Fax: +48 58 73 56 110.

E-mail address: rkornijow@mir.gdynia.pl.

Peer review under the responsibility of Institute of Oceanology of the Polish Academy of Sciences.



Production and hosting by Elsevier

<https://doi.org/10.1016/j.oceano.2018.02.004>

0078-3234/© 2018 Institute of Oceanology of the Polish Academy of Sciences. Production and hosting by Elsevier Sp. z o.o. This is an open access article under the CC BY-NC-ND license (<http://creativecommons.org/licenses/by-nc-nd/4.0/>).

1. Introduction

According to the alternative stable state theory, a given system can remain in one of multiple possible states defined by a specific composition of biocoenoses and habitat properties over ecologically-relevant timescales (Holling, 1973; Scheffer and Carpenter, 2003; Scheffer et al., 2001). During the persistence of a given state, a system of ecological feedbacks develops, counteracting the shift into another state. The transition of the ecosystem into another alternative state precedes exceeding ecosystem thresholds, and usually requires the interference of a sufficiently strong driver able to disturb the current balance, and as a consequence lead to profound transformations of the entire system. Transition states, considered unstable, can occur in between. The theory has become an important framework for understanding and managing both terrestrial ecosystems (e.g. grass-dominated vs. shrub dominated), as well as aquatic, freshwater, and marine ecosystems (e.g. clear-water vs. turbid water, kelp forests vs. urchin dominance) (review in Folke et al., 2004).

Ocean ecosystems naturally respond to environmental stress very slowly, and the rate of the occurring processes is distinguished by considerable inertia. Due to such characteristics, the majority of regime shifts in oceans unfold slowly and smooth transitions between equilibrium states are easy to overlook or ignore (Hakanson and Lindgren, 2008; Knowlton, 2004; Lyttimäki and Hildén, 2007; Petraitis and Dudgeon, 2004). The stability of open zones of oceans contrasts with the dynamics of processes occurring in coastal lagoons and estuaries. They are transitional zones where the influences of the aquatic and terrestrial, as well as freshwater and marine environment clash (Perez-Ruzafa et al., 2011). This is additionally combined with the destabilising effect of human activity, usually strongly evident in these areas. In such conditions, the risk of a shift from one state into another is particularly high (Viaroli et al., 2008). Therefore, it is important not only to define the current state of lagoons, but also to determine the rate of changes and drivers causing them, as well as the ecological thresholds exceeding of which can result in a shift to a new state (Lyttimäki and Hildén, 2007). The knowledge of such conditions can permit management of resources preventing the transition into another state, and therefore dramatic changes in the biocoenosis and the provision of ecosystem services to the coastal communities (Hughes et al., 2013; Mollmann et al., 2015). On the other hand, such knowledge can provide the basis for programmes aimed at the management or restoration of the degraded systems (Hakanson and Bryhn, 2008; Jeppesen et al., 1994; Moss, 1994).

In spite of high interest in the stable states concept among marine ecologists, attempts of its implementation aimed at the explanation of phenomena observed in the lagoons and estuaries of the Baltic Sea have been undertaken only in several cases and in a limited scope (Dahlgren and Kautsky, 2004; Munkes, 2005; Rosqvist et al., 2010). This paper is the first attempt of implementation of the theory in reference to a Baltic lagoon, taking into consideration the majority of trophic levels. It concerns the Vistula Lagoon, the second largest and one of the most thoroughly investigated lagoons in the region. The study is based on information included in

publications issued over the last 60 years. The objective of the study was to organise knowledge available in the literature regarding the lagoon's ecosystem in order to provide the basis for: i. defining the (current and past) state of the lagoon in the context of the alternative state theory and regime shifts, ii. analysing drivers and buffer mechanisms maintaining a given state, with consideration of bottom-up and top-down regulations, and iii. presenting chances for the improvement of the ecological status of the lagoon, and diagnosing potential threats to the ecosystem which can undermine them. In the paper, alternative states correspond to situations in which one of the groups of primary producers is dominant, namely macrophytes (corresponding to macrophyte-dominated state) or phytoplankton (phytoplankton-dominated state) (Scheffer and Carpenter, 2003; Scheffer et al., 1993).

2. Material and methods

The Vistula Lagoon is located in the south-eastern part of the Baltic Sea. It is a strongly elongated, N–S oriented water body with a length of 91 km, width from 7 to 11 km, and surface area of 838 km². The eastern part of the lagoon with an area of 328 km² is located on the Polish side (Fig. 1), and the remaining part on the Russian side. To the north, it is separated from the open sea by the Vistula Spit – a shallow belt of sandy land with a width of 1–2 km and length of approximately 50 km. Contact with marine waters occurs through the Baltiysk Strait (the inlet length, width and depth: 2 km, 400 m and 10–12 m, respectively). The extensive surface area of the lagoon contrasts with its low depth (mean depth 2.5 m; max. depth 5.2 m).

The shoreline of the lagoon on the Polish side is weakly developed. The only bay strongly extending into the land is the Elbląg Bay, located in the south-western part of the lagoon, and fed by the Elbląg River (Fig. 1). It has an area of 7.23 km², and is very shallow (max. depth in the central area of the bay usually not exceeding approximately 0.8 m).

The lagoon is fed by several rivers draining an area of 23,871 km². In comparison to the lagoon's water surface area, the drainage area is exceptionally large (Łomniewski, 1958). More than half of the area is under agricultural use, and approximately 25% is covered by forests. The total number of residents in the lagoon's catchment slightly exceeds one million. Industry is not extensively developed.

Until the end of the 19th century, the Vistula Lagoon was nearly a freshwater basin supplied mainly by two rivers: Vistula and Pregolya. In 1895, for the purpose of protection of areas located at the mouth of the delta of the Vistula River against flood, a new mouth of the river to the Baltic Sea was dug. Moreover, a cascading system of four locks and weirs was constructed on the Nogat River (a distributary channel of the Vistula River) the main stream feeding the lagoon at the time (Łomniewski, 1958). This reduced the inflow of waters from the Vistula River to the lagoon 10 times, resulting in a gradual increase in the salinity of the lagoon waters. Nowadays, the highest salinity, reaching 6.5‰, is observed in the vicinity of the Baltiysk inlet. It gradually decreases towards the east and Western, reaching values close to zero at the mouths of the largest rivers.

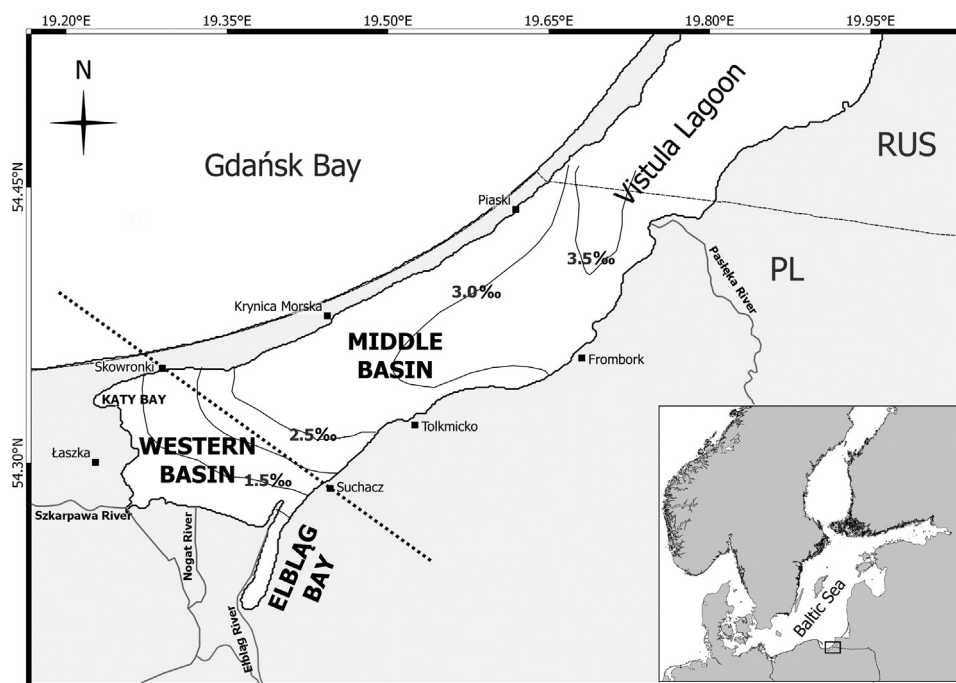


Figure 1 The Vistula Lagoon with marked oligohaline and mesohaline regions (Western and Middle basins, respectively). After Szarejko-Lukasiewicz (1959), modified.

The water level in the lagoon is subject to considerable fluctuations with an amplitude of up to 1.2 m, particularly in the period of autumn-winter storms (Chubarenko et al., 2012). They result from water exchange with the Baltic Sea and strong winds. The large surface area of the lagoon and its low depth favour continuous water mixing, and therefore intensive sediment resuspension. Sediments on the eastern and western ends of the lagoon and in its central part at a depth from approximately 2 m are muddy. Along the southern and northern shores, up to a depth of approximately 1.5–2 m, sandy fractions are dominant, locally with a small admixture of fine loamy fractions.

The lagoon is under the influence of both maritime and continental climate, with air temperature that can attain high annual amplitudes from -31°C to 36°C . The ice cover usually persists for only several days in mild winters, and from December until March in the coldest years.

Large scale research on the ecosystem of the Vistula Lagoon commenced at the beginning of the 1950s. It particularly focused on the determination of the habitat and food conditions of fish, and other issues related to fishery. In addition, monitoring research was conducted by the state environmental protection services. As a result, the lagoon became one of the most thoroughly investigated Baltic lagoons. The present paper focuses on the Polish part of the lagoon. It is based on literature, particularly published mostly after 2010, and concerning: physical–chemical properties of waters and sediments, plankton, macrophytes, macroinvertebrates, fish and birds. In the case of lack of publications from the period, older papers were used, provided that information included in them is still valid.

For the purpose of the study, the lagoon was divided into the Western and Middle basins (Fig. 1). The division was performed based on criteria such as: salinity, exposure to wind, nature of bottom sediments, and occurrence and distribution of vegetation.

3. Results

3.1. Nutrient load

Due to the large area of the catchment of the Vistula Lagoon and predominance of its agricultural use, very high amounts of nutrients are supplied to the lagoon every year. The total load from drainage basin amounts to 16 g of nitrogen and 1.2 g m^{-2} of the surface area of the water body (Witek et al., 2010). The performed balance of nutrients flow suggests that the primary source of nitrogen and phosphorus for primary producers is not the direct supply of nutrients from the catchment, but the mineralisation of organic matter, occurring in sediments and the water column, related to continuous resuspension. As a result of the mineralisation, from 15 to 20% of nitrogen, and as much as 20–40% of phosphorus contained in the sediments is released back to the water (Witek et al., 2010). The spatial distribution of nutrients in the lagoon is relatively even, with slightly increased values of N concentrations in the Middle Basin (Table 1).

According to Witek et al. (2010), the limitation of primary production with phosphorus occurs in spring, when phosphates are exhausted by phytoplankton, and nitrogen is still available. In late spring and summer, nitrogen compounds become the limiting factor, possibly favouring the development of cyanobacteria.

Table 1 Characteristics of the Western and Middle basins of the Vistula Lagoon. The physical–chemical data are the means \pm SD (standard deviation) and ranges of monthly measurements at two sites located in the Western Basin and seven in the Middle Basin from May to October 2013. Data provided by the Institute of Meteorology and Water Management National Research Institute, Maritime Branch of Gdynia. SDD – Secchi disc depth.

Parameter	Western Basin	Middle Basin
Max. depth [m]	1–2	3–4
Wind exposure	From low to medium	High
Sediments	Muddy, organic	Sandy to ca. 1.5 m, deeper muddy
Salinity [‰]	1.1 \pm 0.3 (0.3–1.8)	2.6 \pm 0.6 (1.4–3.7)
N_{tot} [mg l ⁻¹]	2.1 \pm 0.8 (1.5–4.5)	2.3 \pm 0.4 (1.1–3.2)
P_{tot} [mg l ⁻¹]	0.11 \pm 0.04 (0.06–0.18)	0.10 \pm 0.04 (0.05–0.19)
SDD [m]	0.49 \pm 0.20 (0.3–1.5)	0.39 \pm 0.15 (0.2–0.7)
Chl.-a [μ g l ⁻¹]	48.27 \pm 22.9 (13.0–93.2)	54.3 \pm 23.8 (8.9–106.6)

3.2. Light availability

Water transparency measured by Secchi disc depth (SDD) is slightly higher in the Western Basin than in the Middle one, conversely as chlorophyll-*a* concentrations (Table 1). More transparent water in the Western Basin was noticed earlier by other authors (Pliński and Simm, 1978; Renk et al., 2001; Ringer, 1959). Relatively low SDD values resulted not only from the concentration of chlorophyll but also the presence of abiotic resuspended particles.

The compensation point, determined by multiplying values of SDD by the number 3 (Holmes, 1970), depending on the analysed region of the lagoon, amounted from 117 to 147 cm. The upper range corresponds to a depth at which charales were recorded in the Kały Bay (Western Basin) in 2013 (Kornijów, 2018). Some macrophytes, however,

especially of the genus *Potamogeton* in the Western Basin, grow at a depth of more than 2 m.

3.3. Communities

3.3.1. Phytoplankton

The phytoplankton of the lagoon is dominated by cyanobacteria, slightly more abundant in the Middle than in the Western Basin (Fig. 2). In the latter, a higher contribution is reached by diatoms and green algae. Cyanobacterial blooms occur mostly in the summer period, particularly in the Middle Basin (Dmitrieva and Semenova, 2012; Nawrocka and Kobos, 2011). They include several species which can produce cyanobacterial toxins (Rybicka, 2005).

3.3.2. Zooplankton

The structure of zooplankton abundance in both basins considerably differs (Fig. 3). Cladocera are predominant in the Western and Copepoda in the Middle Basin. Rotifera are relatively more abundant in the Western Basin. Cladocera include mostly numerous small (*Bosmina longirostris*, *Chydorus sphaericus*, *Ceriodaphnia* sp.) and large filtrators (*Diapanosoma brachyurum* and *Daphnia* sp.), as well as predatory *Leptodora kindtii*. The most abundant Copepoda species, considered as inefficient filtrators, are *Eurytemora affinis* and *Acartia tonsa*. The highest contribution in the abundance of Rotatoria is reached by small bodied omnivorous taxa: *Keratella cochlearis*, *Keratella cochlearis tecta* and *Filinia longiseta* (Grzyb, 2012; Paturej and Gutkowska, 2015; Paturej et al., 2017).

3.3.3. Macrophytes

Emergent vegetation is well developed in both basins, forming a belt with a width from several tens to several hundred metres up to a depth of approximately 1 m (Fig. 4). Its higher qualitative variability and cover occurs in the Western Basin (Kornijów, 2018). Here, emergent vegetation occurs practically over the entire length of the shore (except for ports). In some places it is composed of two lateral belts: internal, including reed (*Phragmites australis*) and cattail (*Typha*

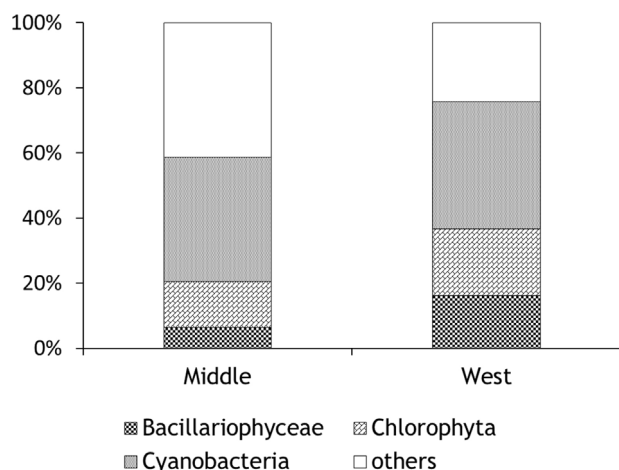


Figure 2 Relative biomass of the main phytoplankton groups in the Western and Middle basins. Mean values from the period 2010–2014, based on data collected by the Province Inspectorate of Environmental Protection in Elbląg and the National Marine Fisheries Research Institute (unpublished).

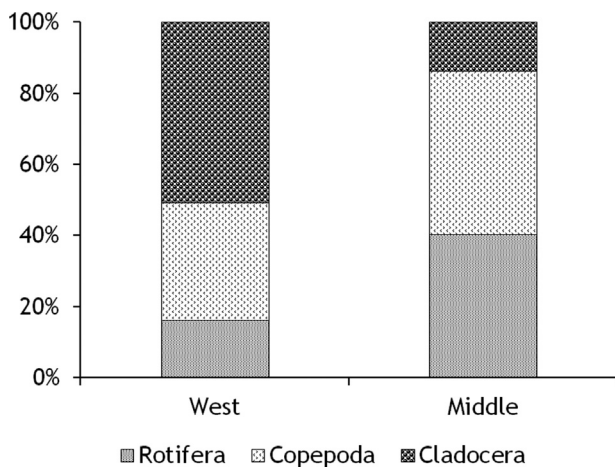


Figure 3 Relative abundance of the main zooplankton groups in the Western and Middle basins. After Paturej and Kruk (2011), modified.

angustipholia), and external, composed of lakeshore bulrush (*Schoenoplectus lacustris*). The zone between the belts, protected from wave action, with a width from several tens to several hundred metres, includes patches of elodeids and nymphaeids. Such a vegetation pattern, developed under the influence of wave energy, is called large-lake phytolittoral.

In the Middle Basin, patches of emergent vegetation are dominated by reed. They cover approximately 80% of the shore (Pawlikowski and Kornijów, 2018). In places free from reed, sandy beaches occur, developing the psammolittoral.

Submerged and floating-leaved vegetation is well developed only in the Western Basin, and especially in the Elbląg

Bay located in its southern part (Kornijów, 2018). Approximately half of the bay's water surface is covered by carpets of fringed water-lily (*Nymphoides peltata*) with an admixture of yellow water-lily (*Nuphar lutea*) (Figs. 4 and 5). Under and among them, elodeid assemblages occur, particularly composed of: Eurasian water-milfoil (*Myriophyllum spicatum*), rigid hornwort (*Ceratophyllum demersum*), Canadian pondweed (*Elodea canadensis*), horned pondweed (*Zanichella palustris*) and curled pondweed (*Potamogeton crispus*). In the remaining areas of the Western Basin, the occurrence of variable submerged and floating-leaved assemblages is limited to a relatively narrow (dozen of metres) near-shore belt (Gajewski, 2010).

In the Middle Basin, practically no nymphaeids occur, and elodeids develop resistant to water motion and drying out clusters of perfoliate pondweed (*Potamogeton perfoliatus*) with an admixture of sago pondweed (*P. pectinatus*) with a diameter from several to several hundred metres, growing up to a depth of approximately 1.2 m (Figs. 5 and 6).

3.3.4. Macroinvertebrates

In both basins, in terms of density, benthos is dominated by detritivorous Tubificinae and larvae of Chironomidae (Kornijów and Pawlikowski, 2015; Rychter and Jabłońska-Barna, 2018). Bivalve *Dreissena polymorpha* is locally encountered on hard bottom. Invasive crabs *Rhithropanopeus harrisi* prefer more saline Middle Basin and *Eriocheir sinensis* overgrown areas, and mouths of rivers (Jabłońska-Barna et al., 2013; Wójcik-Fudalewska and Normant-Saremba, 2016). The biomass structure is dominated by two alien species: bivalve clam *Rangia cuneata* and polychaete *Mareznelleria* sp. (Ezhova et al., 2005; Rychter and Jabłońska-Barna, 2018; Warzocha et al., 2016). The nectobenthos of near-shore

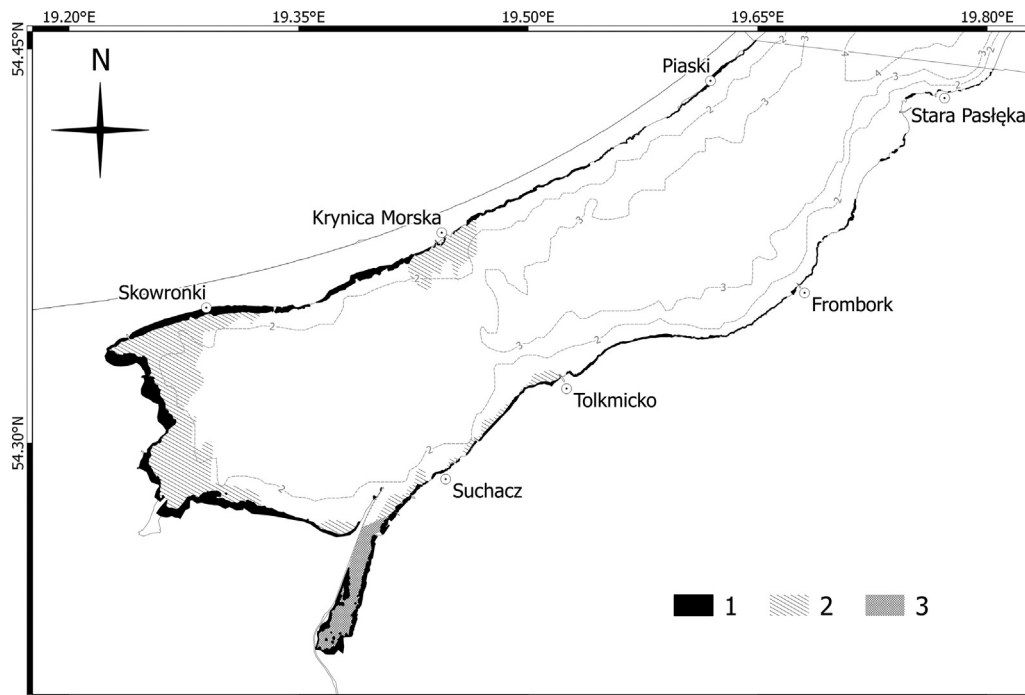


Figure 4 Distribution of emergent vegetation (1), and vegetation with dominance of submerged (2) and floating leaved (3) macrophytes in the Vistula Lagoon. According to Gajewski (2010).



Figure 5 Poor vegetation in the southern part of the Middle Basin shore; monotonous belt of *Phragmites australis* and scattered patches of *Potamogeton perfoliatus*, 2013.08.02 (to the left), and diverse and luxuriantly developed vegetation in the Elbląg Bay (Western Basin); extensive patches of *Nymphoides peltata* and *Myriophyllum spicatum*, 2012.07.27 (to the right).

shallow areas covered with vegetation, except for the least saline parts of the Western Basin, includes abundant predatory shrimp *Palaemon elegans* and filter feeder mysid *Neomysis integer*.

3.3.5. Fish

The ichthyofauna of the lagoon is composed mostly of freshwater species (Nermer et al., 2011; Psuty and Wilkońska, 2009). Marine fish such as flounder (*Platichthys flesus*), turbot (*Scophthalmus maximus*), and Atlantic herring (*Clupea harengus*) occur in the lagoon periodically and mostly in the Middle Basin. The former two practice irregular food migrations. Herring arrives in spring (March–May) and autumn (September–October) for spawning. In those periods, the fish may constitute approximately 80% of harvested fish biomass.

Non-piscivores (except for herring) in the lagoon are dominated by ruffe (*Gymnocephalus cernua*) and roach (*Rutilus rutilus*) (Fig. 7). In the Western Basin, bleak (*Alburnus alburnus*), European smelt (*Osmerus operlanus*)

and silver bream, and in the Middle Basin three-spined stickleback (*Gasterosteus aculeatus*) are also abundant. Greater differences between the two parts of the lagoon occur in the dominance structure of piscivorous fish. An evident division of influence is observed – pikeperch dominates in the Middle, and perch in the Western Basin (Fig. 7).

The percentage of piscivores in the total biomass of planktivorous and predatory fish in the Western Basin amounts to 31% throughout the year (Nermer et al., 2011). In the Middle Basin, their percentage is similar (32%) with the exception of spring and autumn when herring arrives for spawning. Then the value is very low (2%).

3.3.6. Birds

The lagoon together with the adjacent wetlands overgrown by reed beds and riparian forests, and river mouths constitute a well-known refuge of water and wetland birds. The most abundant herbivores include ducks (among others: *Netta rufina*, *Anas clypeata*, *Anas platyrhynchos*, *Anas querquedula*,



Figure 6 Strong winds in the Middle Basin lead to extremely low or high water levels persisting from several hours to several days. Their destructive force limits the possibilities of colonisation by macrophytes, 2013.07.10.

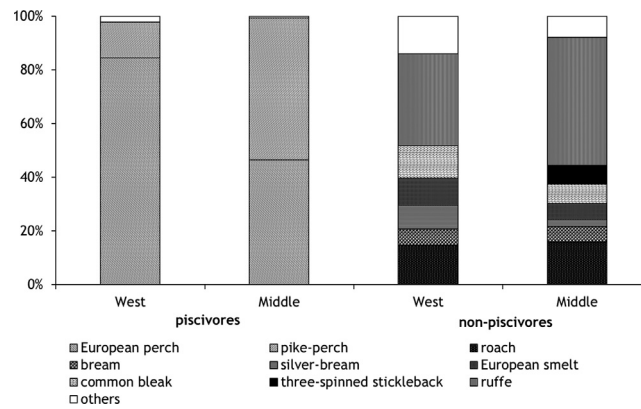


Figure 7 Relative abundance of piscivores (to the left) and non-piscivores without herring (to the right) in the Western and Middle basins.

Based on the data in Nermer et al. (2011).

and *Aythya ferina*), Canada goose (*Branta canadensis*), coot (*Fulica atra*), and mute swan (*Cygnus olor*) (Goc and Mokwa, 2012). The highest numbers of birds, estimated for a total from several to tens thousand individuals, occur in the Western Basin, particularly in the Elbląg Bay and at the mouth of the rivers. Predatory birds feeding on fish particularly include white-tailed eagle *Haliaeetus albicilla* the abundance of which including juvenile individuals is estimated for 40–50 individuals, seagulls (*Hydrocoloeus minutus*), terns (*Chlidonias niger*, *C. hybridus*), herons (*Ardea cinerea*, *Egretta alba*, *Botaurus stellaris*, *Ixobrychus minutus*), grebes (*Podiceps cristatus*) and cormorants (*Phalacrocorax carbo*). The cormorant colony, one of the largest in Europe, is estimated for approximately 11,000 couples (Goc and Mokwa, 2012).

4. Discussion

4.1. Alternative states and driving forces

The recorded differences in primary producers, and especially in the development of macrophyte communities between designated parts of the lagoon allow for ascribing a different alternative state to each of them (Table 2). The Western Basin currently shows the features of the transition state, the Elbląg Bay located in its south part – the macrophyte-dominated state, and the Middle Basin – the phytoplankton-dominated state.

Only the Elbląg Bay has retained its macrophyte-dominated state until now. It is the most freshwater region,

Table 2 Characteristic features determining the alternative status of distinguished basins. EMV – emergent vegetation, SUV – submerged vegetation, FLV – floating-leaved vegetation.

Parameter Status	Western Basin (Elbląg Bay) Macrophyte-dominated	Western Basin (other area) Transition state	Middle Basin Phytoplankton-dominated
EMV	A continuous belt, with domination of: <i>Phragmites communis</i> , <i>Schoenoplectus lacustris</i> and <i>Typha angustifolia</i>	A continuous or two parallel belts composed mostly <i>P. communis</i> and <i>S. lacustris</i>	Intermittent monospecific belt of <i>P. communis</i>
SUV	Vast patches rich in species, with domination of <i>Ceratophyllum demersum</i> and <i>Myriophyllum spicatum</i> , covering over 40% of bottom surface	From large patches (<i>Nitellopsis obtusa</i>) (Bay Kały) to several dozen metres belts of outside emergent macrophytes (mostly <i>Potamogeton perfoliatus</i> and <i>C. demersum</i>)	Small or medium-sized scattered patches of <i>P. perfoliatus</i> and <i>Stuckenia pectinata</i>
FLV	Extensive beds, mostly of <i>Nymphoides peltata</i> with admixture of <i>Nuphar lutea</i> , covering about 80% of water surface	From extensive (Bay Kały) to small stands, mostly <i>N. lutea</i>	Hardly present (<i>N. lutea</i>)
Phytoplankton	Elevated percentage of diatoms, cyanobacterial blooms occasional	Elevated percentage of diatoms and chlorophytes, cyanobacterial blooms frequent in summer	High percentage of cyanobacteria, cyanobacterial blooms frequent in summer
Transparency	From high to medium	From medium to low	Low

largely isolated from the influence of the main basin of the lagoon. At least since the 1950s emergent vegetation has surrounded the bay with a wide and almost continuous ring, and nymphaeids and elodeids have covered more than half of the bottom area (Pliński, 1995; Pliński et al., 1978, and own observations). The macrophyte-dominated state in the bay is maintained in spite of many years (1970–1990) of strong nutrient supply by the Elbląg River (Cieśliński, 2002), as well as supply of faeces of thousands of individuals of waterfowl (Goc and Mokwa, 2012). The vegetation is evidently not impoverished as a result of herbivory by birds, frequently considered as the cause of failure of restoration measures (Phillips et al., 2016).

The literature data suggest that the present transition state of the remaining area of the Western Basin has been lasting since the early 1980s. Before, the area showed many features of macrophyte-dominated state, similarly as the Elbląg Bay. A very wide belt of emergent vegetation of several hundred metres over km-long sections was divided by an open water zone developing large-lake littoral. It was inhabited by luxuriantly developed floating-leaved and submerged vegetation, including extensive meadows of various species of charales (Pliński et al., 1978; Szarejko, 1955). The external belt of helophytes is currently residual, and submerged vegetation severely impoverished qualitatively has been limited to an intermittent belt of approximately a dozen metres wide on the external side of the emergent vegetation.

The shift of the prevailing area of the Western Basin from the macrophyte-dominated to transition state probably occurred as a consequence of interference from many human interactions. For several decades the waters had been supplied with domestic and industrial sewage. The 1970s was also a period of intensified application of mineral fertilisers. As a consequence, the concentration of nutrients in water gradually increased (Margoński and Horbowa, 2003; Różańska and Wiktor, 1978). This, however, did not lead to more prosperous development of phytoplankton (Latała, 1978; Pliński and Simm, 1978; Renk et al., 2001; Witek et al., 2010), probably due to bad light conditions caused by resuspension and substantial dynamics of salinity and water level fluctuations. Notice that the shift from the macrophyte-dominated to phytoplankton-dominated state did not occur in the Elbląg Bay in spite of an approximate, or even higher load of nutrients (Cieśliński, 2002). Therefore, the shrinkage of macrophytes with gradually increasing nutrient load, the mechanism suggested by some authors (Dahlgren and Kautsky, 2004; Krause-Jensen et al., 2008; Munkes, 2005), probably was not determined by excessive development of algae.

Another concept assumes that the shift from one state to another occurs as a result of the disturbance of the environment's resilience (defined as the magnitude of perturbation that a system can absorb) caused by a strong external driver (Holling, 1973). Based on such an assumption, the nutrients are not the driver themselves, but they influence the threshold for the actual drivers causing the switch (Folke et al., 2004; Moss, 2007; Phillips et al., 2016). In the analysed case, there must have been at least several such drivers with combined and synergistic effects. The most important one seems to be the effect of hydro-engineering dredging works, conducted for several years in the first half of the 1980s along the western shore of the lagoon. Their side effect is always

strong water turbidity, as well as release of nutrients and pollutants from sediments over a considerably larger area than that directly affected by such works. After conducting the works, part of the phytolittoral with elodeid and nymphaeid assemblages disappeared (Chmara, 2012; Goc and Mokwa, 2012). The negative effect of dredging works on the vegetation is confirmed by the disappearance of the extensive meadows of *Nitellopsis obtuse* in 2014 in the Kały Bay. The works had been conducted one year before at the mouth of the Elbląg River and at the inlet to the Kały Bay. The dredging must have affected not only plants, but also other organisms. For example, its long-term negative effect on the spawning grounds of pikeperch, and a strong decrease in its abundance in the Vistula Lagoon was documented by Borowski and Dąbrowski (1998). This might have resulted in the weakening of the cascade effect. Already before, in the 1950s and 1960s, the positive effect of predatory fish on the environment had been strongly limited due to the collapse of the population of pike (Psuty-Lipska and Borowski, 2003).

Chemical compound tributyltin could have also contributed to the degradation of the vegetation. In the 1970s and 1980s it was commonly applied for the protection of nets against invasive hydroid *Cordylophora caspia* almost throughout the lagoon. Tributyltin proved to be harmful not only for invertebrates and fish, but also for plants (Brooke et al., 1986). Sayer et al. (2006) suggest that this compound may promote the replacement of macrophytes by phytoplankton through reducing populations of grazing organisms in water bodies already affected by eutrophication.

Whereas shading by periphyton does not seem to be a driver completely eliminating macrophytes, it undoubtedly contributed to the worsening of the plants' condition. Weakened plants could more easily yield to the pressure of omnivorous/herbivorous invertebrates (Bakker et al., 2016; Hidding et al., 2016). Next to crustaceans (Chinese mitten crab *E. sinensis*, dwarf crab *R. harrisi*, and spiny-cheek crayfish *Orconectes limosus*), they also include several species of Amphipoda. The latter reach considerably smaller sizes, but they inhabit plants in enormous numbers, so their cumulative effect can be substantial (Kornijów, 1996).

The Western Basin currently remains in a transition state balancing between the phyto- and macrophyte-dominated state. Periodically, underwater meadows of elodeids and charales develop over extensive areas, particularly in the Kały Bay protected from wind. Further dredging works, however, lead to their repeated destruction. Each time, this entails the loss of a chance, or at least long-term delay, of gradual, progressing eastwards, improvement of water quality. The plants, and particularly charales, play an important role in the restoration of degraded water bodies, influencing sedimentation and nutrients concentration (Blindow et al., 2014; Van den Berg and Coops, 1999). In addition macrophytes stabilise and oxygenate sediments, and therefore limit internal supply of phosphorus compounds. Moreover, they compete with phytoplankton for nutrients, have an allelopathic effect on algae, and provide habitat structure limiting the strength of the top-down effect of fish on zooplankton, controlling the development of phytoplankton (e.g., Blindow et al., 2014; Moss et al., 1996; Phillips et al., 2016).

The Middle Basin is phytoplankton-dominated, and has remained as such for at least 60 years. Currently, similarly as in the 1950s (Ringer, 1959), its bottom is overgrown by locally

large-sized (several hundred metres in diameter), although together not exceeding 5% of the littoral area, patches of *P. perfoliatus*, particularly along the southern shore. Beginning from July, the surface of plants is covered by a thick layer of periphyton. Its abundance can be explained by complete lack of snails (unpublished), considered as the most efficient grazers (Underwood, 1991). The time of the existence of shaded elodeids and nymphaeids in the central part of the lagoon was reduced, and currently lasts for approximately three months (Pawlikowski and Kornijów, 2018). This is a typical manifestation of excessive fertility of the water body, called the “sandwich effect” (Sayer et al., 2010) due to the fact that the period before the appearance of plants and after their disappearance is characterised by strong development of phytoplankton.

The tendency for higher than average concentrations of phytoplankton in more saline Middle Basin can be related to different dominance structure of filtering zooplankton, higher predation pressure on zooplankton, and in consequence lower grazing capacity than in the less saline western part of the lagoon (Jeppesen et al., 1994; Moss, 1994). In contrast to the Western Basin, in the Middle one, crustation zooplankton does not include efficient filter-feeding cladocerans such as: *Daphnia* sp., *Bosmina* sp., and *Ceriodaphnia quadrangula*. Instead, it is dominated by omnivorous *E. affinis* and *A. tonsa*, prosperous in estuaries with highly suspended particulate matter dominated by non-living particles (Richman et al., 1977; Tackx et al., 2003). In the absence of Cladocera, efficient filtrators Rotatoria predominate, freed from food competition. Due to lack of elodeids, water turbidity remains the only refuge for zooplankton against fish predation (Horppila and Liljendahl-Nurminen, 2005). In addition to freshwater fish, stickleback *G. aculeatus* and ziege *Pelecus cultratus* constitute permanent components of the planktivorous ichthyofauna. In spring, zooplankton is additionally strongly affected by Baltic herring *C. harengus* (Dmitrieva and Semenova, 2012; Grzyb, 2012) spawning in more saline regions of the lagoon (Nermer et al., 2011). First, zooplankton is eaten by shoals of adult fish, and then for at least approximately three months also by their larvae and fry until they leave the lagoon. The larvae reach very high densities, even up to more than one hundred individuals per m³ (Grzyb, 2012), and are able to remove approximately 50% of zooplankton standing stock (Nauhenko, 2009). This is probably the cause of the strong decrease in the abundance of zooplankton observed in June (Grzyb, 2012). In addition to planktivorous fish, in the more saline Middle Basin in the open water zone, predatory cladocerans *Cercopagis pengoi* are occasionally abundant, and in the littoral phytophilous crustaceans *N. integer* and *P. elegans*. They may exert an additional top-down impact on zooplankton (Jeppesen et al., 1994; Lehtiniemi and Gorokhova, 2008; Lesutiene et al., 2014; Moss, 1994). In consequence, higher cumulative predation by invertebrates and fish may lead to low zooplankton/phytoplankton ratio, and accelerate eutrophication processes.

The above discussion concerns the role of different drivers in the transition from one state to another, or in the maintenance of the already existing one in the designated parts of the Vistula Lagoon. It is also worth mentioning the top-down causal factor common for the entire lagoon area, particularly strong from the mid 1980s. That includes piscivorous birds,

including large white-tailed eagle and many smaller such as: herons, seagulls, grebes, and in particular cormorants – highly efficient predators, even in turbid waters (Gremillet et al., 2012). They control the abundance of mainly small fish such as: ruffe, roach, round goby, or stickleback (Stempniewicz et al., 2003). It is estimated that only the cormorants themselves eat from 1.2 to 2.1 tonnes of fish annually, a biomass comparable to that harvested by fishermen (Kornijów, 2018). Whereas fishermen catch large and economically valuable fish, cormorants mainly prey on small planktivorous species. This may result in the cascading effect leading to reduced pressure of small fish on zooplankton and an increase in zooplankton grazing on phytoplankton. Remains of undigested fish are not returned to water in the form of faeces. They are deposited on land. Therefore, cormorants also contribute to continuous export of nutrients from the aquatic environment. There is at least one example of water quality remarkably improved by the activity of cormorants (Leah et al., 1980).

4.2. Implications for the theory

According to the alternative stable states theory, an ecosystem can remain in one of the states in a broad range of nutrient concentrations (Scheffer et al., 1993). The Vistula Lagoon constitutes an interesting case in which at very approximate nutrient concentrations, but under different hydromorphological, hydrological, and anthropopressure conditions, three different, alternative states developed and co-existed in a single water body. Such a theoretical possibility was earlier considered by Knowlton (2004). Drivers considered to determine the distinguished alternative states are listed in an arbitrarily accepted order (from the most to the least important) in Table 3.

The dominant driver regulating the structure and processes occurring in the lagoon seems to be wave exposure. Only inconsiderable wave action, such as that in the sheltered Elbląg Bay, permits the existence of the macrophyte-dominated state (Figs. 4 and 5). In the exposed central part of the basin, where waves periodically reach a height of up to 1.5 m (Chubarenko et al., 2012), such a state is very unlikely, irrespective of the level of nutrient concentrations (Coops et al., 1991). The destructive effect of wave action on macrophytes and other organisms is magnified by substantial water level fluctuations reaching up to 1.2 m, which periodically permit eroding of deeper located parts of the bottom (Fig. 6). Moreover, wave energy causes resuspension which on the one hand worsens the light conditions and constrains the re-establishment of macrophytes (Green and Coco, 2014; Lawson et al., 2007), and on the other hand magnifies the internal supply of nutrients (Sondergaard et al., 1992), stimulating the development of phytoplankton and periphyton. The Vistula Lagoon can be therefore included to typical coastal water bodies, maintained first of all by physical constraint (Perez-Ruzafa et al., 2011). Water salinity is the second in terms of strength of effect. It determines the structure of biocoenoses, including the contribution of filtrators and predators, and indirectly affects the strength of top-down regulation (Jeppesen et al., 1994; Moss, 1994). The next driver, third in terms of “importance” are bottom-up regulations. They influence the development of vegetation and associated biota

Table 3 The major drivers at four-scale magnitude (low, medium, significant, high) of the distinguished states in particular areas of the Vistula Lagoon.

Area Status	Western Basin (including Elbląg Bay) Macrophyte-dominated/transition state	Middle Basin Phytoplankton-dominated
Wind and wave exposure	From low to medium – shores protected to the west	High – unprotected shores, periodically strong winds from the Baltic Sea, storms
Salinity	From low to medium – salinity < 2 PSU, periodical inflow of more saline waters from the east	High – salinity > 2–5 PSU
Bottom-up forces	From high (nutrient supply by bird faeces in Elbląg Bay) to medium – inflow of nutrients from rivers, periodical resuspension and internal supply of phosphorus	High – permanent resuspension and internal supply of phosphorus compounds
Anthropogenic impact (fishery, toxins, boating, pollution, hydro-engineering works)	From low (Elbląg Bay as a reserve) to high until the first half of the 2000s, currently moderate	High until the first half of the 2000s, currently moderate
Multi-level top-down regulations	Significant – very abundant: piscivorous birds, strong pikeperch and perch population, effective grazers (Cladocera)	Medium – very abundant: piscivorous birds, strong pikeperch and perch population, numerous but ineffective phytoplankton grazers (Copepoda, Rotatoria)
Pressure of predators on zooplankton	From low (refuge effect by vegetation structure in Elbląg Bay) to medium – mainly freshwater fish	High – freshwater and marine fish, predatory crustaceans
Herbivory on elodeids/nymphaeids	High – abundant: waterfowl, crayfish, insect larvae, amphipods	Low – low density of waterfowl, abundant: crayfish, insect larvae, amphipods. No snails

particularly in regions of the lagoon protected from wind. A similar conclusion was presented by Viaroli et al. (2008) investigating the role of different drivers determining the state of eutrophic Mediterranean coastal lagoons.

The importance of the drivers concerning trophic interactions, summed up in Table 3 was discussed in Section 4.1.

4.3. Implications for management

The aforementioned drivers with proposed hierarchical order of importance (Table 2) constitute a mutually supplementing system determining the current state of particular regions of the lagoon (Table 2). Their knowledge can be helpful in the development of programmes concerning: restoration measures, environmental impact assessments, or sustainable management of the lagoon's resources. The specification of guidelines for the improvement of the ecological state for particular areas of the Vistula Lagoon should consider not only the presence of the aforementioned drivers, but also conditions such as: the vast surface area of the lagoon, shallowness of its basin and the related susceptibility to resuspension, and already strengthened feedback mechanisms (among others: dominance of phytoplankton, high percentage of cyanobacteria, fine-grained stirred-up sediments difficult to colonise by macrophytes, presence of hydrogen sulphide in sediments as the effect of excessive concentration of organic matter, and high top-down pressure on zooplankton). They can slow down the improvement processes or even make them impossible. The above suggests the obvious conclusion that the possibilities of improvement of ecological

conditions in the lagoon, including causing the shift from the phytoplankton-dominated to macrophyte-dominated state, are very limited. It is practically impossible to reduce the strength of the first driver in the hierarchy, namely wave exposure. The application of solutions aimed at limiting the destructive effect of waves, proposed for lakes, e.g. deepening, wind reducing barriers, sand capping of the sediment, changes in the water level, and alterations to the shoreline profile (Penning et al., 2013) is hardly possible in the case of the Vistula Lagoon due to its size. Therefore, it is worth emphasising the role the reed rush in the lagoon plays in wave attenuation and development of habitat conditions. The wide belts of reed occurring on many sections of the Vistula Lagoon, with a mean density of $70 \text{ stems m}^{-2} \pm 18 \text{ SD}$, can substantially modify water insolation, temperature, and oxygenation, as well as the grain size and chemical composition of sediments (Pawlikowski and Kornijów, 2018). Near-shore reed beds, similarly as submerged vegetation, are also important for the protection of shores against erosion, and as a filter for nutrients and organic material flushed from the catchment (Berthold et al., 2018; Christianen et al., 2013; Moller et al., 2011; Rupprecht et al., 2017). Due to this, all human activities should be conducted in a way minimising the impact on both aquatic and riparian vegetation.

According to English and Danish researchers (Jeppesen et al., 1994; Moss, 1994), water quality can be considerably improved by a reduction of salinity to a level below 2‰. It can even lead to a switch from the phytoplankton to macrophyte-dominated state. It may seem that the postulate of a decrease in water salinity in the Vistula Lagoon is not feasible

considering the scale of the undertaking. Examples of practical application of such a solution in coastal lagoons are known, however. In the Ringkøbing Fjord on the western coast of Denmark, water salinity is driven by sluice management. Due to a small change in water salinity over a period of two years, the ecosystem changed from a nutrient-driven turbid green water to a grazing-controlled clear water (Hakanson and Bryhn, 2008). Notice also that in the past, human activity has already led to a substantial change in the salinity of the Vistula Lagoon, unfortunately involving its increase. This occurred over the last hundred years, after the construction of locks and weirs in the early 20th century, blocking the inflow of the Vistula River to the lagoon, and redirecting the main river water masses directly to the Baltic Sea. It is justified to claim that the reduction of the inflow of waters from the Vistula River to the lagoon in the 20th century saved the ecosystem from total degradation in the period 1970s–1990s when the inflowing rivers were extremely polluted and resembled sewers (Glasby and Szefer, 1998). The currently existing hydro-technical infrastructure would probably permit a controlled increase in the supply of freshwater to the lagoon and a decrease in salinity. The analysis of the justification of such a solution, similarly as the resulting far-reaching consequences, exceeds the thematic scope of this paper.

According to Jeppesen et al. (2007), measures other than a decrease in salinity, including those leading to a change in the dominance structure of fish and strengthening of the cascade effect, are inefficient in the case of salinity exceeding 2‰, and do not result in the improvement of water quality. Consider, however, that sustaining the current pressure of zooplankton on phytoplankton requires keeping the abundance of planktivorous/omnivorous fish on a relatively low level, possibly through the maintenance of numerous stock of predatory fish with relevant age structure (Eriksson et al., 2009; Sieben et al., 2011). In the case of the Vistula Lagoon, this particularly concerns pikeperch and perch. Their contribution in the total biomass of planktivorous and predatory fish in the lagoon for most of the year amounts to approximately 30%. It is assumed that effective top-down pressure, which can translate into efficient phytoplankton control by zooplankton through the cascade effect, requires at least 50% share of predators in the fish biomass (Moss et al., 1996). In the analysed case, also very strong pressure of piscivorous birds needs to be taken into account, including cormorants having a synergic effect on fish populations, together with predatory fish.

Pikeperch, unlike pike, is a species well adapted to turbid waters due to the specific eye structure and well developed sense of smell (Sandstrom and Karas, 2002). Although perch is a typically visual predator, well adapted to macrophyte dominated habitats (Kornijów et al., 2016), it also thrives in the lagoon, perhaps due to the fact that strongly increased water turbidity only occurs periodically as a result of resuspension. Both of the species control the abundance of not only small planktivorous fish, but also zooplanktivorous crustaceans *N. integer* and *Palaemon elegance* (unpublished). Unfortunately, in spite of more than a threefold reduction of the number of fishing vessels in the 2000s, and implementation of a number of fishing restrictions concerning fishing gears and catch limits, the population of both of the species has been showing symptoms of overfishing over the recent years.

This is suggested by a relatively high contribution of individuals only from two or three age classes (age groups 3–5), and low contribution of those with large sizes (Psuty and Wilkońska, 2009). The situation is so serious it may lead to the collapse of the populations of those species of key importance for the functioning of the lagoon. On the other hand, as a result of lack of interest of fishermen (and shortage of large pikeperch), the populations of cyprinid fish: roach and bream, include numerous older individuals. At this stage of life, they are benthivorous, and can intensify bioresuspension (Tatrai et al., 1997). Moreover, they contribute to the spawning success of the population, and their planktivorous juvenile stages increase the feeding pressure on zooplankton. It is therefore needed to limit and control the abundance of large cyprinid fish which remain outside the feeding spectrum of the currently dominating age groups of perch and pikeperch. A solution could be a decrease in the fishing pressure on pikeperch, and an increase in the size-limit. An increase in the abundance of European catfish, present in the lagoon, through fish stocking could be considered, too. The fish, however, grows slowly and over a long period of time. In the conditions of substantial fishing pressure, this largely limits the chance of reaching sufficient sizes by a high number of individuals to efficiently control the population of large cyprinids. Meanwhile, next to fishermen, also white-tailed eagles, numerous in the area, may play a substantial role in controlling the abundance of large cyprinids (Ekblad et al., 2016).

Considerable improvement of water quality and transformation of biocoenosis might occur independently from human measures as a result of the bio-engineering activity of the alien bivalve *R. cuneata*. This thermophilous clam originating from the Gulf of Mexico has been present in the Vistula Lagoon for approximately 8 years. It reaches a length of 4–5 cm and shows fast rate of growth of even 20–25 mm in the first year of life. As a non-selective filtrator, it feeds both on phytoplankton and abioses-ton. Harsh winters lead to high mortality of the clam population. However, it rapidly regenerates in the following years (Kornijów et al., 2018; Warzocha et al., 2016), reaching abundances of up to 1000 ind. m⁻². The literature provides examples of positive effect of *R. cuneata* on sediment stabilisation, limiting the development of phytoplankton, and as a consequence improvement of water transparency and reconstruction of elodeid assemblages (Cercio and Noel, 2010; Shaffer et al., 2009). Considering the relatively long time of water retention and small depth of the Vistula Lagoon, the occurrence of a similar effect can be presumed. This is suggested by the observation in 2017 of the co-occurrence of very high density of *Rangia* in the central part of the lagoon (mean: 1147 ± 353 SD) and exceptionally high Secchi disc depth values in August and September (180 and 140 cm, respectively; own unpublished data) as compared to the multiannual mean value amounting to only approximately 40 cm.

Taking into consideration local hydromorphological and hydrological factors, as well as the composition of biocoenoses, the Western Basin, most freshwater part of the Vistula Lagoon seems to have the greatest chance for restoring the macrophyte-dominated state. The process would probably be already advanced if not for the dredging works conducted every several years. Further hydro-technical works planned for the period 2018–2022 can have a similar effect on the

environment, but at a considerably greater scale of the entire lagoon. They involve digging the canal through the Vistula Spit, and construction of a waterway with a depth of 5 m, width from 60 to 100 m, and length, depending on the finally arranged location, from 9 to 26 km in the western part of the lagoon. The execution of the waterway itself, and its further necessary periodical deepening (due to the shallow character of the water body and susceptibility to resuspension) may lead to serious cascade of changes in the environment and food chain, resulting in complete degradation of the ecosystem (Kornijów, 2018).

The phytoplankton-dominated state present in the major area of the Vistula Lagoon does not mean that the situation cannot become even worse. In the conditions of both the macrophyte-dominated and phytoplankton-dominated states, a broad spectrum of habitat conditions can occur, depending on among others the dominance structure of primary producers (Moss et al., 1996). Consequences of the phytoplankton-dominated state of extremely degraded hypertrophic water bodies are various, and always troublesome. Chlorophyll-*a* concentrations can be even several times higher than in the Vistula Lagoon. High concentrations of cyanobacterial toxins are maintained throughout the year, constituting a threat to the wildlife and people. The species diversity of biocoenoses is strongly reduced. The fish stock is limited to several economically useless species, and the smell of decomposing algae extends many kilometres around the water body. Such situations are encountered in hypertrophic lakes and lagoons (Pawlik-Skowronska et al., 2008; Witek et al., 2010). In spite of remaining in the phytoplankton-dominated state over the majority of its area, the Vistula Lagoon still shows features of a eutrophic and not hypertrophic water body (Margoński and Horbowa, 2003; Nawrocka and Kobos, 2011; Witek et al., 2010), and it can remain this way under the condition of sustainable use of its resources and conducting pro-ecological investment policy, if not considering the possibilities of improvement of the state of the lagoon, at least aiming at not increasing the current environmental threats.

Acknowledgements

The work was conducted as a part of statutory activities of the Department of Fishery Oceanography and Marine Ecology of the National Marine Fisheries Research Institute, project number: Dot16/Vistula. I am grateful to Dr. Aleksander Drgas, Dr. Jacek Malicki and Prof. Tomasz Linkowski for their helpful comments at the early stage of the manuscript. MSc Krzysztof Pawlikowski kindly helped in preparing the drawings.

References

- Bakker, E.S., Wood, K.A., Pages, J.F., Veen, G.F., Christianen, M.J.A., Santamaria, L., Nolet, B.A., Hilt, S., 2016. Herbivory on freshwater and marine macrophytes: a review and perspective. *Aquat. Bot.* 135, 18–36, <http://dx.doi.org/10.1016/j.aquabot.2016.04.008>.
- Berthold, M., Karstens, S., Buczek, U., Schumann, R., 2018. Potential export of soluble reactive phosphorus from a coastal wetland in a cold-temperate lagoon system: buffer capacities of macrophytes and impact on phytoplankton. *Sci. Tot. Env.* 616–617, 46–54, <http://dx.doi.org/10.1016/j.scitotenv.2017.10.244>.
- Blindow, I., Hargeby, A., Hilt, S., 2014. Facilitation of clear-water conditions in shallow lakes by macrophytes: differences between charophyte and angiosperm dominance. *Hydrobiologia* 737 (1), 99–110, <http://dx.doi.org/10.1007/s10750-013-1687-2>.
- Borowski, W., Dąbrowski, H., 1998. The influence of dredging on the ecological value of pikeperch and common bream spawning grounds near Gold Island in the Vistula Lagoon. *Rep. Sea Fish. Inst.* 1997. 102–110.
- Brooke, L.T., Call, D.J., Poirier, S.H., Markee, T.P., Lindberg, C.A., McCauley, D.J., Simonson, P.G., 1986. Acute toxicity and chronic effects of bi(tri-butyltin) oxide to several species of freshwater organisms. *Center for Lake Superior Environmental Studies Report*, Univ. Wisconsin, Superior, WI, p. 20.
- Cerco, C.F., Noel, M.R., 2010. Monitoring, modeling, and management impacts of bivalve filter feeders in the oligohaline and tidal fresh regions of the Chesapeake Bay system. *Ecol. Model.* 221 (7), 1054–1064, <http://dx.doi.org/10.1016/j.ecolmodel.2009.07.024>.
- Chmara, R., 2012. Vegetation and habitats. In: Przewoźniak, M. (Ed.), *Environmental Impact Assessment of the Long-term Program. Construction of a Waterway Connecting the Vistula Lagoon with the Gdańsk Bay*. *Biuro Projektów i Wdrożeń Ekologicznych PROEKO*, 132–139, (in Polish).
- Christianen, M.J.A., van Belzen, J., Herman, P.M.J., van Katwijk, M. M., Lamers, L.P.M., van Leent, P.J.M., Bouma, T.J., 2013. Low-canopy seagrass beds still provide important coastal protection services. *PLoS ONE* 8 (5), e62413, <http://dx.doi.org/10.1371/journal.pone.0062413>.
- Chubarenko, B.V., Leitsina, L.V., Esiukova, E.E., Kurennoy, D.N., 2012. Model analysis of the currents and wind waves in the Vistula Lagoon of the Baltic Sea. *Oceanology* 52 (6), 748–753, <http://dx.doi.org/10.1134/S000143701206001x>.
- Cieśliński, R., 2002. An attempt to assess the impact of pollutants from the territory of Elbląg City on the water quality of Elbląg River. In: Górka, Z.Z., Jelonek, A. (Eds.), *Geographical Determinants of the Development of Małopolska*, Inst. Geogr. Spatial Manage., Jagiellonian Univ., Kraków, 139–145, (in Polish).
- Coops, H., Boeters, R., Smit, H., 1991. Direct and indirect effects of wave attack on helophytes. *Aquat. Bot.* 41 (4), 333–352, [http://dx.doi.org/10.1016/0304-3770\(91\)90052-7](http://dx.doi.org/10.1016/0304-3770(91)90052-7).
- Dahlgren, S., Kautsky, L., 2004. Can different vegetative states in shallow coastal bays of the Baltic Sea be linked to internal nutrient levels and external nutrient load? *Hydrobiologia* 514 (1–3), 249–258, http://dx.doi.org/10.1007/978-94-017-0920-0_23.
- Dmitrieva, O.A., Semenova, A.S., 2012. Seasonal dynamics and trophic interactions of phytoplankton and zooplankton in the Vistula Lagoon of the Baltic Sea. *Oceanology* 52 (6), 785–789, <http://dx.doi.org/10.1134/S0001437012060033>.
- Ekblad, C.M.S., Sulkava, S., Stjernberg, T.G., Laaksonen, T.K., 2016. Landscape-scale gradients and temporal changes in the prey species of the white-tailed eagle (*Haliaeetus albicilla*). *Ann. Zool. Fenn.* 53 (3–4), 228–240.
- Eriksson, B.K., Ljunggren, L., Sandstrom, A., Johansson, G., Mattila, J., Rubach, A., Raberg, S., Snickars, M., 2009. Declines in predatory fish promote bloom-forming macroalgae. *Ecol. Appl.* 19 (8), 1975–1988, <http://dx.doi.org/10.1890/08-0964.1>.
- Ezhova, E., Żmudziński, L., Maciejewska, K., 2005. Long-term trends in the macrozoobenthos of the Vistula Lagoon, southeastern Baltic Sea. *Species composition and biomass distribution*. *Bull. Sea Fish. Inst.* 1, 55–73.
- Folke, C., Carpenter, S., Walker, B., Scheffer, M., Elmqvist, T., Gunderson, L., Holling, C.S., 2004. Regime shifts, resilience, and biodiversity in ecosystem management. *Annu. Rev. Ecol. Evol. Syst.* 35, 557–581, <http://dx.doi.org/10.1146/annurev.ecolsys.35.021103.105711>.
- Gajewski, L. (Ed.), 2010. *Research of the Vistula Lagoon bottom (including the Elbląg Bay)*. Final Report. Report No. 334. Maritime Inst., Gdańsk; Maritime Office, Gdynia, 1–96, (in Polish).

- Glasby, G.P., Szefer, P., 1998. Marine pollution in Gdańsk Bay, Puck Bay and the Vistula Lagoon, Poland: an overview. *Sci. Total Environ.* 212 (1), 49–57.
- Goc, M., Mokwa, T., 2012. Birds. In: Przewoźniak, M. (Ed.), *Construction of a waterway connecting the Vistula Lagoon with the Gdańsk Bay*, Biuro Projekt. Wdroż. Ekol. PROEKO, 145–155, (in Polish).
- Green, M.O., Coco, G., 2014. Review of wave-driven sediment resuspension and transport in estuaries. *Rev. Geophys.* 52 (1), 77–117, <http://dx.doi.org/10.1002/2013rg000437>.
- Gremillet, D., Nazirides, T., Nikolaou, H., Crivelli, A.J., 2012. Fish are not safe from great cormorants in turbid water. *Aquat. Biol.* 15 (2), 187–194, <http://dx.doi.org/10.3354/ab00430>.
- Grzyb, A., 2012. The “match-mismatch” phenomenon and the effect of larval density as a proposal to explain the herring recruitment mechanism in the Vistula Lagoon. (PhD Thesis). Inst. Inland Fish, Olsztyn, (in Polish).
- Hakanson, L., Bryhn, A.C., 2008. Goals and remedial strategies for water quality and wildlife management in a coastal lagoon – a case-study of Ringkobing Fjord, Denmark. *J. Environ. Manage.* 86 (3), 498–519, <http://dx.doi.org/10.1016/j.jenvman.2006.12.006>.
- Hakanson, L., Lindgren, D., 2008. On regime shifts and budgets for nutrients in the open Baltic Proper: evaluations based on extensive data between 1974 and 2005. *J. Coast. Res.* 24 (4c), 246–260, <http://dx.doi.org/10.2112/07-0870.1>.
- Hidding, B., Bakker, E.S., Hootsmans, M.J.M., Hilt, S., 2016. Synergy between shading and herbivory triggers macrophyte loss and regime shifts in aquatic systems. *Oikos* 125 (10), 1489–1495, <http://dx.doi.org/10.1111/oik.03104>.
- Holling, C.S., 1973. Resilience and stability of ecological systems. *Annu. Rev. Ecol. Syst.* 4, 1–23, <http://dx.doi.org/10.1146/annurev.es.04.110173.000245>.
- Holmes, R.W., 1970. The Secchi disk in turbid coastal waters. *Limnol. Oceanogr.* 15 (5), 688–694.
- Horpilla, J., Liljendahl-Nurminen, A., 2005. Clay-turbid interactions may not cascade – a reminder for lake managers. *Restor. Ecol.* 13 (3), 242–246, <http://dx.doi.org/10.1111/j.1526-100X.2005.00031.x>.
- Hughes, T.P., Carpenter, S., Rockstrom, J., Scheffer, M., Walker, B., 2013. Multiscale regime shifts and planetary boundaries. *Trends Ecol. Evol.* 28 (7), 389–395, <http://dx.doi.org/10.1016/j.tree.2012.08.022>.
- Jabłońska-Barna, I., Rychter, A., Kruk, M., 2013. Biocontamination of the western Vistula Lagoon (south-eastern Baltic Sea, Poland). *Oceanologia* 55 (3), 751–763, <http://dx.doi.org/10.5697/oc.55-3.751>.
- Jeppesen, E., Sondergaard, M., Kanstrup, E., Petersen, B., Eriksen, R.B., Hammershoj, M., Mortensen, E., Jensen, J.P., Have, A., 1994. Does the impact of nutrients on the biological structure and function of brackish and fresh-water lakes differ? *Hydrobiologia* 275 (1), 15–30, <http://dx.doi.org/10.1007/BF00026696>.
- Jeppesen, E., Sondergaard, M., Pedersen, A.R., Jurgens, K., Strzelczak, A., Lauridsen, T.L., Johansson, L.S., 2007. Salinity induced regime shift in shallow brackish lagoons. *Ecosystems* 10 (1), 48–58, <http://dx.doi.org/10.1007/s10021-006-9007-6>.
- Knowlton, N., 2004. Multiple “stable” states and the conservation of marine ecosystems. *Prog. Oceanogr.* 60 (2–4), 387–396, <http://dx.doi.org/10.1016/j.poccean.2004.02.011>.
- Kornijów, R., 1996. Cumulative consumption of the lake macrophyte *Elodea* by abundant generalist invertebrate herbivores. *Hydrobiologia* 319, 185–190, <http://dx.doi.org/10.1007/Bf00013731>.
- Kornijów, R., 2018. Chapter 7.8. Trophic interactions versus salinity and water quality in the Vistula Lagoon. Current status and threats. In: Bolatek, J. (Ed.), *The Vistula Lagoon at the Beginning of the 21st Century*. PWN, Warsaw (in press, in Polish).
- Kornijów, R., Measey, G.J., Moss, B., 2016. The structure of the littoral: effects of waterlily density and perch predation on sediment and plant-associated macroinvertebrate communities. *Freshw. Biol.* 61 (1), 32–50, <http://dx.doi.org/10.1111/fwb.12674>.
- Kornijów, R., Pawlikowski, K., 2015. Three-dimensional microdistribution of *Chironomus balatonicus* larvae (Chironomidae, Diptera) in soft sediments from the Vistula Lagoon (South Baltic Sea). *Ann. Limnol. – Int. J. Limnol.* 51 (4), 343–349, <http://dx.doi.org/10.1051/limn/2015034>.
- Kornijów, R., Pawlikowski, K., Drgas, A., Rolbiecki, L., Rychter, A., 2018. Mortality of post-settlement clams *Rangia cuneata* (Macrtridae, Bivalvia) at an early stage of invasion in the Vistula Lagoon (South Baltic) due to biotic and abiotic factors. *Hydrobiologia*, 13 pp. <http://dx.doi.org/10.1007/s10750-017-3489-4>.
- Krause-Jensen, D., Sagert, S., Schubert, H., Bostrom, C., 2008. Empirical relationships linking distribution and abundance of marine vegetation to eutrophication. *Ecol. Indic.* 8 (5), 515–529, <http://dx.doi.org/10.1016/j.ecolind.2007.06.004>.
- Latała, A., 1978. Chlorophyll content in the waters of the Vistula Lagoon. *Stud. Mat. Oceanol., Biol. Morza* 21 (4), 82–94.
- Lawson, S.E., Wiberg, P.L., McGlathery, K.J., Fugate, D.C., 2007. Wind-driven sediment suspension controls light availability in a shallow coastal lagoon. *Estuar. Coast.* 30 (1), 102–112, <http://dx.doi.org/10.1007/BF02782971>.
- Leah, R.T., Moss, B., Forrest, D.E., 1980. The role of predation in causing major changes in the limnology of a hyper-eutrophic Lake. *Int. Rev. Ges. Hydrobiol.* 65 (2), 223–247, <http://dx.doi.org/10.1002/iroh.19800650205>.
- Lehtiniemi, M., Gorokhova, E., 2008. Predation of the introduced cladoceran *Cercopagis pengoi* on the native copepod *Eurytemora affinis* in the northern Baltic Sea. *Mar. Ecol. Prog. Ser.* 362, 193–200, <http://dx.doi.org/10.3354/meps07441>.
- Lesutiene, J., Gasiunaite, Z.R., Strikaityte, R., Ziliene, R., 2014. Trophic position and basal energy sources of the invasive prawn *Palaemon elegans* in the exposed littoral of the SE Baltic Sea. *Aquat. Invasions* 9 (1), 37–45, <http://dx.doi.org/10.3391/ai.2014.9.1.03>.
- Lyytimäki, J., Hildén, M., 2007. Thresholds of sustainability: policy challenges of regime shifts in coastal areas. *Sustainability Sci. Pract. Policy* 3 (2), 61–69, <http://dx.doi.org/10.1080/15487733.2007.11908007>.
- Łomniewski, K., 1958. *The Firth of Vistula*. PWN, Warsaw, 106 pp. (in Polish).
- Margoński, P., Horbowa, K., 2003. Are there trends in water quality, chlorophyll *a* and zooplankton of the Vistula Lagoon (Southern Baltic Sea) as a result of changes in nutrient loads? In: *Dublin ECSA 9 Nutrients*, 6–162. Diffuse Pollution Conference ECSA 9 Nutrients, Dublin, 6–14.
- Moller, I., Mantilla-Contreras, J., Spencer, T., Hayes, A., 2011. Microtidal coastal reed beds: hydro-morphological insights and observations on wave transformation from the southern Baltic Sea. *Estuar. Coast. Shelf Sci.* 92 (3), 424–436, <http://dx.doi.org/10.1016/j.ecss.2011.01.016>.
- Mollmann, C., Folke, C., Edwards, M., Conversi, A., 2015. Marine regime shifts around the globe: theory, drivers and impacts. *Philos. Trans. R. Soc. B* 370 (1659), <http://dx.doi.org/10.1098/rstb.2013.0260>.
- Moss, B., 1994. Brackish and freshwater shallow lakes – different systems or variations on the same theme? *Hydrobiologia* 275 (1), 1–14, <http://dx.doi.org/10.1007/BF00026695>.
- Moss, B., 2007. The art and science of lake restoration. *Hydrobiologia* 581 (1), 15–24, <http://dx.doi.org/10.1007/s10750-006-0524-2>.
- Moss, B., Madgwick, J., Phillips, G., 1996. *A Guide to the Restoration of Nutrient-enriched Shallow Lakes*. Broads Authority, 18 Colegate, Norwich, Norfolk, 180 pp.
- Munkes, B., 2005. Eutrophication, phase shift, the delay and the potential return in The Greifswalder Bodden, Baltic Sea. *Aquat. Sci.* 67 (3), 372–381, <http://dx.doi.org/10.1007/s00027-005-0761-x>.
- Naumenko, E.N., 2009. Zooplankton in different types of estuaries (using Curonian and Vistula estuaries as an example). *Inland*

- Water Biol. 2 (1), 72–81, <http://dx.doi.org/10.1134/S1995082909010118>.
- Nawrocka, L., Kobos, J., 2011. The trophic state of the Vistula Lagoon: an assessment based on selected biotic and abiotic parameters according to the Water Framework Directive. *Oceanologia* 53 (3), 881–894, <http://dx.doi.org/10.5697/oc.53-3.881>.
- Nermer, T., Grochowski, A., Fey, D., Ramutkowski, M., Szymanek, L., Lejk, A., Psuty, I., 2011. *Inventory of ichthyofauna in the Polish part of the Vistula Lagoon, including the Elbląg Bay*. Nat. Mar. Fish. Inst. Gdynia, 111 pp. (in Polish).
- Paturej, E., Gutkowska, A., 2015. The effect of salinity levels on the structure of zooplankton communities. *Arch. Biol. Sci.* 67 (2), 483–492, <http://dx.doi.org/10.2298/abs140910012p>.
- Paturej, E., Gutkowska, A., Koszalka, J., Bowszys, M., 2017. Effect of physicochemical parameters on zooplankton in the brackish, coastal Vistula Lagoon. *Oceanologia* 59 (1), 49–56, <http://dx.doi.org/10.1016/j.oceano.2016.08.001>.
- Paturej, E., Kruk, M., 2011. The impact of environmental factors on zooplankton communities in the Vistula Lagoon. *Oceanol. Hydrobiol. Stud.* 40 (2), 37–48, <http://dx.doi.org/10.2478/s13545-011-0015-6>.
- Pawlik-Skowronska, B., Pirszel, J., Kornijów, R., 2008. Spatial and temporal variation in microcystin concentrations during perennial bloom of *Planktothrix agardhii* in a hypertrophic lake. *Ann. Limnol. – Int. J. Limnol.* 44 (2), 145–150, <http://dx.doi.org/10.1051/Limn:2008015>.
- Pawlikowski, K., Kornijów, R., 2018. *Role of macrophytes in structuring littoral habitats in the Vistula Lagoon (South Baltic)*. *Oceanologia* (in press).
- Penning, W.E., Genseberger, M., Uittenbogaard, R.E., Cornelisse, J. C., 2013. Quantifying measures to limit wind-driven resuspension of sediments for improvement of the ecological quality in some shallow Dutch lakes. *Hydrobiologia* 710 (1), 279–295, <http://dx.doi.org/10.1007/s10750-012-1026-z>.
- Perez-Ruzafa, A., Marcos, C., Perez-Ruzafa, I.M., Perez-Marcos, M., 2011. Coastal lagoons: “transitional ecosystems” between transitional and coastal waters. *J. Coast. Conserv.* 15 (3), 369–392, <http://dx.doi.org/10.1007/s11852-010-0095-2>.
- Petratits, P.S., Dudgeon, S.R., 2004. Detection of alternative stable states in marine communities. *J. Exp. Mar. Biol. Ecol.* 300 (1–2), 343–371, <http://dx.doi.org/10.1016/j.jembe.2003.12.026>.
- Phillips, G., Willby, N., Moss, B., 2016. Submerged macrophyte decline in shallow lakes: what have we learnt in the last forty years? *Aquat. Bot.* 135, 37–45, <http://dx.doi.org/10.1016/j.aquabot.2016.04.004>.
- Pliński, M., 1995. *Vascular plants of the northern part of the Vistula Lagoon*. *Bull. Marit. Inst.* 22 (2), 81–87.
- Pliński, M., Kreńska, B., Wnorowski, T., 1978. *Floristic relations and biomass of vascular plants in the Vistula lagoon*. *Stud. Mater. Oceanol., Biol. Morza* 21 (4), 161–196, (in Polish).
- Pliński, M., Simm, A., 1978. *Seasonal fluctuations in the composition, distribution and quantity of phytoplankton in the Vistula Lagoon in 1974 and 1975*. *Stud. Mater. Oceanol., Biol. Morza* 4 (21), 53–80.
- Psuty-Lipska, I., Borowski, W., 2003. *Factors affecting fish assemblages in the Vistula Lagoon*. *Arch. Fish. Mar. Res.* 50 (3), 253–270.
- Psuty, I., Wilkońska, H., 2009. The stability of fish assemblages under unstable conditions: a ten-year series from the Polish part of the Vistula Lagoon. *Arch. Pol. Fish.* 17 (2), 65–76, <http://dx.doi.org/10.2478/v10086-009-0004-1>.
- Renk, H., Ochocki, S., Zalewski, M., Chmielowski, H., 2001. *Environmental factors controlling primary production in the Polish part of the Vistula*. *Rep. Sea Fish. Inst. Gdynia* 152, 77–95.
- Richman, S., Heinle, D.R., Huff, R., 1977. Grazing by adult estuarine Calanoid copepods of Chesapeake Bay. *Mar. Biol.* 42 (1), 69–84, <http://dx.doi.org/10.1007/bf00392015>.
- Ringer, Z., 1959. *An attempt to estimate the biomass of the littoral flora of the Vistula Lagoon based on the studies carried out in 1955*. *Prace Mor. Inst. Rybac. Gdyni* 10/A, 193–214, (in Polish).
- Rosqvist, K., Mattila, J., Sandstrom, A., Snickars, M., Westernbom, M., 2010. Regime shifts in vegetation composition of Baltic Sea coastal lagoons. *Aquat. Bot.* 93 (1), 39–46, <http://dx.doi.org/10.1016/j.aquabot.2010.03.002>.
- Różańska, Z., Wiktor, K., 1978. *Summary of the results of investigations of the Vistula Lagoon in 1974–1975*. *Stud. Mater. Oceanogr., Biol. Morza* 21 (4), 197–204, (in Polish).
- Rupprecht, F., Moller, I.I., Paul, M., Kudella, M., Spencer, T., van Wesenbeeck, B.K., Wolters, G., Jensen, K., Bouma, T.J., Miranda-Lange, M., Schimmels, S., 2017. Vegetation-wave interactions in salt marshes under storm surge conditions. *Ecol. Eng.* 100, 301–315, <http://dx.doi.org/10.1016/j.ecoleng.2016.12.030>.
- Rybicka, D., 2005. *Potentially toxic blue-green algae [Cyanoprokaryota] in the Vistula Lagoon*. *Oceanol. Hydrobiol. Stud.* 34 (Suppl. 3), 161–176.
- Rychter, A., Jabłońska-Barna, I., 2018. *Chapter 7.4. Macrozoobenthos of the Vistula Lagoon*. In: Bolalek, J. (Ed.), *The Vistula Lagoon at the Beginning of the 21st Century*. PWN, Warsaw (in press, in Polish).
- Sandstrom, A., Karas, P., 2002. Effects of eutrophication on young-of-the-year freshwater fish communities in coastal areas of the Baltic. *Environ. Biol. Fish.* 63 (1), 89–101, <http://dx.doi.org/10.1023/A:1013828304074>.
- Sayer, C.D., Davidson, T.A., Jones, J.I., 2010. Seasonal dynamics of macrophytes and phytoplankton in shallow lakes: a eutrophication-driven pathway from plants to plankton? *Freshw. Biol.* 55 (3), 500–513, <http://dx.doi.org/10.1111/j.1365-2427.2009.02365.x>.
- Sayer, C.D., Hoare, D.J., Simpson, G.L., Henderson, A.C.G., Liptrot, E.R., Jackson, M.J., Appleby, P.G., Boyle, J.F., Jones, J.I., Waldock, M.J., 2006. TBT causes regime shift in shallow lakes. *Environ. Sci. Technol.* 40 (17), 5269–5275, <http://dx.doi.org/10.1021/es060161o>.
- Scheffer, M., Carpenter, S., Foley, J.A., Folke, C., Walker, B., 2001. Catastrophic shifts in ecosystems. *Nature* 413 (6856), 591–596, <http://dx.doi.org/10.1038/35098000>.
- Scheffer, M., Carpenter, S.R., 2003. Catastrophic regime shifts in ecosystems: linking theory to observation. *Trends Ecol. Evol.* 18 (12), 648–656, <http://dx.doi.org/10.1016/j.tree.2003.09.002>.
- Scheffer, M., Hosper, S.H., Meijer, M.L., Moss, B., Jeppesen, E., 1993. Alternative equilibria in shallow lakes. *Trends Ecol. Evol.* 8 (8), 275–279, [http://dx.doi.org/10.1016/0169-5347\(93\)90254-M](http://dx.doi.org/10.1016/0169-5347(93)90254-M).
- Shaffer, G.P., Day, J.W., Mack, S., Kemp, G.P., van Heerden, I., Poirrier, M.A., Westernphal, K.A., FitzGerald, D., Milanese, A., Morris, C.A., Bea, R., Penland, P.S., 2009. The MRGO navigation project: a massive human-induced environmental, economic, and storm disaster. *J. Coast. Res.* 54 (SI), 206–224, <http://dx.doi.org/10.2112/Si54-004.1>.
- Sieben, K., Rippen, A.D., Eriksson, B.K., 2011. Cascading effects from predator removal depend on resource availability in a benthic food web. *Mar. Biol.* 158 (2), 391–400, <http://dx.doi.org/10.1007/s00227-010-1567-5>.
- Sondergaard, M., Kristensen, P., Jeppesen, E., 1992. Phosphorus release from resuspended sediment in the shallow and wind-exposed Lake Arreso, Denmark. *Hydrobiologia* 228 (1), 91–99, <http://dx.doi.org/10.1007/BF00006480>.
- Stempniwicz, L., Martyniak, A., Borowski, W., Goc, M., 2003. *Fish stocks, commercial fishing and cormorant predation in the Vistula Lagoon, Poland*. In: Cowx, I.G. (Ed.), *Interactions Between Fish and Birds, Implications for Management*. Blackwell Sci. Ltd., Oxford, 51–64.
- Szarejko, D., 1955. *The Vistula Lagoon vegetation*. *Rep. Sea Fish. Inst. Gdynia* 8, 235–254, (in Polish).
- Szarejko-Lukasiewicz, D., 1959. *Hydrographic investigations of the Firth of Vistula in 1953–1954*. *Rep. Sea Fish. Inst. Gdynia* 10/A, 215–228, (in Polish).

- Tackx, M.L.M., Herman, P.J.M., Gasparini, S., Irigoien, X., Billiones, R., Daro, M.H., 2003. Selective feeding of *Eurytemora affinis* (Copepoda, Calanoida) in temperate estuaries: model and field observations. *Estuar. Coast. Shelf Sci.* 56 (2), 305–311, [http://dx.doi.org/10.1016/s0272-7714\(02\)00182-8](http://dx.doi.org/10.1016/s0272-7714(02)00182-8).
- Tatrai, I., Olah, J., Paulovits, G., Matyas, K., Kawiecka, B.J., Jozsa, V., Pekar, F., 1997. Biomass dependent interactions in pond ecosystems: responses of lower trophic levels to fish manipulations. *Hydrobiologia* 345 (2–3), 117–129, <http://dx.doi.org/10.1023/A:1002919305978>.
- Underwood, G.J.C., 1991. Growth enhancement of the macrophyte *Ceratophyllum demersum* in the presence of the snail *Planorbis planorbis* – the effect of grazing and chemical conditioning. *Freshw. Biol.* 26 (2), 325–334, <http://dx.doi.org/10.1111/j.1365-2427.1991.tb01738.x>.
- Van den Berg, M.S., Coops, H., 1999. Stoneworts: valuable for water management. RIZA report 98.055, 40 pp., <https://trove.nla.gov.au/version/42922289>.
- Viaroli, P., Bartoli, M., Giordani, G., Naldi, M., Orfanidis, S., Zaldivar, J.M., 2008. Community shifts, alternative stable states, biogeochemical controls and feedbacks in eutrophic coastal lagoons: a brief overview. *Aquat. Conserv.* 18 (S1), 105–117, <http://dx.doi.org/10.1002/aqc.956>.
- Warzocha, J., Szymanek, L., Witalis, B., Wodzinowski, T., 2016. The first report on the establishment and spread of the alien clam *Rangia cuneata* (Mactridae) in the Polish part of the Vistula Lagoon (southern Baltic). *Oceanologia* 58 (1), 54–58, <http://dx.doi.org/10.1016/j.oceano.2015.10.001>.
- Witek, Z., Zalewski, M., Wielgat-Rychert, M., 2010. *Nutrient stocks and fluxes in the Vistula Lagoon at the end of the twentieth century*. Pomeranian Univ., Słupsk-Gdynia, 186 pp.
- Wójcik-Fudalewska, D., Normant-Saremba, M., 2016. Long-term studies on sex and size structures of the non-native crab *Eriochelir sinensis* from Polish coastal waters. *Mar. Biol. Res.* 12 (4), 412–418, <http://dx.doi.org/10.1080/17451000.2016.1148820>.

Available online at www.sciencedirect.com

ScienceDirect

journal homepage: www.journals.elsevier.com/oceanologia/

ORIGINAL RESEARCH ARTICLE

Comparison of the burial rate estimation methods of organic and inorganic carbon and quantification of carbon burial in two high Arctic fjords

Katarzyna Koziowska*, Karol Kuliński, Janusz Pempkowiak

Institute of Oceanology Polish Academy of Sciences, Sopot, Poland

Received 7 February 2018; accepted 23 February 2018

Available online 12 March 2018

KEYWORDS

Spitsbergen;
Carbon deposition;
Pore water;
Dissolved carbon species;
Return flux;
Carbon accumulation;
Sedimentary carbon

Summary Quantifying the burial of organic carbon (OC) and inorganic carbon (IC) species in marine sediments contribute to a better understanding of carbon cycle. This is especially important in the Arctic, where carbon deposition is relatively high and expected to change with climate warming. This study aimed to quantify the burial rates of OC and IC in the sediments of two high-latitude fjords – Hornsund and Kongsfjorden (European Arctic). Comparison of the results from three methods quantifying carbon burial in marine sediments was carried out.

Sediment cores, pore water, and over-bottom water samples were analyzed for OC and IC. The burial rates were established by considering: carbon deposition to sediments minus carbon return flux, carbon deposited to sediments 80–100 years ago and carbon deposited to sediments recently. The radiolead method was employed for sediment dating. Carbon return flux was obtained using dissolved carbon species concentrations in pore water and over-bottom water.

Sediment linear and mass accumulation rates in the fjords were 0.12–0.20 cm y⁻¹ and 1160–2330 g m⁻² y⁻¹. The OC burial rates were 19.3–30.3 g OC m⁻² y⁻¹ in Hornsund and 5.7–10.0 g OC m⁻² y⁻¹ in Kongsfjorden. IC burial was taken as equal to IC deposition and ranged from 10.7 to 20.8 g IC m⁻² y⁻¹ in Hornsund and 19.4–45.7 g IC m⁻² y⁻¹ in Kongsfjorden. The “return flux” model seems most appropriate for carbon burial rate studies. The data demonstrated that OC burial dominates in Hornsund, while in Kongsfjorden, IC burial is more important. © 2018 Institute of Oceanology of the Polish Academy of Sciences. Production and hosting by Elsevier Sp. z o.o. This is an open access article under the CC BY-NC-ND license (<http://creativecommons.org/licenses/by-nc-nd/4.0/>).

* Corresponding author at: Institute of Oceanology Polish Academy of Sciences, ul. Powstańców Warszawy 55, Sopot, Poland. Tel.: +48 587311931.

E-mail address: kkozio@iopan.gda.pl (K. Koziowska).

Peer review under the responsibility of Institute of Oceanology of the Polish Academy of Sciences.



<https://doi.org/10.1016/j.oceano.2018.02.005>

0078-3234/© 2018 Institute of Oceanology of the Polish Academy of Sciences. Production and hosting by Elsevier Sp. z o.o. This is an open access article under the CC BY-NC-ND license (<http://creativecommons.org/licenses/by-nc-nd/4.0/>).

1. Introduction

Carbon dioxide is a trace component of the atmosphere that has a major role in the greenhouse effect (IPCC, 2013). As carbon dioxide is an important component of carbon cycling, the quantification of sinks, sources, and fluxes that influence its concentration in the atmosphere is important, especially in the context of future CO₂ concentrations in the atmosphere and predictions of future climate.

Marine sediments constitute the most important long-term sink of carbon worldwide, while Arctic sediments preserve much of the deposited carbon (Smith et al., 2015). This is apparently facilitated by large loads of carbon delivered from land (Smeaton et al., 2016) and integrated in a short time period primary production (Stein and Macdonald, 2004), which supports organic carbon (OC) and inorganic carbon (IC) deposition to sediments (Koziarowska et al., 2017). It has recently been postulated that the sediments of the high-latitude fjords serve as a sink of OC to an extent that greatly exceeds the fjords' contribution to the Arctic area (Smith et al., 2015). Moreover, recent reports indicate that high loads of IC (carbon in carbonates) are deposited in fjord sediments (Smeaton et al., 2016), while significant part of the loads can be attributed to biogenic carbonates (Koziarowska et al., 2017).

Both OC and IC species that originate either from primary production or are delivered from land are readily deposited to the bottom sediments (Teske et al., 2011). The former are intensively mineralized in the water column and at the sediment–water interface (Holding et al., 2017; Teske et al., 2011), where the redox conditions determine the efficiency of mineralization and biogenic element exchange between sediments and the overlying water (Ingall et al., 2005; Jorgensen et al., 2005). The load of biogenic carbonates originating from numerous carbonate-secreting organisms, such as coccolithophores, barnacles, echinoids, and bivalves, reaches the sediments and is largely unaffected when buried there (Andrulleit et al., 1996; Freiwald, 1998).

Recently, a major effort has been directed toward establishing the rate of OC deposition and its burial in surface sediments (Smeaton et al., 2016; Smith et al., 2015). To calculate OC burial in sediments, most often, the product of the sediment mass accumulation rate (MAR) and the concentration of OC in sediments have been used. OC mineralization in sediments has been either neglected or estimated based on the difference between contemporary and preindustrial OC delivery to surface sediments (Kuliński et al., 2014; Zaborska et al., 2016); in practice, the OC load in a sediment layer deposited 80–100 years ago is taken as equal to the burial rate. The former approach (ignoring mineralization) is valid for short-term carbon preservation in sediments, while the latter is subject to uncertainties caused by the unspecified effects of glacier surges and the primary production changes caused by the recent warming of the Arctic. Due to the global warming, and, in the consequence, substantially increased primary production (Arrigo et al., 2008; Fernandez-Mendez et al., 2015), the surface sediments have been enriched with autochthonous labile OC that is eventually mineralized and/or decomposed, while the dissolved IC (DIC) and dissolved OC (DOC) species resulting from those processes return to the seawater overlying the sediments.

The problem concerning quantifying burial rates in view of the recent increase of OC in marine surface sediments has been resolved by measuring the return flux of OC and IC species from sediments to the overlying seawater (Arndt et al., 2013; Kuliński and Pempkowiak, 2012; Winogradow and Pempkowiak, 2018). The actual burial of carbon is obtained by subtracting the carbon return flux from the carbon deposition to sediments. Burial of carbonates is much easier to quantify, as they do not undergo any microbial processes in the surface sediments. The only way to reduce the concentration of carbonates in sediments would involve a significant pH decrease; pH, although low, is relatively constant in pore waters (Mucci et al., 2000). Despite the straightforward measurement technique, the sedimentary carbonate deposition and burial in sediments of the Arctic fjords have seldom been quantified (Freiwald, 1998; Koziarowska et al., 2017; Smeaton et al., 2016). Thus, the burial of both OC and IC in the fjords' sediments remains to be assessed.

The purpose of this study was to quantify the OC and IC burial rates in the subsurface sediments of the two high-latitude fjords – Hornsund and Kongsfjorden – localized on the western shores of Spitsbergen, the main island of the Svalbard archipelago, European Arctic. OC and IC concentrations were measured in the subsequent layers of sediment cores collected at two sampling stations along each fjord axis, in pore water separated from the surface core layers and seawater overlying sediments. Carbon deposition was equal to the product of the sediment MAR and carbon concentration in sediments. The sediment accumulation rate (SAR) and age of the sediment layers, required for assessing carbon deposition, were obtained using the ²¹⁰Pb method, which was validated with the distribution of ¹³⁷Cs. The return fluxes of both DOC and DIC were calculated as diffusion flows from pore water of the uppermost sediment layer to water overlying sediments using Fick's first law of diffusion. The carbon burial rates were calculated based on all three available approaches, as follows: (I) the difference between carbon deposition to sediments and the carbon return flux; (II) carbon deposited to sediments approximately 80–100 years ago, as this is considered enough time for mineralization of the labile OC in sediments (for further calculations, we took samples from about 1930 AD); and (III) carbon deposited to sediments recently.

2. Study area

The study was carried out in Hornsund and Kongsfjorden on the west coast of Spitsbergen. *Hornsund* is the southernmost fjord; it is a medium-sized fjord characterized by a complex coastline including 14 tidewater glaciers entering it directly. The fjord is influenced by two main current systems. The first, the coastal Sørkapp Current, carries less saline and cold Arctic-type waters, while the other, the West Spitsbergen Current (WSC), carries relatively warm and saline Atlantic water (Piechura et al., 2001; Swerpel, 1985). In Hornsund, however, the influence of WSC is less pronounced, due to strong pressure from waters of the Sørkapp Current. The SARs vary significantly, with a decreasing trend toward the mouth of the fjord. In the inner part (Brepollen), the rate is about 0.7 cm y⁻¹ (Szczeniński et al., 2006; Zaborska et al., 2016); in the central part, it ranges from 0.2 cm y⁻¹ (Pawłowska et al.,

2017; Zaborska et al., 2016, 2017) to 0.5 cm y^{-1} (Szczeniński et al., 2006); and it is 0.17 cm y^{-1} in the outer part (Zaborska et al., 2017). The sediments are mainly composed of sandy mud in the inner part (close to the glacier fronts) and mud in the outer part of the fjord (Gorlich, 1986). The highest concentration of sedimentary OC is about 20 mg g^{-1} at the innermost part of the fjord and 14 mg g^{-1} at the fjord mouth (Koziarowska et al., 2016; Zaborska et al., 2016). Hornsund is characterized by a relatively high primary production – from 120 to $220 \text{ g C m}^{-2} \text{ y}^{-1}$ (Piwoż et al., 2009; Smoła et al., 2017).

Kongsfjorden is a relatively small fjord with a wide opening to the open ocean. The area is divided into two parts by a sill – an outer part strongly affected by the WSC and an inner part under the influence of five tidewater glaciers (Promińska et al., 2017). Due to the large supply of mineral material with freshwater from melting glaciers in the inner part, the SARs differ significantly along the fjord axis. In the inner part, the SAR is estimated at $6\text{--}8 \text{ cm y}^{-1}$ (Elverhoi et al., 1983); in the central part, SARs of 0.1 cm y^{-1} (Elverhoi et al., 1983), 0.20 cm y^{-1} (Koziarowska et al., 2017), 0.24 cm y^{-1} (Kuliński et al., 2014), and $0.38\text{--}0.41 \text{ cm y}^{-1}$ (Zaborska et al., 2016) have been reported; and in the outer part of the fjord, the rate ranges from 0.04 cm y^{-1} (Elverhoi et al., 1983) to 0.13 cm y^{-1} (Koziarowska et al., 2017; Kuliński et al., 2014). Large differences in the reported SAR values arise from the different distances of sampling stations from the glacier front. Surface sediments are dominated by silt fractions (Bijoy Nandan et al., 2016), silts, and silty clays (Zaborska et al., 2006), while below a water depth of $30\text{--}40 \text{ m}$, sediments are composed of fairly uniform mud (Włodarska-Kowalczyk and Pearson, 2004). The total carbon (TC) concentration is relatively constant across the fjord, as it ranges between 30 and 40 mg g^{-1} (Bijoy Nandan et al., 2016; Koziarowska et al., 2017). The amount of OC in the surface sediments increases along the fjord axis from less than 1 mg g^{-1} close to the glacier front to over 20 mg g^{-1} at the fjord mouth (Bijoy Nandan et al., 2016; Kędra et al., 2010; Koziarowska et al., 2017; Kuliński et al., 2014; Włodarska-Kowalczyk and Pearson, 2004). Primary production is much lower than it is in Hornsund, as it ranges between $20 \text{ g C m}^{-2} \text{ y}^{-1}$ (Piwoż et al., 2009) and $50 \text{ g C m}^{-2} \text{ y}^{-1}$ (Hop et al., 2002).

3. Experimental

3.1. Sampling and general flow of analyses

Sediment cores were collected using a Nemisto gravity corer at two stations in each fjord (H1, H2 in Hornsund and Kb1, Kb2 in Kongsfjorden), located in the outer and central parts of the fjords (Fig. 1). Locations of sampling stations were carefully selected to reduce the impact of land – namely a direct discharge of freshwater and mineral material, and consequently, a rapid and/or irregular accumulation of sediments.

At each sampling station, a sediment core with undisturbed overlying bottom water was collected and prepared for the analyses, as shown in Fig. 2. Briefly, bottom water overlying the sediment was sampled for DIC and DOC analyses 5 cm above the sediment surface. Following this, the core was sliced into 10-mm -thick layers, and the obtained sediment samples were frozen (-20°C). In the laboratory, sediment samples were centrifuged (15 min , 5000G), and pore

water from the uppermost layers was used for DIC and DOC measurements. The moisture-deprived sediment samples were used for analyses of OC and IC concentrations and ^{210}Pb and ^{137}Cs activity concentrations. All the analyses were carried out in the Marine Biogeochemistry Laboratory of the Institute of Oceanology of the Polish Academy of Sciences, in Sopot, using the methods described concisely below. In the case of Kongsfjorden, the same stations were sampled previously by Koziarowska et al. (2017) for studies related to sediment accumulation rates, OC and IC provenience.

3.2. ^{210}Pb and ^{137}Cs activity concentrations analyses

Measurements of ^{210}Pb activity concentration were performed following the procedure developed by Flynn (1968) and adopted by Pempkowiak (1991) and Zaborska et al. (2007). Here, 200 mg of dry and homogenous material was spiked with a ^{209}Po chemical yield tracer with known activity and digested using 12 M hydrofluoric acid (3 mL) and concentrated perchloric acid (2 mL). Isotopes of polonium were spontaneously deposited on a silver disk. After deposition, the disks were analyzed for ^{210}Po and ^{209}Po in a multichannel analyzer (Canberra, United States) equipped with a Si/Li detector. The activity concentrations of ^{210}Po in the sediment samples were calculated based on chemical recovery by comparing the measured and spiked activities of ^{209}Po . Quality control was based on measurements of blanks and standards (IAEA-300 and IAEA-326) and spiked samples to verify the chemical recovery and the efficiency of detection.

The ^{137}Cs activity concentrations were measured in a γ -spectrometer (Canberra, United States) equipped with a high-purity Ge detector. Sediment samples were packed in a vessel of standard geometry ($65 \text{ mm } \varphi \times 10 \text{ mm}$) and counted for at least 24 h . The counting error was lower than 10% . Calibration of the counter was performed based on the reference materials obtained from IAEA (IAEA-300 and IAEA-385).

3.2.1. Linear sediment accumulation rates [cm y^{-1}]

Linear SARs were determined from profiles of excess ^{210}Pb activity concentration ($^{210}\text{Pb}_{\text{ex}} = ^{210}\text{Pb}_{\text{total}} - ^{210}\text{Pb}_{\text{supported}}$) vs. porosity-corrected sediment depth. The rates were calculated from the sections of profiles with exponential decreases in $^{210}\text{Pb}_{\text{ex}}$ vs. sediment depth (Zaborska et al., 2007).

3.2.2. Sediment mass accumulation rates [$\text{g m}^{-2} \text{ y}^{-1}$]

Sediment MARs were determined from the activity concentrations of the $^{210}\text{Pb}_{\text{ex}}$ profiles after earlier transformation of the linear depth in sediments to the “mass” depth using the consecutive layers' specific mass and linear depth in sediments (Robbins, 1978; Zaborska et al., 2008).

3.3. Total carbon (TC), organic carbon (OC), and inorganic carbon (IC) analyses in sediment samples

The analyses of TC and OC concentrations were performed using an Elemental Analyzer Flash EA 1112 Series combined with a Delta V Advantage (Thermo Electron Corp., Germany) isotopic ratio mass spectrometer (IRMS). Measurements were

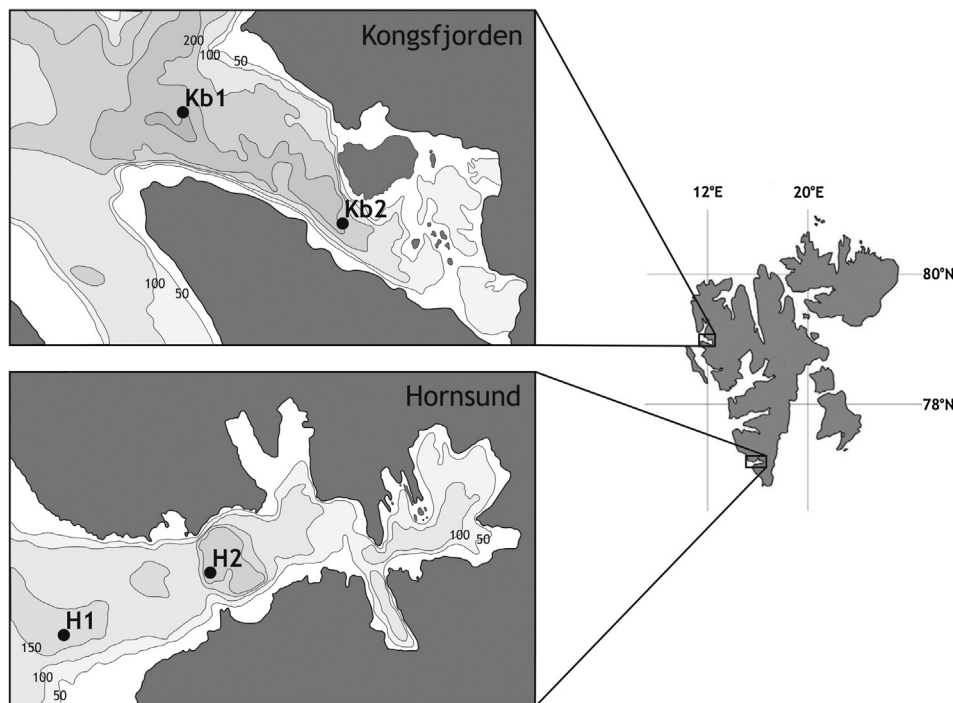


Figure 1 Locations of sampling stations in the Hornsund and the Kongsfjorden.

performed according to the method described by Kuliński et al. (2014). Briefly, about 30 mg (10- μ g accuracy) of freeze-dried and homogenized sediments were weighed into silver capsules. For OC concentration measurements, samples were acidified with 2 M hydrochloric acid to remove carbonates and dried at 60°C for 24 h (the procedure was repeated until a constant sample weight was achieved). The OC and IC measurements were calibrated against certified reference materials consisting of environmental samples (marine sediments; Flußsediment) provided by HEKatech GmbH (Germany). The precisions of the TC and OC measurements, given as relative

standard deviations, were better than $\pm 1.6\%$ and $\pm 1.4\%$ ($n = 5$), respectively. Concentrations of IC were measured as differences between TC and OC concentrations.

3.4. Dissolved inorganic carbon (DIC), dissolved organic carbon (DOC), and light absorption spectra analyses in water samples

The DIC and DOC concentrations were measured in a TOC-L analyzer (Shimadzu Corp., Japan). The DOC analyses were conducted using a high-temperature (680°C) oxidation

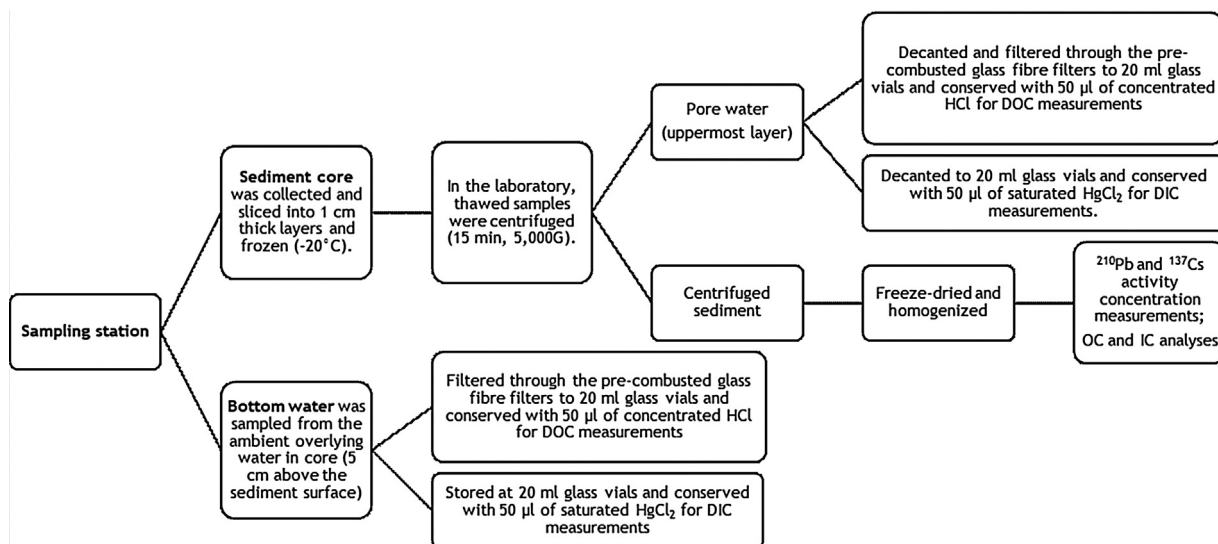


Figure 2 Flowchart of the analyses.

method and Pt catalyst. Quality control consisted of the regular analysis of blanks, as well as accuracy and precision checks based on comparisons with the reference material – North Atlantic water obtained from the Hansell Laboratory (recovery: 95%, precision characterized by relative standard deviation [RSD]: $\pm 0.8\%$; $n = 5$). The DIC concentrations were measured using a method based on sample acidification and detection of the evolving CO_2 in a nondispersive infrared (NDIR) detector. The accuracy and precision were based on the analyses of the reference material – natural seawater obtained from the Marine Physical Laboratory, University of California, San Diego (recovery: 98.5%, RSD: $\pm 1.3\%$; $n = 5$).

To assess quality of organic matter (OM) dissolved in the pore water, absorption spectra of pore water in the visible (Vis) and ultraviolet (UV) spectrum range were recorded with a UV–Vis Spectrophotometer (Hitachi, Japan) in the range of 200–800 nm. The measurements were performed in a 10-mm-length quartz cuvette against distilled water.

3.5. Calculations

3.5.1. Carbon deposition to sediments

Carbon deposition to sediments was calculated as a product of sediment MAR and OC and/or IC concentrations in the subsequent sediment layers.

3.5.2. Carbon return flux

Diffusion of dissolved carbon species from sediments into the over-bottom seawater was estimated based on Fick's first law of diffusion (Ullman and Aller, 1982):

$$J = -\phi \cdot D_{\text{sed}} \cdot \frac{\Delta c}{\Delta x},$$

where J is the diffusion flux of DIC or DOC [$\mu\text{g cm}^{-2} \text{s}^{-1}$], ϕ is the porosity of the sediment (%), D_{sed} is the sediment diffusion coefficient DIC or DOC [$\text{cm}^2 \text{s}^{-1}$], and $\Delta c/\Delta x$ is the DIC or DOC concentration gradient between pore water of the surface-most sediment layer and seawater overlying sediments [$\mu\text{g cm}^{-3}/\text{cm}$].

The sediment diffusion coefficients derived from the literature were $6.32 \times 10^{-6} \text{ cm}^2 \text{ s}^{-1}$ for DIC (Martin and McCorkle, 1993) and $1.22 \times 10^{-6} \text{ cm}^2 \text{ s}^{-1}$ for DOC (Holcombe et al., 2001).

3.5.3. Carbon burial rate

Three approaches were used to establish the carbon burial rate ($C_{\text{BR(I); II; III}}$) in bottom sediments, as follows:

- I. $C_{\text{BR(I)}}$ was determined as the difference between the OC accumulation in the surface-most sediments and the sum of return fluxes of both DIC and DOC; for IC, we assumed that its accumulation was equal to burial;
- II. $C_{\text{BR(II)}}$ was taken as the IC and OC accumulated in sediments of the approximately 80–100-year-old core layer (for further calculations, we took samples from about 1930 AD; depending on the SAR, the layer is found at a depth of 15–30 cm below the sediment water interface); this approach assumes that after this time from deposition, carbon no longer undergoes quantitative changes; and
- III. $C_{\text{BR(III)}}$ was taken as carbon deposition to the surface-most sediment layer.

4. Results

4.1. Sediment dating

The linear SAR at station H1 was 0.12 cm y^{-1} , while it was 0.19 cm y^{-1} at station H2. At the sediment depths of 15–16 cm and 17–18 cm, respectively, the activity concentration of $^{210}\text{Pb}_{\text{total}}$ reached the values assigned to the supported radiolabel (Fig. 3). The linear SAR obtained in this study was in the range reported previously by Pawłowska et al. (2017). The vertical profiles of ^{210}Pb indicated that the uppermost 6 cm of sediments in the outer part of the fjord and the uppermost 5 cm in the fjord central part were mixed. The respective values for Kongsfjorden were 0.13 cm y^{-1} at station Kb1 and 0.20 cm y^{-1} at station Kb2, representing faster sedimentation. These rates were in the range reported by Elverhoi et al. (1983) and Kuliński et al. (2014). The SAR results were also positively validated by radiocesium measurements. The depth of the ^{137}Cs appearance in the cores layers dated to about 1950 AD was taken as a proof that sediment mass accumulation rates are sufficiently accurate. The measured ^{137}Cs activity concentrations ranged from <0.1 to 6.4 Bq kg^{-1} and were comparable to results reported previously by Zaborska (2017) (Fig. 3). The MAR calculation in Hornsund indicated that 1310 g, at station H1, and 2330 g, at station H2, of sedimentary material is annually deposited in every square meter of this region of the fjord. In the case of Kongsfjorden, the sediment MAR results amounted to $1160 \text{ g m}^{-2} \text{ y}^{-1}$ in the outer part of the fjord and $1950 \text{ g m}^{-2} \text{ y}^{-1}$ in the central part. The differences of mass SAR in the fjords indicate different loads of the suspended matter reaching the sea floor, and they can, most likely, be assigned to different levels of proximity to, and activity of, glaciers.

4.2. Carbon concentrations in sediments, pore water, and over-bottom water

4.2.1. Sedimentary carbon concentrations

The OC concentrations in sediments ranged between 5.0 mg g^{-1} and 19.0 mg g^{-1} (0.5% and 1.9%, respectively; Fig. 4a) – values close to the concentrations previously reported for sediments of the Svalbard fjords (Koziarowska et al., 2016; Kuliński et al., 2014; Szczuciński et al., 2009; Winkelmann and Knies, 2005; Zaborska et al., 2006). There were no significant differences between the two stations in Hornsund. However, in Kongsfjorden, the Kb2 station was characterized by significantly lower sedimentary OC concentrations. All vertical profiles, especially those from the central parts of the fjords, indicated increasing OC concentrations in the upper sections of the cores.

There were significant differences between fjords concerning IC concentrations. These were lower in Hornsund (8.0 – 13.8 mg g^{-1}) and higher in Kongsfjorden (16.8 – 29.5 mg g^{-1} ; Fig. 4b; Koziarowska et al., 2017).

4.2.2. DIC and DOC concentrations

DOC concentrations in pore water of the surface sediment layers varied between 84.0 and 243.8 mg L^{-1} (Table 1). DOC concentrations differed significantly between the fjords: the lowest were measured at station H1, while the highest were found at Kb2. The obtained results are much higher than

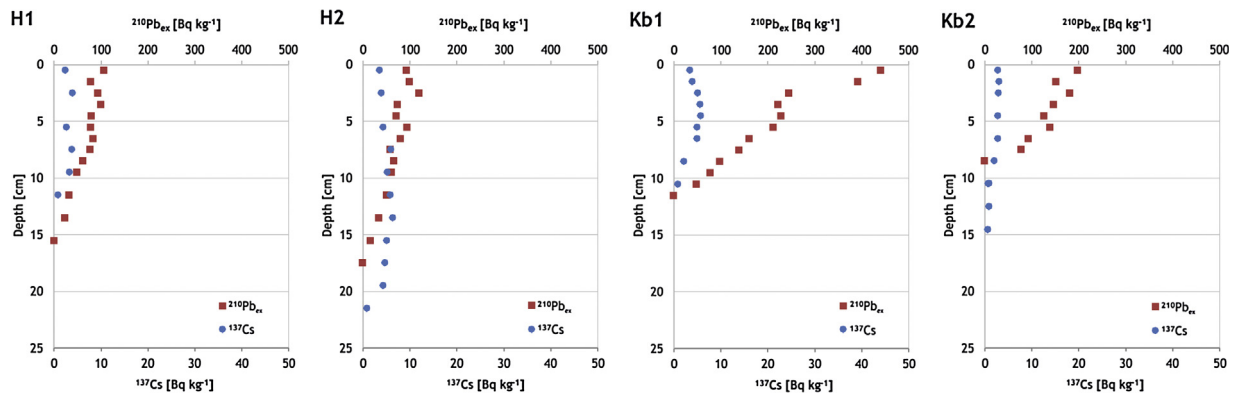


Figure 3 Vertical profiles of $^{210}\text{Pb}_{\text{ex}}$ (scale – upper X-axis) and ^{137}Cs (scale – lower X-axis) activity concentrations plotted against depth below sediment-water interface.

those reported previously in high latitude marine sediments – Hulth et al. (1996) reported a range of 5–100 mg L^{-1} , while Mucci et al. (2000) results were 5–30 mg L^{-1} . DIC concentrations were much lower than those of DOC, as they varied in the range of 26.5–37.5 mg L^{-1} in Kongsfjorden and 30.2–32.3 mg L^{-1} in Hornsund (Table 1). Concentrations measured in the Svalbard fjords in this study are close to the concentrations previously measured in the pore water of Arctic sediments, for example, 22–38 mg L^{-1} (Glud et al., 1998).

4.3. Accumulation rates of organic (OC_{AR}) and inorganic (IC_{AR}) carbon

The results of sediment MARs were lower in the central parts of the fjords (1310 and 1160 $\text{g m}^{-2} \text{y}^{-1}$ in Hornsund and Kongsfjorden, respectively) than at the mouth of the fjords (2330 and 1950 $\text{g m}^{-2} \text{y}^{-1}$). The combination of MAR

distribution and OC concentration profiles caused OC_{AR} to be different along the Hornsund axis; it ranged from 20.6 to 24.3 $\text{g OC m}^{-2} \text{y}^{-1}$ at H1 and from 32.4 to 40.5 $\text{g OC m}^{-2} \text{y}^{-1}$ at H2. In Kongsfjorden, despite differences in these two features (MARs and OC concentrations), OC_{AR} was quite similar and ranged from 15.4 to 20.8 $\text{g OC m}^{-2} \text{y}^{-1}$ at Kb1 and from 9.7 to 20.3 $\text{g OC m}^{-2} \text{y}^{-1}$ at Kb2 (Fig. 5a). These values are in the range of previously reported results for the Svalbard fjords (Kuliński et al., 2014; Winkelmann and Knies, 2005; Zaborska et al., 2016).

The IC_{AR} results differed significantly between the fjords and sampling stations; higher loads of IC were accumulated in Kongsfjorden sediments (19.4–23.0 $\text{g IC m}^{-2} \text{y}^{-1}$ and 41.4–57.5 $\text{g IC m}^{-2} \text{y}^{-1}$ at Kb1 and Kb2, respectively) and lower in Hornsund (10.7–13.1 and 20.8–32.1 $\text{g IC m}^{-2} \text{y}^{-1}$ at H1 and H2, respectively; Fig. 5b). Significant variations in the carbon accumulation rates could also be observed in the vertical

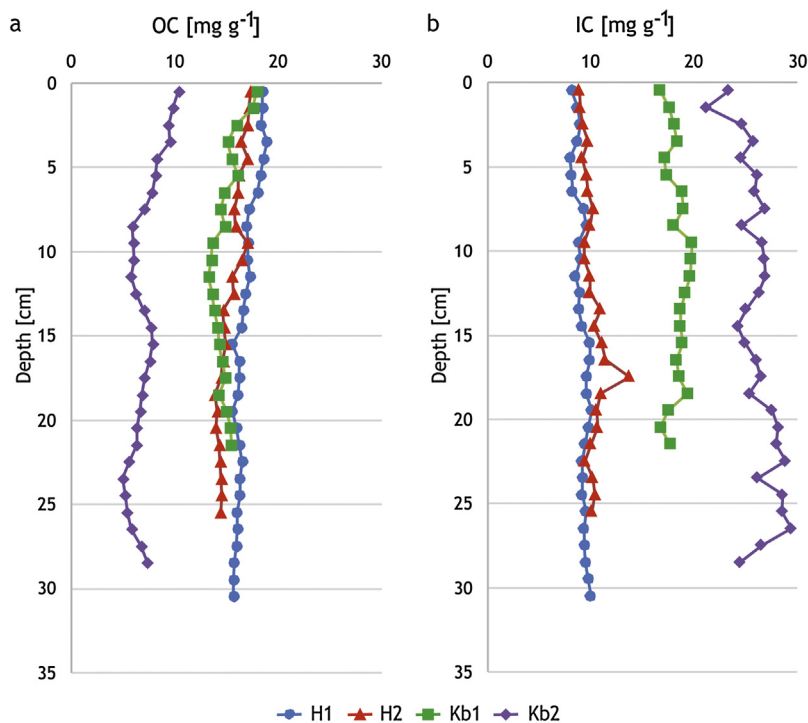


Figure 4 Sedimentary organic carbon (OC) (a) and sedimentary inorganic carbon (IC) (b) versus depth in the investigated sediment cores.

Table 1 Concentrations of dissolved organic carbon (DOC) and dissolved inorganic carbon (DIC) in pore water of the surface-most sediment layer and seawater overlying sediments in the investigated cores.

Stations	Pore water [mg L^{-1}]		Sea water [mg L^{-1}]	
	DOC	DIC	DOC	DIC
H1	84.0	30.2	1.9	25.4
H2	192.6	32.3	0.8	25.2
Kb1	231.3	26.5	1.1	25.3
Kb2	243.8	37.5	2.3	25.4

profiles. Both OC_{AR} and IC_{AR} showed larger variations in the sampling stations located in the central parts of the fjords (H2 and Kb2) than these in the fjords' mouths.

It is characteristic for OC_{AR} to increase toward the sediment surface, while IC_{AR} decreases. The stations located in the outer parts of the fjords (H1 and Kb1) were characterized by a relatively constant amount of deposited carbon over the last century. This was not the case for the central parts in the two fjords. This indicates a much higher dynamics of processes in the central regions than in the open parts of the fjords.

4.4. Carbon return flux (C_{RF})

Carbon return flux from bottom sediments to the water column was determined as the amount of carbon species diffusing from sediment pore water to the over-bottom seawater based on Fick's first law of diffusion. The porosity was equal to 0.76–0.81 and these are typical values for muddy

sediments (Robbins, 1978). The obtained C_{RF} results were in the range of 5.0–10.2 $\text{g m}^{-2} \text{y}^{-1}$ in Hornsund (stations H1 and H2) and 10.9–14.6 $\text{g m}^{-2} \text{y}^{-1}$ in Kongsfjorden (stations Kb1 and Kb2; Table 2). The results showed that lower contribution in the TC return flux had DIC, only 3–24% (0.3–3.0 $\text{g m}^{-2} \text{y}^{-1}$). More significant were the OC return fluxes, which were 3.8 $\text{g m}^{-2} \text{y}^{-1}$ and 8.6 $\text{g m}^{-2} \text{y}^{-1}$ at stations H1 and H2 and 10.6 $\text{g m}^{-2} \text{y}^{-1}$ and 11.6 $\text{g m}^{-2} \text{y}^{-1}$ at stations Kb1 and Kb2, respectively. This is contrary to findings from the Baltic Sea, where the DIC return flux predominates (Kuliński and Pempkowiak, 2012).

4.5. Carbon burial in sediments (C_{BR})

4.5.1. $\text{C}_{\text{BR(I)}}$ based on deposition and return flux

The OC burial rates are presented in Tables 3 and 4. The values differed significantly for both fjords, as they were in the range of 19.3–30.3 $\text{g OC m}^{-2} \text{y}^{-1}$ in Hornsund and 5.7–10.0 $\text{g OC m}^{-2} \text{y}^{-1}$ in Kongsfjorden (Table 3). In addition, the $\text{IC}_{\text{BR(I)}}$ varied in both fjords and stations (10.7 $\text{g IC m}^{-2} \text{y}^{-1}$, 20.8 $\text{g IC m}^{-2} \text{y}^{-1}$, 19.4 $\text{g IC m}^{-2} \text{y}^{-1}$, and 45.7 $\text{g IC m}^{-2} \text{y}^{-1}$ at H1, H2, Kb1, and Kb2, respectively).

Despite differences in the MARs and both OC and IC concentrations, the values of $\text{C}_{\text{BR(I)}}$, defined as the sum of the organic and inorganic fractions buried in the outer and central parts of both fjords, were surprisingly similar. They were 29.4–30.0 $\text{g m}^{-2} \text{y}^{-1}$ at the outer parts and 51.1–51.4 $\text{g m}^{-2} \text{y}^{-1}$ in the central parts of the investigated fjords (Table 3).

4.5.2. $\text{C}_{\text{BR(II)}}$ based on the concentrations in subsurface sediments

The OC burial rate, determined by multiplying MAR by the OC concentration in sediment layers accumulated about

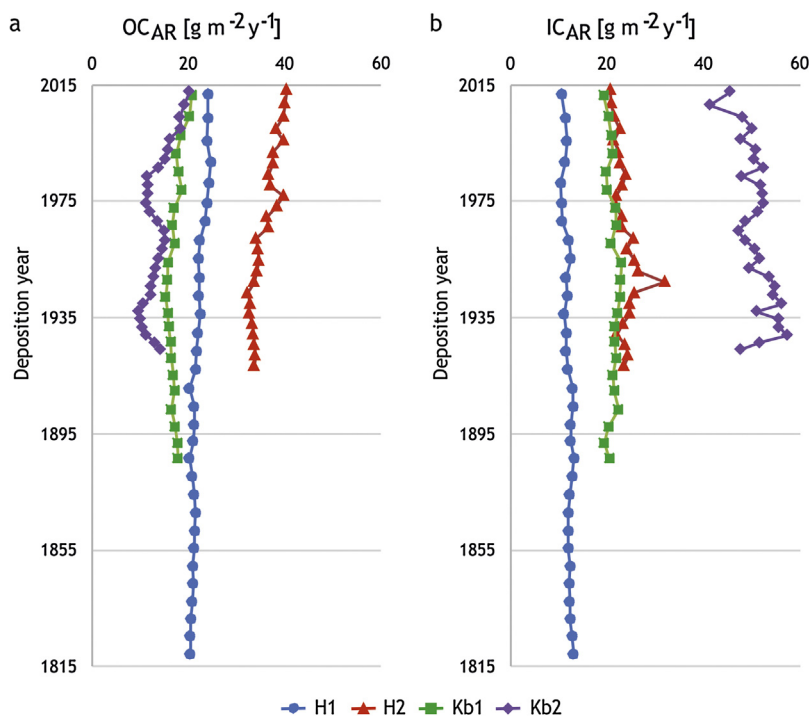


Figure 5 Vertical profiles of organic (OC_{AR}) (a) and inorganic (IC_{AR}) (b) carbon accumulation rates in the investigated sediment cores plotted against the sediment layer deposition.

Table 2 Results of porosity, diffusion flux (J) of dissolved organic carbon (DOC) and dissolved inorganic carbon (DIC), carbon return flux (C_{RF}).

Station	Porosity	J_{DOC} [$g\ m^{-2}\ y^{-1}$]	J_{DIC} [$g\ m^{-2}\ y^{-1}$]	C_{RF} [$g\ m^{-2}\ y^{-1}$]
H1	0.78	3.8	1.2	5.05
H2	0.76	8.6	1.6	10.2
Kb1	0.78	10.6	0.3	10.9
Kb2	0.81	11.6	3.0	14.6

Table 3 Results of the mass accumulation rate (MAR), organic carbon accumulation rate (OC_{AR}), carbon return flux (C_{RF}), organic carbon burial rate ($OC_{BR(I)}$), efficiency of $OC_{BR(I)}$, inorganic carbon burial rate ($IC_{BR(I)}$), and total carbon burial rate ($TC_{BR(I)}$) in the investigated cores.

Station	MAR [$g\ m^{-2}\ y^{-1}$]	OC_{AR} [$g\ m^{-2}\ y^{-1}$]	C_{RF} [$g\ m^{-2}\ y^{-1}$]	$OC_{BR(I)}$ [$g\ m^{-2}\ y^{-1}$]	Efficiency of $OC_{BR(I)}$ [%]	$IC_{BR(I)}$ [$g\ m^{-2}\ y^{-1}$]	$TC_{BR(I)}$ [$g\ m^{-2}\ y^{-1}$]
H1	1310	24.3	5.0	19.3	79.5	10.7	30.0
H2	2330	40.5	10.2	30.3	74.7	20.8	51.1
Kb1	1160	20.8	10.9	10.0	47.8	19.4	29.4
Kb2	1950	20.3	14.6	5.7	27.9	45.7	51.4

Table 4 Burial rates of total carbon (TC), organic carbon (OC) and inorganic carbon (IC) in the investigated sediments assessed by methods: I (carbon deposition minus carbon return flux), II (carbon deposition in the sediment layer dated 1930 AD), and III (contemporary carbon deposition).

Station	OC_{BR} [$g\ m^{-2}\ y^{-1}$]			IC_{BR} [$g\ m^{-2}\ y^{-1}$]			TC_{BR} [$g\ m^{-2}\ y^{-1}$]		
	I	II	III	I	II	III	I	II	III
H1	19.3	22.1	24.3	10.7	11.7	10.7	30.0	33.8	35.0
H2	30.3	33.4	40.5	20.8	23.4	20.8	51.1	56.8	61.3
Kb1	10.0	16.1	20.8	19.4	21.7	19.4	29.4	37.8	40.2
Kb2	5.7	10.6	20.3	45.7	55.8	45.7	51.4	66.4	66.0

1930 AD, ranged from 22.1 to 33.4 $g\ OC\ m^{-2}\ y^{-1}$ in Hornsund and 10.6 to 16.1 $g\ OC\ m^{-2}\ y^{-1}$ in Kongsfjorden. The results differ from those obtained using carbon return flux (method I, see Section 4.5.1), as they are slightly higher in Hornsund and significantly higher in Kongsfjorden. In the case of $IC_{BR(II)}$, the obtained results were higher than those calculated using methods I and III. In Hornsund, the values varied from 11.7 to 23.4 $g\ IC\ m^{-2}\ y^{-1}$, while they were in the range of 21.7–55.8 $g\ IC\ m^{-2}\ y^{-1}$ in Kongsfjorden. The values of $TC_{BR(II)}$ (sum of $IC_{BR(II)}$ and $OC_{BR(II)}$) were comparable in the outer and central parts of both fjords and varied between 33.8 and 37.8 $g\ m^{-2}\ y^{-1}$ in the outer parts and 56.8 and 66.4 $g\ m^{-2}\ y^{-1}$ in the central parts of Hornsund and Kongsfjorden, respectively.

4.5.3. $C_{BR(III)}$ based on the contemporary carbon deposition

The results of $OC_{BR(III)}$, assessed as carbon deposition at the top-most sediment layers, were 24.3–40.5 $g\ OC\ m^{-2}\ y^{-1}$ in Hornsund and 20.3–20.8 $g\ OC\ m^{-2}\ y^{-1}$ in Kongsfjorden. These values are larger than the results obtained using the two methods described above (methods I and II, see Sections 4.5.1 and 4.5.2), especially at station Kb2 in Kongsfjorden, where the return flux was the highest. The results are also

larger than the OC burial rate obtained by Zaborska et al. (2016) and Kuliński et al. (2014). In the case of $IC_{BR(III)}$, the obtained results were the same as those calculated using method I. This is due to the assumption that sedimentary IC is stable and not subject to removal processes. The values of $TC_{BR(III)}$ were higher than those calculated using methods I and II, as they varied from 35.0 to 61.3 $g\ m^{-2}\ y^{-1}$ in Hornsund and 40.2 to 66.0 $g\ m^{-2}\ y^{-1}$ in Kongsfjorden. The results of the OC, IC, and TC burial rates obtained using the three methods are presented in Table 4.

4.6. Absorption spectra in the visible (Vis) and ultraviolet (UV) ranges

Absorption spectra of pore waters from the surface-most sediment layers (0–1 cm) from Kongsfjorden are presented in Fig. 6. In the 260–300 nm range, a clear absorption peak can be seen (Fig. 6a). The shapes of the absorption spectra resemble those of humic substances (Schnitzer and Khan, 1972), including those recorded for humic substances from marine sediments (Pempkowiak and Szponar, 1993).

Based on the measured pore water absorbances and mass absorption coefficients (MAC) of the aquatic humic acids separated from seawater (4.3 and 7.8 $cm^2\ mg^{-1}$ at wavelengths

260 and 300 nm; [Stoumer and Harvey, 1974](#)), it was calculated that concentration of humic substances in pore water range from 12 to 32 mg L⁻¹ at station Kb1 and from 11 to 22 mg L⁻¹ at Kb2. As no MACs for humic substances from the fjords, or even Arctic, pore waters are available, the reported humic substances concentration ranges should be regarded as preliminary. However even these preliminary calculations suggest that humic substances can play an important role in the DOC return flux from sediments.

Unfortunately, corresponding pore water samples from Hornsund were lost during transportation.

5. Discussion

Studies suggest that climate warming, and consequently, the reduction of sea ice in summer together with an increase of the annual availability of light, may cause an expansion of the area favorable for phytoplankton growth and may enhance the pelagic primary production in the Arctic ([Fernandez-Mendez et al., 2015](#)). [Arrigo et al. \(2008\)](#) reported that annual primary production in the Arctic Ocean in 2007 was 23% higher than in 1998–2002, therefore an export of particulate OC is likely to have increased ([Lalande et al., 2009](#)).

Assessment of the consequences of those processes for both historical and present-day equilibriums is under way ([Cochrane et al., 2009](#); [Renaud et al., 2007, 2008](#)). Due to the influence of warm Atlantic waters, Kongsfjorden can be considered a “warm fjord,” while Hornsund is a “cold” one; thus, the different intensities of the processes in the two fjords may represent possible effects of the climate change in the Arctic.

5.1. Efficiency of carbon burial in bottom sediments

The terms *OC deposition rate* and *OC burial rate* are often used interchangeably ([St-Onge and Hillaire-Marcel, 2001](#)), but these are terms that describe two separate phenomena, as a fraction of the deposited OM is mineralized. To establish the OC burial rate, it is necessary to determine the amount of OC deposited to sediments and subtract from it the amount of carbon that is mineralized and/or hydrolyzed in surface sediments and diffuses back to seawater overlying sediments, as a dissolved carbon species return flux.

It is worth emphasizing that there are different approaches to determining the OC burial rate in sediments. [St-Onge and Hillaire-Marcel \(2001\)](#) identified carbon burial as equal to carbon deposition to sediments, while [Kuliński et al. \(2014\)](#) and [Zaborska et al. \(2016\)](#) defined burial as a deposition in subsurface sediments (e.g. deposition in the sediment layer dated as about 80–100 years old – the time believed to be long enough for mineralization of the labile OC in sediments). The former approach is valid for short-term carbon preservation in sediments, while the latter considers mineralization and hydrolysis but is subject to possible serious errors caused by an unspecified effect of glacier surges and the primary production changes caused by the recent climate warming. Recently, the burial rate has been defined as a difference between the carbon deposited to sediments and the return flux of dissolved carbon species from sediments to the overlying water ([Kuliński and Pempkowiak, 2012](#)). Thus, the comparison of carbon burial rates from different publications and calculated in different ways must be treated with caution. The burial rates are likely sensitive and susceptible to environmental changes related to global alterations, such as a decrease in ice cover, increase in freshwater supplies, or changes in the functioning of fjords' ecosystems ([Węstawski et al., 2017](#)).

In this study, carbon burial rates were evaluated using three different approaches, as described above. The data presented in [Table 4](#) demonstrate that the values obtained by the three methods are often comparable. The biggest differences in the obtained values were seen in the case of the OC burial rate (especially in sampling stations from Kongsfjorden), probably due to a much higher dynamics of the processes associated with OC (mineralization and/or hydrolysis) in surface sediments than with IC. In addition, methods II and III are vulnerable to OC concentration changes caused by factors other than sedimentary OM mineralization, such as inflow changes of the mineral material and/or fluctuation of OM deposition to sediments. Therefore, we think that the most accurate calculations are those using the carbon return flux method (I), and below, we only discuss and interpret the data calculated using the first method.

Substantial differences of $OC_{BR(I)}$ are characteristic of the study area. Differences in the $OC_{BR(I)}$ in Hornsund and Kongsfjorden may be due to the different intensities of primary production in the two areas – which is much higher in Hornsund and lower in Kongsfjorden ([Hop et al., 2002](#); [Piwosz](#)

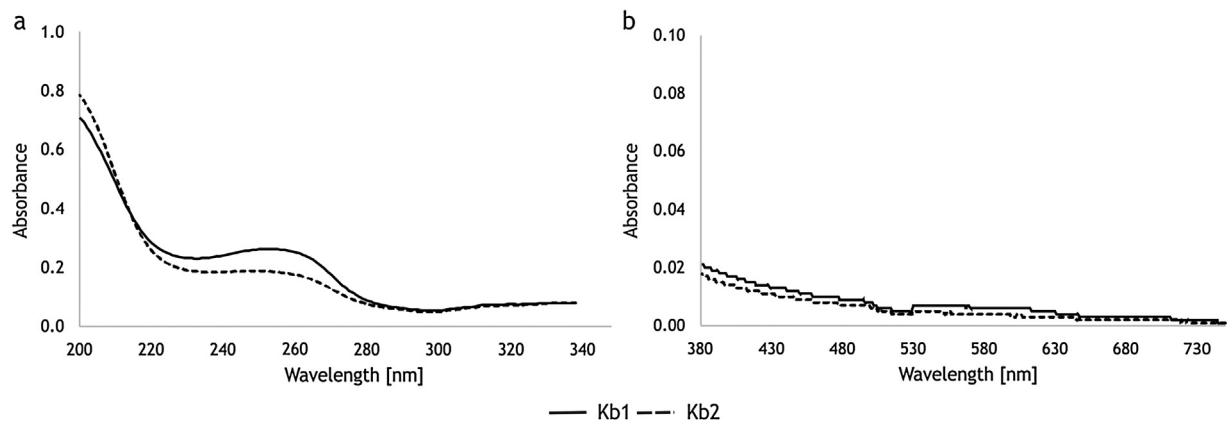


Figure 6 Absorption spectra of pore-water from the top-most sediment layers: (a) ultraviolet (UV), (b) visible (Vis).

et al., 2009). Another reason for this may be the provenience of OM. Zaborska et al. (2016) reported that sediments in Hornsund contain twice as much terrestrial carbon as Kongsfjorden sediments. Furthermore, Koziarowska et al. (2016) estimated that 69–75% of sedimentary OM in the central and outer parts of Hornsund is of terrestrial origin. This high contribution of land-derived OM in Hornsund sediments (Koziarowska et al., 2016) is especially important, if its high resistance to mineralization is taken into account (Antonio et al., 2010). Consequently, the mineralization rate in Hornsund sediments is lower (low carbon return flux), and the efficiency of $OC_{BR(I)}$ is higher. This suggests that it is not only the quantity of OM deposited into sediments that influences the OC burial rate, but also the OM source (marine vs. terrestrial). Thus, the efficiency of carbon burial rates is different in the investigated fjords; higher values were found in Hornsund – 79.5% at H1 and 74.7% at H2 – while lower rates were observed in Kongsfjorden – 47.8% at Kb1 and 27.9% at Kb2 (Table 3). In addition, the difference in $OC_{BR(I)}$ between the fjords may be due to other environmental conditions, like: water depth, water temperature, activity of benthic organisms, and/or oxygen availability (Promińska et al., 2017). Interestingly, lower burial efficiencies and higher return fluxes were found at stations located in the central parts of both fjords. This may confirm the hypothesis that the observed increase of OC_{AR} toward the sediment surface in the vertical profiles at stations H2 and Kb2 is caused by an increasing contribution of labile OM.

The IC burial rates were calculated by assuming that the amount of IC deposited to the sediments is equal to its burial rate, as carbonates can be removed from sediments only due to a pH decrease, and the pH, although low, is relatively constant in near bottom waters (Mucci et al., 2000). The lower IC concentrations in Hornsund indicate a low carbonate supply from the mainland and/or small in situ production by calcareous organisms. In Kongsfjorden, high IC concentrations in the central part (Kb2) are likely the effect of land-derived carbonates supplied by glaciers that, when moving, scratch the land surface rich in limestone in that region. The problem has already been discussed in detail by Koziarowska et al. (2017). In Hornsund, the differences of $TC_{BR(I)}$ between stations are caused mainly by different MARs, while in Kongsfjorden, the differences are due to both different MARs and different IC concentrations.

To conclude, OC burial dominates in the Hornsund sediments, while IC burial is more intensive in Kongsfjorden.

5.2. Carbon burial – the global perspective

As scarce reports on IC deposition to fjord sediments are available, in this section, just the OC burial rate established by considering the return flux is compared ($OC_{BR(I)}$). The obtained results are comparable, yet not identical, to those reported earlier in the Svalbard region (Kuliński et al., 2014; Winkelmann and Knies, 2005; Zaborska et al., 2016) (Table 5). Minor differences in $OC_{BR(I)}$ are likely due to slightly different location of the sampling stations – closer or farther from the shore and/or glacier front; however, the general pattern is similar, with higher OC burial rate values in Hornsund than in Kongsfjorden. For other Arctic regions, variation of OC burial is more visible; in the cases of the Barents Sea (Carroll et al., 2008), Young Sund in the Greenland Sea (Rysgaard and Nielsen,

2006), and Gulf of St. Lawrence (Silverberg et al., 2000), the OC burial rates are comparable to those for Kongsfjorden reported in this study. The results from glaciated and non-glaciated fjords in Southeast Alaska (Cui et al., 2016) and the Saguenay Fjord, Canada (St-Onge and Hillaire-Marcel, 2001) were characterized by much higher and more varied rates ($13–1113 \text{ g OC m}^{-2} \text{ y}^{-1}$). In other regions (mid-latitude fjords), the OC burial rate was slightly lower due to the smaller MAR (Knudson et al., 2011; Muller, 2001; Muzuka and Hillaire-Marcel, 1999; Pickrill, 1993; Smeaton et al., 2016; Smith et al., 2015), as MARs strongly influence the amount of carbon deposited to the seafloor. Most of the Patagonia (Chile) fjords are characterized by OC_{AR} and OC_{BR} in similar ranges to those measured in the frame of the present study. For example, the Jacaf Fjord ($OC_{AR} = 33.4–40.8 \text{ g m}^{-2} \text{ y}^{-1}$; $OC_{BR} = 21.0–25.7 \text{ g m}^{-2} \text{ y}^{-1}$) is characterized by rates similar to those in Hornsund, while the OC_{BR} in the Aisén Fjord ($OC_{AR} = 10.5–20.7 \text{ g m}^{-2} \text{ y}^{-1}$; $OC_{BR} = 6.6–13.1 \text{ g m}^{-2} \text{ y}^{-1}$) resembles Kongsfjorden in this respect (Sepulveda et al., 2011).

Reported carbon burial rates often lack definitions. In addition, the methodology used to calculate the rates is not included or lacking detail; thus, direct comparisons of data originating from recent reports may be misleading. Nevertheless, it may be concluded that the OC_{BR} values in the Svalbard fjords sediments vary in the range of $5–40 \text{ g m}^{-2} \text{ y}^{-1}$. The actual rate depends on the number of glaciers and their activity in the watershed, proximity of sampling locations to glacier fronts, water depth, and intensity of both primary production and OM mineralization.

5.3. Sources of DIC and DOC in pore water

It is generally accepted that DIC in bottom waters is composed of carbon dioxide and bicarbonate ions. Carbon dioxide is produced during OM mineralization. Then, it reacts with carbonates, giving bicarbonate ions. The relatively small concentrations of DIC measured in the pore water of the studied fjords indicate that mineralization processes in the sediments are weak. In contrast, the DOC concentrations measured in pore water of the studied area sediments are larger than the DOC concentrations in the pore water of the Baltic sediments by nearly an order of magnitude (Kuliński and Pempkowiak, 2012). A plausible explanation for this is that the dissolved organic substances originate as products of sedimentary OM hydrolysis and/or desorption from the solid phase. It is further argued that the dissolved organic substances released from sediments are refractory in nature.

The absorption curves of pore water, presented in Fig. 6, can be interpreted as resulting from the presence of dissolved fulvic acids – the water-soluble fraction of humic substances. Thus, such high concentrations of DOC in pore waters may be explained by, for example, the presence of large amounts of fulvic substances, which are relatively resistant to biological degradation (Schnitzer, 1991). Both humic acids and fulvic acids are refractory, as they result from a prolonged biochemical stabilization. This explanation agrees well with the previously mentioned high contribution of the land-derived OM in the Hornsund sediments (Koziarowska et al., 2016). This fraction of sedimentary OM is apparently brought to sediments as a part of soil particles. Thus, it is possible that dissolved organic substances present

Table 5 Sediment accumulation rate (SAR), mass accumulation rate (MAR), organic carbon accumulation rate (OC_{AR}), OC burial rate (OC_{BR}) and OC_{BR} efficiency in this study compared with global fjords.

Region	SAR [cm y ⁻¹]	MAR [g m ⁻² y ⁻¹]	OC _{AR} [g m ⁻² y ⁻¹]	OC _{BR} [g m ⁻² y ⁻¹]	OC _{BR} efficiency [%]	Reference
Svalbard						
Kongsfjorden	0.13–0.20	1160–1950	20.3–20.8	5.7–10.0	28–48	This study
	0.13–0.23	1350–3200	16.6–16.8	9–13	54–69 ^a	Kuliński et al. (2014)
	0.38–0.41	5491–6279	29.5–35.3	15.4–15.9	45–53 ^a	Zaborska et al. (2016)
Hornsund	0.12–0.19	1310–2330	24.3–40.5	19.3–30.3	75–79	This study
	0.22–0.24	2916–3299	38–42	35.5–38.6	84–98 ^a	Zaborska et al. (2016)
Storfjorden	0.18	570–2240	11–46	–	–	Winkelmann and Knies (2005)
Arctic region						
Barents Sea	0.03–0.4	320–650	–	3.7–8.5	5–7 ^d	Carroll et al. (2008)
Young Sund (Greenland Sea)	0.04–0.23	–	–	7.2	–	Rysgaard and Nielsen (2006)
Glaciated fiord (SE Alaska)	–	90,000–3,300,000	–	30–1113	–	Cui et al. (2016)
Non-glaciated fiord (SE Alaska)	–	–	–	13–82	–	Cui et al. (2016)
Saguenay fjord (Canada)	0.2–1.5	–	24–291	24–291	–	St-Onge and Hillaire-Marcel (2001)
Gulf of St. Lawrence (Canada)	0.08	~285	–	5.5–6.4	3.5 ^d	Silverberg et al. (2000)
Gulf of St. Lawrence (Canada)	1.0–1.5	–	0.7–2.5	–	–	Muzuka and Hillaire-Marcel (1999)
Labrador Sea	0.2–2.8	–	0.02–1.5	–	–	Muzuka and Hillaire-Marcel (1999)
Other regions						
Nordåsvannet fjord (Norway)	0.04–0.22	44.6–261.5	1.9–19.5	–	–	Muller (2001)
Loch Sunart (Scotland)	0.02–0.09	–	3.0–32.1	1.9–25.7 ^b	–	Smeaton et al. (2016)
Patagonia fjords (Chile)	0.14–0.47	–	1.9–40.8	1.2–34.8	63	Sepulveda et al. (2011)
Fiorland (New Zealand)	0.06–0.38	51–1140	2.3–23.2	1.8–18.6 ^c	–	Smith et al. (2015), Knudson et al. (2011), Pickrill (1993)

^a Difference in OC concentration between the surface layer and deepest layer.

^b Burial rate calculated assuming a burial efficiency of 63% (Sepulveda et al., 2011).

^c Burial rate calculated assuming a burial efficiency of 80% (Bernier, 1980).

^d Share of primary production buried in sediments.

in pore water are fulvic acids – products of desorption and/or hydrolyzation of terrestrial OM brought to the fjord sediments as a suspension, as well as residues of the autochthonous OM mineralization and humification.

5.4. Future challenges

This research quantified OC and IC burial in bottom sediments of two high Arctic fjords, Hornsund and Kongsfjorden, which differ significantly in terms of their hydrological features, activity, and number of surrounding glaciers, as well as primary production. At the same time, this study organized the knowledge on the meaning of carbon burial. It clearly defined carbon burial as the difference between carbon deposition and carbon return flux. This is especially important for quantifying burial of OC that undergoes mineralization, decomposition, and/or hydrolysis during early diagenesis.

Since it was shown that Arctic fjords are important regions in the global carbon cycle (Smith et al., 2015), quantification of carbon burial in sediments of these regions is of key

importance. There are different environmental consequences of burial for different carbon species (organic vs. inorganic) and origins (marine vs. terrestrial). Thus, it is important for the accurate quantification of carbon burial performed in this study to be followed by detailed study on the provenience of both IC and OC. It is well known that burial of marine OC, as the last link of the biological pump, contributes significantly to the reduction of atmospheric CO₂. In the case of terrestrial OC burial, carbon only changes the location from the terrestrial (soils) to the marine (sediments). Supply, transformations, and burial of carbonates, depending on their sources, may generate contrary mechanisms. The discharge of carbonates from land may lead to their partial dissolution in seawater, and consequently, to an increase in total alkalinity. This increases the uptake or lowers emission of CO₂ from/to the atmosphere. In contrast, the formation of biogenic carbonates reduces alkalinity and leads to the opposite effects.

It is not clear how to distinguish between terrestrial and biogenic IC. Recently an effort to do this for Kongsfjorden sediments was carried out by Koziarowska et al. (2017). In the

case of the organic fraction ratio of carbon stable isotopes represent a tool commonly used for distinguishing between marine and terrigenous sources. However, numerous studies report limitations of this method for high latitudes (Bourgeois et al., 2016; Kuliński et al., 2014; Kumar et al., 2016). Thus, separate quantification of marine and terrestrial OC and IC burial is still a challenge for high Arctic regions.

6. Conclusions

In this study, surface sediments of two high-latitude Arctic fjords, Hornsund and Kongsfjorden, were assessed as a sink of both IC and OC. The burial rate of carbon was taken as a measure of the actual carbon sink. Moreover, comparison of the results from three methods quantifying carbon burial in marine sediments was carried out.

The $OC_{BR(I)}$ differed significantly in the two investigated fjords, as it equaled 19.3–30.3 g OC m⁻² y⁻¹ in Hornsund and 5.7–10.0 g OC m⁻² y⁻¹ in Kongsfjorden. This was accompanied with a higher efficiency of OC burial in Hornsund (75–80%) than in Kongsfjorden (30–50%). The higher carbon burial efficiency in the former indicates that more OC reaching sediments is permanently buried in sediments, a feature attributed to the higher contribution of land-delivered OM there. The burial rate of IC was much smaller in Hornsund and much higher in Kongsfjorden than OC burial was, a feature attributed to both varying SARs and concentrations of carbonates in sediments. The latter reason may result from the larger activity of calciferous organisms and spread of carbonates in the Kongsfjorden catchment area than in Hornsund. The study showed that the values obtained by the three tested methods in separate cores may differ and/or be comparable. On the other hand, by definition, just the 'return flux' method simultaneously takes into account processes that likely affect carbon concentration in sediments: diffusion, mineralization and/or hydrolysis, while it is not vulnerable to OC concentration changes caused by e.g. dynamics of mineral material and/or OC deposition to sediments.

The DOC occurrence in pore water was attributed to hydrolysis and the desorption of biochemically refractory, possibly high-molecular substances, from sediment mineral particles. The absorption spectra indicated that the organic substances released from sediments are likely fulvic acids. This implies that organic substances are delivered to sediments and accumulated in the sediments already as refractory carbon species adsorbed to mineral particles.

Acknowledgements

Katarzyna Koziarowska's participation in the study was supported by the Centre for Polar Studies, KNOW – Leading National Research Centre, Sosnowiec, Poland. Financial support from the National Science Centre, Poland, grant no. 2015/19/N/ST10/01652, and the statutory activities of the Institute of Oceanology (Sopot, Poland) are acknowledged.

References

Andrzejewicz, H., Freiwald, A., Schafer, P., 1996. Bioclastic carbonate sediments on the southwestern Svalbard shelf. *Mar. Geol.* 134 (3–4), 163–182, [http://dx.doi.org/10.1016/0025-3227\(96\)00044-8](http://dx.doi.org/10.1016/0025-3227(96)00044-8).

Antonio, E.S., Kasai, A., Ueno, M., Won, N., Ishihi, Y., Yokoyama, H., Yamashita, Y., 2010. Spatial variation in organic matter utilization by benthic communities from Yura River-Estuary to offshore of Tango Sea, Japan. *Estuar. Coast. Shelf Sci.* 86 (1), 107–117, <http://dx.doi.org/10.1016/j.ecss.2009.10.020>.

Arndt, S., Jorgensen, B.B., LaRowe, D.E., Middelburg, J.J., Pancost, R.D., Regnier, P., 2013. Quantifying the degradation of organic matter in marine sediments: a review and synthesis. *Earth-Sci. Rev.* 123, 53–86, <http://dx.doi.org/10.1016/j.earscirev.2013.02.008>.

Arrigo, K.R., van Dijken, G., Pabi, S., 2008. Impact of a shrinking Arctic ice cover on marine primary production. *Geophys. Res. Lett.* 35 (L19603), <http://dx.doi.org/10.1029/2008GL035028>.

Berner, R.A., 1980. *Early Diagenesis: A Theoretical Approach*. Princeton Univ. Press, Princeton, 1–241.

Bijoy Nandan, S., Krishnapriya, P.P., Akhilesh, V., Asha, C.V., Jayachandran, P.R., Krishnan, K.P., 2016. Benthic Faunal assemblage of the Arctic Kongsfjorden System, Norway. *Int. J. Mar. Sci.* 6, 1–8, <http://dx.doi.org/10.5376/ijms.2016.06.0054>.

Bourgeois, S., Kerherve, P., Calleja, M.L., Many, G., Morata, N., 2016. Glacier inputs influence organic matter composition and prokaryotic distribution in a high Arctic fjord (Kongsfjorden, Svalbard). *J. Marine Syst.* 164, 112–127, <http://dx.doi.org/10.1016/j.jmarsys.2016.08.009>.

Carroll, J., Zaborska, A., Papucci, C., Schirone, A., Carroll, M.L., Pempkowiak, J., 2008. Accumulation of organic carbon in western Barents Sea sediments. *Deep-Sea Res. II* 55 (20–21), 2361–2371, <http://dx.doi.org/10.1016/j.dsr2.2008.05.005>.

Cochrane, S.K.J., Denisenko, S.G., Renaud, P.E., Emblow, C.S., Ambrose, W.G., Ellingsen, I.H., Skarohamar, J., 2009. Benthic macrofauna and productivity regimes in the Barents Sea – ecological implications in a changing Arctic. *J. Sea Res.* 61 (4), 222–233, <http://dx.doi.org/10.1016/j.seares.2009.01.003>.

Cui, X.Q., Bianchi, T.S., Jaeger, J.M., Smith, R.W., 2016. Biospheric and petrogenic organic carbon flux along southeast Alaska. *Earth Planet. Sci. Lett.* 452, 238–246, <http://dx.doi.org/10.1016/j.epsl.2016.08.002>.

Elverhoi, A., Lonne, O., Selander, R., 1983. Glacimarine sedimentation in a modern fjord environment. *Polar Res.* 1, 127–149, <http://dx.doi.org/10.3402/polar.v1i2.6978>.

Fernandez-Mendez, M., Katlein, C., Rabe, B., Nicolaus, M., Peeken, I., Bakker, K., Flores, H., Boetius, A., 2015. Photosynthetic production in the central Arctic Ocean during the record sea-ice minimum in 2012. *Biogeosciences* 12, 3525–3549, <http://dx.doi.org/10.5194/bg-12-3525-2015>.

Flynn, W.W., 1968. The determination of low levels of 210Po in environmental materials. *Anal. Chim. Acta* 43 (2), 221–227, [http://dx.doi.org/10.1016/S0003-2670\(00\)89210-7](http://dx.doi.org/10.1016/S0003-2670(00)89210-7).

Freiwald, A., 1998. *Modern nearshore cold-temperate calcareous sediments in the Troms District, Northern Norway*. *J. Sediment. Res.* 68 (5), 763–776.

Glud, R.N., Holby, O., Hoffmann, F., Canfield, D.E., 1998. Benthic mineralization and exchange in Arctic sediments (Svalbard, Norway). *Mar. Ecol.-Prog. Ser.* 173, 237–251, <http://dx.doi.org/10.3354/meps173237>.

Gorlich, K., 1986. *Glacimarine sedimentation of muds in Hornsund Fjord, Spitsbergen*. *Ann. Soc. Geologor. Polon.* 56 (3–4), 433–477.

Holcombe, B.L., Keil, R.G., Devol, A.H., 2001. Determination of pore-water dissolved organic carbon fluxes from Mexican margin sediments. *Limnol. Oceanogr.* 46 (2), 298–308, <http://dx.doi.org/10.4319/lo.2001.46.2.0298>.

Holding, J.M., Duarte, C.M., Delgado-Huertas, A., Soetaert, K., Vonk, J.E., Agusti, S., Wassmann, P., Middelburg, J.J., 2017. Autochthonous and allochthonous contributions of organic carbon to microbial food webs in Svalbard fjords. *Limnol. Oceanogr.* 62 (2), 1307–1323, <http://dx.doi.org/10.1002/lno.10526>.

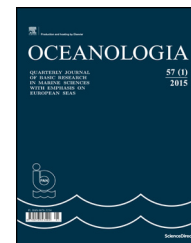
Hop, H., Pearson, T., Hegseth, E.N., Kovacs, K.M., Wiencke, C., Kwaśniewski, S., Eiane, K., Mehlum, F., Gulliksen, B., Włodarska-Kowalczyk, M., Lydersen, C., Węstawski, J.M., Cochrane, S.,

- Gabrielsen, G.W., Leakey, R.J.G., Lonne, O.J., Zajączkowski, M., Falk-Petersen, S., Kendall, M., Wangberg, S.A., Bischof, K., Voronkov, A.Y., Kovaltchouk, N.A., Wiktor, J., Poltermann, M., di Prisco, G., Papucci, C., Gerland, S., 2002. The marine ecosystem of Kongsfjorden, Svalbard. *Polar Res.* 21 (1), 167–208, <http://dx.doi.org/10.1111/j.1751-8369.2002.tb00073.x>.
- Hulth, S., Hall, P.O.J., Blackburn, T.H., Landen, A., 1996. Arctic sediments (Svalbard): pore water and solid phase distributions of C, N, P and Si. *Polar Biol.* 16 (6), 447–462.
- Ingall, E., Kolowith, L., Lyons, T., Hurtgen, M., 2005. Sediment carbon, nitrogen and phosphorus cycling in an anoxic fjord. Effingham Inlet, British Columbia. *Am. J. Sci.* 305 (3), 240–258, <http://dx.doi.org/10.2475/ajs.305.3.240>.
- IPCC, 2013. *Climate Change 2013: The Physical Science Basis. Contribution of Working Group I to the Fifth Assessment Report of the Intergovernmental Panel on Climate Change.* Cambridge University Press, Cambridge, United Kingdom and New York, NY, USA.
- Jorgensen, B.B., Glud, R.N., Holby, O., 2005. Oxygen distribution and bioirrigation in Arctic fjord sediments (Svalbard, Barents Sea). *Mar. Ecol.-Prog. Ser.* 292, 85–95, <http://dx.doi.org/10.3354/meps292085>.
- Kędra, M., Włodarska-Kowalczyk, M., Węstawski, J.M., 2010. Decadal change in macrobenthic soft-bottom community structure in a high Arctic fjord (Kongsfjorden, Svalbard). *Polar Biol.* 33 (1), 1–11, <http://dx.doi.org/10.1007/s00300-009-0679-1>.
- Knudson, K.P., Hendy, I.L., Neil, H.L., 2011. Re-examining Southern Hemisphere westerly wind behavior: insights from a late Holocene precipitation reconstruction using New Zealand fjord sediments. *Quat. Sci. Rev.* 30, 3124–3138, <http://dx.doi.org/10.1016/j.quascirev.2011.07.017>.
- Koziarowska, K., Kuliński, K., Pempkowiak, J., 2016. Sedimentary organic matter in two Spitsbergen fjords: Terrestrial and marine contributions based on carbon and nitrogen contents and stable isotopes composition. *Cont. Shelf Res.* 113, 38–46, <http://dx.doi.org/10.1016/j.csr.2015.11.010>.
- Koziarowska, K., Kuliński, K., Pempkowiak, J., 2017. Distribution and origin of inorganic and organic carbon in the sediments of Kongsfjorden, Northwest Spitsbergen, European Arctic. *Cont. Shelf Res.* 150, 27–35, <http://dx.doi.org/10.1016/j.csr.2017.08.023>.
- Kuliński, K., Pempkowiak, J., 2012. Carbon Cycling in the Baltic Sea. Springer, Berlin, 1–129, <http://dx.doi.org/10.1007/978-3-642-19388-0>.
- Kuliński, K., Kędra, M., Legeżyńska, J., Gtuchowska, M., Zaborska, A., 2014. Particulate organic matter sinks and sources in high Arctic fjord. *J. Marine Syst.* 139, 27–37, <http://dx.doi.org/10.1016/j.jmarsys.2014.04.018>.
- Kumar, V., Tiwari, M., Nagoji, S., Tripathi, S., 2016. Evidence of Anomalous Low delta C-13 of Marine Organic Matter in an Arctic Fjord. *Sci. Rep.* 6, <http://dx.doi.org/10.1038/srep36192>.
- Lalande, C., Belanger, S., Fortier, L., 2009. Impact of a decreasing sea ice cover on the vertical export of particulate organic carbon in the northern Laptev Sea, Siberian Arctic Ocean. *Geophys. Res. Lett.* 36 (L21604), <http://dx.doi.org/10.1029/2009GL040570>.
- Martin, W.R., McCorkle, D.C., 1993. Dissolved organic carbon concentrations in marine pore waters determined by high-temperature oxidation. *Limnol. Oceanogr.* 38 (7), 1464–1479.
- Mucci, A., Sundby, B., Gehlen, M., Arakaki, T., Zhong, S., Silverberg, N., 2000. The fate of carbon in continental shelf sediments of eastern Canada: a case study. *Deep-Sea Res.* II 47, 733–760.
- Muller, A., 2001. Geochemical expressions of anoxic conditions in Nordasvannet, a land-locked fjord in western Norway. *Appl. Geochem.* 16 (3), 363–374, [http://dx.doi.org/10.1016/s0883-2927\(00\)00024-x](http://dx.doi.org/10.1016/s0883-2927(00)00024-x).
- Muzuka, A.N.N., Hillaire-Marcel, C., 1999. Burial rates of organic matter along the eastern Canadian margin and stable isotope constraints on its origin and diagenetic evolution. *Mar. Geol.* 160 (3–4), 251–270, [http://dx.doi.org/10.1016/s0025-3227\(99\)00022-5](http://dx.doi.org/10.1016/s0025-3227(99)00022-5).
- Pawłowska, J., Łącka, M., Kucharska, M., Szymańska, N., Koziarowska, K., Kuliński, K., Zajączkowski, M., 2017. Benthic foraminifera contribution to fjord modern carbon pools: a seasonal study in Adventfjorden, Spitsbergen. *Geobiology* 15 (5), 704–714, <http://dx.doi.org/10.1111/gbi.12242>.
- Pempkowiak, J., 1991. Enrichment factors of heavy-metals in the Southern Baltic surface sediments dated with Pb210 and Cs137. *Environ. Int.* 17 (5), 421–428, [http://dx.doi.org/10.1016/0160-4120\(91\)90275-u](http://dx.doi.org/10.1016/0160-4120(91)90275-u).
- Pempkowiak, J., Szponar, Z., 1993. The complexing capacities of humic substances isolated from Baltic sediments and their molecular weight fractions towards copper (II) and iron (III). *Oceanologia* 34, 39–47.
- Pickrill, R.A., 1993. Sediment yields in Fjordland. *J. Hydrol.* 31 (1), 39–55.
- Piechura, J., Beszczynska-Moller, A., Osinski, R., 2001. Volume, heat and salt transport by the West Spitsbergen Current. *Polar Res.* 20 (2), 233–240, <http://dx.doi.org/10.1111/j.1751-8369.2001.tb00061.x>.
- Piwosz, K., Walkusz, W., Hapter, R., Wieczorek, P., Hop, H., Wiktor, J., 2009. Comparison of productivity and phytoplankton in a warm (Kongsfjorden) and a cold (Hornsund) Spitsbergen fjord in mid-summer 2002. *Polar Biol.* 32 (4), 549–559, <http://dx.doi.org/10.1007/s00300-008-0549-2>.
- Promińska, A., Cisek, M., Walczowski, W., 2017. Kongsfjorden and Hornsund hydrography – comparative study based on a multiyear survey in fjords of west Spitsbergen. *Oceanologia* 59 (4), 397–412, <http://dx.doi.org/10.1016/j.oceano.2017.07.003>.
- Renaud, P.E., Morata, N., Ambrose, W.G., Bowie, J.J., Chiuchiolo, A., 2007. Carbon cycling by seafloor communities on the eastern Beaufort Sea shelf. *J. Exp. Mar. Biol. Ecol.* 349 (2), 248–260, <http://dx.doi.org/10.1016/j.jembe.2007.05.021>.
- Renaud, P.E., Morata, N., Carroll, M.L., Denisenko, S.G., Reigstad, M., 2008. Pelagic-benthic coupling in the western Barents Sea: processes and time scales. *Deep-Sea Res.* II 55, 2372–2380, <http://dx.doi.org/10.1016/j.dsr2.2008.05.017>.
- Robbins, J.A., 1978. Geochemical and geophysical applications of radioactive lead. In: Nriagu, J.O. (Ed.), *Biogeochemistry of Lead in the Environment.* Elsevier, Amsterdam, 285–393.
- Rysgaard, S., Nielsen, T.G., 2006. Carbon cycling in a high-arctic marine ecosystem – Young Sound, NE Greenland. *Prog. Oceanogr.* 71 (2–4), 426–445, <http://dx.doi.org/10.1016/j.pcean.2006.09.004>.
- Schnitzer, M., 1991. Soil organic matter – the next 75 years. *Soil Sci.* 151 (1), 41–58, <http://dx.doi.org/10.1097/00010694-199101000-00008>.
- Schnitzer, M., Khan, S.U., 1972. *Humic Substances in the Environment. Books on Demand.*
- Sepulveda, J., Pantoja, S., Hughen, K.A., 2011. Sources and distribution of organic matter in northern Patagonia fjords, Chile (similar to 44–47 degrees S): a multi-tracer approach for carbon cycling assessment. *Cont. Shelf Res.* 31 (3–4), 315–329, <http://dx.doi.org/10.1016/j.csr.2010.05.013>.
- Silverberg, N., Sundby, B., Mucci, A., Zhong, S., Arakaki, T., Hall, P., LandeHn, A., Tengberg, A., 2000. Remineralization of organic carbon in eastern Canadian continental margin sediments. *Deep-Sea Res.* II 47 (3–4), 699–731, [http://dx.doi.org/10.1016/S0967-0645\(99\)00123-X](http://dx.doi.org/10.1016/S0967-0645(99)00123-X).
- Smeaton, C., Austin, W.E.N., Davies, A.L., Baltzer, A., Abell, R.E., Howe, J.A., 2016. Substantial stores of sedimentary carbon held in mid-latitude fjords. *Biogeosciences* 13 (20), 5771–5787, <http://dx.doi.org/10.5194/bg-13-5771-2016>.
- Smith, R.W., Bianchi, T.S., Allison, M., Savage, C., Galy, V., 2015. High rates of organic carbon burial in fjord sediments globally. *Nat. Geosci.* 8 (6), 446–450, <http://dx.doi.org/10.1038/ngeo2421>.
- Smola, Z., Tatarek, A., Wiktor, J., Wiktor Jr., J., Hapter, R., Kubiszyn, A., Węstawski, J.M., 2017. Primary producers and production in

- Hornsund and Kongsfjorden – comparison of two fjord systems. *Pol. Polar Res.* 38 (3), 351–373, <http://dx.doi.org/10.1515/popore-2017-0013>.
- Stein, R., Macdonald, R.W., 2004. *The Organic Carbon Cycle in Arctic Ocean*. Springer.
- St-Onge, G., Hillaire-Marcel, C., 2001. Isotopic constraints of sedimentary inputs and organic carbon burial rates in the Saguenay Fjord, Quebec. *Mar. Geol.* 176 (1–4), 1–22, [http://dx.doi.org/10.1016/S0025-3227\(01\)00150-5](http://dx.doi.org/10.1016/S0025-3227(01)00150-5).
- Stoumermer, D., Harvey, G., 1974. Humic substances from seawater. *Nature* 250, 480–481, <http://dx.doi.org/10.1038/250480a0>.
- Swerpel, S., 1985. The Hornsund fjord: water masses. *Pol. Polar Res.* 6 (4), 475–496.
- Szczuciński, W., Schettler, G., Zajączkowski, M., 2006. Sediment accumulation rates, geochemistry and provenance in complex High Arctic fjord, Hornsund, Svalbard. In: Fourth ESF SEDIFLUX Science Meeting & First Workshop of I.A.G./A.I.G. SEDIBUD: Source to Sink Fluxes and Sediment Budgets in Cold Environments. NGF Abstracts and Proceeding of the Geological Society of Norway 4. p. 65.
- Szczuciński, W., Zajączkowski, M., Scholten, J., 2009. Sediment accumulation rates in subpolar fjords – impact of post-Little Ice Age glaciers retreat, Billefjorden, Svalbard. *Estuar. Coast. Shelf Sci.* 85 (3), 345–356, <http://dx.doi.org/10.1016/j.ecss.2009.08.021>.
- Teske, A., Durbin, A., Ziervogel, K., Cox, C., Arnosti, C., 2011. Microbial community composition and function in permanently cold seawater and sediments from an Arctic Fjord of Svalbard. *Appl. Environ. Microbiol.* 77 (6), 2008–2018, <http://dx.doi.org/10.1128/aem.01507-10>.
- Ullman, W.J., Aller, R.C., 1982. Diffusion-coefficients in nearshore marine-sediments. *Limnol. Oceanogr.* 27 (3), 552–556, <http://dx.doi.org/10.4319/lo.1982.27.3.0552>.
- Węstawski, J.M., Buchholz, F., Gtuchowska, M., Weydmann, A., 2017. Ecosystem maturation process follows the warming of the Arctic fjords. *Oceanologia* 59 (4), 592–602, <http://dx.doi.org/10.1016/j.oceano.2017.02.002>.
- Winkelmann, D., Knies, J., 2005. Recent distribution and accumulation of organic carbon on the continental margin west off Spitsbergen. *Geochem. Geophys. Geosyst.* 6, <http://dx.doi.org/10.1029/2005gc000916>.
- Winogradow, A., Pempkowiak, J., 2018. Characteristic of sedimentary organic matter in coastal and depositional areas in the Baltic Sea. *Estuar. Coast. Shelf Sci.* 204, 66–75, <http://dx.doi.org/10.1016/j.ecss.2018.02.011>.
- Włodarska-Kowalczyk, M., Pearson, T.H., 2004. Soft-bottom macrobenthic faunal associations and factors affecting species distributions in an Arctic glacial fjord (Kongsfjord, Spitsbergen). *Polar Biol.* 27 (3), 155–167, <http://dx.doi.org/10.1007/s00300-003-0568-y>.
- Zaborska, A., 2017. Sources of ¹³⁷Cs to an Arctic fjord (Hornsund, Svalbard). *J. Environ. Radioact.* 180, 19–26, <http://dx.doi.org/10.1016/j.jenvrad.2017.09.021>.
- Zaborska, A., Beszczynska-Moller, A., Włodarska-Kowalczyk, M., 2017. History of heavy metal accumulation in the Svalbard area: distribution, origin and transport pathways. *Environ. Pollut.* 231 (1), 437–450, <http://dx.doi.org/10.1016/j.envpol.2017.08.042>.
- Zaborska, A., Carroll, J., Papucci, C., Pempkowiak, J., 2007. Inter-comparison of alpha and gamma spectrometry techniques used in Pb-210 geochronology. *J. Environ. Radioact.* 93 (1), 38–50, <http://dx.doi.org/10.1016/j.jenvrad.2006.11.007>.
- Zaborska, A., Carroll, J., Papucci, C., Torricelli, L., Carroll, M.L., Walkusz-Miotk, J., Pempkowiak, J., 2008. Recent sediment accumulation rates for the Western margin of the Barents Sea. *Deep-Sea Res. II* 55 (20–21), 2352–2360, <http://dx.doi.org/10.1016/j.dsr2.2008.05.026>.
- Zaborska, A., Pempkowiak, J., Papucci, C., 2006. Some sediment characteristic and sedimentation rates in an Arctic fjord (Kongsfjorden, Svalbard). *Rocz. Ochr. Sr.* 8, 79–96.
- Zaborska, A., Włodarska-Kowalczyk, M., Legeżyńska, J., Jankowska, E., Winogradow, A., Deja, K., 2016. Sedimentary organic matter sources, benthic consumption and burial in west Spitsbergen fjords – Signs of maturing of Arctic fjordic systems? *J. Marine Syst.* 180, 112–123, <http://dx.doi.org/10.1016/j.jmarsys.2016.11.005>.

Available online at www.sciencedirect.com

ScienceDirect

journal homepage: www.journals.elsevier.com/oceanologia/

SHORT COMMUNICATION

Characterization of light absorption coefficient of red *Noctiluca scintillans* bloom in the South Eastern Arabian Sea

Sudheeshan Sushama Shaju ^{a,*}, Raghunadha Rao Akula ^a, Thajudeen Jabir ^b

^a Naval Physical and Oceanographic Laboratory (DRDO), Kochi, India

^b Department of Marine Biology Microbiology and Biochemistry, Cochin University of Science and Technology, Kochi, India

Received 27 June 2017; accepted 20 December 2017

Available online 8 January 2018

KEYWORDS

Noctiluca scintillans;
Phytoplankton
absorption coefficient;
Upwelling;
Oil sardine;
South Eastern Arabian
Sea (SEAS)

Summary The red *Noctiluca scintillans* bloom was observed off Cochin in the South Eastern Arabian Sea (SEAS), affecting a very large area during July–August 2016. The surface water samples from the bloom region were collected to study the physical, biological and light absorption characteristics. The bloom affects the food chain by their voracious predation on the species of both first and second trophic levels. The *N. scintillans* cell density during the bloom was estimated at 4.73×10^5 cells l^{-1} . In the phytoplankton absorption coefficient spectra, the accessory pigments displayed peaks in the 488–558 nm regions, which represent the characteristic carotenoid pigment (red colored pigment) for the bloom of red *Noctiluca*. Signature of the coastal upwelling was found from the salinity and temperature distribution, which was measured prior to the bloom occurrence. From the sea surface temperature (SST), it is also confirmed the presence of fresh water from the Cochin estuary. Increased productivity near coastal region, along with episodic events of strengthening of the upwelling, favors the proliferation of smaller diatoms. The plankton succession from smaller diatoms to larger diatoms and dinoflagellates, favors the proliferation of the red *Noctiluca*. The occurrence of blooms of red *N. scintillans*, which feed on phytoplankton, mainly diatoms, and other dinoflagellates, could be a threat to larvae of oil sardine during the upwelling period, and may negatively impact on the commercially important fishery of oil sardine, in this region.

© 2018 Institute of Oceanology of the Polish Academy of Sciences. Production and hosting by Elsevier Sp. z o.o. This is an open access article under the CC BY-NC-ND license (<http://creativecommons.org/licenses/by-nc-nd/4.0/>).

* Corresponding author at: Naval Physical and Oceanographic Laboratory (DRDO), Kochi 682021, India.

E-mail address: shaju.peringammala@gmail.com (S.S. Shaju).

Peer review under the responsibility of Institute of Oceanology of the Polish Academy of Sciences.



Production and hosting by Elsevier

<https://doi.org/10.1016/j.oceano.2017.12.002>

0078-3234/© 2018 Institute of Oceanology of the Polish Academy of Sciences. Production and hosting by Elsevier Sp. z o.o. This is an open access article under the CC BY-NC-ND license (<http://creativecommons.org/licenses/by-nc-nd/4.0/>).

Noctiluca scintillans (Macartney) Kofoid & Swezy 1921, a marine planktonic dinoflagellate, is one of the most important and abundant red tide organisms. It has a worldwide distribution and occurs in two forms. Red *Noctiluca* is heterotrophic and acts as a microzooplankton grazer in the food web. Green *Noctiluca* contains the photosynthetic symbiont *Pedinomonas noctilucae* (Subrahmanyam) Sweeney, 1976 (Prasinophyte), also feeds on other plankton. Red *Noctiluca* occurs over a wide temperature range from 10 to 25°C and at salinities higher than 28 psu. It is particularly abundant in high productivity areas such as upwelling or eutrophic areas where diatoms dominate, since they are its preferred food source. Green *Noctiluca* is restricted to a temperature range of 25–30°C and occurs mainly in tropical waters of the south-east Asia, Bay of Bengal (east coast of India), eastern, western and northern Arabian Sea and Red Sea (Baliarsingh et al., 2016; Gomes et al., 2014; Harrison et al., 2011; Turkoglu, 2013). The red *N. scintillans* lacks symbiotic association with diatoms and its red color is due to the grazing of diatoms, which contains carotenoids (Balch and Haxo, 1984). The red *N. scintillans* blooms affects the food chain by their voracious predation on the species of both first and second trophic level (Baliarsingh et al., 2016; Padmakumar et al., 2016). Blooms of *N. scintillans* have been linked to massive mortality of fish and marine invertebrates. Although this species does not produce toxin, it has been found to accumulate toxic levels of ammonia, acting as killing agent in blooms and deteriorating the water quality (Sahayak et al., 2005). Identification of phytoplankton types on the basis of absorption spectra is a challenge for the Harmful Algal Bloom (HAB) monitoring. This study is an approach to improve the knowledge of the optical characteristics of important HAB species in South Eastern Arabian Sea (SEAS) and to provide information on the possible effect on the fishery.

The coastal waters of SEAS were largely influenced by freshwater discharge and seasonally reversing monsoon. The summer (southwest) monsoon extends from June to September whereas the winter (northeast) monsoon extends from November to February. The upwelling process, supported by the southerly current observed along the coastal waters during the southwest monsoon, results in maximum primary production (Habebrehman et al., 2008; Joshi and Rao, 2012). A seasonal hypoxia arises due to increased oxygen demand for mineralization of organic matter following high surface production (Gupta et al., 2016). The Cochin backwater is the largest estuarine system of the southwest coast of India, and receives $1.04 \times 10^5 \text{ m}^3$ of industrial and 260 m^3 of domestic wastes per day without treatment (Gupta et al., 2009). During southwest monsoon, the hydrographic parameters are significantly influenced by strong freshwater influx (Srinivas and Dineshkumar, 2006).

The surface water samples were collected onboard INS *Sagardhwani* on 21st July at the CTD stations and on 2nd August 2016, a representative water sample from the bloom patches were also collected to estimate the Chlorophyll *a* (Chl-*a*) concentration. For this, the collected samples were filtered through 25 mm Whatman GF/F filter under low vacuum (100–1000 ml based on the concentration visually seen from the filter paper) and extracted with 90% acetone and analysis were done by using Turner Designed 10AU Fluorometer. Also surface water samples from the bloom region were collected for the measurements absorption

characteristics. The light absorption coefficient of phytoplankton [$aph(\lambda)$] was measured using a quantitative glass fiber filter technique (QFT) and standard procedures (Hoepffner and Sathyendranath, 1993; Shaju et al., 2015; Vijayan and Somayajula, 2014). In brief, surface water samples collected were filtered through 25 mm Whatman GF/F filter under low vacuum and the filtrate measured against a blank filter using a Shimadzu UV-VIS spectrophotometer attached to an integrating sphere following the protocol of Mitchell (1990). The wavelength scan was done from 300 nm to 750 nm with the resolution of 1 nm before and after rinsing the filter paper with warm methanol for one hour to determine the detrital absorption (Kishino et al., 1985). For each of the measured spectra, the optical density obtained at 750 nm was subtracted from that of all other wavelengths. Optical density of the total suspended matter was corrected for the pathlength amplification (β effect) and converted into light absorption coefficients by the total particulate matter [$ap(\lambda)$] (m^{-1}) and detritus matter [$ad(\lambda)$] (m^{-1}), i.e. before and after extraction with methanol, respectively (Cleveland and Weidemann, 1993; Kyewalyanga et al., 1998). The plankton absorption component [$aph(\lambda)$] was derived as a difference between the particulate and detritus absorptions of the total particulate matter by subtraction $ad(\lambda)$ from $ap(\lambda)$ (Bricaud et al., 2004; Kishino et al., 1985). Samples were also collected from the bloom area to identify the phytoplankton composition. Inverted microscope (Leica Generic DMIL) with phase contrast was used to estimate the phytoplankton diversity and abundance using standard identification keys (Tomas, 1997). In this study, light absorption characteristics of red tide were analyzed based on the pigments in the bloom samples by the decomposition of phytoplankton absorption coefficient spectra using the 4th derivative analysis (Shaju et al., 2015). The fourth derivative of $aph(\lambda)$ was calculated by applying the 41 point fourth degree polynomial smoothing and then by differentiation using the Savitzky–Golay method (Savitzky and Golay, 1964). The polynomial smoothing was applied because differentiation tends to amplify the effects of high frequency noise in the spectra (Aguirre-Gómez et al., 2001). The procedure was carried out using the Origin 8.0 scientific analysis software. Peaks in the fourth derivative curves were selected using the peak finder tool in the software. The physical conditions prevailing in the area were measured using the conductivity temperature depth (CTD) profiler Idronaut Ocean Seven 320 plus system on 21st July 2016. Microwave+Infra-red (IR) Optimally Interpolated (OI) Sea Surface Temperature (SST) data obtained by Remote Sensing Systems sponsored by National Oceanographic Partnership Program (NOPP) and the NASA Earth Science Physical Oceanography Program, available at www.remss.com/measurements/sea-surface-temperature were also used in this study.

Reddish discoloration of coastal waters off Cochin, at 09°48'N and 76°03'E, was observed from the vessel MV *Pra-shikshani* on 28th July 2016 and subsequently, on 2nd August, from INS *Sagardhwani* (Fig. 1). The species causing the bloom was identified as the *N. scintillans* (Macartney) Kofoid and Swezy, 1921 (Fig. 2a), which is a heterotrophic dinoflagellate and one of the abundant “red tide” organisms in the tropical, subtropical, temperate coastal waters (Sriwoon et al., 2008) and upwelling regions (Dela-Cruz et al., 2008). The red patches of the bloom (Fig. 2b) were observed in a vast area

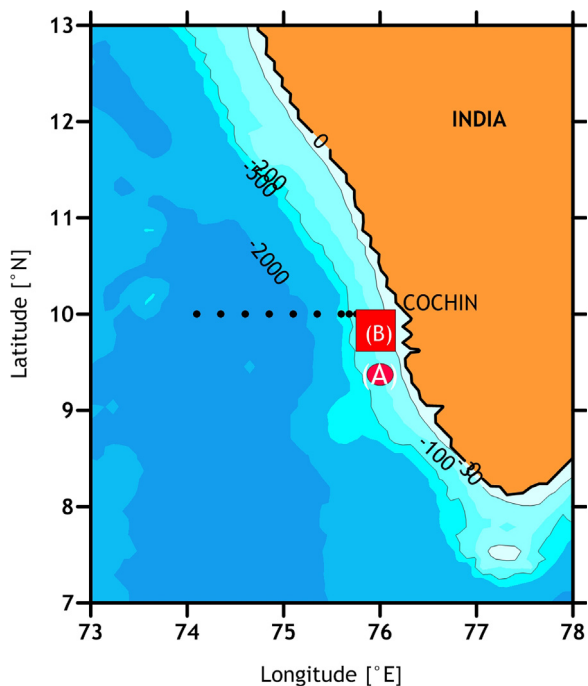


Figure 1 Map of the study area showing the hydrographic stations (dotted points) sampled one week before the first observation of the bloom (A – indicates bloom observation on 28th July 2016 onboard MV *Prashikshani*, B – indicates bloom observation on 2nd August 2016 onboard INS *Sagardwani*).

extending from 09°55' to 09°57'N and 75°59' to 76°03'E. The red *N. scintillans* blooms were last reported in the coastal waters of SEAS in 2004 and 2008 (Baliarsingh et al., 2016; Joseph et al., 2008; Padmakumar et al., 2016) whereas the green *N. scintillans* blooms were regularly reported in the coastal regions of the northern Arabian Sea (Baliarsingh et al., 2016; Gomes et al., 2014). This study attempts the bio-optical characterization of *N. scintillans* bloom in the SEAS and discusses its possible impacts on the food web and sardine fishery of the region.

The water column salinity and temperature distribution along 10°N, prior to the bloom occurrence is given in Fig. 3a and b and it has shown signature of coastal upwelling from the up sloping of salinity and temperature contours. A low saline patch was observed near the coast in the upper few meters in the salinity distribution, which would have been generated due to the freshwater influx from the estuary (Jyothibabu et al., 2006; Madhupratap, 1987). This cold less saline surface water from Cochin estuary normally carries high nutrients that help in the increased productivity during summer monsoon near the coast. Prior to the bloom initiation, Chl-*a* concentration varied from 0.28 to 0.42 mg m⁻³ with an average value of 0.34 ± 0.05 mg m⁻³ in the offshore region and from 0.55 to 4.16 mg m⁻³ with an average concentration of 1.47 ± 1.37 mg m⁻³ in the near coastal waters off Cochin. This increased productivity and episodic events of low SST visible from the time series SST (Fig. 4). The effect of intense upwelling as evidenced from data distribution along the near coastal region, favors the proliferation of smaller diatoms (Sahayak et al., 2005). The plankton succession from smaller diatoms to larger diatoms and dinoflagellates, favors the proliferation of red *Noctiluca* bloom.



Figure 2 Bloom of red *Noctiluca scintillans* as (a) microscopic picture of the *Noctiluca scintillans*, a line indicates the 200 μm length (b) large patches extending to the vast area.

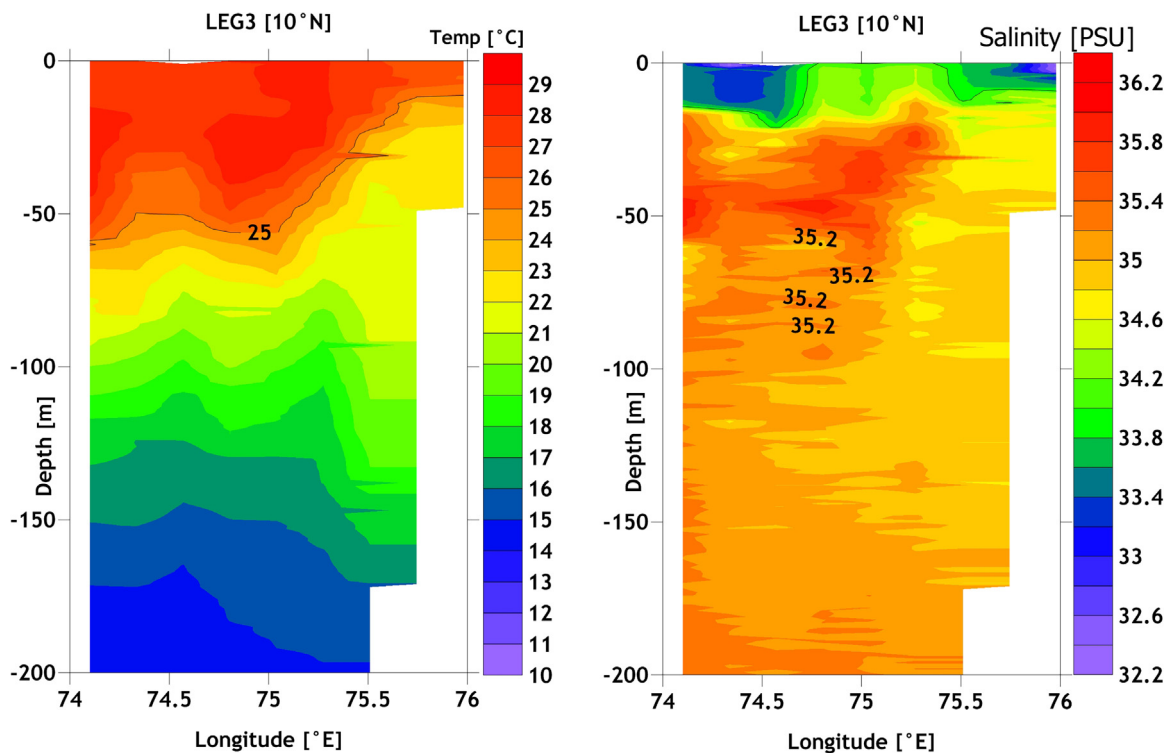


Figure 3 Longitude depth section of (a) temperature ($^{\circ}\text{C}$) and (b) salinity (psu) along 10°N in the off Cochin region measured onboard INS Sagardwani on 21st July 2016.

The density of *N. scintillans* was found to be 4.73×10^5 cells l^{-1} and the measured Chl-*a* concentration varied from 0.73 to 1.47 mg m^{-3} in the bloom region. This is comparable to the bloom event of the southeastern Black Sea on April 2011 with cell number ranges between 1.1×10^3 to 6.81×10^6 cell l^{-1} (Kopuz et al., 2014) and Sea of Marmara with cell density of 2.20×10^6 cell l^{-1} (Turkoglu, 2013). Other phytoplankton species in the bloom area were *Ceratium* sp., *Rhizosolenia* sp., *Porocentrum* sp., *Thalassiosira* sp., *Nitzschia* sp. and *Dinophysis* sp. The percentage composition of *N. scintillans*, diatoms and other dinoflagellates in the bloom waters were 72.67%, 10.92% and 16.32% respectively. A very low species diversity and abundance of other dinoflagellates and diatoms were observed. The diatom, *Thalassiosira* sp. was notable, since it is considered to be the most preferred prey species of the red *N. scintillans* (Baliarsingh et al., 2016; Sahayak et al., 2005).

A representation of the measured phytoplankton absorption coefficient spectra [$a_{ph}(\lambda)$] from the water samples collected from the bloom and its fourth derivative are given in Fig. 5. Absorption maxima for the pigment Chl-*a* in the phytoplankton absorption spectrum were found around wavelengths of 444 and 676 nm, while accessory pigments displayed their absorption peaks in the 488–558 nm regions, which represents characteristic carotenoid (red pigment) for the red *Noctiluca* bloom. The optical measurements from the Belgian coastal waters during a red *Noctiluca* bloom event on 2015 also showed the same results with a maximum absorption at 488 nm which corresponds to the carotenoids (Astorceca et al., 2005). Karabashev and Evdoshenko (2016) identified that the high content of accessory pigments makes inequalities in remote sensing reflectance (R_{rs}). It was also

found that $R_{rs}(488) < R_{rs}(531)$ and $R_{rs}(488) < R_{rs}(469)$. Absorption and reflectance values and effect of R_{rs} deficit due to accessory pigments and their relations give indication of the bloom for the ocean color application and products.

The accessory pigment carotenoid showed an absorption peak at 488 nm and sharper decrease from 528 nm to 580 nm which matches with the earlier reports (Van Mol et al., 2007). The small peaks in the 560–619 nm regions could be accounted for the degradation products and Chl-*c*. Carotenoids, particularly fucoxanthin peaks, could be identified in the 528 nm region in the derivative spectra. The diadinoxanthin and carotene peaks were identified at 488, 528 nm. Phycoerythrobilin peak was observed at 558 nm. Smaller peaks were observed in the 590 nm and also at 615, 619, 635 and 647 nm. The shape and magnitude of the phytoplankton absorption spectrum reflect the pigment composition and its concentrations related to the phytoplankton class. The phytoplankton absorption spectrum modifies the remote sensing reflectance and contributes to the satellite detection of the bloom. Green *N. scintillans* bloom has been identified through remote sensing reflectance spectra, in the northern Arabian Sea (Dwivedi et al., 2016) and in coastal waters of the northeast coast of India (Baliarsingh et al., 2016). But no studies have been reported on the red *N. scintillans* bloom absorption spectral characteristics in the SEAS. Karabashev and Evdoshenko (2016) also identified that a better spectral resolution made it possible to distinguish the second shortwave remote sensing reflectance (R_{rs}) minimum at 488 nm for the cyanobacterial bloom of 2005 in the Baltic Sea and this can be applied to the *Noctiluca* bloom. The absorption peak identified from the phytoplankton absorption coefficient spectra between 488 and 558 nm regions

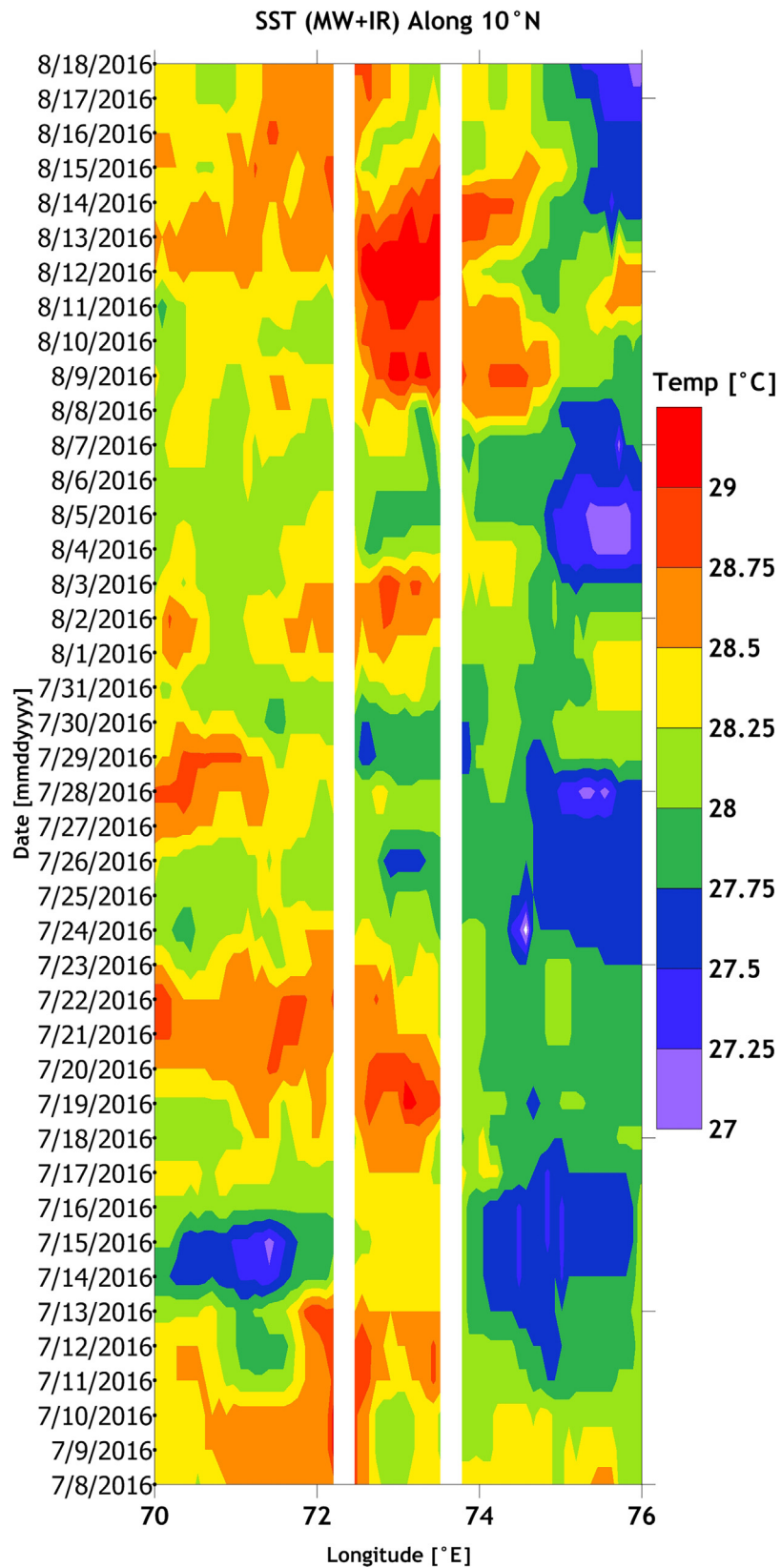


Figure 4 Hovmöller diagram of Sea Surface Temperature (SST) Microwave+Infrared (MW+IR) (°C) from 8th July to 18th August 2016 during the month of bloom period over 10°N latitude.

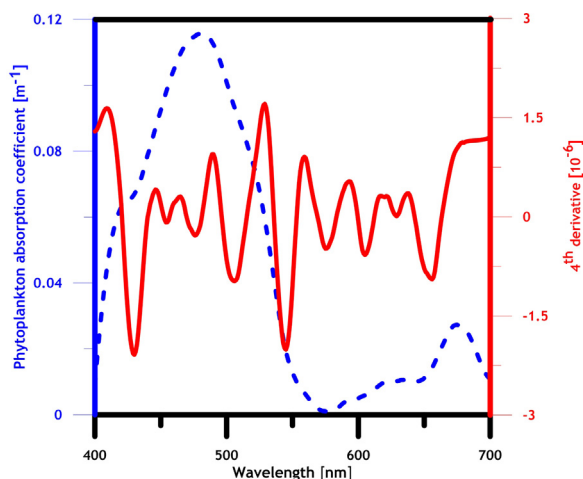


Figure 5 Phytoplankton absorption coefficient spectrum in the visible wavelength of the *Noctiluca scintillans* bloom sample (blue dotted line) and the spectra showing the 4th derivative of the phytoplankton absorption coefficient (red smooth line) against wavelength (nm).

along with the red region can be used for the specific identification of red *N. scintillans* bloom.

Frequent occurrence of diatom blooms affects the fishery resources (Boalch, 1984; Sanseverino et al., 2016). Central Marine Fisheries Research Institute (CMFRI), India, reported a drastic decline in the catch of oil sardine along southwest coast (CMFRI Newsletter, 2015; CMFRI News, 2016), ascribed to the impact of climatic change and related ecosystem changes. The occurrence of blooms of red *N. scintillans*, which graze on phytoplankton, mainly diatoms, and other dinoflagellates, becomes a threat to the food availability of larvae, juveniles and adults of the oil sardine as they also prefer the smaller phytoplanktons during the upwelling period (Padmakumar et al., 2016; Umani et al., 2004) thus would be making it as one of the major reasons for the decline in the oil sardine catch. According to CMFRI (CMFRI Newsletter, 2015; CMFRI News, 2016), the fall in oil sardine catch cause revenue loss to the tune of USD 30 million. The monitoring of Harmful Algal Blooms (HABs) using satellite observations and their early detection still have constraints due to difficulties in identifying phytoplankton functional types. This paper identifies the characteristic pigment of red *N. scintillans* in an upwelling region by optical measurements, which allows the synoptic monitoring of the bloom through satellite platform. Considering the high economic and ecological impacts in the coastal region, more studies on the plankton community structure, physical processes and monitoring of algal bloom using remote sensing would be needed.

Acknowledgements

We thank the Director of the Naval Physical and Oceanographic Laboratory for providing the necessary facilities and the officers and men of INS *Sagardhwani* for the help rendered for onboard sampling. First author thanks DRDO,

Ministry of Defence, Government of India for providing Research Associate Fellowship. Authors express special thanks to Dr. Sanilkumar K.V., Group Director, Ocean Sciences Division, Naval Physical and Oceanographic Laboratory, Kochi for the encouragement of the work, help-rendered and critical evaluation of the manuscript. We also thank Dr. Vipin P.M. for the bloom observation from MV *Prashikshani*.

References

- Aguirre-Gómez, R., Weeks, A.R., Boxall, S.R., 2001. The identification of phytoplankton pigments from absorption spectra. *Int. J. Remote Sens.* 22 (2–3), 315–338, <http://dx.doi.org/10.1080/014311601449952>.
- Astoreca, R., Rousseau, V., Ruddick, K., Mol, B.V., Parent, J., Lancelot, C., 2005. Optical properties of algal blooms in an eutrophicated coastal area and its relevance to remote sensing. In: *Proc. SPIE 5885, Optics and Photonics: Remote Sensing of the Coastal Oceanic Environment*, San Diego, CA, USA, <http://dx.doi.org/10.1117/12.615160>.
- Balch, W.M., Haxo, F.T., 1984. Spectral properties of *Noctiluca miliaris* Suriray, a heterotrophic dinoflagellate. *J. Plankton Res.* 6 (3), 515–525, <http://dx.doi.org/10.1093/plankt/6.3.515>.
- Baliarsingh, S.K., Lotliker, A.A., Trainer, V.L., Wells, M.L., Parida, C., Sahu, B.K., Srichandan, S., Sahoo, S., Sahu, K.C., Kumar, T.S., 2016. Environmental dynamics of red *Noctiluca scintillans* bloom in tropical coastal waters. *Mar. Pollut. Bull.* 111 (1–2), 277–286, <http://dx.doi.org/10.1016/j.marpolbul.2016.06.103>.
- Boalch, G.T., 1984. Algal blooms and their effects on fishing in the English Channel. In: Bird, C.J., Ragan, M.A. (Eds.), *Eleventh International Seaweed Symposium. Developments in Hydrobiology*, Vol 22. Springer, Dordrecht, 449–452, http://dx.doi.org/10.1007/978-94-009-6560-7_89.
- Bricaud, A., Claustre, H., Ras, J., Oubelkheir, K., 2004. Natural variability of phytoplanktonic absorption in oceanic waters: influence of the size structure of algal populations. *J. Geophys. Res.* 109, C11010, <http://dx.doi.org/10.1029/2004JC002419>.
- Cleveland, J.B.S., Weidemann, A.D., 1993. Quantifying absorption by aquatic particles: a multiple scattering correction for glass-fiber filters. *Limnol. Oceanogr.* 38 (6), 1321–1327, <http://dx.doi.org/10.4319/lo.1993.38.6.1321>.
- CMFRI News, 2016. The News Minute, Kochi, India, <http://eprints.cmfri.org.in/id/eprint/10917>.
- CMFRI Newsletter, 2015. Kadalamin, No.145, Kochi, India, 28 pp., <http://eprints.cmfri.org.in/id/eprint/10766>.
- Dela-Cruz, J., Middleton, J.H., Suthers, I.M., 2008. The influence of upwelling, coastal currents and water temperature on the distribution of the red tide dinoflagellate, *Noctiluca scintillans*, along the east coast of Australia. *Hydrobiologia* 598 (1), 59–75, <http://dx.doi.org/10.1007/s10750-007-9140-z>.
- Dwivedi, R., Baliarsingh, S.K., Lotliker, A.A., Kumar, T.S., Shenoj, S.S. C., 2016. An optical approach for synoptic monitoring of red *Noctiluca scintillans* bloom and its associates from space. *Environ. Monit. Assess.* 188 (1), 50, <http://dx.doi.org/10.1007/s10661-015-5041-1>.
- Gomes, H.do.R., Goes, J.I., Matondkar, S.G.P., Buskey, E.J., Basu, S., Parab, S., Thoppil, P., 2014. Massive outbreaks of *Noctiluca scintillans* blooms in the Arabian Sea due to spread of hypoxia. *Nat. Commun.* 5, 4862, <http://dx.doi.org/10.1038/ncomms5862>.
- Gupta, G.V.M., Sudheesh, V., Sudharma, K.V., Saravanane, N., Dhanya, V., Dhanya, K.R., Lakshmi, G., Sudhakar, M., Naqvi, S.W.A., 2016. Evolution to decay of upwelling and associated biogeochemistry over the southeastern Arabian Sea shelf. *J. Geophys. Res. Biogeosci.* 121 (1), 159–175, <http://dx.doi.org/10.1002/2015JG003163>.

- Gupta, G.V.M., Thottathil, S.D., Balachandran, K.K., Madhu, N.V., Madeswaran, P., Nair, S., 2009. CO₂ supersaturation and net heterotrophy in a tropical estuary (Cochin, India): influence of anthropogenic effect. *Ecosystems* 12 (7), 1145–1157, <http://dx.doi.org/10.1007/s10021-009-9280-2>.
- Habeebrehman, H., Prabhakaran, M.P., Jacob, J., Sabu, P., Jayalakshmi, K.J., Achuthankutty, C.T., Revichandran, C., 2008. Variability in biological responses influenced by upwelling events in the eastern Arabian Sea. *J. Mar. Syst.* 74 (1), 545–560, <http://dx.doi.org/10.1016/j.jmarsys.2008.04.002>.
- Harrison, P.J., Furuya, K., Glibert, P.M., Xu, J., et al., 2011. Geographical distribution of red and green *Noctiluca scintillans*. *Chin. J. Oceanol. Limnol.* 29 (4), 807–831, <http://dx.doi.org/10.1007/s00343-011-0510-z>.
- Hoepffner, N., Sathyendranath, S., 1993. Determination of the major groups of phytoplankton pigments from the absorption spectra of total particulate matter. *J. Geophys. Res. Ocean.* 98 (C12), 22789–22803, <http://dx.doi.org/10.1029/93JC01273>.
- Joseph, T., Shaiju, P., Laluraj, C.M., Balachandran, K.K., Nair, M., George, R., Nair, K.K.C., Sahayak, S., Prabhakaran, M.P., 2008. Nutrient environment of red tide-infested waters off south-west coast of India. *Environ. Monit. Assess.* 143 (1–3), 355–361, <http://dx.doi.org/10.1007/s10661-007-9938-1>.
- Joshi, M., Rao, A.D., 2012. Response of southwest monsoon winds on shelf circulation off Kerala coast, India. *Cont. Shelf Res.* 32, 62–70, <http://dx.doi.org/10.1016/j.csr.2011.10.015>.
- Jyothibabu, R., Madhu, N.V., Jayalakshmi, K.V., Balachandran, K.K., Shiyas, C.A., Martin, G.D., Nair, K.K.C., 2006. Impact of freshwater influx on microzooplankton mediated food web in a tropical estuary (Cochin backwaters – India). *Estuar. Coast. Shelf Sci.* 69 (3–4), 505–518, <http://dx.doi.org/10.1016/j.ecss.2006.05.013>.
- Karabashev, G.S., Evdoshenko, M.A., 2016. Narrowband shortwave minima in spectra of backscattered light from the sea obtained from ocean color scanners as a remote indication of algal blooms. *Oceanologia* 58 (4), 279–291, <http://dx.doi.org/10.1016/j.oceano.2016.05.001>.
- Kishino, M., Takahashi, M., Okami, N., Ichimura, S., 1985. Estimation of the spectral absorption coefficients of phytoplankton in the sea. *Bull. Mar. Sci.* 37 (1), 634–642.
- Kopuz, U., Feyzioglu, A.M., Valente, A., 2014. An unusual red-tide event of *Noctiluca scintillans* (Macartney) in the Southeastern Black Sea. *Turk. J. Fish. Aquat. Sci.* 14, 261–268, http://dx.doi.org/10.4194/1303-2712-v14_1_28.
- Kyewalyanga, M.N., Platt, T., Sathyendranath, S., Lutz, V.A., Stuart, V., 1998. Seasonal variations in physiological parameters of phytoplankton across the North Atlantic. *J. Plankton Res.* 20 (1), 17–42.
- Madhupratap, M., 1987. Status and strategy of zooplankton of tropical Indian estuaries: a review. *Bull. Plankton Soc. Japan* 34, 65–81.
- Mitchell, B.G., 1990. Algorithms for determining the absorption coefficient of aquatic particulates using the quantitative filter technique (QFT). In: *Proceedings volume – Ocean Optics X, Orlando, FL, USA, 137–148*.
- Padmakumar, K.B., Thomas, L.C., Vijayan, A., Sudhakar, M., 2016. “Crab Jubilee” subsequent to red tide of *Noctiluca scintillans* along the central Kerala coast (SW coast of India). *Indian J. Geomarine Sci.* 45 (11), 1549–1551.
- Sahayak, S., Jyothibabu, R., Jayalakshmi, K.J., Habeebrehman, H., Sabu, P., Prabhakaran, M.P., Jasmine, P., Shaiju, P., Rejomon, G., Thresamma, J., et al., 2005. Red tide of *Noctiluca miliaris* off south of Thiruvananthapuram subsequent to the “stench event” at the southern Kerala coast. *Curr. Sci.* 89 (9), 1472–1473.
- Sanseverino, I., Conduto, D., Pozzoli, L., Dobricic, S., Lettieri, T., 2016. Algal Bloom and its Economic Impact. Publ. Office EU, Italy, 26–30, <http://dx.doi.org/10.2788/660478>.
- Savitzky, A., Golay, M.J.E., 1964. Smoothing and differentiation of data by simplified least-squares procedures. *Anal. Chem.* 36 (8), 1627–1639, <http://dx.doi.org/10.1021/ac60214a047>.
- Shaju, S.S., Minu, P., Srikanth, A.S., Ashraf, P.M., Vijayan, A.K., Meenakumari, B., 2015. Decomposition study of in vivo phytoplankton absorption spectra aimed at identifying the pigments and the phytoplankton group in complex case 2 coastal waters of the Arabian Sea. *Oceanol. Hydrobiol. Stud.* 44 (3), 282–293, <http://dx.doi.org/10.1515/ohs-2015-0027>.
- Srinivas, K., Dineshkumar, P.K., 2006. Atmospheric forcing on the seasonal variability of sea level at Cochin, Southwest Coast of India. *Cont. Shelf Res.* 26 (10), 1113–1133, <http://dx.doi.org/10.1016/j.csr.2006.03.010>.
- Sriwong, R., Pholpunthin, P., Lirdwitayaprasit, T., Kishino, M., Furuya, K., 2008. Population dynamics of green *Noctiluca scintillans* (Dinophyceae) associated with the monsoon cycle in the upper Gulf of Thailand. *J. Phycol.* 44 (3), 605–615, <http://dx.doi.org/10.1111/j.1529-8817.2008.00516.x>.
- Tomas, C.R., 1997. *Identifying Marine Phytoplankton*. Acad. Press, San Diego, 858 pp.
- Turkoglu, M., 2013. Red tides of the dinoflagellate *Noctiluca scintillans* associated with eutrophication in the Sea of Marmara (the Dardanelles, Turkey). *Oceanologia* 55 (3), 709–732, <http://dx.doi.org/10.5697/oc.55-3.709>.
- Umani, S.F., Beran, A., Parlato, S., Virgilio, D., Zollet, T., De Olazabal, A., Lazzarini, B., Cabrini, M., 2004. *Noctiluca scintillans* Macartney in the Northern Adriatic Sea: long-term dynamics, relationships with temperature and eutrophication, and role in the food web. *J. Plankton Res.* 26 (5), 545–561.
- Van Mol, B., Ruddick, K., Astoreca, R., Park, Y., Nechad, B., 2007. Optical detection of a *Noctiluca scintillans* bloom. *EARSelEProc.* 6, 130–137.
- Vijayan, A.K., Somayajula, S.A., 2014. Effect of accessory pigment composition on the absorption characteristics of dinoflagellate bloom in a coastal embayment. *Oceanologia* 56 (1), 107–124, <http://dx.doi.org/10.5697/oc.56-1.107>.



Available online at www.sciencedirect.com

ScienceDirect

journal homepage: www.journals.elsevier.com/oceanologia/



SHORT COMMUNICATION

First record of the deep-water shark *Etmopterus spinax* (Chondrichthyes: Etmopteridae) from the southern Baltic Sea (Pomeranian Bay)

Beata Więcaszek, Ewa Sobecka, Remigiusz Panicz, Sławomir Keszka, Klaudia Górecka, Angelika Linowska*

West Pomeranian University of Technology in Szczecin, Szczecin, Poland

Received 29 September 2017; accepted 1 February 2018

Available online 14 February 2018

KEYWORDS

Etmopterus spinax;
Anisakis simplex;
Pomeranian Bay;
Southern Baltic Sea;
Inflow from the North
Sea

Summary *Etmopterus spinax* is a deep-sea shark species that inhabits the northeast Atlantic and the western Mediterranean Sea. Skagerrak and Kattegat are reported to be part of the distribution of the species, but it has never been noted in the southern Baltic. Lacking any commercial value and commonly discarded in trawl and longline fisheries, *E. spinax* has been poorly studied. We reported on the first record of one specimen of *E. spinax* caught in the Pomeranian Bay on October 13, 2016 at a depth of 10 m. It was a female measuring 42.7 cm in total length. The morphological examination of the specimen was supported with COI barcode analysis, whereas species assignment to the population of origin was conducted based on a control region (CR) sequence of mtDNA. COI and CR sequence searches against GeneBank confirmed its identity as *E. spinax* and revealed that the specimen shared identical haplotypes with fish from populations in the Azores, Rockall Trough, and west of Ireland in the northeast Atlantic. The stomach contents, parasitic fauna, and hepatosomatic index of the individual were also examined. Only one L3 larval *Anisakis simplex* nematode specimen was collected from the stomach lumen of the shark. The specimen could have arrived in the Pomeranian Bay along with an inflow

* Corresponding author at: Department of Hydrobiology, Ichthyology and Biotechnology of Breeding, Faculty of Food Sciences and Fisheries, West Pomeranian University of Technology in Szczecin, K. Królewicza st. 4, 71-550 Szczecin, Poland. Tel.: +48 91 449 66 93.

E-mail addresses: Beata.Wiecaszek@zut.edu.pl (B. Więcaszek), Ewa.Sobecka@zut.edu.pl (E. Sobecka), Remigiusz.Panicz@zut.edu.pl (R. Panicz), Sławomir.Keszka@zut.edu.pl (S. Keszka), Klaudia.Gorecka@zut.edu.pl (K. Górecka), Angelika.Linowska@zut.edu.pl (A. Linowska). Peer review under the responsibility of Institute of Oceanology of the Polish Academy of Sciences.



Production and hosting by Elsevier

<https://doi.org/10.1016/j.oceano.2018.02.001>

0078-3234/© 2018 Institute of Oceanology of the Polish Academy of Sciences. Production and hosting by Elsevier Sp. z o.o. This is an open access article under the CC BY-NC-ND license (<http://creativecommons.org/licenses/by-nc-nd/4.0/>).

from the North Sea. In December 2014, a strong Major Baltic Inflow brought large amounts of water into the Baltic Sea, followed by some inflows of moderate intensity.

© 2018 Institute of Oceanology of the Polish Academy of Sciences. Production and hosting by Elsevier Sp. z o.o. This is an open access article under the CC BY-NC-ND license (<http://creativecommons.org/licenses/by-nc-nd/4.0/>).

The velvet belly lanternshark, *Etmopterus spinax* (L., 1758), is a deep-sea bioluminescent squaloid shark (Claes and Mallefet, 2009) found predominantly in the northeast Atlantic, the western Mediterranean Sea and in deep waters off southern Africa (south of Senegal) at depths of 70–2000 m and most abundantly at 200–500 m (Compagno et al., 2005). According to McEachran and Branstetter (1984), it occurs rarely in the North Sea and is absent from the Baltic; however, Bergstad et al. (2003) report that this species is a characteristic member of the Skagerrak deep-water fish assemblage at depths of 300–700 m, while Compagno (1984) report Skagerrak and Kattegat to be part of the distribution of the species. *E. spinax* is a non-commercial species that is caught only as by-catch in bottom trawls fishing for *Nephrops norvegicus* (L. 1758) and *Pandalus borealis* Krøyer, 1838 in the Skagerrak and Kattegat by Swedish fishermen. All specimens are probably discarded, which limits the data that is available. It has never been recorded in logbooks. However, in Swedish waters, bottom-trawls are required to have a selective grid that should help to reduce by-catch of *E. spinax* (Coelho et al., 2009).

Data from the Mediterranean Sea and the eastern central and south Atlantic indicate that the species is caught relatively commonly in scientific trawl surveys, and since there is no evidence that the population has declined there, its IUCN Red List status is least concern (LC) (Coelho et al., 2009). However, the over-exploitation of shelf fish stocks has triggered many fisheries to exploit marine resources at ever greater ocean depths (Morato et al., 2006), and this species is considered vulnerable to over-fishing because of its late maturity (Coelho and Erzini, 2008). Furthermore, the reproductive cycle in *E. spinax* has been suggested to last from two to three years before viviparous parturition, which suggests this species has low fecundity. Occurring frequently as by-catch in deep-water fisheries landing crustaceans and teleosts, the species is exposed to relatively high levels of mortality (Porcu et al., 2014). Therefore, lacking any commercial value and commonly discarded in trawl and longline fisheries, *E. spinax* has been poorly studied (Coelho and Erzini, 2008).

According to Klimpel and Palm (2002), parasitological studies on deep-water chondrichthyans from the northeastern Atlantic are scarce. To date, no parasitic investigations of this species have been done in the Baltic Sea area.

The aim of the study was to present the first record of *E. spinax* in the Pomeranian Bay, which is the first time it has been noted in the southern Baltic, as well as to assign its population of origin through genetic studies. Additionally, the stomach contents, parasitic fauna, and hepatosomatic index were examined.

One specimen of the deep-water shark *E. spinax* was caught in the Pomeranian Bay (western Baltic; 54°04'80"N

14°44'00"E) on October 13, 2016, at a depth of 10 m with a cod gillnet (110 mm mesh size).

The Pomeranian Bay (Arkona Basin) is a large, shallow basin off the Polish and German coasts, no more than 30 m deep. It is a highly dynamic environment and is one of the most important ecological areas in the southwestern Baltic Sea. Salinity does not deviate from that prevailing in southern Baltic surface waters (7 psu) (Czugała and Woźniczka, 2010).

Sixteen diagnostic metric characters were studied, according to McEachran and Branstetter (1984) and Compagno et al. (2005), to the nearest mm. Weight was measured to the nearest 0.1 g.

Material for the genetic study consisted of muscle tissue fragments collected during morphological examinations of *E. spinax*. DNA was isolated using the peqGOLD Tissue DNA Mini Kit (PeqLab, Germany) following the manufacturer's instructions. Qualitative and quantitative assessment of the isolates was conducted by separation on 1.5% agarose gel and spectrophotometric assays using NanoDrop 2000 (Thermo Scientific). In order to confirm the morphological identification of the specimen, a PCR assay was performed based on the mitochondrial DNA (mtDNA) marker cytochrome oxidase subunit 1 (COI). COI sequences were amplified based on FishF2_t1 and FishR2_t1 primers according to the method described by Ivanova et al. (2007). Additionally, Elasmocr15642 and Elasmocr16638 primers were used to amplify the control region (CR) of mtDNA, and these were used to assign the specimen to populations identified in a paper published by Stonero et al. (2003). Both PCR reactions were prepared based on GoTaq[®] G2 Flexi DNA Polymerase (Promega) and subjected to a heating-cooling treatment using a thermal cycler GeneAmp PCR system 9700 thermocycler (Applied Biosystems). The results of amplification were assessed by separating the samples on 1.5% agarose gel. The COI and CR PCR products were bidirectionally sequenced using Genomed (Warsaw, Poland) and assembled with Geneious 8.1.6 (Kearse et al., 2012). Then the GeneBank database was searched BALST for matches.

The stomach content was also examined, and the hepatosomatic index (HSI) (%), which is the ratio between liver weight and fish weight, was calculated as follows:

$$HSI = 100 \times \frac{LW}{W},$$

where LW – liver weight (g) and W – fish wet weight (g).

The parasitological examination focused on the skin, vitreous humor, eye lens, mouth, buccal and nasal cavities, gills, gastrointestinal tract, kidney, peritoneum, and muscles. The nematode was isolated and transferred to glycerin

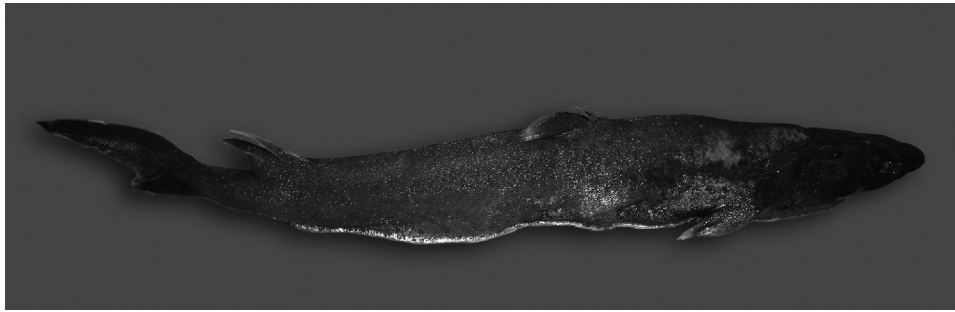


Figure 1 The specimen studied from the Pomeranian Bay.

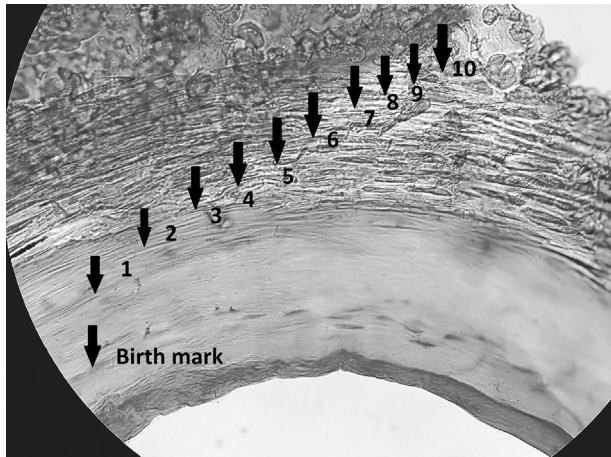


Figure 2 Age validation of *Etmopterus spinax* female collected in the Pomeranian Bay.

to increase transparency. Vertebrae for age determination were removed from the specimen examined from the cervical regions. First, a thin section through the center of the centrum was prepared, then it was stained with hematoxylin and eosin, embedded in a hard epoxy and mounted onto a microscope slide (Campana, 2014). The age was determined under the microscope Motic BA 210 (at 100 \times magnification).

The *E. spinax* specimen examined was a female 42.7 cm in total length TL (Fig. 1) and 311.6 g in weight (gutted weight was 229.5 g). The fish specimen was ten years old (Fig. 2).

Head length (HL) was 21.17% of TL. The snout of the individual examined was long (47.49% of HL). The nostrils were located about midway from the snout tip to the eye (slightly closer to the eye – 54.35%). The eye diameter was long (25.43% of HL), but it was not longer than the distance from the snout tip to the eye (28.34%). The mouth width (43.55% of HL) was slightly less than snout length (47.49% of HL). The spiracle was above and behind the eye (Fig. 3). The gill openings were similar in size to the spiracle (7.06% of HL each), and they were less than one-third of eye length. The interdorsal space was short (21.47% of TL) and was much shorter than the pectoral-pelvic fin distance (34.15%). The bases of dorsal fins D_2 and D_1 were 8.16% and 5.19% of TL, while the heights of D_2 and D_1 were 7.71% and 5.65% of TL, respectively. Similarly, the spine in D_2 was higher than that in D_1 (6.40% and 4.27% of TL, respectively). The distance from the pelvic insertions to the ventral caudal origin was slightly

longer than that from the tip of the snout to the first gill openings (20.96% and 17.55%, respectively). The morphological characters of the specimen described in this work correspond to data reported in McEachran and Branstetter (1984) and Compagno et al. (2005), with the exception of the eye diameter dimension, which in the current study was not longer than the distance from the snout tip to the eye.

BLAST analysis of the COI barcode confirmed the identity of the collected specimen as *E. spinax*, and the barcode for this species was previously submitted to GenBank (i.e., KJ128486.1). Specimen assignment to the population of origin based on the 913 bp sequence of CR revealed that, according to work published by Gubili et al. (2016), the *E. spinax* specimen collected in the Baltic Sea shared identical sequences (haplotypes) with fish collected in the north Atlantic, from the Azores (KX494600.1, KX494606.1, KX494607.1, KX494608.1), the Rockall Trough (KX494695.1, KX494680.1), and west of Ireland (KX494644.1, KX494637.1, KX494634.1).

Velvet belly lanternsharks from these populations had significantly negative F_u 's F_s values, but only that from Ireland also exhibited a unimodal distribution, suggesting population expansion for the CR. It is interesting that the haplotype identified in the specimen examined was not described in regions that are geographically adjacent (i.e., Norway or the North Sea), but in Atlantic basins. One of the reasons for this could be the small sample size of Norwegian sample collection or the lower level of haplotype diversity of the North Sea samples. The results presented by Gubili et al. (2016) demonstrating high levels of connectivity and gene-flow in this species across the northeast Atlantic suggest similar events among populations from the eastern North Sea and the Baltic Sea.

Previous genetic work has produced little evidence of population structure in members of deep-water shark groups with gene-flow occurring at all but the largest oceanic distances assessed, which supports the generally held paradigm of high connectivity and low population structure in marine species (Ward et al., 1994). Recently, the study by Gubili et al. (2016) demonstrated high levels of gene-flow in *E. spinax* across the northeast Atlantic, adding to a relatively limited literature examining the population genetics and phylo-geography of potentially vulnerable deep-sea sharks. Furthermore, the significant population sub-division observed between Atlantic and Mediterranean lanternsharks highlights the potentially significant role of bathymetry as a barrier to connectivity, with important implications for fisheries management.



Figure 3 Head of the specimen studied, with the spiracle above the eye.

The diet of *E. spinax* has been analyzed as follows: crustaceans 74.8%, fishes 16.9%, cephalopods 6.9%, polychaetes 0.9%, and others 0.5% (Cecchi et al., 2004). In this work, the stomach of the specimen studied was empty, and only one nematode *Anisakis simplex* (Rudolphi, 1809) L3 larva from the stomach lumen was identified. The larvae of this nematode occur in marine fish (mainly in herring, mackerel, and cod-like families), in which they migrate from the stomach to the body cavity and locate in the intestine, as well as on the peritoneum and under the liver and gonad capsules. The larva found in *E. spinax* specimen was dead, hence its presence in the empty stomach.

The larvae of *A. simplex* in this host was first identified by Klimpel and Palm (2002) in specimens from the Norwegian Deep. In addition to internal parasites such as the nematode larvae of two species (*A. simplex*) and *Hysterothylacium aduncum* (Rudolphi, 1802) and three species of tapeworms, they found two monogenean species that are ectoparasites. *A. simplex* and *H. aduncum* are listed in the Baltic Proper (in the Gulf of Finland, the Gulf of Gdańsk, and the Pomeranian Bay; Unger et al., 2014). It is worth mentioning that nematodes exhibit great flexibility with regard to environmental changes. No ectoparasites were found in the specimen examined; however, since they are more sensitive to environmental changes, they could have died while their host was in the low-saline waters of the Baltic Proper. It is not known how long the specimen was in Baltic Sea waters, or whether the nematode infection occurred in the Baltic Sea, because there was no prey in the stomach. The infection could have occurred in the North Sea by swallowing the larva along with its first intermediate host, such as marine planktonic copepods (euphausiids), or it could have occurred in the Baltic Sea via teleosts as intermediate or paratenic hosts (Klimpel and Palm, 2002).

The HSI presented in this work is in agreement with Porcu et al. (2014). According to their work, the liver of *E. spinax* is relatively small at 11.5% and 10.3% of total body weight in females and males, respectively (11.07% in the present study). HSI values are higher in mature females, but it decreases during pregnancy, and a slight increase is observed in spent females.

The specimen of *E. spinax* studied in this work was found in the Pomeranian Bay trapped in a cod gillnet at a depth of

10 m. The velvet belly lanternshark, however, is usually found on, near, or well above the substrate from 70 to 2000 m, although mostly between depths of 200 and 500 m (Compagno, 1984). In the northeast Atlantic, *E. spinax* has been caught at depths of 400–1000 m (Merrett et al., 1991). It is known to segregate by size into different depths with large, mature females found at the greatest depths (Gibson et al., 2006). In general, smaller (<30 cm) individuals tend to occur at depths of less than 500 m, while mature individuals are found at moderate depths (500–600 m) (Coelho et al., 2009). This may suggest that these mature sharks are being affected more by commercial deep-water fisheries than other life stages of *E. spinax* that are found in shallower waters. The female *E. spinax* examined in this study can be considered large, because specimens of this species rarely exceed 45 cm (Compagno, 1984). The age determined of specimen examined (ten years) is in agreement with Gennari and Scacco (2007) from the Tyrrhenian Sea (ten years old females were of 37.5–42.0 cm TL) and in Coelho and Erzini (2008) from the waters off Portuguese coast (ten years old females were of 41.1 cm TL).

The specimen collected could have arrived in the Pomeranian Bay along with an inflow from the North Sea. In December 2014, a strong Major Baltic Inflow (MBI), classified as a rare, very strong event, brought large amounts of saline water into the Baltic Sea (Naumann et al., 2016). In November 2015, a series of twelve low-pressure cells crossed the Baltic Sea. During the winter of 2015–2016, again two MBIs of moderate intensity followed the previous one. In this warm winter, only one phase of cold continental weather conditions triggered an outflow at the beginning of January. Afterward, warm maritime weather continued again with storms at the end of January and the beginning of February. In September 2016, a baroclinic inflow was observed at the Darss Sill (Naumann et al., 2016).

A better understanding of the biology, ecology, population structure, and migratory activity of deep-water chondrichthyans is needed to make reliable predictions on the long-term effects of fishing and to ensure that these species are sustainably managed in the future (Cunha et al., 2012).

Acknowledgments

Authors thank Prof. Małgorzata Sobczak for technical support in the microscope slide preparation of the *E. spinax* vertebrae.

References

- Bergstad, O.A., Wik, Å.D., Hildre, Ø., 2003. Predator–prey relationships and food sources of the Skagerrak deep-water fish assemblage. *J. Northw. Atl. Fish. Sci.* 31, 165–180.
- Campana, S.E., 2014. Age determination of elasmobranchs, with special reference to Mediterranean species: a technical manual. *Studies and Reviews. General Fisheries Commission for the Mediterranean*. No. 94. FAO, Rome, p. 38.
- Cecchi, E., Mancusi, C., Pajetta, R., Serena, F., 2004. Contributo alla conoscenza della biologia di *Etmopterus spinax* (Linnaeus, 1758) (Chondrichthyes, Etmopteridae). *Biol. Mar. Medit.* 11 (2), 564–568.
- Claes, J.M., Mallefet, J., 2009. Hormonal control of luminescence from lantern shark (*Etmopterus spinax*) photophores. *J. Exp. Biol.* 212, 3684–3692, <http://dx.doi.org/10.1242/jeb.034363>.
- Coelho, R., Erzini, K., 2008. Identification of deep water lantern sharks (Chondrichthyes: Etmopteridae) using morphometric data and multivariate analysis. *J. Mar. Biol. Assoc. UK* 88 (1), 199–204, <http://dx.doi.org/10.1017/S0025315408000271>.
- Coelho, R., Blasdale, T., Mancusi, C., Serena, F., Guallart, J., Ungaro, N., Litvinov, F., Crozier, P., Stenberg, C., 2009. *Etmopterus spinax*. In: The IUCN Red List of Threatened Species. , <http://dx.doi.org/10.2305/IUCN.UK.2009-2.RLTS.T161388A5412576.en>.
- Compagno, L.J.V., 1984. *Sharks of the World: An Annotated and Illustrated Catalogue of Shark Species Known to Date*. Vol. 4, Pt. 1. Hexanchiformes to Lamniformes. FAO, Rome.
- Compagno, L.J.V., Dando, M., Fowler, S., 2005. *Sharks of the World*. Harper Collins Publ. Ltd., London, 368 pp.
- Cunha, R.L., Coscia, I., Madeira, C., Mariani, S., Stefanni, S., Castilho, R., 2012. Ancient divergence in the trans-oceanic deep-sea shark *Centroscymnus crepidater*. *PLoS ONE* 7 (11), e49196, <http://dx.doi.org/10.1371/journal.pone.0049196>.
- Czugała, A., Woźniczka, A., 2010. The River Odra estuary – another Baltic Sea area colonized by the round goby *Neogobius melanostomus* Pallas, 1811. *Aquat. Invent.* 5 (Suppl. 1), 61–65, <http://dx.doi.org/10.3391/ai.2010.5.S1.014>.
- Gennari, E., Scacco, U., 2007. First age and growth estimates in the deep water shark, *Etmopterus spinax* (Linnaeus, 1758), by deep coned vertebral analysis. *Mar. Biol.* 1–8, <http://dx.doi.org/10.1007/s00227-007-0769-y>.
- Gibson, C., Valenti, S.V., Fowler, S.L., Fordham, S.V., 2006. The conservation status of northeast Atlantic chondrichthyans. In: Report of the IUCN Shark Specialist Group Northeast Atlantic Regional Red List Workshop. IUCN SSC Shark Specialist Group, Newbury.
- Gubili, C., Macleod, K., Perry, W., Hanel, P., Batzakis, I., Farrell, E. D., Lynghammar, A., Mancusi, C., Mariani, S., Menezes, G.M., Neat, F., Scarcella, G., Griffiths, A.M., 2016. Connectivity in the deep: phylogeography of the Velvet Belly Lanternshark. *Deep Sea Res. I* 115, 233–239, <http://dx.doi.org/10.1016/j.dsr.2016.07.002>.
- Ivanova, N.V., Zemlak, T.S., Hanner, R.H., Hebert, P.D.N., 2007. Universal primer cocktails for fish DNA barcoding. *Mol. Ecol. Notes* 7, 544–548.
- Kearse, M., Moir, R., Wilson, A., Stones-Havas, S., Cheung, M., Sturrock, S., Buxton, S., Cooper, A., Markowitz, S., Duran, C., Thierer, T., Ashton, B., Mentjies, P., Drummond, A., 2012. Genious Basic: an integrated and extendable desktop software platform for the organization and analysis of sequence data. *Bioinformatics* 28 (12), 1647–1649.
- Klimpel, S., Palm, H.W., 2002. Metazoan parasites and food composition of juvenile *Etmopterus spinax* (L., 1758) (Dalatiidae, Squaliformes) from Norwegian Deep. *Parasitol. Res.* 89, 245–251.
- McEachran, J.D., Branstetter, S., 1984. Squalidae. In: Whitehead, P. J.P., Bauchot, M.L., Hureau, J.C., Nielsen, J., Tortonese, E. (Eds.), *Fishes of the Northeastern Atlantic and the Mediterranean*, vol. 2. Unesco, Paris, 128–147.
- Merrett, N.R., Gordon, J.D.M., Stehmann, M., Haedrich, R.L., 1991. Deep demersal fish assemblage structure in the Porcupine Seabight (Eastern North Atlantic): slope sampling by three different trawls compared. *J. Mar. Biol. Assoc. UK* 71 (3), 329–358.
- Morato, T., Watson, R., Pitcher, T.J., Pauly, D., 2006. Fishing down the deep. *Fish Fish.* 7, 24–34.
- Naumann, M., Nausch, G., Mohrholz, V., 2016. Water Exchange between the Baltic Sea and the North Sea, and conditions in the Deep Basins. HELCOM Baltic Sea Environment Fact Sheets <http://www.helcom.fi/baltic-sea-trends/environment-fact-sheets>.
- Porcu, C., Marongiu, M.F., Follasa, M.C., Bellodi, A., Mulas, A., Pesci, P., Cau, A., 2014. Reproductive aspects of the velvet belly *Etmopterus spinax* (Chondrichthyes: Etmopteridae), from the Central Western Mediterranean Sea, Notes on game-to genesis and oviducal gland microstructure. *Mediterr. Mar. Sci.* 15, 313–326, <http://dx.doi.org/10.12681/mms.559>.
- Stonero, D.S., Grady, J.M., Priede, K.A., Quattro, J.M., 2003. Amplification primers for the mitochondrial control region and sixth intron of the nuclear-encoded lactate dehydrogenase A gene in elasmobranch fishes. *Conserv. Genet.* 4 (6), 805–808.
- Unger, P., Klimpel, S., Lang, T., Palm, H.W., 2014. Metazoan parasites from herring (*Clupea harengus* L.) as biological indicators in the Baltic Sea. *Acta Parasitol.* 59 (3), 518–528.
- Ward, R.D., Woodward, M., Skibinski, D.O.F., 1994. A comparison of genetic diversity levels in marine, freshwater, and anadromous fishes. *J. Fish Biol.* 44, 213–232.